Title
Anionic N-Heterocyclic Carbenes Featuring Carboranes: Reactivity and Catalysis

Author
Raviprolu, Varun Tej

Publication Date
2023

Peer reviewed|Thesis/dissertation

UNIVERSITY OF CALIFORNIA
RIVERSIDE

Anionic N-Heterocyclic Carbenes Featuring Carboranes: Reactivity and Catalysis

A Dissertation submitted in partial satisfaction
of the requirements for the degree of

Doctor of Philosophy

in

Chemistry

by

Varun Tej Raviprolu

September 2023

Dissertation Committee:
Dr. Vincent Lavallo, Chairperson
Dr. Matthew Conley
Dr. William Hill Harman

The Dissertation of Varun Tej Raviprolu is approved:

Committee Chairperson

University of California, Riverside

Acknowledgements

I express my deep gratitude to my parents for supporting me to achieve what I have today. This wouldn't have been possible without their encouragement in every step I have taken so far. I'm grateful for the motivation and backing I received from my brother, my uncle, grandma and their family over the past decade.

I thank my advisor Dr. Vince Lavallo for welcoming me from India and providing me an opportunity to work in his lab. I thank him for training me into a synthetic chemist and teaching me how to approach as a scientist. A special thanks to Dr. Kou for going far and beyond your way and arranging the head TA position for me. Thanks to Dr. Harman and his student Phil for performing all the CV experiments for me so patiently. I can't thank enough my grad school mentor Dr. Steven Fisher for being so patient with me during my first year and showing me all the synthetic techniques. Thanks to Dr. Jess Estrada for leaving an amazing ligand for me and helping me make it. I thank our alumnus Dr. Sarah Lee for helping me with my grad coursework and introducing me to the world of 10-vertex carbenes. I'm grateful to Pris and Natasha for being so nice about all the supplies and deliveries. I thank our ACIF staff Charlene, Veronica and Lingchao for being kind and helpful about the X-Ray crystallography, the NMR and the EPR.

I was fortunate to learn chemistry from Dr. K.S Nagarajan, my chemistry professor. Thanks to his great lectures, I developed a love for inorganic chemistry. I can never forget the guidance I received from my friends and professors at NIT Rourkela for further nurturing my knowledge and recommending me to graduate programs.

My lab mates through the past 6 years created an amazing atmosphere and I never felt away from home. I thank Anton for being a great friend and support to me over the years. I miss making fun of you. I'm indebted to Sergio, Aaron and Stephen for all the rides, help in the lab and staying with me during my hard times. I miss all the fun we had in the lab.

I thank my friend Akhil for being a great motivation and encouragement over the past decade. Thanks for all the never-ending conversations we had and helping me navigate through this challenging journey. Thanks to my friends Srivatsav, Ankush and Geeth for supporting in multiple ways before and during my PhD journey. I express gratitude to my friends Harish, Girish, Satish and Karthik for the fun we had over the phone and during my visits to India. I appreciate you all being there for me during tough times.

Lastly, I appreciate my dad's efforts in aspiring me to grow into a successful person in life. I wish you're here for this celebration. I dedicate this dissertation to him for everything he has done for me.

The text, figures and schemes for the following chapters have been reproduced, in part or in their entirety, from the following published or submitted manuscripts.

Chapter-2: A Weakly Coordinating yet Functional Au(I) Complex: Access to Organometallic Ion-Pairs

S.P. Fisher, S. McArthur, V. Tej, S. Lee, A. Chan, I. Banda, A. Gregory, K. Berkely, C. Tsay, A. Rheingold, G. Guisado-Barrios, V. Lavallo; "Strongly Coordinating Ligands to Form Weakly Coordinating yet Functional Organometallic Anions", *J. Am. Chem. Soc*., **2020**, 142, 1, 251-256.

Chapter-4: Fusing 10-vertex *Closo*-Carborane Anions with N-Heterocyclic Carbenes

V. Tej, S. Lee, I. Banda, A. Gregory, S. McArthur, S.P. Fisher, V. Lavallo; "Fusing 10-vertex closo-Carborane Anions with N-Heterocyclic Carbenes", *Chem. Commun*., **2022**, 58, 10580-10582.

Chapter-7: When the Ferrocene Analogy Breaks Down: Promiscuous Behavior of Dicarbollide Derivatives

V. Tej, P. Farias, V. Carta, H. Harman, V. Lavallo; "When the Ferrocene Analogy Breaks Down: Metallocene Transmetalation Chemistry", *Angew. Chem. Int. Ed*., **2023**, Accepted

ABSTRACT OF THE DISSERTATION

Anionic N-Heterocyclic Carbenes Featuring Carboranes: Reactivity and Catalysis

by

Varun Tej Raviprolu

Doctor of Philosophy, Graduate Program in Chemistry
University of California, Riverside, September 2023
Dr. Vincent Lavallo, Chairperson

Carbenes are neutral, divalent, six electron carbon species. Although initially perceived as reaction intermediates, pioneering work from Bertrand showed that they can be isolated in the laboratory. Further, Arduengo isolated N-Heterocyclic Carbenes (NHCs), a stable variety of persistent carbenes usually flanked by bulky aryl groups. These compounds have become popular as strongly coordinating ligands for transition metals producing some of the most active catalysts so far. Since then, there has been a growing interest in the development of NHCs for transition metal catalysis. Over the past few years, our lab has been developing NHCs featuring weakly coordinating Carborane anions. Due to the inherent charge on these molecules, the resulting NHCs are overall mono or dianionic depending on the number of carboranes in the molecule.

To impart more robust nature for reactivity investigations, the dianionic 12-vertex *closo* carboranyl NHCs were hexahalogenated. The monoanionic Au(I) complex of this NHC is itself a weakly coordinating anion allowing us to pair it with a variety of main-group and organometallic cations. The synthetic utility of these ion-pairs was demonstrated by a tandem hydroamination of alkynes followed by the hydrosilylation of the imines using a Au(I)/N-methyl benzothiazolium system. The scope of these carboranyl NHCs was then expanded to the 10-vertex *closo* carborane where stable NHCs bearing this carborane were synthesized using novel synthetic methods. Perchlorination of this carbene, including the backbone bearing the imidazolylidene ring rendered an unprecedented water stable carbene. Moreover, we show the 10-vertex carboranyl NHC is a strong ligand through synthesis of the corresponding Cu(I) and Au(I) complexes.

The dicarbollide ligand, derived from the *o*-carborane was then functionalized to produce the bis(dicarbollide)iron appended NHCs, the isolobal equivalents of ferrocene. Despite the long-established analogy with ferrocenes, these complexes were seen to behave in a promiscuous way. An unusual transmetalation reaction with other transition metals was discovered to produce the first examples of metallacarborane appended NHCs. Coordination of these NHCs with Cu(I) produced bimetallic complexes with a rare coordination environment. The promiscuous nature of the dicarbollide-NHC ligands was further illustrated by their diverse reactivity with a Pd(II) precursor.

Table of Contents

List of Figures

Chapter-1:

Chapter-2:

Chapter 3:

Chapter-4:

List of Schemes

Chapter-1

Chapter-2

Chapter-3

List of Tables

Chapter 1: Introduction

1.1 Background

Benzene (Fig. **1**), a simple aromatic hydrocarbon was first isolated as a liquid from compressed coal gas in 1825 by Michael Faraday.[1] However, the structure of benzene remained elusive till 1865 when kekule proposed a cyclic arrangement of six carbon atoms connected to each other through alternative single and double bonds. In 1931, Linus Pauling proposed benzene had a single structure which is a resonance combination of the two possible structures with alternating single and double bonds.[2] Around the same time, Huckel defined cyclic planar molecules that have 4n+2 π electrons in conjugation as aromatic compounds, commonly called arenes.[3]

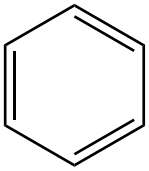

Fig. **1.1** Benzene

In the presence of an external magnetic field, the absolute magnetic shielding at the center of the ring directly correlates with the aromaticity of the arene. The Nucleus-Independent Chemical Shift (NICS) calculations that compute the magnetic shielding could thus be used to quantify the aromaticity of the arenes. The negative and positive NICS values indicate aromaticity and antiaromaticity of a compound respectively. For instance, benzene has a NICS value of -9.7 suggesting it's highly aromatic nature.[4] Arenes with heteroatoms like pyrrole and thiophene have NICS values of -15.1 and -13.6 respectively.[4] The contribution of the heteroatom lone pairs in ring conjugation increases the aromaticity of the arene and is reflected in its higher NICS values compared to benzene.

Another characteristic of arenes is the classical electrophilic aromatic substitution reaction (EAS) (Scheme **1.1**). In the presence of a lewis acid, the hydrogen atom of the arene is replaced by an electrophile. Every year, tons of benzene derivatives like alkyl, nitro and

halobenzenes are manufactured using this reaction. The electronic properties of arenes can be manipulated by functionalizing them with appropriate electron donating or electron withdrawing groups. The *ortho* and *para* positions of the cyclic ring are functionalized with bulky groups like isopropyl and *t*-butyl to make the arene sterically bulky.

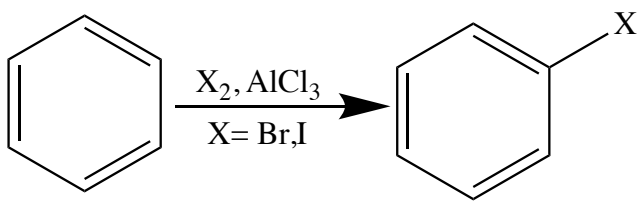

Scheme **1.1** Electrophilic Aromatic Substitution of benzene

The use of sterically bulky aryl groups is more pronounced in the context of ligand design in organometallic chemistry.[5] Steric control has been one of the central design principles in producing some of the highly active metal catalysts so far.[6-7] The fine tuning of steric and electronic properties of the ancillary ligands changes the properties and reactivity at the metal center. Bulky aryl groups like the 2,4,6-trimethylphenyl (mesityl), 2,6-diisopropylphenyl (dipp) (Fig. **1.2**) are commonly employed to alter the steric properties in diimine, phosphine, NacNac ligands among others.[8-12] Further, ancillary ligands with bulky aryl groups influence the chemo and the regioselectivity of the product outcome and in some cases help stabilizing the active catalyst.[13-14]

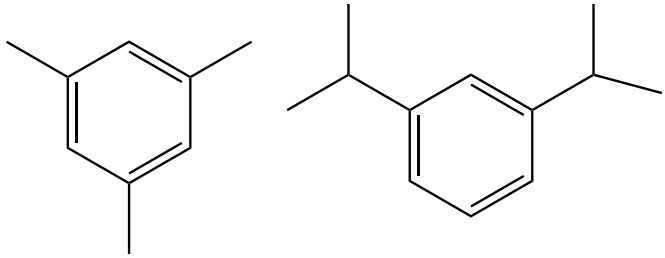

Fig. **1.2** Bulky groups used in ancillary ligand design

1.2 Carboranes

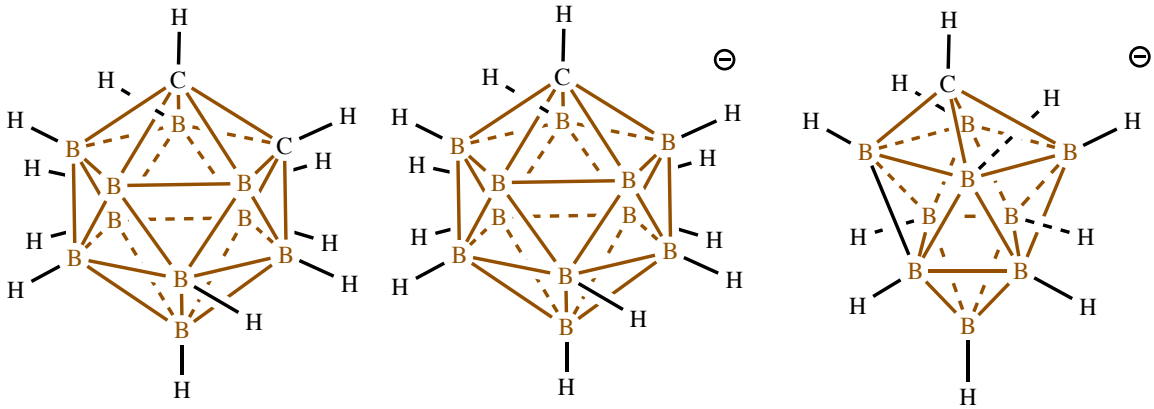

Fig. **1.3** The 12 and 10 vertex Carboranes

Another alternative to the steric tuning of aryl groups is employing an interesting class of molecules called Carboranes (Fig. **1.3**).[15-17] These are bulky polyhedral boranes usually with at least one carbon vertex. Each boron and the carbon have an exo B-H and C-H bond respectively. The electrons in the cage are highly delocalized due to the multi-centered bonding between different B-B, B-C or B-H-B units. Hence the bonding inside the cage cannot be described by the classical two centered two electron bond.[18] These compounds are highly thermally stable; some carboranes do not decompose up to temperatures of about 600ºC. Depending on the number of carbon and boron atoms, these clusters could be anionic or neutral. Fig. **1.3** shows the neutral o-carborane **1**[19], the anionic carba-*closo*-dodecaborate **2**[20] and the carba-*closo*-decaborate clusters **3.**[21] **1** and **2** are examples of icosahedral carboranes meaning the clusters have twelve vertices. The neutral cluster **1** has ten borons and two carbons while **2** has eleven borons and one carbon making it anionic.

The cluster **3** is a smaller analogue of **2** with nine borons and one carbon and is anionic as well.

In the borane nomenclature, the clusters **1**-**3** are termed *closo* implying they look closed and are examples of complete polyhedra.[22] The clusters that lack one vertex are termed *nido* and the clusters that lack two vertices are called *arachno*. The presence of delocalized electrons in these clusters resembles that in arenes. However, these compounds are non-planar, hence they are often referred to as 'three dimensional aromatic compounds.' This is further corroborated by the NICS calculations-the values for carborane **1** derivatives are in the range of -34 indicating the high aromatic nature of these compounds.[23] Moreover, in the presence of elemental halogens and bronsted acids, the boron atoms of the clusters undergo halogenation analogous to the electrophilic aromatic substitution reactions in arenes (Scheme **1.2**).[24] The reactivity pattern was found to be very similar to that of arenes justifying the term three-dimensional aromaticity.

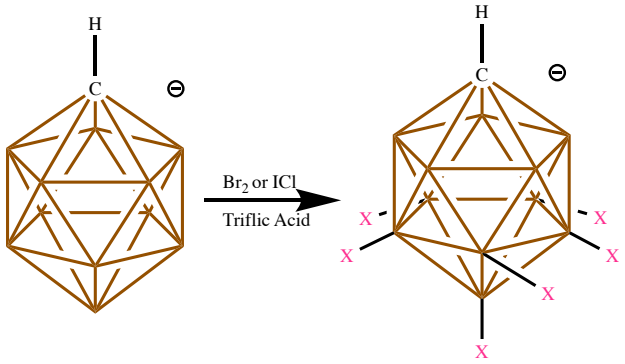

Scheme **1.2** Hexahalogenation of *closo* carborane anions

Due to the inductive effect of the carbon atom, the antipodal boron vertex and the lower pentagonal belt of the carborane are more nucleophilic-evident by the faster rate of halogenation of the antipode and the lower belt in electrophilic aromatic substitution like reaction compared to the upper pentagonal belt. This property allows the selective isolation of the clusters that are partially halogenated with Br or I (harder with Cl due to the faster rate of halogenation) when the reaction conditions and progress are carefully monitored.

The property that made the anionic carboranes widely applicable in synthetic chemistry is their weakly coordinating behavior. The highly delocalized electron cloud in the anionic carboranes, particularly **2** yields in very weak coordination to the counter-cation they are paired with. Hence, classically they were used as Weakly Coordinating Anions (WCAs) to stabilize highly reactive cations as pioneered by the work of Prof. Reed at University of California, Riverside.[25-26] The halogenation of the clusters renders them less nucleophilic, more robust and more weakly coordinating due to the electron-withdrawing effect imparted by the halogens.

The fully chlorinated carborane **2** (Cl_{11}) was used to isolate the benzenium ($C_6H_7^+$) cation, fullerenium (HC_{60}^+) cation, the triisopropyl silylium and *t*-butyl cation.[27-30] Moreover, the isolation of a free proton H^+ was possible with this anion and the compound behaves as a super acid.[31] Other than stabilizing reactive cations, carboranes were applied in material sciences and in medicine as a boron source in boron neutron capture therapy.[32-36] Deviating from their classical applications, our lab started investigating carboranes as substituents for ancillary ligands.[16-17] The inherent charge and the steric bulk of these molecules would impart novel coordination environments around metal centers and potentially influence the catalytic activity of transition metals complexes.

1.3 Carboranes in Ligand Design

While the cluster **1** is very widely used as a ligand substituent, it has certain drawbacks that limit its utility in ligand design. The B-H bonds on **1** are more susceptible to oxidative additions on to metal centers producing cyclometalated products. However, the anionic carboranes **2** and **3** are more resistant to the cluster B-H oxidative addition. Hence incorporating **2** and **3** in ligand scaffolds should result in more stable metal complexes and higher catalytic activity. One earlier report of using **2** as ligand substituent came from Strauss and co-workers (Scheme **1.3**).[37] They treated the nBu_4N^+ salt of F_{11} cluster with Cu(mesityl)$_n$ in the presence of nBu_4NCl as a chloride source to produce the $F_{11}CuCl$ complex where Cu was attached to the cluster carbon atom. Later, several other groups reported Cu, Ag, Zn and Hg complexes of Cl_{11}, Br_{11} clusters, where the metal atom was bonded to the cluster carbon.[38-40] However, most of these compounds represent carborane functionalized metal complexes rather than carborane ancillary ligand complexes. The first example of a carborane ancillary ligand came from Reed's group in 1993 with their reported carborane functionalized phosphine ligand.[41] Following this, our group reported a more electron donating phosphine with cluster **3** (Fig. **1.4**).[42]

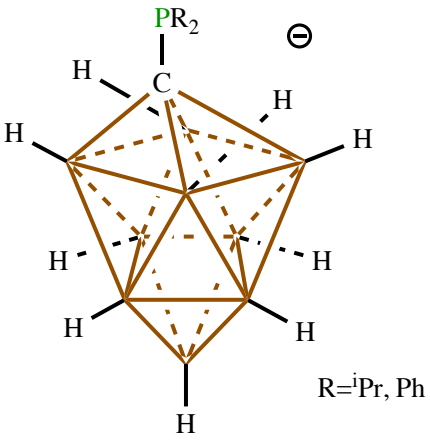

Fig. **1.4** The 10-vertex carborane appended phosphine

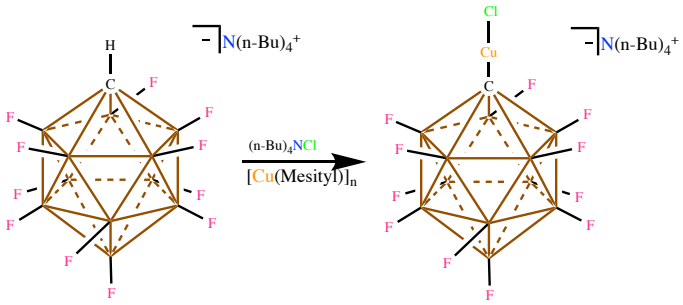

Scheme **1.3** Synthesis of carborane appended Cu complex

1.4 N-Heterocyclic Carbenes

Over the past couple decades, carbene ligands have become very popular choice of ancillary ligands for transition metal complexes.[43-48]

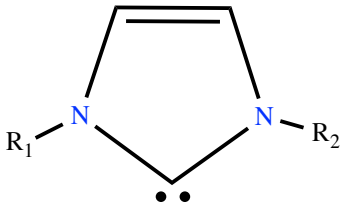

R_1,R_2 = Mesityl, Dipp

Fig. **1.5** The generic structure of N-Heterocyclic Carbene

Carbenes were initially thought of as reaction intermediates impossible to isolate till a stable carbene was first isolated by Guy Bertrand in 1988.[49] Later in 1991, Arduengo reported the N-Heterocyclic Carbenes (NHCs) as more robust singlet carbenes and characterized them using X-Ray diffraction and NMR spectroscopy.[50] The NHCs usually feature bulky aryl substituents on the nitrogens that help prevent the dimerization of the carbene to the olefin, known as the Wanzlick equilibrium.[51] The stability of these carbenes primarily arises from the π electron donation of the nitrogens into the empty p-orbital of the carbene carbon. Further, a diverse library of NHCs can be synthesized with ease by slightly varying the starting materials and reaction conditions. This, coupled with their strong sigma donating properties have made the NHCs one of the strongly coordinating ligands to transition metals, stronger than phosphines.

1.5 Closo Carboranyl NHCs

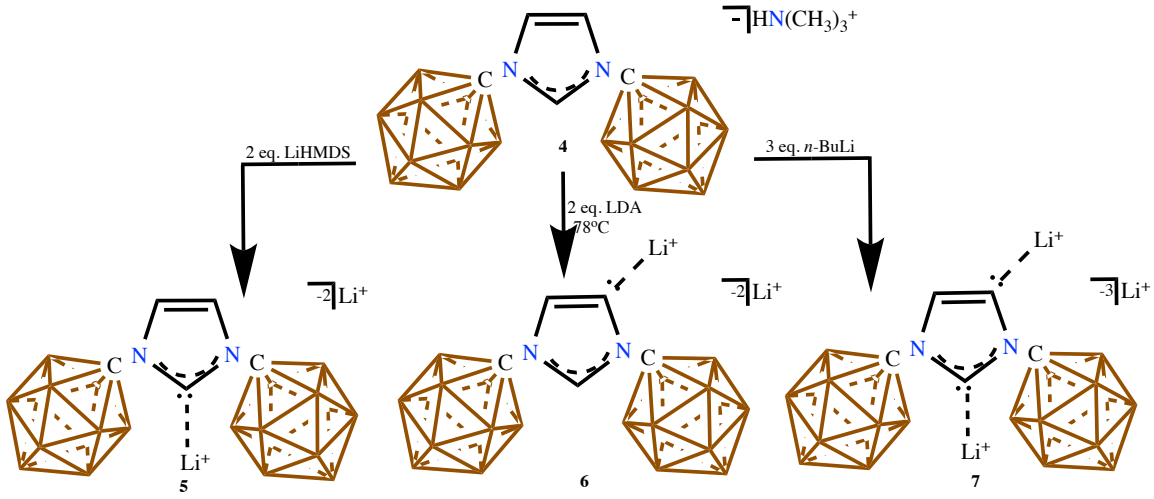

Scheme **1.4** Deprotonation of imidazolium **4** to produce normal **5**, abnormal **6** and paranormal **7** carbenes

Carboranes are sterically bulkier than the Mes or Dipp groups used in NHC design. Hence, it should be possible to synthesize stable NHCs appending carboranes onto the imidazolium ring nitrogens. Moreover, the inherent charge of the anionic clusters **2** and **3** would render the NHC dianionic, making them more electron rich. Our group envisioned these anionic NHCs can act as stable anionic ligands for transition metal complexes. Subsequently in 2014, our group reported the first ever carborane functionalized NHCs where the bulky aryl groups were replaced by cluster **2**.[52] (Scheme **1.4**). The anionic charge of the two carborane clusters rendered the NHC dianionic overall. Depending on the base and the reaction conditions, they could isolate three classes of carbenes from the same imidazolium precursor-normal **5**, abnormal **6** and the paranormal **7** NHCs. When the trimethylammonium salt of the imidazolium was treated with two equivalents of LiHMDS, it produced the normal carbene where the C-2 proton was deprotonated. Deprotonation with 2 equivalents of LDA at low temperature resulted in deprotonation at C-5 position producing the abnormal carbene. Deprotonation with 3 equivalents of *n*-BuLi produced the carbene deprotonated at both C-2 and C-5 positions called the paranormal carbene (Scheme

1.4). In solid state, the carbene lone-pair is coordinated to one of the Li^+ counter-cations. Hence, these anionic NHCs are technically carbenoids. This presents the significance of appending carboranes, since isolating different classes of carbenes wasn't something possible with classical NHCs appending aryl groups. The inherent charge and sterics of the carboranes likely resulted in this unconventional behavior.

Later, our group reported unsymmetrical imidazoliums where one of the ring nitrogens is

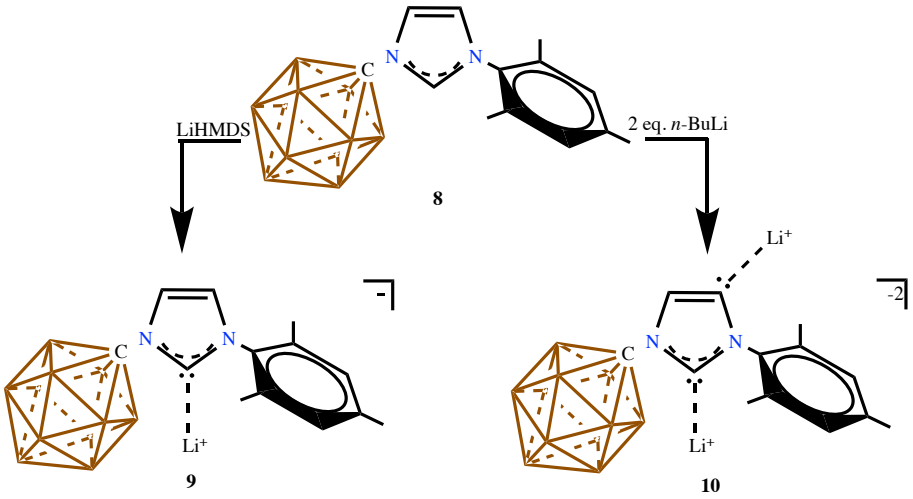

Scheme **1.5** Synthesis of unsymmetrical normal NHC **9** and paranormal NHC **10**

appended by an aryl group (mesityl) and the other with carborane **2**.[53] The charge balance here produces a zwitterionic imidazolium which upon deprotonation with 1 equivalent of LiHMDS produced the normal carbene **9**. Deprotonation with two equivalents of *n*-BuLi afforded the doubly deprotonated paranormal NHC **10** (Scheme **1.5**). The electronic and steric effects imparted by the carborane are apparent here: the backbone of the imidazolium ring was selectively deprotonated at the carbon closer to the mesityl ring.

Subsequently, our group alumni Dr. Fisher explored the possibility of employing the dianionic NHC **5** as an ancillary ligand for transition metal complexes. Treatment of NHC with $ClAuSMe_2$ in PhF at -40°C produced the Au(I) complex of the NHC **11** (Scheme **1.6**).[54] Later, this compound was made in a two-step process producing more yield.

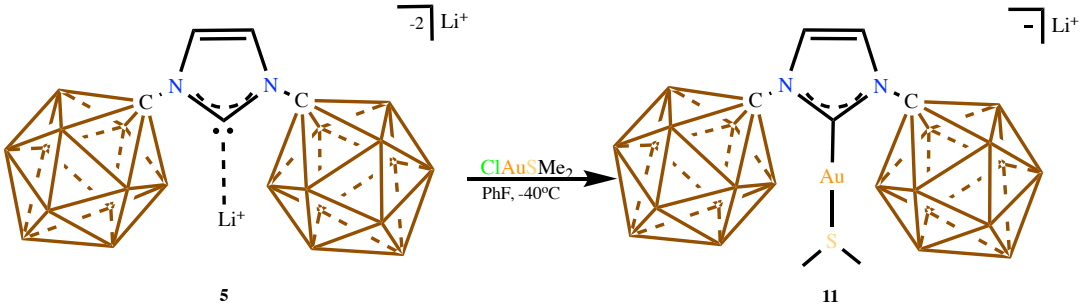

5 11

Scheme **1.6** Synthesis of anionic Au(I) complex **11**

Initially, the NHC was treated with $ClAuSMe_2$ in THF to produce the NHC-Au-Cl complex. This was dissolved in DCM and treated with SMe_2 to precipitate LiCl producing the NHC-Au-SMe_2 complex.

1.6 Nido Carboranes as Cp Mimics

Like previously discussed, the *o*-carborane is susceptible to B-H oxidative addition more so than the corresponding anionic *closo* clusters. This precludes the synthesis of imidazoliums like **5** with *o*-carborane. However, the interesting property of *o*-carborane is its boron vertex extrusion when refluxed in alcohols in the presence of a base. Discovered by Prof. Hawthorne at the University of California, Riverside, this deboronation reaction produces the anionic *nido* carborane **12** with a bridging hydride that's fluxional between the three borons on the open face of the cluster (Scheme **1.7**).[55]

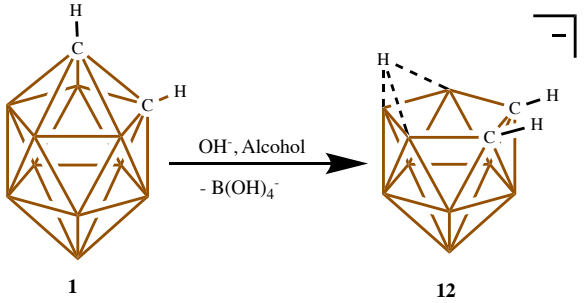

1 12

Scheme **1.7** Deboronation of the o-carborane

The bridging hydride could be deprotonated with a strong base like NaH to produce a dianionic cluster species termed the 'dicarbollide' by Hawthorne. The

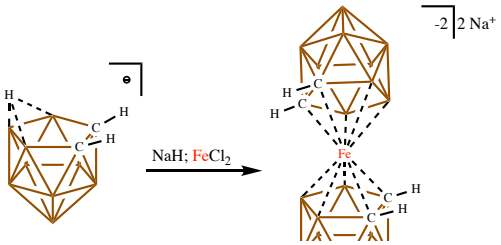

Scheme **1.8** Synthesis of bis(dicarbollide)iron **13**

13

dicarbollide upon treatment with $FeCl_2$ produced the bis(dicarbollide) iron **13**, the ferrocene analogue of carboranes (Scheme **1.8**).[56] This work established that the dicarbollides mimic the behavior of cyclopentadienyl (Cp) ligand. Further, the group reported the cobalt and nickel analogues of this compound.[56] The dianionic bis(dicarbollide) iron and cobalt complexes behave as one electron oxidants and reductants respectively analogous to their Cp counterparts.

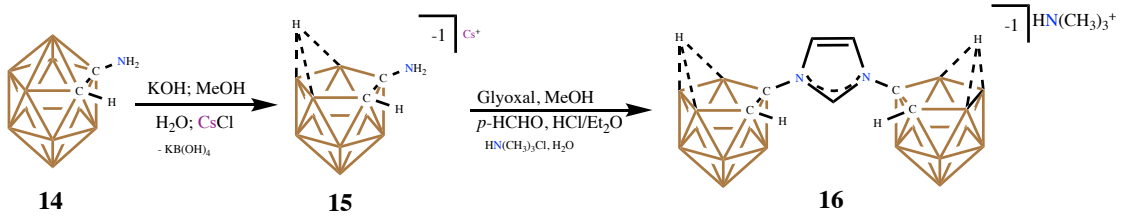

Scheme **1.9** Synthesis of symmetrical imidazolium **16**

1.7 Nido Carboranyl NHCs

Considering the Cp like behavior of the dicarbollide, our lab alumni envisioned an NHC with nitrogens appending a dicarbollide unit would be an interesting ancillary ligand. This ligand would not only possess the σ donating properties of the carbene, but the ability of the dicarbollide to form π complexes as well. Subsequently, Dr. Estrada synthesized the o-carboranyl amine **14** and subjected it to deboronation conditions to produce the *nido* dicarbollyl amine **15**. The amine when treated with glyoxal and p-formaldehyde in HCl/ether produced the imidazolium **16** (Scheme **1.9**). When both the bridging hydrides of the dicarbollides and the iminium C-2 proton of **16** were deprotonated, it produced the tetraanionic NHC **17** (Scheme **1.10**) which had poor solubility and hard to characterize.

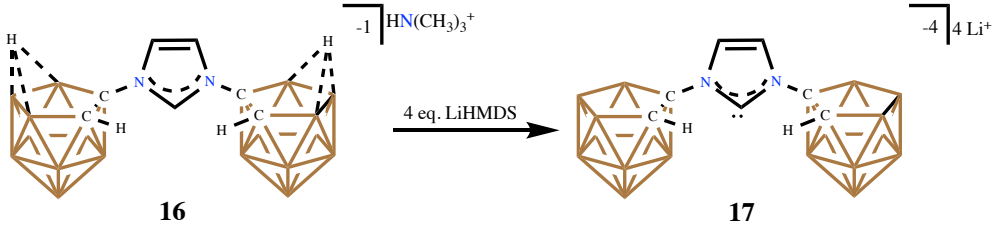

Scheme **1.10** Synthesis of unsymmerical imidazolium **17**

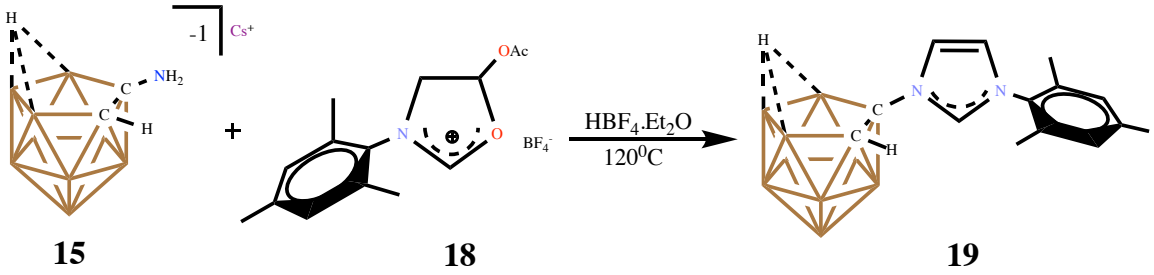

Scheme **1.11** Synthesis of unsymmetrical imidazolium **19**

Alternatively, Dr. Estrada considered replacing one of the dicarbollide units by a mesityl group to enhance the solubility. To synthesize this unsymmetrical imidazolium, the anionic *nido* amine **15** was treated with the N-mesityl oxazolinium tetrafluoroborate salt **18** reported by Furstner et al (Scheme **1.11**).[57] The bridging hydride of the dicarbollide had a pk_a of 13 while the C-2 iminium proton of imidazolium has a pk_a of around 25. Hence, the deprotonation of this imidazolium with one equivalent of NaHMDS produced the monoanionic dicarbollide fused imidazolium **20**. Deprotonation with two equivalents of NaHMDS produced the dianionic dicarbollide fused NHC **21** (Scheme **1.12**).[58]

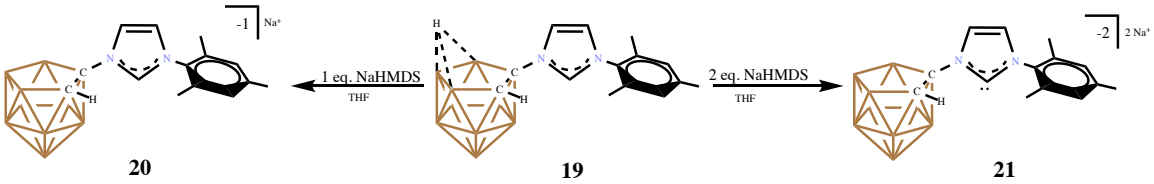

Scheme **1.12** Synthesis of dicarbollide fused imidazolium **20** and NHC **21**

The coordination chemistry of the ligands **20** and **21** will be discussed in chapters **7** and **8**.

1.8 Experimental

General Considerations:

All manipulations were carried out using standard Schlenk or glovebox techniques under a dinitrogen atmosphere (industrial grade, glovebox) or purified elemental argon

(99.995%, Schlenk line) unless otherwise stated. Dry solvents were obtained via distillation under argon from calcium hydride (acetonitrile, fluorobenzene, methylene chloride), sodium-potassium alloy (diethyl ether), potassium (benzene) or potassium using benzophenone ketyl radical as an indicator (tetrahydrofuran). Pentane and toluene were collected from a solvent purification system by SG Waters USA, LLC utilizing a fifteen minute argon sparge followed by passage though activated aluminum. The amine **15**[59] and the salt **18**[57] were synthesized according to literature procedures. Unless specifically stated, reagents were purchased from commercial vendors and used without further purification. Nuclear magnetic resonance (NMR) spectroscopy was carried out using: Bruker Avance 300 MHz, Bruker Avance 600 MHz, and Bruker NEO 400 MHz (Prodigy LN2 cryoprobe), Varian Inova 500 MHz and Bruker NEO 600 (CP-MAS). NMR chemical shifts are reported in parts per million (ppm) with ^{1}H and ^{13}C chemical shifts referenced to the residual non-deutero solvent. The ^{11}B-^{1}H coupling constants from ^{11}B spectra are reported when possible. Infrared spectroscopy was recorded on a Bruker ALPHA FTIR Spectrometer or Thermo Fisher Nicolet FTIR Spectrometer. High-resolution mass spectrometry (HRMS) was collected on an Agilent Technologies 6210 (TOF LC/MS) featuring a direct injection with multimode electrospray ionization/atmospheric-pressure chemical ionization (ESI/APCI). Melting points were obtained on a Büchi Model B-545.

Synthesis of **19**:

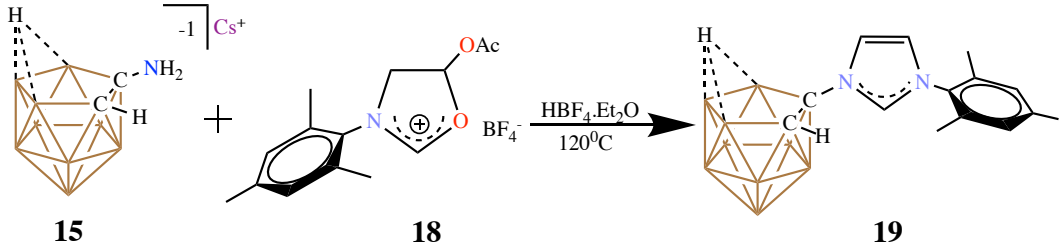

15 **18** **19**

This compound was made by a slight adaptation from the literature protocol.[58] In a nitrogen filled glove box, the *nido* amine **15** (1.0g, 3.5 mmol) was added to the oxazolinium salt **18** (1.17g, 3.5 mmol) in a teflon walled pressure vessel. The solids were dissolved in acetonitrile (20 mL) and the teflon vessel was sealed, brought outside the glove box and heated to 70^{o}C in an oil bath overnight. The vessel was then cooled to room temperature and $HBF_4.Et_2O$ (0.55 mL) was added under a stream of argon. The vessel was sealed again and heated to 120^{0}C overnight. The vessel was then cooled to room temperature and vacuum filtered to remove the insoluble salts. The concentrate was then dissolved in dichloromethane (30 mL) and washed with water in a separatory funnel. The crude dichloromethane solution was then allowed to pass through a plug of silica gel and the solvent pumped down *in vacuo*. The solid was then dissolved in about 15 mL acetonitrile and left in the freezer overnight to produce 0.6g of **19** as sharp brown crystals. The spectra matched with those reported in the literature.

1.9 *References*

1. Faraday, M., XX. On new compounds of carbon and hydrogen, and on certain other products obtained during the decomposition of oil by heat. *Philosophical Transactions of the Royal Society of London* **1997,** *115*, 440-466.

2. Pauling, L.; Wheland, G. W., The Nature of the Chemical Bond. V. The Quantum-Mechanical Calculation of the Resonance Energy of Benzene and Naphthalene and the Hydrocarbon Free Radicals. *The Journal of Chemical Physics* **2004,** *1* (6), 362-374.

3. Hückel, E., Quantentheoretische Beiträge zum Benzolproblem. *Zeitschrift für Physik* **1931,** *70* (3), 204-286.

4. Schleyer, P. v. R.; Maerker, C.; Dransfeld, A.; Jiao, H.; van Eikema Hommes, N. J. R., Nucleus-Independent Chemical Shifts: A Simple and Efficient Aromaticity Probe. *Journal of the American Chemical Society* **1996,** *118* (26), 6317-6318.

5. Izquierdo, F.; Manzini, S.; Nolan, S. P., The use of the sterically demanding IPr* and related ligands in catalysis. *Chemical Communications* **2014,** *50* (95), 14926-14937.

6. Ogba, O. M.; Warner, N. C.; O'Leary, D. J.; Grubbs, R. H., Recent advances in ruthenium-based olefin metathesis. *Chemical Society Reviews* **2018,** *47* (12), 4510-4544.

7. Vougioukalakis, G. C.; Grubbs, R. H., Ruthenium-Based Heterocyclic Carbene-Coordinated Olefin Metathesis Catalysts. *Chemical Reviews* **2010,** *110* (3), 1746-1787.

8. Stender, M.; Wright, R. J.; Eichler, B. E.; Prust, J.; Olmstead, M. M.; Roesky, H. W.; Power, P. P., The synthesis and structure of lithium derivatives of the sterically encumbered β-diketiminate ligand [{(2,6-Pri2H3C6)N(CH3)C}2CH]−, and a modified synthesis of the aminoimine precursor. *Journal of the Chemical Society, Dalton Transactions* **2001,** (23), 3465-3469.

9. Aranyos, A.; Old, D. W.; Kiyomori, A.; Wolfe, J. P.; Sadighi, J. P.; Buchwald, S. L., Novel Electron-Rich Bulky Phosphine Ligands Facilitate the Palladium-Catalyzed Preparation of Diaryl Ethers. *Journal of the American Chemical Society* **1999,** *121* (18), 4369-4378.

10. Su, M.; Buchwald, S. L., A Bulky Biaryl Phosphine Ligand Allows for Palladium-Catalyzed Amidation of Five-Membered Heterocycles as Electrophiles. *Angewandte Chemie International Edition* **2012,** *51* (19), 4710-4713.

11. Zarate, C.; Yang, H.; Bezdek, M. J.; Hesk, D.; Chirik, P. J., Ni(I)–X Complexes Bearing a Bulky α-Diimine Ligand: Synthesis, Structure, and Superior Catalytic Performance in the Hydrogen Isotope Exchange in Pharmaceuticals. *Journal of the American Chemical Society* **2019,** *141* (12), 5034-5044.

12. Deng, L.; Woo, T. K.; Cavallo, L.; Margl, P. M.; Ziegler, T., The Role of Bulky Substituents in Brookhart-Type Ni(II) Diimine Catalyzed Olefin Polymerization: A Combined Density Functional Theory and Molecular Mechanics Study. *Journal of the American Chemical Society* **1997,** *119* (26), 6177-6186.

13. Kim, S.-T.; Kim, S.; Baik, M.-H., How bulky ligands control the chemoselectivity of Pd-catalyzed N-arylation of ammonia. *Chemical Science* **2020,** *11* (4), 1017-1025.

14. Haines, B. E.; Saito, Y.; Segawa, Y.; Itami, K.; Musaev, D. G., Flexible Reaction Pocket on Bulky Diphosphine–Ir Complex Controls Regioselectivity in para-Selective C–H Borylation of Arenes. *ACS Catalysis* **2016,** *6* (11), 7536-7546.

15. Grimes, R. N., Chapter 1 - Introduction and History. In *Carboranes (Third Edition)*, Grimes, R. N., Ed. Academic Press: Boston, 2016; pp 1-5.

16. Fisher, S. P.; Tomich, A. W.; Lovera, S. O.; Kleinsasser, J. F.; Guo, J.; Asay, M. J.; Nelson, H. M.; Lavallo, V., Nonclassical Applications of closo-Carborane Anions: From Main Group Chemistry and Catalysis to Energy Storage. *Chemical Reviews* **2019,** *119* (14), 8262-8290.

17. Fisher, S. P.; Tomich, A. W.; Guo, J.; Lavallo, V., Teaching an old dog new tricks: new directions in fundamental and applied closo-carborane anion chemistry. *Chemical Communications* **2019,** *55* (12), 1684-1701.

18. Grimes, R. N., Chapter 2 - Structure and Bonding. In *Carboranes (Third Edition)*, Grimes, R. N., Ed. Academic Press: Boston, 2016; pp 7-18.

19. Grimes, R. N., Chapter 9 - Icosahedral Carboranes: 1,2-C2B10H12. In *Carboranes (Third Edition)*, Grimes, R. N., Ed. Academic Press: Boston, 2016; pp 283-502.

20. Grimes, R. N., Chapter 8 - Icosahedral Carboranes: Closo-CB11 Clusters. In *Carboranes (Third Edition)*, Grimes, R. N., Ed. Academic Press: Boston, 2016; pp 249-281.

21. Grimes, R. N., Chapter 6 - Ten-Vertex Carboranes. In *Carboranes (Third Edition)*, Grimes, R. N., Ed. Academic Press: Boston, 2016; pp 139-178.

22. Grimes, R. N., Chapter 3 - Synthesis and Reactivity: An Overview. In *Carboranes (Third Edition)*, Grimes, R. N., Ed. Academic Press: Boston, 2016; pp 19-22.

23. Schleyer, P. v. R.; Najafian, K., Stability and Three-Dimensional Aromaticity of closo-Monocarbaborane Anions, CBn-1Hn-, and closo-Dicarboranes, C2Bn-2Hn. *Inorganic Chemistry* **1998,** *37* (14), 3454-3470.

24. Xie, Z.; Tsang, C.-W.; Sze, E. T.-P.; Yang, Q.; Chan, D. T. W.; Mak, T. C. W., Highly Chlorinated, Brominated, and Iodinated Icosahedral Carborane Anions: 1-H-

CB11X11-, 1-CH3-CB11X11- (X = Cl, Br, I); 1-Br-CB11Br11. *Inorganic Chemistry* **1998,** *37* (25), 6444-6451.

25. Reed, C. A., H+, CH3+, and R3Si+ Carborane Reagents: When Triflates Fail. *Accounts of Chemical Research* **2010,** *43* (1), 121-128.

26. Reed, C. A., Carboranes: A New Class of Weakly Coordinating Anions for Strong Electrophiles, Oxidants, and Superacids. *Accounts of Chemical Research* **1998,** *31* (3), 133-139.

27. Reed, C. A.; Bolskar, R. D., Discrete Fulleride Anions and Fullerenium Cations. *Chemical Reviews* **2000,** *100* (3), 1075-1120.

28. Reed, C. A.; Kim, K.-C.; Stoyanov, E. S.; Stasko, D.; Tham, F. S.; Mueller, L. J.; Boyd, P. D. W., Isolating Benzenium Ion Salts. *Journal of the American Chemical Society* **2003,** *125* (7), 1796-1804.

29. Reed, C. A.; Xie, Z.; Bau, R.; Benesi, A., Closely Approaching the Silylium Ion (R3Si+). *Science* **1993,** *262* (5132), 402-404.

30. Kato, T.; Reed, C. A., Putting tert-Butyl Cation in a Bottle. *Angewandte Chemie International Edition* **2004,** *43* (22), 2908-2911.

31. Juhasz, M.; Hoffmann, S.; Stoyanov, E.; Kim, K.-C.; Reed, C. A., The Strongest Isolable Acid. *Angewandte Chemie International Edition* **2004,** *43* (40), 5352-5355.

32. Axtell, J. C.; Kirlikovali, K. O.; Djurovich, P. I.; Jung, D.; Nguyen, V. T.; Munekiyo, B.; Royappa, A. T.; Rheingold, A. L.; Spokoyny, A. M., Blue Phosphorescent Zwitterionic Iridium(III) Complexes Featuring Weakly Coordinating nido-Carborane-Based Ligands. *Journal of the American Chemical Society* **2016,** *138* (48), 15758-15765.

33. Wang, Y.; Spokoyny, A. M., Abiotic Main Group Pharmacophore Renders a New Class of Antimicrobial Agents. *ACS Central Science* **2022,** *8* (3), 309-311.

34. Mills, H. A.; Jones, C. G.; Anderson, K. P.; Ready, A. D.; Djurovich, P. I.; Khan, S. I.; Hohman, J. N.; Nelson, H. M.; Spokoyny, A. M., Sterically Invariant Carborane-Based Ligands for the Morphological and Electronic Control of Metal–Organic Chalcogenolate Assemblies. *Chemistry of Materials* **2022,** *34* (15), 6933-6943.

35. Jung, D.; Muni, M.; Marin, G.; Ramachandran, R.; El-Kady, M. F.; Balandin, T.; Kaner, R. B.; Spokoyny, A. M., Enhancing cycling stability of tungsten oxide supercapacitor electrodes via a boron cluster-based molecular cross-linking approach. *Journal of Materials Chemistry A* **2020,** *8* (35), 18015-18023.

36. Reddy, V. J.; Roforth, M. M.; Tan, C.; Reddy, M. V. R., Synthesis of Functionalized Carboranes as Potential Anticancer and BNCT Agents. *Inorganic Chemistry* **2007,** *46* (2), 381-383.

37. Ivanov, S. V.; Rockwell, J. J.; Polyakov, O. G.; Gaudinski, C. M.; Anderson, O. P.; Solntsev, K. A.; Strauss, S. H., Highly Fluorinated Weakly Coordinating Monocarborane Anions. 1-H-CB11F11-, 1-CH3-CB11F11-, and the Structure of [N(n-Bu)4]2[CuCl(CB11F11)]. *Journal of the American Chemical Society* **1998,** *120* (17), 4224-4225.

38. Zhang, K.; Shen, Y.; Liu, J.; Spingler, B.; Duttwyler, S., Crystal structure of a carborane endo/exo-dianion and its use in the synthesis of ditopic ligands for supramolecular frameworks. *Chemical Communications* **2018,** *54* (14), 1698-1701.

39. Wehmschulte, R. J.; Wojtas, L., Cationic Ethylzinc Compound: A Benzene Complex with Catalytic Activity in Hydroamination and Hydrosilylation Reactions. *Inorganic Chemistry* **2011,** *50* (22), 11300-11302.

40. Tsang, C.-W.; Yang, Q.; Mak, T. C. W.; Xie, Z., Synthesis and crystal structure of silver and argentate complexes of mixed halocarborane anions, (C5H5N)2Ag(1-H□CB11Br5I6)(C5H5N) and [{(CH3CN)4Ag3}{Ag(CB11I5Br6)2}]n. *Applied Organometallic Chemistry* **2003,** *17* (6-7), 449-452.

41. Jelinek, T.; Baldwin, P.; Scheidt, W. R.; Reed, C. A., New weakly coordinating anions. 2. Derivatization of the carborane anion CB11H12. *Inorganic Chemistry* **1993,** *32* (10), 1982-1990.

42. Estrada, J.; Lugo, C. A.; McArthur, S. G.; Lavallo, V., Inductive effects of 10 and 12-vertex closo-carborane anions: cluster size and charge make a difference. *Chemical Communications* **2016,** *52* (9), 1824-1826.

43. Marion, N.; Navarro, O.; Mei, J.; Stevens, E. D.; Scott, N. M.; Nolan, S. P., Modified (NHC)Pd(allyl)Cl (NHC = N-Heterocyclic Carbene) Complexes for Room-Temperature Suzuki−Miyaura and Buchwald−Hartwig Reactions. *Journal of the American Chemical Society* **2006,** *128* (12), 4101-4111.

44. Kelly Iii, R. A.; Clavier, H.; Giudice, S.; Scott, N. M.; Stevens, E. D.; Bordner, J.; Samardjiev, I.; Hoff, C. D.; Cavallo, L.; Nolan, S. P., Determination of N-Heterocyclic Carbene (NHC) Steric and Electronic Parameters using the [(NHC)Ir(CO)2Cl] System. *Organometallics* **2008,** *27* (2), 202-210.

45. Martin, A. R.; Makida, Y.; Meiries, S.; Slawin, A. M. Z.; Nolan, S. P., Enhanced Activity of [Ni(NHC)CpCl] Complexes in Arylamination Catalysis. *Organometallics* **2013,** *32* (21), 6265-6270.

46. Lazreg, F.; Nahra, F.; Cazin, C. S. J., Copper–NHC complexes in catalysis. *Coordination Chemistry Reviews* **2015,** *293-294*, 48-79.

47. Colacino, E.; Martinez, J.; Lamaty, F., Preparation of NHC–ruthenium complexes and their catalytic activity in metathesis reaction. *Coordination Chemistry Reviews* **2007,** *251* (5), 726-764.

48. Visbal, R.; Laguna, A.; Gimeno, M. C., Simple and efficient synthesis of [MCI(NHC)] (M = Au, Ag) complexes. *Chemical Communications* **2013,** *49* (50), 5642-5644.

49. Igau, A.; Grutzmacher, H.; Baceiredo, A.; Bertrand, G., Analogous .alpha.,.alpha.'-bis-carbenoid, triply bonded species: synthesis of a stable .lambda.3-phosphino carbene-.lambda.5-phosphaacetylene. *Journal of the American Chemical Society* **1988,** *110* (19), 6463-6466.

50. Arduengo, A. J., III; Harlow, R. L.; Kline, M., A stable crystalline carbene. *Journal of the American Chemical Society* **1991,** *113* (1), 361-363.

51. Wanzlick, H. W., Aspects of Nucleophilic Carbene Chemistry. *Angewandte Chemie International Edition in English* **1962,** *1* (2), 75-80.

52. El-Hellani, A.; Lavallo, V., Fusing N-Heterocyclic Carbenes with Carborane Anions. *Angewandte Chemie International Edition* **2014,** *53* (17), 4489-4493.

53. Asay, M. J.; Fisher, S. P.; Lee, S. E.; Tham, F. S.; Borchardt, D.; Lavallo, V., Synthesis of unsymmetrical N-carboranyl NHCs: directing effect of the carborane anion. *Chemical Communications* **2015,** *51* (25), 5359-5362.

54. Fisher, S. P.; El-Hellani, A.; Tham, F. S.; Lavallo, V., Anionic and zwitterionic carboranyl N-heterocyclic carbene Au(i) complexes. *Dalton Transactions* **2016,** *45* (24), 9762-9765.

55. Hawthorne, M. F.; Young, D. C.; Garrett, P. M.; Owen, D. A.; Schwerin, S. G.; Tebbe, F. N.; Wegner, P. A., Preparation and characterization of the (3)-1,2- and (3)-1,7-dicarbadodecahydroundecaborate(-1) ions. *Journal of the American Chemical Society* **1968,** *90* (4), 862-868.

56. Hawthorne, M. F.; Young, D. C.; Andrews, T. D.; Howe, D. V.; Pilling, R. L.; Pitts, A. D.; Reintjes, M.; Warren, L. F., Jr.; Wegner, P. A., .pi.-Dicarbollyl derivatives of the transition metals. Metallocene analogs. *Journal of the American Chemical Society* **1968,** *90* (4), 879-896.

57. Fürstner, A.; Alcarazo, M.; César, V.; Lehmann, C. W., Convenient, scalable and flexible method for the preparation of imidazolium salts with previously inaccessible substitution patterns. *Chemical Communications* **2006,** (20), 2176-2178.

58. Estrada, J.; Lavallo, V., Fusing Dicarbollide Ions with N-Heterocyclic Carbenes. *Angewandte Chemie International Edition* **2017,** *56* (33), 9906-9909.

59. Tsuji, M., On Attempts at Generation of Carboranyl Carbocation. *The Journal of Organic Chemistry* **2003,** *68* (25), 9589-9597.

Chapter 2: A Weakly Coordinating yet Functional Au(I) Complex: Access to Organometallic Ion-Pairs

2.1 Introduction

In the previous chapter, we have seen how the carborane **2** can be appended onto imidazolium ring to produce carboranyl NHCs. Further, we discussed how NHC can be employed as a ligand for the Au(I) complex **11**. Apart from the traditional organometallic catalysis, the distinct advantage of introducing carboranyl NHCs is that the complex **11**is overall anionic. This means, the Li^+ cation could be switched to other transition metal cations. However, to do this, the Au(I) complex needs to be more robust, and this could be achieved by perhalogenating the imidazoliums inspired by the work of Reed.[1] Since halogenating the carboranes imparts more robust and weakly coordinating nature, our lab alumni sought at synthesizing the partially brominated and iodinated imidazoliums **22**. We envisioned the ensuing NHCs would be more stable and serve as platforms for novel reactivity by playing with the cation.

2.2 Hexahalogenation of Imidazoliums

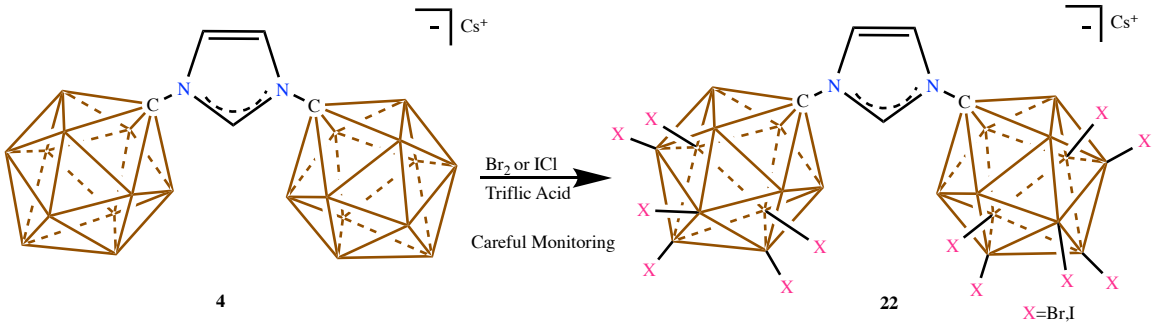

Scheme **2.1** Hexahalogenation of the imidazolium **4**

To do this, the anionic imidazolium **4** was treated with bromine and triflic acid and heated at 50°C over 3-5 days. Careful monitoring led to isolating the partially brominated imidazolium **22Br$_{12}$**. Similarly, treating the imidazolium **4** with ICl and triflic acid and

heating at 50°C for 24h cleanly afforded the partially iodinated imidazolium **22I$_{12}$**. (Scheme **2.1**).

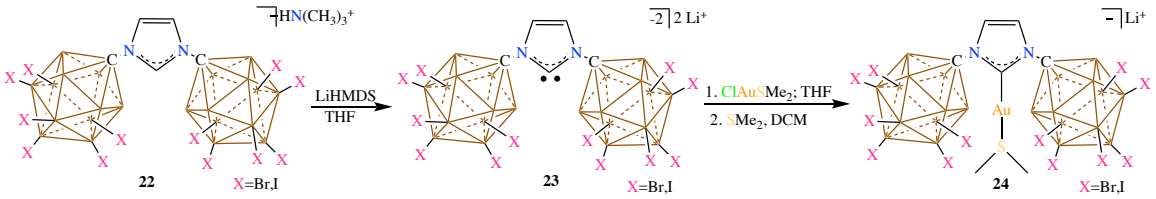

Scheme **2.2** Synthesis of the NHC **23** and the Au(I) complex **24** of halogenated carboranyl imidazolium **22**

Following this, the normal carbene **23** was made by deprotonation using LiHMDS in THF. Interestingly, in solid-state, the NHC **23** was a true carbene; not a carbenoid. This is likely due to the steric bulk imposed by the hexahalogenation. The Au(I) complex **24** was then made by treating **23** with ClAuSMe$_2$ in THF, followed by treatment with SMe$_2$ in DCM (Scheme **2.2**).

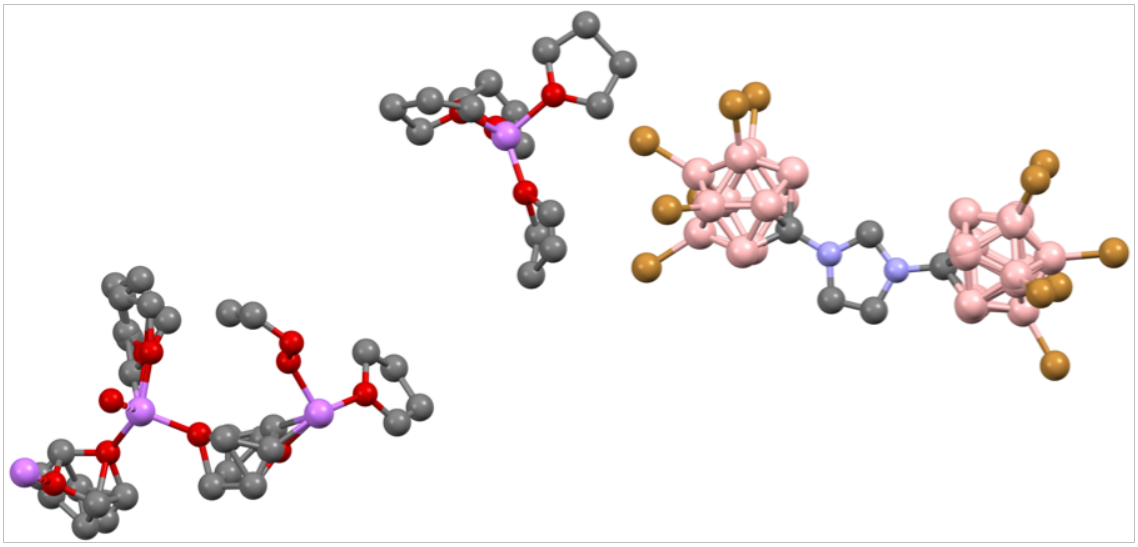

Fig. **2.1** X-Ray Structure of the NHC **23Br$_{12}$.** Hydrogen atoms omitted for clarity. N=Blue, B=pink, Li=purple, O=red, Br=brown

2.3 NHC-Au(I) Complex as a Weakly Coordinating Anion

One way to visualize complex **24** is the entire anionic complex could act as a potential weakly coordinating anion to some extent, owing to the presence of two extremely weakly coordinating carboranes. If this were true, the Li^+ could be switched to more reactive cations. Since the Ag^+ salts are known to induce the abstraction of halides from transition metal complexes, we wanted to synthesize the Ag^+ salt of **24** as a precursor for pairing reactive cations with it.

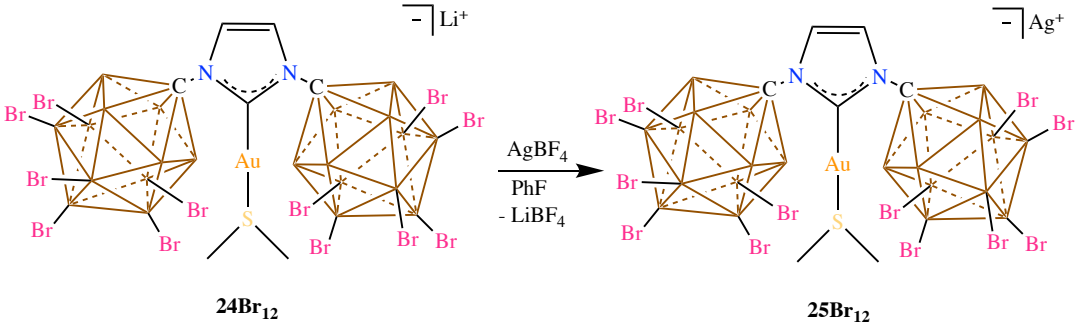

Scheme **2.3** Synthesis of **25Br$_{12}$** from **24Br$_{12}$**

To make the Ag^+ salt, **24** was treated with $AgBF_4$ in fluorobenzene (Scheme **2.3**). The precipitate obtained had **25** and the $LiBF_4$ byproduct. Clean **25** was isolated after washing the $LiBF_4$ byproduct in ether, confirmed by the absence of $LiBF_4$ in ^7Li, ^{11}B and ^{19}F NMRs.

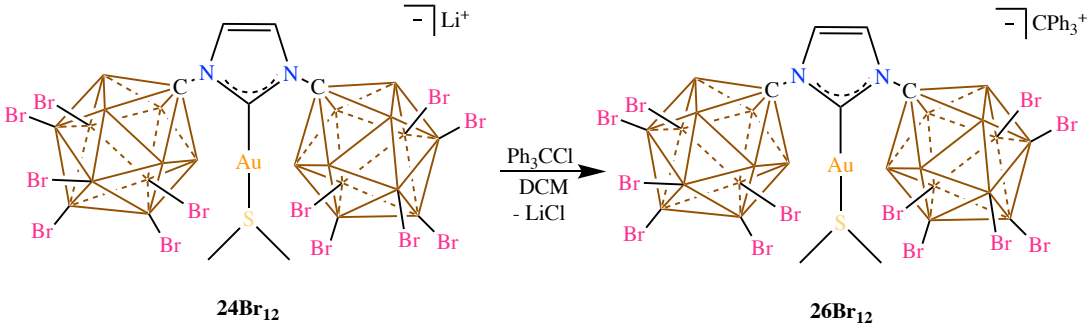

Scheme **2.4** Synthesis of **26Br$_{12}$** from **24Br$_{12}$**

After the successful synthesis of the **25**, we wanted to use it as a halide abstracting reagent from CPh_3Cl (trityl chloride). When **24 or 25** were treated with the trityl chloride in acetonitrile, the salt metathesis was observed. However, the analysis of the supernatant by ^1H NMR showed the presence of $HCPh_3$. After many control experiments, Dr. Fisher understood that the THF coordinated to the Li^+ or Ag^+ cations acted as a hydride source by a lewis-acid mediated ring opening thus quenching the trityl cation. To circumvent this issue, the coordinated THF was displaced by acetonitrile by pumping down the acetonitrile solution of **24** under vacuum for three times. When the acetonitrile coordinated **24** was treated with trityl chloride in dichloromethane, a precipitate was observed (Scheme **2.4**). Filtering and analyzing the solution showed the clean formation of the trityl salt of the Au(I) complex **26** by multinuclear NMR analysis. In the solid-state structure, the closest interaction distance between the anion and cation was about 2.97A which is out of range for any kind of covalent interaction (Fig. **2.2**). This concludes that the complex **24** can behave as a weakly coordinating anion.

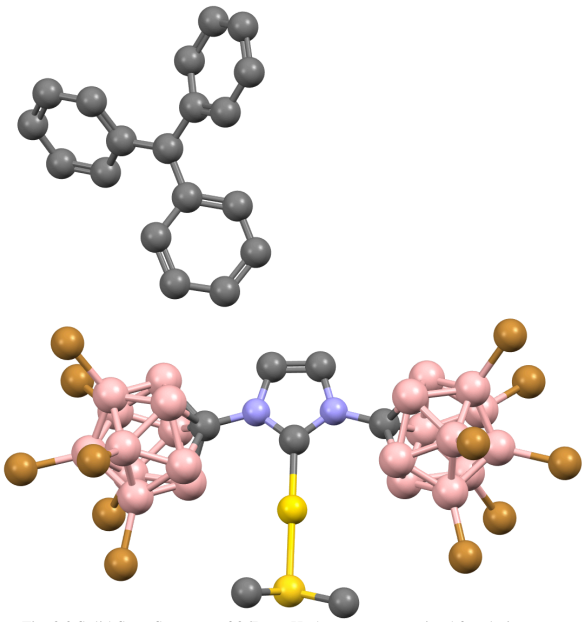

Fig. **2.2** Solid-State Structure of **26Br$_{12}$.** Hydrogen atoms omitted for clarity. N=Blue, Au=gold, S=yellow, B=pink, Br=brown

To investigate the possibility of pairing up more reactive cations with **24**, the trityl salt was used to abstract a hydride from triethylsilane potentially making a silylium cation. The silylium cations are highly electrophilic, lewis acidic and have a strong tendency to bind to solvents or halogens of the counteranions. Previously the Cl_{11} and the Cl_6 clusters were used to isolate the silylium cations by Reed.[2] The solid-state structures of these compounds revealed a weak interaction with the cluster halogens and hence Reed coined the term 'silylium like'meaning the silylium orbital is not vacant and contains a weakly interacting ligand.[1]

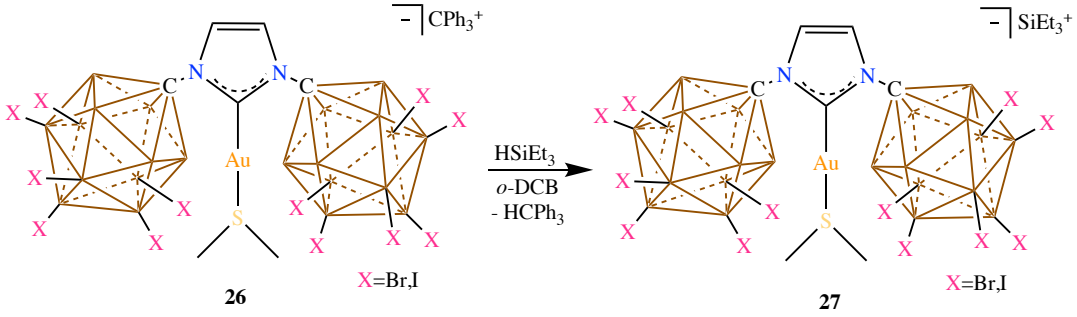

26 **27**

Scheme **2.5** Synthesis of **27** from **26**

Inspired by this work, we treated the trityl salt **26** with triethylsilane in o-dichlorobenzene. The strong orange color of the trityl disappeared in a few mins indicating the quenching of the cation by the hydride from the silane. The ^{1}H NMR showed the formation of triphenylmethane suggesting the abstraction of hydride by the trityl. The close examination of the NHC backbone and the SMe_2 peaks showed two peaks very close to each other indicating the presence of two very closely related silylium like species in the solution. The ^{13}C NMR spectrum displayed two sets of close ethyl peaks from the triethylsilylium cation corroborating the existence of two silylium like species. The ^{29}Si-^{1}H HSQC NMR displays two peaks as well concluding the existence of two species in the solution.

This phenomenon was previously observed by Reed with the silylium and methyl like species and could be explained via the population of species coordinating to the antipodal B-X vs the lower pentagonal belt B-X bonds.[3-4] Since the ^{29}Si NMR shifts are not in the range for simple B-X silylium adducts, the existence of another silylium species in the solution could likely be explained due to the formation of a silylium-SMe_2 adduct.[5-6] All attempts to obtain a single crystal X-Ray structure of this compound were unsuccessful likely due to the low solubility and the incompatibility of the species in most solvents.

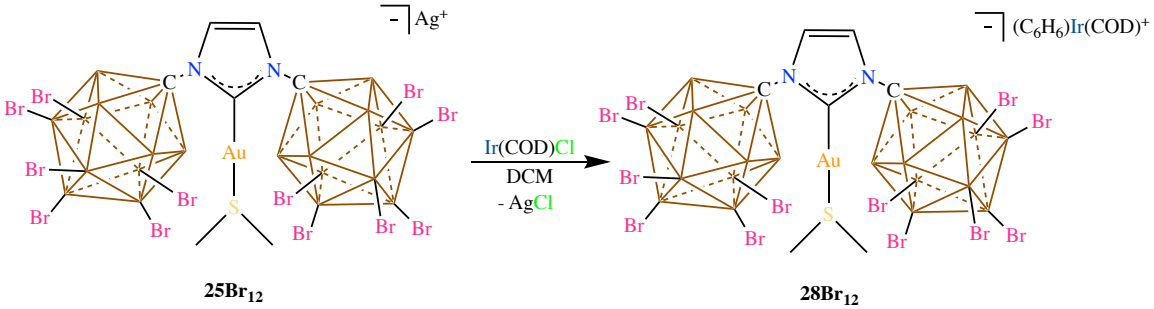

25Br$_{12}$ **28Br$_{12}$**

Scheme **2.6** Synthesis of the ion-pair **28Br$_{12}$** from **25Br$_{12}$**

Since the anion **24** allows pairing of reactive main group cations, we envisioned it would allow the pairing of reactive organometallic cations as well. Subsequently, to a suspension of **25Br$_{12}$** in dichloromethane, a DCM solution of $[Ir(COD)Cl]_2$ was added expecting the formation of an Ir cation after the Ag^+ salt abstracts the chloride. To coordinatively saturate the Ir cation, a drop of benzene was added expecting the formation of the classical $[\eta^6(C_6H_6)Ir(COD)]$ cation (Scheme **2.6**).[7-8] The reaction mixture was filtered to remove AgCl after an hour. The ^{1}H NMR showed a clean formation of Au^-/Ir^+ ion-pair, the shifts were comparable to the cation reported in the literature. The ion-pair was unambiguously characterized using multinuclear and 2D NMR correlation, single crystal X-Ray diffraction and mass spectrometry.

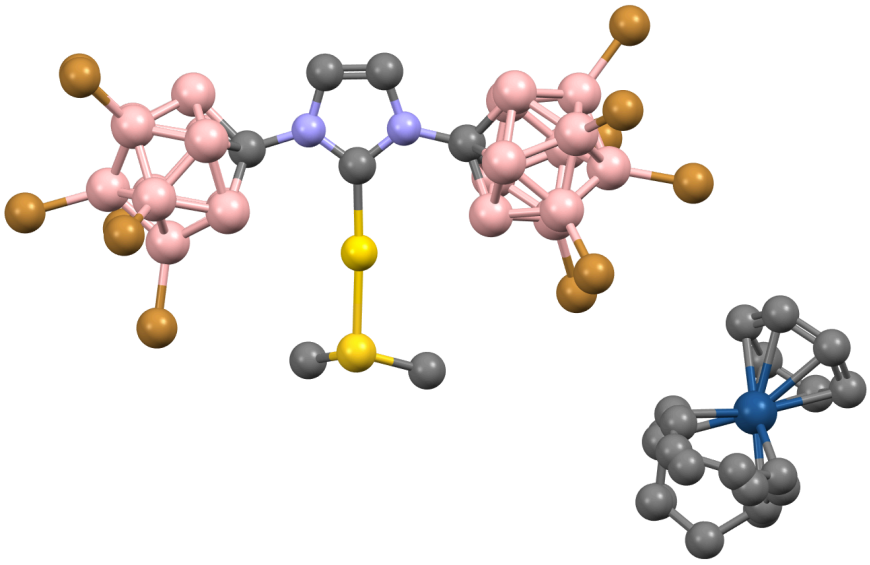

Fig. **2.3** Solid-State Structure of **28.** Hydrogen atoms omitted for clarity. N=Blue, B=pink, Au=gold, S=yellow, Br=brown, Ir= ocean blue

2.4 NHC-Au(I) Complex as a Catalyst

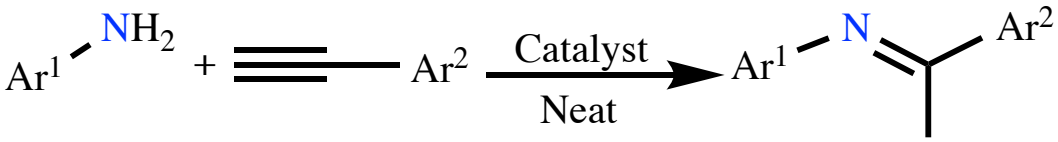

Scheme **2.7** Hydroamination of amines with alkynes

After establishing **24** as a weakly coordinating organometallic anion, we turned our attention towards its catalytic activity. Since Au(I) complexes are known to activate alkynes and catalyze hydroamination reactions,[9-12] we wanted to probe if **24** could perform the same. Subsequently, we reacted mesityl amine with phenyl acetylene in the presence of 5 mol% of **24I$_{12}$** and monitored the formation of the corresponding imine. Although not much conversion was observed at room temperature, heating to 80^{o}C showed a significant formation of the imine. Surprisingly, more than 99% of the starting materials were converted to the imine in less than an hour. Delighted by the results, we continued

evaluating the catalytic performance of both **24Br$_{12}$** and **24I$_{12}$** for hydroamination reaction and the results are summarized in the table below.

Entry	Catalyst	Ar^1	Ar^2	Catlyst Loading (%)	t (h)	T (°C)	Yield (%)	TON
1	**Br$_{12}$[Li]**	Mes	MeO-C$_6$H$_4$	0.01	24h	80	66	66000
2	**I$_{12}$[Li]**	Mes	MeO-C$_6$H$_4$	0.001	24h	80	90	90000
3	**Br$_{12}$[Li]**	Dipp	F-C$_6$H$_4$	0.001	24h	80	87	87000
4	**I$_{12}$[Li]**	Dipp	F-C$_6$H$_4$	0.1	24h	80	68	68000
5	**Br$_{12}$[Li]**	Dipp	MeO-C$_6$H$_4$	0.01	24h	80	93	93000
6	**I$_{12}$[Li]**	Dipp	MeO-C$_6$H$_4$	0.001	24h	80	88	88000

Table **2.1** Hydroamination of alkynes with amines

From the Table **2.1**, it can be asserted that these weakly coordinating anions display high catalytic activity. The turnover numbers (TON) for some reactions approached as high as 90,000 with yields close to 95% and in some cases perform similar to our previously reported Au(I) phosphine catalyst.[13] This is mostly due to the enhanced π acidity at Au(I) due to the electron withdrawing inductive effects of the halogens.

2.5 Conclusion

In conclusion, the NHC-Au complex **24** behaves as a weakly coordinating anion yet highly active catalyst. This allowed the isolation of ion-pairs of this anion with reactive main group and organometallic cations. This represents a new paradigm in the ligand and molecular design using carboranes. Pairing of reactive cations with the catalytically functional anion let us perform tandem catalytic reactions which will be discussed in the following chapter.

2.6 Experimental

General Considerations:

All manipulations were carried out using standard Schlenk or glovebox techniques under a dinitrogen atmosphere (industrial grade, glovebox) or purified elemental argon (99.995%, Schlenk line) unless otherwise stated. Dry solvents were obtained via distillation under argon from calcium hydride (acetonitrile, fluorobenzene, methylene chloride), sodium-potassium alloy (diethyl ether), potassium (benzene) or potassium using benzophenone ketyl radical as an indicator (tetrahydrofuran). Pentane and toluene were collected from a solvent purification system by SG Waters USA, LLC utilizing a fifteen minute argon sparge followed by passage though activated aluminum. The imidazolium **4** was prepared according to the literature procedure.[14] Unless specifically stated, reagents were purchased from commercial vendors and used without further purification. Nuclear magnetic resonance (NMR) spectroscopy was carried out using: Bruker Avance 300 MHz, Bruker Avance 600 MHz, and Bruker NEO 400 MHz (Prodigy LN2 cryoprobe), Varian Inova 500 MHz and Bruker NEO 600 (CP-MAS). NMR chemical shifts are reported in parts per million (ppm) with ^{1}H and ^{13}C chemical shifts referenced to the residual non-deuterated solvent. The ^{11}B-^{1}H coupling constants from ^{11}B spectra are reported when possible. Infrared spectroscopy was recorded on a Bruker ALPHA FTIR Spectrometer or Thermo Fisher Nicolet FTIR Spectrometer. High-resolution mass spectrometry (HRMS) was collected on an Agilent Technologies 6210 (TOF LC/MS) featuring a direct injection with multimode electrospray ionization/atmospheric-pressure chemical ionization

(ESI/APCI). Melting points were obtained on a Büchi Model B-545. Complete crystallographic data for compounds **25**, **23Br$_{12}$**, **26Br$_{12}$, 28** are available free of charge from the Cambridge Crystallographic Data Center. These structures can be accessed at: http://www.ccdc.cam.ac.uk/.

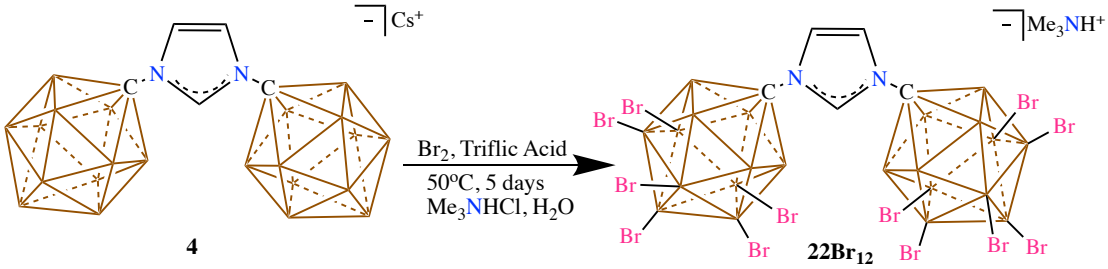

4 **22Br$_{12}$**

Scheme **2.8** Synthesis of **22Br$_{12}$**

4 (1.0 g, 2.06 mmol) and a stir bar was placed in a 100 mL round bottom flask and bromine (10 mL) followed by triflic acid (5 mL) was added. The reaction was heated at 50 °C for 5 days (completion of the reaction is determined by mass spectroscopy). The reaction was filtered on a medium porosity fritted funnel and washed with 10 mL of dichloromethane. The solid on the fritted funnel was then dissolved in ethyl acetate and water (150 mL) was added to the ethyl acetate solution and was titrated with 10% aqueous sodium sulfite solution. The organic layer was separated, and the aqueous solution was extracted with another 100 mL of ethyl acetate. The organic layers were combined and then pumped down to dryness. Further purification can be accomplished by crystallization from THF and hexanes.

Cation exchange was performed by suspending the solid in water, with a few milliliters of acetone, and then adding excess $(CH)_3NHCl$. The suspension was stirred 15 hours and the white solid was collected by filtration giving **22Br$_{12}$[Me$_3$NH$^+$]**. *Note: a mixture of over and under brominated products can be separated by repeated crystallization from THF*

and hexane). ^{1}H NMR (300 MHz, acetone-d_6, 25°C): δ = 9.54 (t,$^{4}J(H,H)$= 1.8 Hz, 1H), 8.00 (d,$^{4}J(H,H)$= 1.8 Hz, 2H), 3.04 (s, 9H) ppm. ^{1}H[^{11}B] NMR (300 MHz, acetone-d_6, 25°C): δ = 9.54 (t,$^{4}J(H,H)$= 1.8 Hz, 1H), 8.00 (d,$^{4}J(H,H)$= 1.8 Hz, 2H), 3.04 (s, 9H), 2.87 (bs, B-H, 10H) ppm. ^{11}B[^{1}H] NMR (128 MHz, acetone-d_6, 25 °C): δ = -1.5, -10.2, -18.6 ppm. ^{11}B NMR (128 MHz, acetone-d_6, 25 °C): δ = -1.5, -10.2, -18.6 ($^{1}J(B,H)$= 132.1 Hz) ppm. ^{13}C[^{1}H] NMR (151 MHz, acetone-d_6, 25°C): δ = 138.9, 124.9, 45.4 ppm (*carborane C not detected*). HRMS (negative mode ESI/APCI) [M*$^{-}$] m/z Calc: C5 H13 B22 I12 N2 = 1861.1852 : Found = 1861.1594, [M-H^{-}] m/z Calc: 1862.1703 : Found = 1862.1559. Melting Point: > 315 °C.

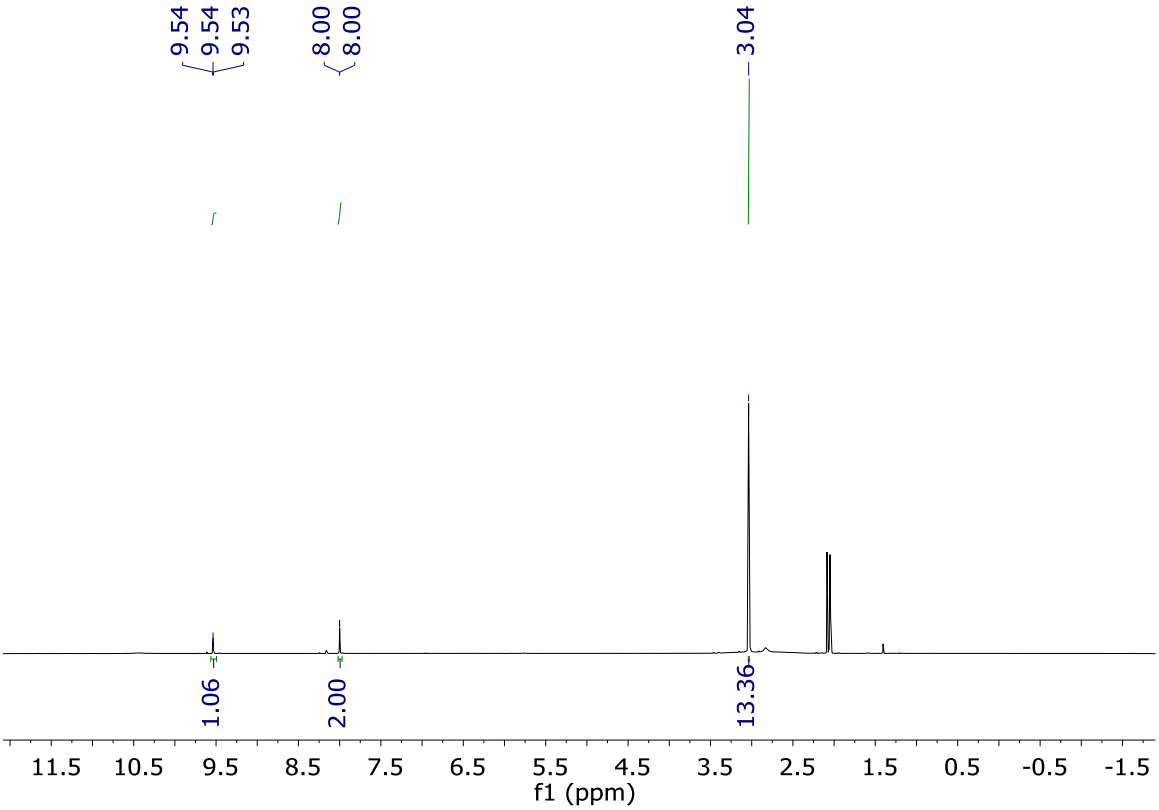

Fig. **2.1** ^{1}H NMR-spectrum of **22Br$_{12}$[Me$_3$NH^{+}]** in acetone-d_6

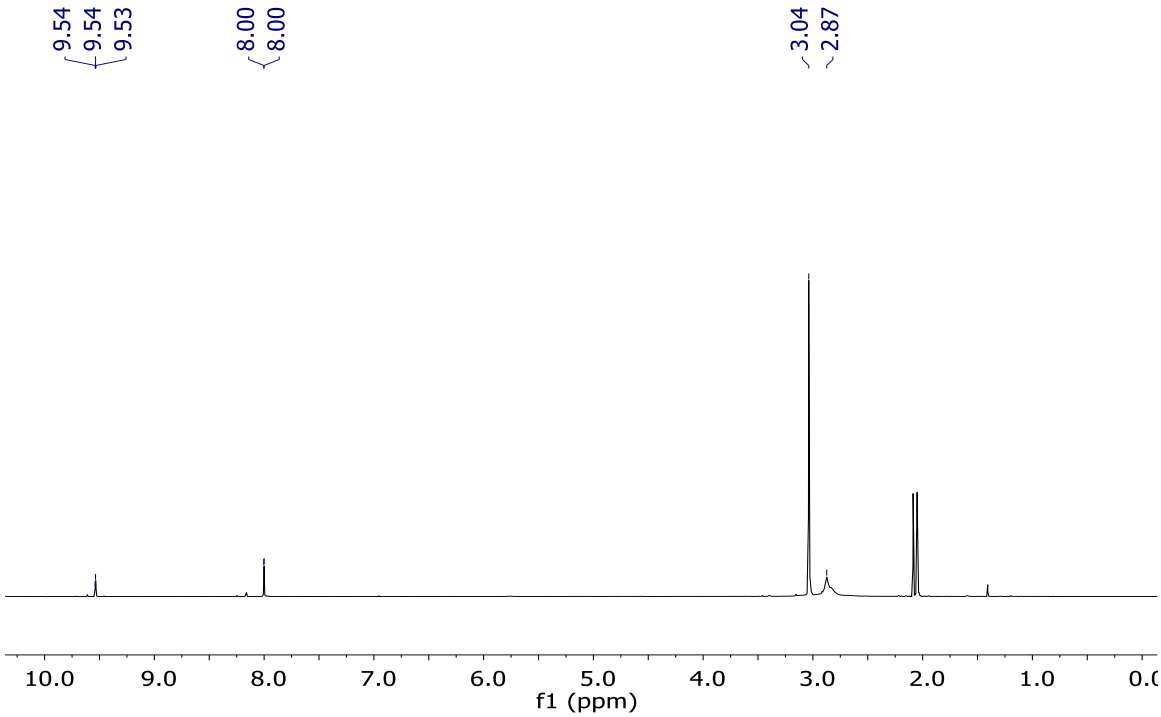

Fig. **2.2** $^{1}H[^{11}B]$ NMR-spectrum of **$22Br_{12}[Me_3NH^+]$** in acetone-d_6

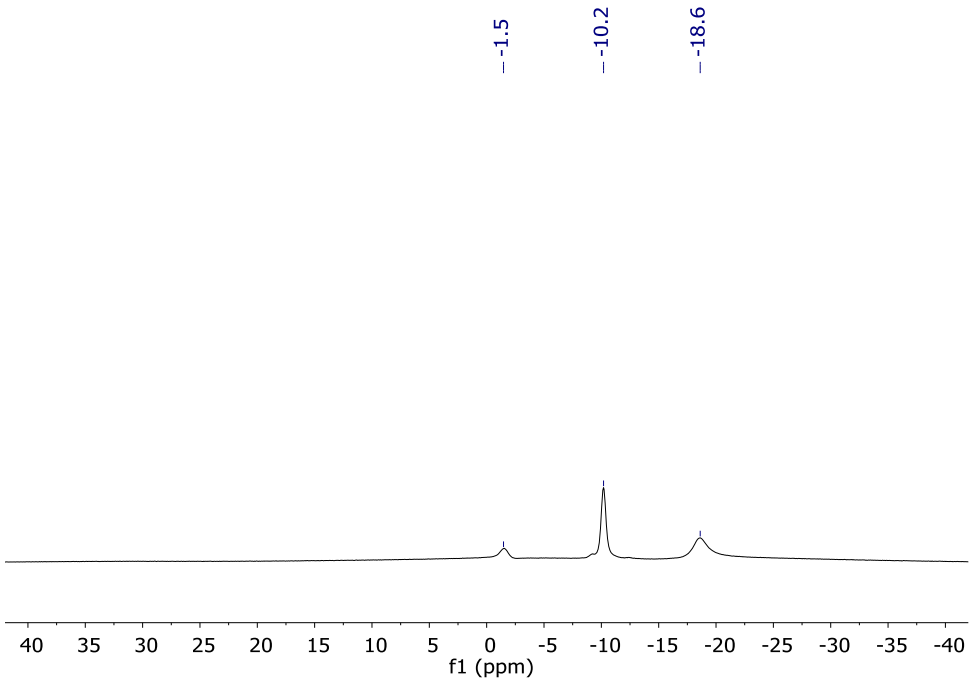

Fig. **2.3** $^{11}B[^{1}H]$ NMR-spectrum of **$22Br_{12}[Me_3NH^+]$** in acetone-d_6

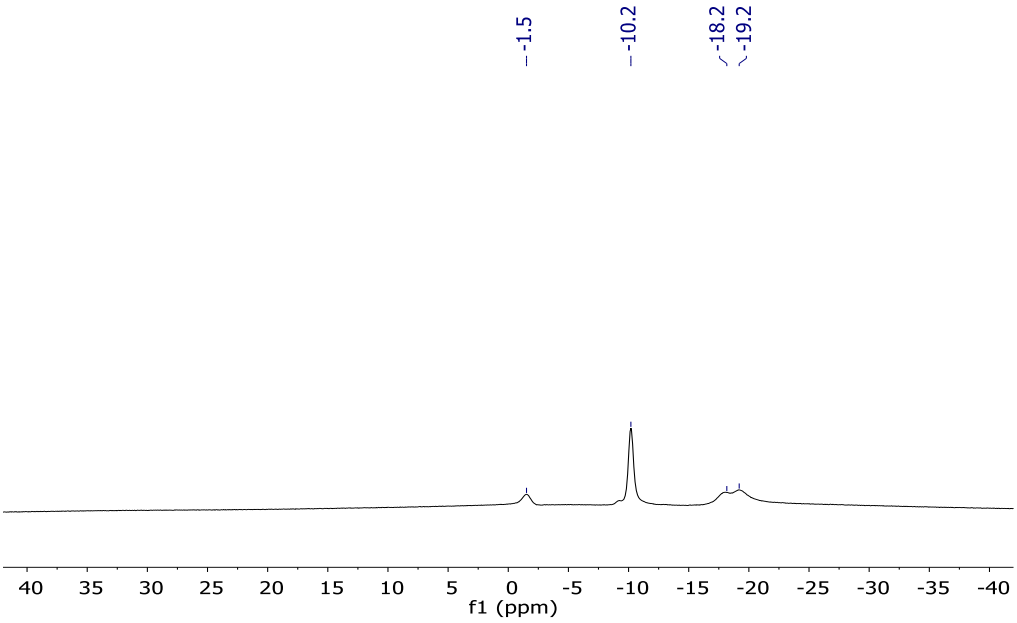

Fig. **2.4** ^{11}B NMR-spectrum of **22Br$_{12}$[Me$_3$NH$^+$]** in acetone-d$_6$

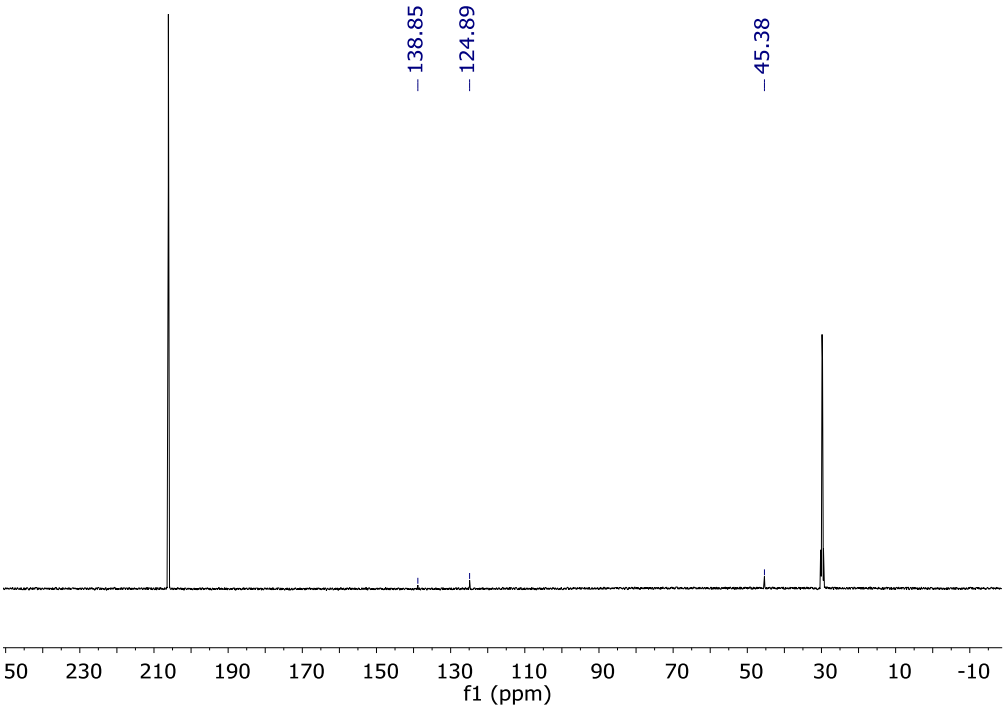

Fig. **2.5**. ^{13}C[^{1}H] NMR-spectrum of **22Br$_{12}$[Me$_3$NH$^+$]** in acetone-d$_6$

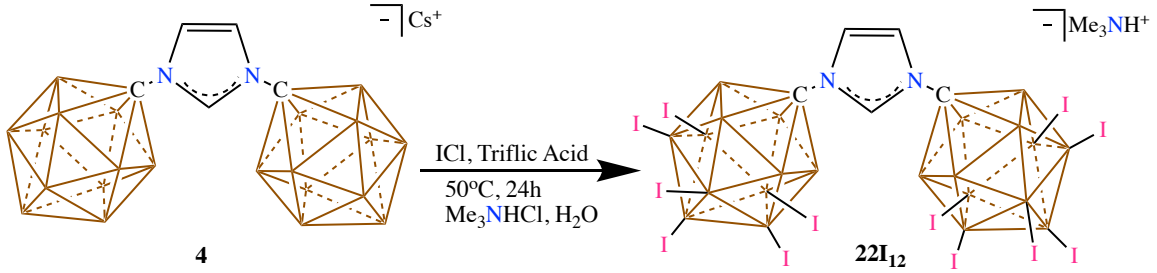

Scheme **2.9** Synthesis of **22I$_{12}$**

4 (1.00 g, 2.06 mmol) and a stir bar was placed in a 100 mL round bottom flask and 20 mL of ICl and 20 mL of triflic acid was added. The reaction was heated to 50°C and stirred open to atmosphere for 24 hours. The reaction mixture was carefully quenched with saturated sodium sulfite solution then extracted with ethyl acetate (*note: the reaction mixture violently reacts with sodium sulfite at room temperature*). The organic layer was washed with brine followed by water, then pumped down to dryness. A beaker was equipped with a stir bar and the solid was suspended in water. To the suspension a solution of Me_3NHCl (excess) was added and the mixture stirred overnight (12 hours). The next morning the mixture was filtered and the solid was washed with DI water then dried under high vacuum at 80 °C for 2 hours. The yield of the dried product, **22I$_{12}$[Me$_3$NH$^+$]**, was 94% (3.41 g, 1.71 mmol). ^{1}H NMR (400 MHz, acetone-d$_6$, 25°C): δ = 9.72 (t,^{4}*J(H,H)*= 1.7 Hz, 1H), 8.02 (d,^{4}*J(H,H)*= 1.7 Hz, 2H), 3.15 (s, 9H) ppm. ^{1}H[^{11}B] NMR (300 MHz, acetone-d$_6$, 25°C): δ = 9.72 (t,^{4}*J(H,H)*= 1.7 Hz, 1H), 8.02 (d,^{4}*J(H,H)*= 1.7 Hz, 2H), 3.44 (bs, B-H, 10H), 3.15 (s, 9H) ppm. ^{11}B[^{1}H] NMR (128 MHz, acetonitrile-d$_3$, 25 °C): δ = -6.7, -13.0, -20.2 ppm. ^{11}B NMR (128 MHz, acetonitrile-d$_3$, 25 °C): δ = -6.7, -13.0

($^{1}J(B,H)$= 126.3 Hz), -20.2 ppm. $^{13}C[^{1}H]$ NMR (101 MHz, acetone-d_6, 25°C): δ = 138.3, 124.4, 82.6, 45.9 ppm. Melting Point: >315 °C.

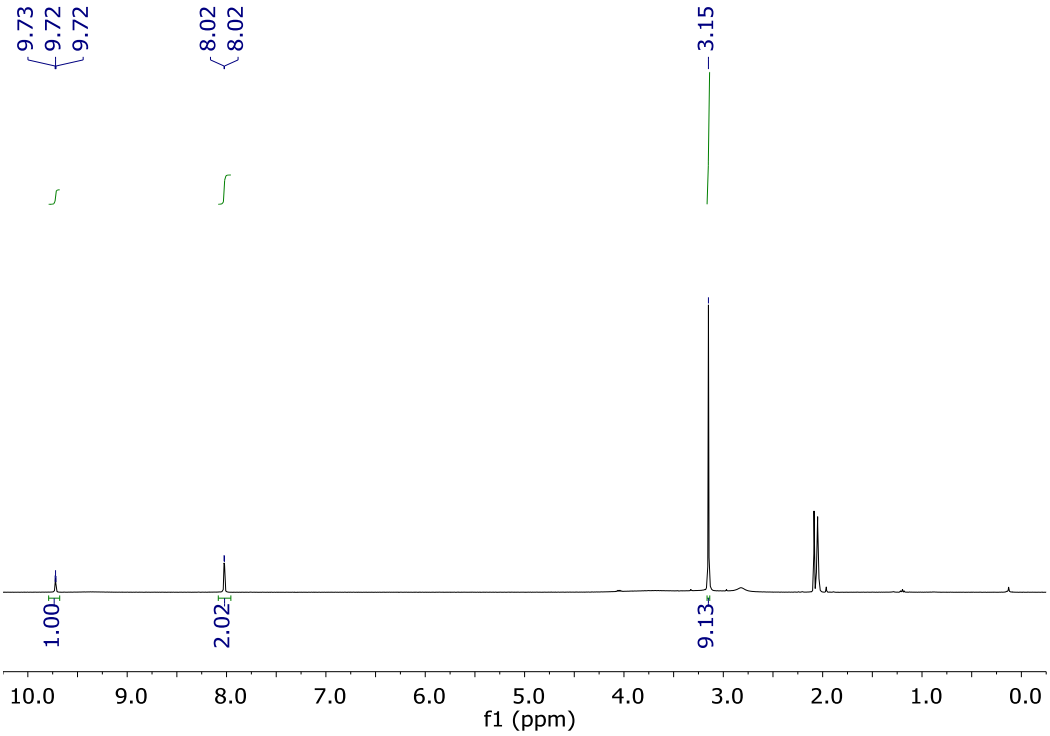

Fig. **2.6** ^{1}H-NMR spectrum of **$22I_{12}[Me_3NH^{+}]$** in acetone-d_6.

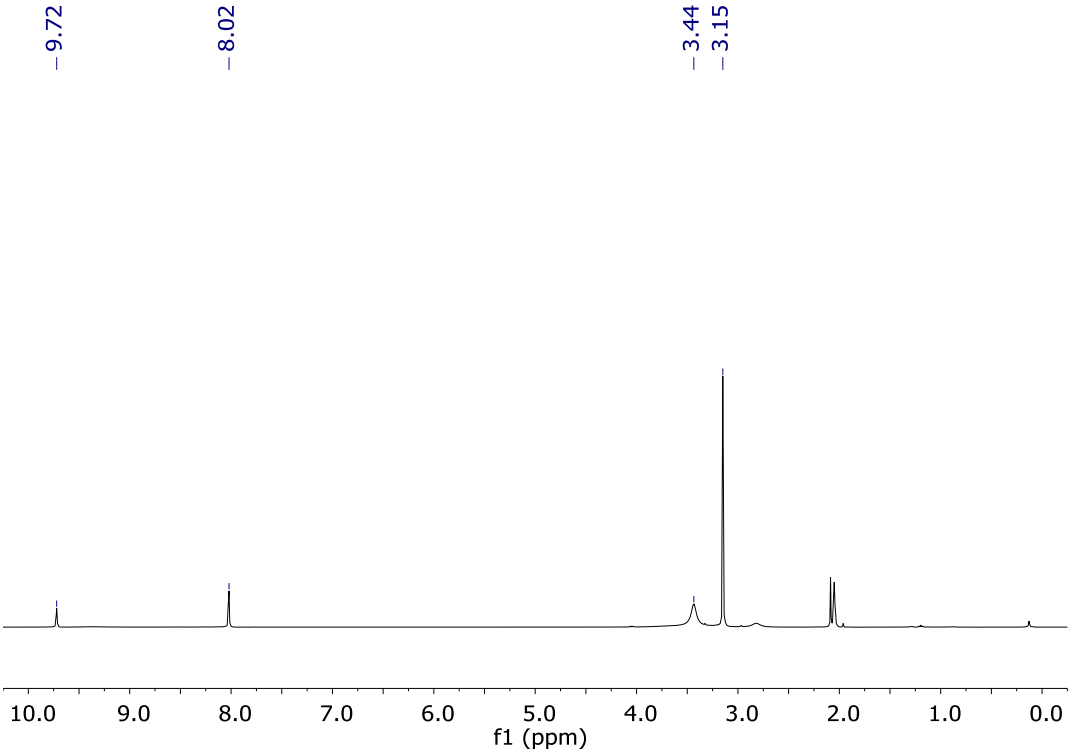

Fig. **2.7** $^{1}H[^{11}B]$-NMR spectrum of **$22I_{12}[Me_3NH^+]$** in acetone-d_6. Note: The B-H resonance can be found at 3.44 ppm.

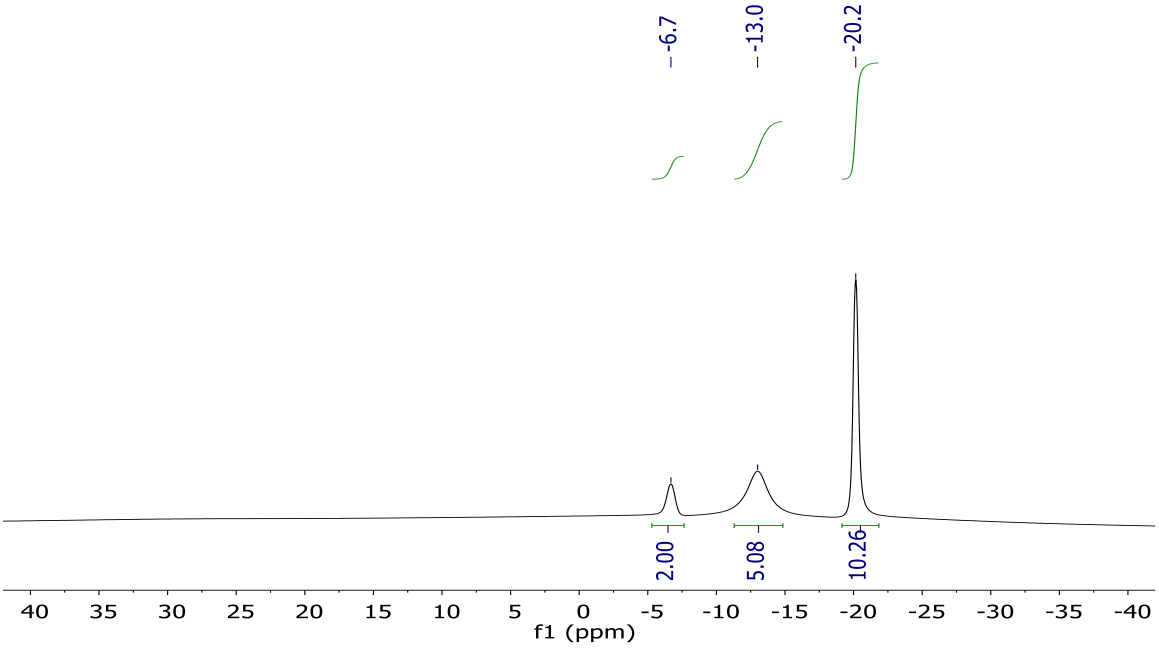

Fig. **2.8** $^{11}B[^{1}H]$-NMR spectrum of **$22I_{12}[Me_3NH^+]$** in acetonitrile-d_3.

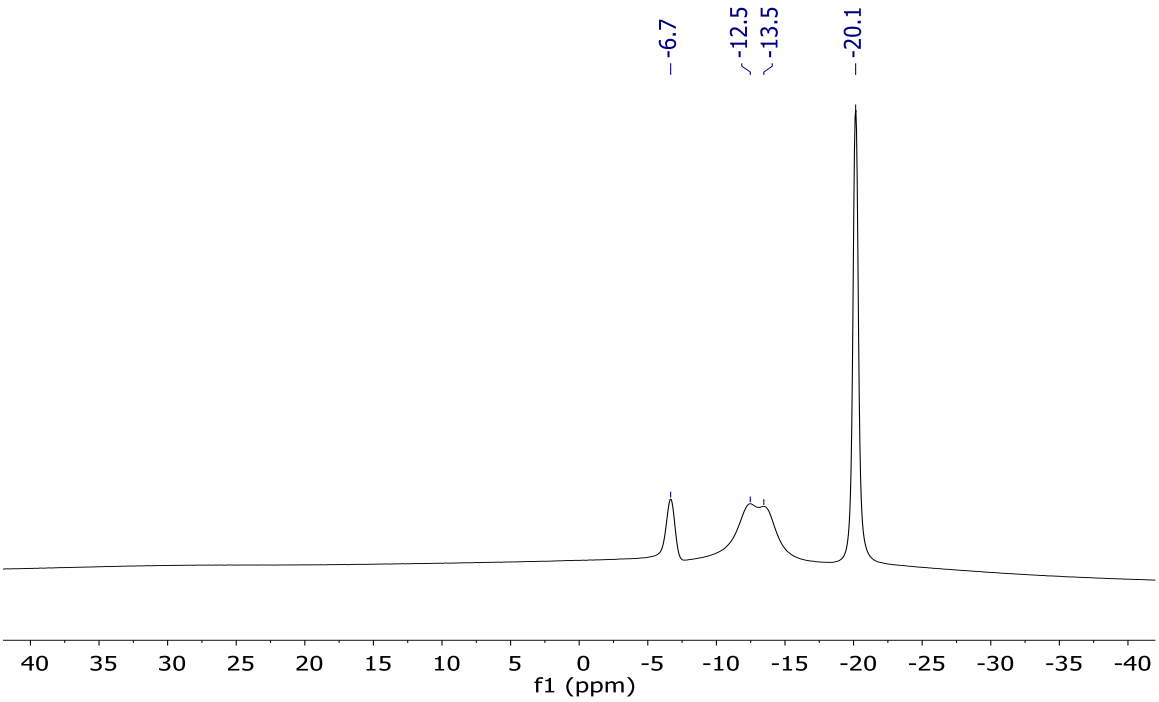

Fig. **2.9** ^{11}B-NMR spectrum of **$22I_{12}[Me_3NH^+]$** in acetonitrile-d_3.

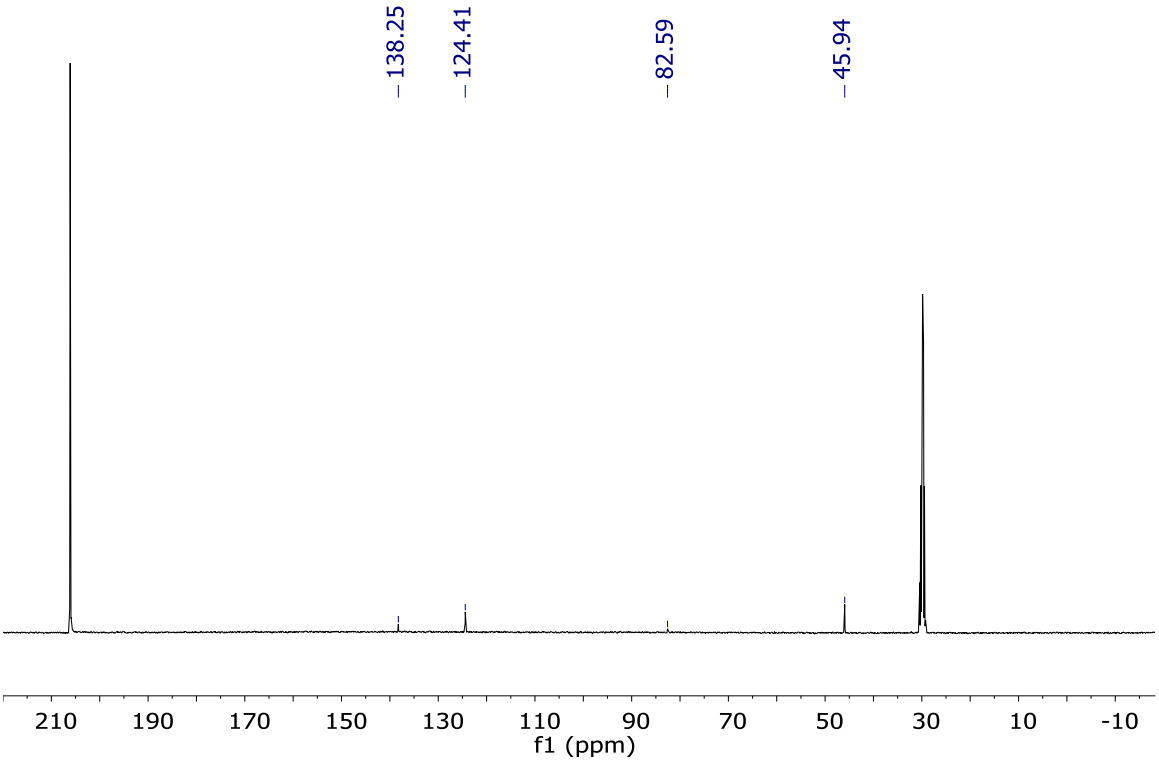

Fig. **2.10** ^{13}C[^{1}H]-NMR spectrum of **$22I_{12}[Me_3NH^+]$** in acetone-d_6.

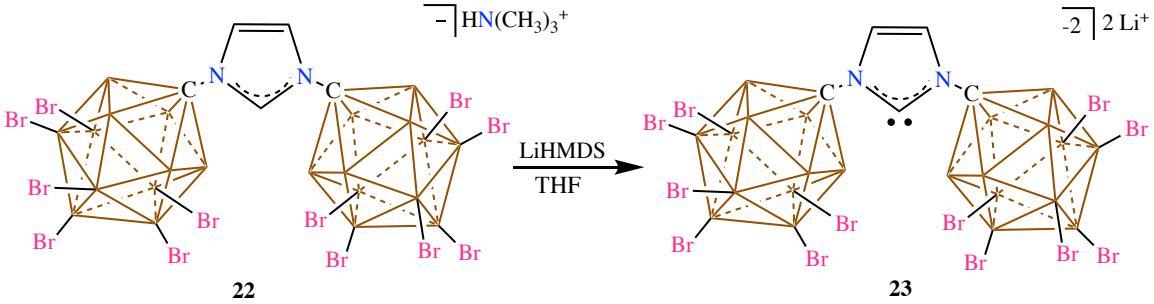

Scheme **2.10** Synthesis of the NHC **23Br$_{12}$**

A glass scintillation vial was equipped with a stir bar and loaded with **22Br$_{12}$[Me$_3$NH$^+$]** (1.0 g, 0.735 mmol) and dissolved in dry THF. A THF solution of LiHMDS (0.307 g, 1.83 mmol) was added slowly and the solution was stirred for 10 minutes at room temperature. After the reaction was over the solvent was pumped down bound dry under vacuum and the solid was washed with Et_2O. The precipitate was allowed to settle, the ether was decanted and the compound was dried under vacuum giving **23Br$_{12}$** 80 % yield, 0.206 g, 0.294 mmol. ^{1}H NMR (600 MHz, acetonitrile-d$_3$, 25°C): δ = 6.98 (s, 2H), 3.50 – 2.00 (bs, 10H, B-H) ppm. ^{1}H[^{11}B] NMR (600 MHz, acetonitrile-d$_3$, 25°C): δ = 6.98 (s, 2H), 2.79 (bs, B-H, 10H) ppm. ^{11}B[^{1}H]-NMR (128 MHz, acetonitrile-d$_3$, 25 °C): δ = -3.4, -10.8, -18.0 ppm. ^{11}B[^{1}H]-NMR (128 MHz, acetonitrile-d$_3$, 25 °C): δ = -3.4, -10.7, -17.8 ($^1J(B,H)$ = 157.8 Hz) ppm. ^{13}C[^{1}H]-NMR (124 MHz, acetonitrile-d$_3$, 25°C): δ = 220.6, 120.1, 87.3 ppm. ^{13}C[^{1}H]-NMR (75 MHz, acetonitrile-d$_3$, 25°C): δ = 220.1, 121.3, 84.9 ppm.

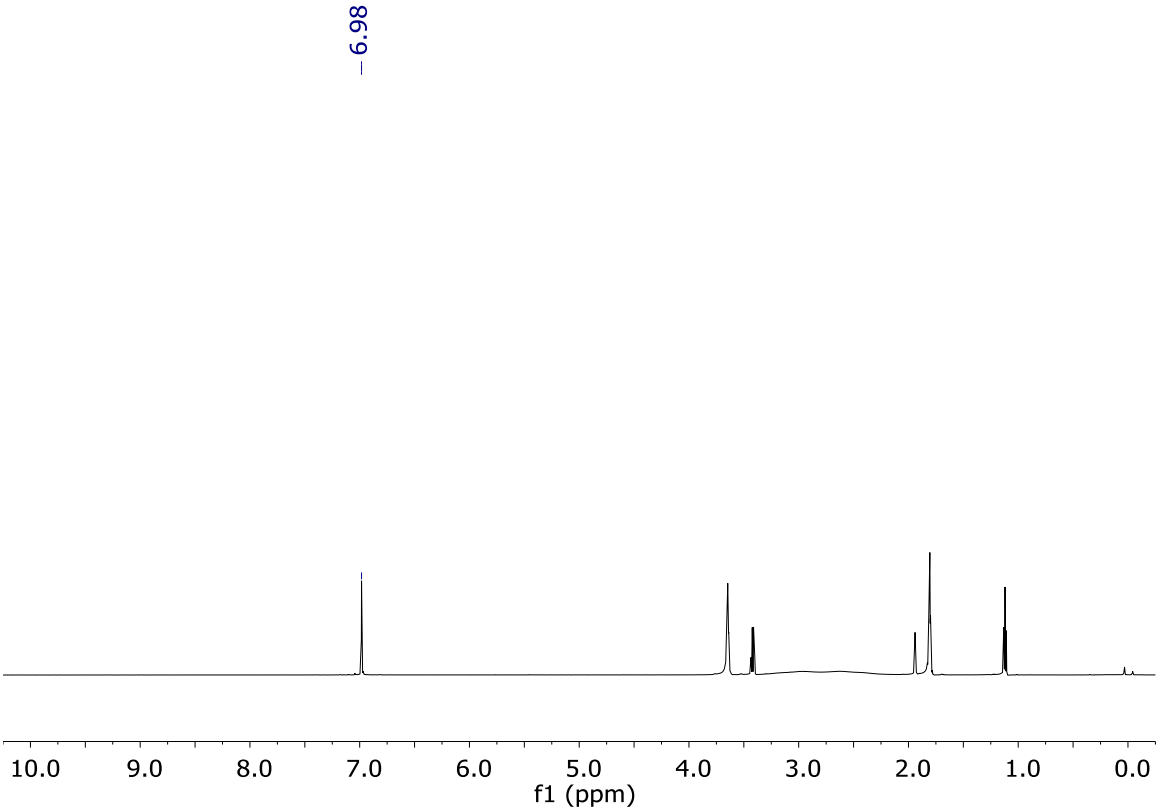

Fig. **2.11** ^{1}H NMR-spectrum of **23Br$_{12}$** in acetonitrile-d$_3$.

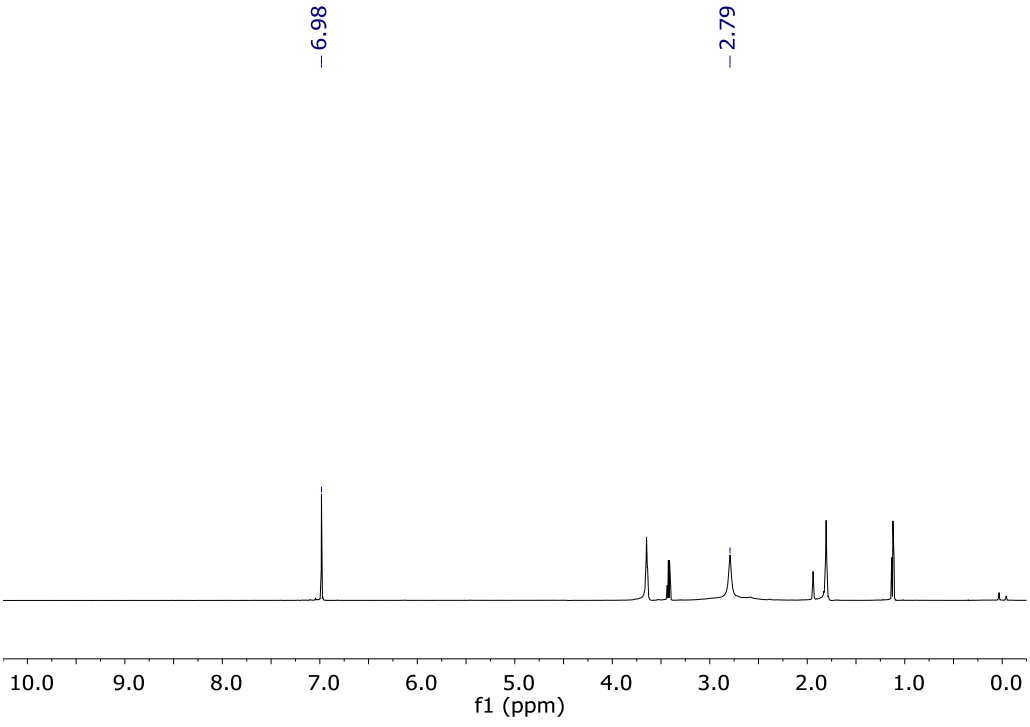

Fig. **2.12** ^{1}H[^{11}B] NMR-spectrum of **23Br$_{12}$** in acetonitrile-d$_3$.

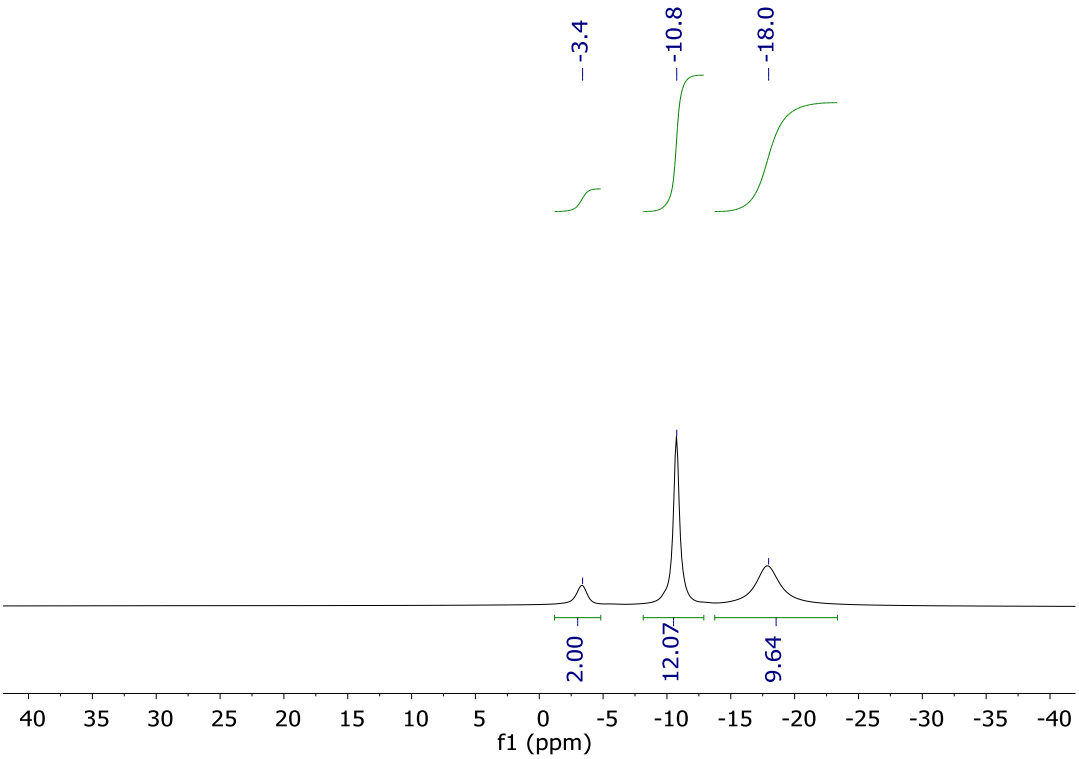

Fig. **2.13** $^{11}B[^{1}H]$ NMR-spectrum of **23Br$_{12}$** in acetonitrile-d$_3$.

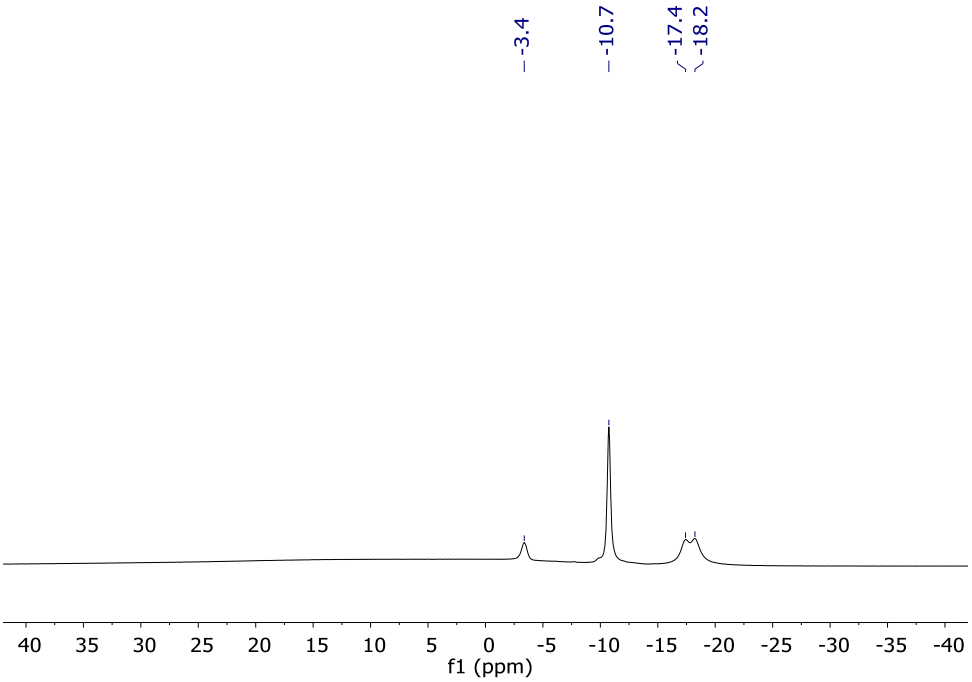

Fig. **2.14** ^{11}B NMR-spectrum of **23Br$_{12}$** in acetonitrile-d$_3$.

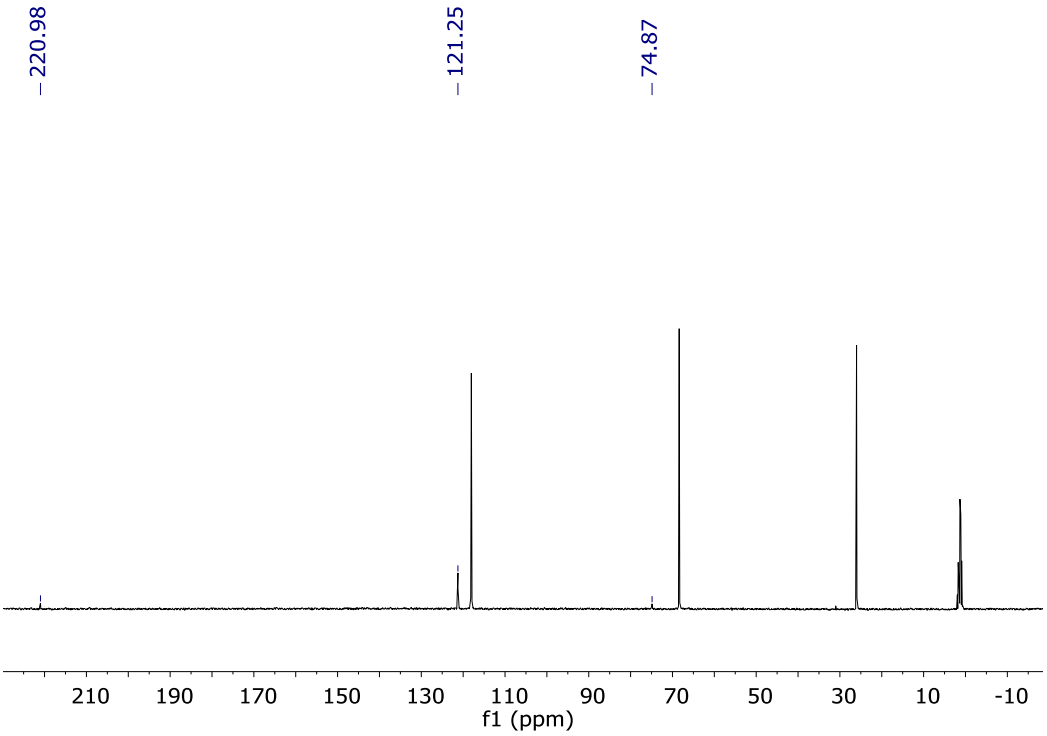

Fig. **2.15** $^{13}C[^{1}H]$ NMR-spectrum of **23Br$_{12}$** in Acetonitrile-d_3.

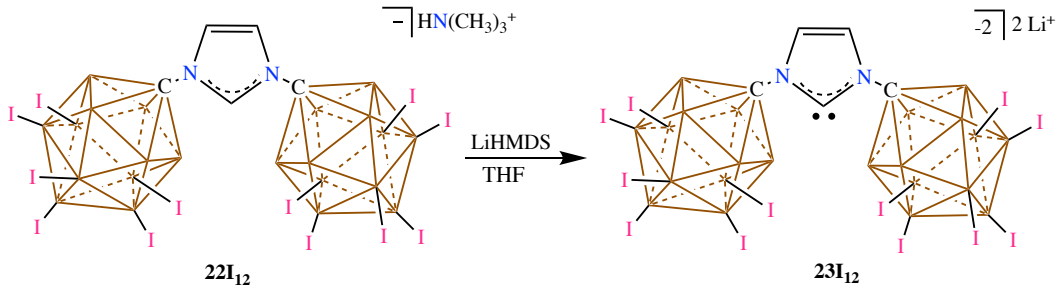

Scheme **2.11** Synthesis of the NHC **23I$_{12}$**

A glass scintillation vial was equipped with a stir bar and loaded with **22I$_{12}$** (2.0 g, 1.04 mmol) and dissolved in dry THF. LiHMDS (0.383 g, 2.29 mmol) was added slowly, and the suspension was stirred for 30 minutes at room temperature. After the reaction was over the solvent was concentrated down and the concentrate was washed with Et_2O (1x, enough to fill the vial). Upon removal of the ether wash the solid was dried on the high vacuum furnishing **23I$_{12}$** in 91% yield, (1.97 grams, 947 mmol). ^{1}H NMR (300 MHz, acetonitrile-d_3, 25°C): δ = 7.00 (s, 2H). $^{1}H[^{11}B]$ NMR (300 MHz, acetonitrile-d_3, 25°C):

δ = 7.00 (s, 2H), 3.35 (bs, B-H, 10H) ppm. $^{11}B[^{1}H]$-NMR (128 MHz, acetonitrile-d_3, 25 °C): δ = -8.3, -12.3, -20.4 ppm. $^{11}B[^{1}H]$-NMR (128 MHz, acetonitrile-d_3, 25 °C): δ = -8.3, -12.3 ($^{1}J(B,H)$ = 123.8 Hz), -20.4 ppm. $^{13}C[^{1}H]$-NMR (124 MHz, THF-h_8, 25°C): δ = 220.6, 120.1, 87.3 ppm. $^{13}C[^{1}H]$-NMR (75 MHz, acetonitrile-d_3, 25°C): δ = 220.3, 121.3, 88.5 ppm.

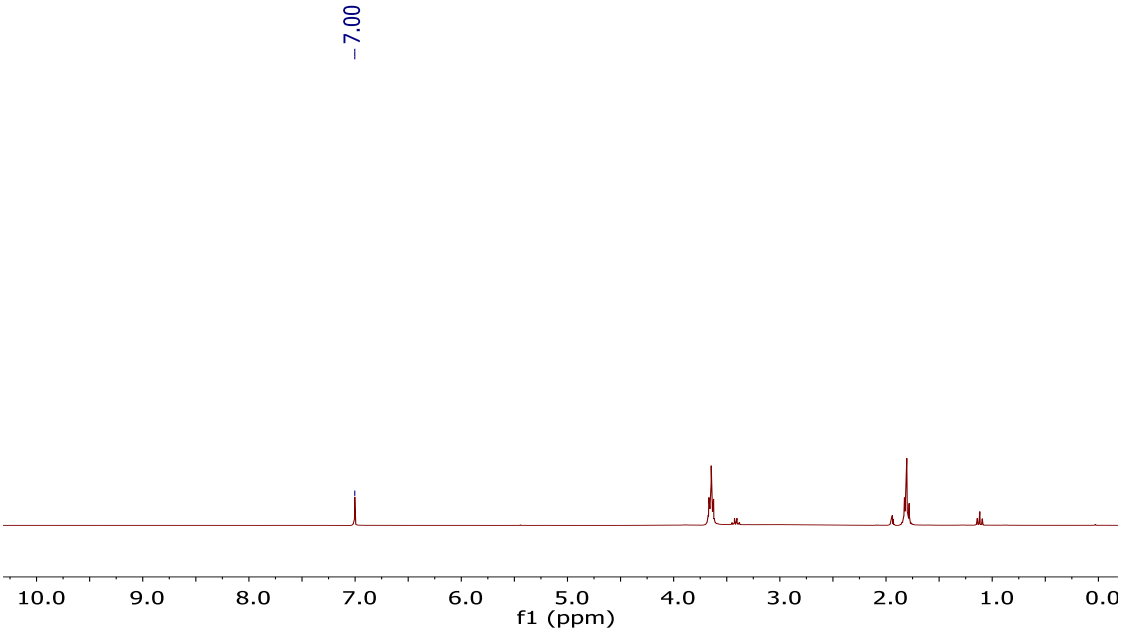

Fig. **2.16** ^{1}H-NMR spectrum of **23I$_{12}$** in acetonitrile-d_3. *Note: tetrahydrofuran and diethyl ether coordinated to the Li^+ ion can be found at 3.6 and 1.8 ppm and 3.4 and 1.1 ppm respectively.*

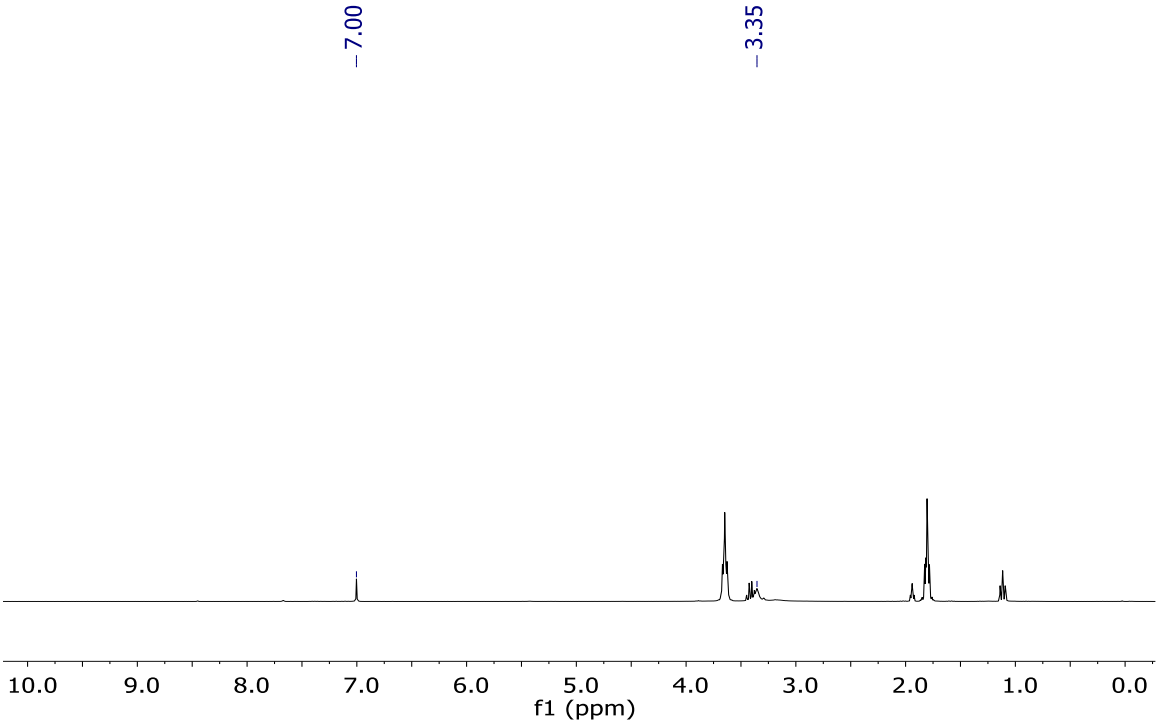

Fig. **2.17** $^{1}H[^{11}B]$ NMR spectrum of **23I$_{12}$** in acetonitrile-d$_3$. *Note: The B-H resonance appears at 3.35 ppm.*

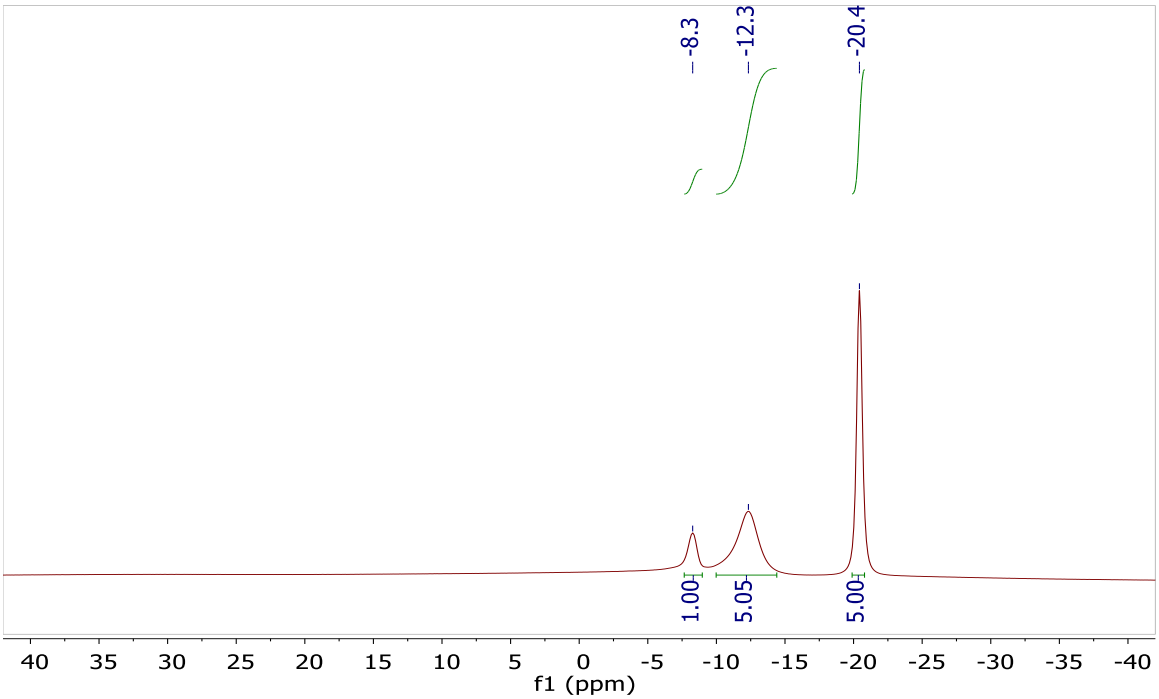

Fig. **2.18** $^{11}B[^{1}H]$ NMR spectrum of **23I$_{12}$** in acetonitrile-d$_3$

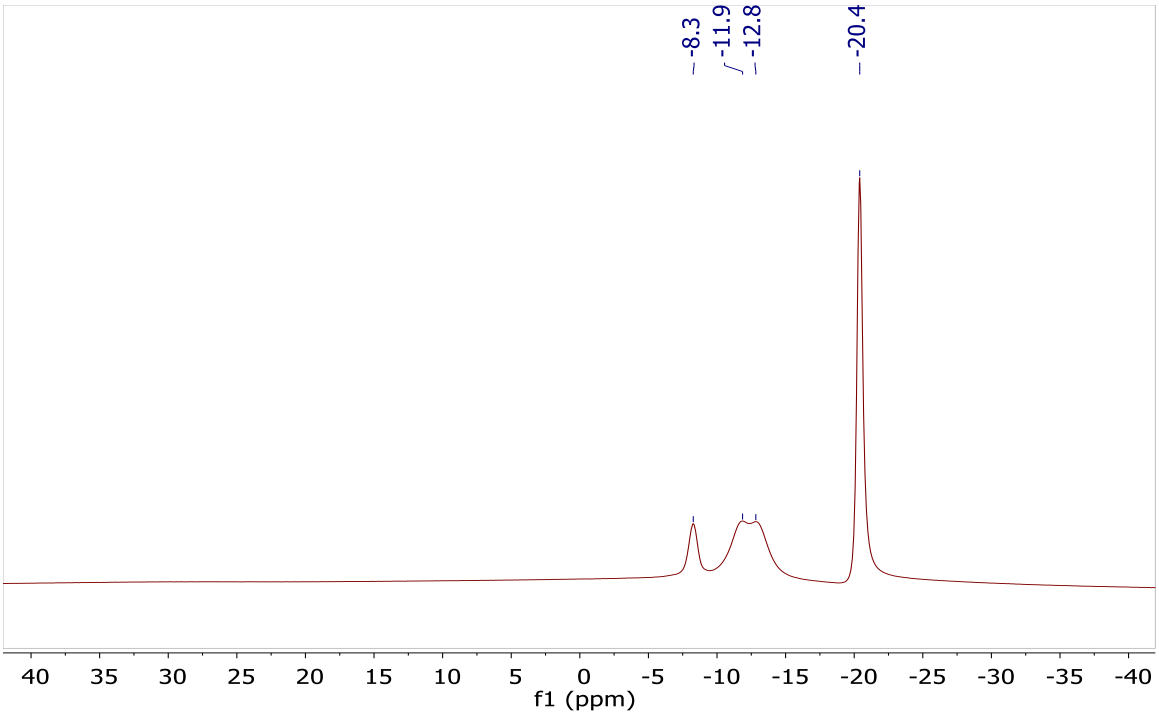

Fig. **2.19** ^{11}B-NMR spectrum of **23I$_{12}$** in acetonitrile-d$_3$.

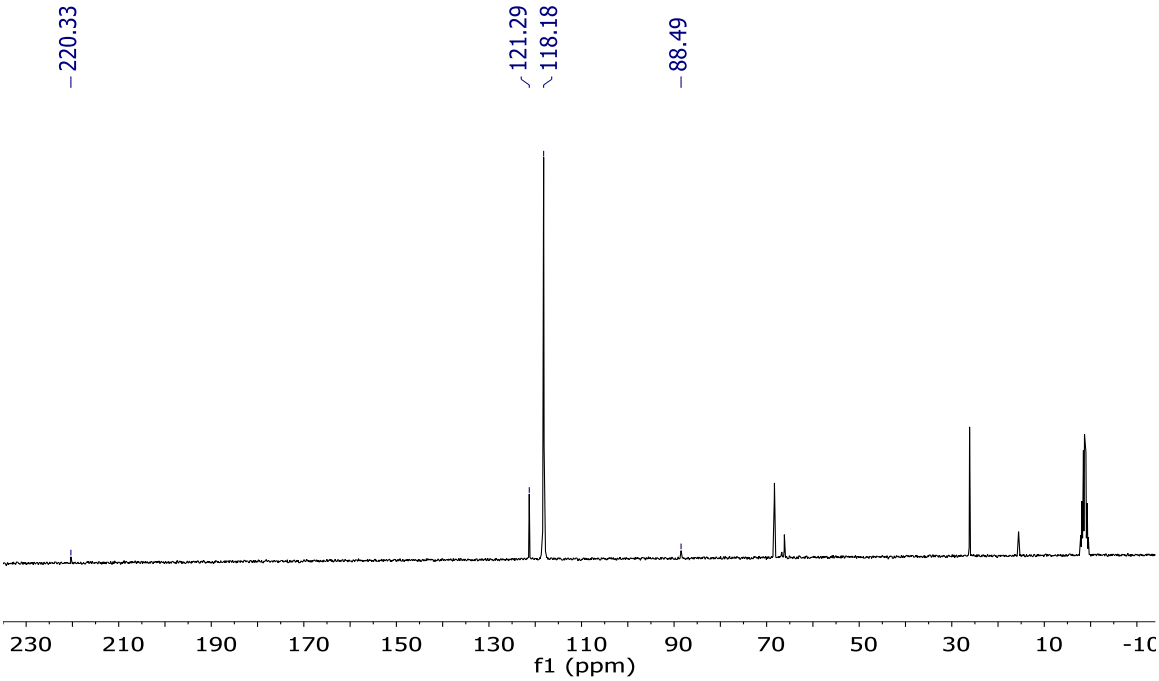

Fig. **2.20** ^{13}C-NMR spectrum of **23I$_{12}$** in acetonitrile-d$_3$. *Note: tetrahydrofuran and diethyl ether coordinated to Li^+ appear at 68 and 26 ppm as well as 66 and 16 ppm respectively.*

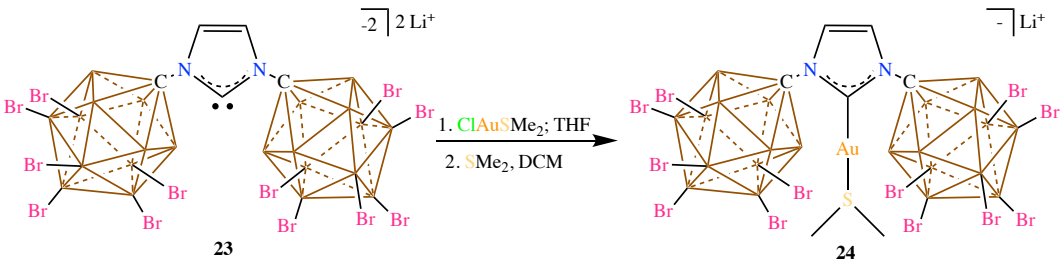

Scheme **2.12** Synthesis of **24Br$_{12}$**

A glass scintillation vial was equipped with a stir bar and loaded with **23Br$_{12}$** (0.300 g, 0.172 mmol). To this, a suspension of dimethylsulfide gold chloride (0.078 g, 0.159 mmol) in THF (2 mL) was added and the reaction was stirred for an hour at room temperature. The solution was then pumped down dry under high vacuum to afford a purple solid. The solid was then suspended in dichloromethane to which freshly distilled dimethylsulfide (1mL, excess) was added. The suspension was stirred overnight and filtered over celite to afford the title compound in 85% yield. ^{1}H NMR (500 MHz, methylene chloride-d$_2$, 25°C): δ = 7.37 (2H, s), 2.93 (6H, s), 3.8 – 2.2 (bs, 10H, B-H) ppm. ^{1}H[^{11}B]-NMR spectrum (300 MHz, methylene chloride-d$_2$, 25°C): δ = 7.37 (2H, s), 3.29 (10H, bs), 2.93 (6H, s) ppm. ^{11}B[^{1}H] NMR (128 MHz, methylene chloride-d$_2$, 25 °C): δ = -1.4, -10.3, -17.8 ppm. ^{11}B NMR (128 MHz, methylene chloride-d$_2$, 25 °C): δ = -1.3, -10.3, -17.8 (broad) ppm. ^{13}C[^{1}H] NMR (126 MHz, methylene chloride-d$_2$, 25 °C): δ = 176.9, 123.7, 71.5, 25.0 ppm. Melting point: 104 – 106 °C.

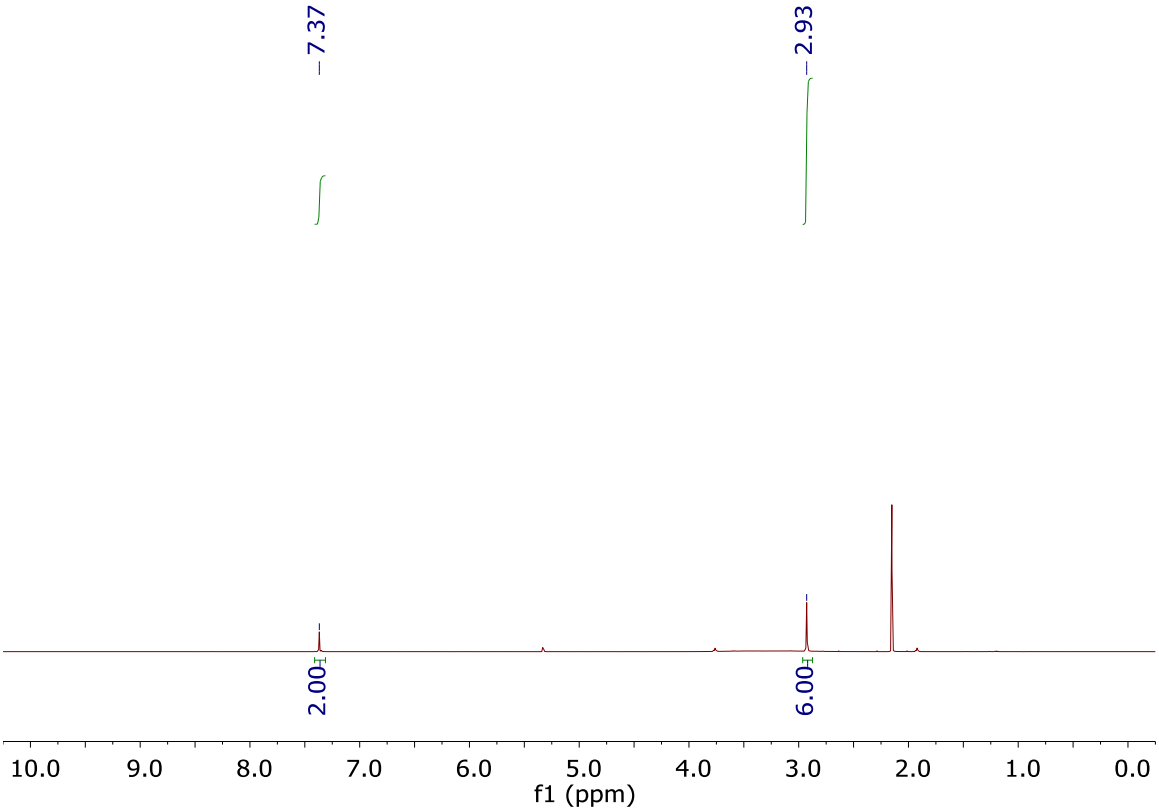

Fig. **2.21** ^{1}H NMR-spectrum of **24Br$_{12}$** in methylene chloride-d$_2$. *Note: acetonitrile and THF are coordinated to the Li$^+$ counter cation at 2.2, 3.8 and 1.9 ppm respectively*.

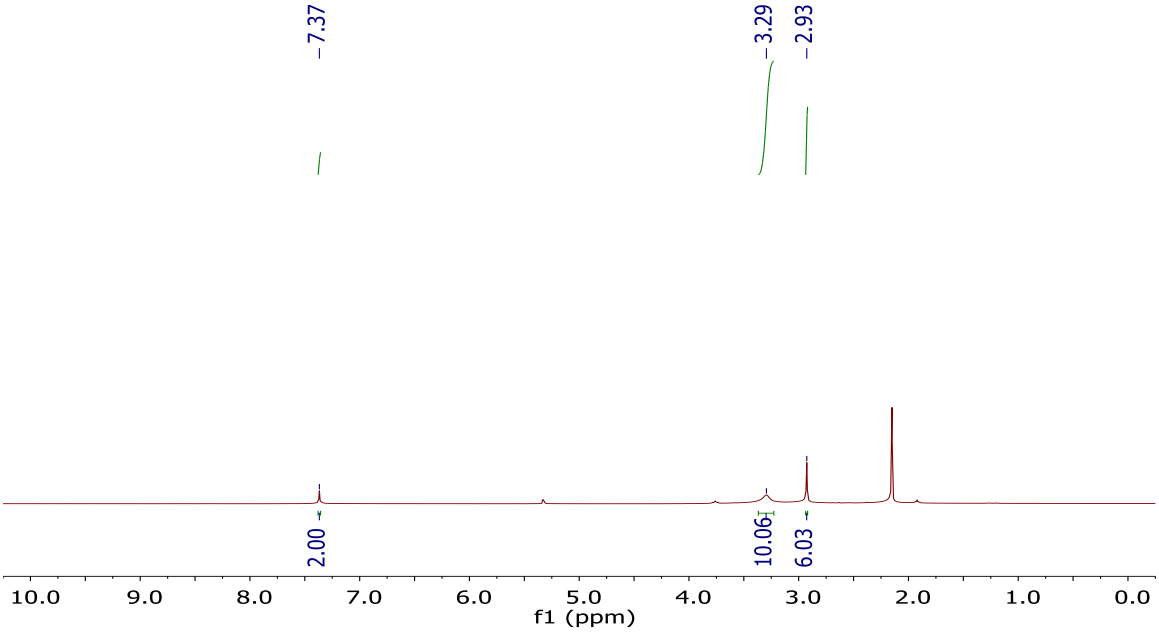

Fig. **2.22** ^{1}H[^{11}B] NMR-spectrum of **24Br$_{12}$** in methylene chloride-d$_2$. *Note: acetonitrile and THF are coordinated to the Li$^+$ counter cation at 2.2, 3.8 and 1.9 ppm respectively.*

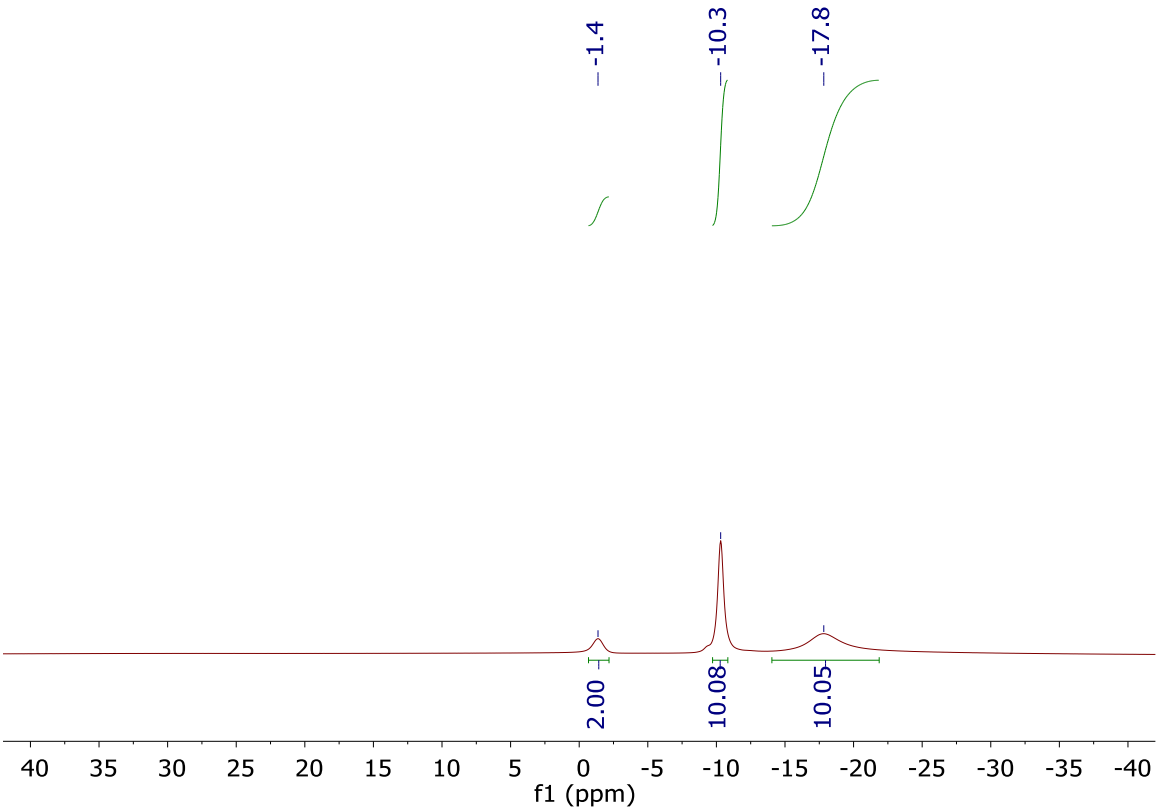

Fig. **2.23** $^{11}B[^{1}H]$ NMR-spectrum of **24Br$_{12}$** in methylene chloride-d_2.

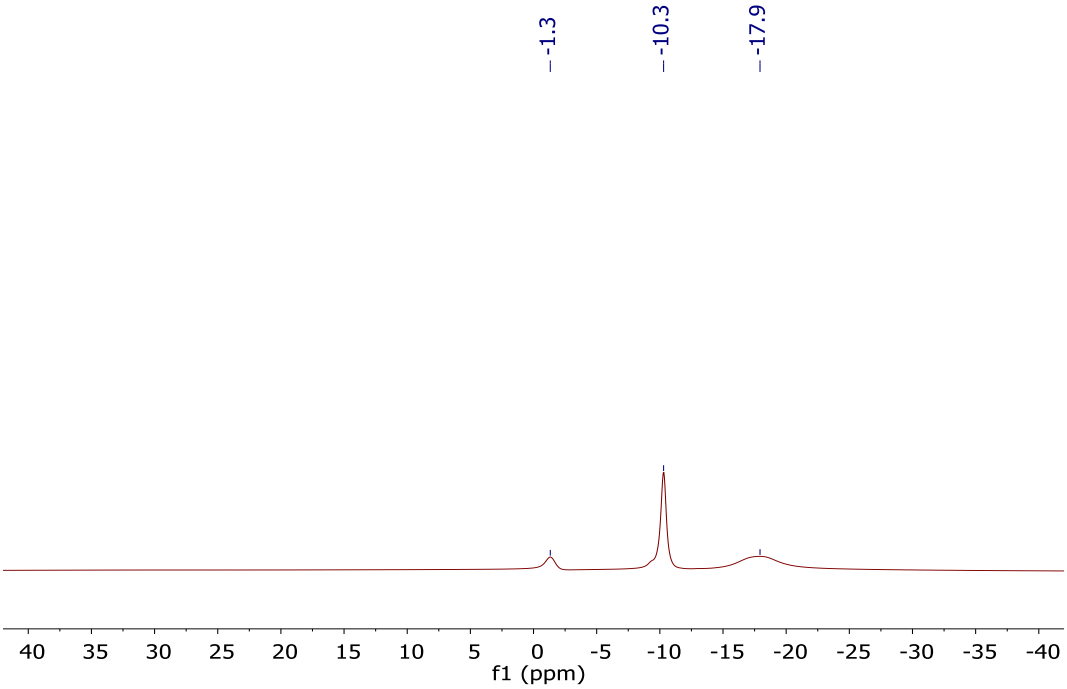

Fig. **2.24** ^{11}B NMR-spectrum of **24Br$_{12}$** in methylene chloride-d_2.

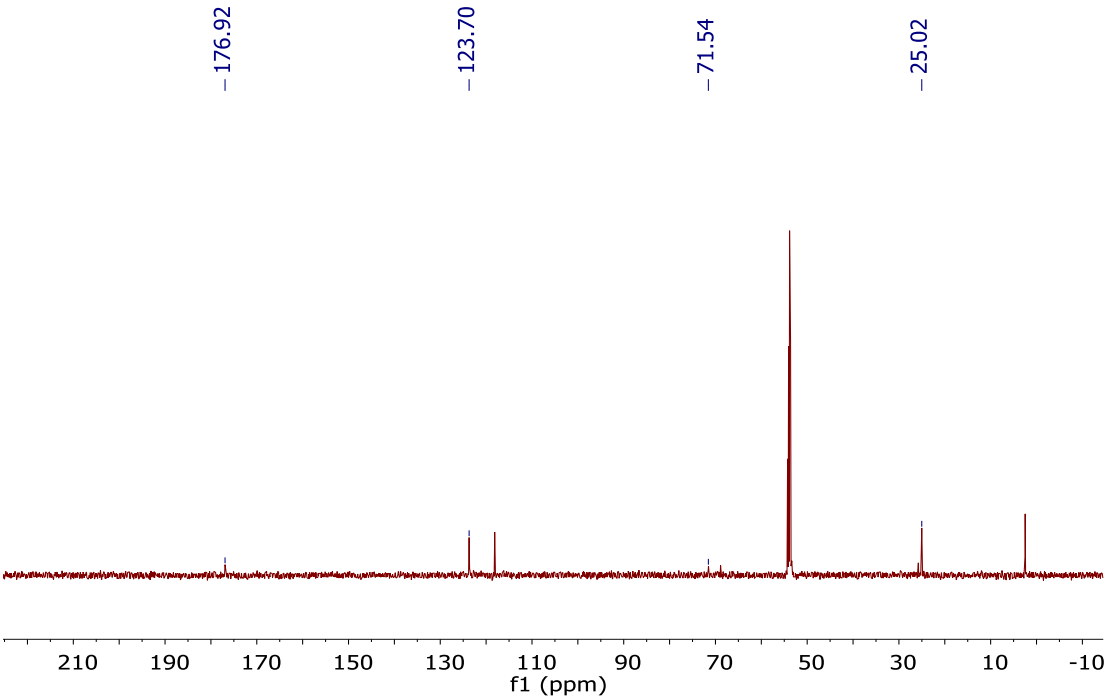

Fig. **2.25** $^{13}C[^{1}H]$ NMR-spectrum of **24Br$_{12}$** in methylene chloride-d$_2$. *Note: acetonitrile and THF coordinated to the Li$^+$ counter cation can be seen at 3, 118 and 26, 69 ppm respectively.*

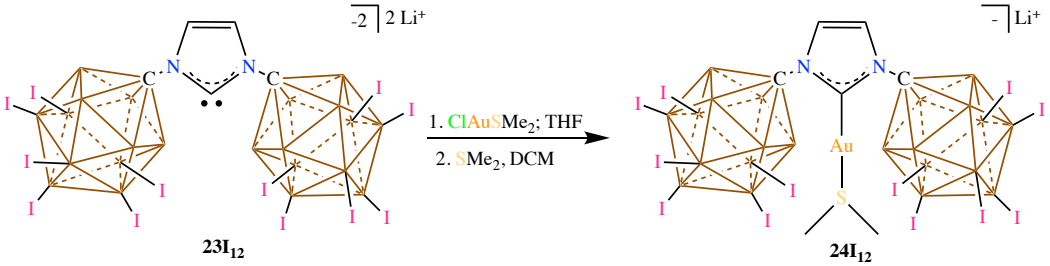

Scheme **2.13** Synthesis of **24I$_{12}$**

A glass scintillation vial was equipped with a stir bar and loaded with **23I$_{12}$** (0.350 g, 0.159 mmol). To this, a suspension of dimethylsulfide gold chloride (0.078 g, 0.159 mmol) in THF (2 mL) was added and the reaction was stirred for an hour at room temperature. The solution was then pumped down dry under high vacuum to afford a purple solid. The solid was then suspended in dichloromethane to which freshly distilled dimethylsulfide (1mL, excess) was added. The suspension was stirred overnight and filtered over celite to afford

the title compound in 85% yield. ^{1}H NMR (400 MHz, methylene chloride-d_2, 25°C): δ = 7.41 (2H, s), 2.97 (6H, s) ppm. ^{1}H[^{11}B]-NMR spectrum (300 MHz, methylene chloride-d_2, 25°C): δ = 7.41 (2H, s), 3.86 (10H, bs), 2.97 (6H, s) ppm. ^{11}B[^{1}H] NMR (128 MHz, methylene chloride-d_2, 25 °C): δ = -6.1, -12.1, -20.0 ppm. ^{11}B NMR (128 MHz, methylene chloride-d_2, 25 °C): δ = -6.2, -12.3 (broad), -20.0 ppm. ^{13}C[^{1}H] NMR (126 MHz, methylene chloride-d_2, 25 °C): δ = 176.0, 123.5, 85.0, 25.2 ppm. Melting point: decomposed at 160 °C.

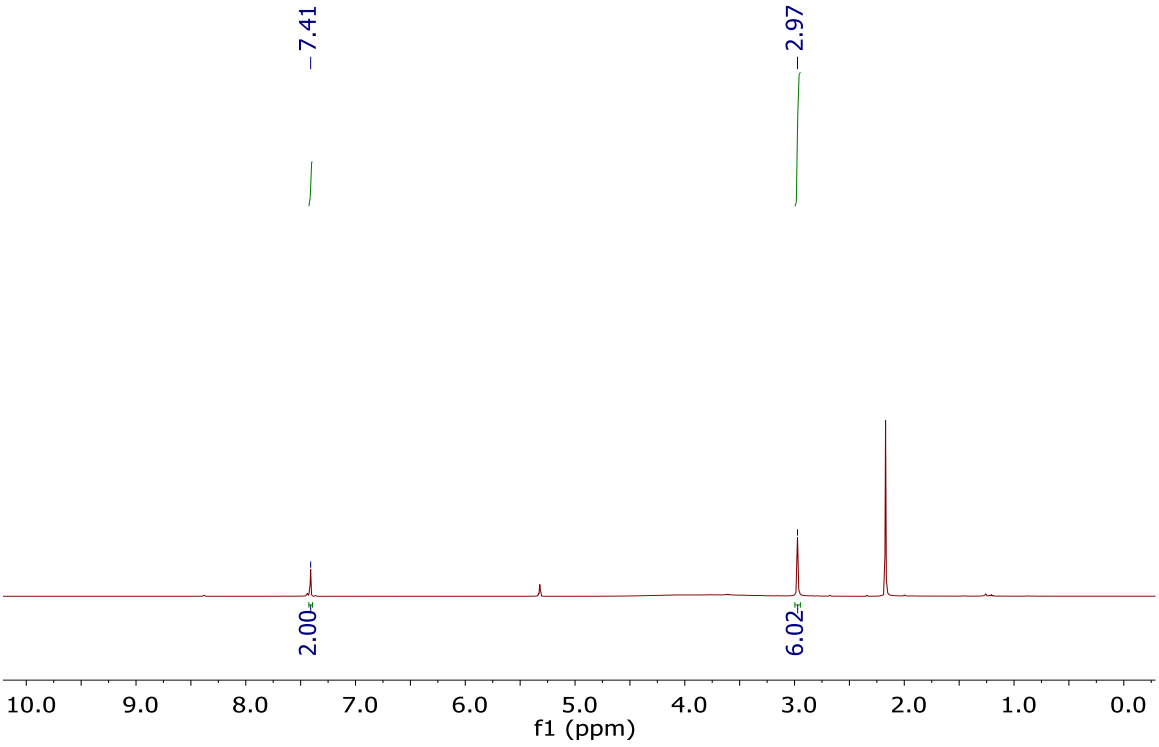

Fig. **2.26.** ^{1}H-NMR spectrum of compound **24I$_{12}$** in methylene chloride-d_2. *Note: acetonitrile coordinated to the lithium cation can be seen at 2.17 ppm.*

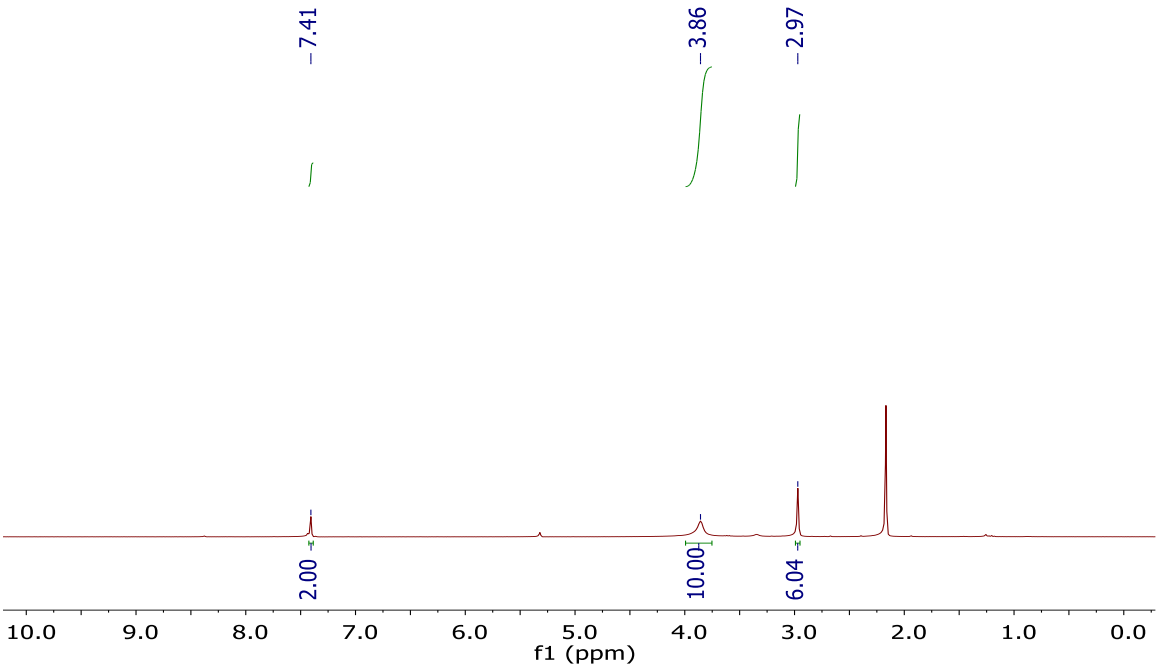

Fig. **2.27** $^{1}H[^{11}B]$-NMR spectrum of compound **24I$_{12}$** in methylene chloride. *Note: the borohydrides show up at 3.86 ppm.*

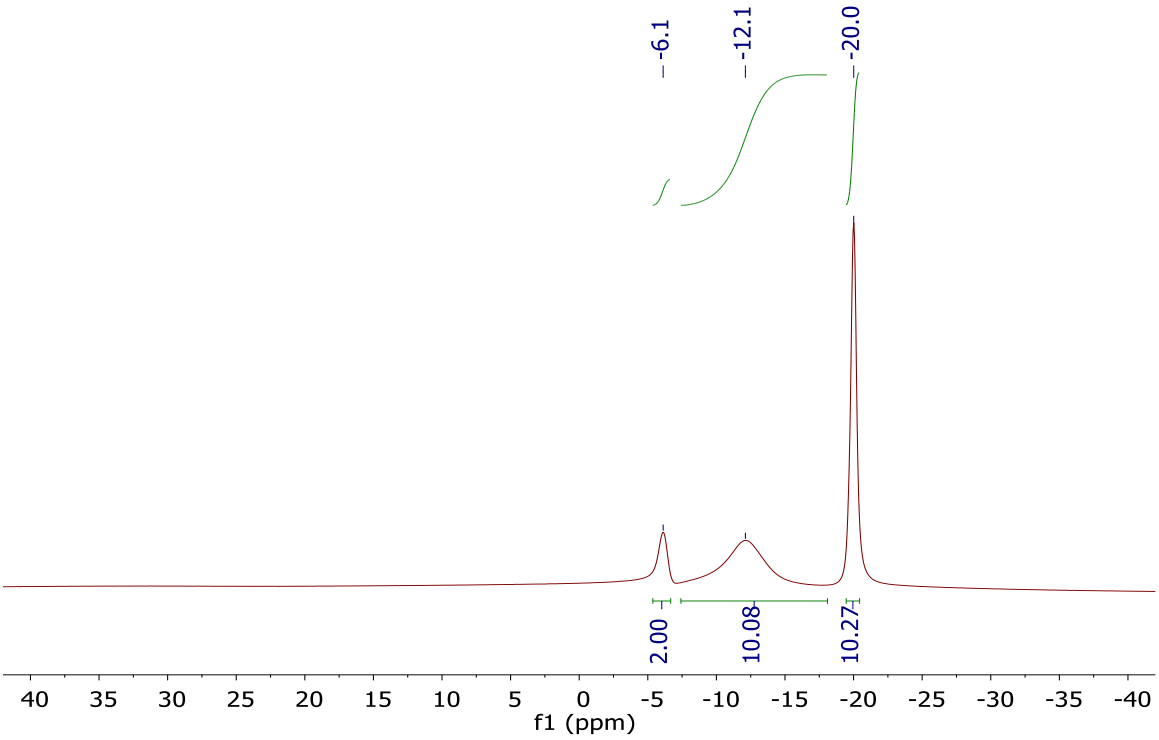

Fig. **2.28** $^{11}B[^{1}H]$-NMR spectrum of compound **24I$_{12}$** in methylene chloride-d_2.

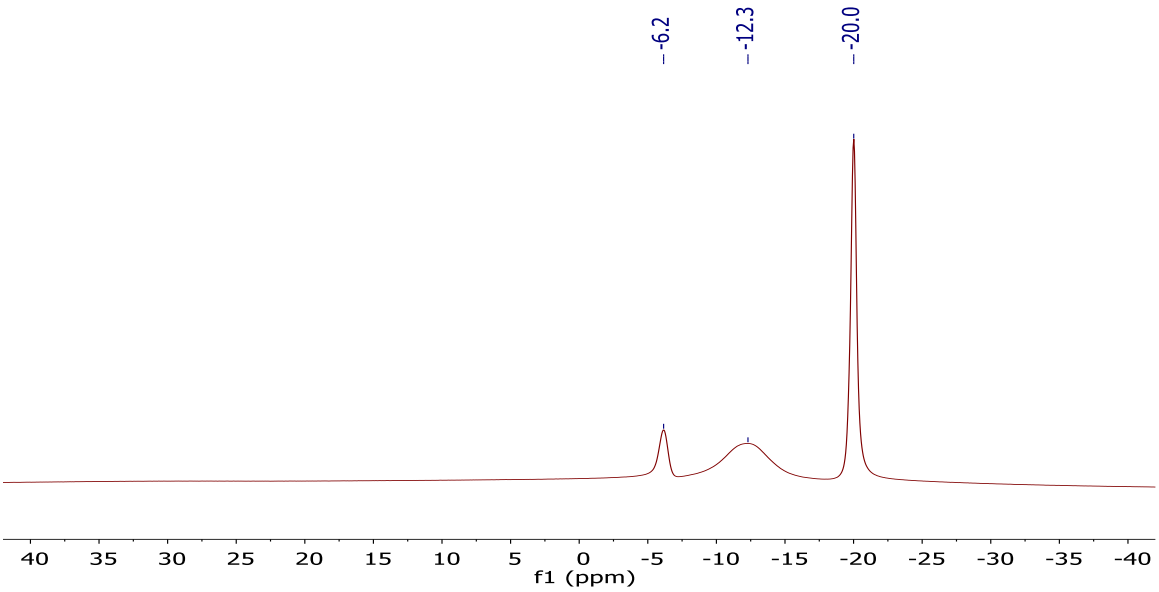

Fig. **2.29** ^{11}B-NMR spectrum of compound **24I$_{12}$** in methylene chloride-d$_2$.

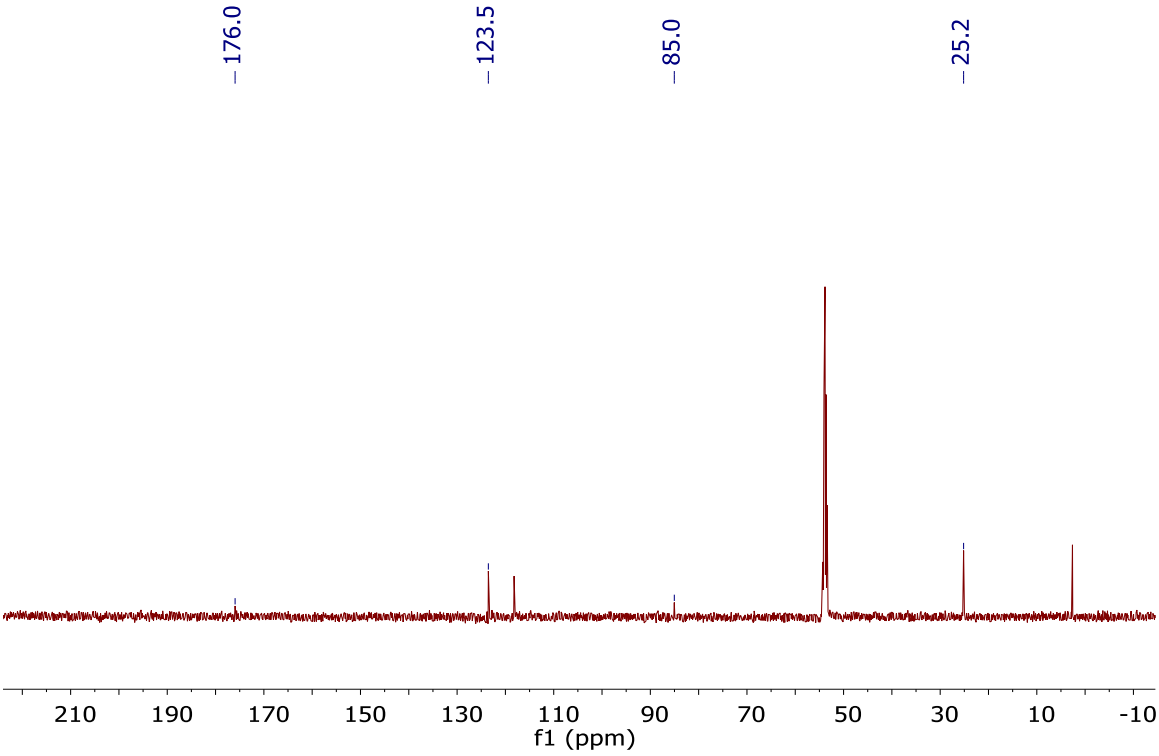

Fig. **2.30** ^{13}C[^{1}H]-NMR spectrum of compound **24I$_{12}$** in methylene chloride-d$_2$. *Note: coordinated acetonitrile can be seen at 2.6 and 118 ppm.*

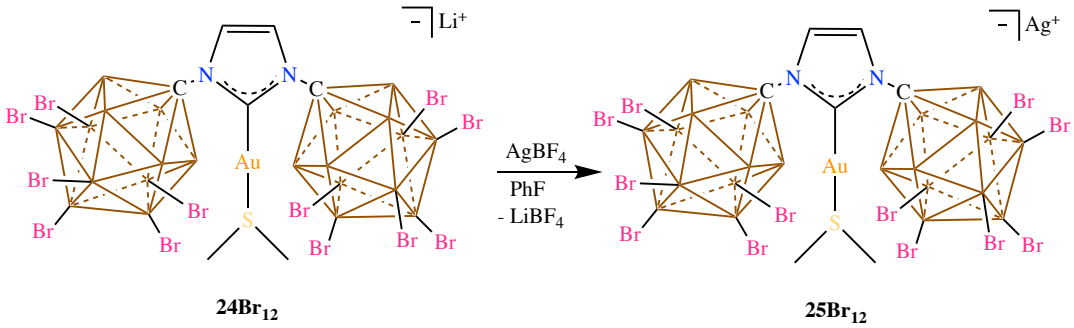

Scheme **2.14** Synthesis of **25Br$_{12}$**

A glass scintillation vial equipped with a stir bar was loaded with **24Br$_{12}$** (267 mg, 143 µmol) and suspended in F-C_6H_5 (4 mL). A solution of $AgBF_4$ (28.5 mg, 146 µmol) in F-C_6H_5 (3 mL) was added dropwise to the suspension containing **24Br$_{12}$** and stirred overnight at room temperature. The F-C_6H_5 supernatant was removed and the solid was pumped down dry under high vacuum. The dry solid was then dissolved in minimal amount of THF and added slowly to a vial filled with diethyl ether (15 mL). The solid was washed in diethyl ether till the $LiBF_4$ was completely removed. The progress of the wash was monitored by ^{7}Li, ^{19}F and ^{11}B NMRs. The remaining solid was pumped down to dryness furnishing **25Br$_{12}$** as a pale purple solid (99.6 mg, 93% yield). *Note: if there is a signal present in the ^{7}Li NMR spectrum but not the ^{19}F NMR spectrum, there was incomplete conversion from Li^+ to Ag^+ (i.e. **24Br$_{12}$** is still present) and the $AgBF_4$ step needs to be repeated.* ^{1}H NMR (600 MHz, acetonitrile-d_3, 25°C): ∂ = 7.47 (s, 2H), 2.79 (s, 6H), 3.8 – 2.5 (bs, 10H) ppm. ^{1}H[^{11}B] NMR (600 MHz, acetonitrile-d_3, 25°C): ∂ = 7.47 (s), 3.29 (bs, H-B), 2.81 (s) ppm. ^{11}B[^{1}H] NMR (192 MHz, acetonitrile-d_3, 25°C): ∂ = -1.7, -10.5, -17.7 ppm. ^{11}B NMR (192 MHz, acetonitrile-d_3, 25°C): ∂ = -1.7, -10.5, -17.6 ($^{1}J(H,B)$ = 107.8 Hz) ppm. ^{13}C[^{1}H] NMR (151 MHz, acetonitrile-d_3, 25°C): ∂ = 177.3, 124.9, 72.3, 24.4 ppm.

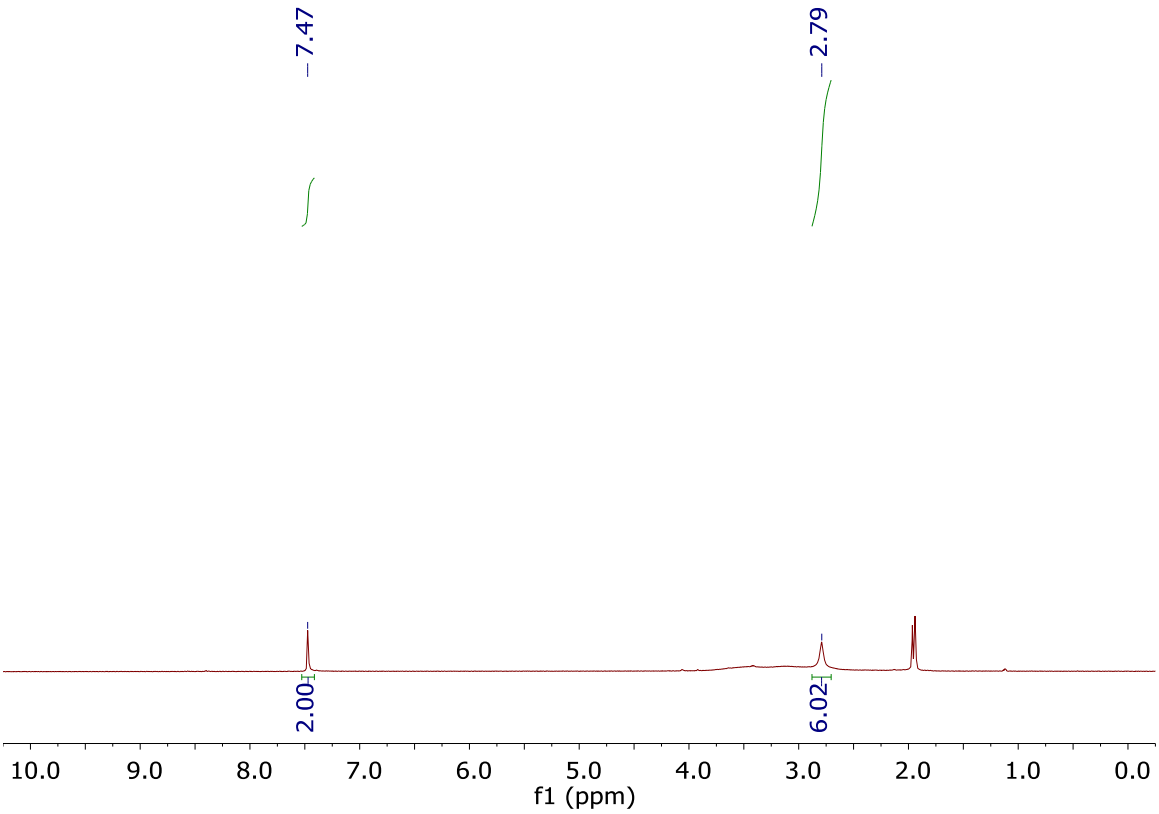

Fig. **2.31** ^{1}H-NMR spectrum of **25Br$_{12}$** in acetonitrile-d$_3$.

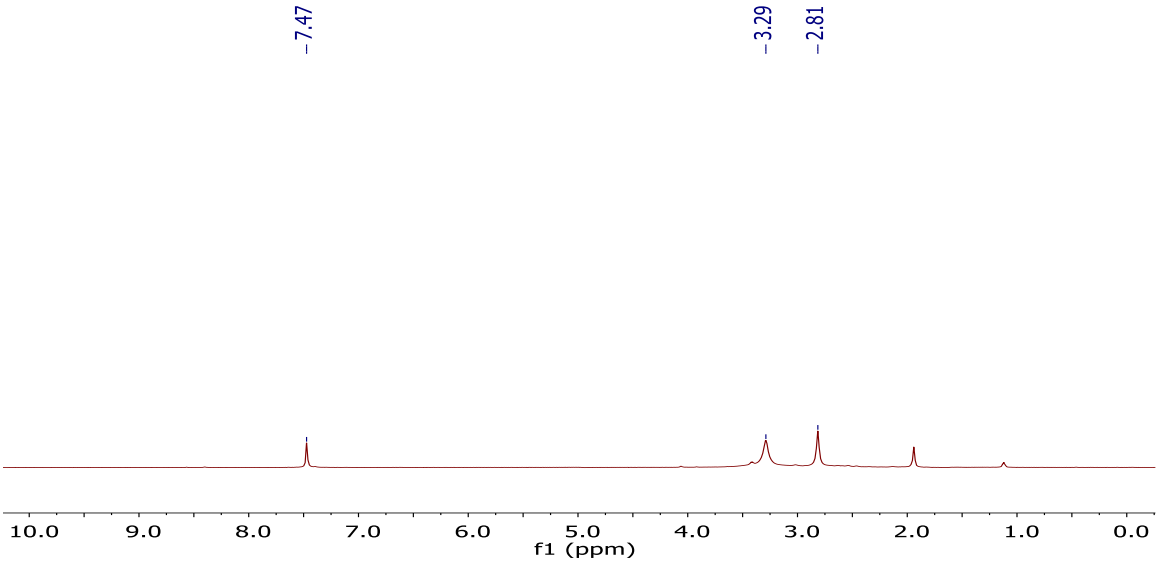

Fig. **2.32** ^{1}H[^{11}B]-NMR spectrum of **25Br$_{12}$** in acetonitrile-d$_3$. *Note: The peak at 3.29 ppm corresponds to B-H resonance, some Et_2O coordinated to the Ag^+ cation appear at 3.42 and 1.12 ppm.*

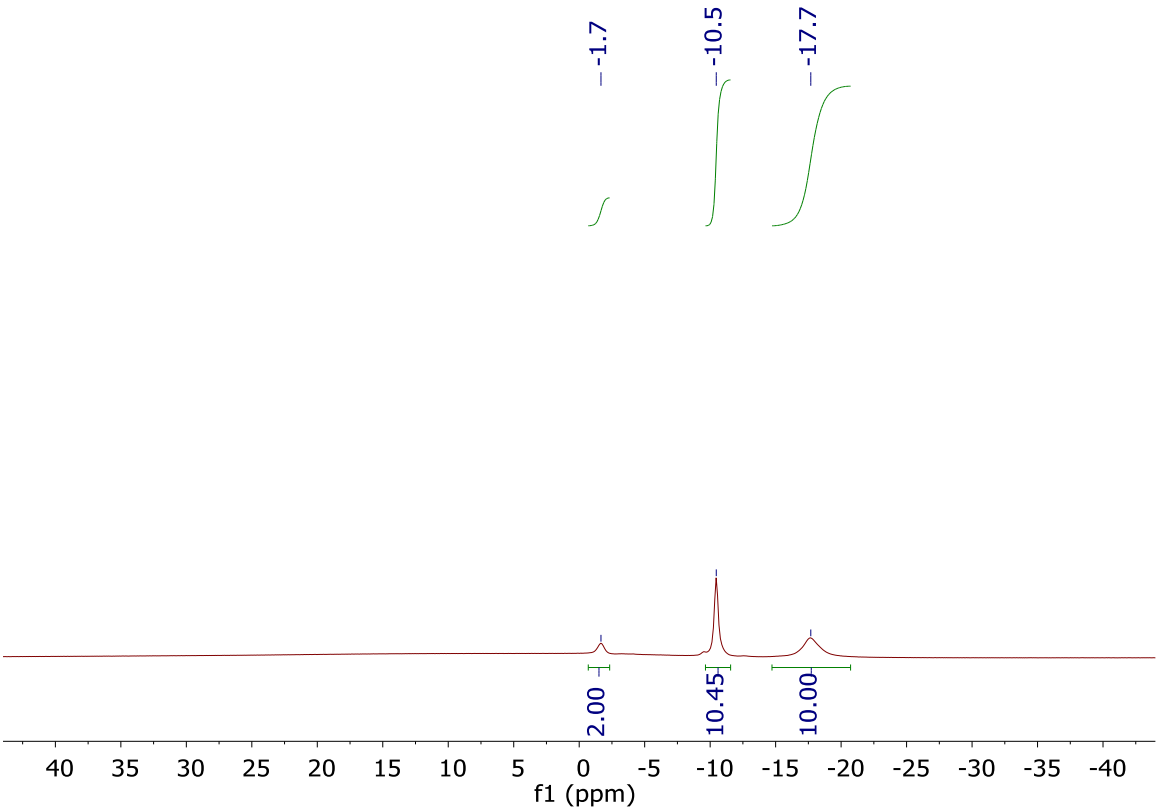

Fig. **2.33** $^{11}B[^{1}H]$-NMR spectrum of **25Br$_{12}$** in acetonitrile-d$_3$.

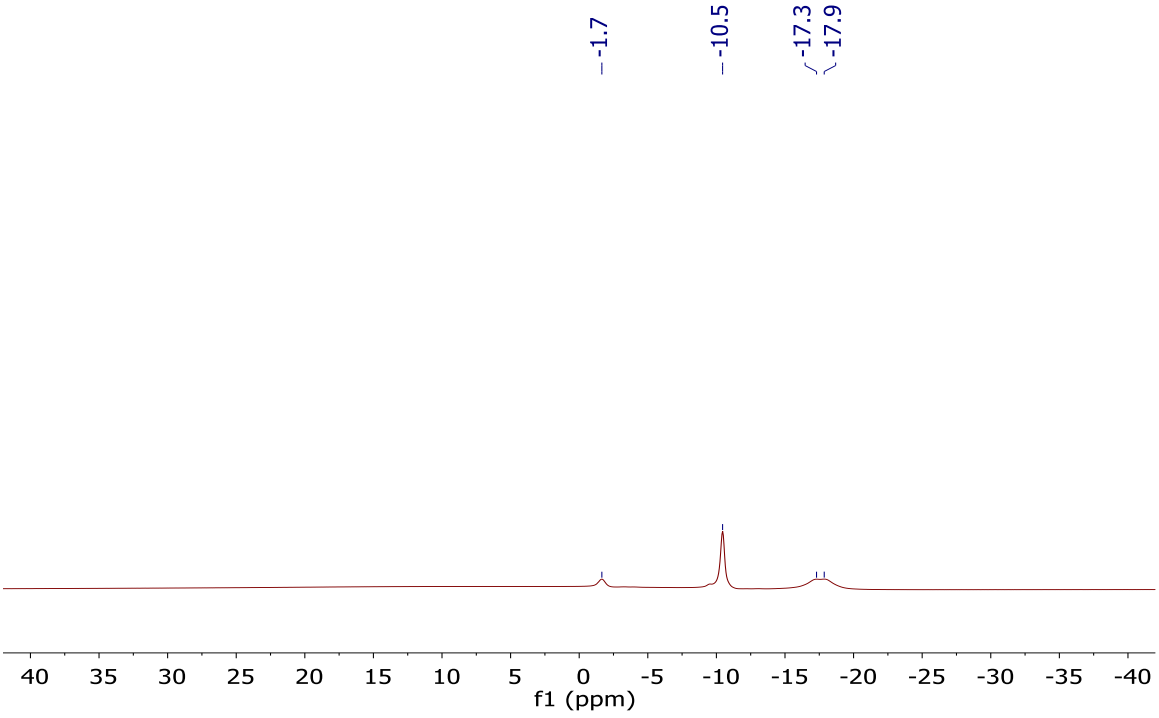

Fig. **2.34** ^{11}B-NMR spectrum of **25Br$_{12}$** in acetonitrile-d$_3$.

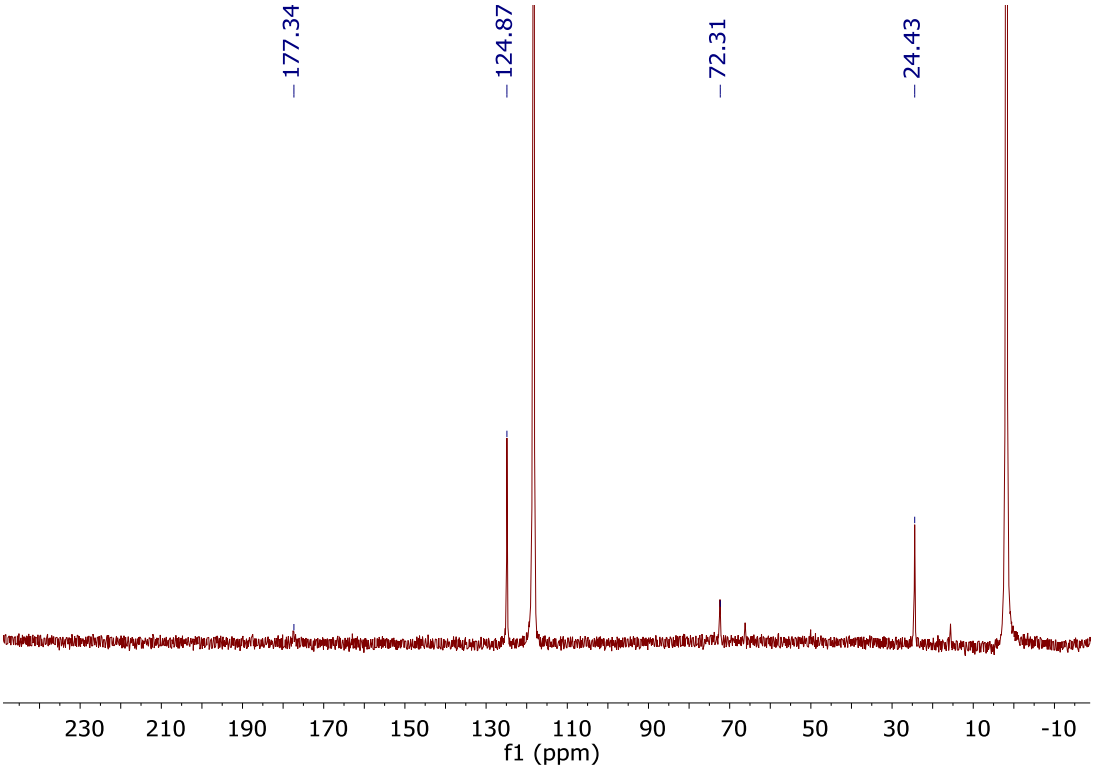

Fig. **2.35** $^{13}C[^{1}H]$-NMR spectrum of **25Br$_{12}$** in acetonitrile-d$_3$. *Note: the peaks at 66.2 and 16.0 ppm correspond to some Et_2O coordinated to the Ag^+ cation.*

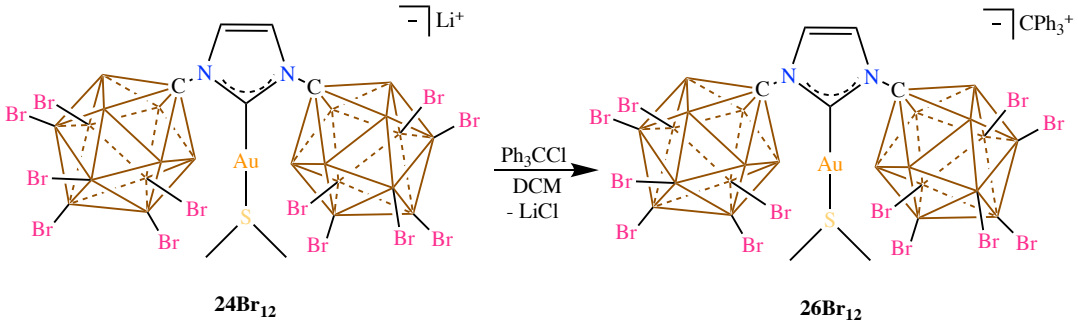

Scheme **2.15** Synthesis of **26Br$_{12}$**

All THF coordinated to the lithium cation is removed by dissolving **24Br$_{12}$** (0.550 g, 0.311 mmol) in acetonitrile then removing the volatiles under vacuum, the process is repeated 3 times. After the THF is removed from the Li^+ cation the solid was suspended in methylene chloride (5 mL). Trityl chloride (123.5 mg, 0.443 mmol) dissolved in methylene chloride (3 mL) was added to the suspension and the reaction changed colors from pale yellow to

bright yellow. The reaction was stirred for one hour at room temperature then filtered. The filtrate was concentrated down to 3 mL then added dropwise to a stirring benzene solution (16 mL) which forms a yellowish top layer and red bottom layer. After stirring for 15 minutes the upper benzene layer was removed and the remaining oil was pumped down to dryness furnishing the **26Br$_{12}$** in 92% yield (488.9 mg). ^{1}H NMR (600 MHz, methylene chloride-d$_2$, 25°C): δ = 8.31 (3H, t, $^{3}J(H,H)$ = 7.5 Hz), 7.93 (6H, t, $^{3}J(H,H)$ = 7.5 Hz), 7.69 (6H, d, $^{3}J(H,H)$ = 7.5 Hz), 7.35 (2H, s), 2.92 (6H, s), 4.2 – 2.2 (bs, 10H, B-H) ppm. ^{1}H[^{11}B]-NMR spectrum (300 MHz, methylene chloride-d$_2$, 25°C): δ = 8.31 (3H, t, $^{3}J(H,H)$ = 7.5 Hz), 7.92 (6H, t, $^{3}J(H,H)$ = 7.5 Hz), 7.70 (6H, d, $^{3}J(H,H)$ = 7.5 Hz), 7.36 (2H, s), 3.28 (10H, bs), 2.92 (6H, s) ppm. ^{11}B[^{1}H] NMR (96 MHz, methylene chloride-d$_2$, 25 °C): δ = -1.4, -10.3, -17.7 ppm. ^{11}B NMR (96 MHz, methylene chloride-d$_2$, 25 °C): δ = -1.3, -10.3 (broad), -17.7 ppm. ^{13}C[^{1}H] NMR (126 MHz, methylene chloride-d$_2$, 25 °C): δ = 211.0, 176.9, 144.0, 143.2, 140.3, 131.2, 123.7, 71.5, 25.0 ppm.

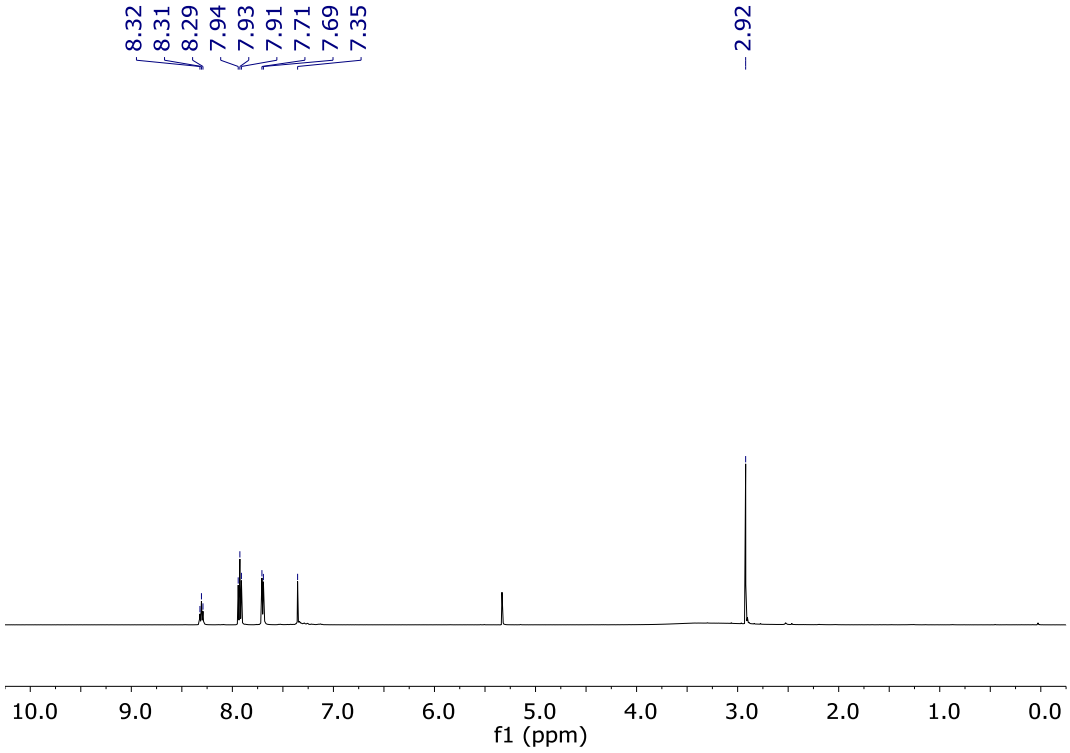

Fig. **2.36** ^{1}H NMR-spectrum of **26Br$_{12}$** in methylene chloride-d$_2$. *Note: Benzene (7.35 ppm) from the wash overlaps with the backbone protons of the NHC ligand.*

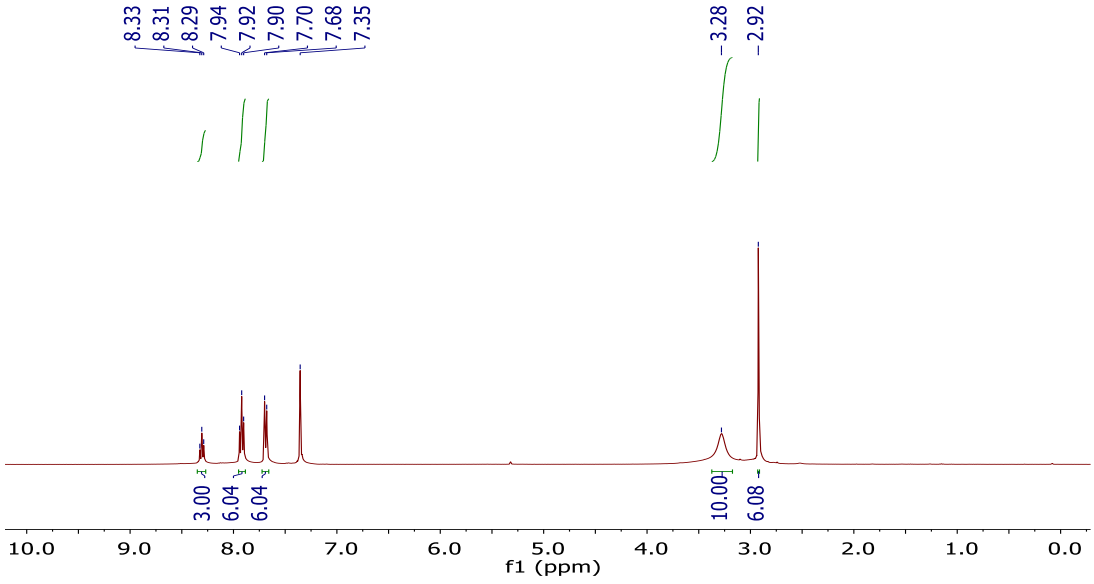

Fig. **2.37** ^{1}H[^{11}B] NMR-spectrum of **26Br$_{12}$** in methylene chloride-d$_2$. *Note: benzene (7.35 ppm) from the wash overlaps with the backbone protons of the NHC ligand.*

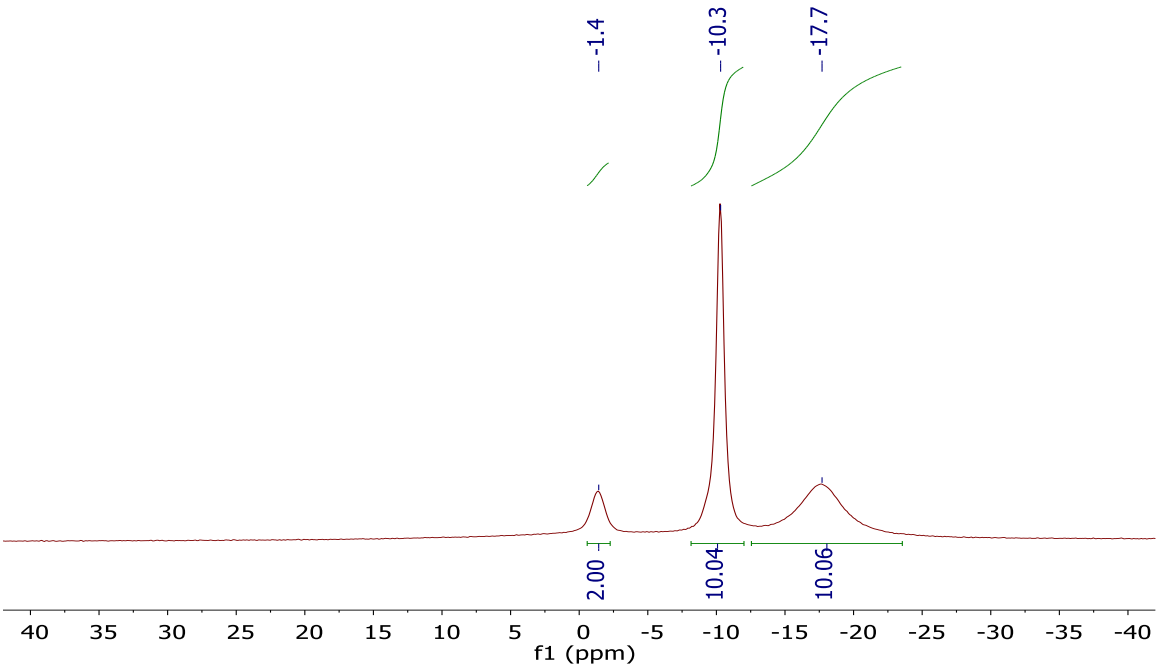

Fig. **2.38** $^{11}B[^{1}H]$ NMR-spectrum of **26Br$_{12}$** in methylene chloride-d_2.

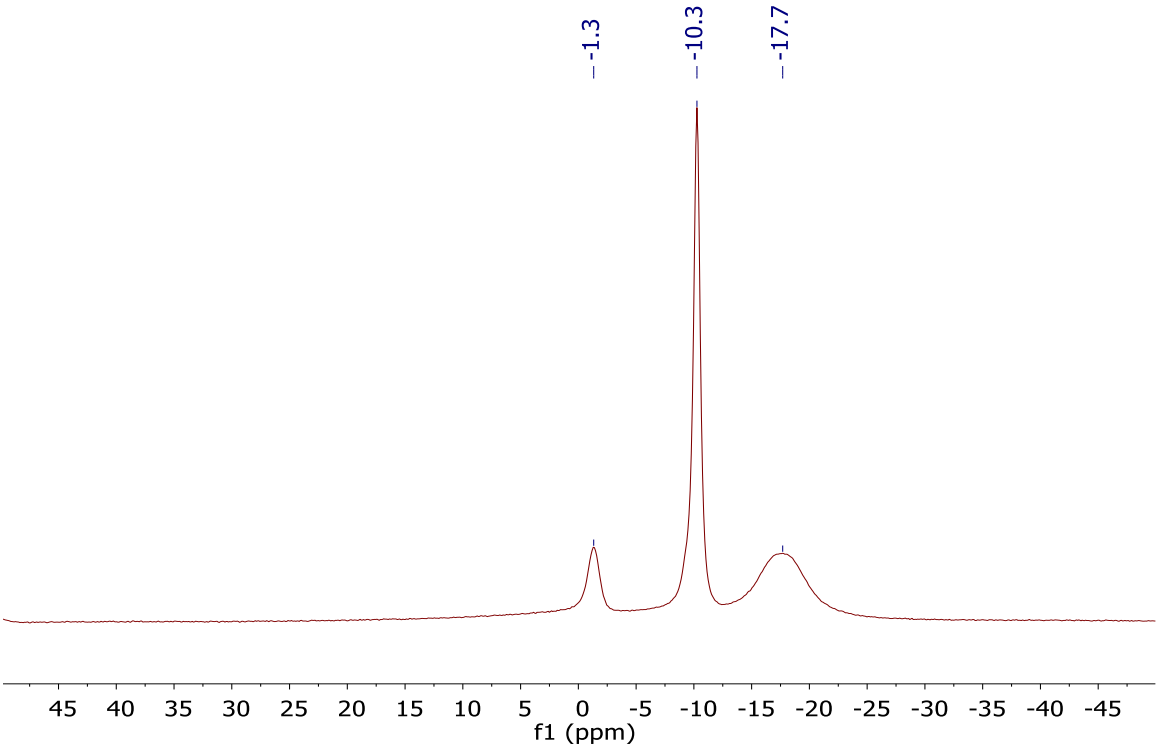

Fig. **2.39** ^{11}B NMR-spectrum of **26Br$_{12}$** in methylene chloride-d_2.

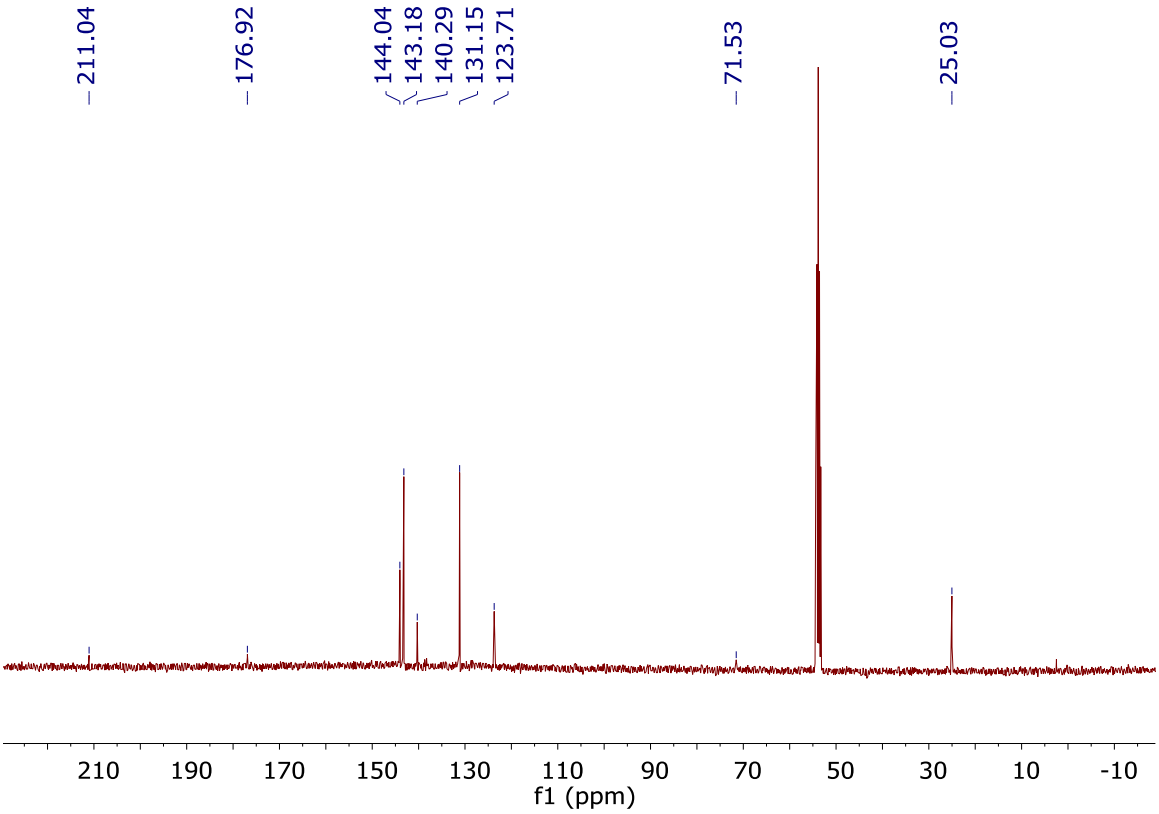

Fig. **2.40** $^{13}C[^{1}H]$ NMR-spectrum of **26Br$_{12}$** in methylene chloride-d$_2$. *Note: the carbene carbon of the NHC ligand appears at 176.9 ppm.*

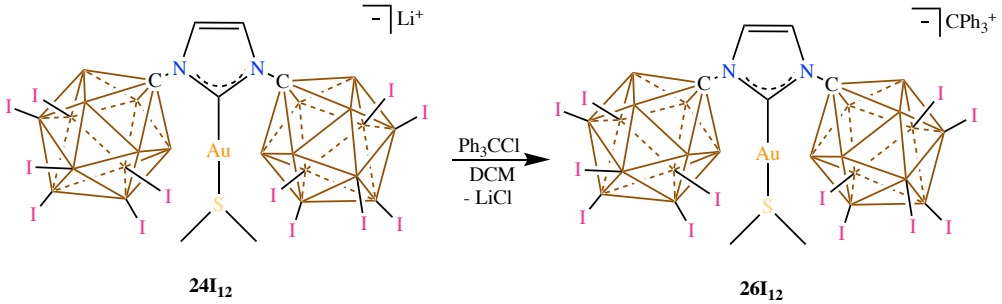

24I$_{12}$ **26I$_{12}$**

Scheme **2.16** Synthesis of **26I$_{12}$**

A glass scintillation vial was equipped with a stir bar and loaded with **24I$_{12}$** (537 mg, 222 µmol) and suspended in acetonitrile (5 mL) and the volatiles removed under vacuum. This process is repeated 3 times. Upon removal of all THF coordinated to the Li^+ cation, the solid was suspended in methylene chloride (5 mL). Trityl chloride (92.9 mg, 334 µmol) dissolved in methylene chloride (3 mL) was added to the suspension and the reaction

changed colors from pale yellow to dark orange red. The reaction was stirred for one hour at room temperature then filtered. The filtrate was concentrated down to 3 mL then added dropwise to a stirring benzene solution (16 mL) which forms a yellowish top layer and red bottom layer. After stirring for 15 minutes, the upper benzene layer was removed and the remaining oil was pumped down to dryness furnishing the **26I$_{12}$** in 94% yield (494 mg, 209 μmol). ^{1}H NMR (600 MHz, methylene chloride-d$_2$, 25°C): δ = 8.32 (3H, t, $^{3}J(H,H)$ = 7.5 Hz), 7.93 (6H, m), 7.70 (6H, d, $^{3}J(H,H)$ = 7.1 Hz), 7.40 (2H, s), 2.97 (6H, s) ppm. ^{1}H[^{11}B]-NMR spectrum (600 MHz, methylene chloride-d$_2$, 25°C): δ = 8.31 (3H, t, $^{3}J(H,H)$ = 7.5 Hz), 7.93 (6H, t, $^{3}J(H,H)$ = 7.5 Hz), 7.70 (6H, d, $^{3}J(H,H)$ = 7.5 Hz), 7.40 (2H, s), 3.84 (10H, bs), 2.97 (6H, s) ppm. ^{11}B[^{1}H] NMR (96 MHz, methylene chloride-d$_2$, 25 °C): δ = -6.1, -12.5, -20.0 ppm. ^{11}B NMR (96 MHz, methylene chloride-d$_2$, 25 °C): δ = -6.2, -12.4 (broad), -20.0 ppm. ^{13}C[^{1}H] NMR (126 MHz, methylene chloride-d$_2$, 25°C): δ = 211.0, 176.0, 144.1, 143.2, 140.3, 131.2, 123.5, 85.0, 25.2 ppm.

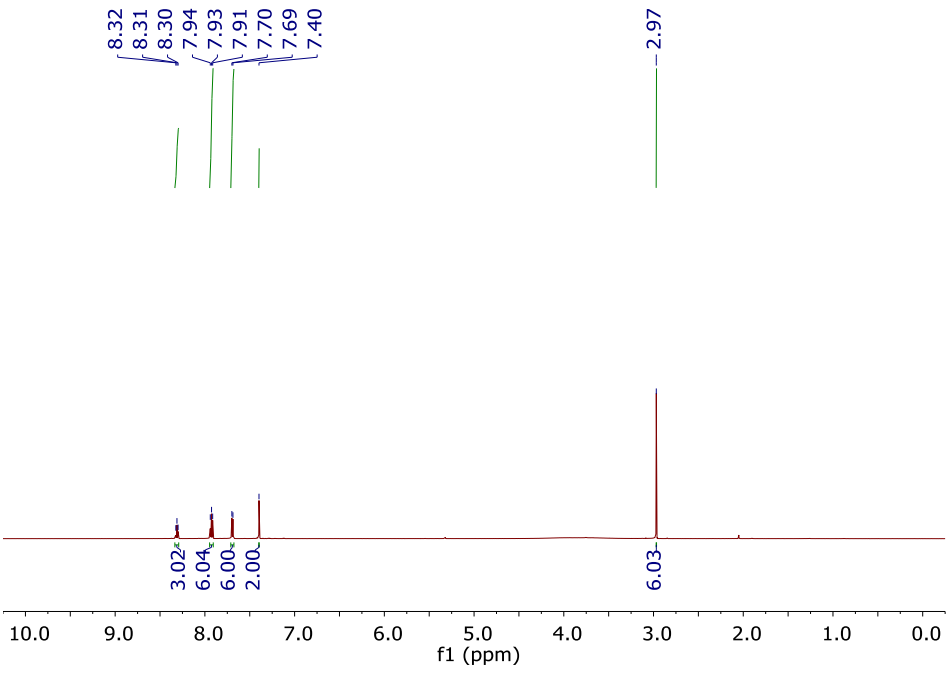

Fig. **2.41** ^{1}H-NMR spectrum of compound **26I$_{12}$** in methylene chloride-d$_2$.

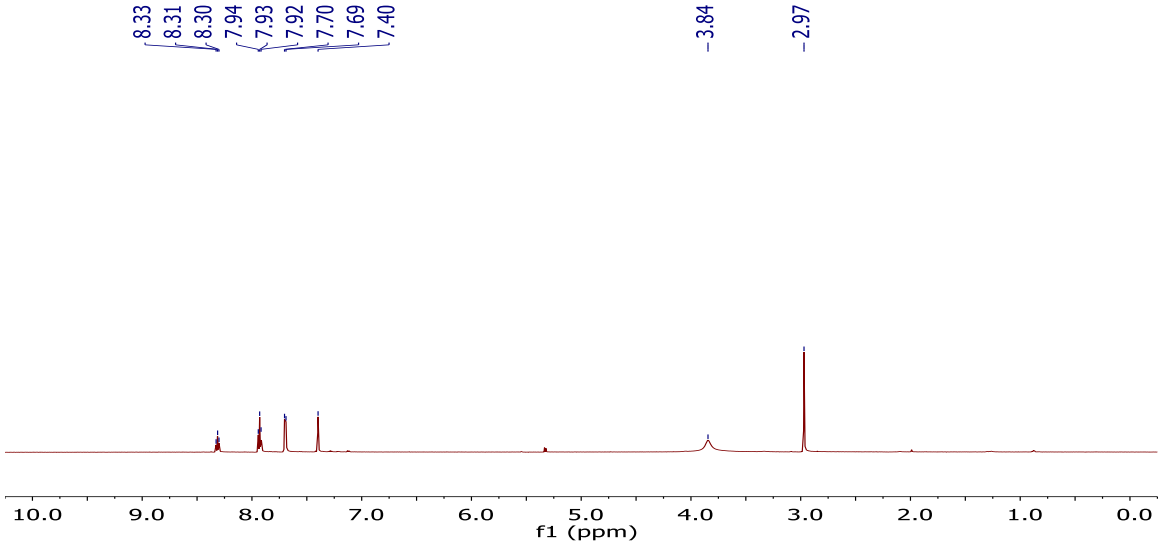

Fig. **2.42** $^{1}H[^{11}B]$-NMR spectrum of compound **26I$_{12}$** in methylene chloride-d_2. *Note: the borohydrides appear at 3.84 ppm.*

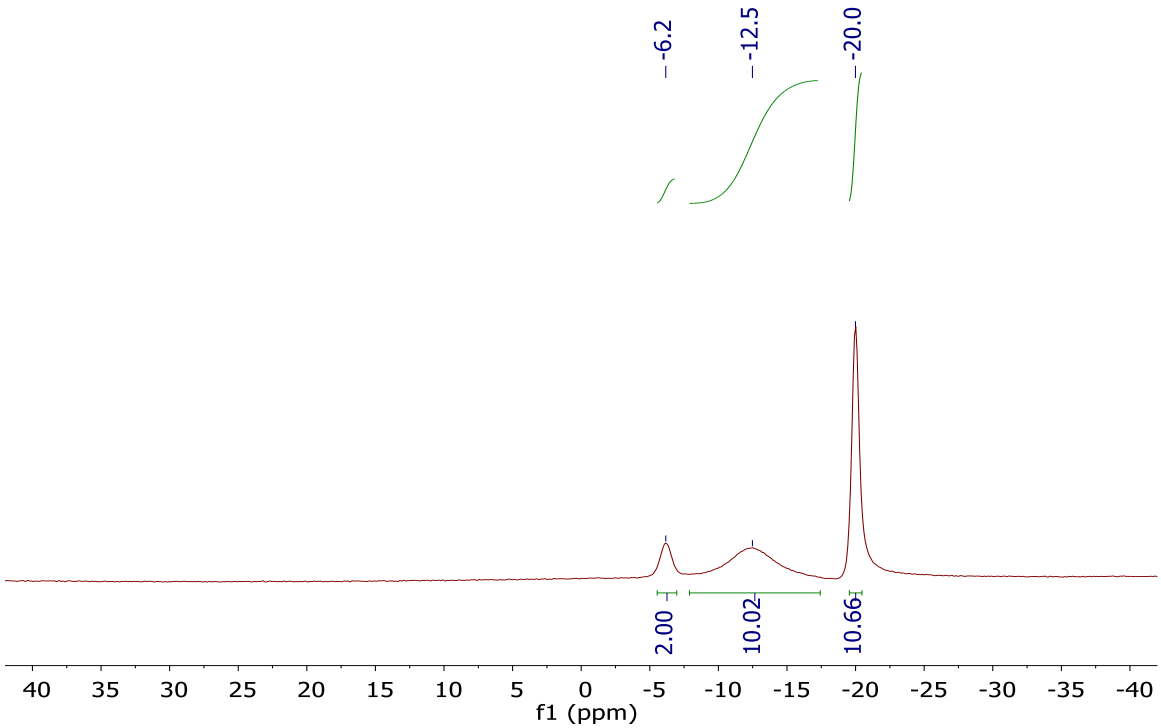

Fig. **2.43** $^{11}B[^{1}H]$-NMR spectrum of compound **26I$_{12}$** in methylene chloride-d_2.

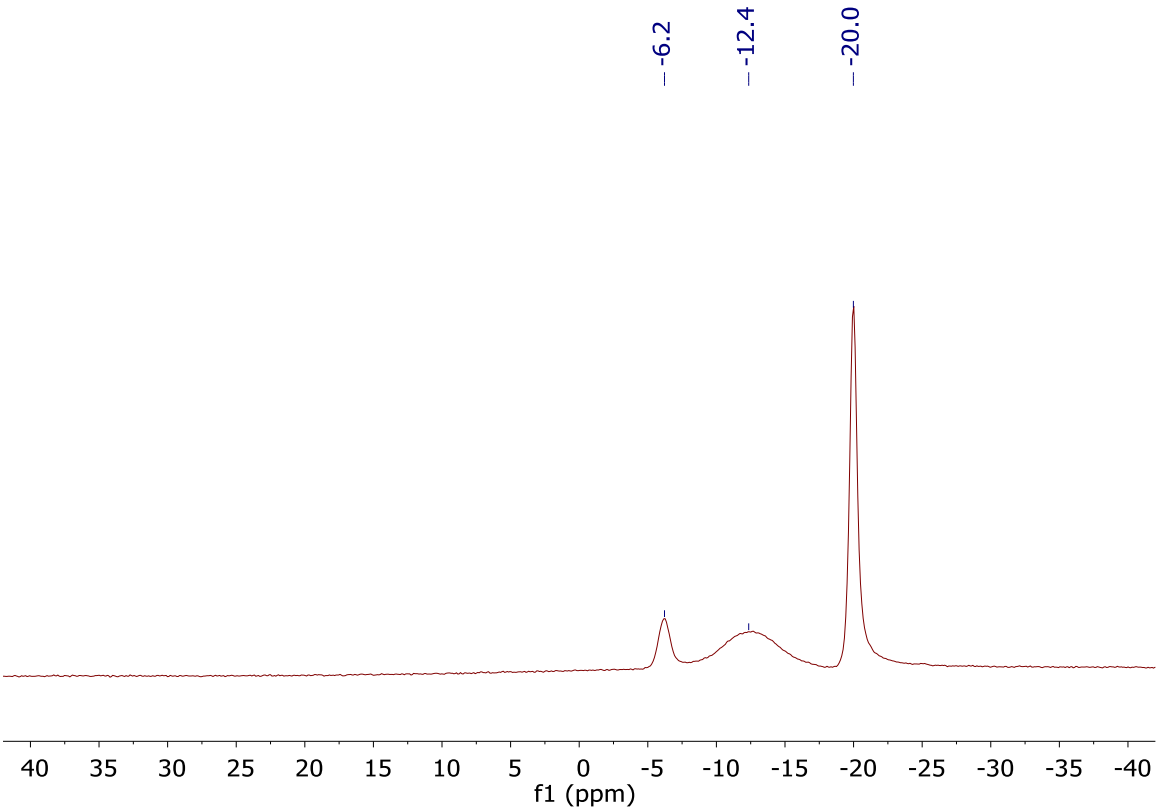

Fig. **2.44** ^{11}B-NMR spectrum of compound **26I$_{12}$** in methylene chloride-d$_2$.

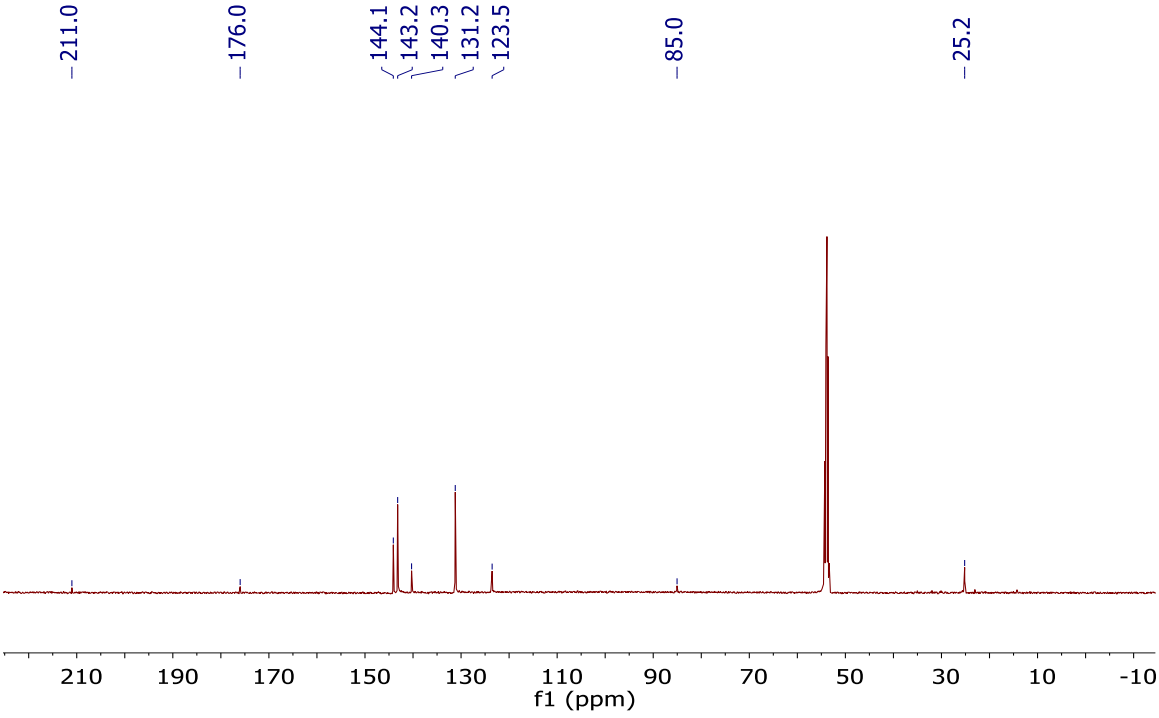

Fig. **2.45** ^{13}C[^{1}H]-NMR spectrum of compound **26I$_{12}$** in methylene chloride-d$_2$.

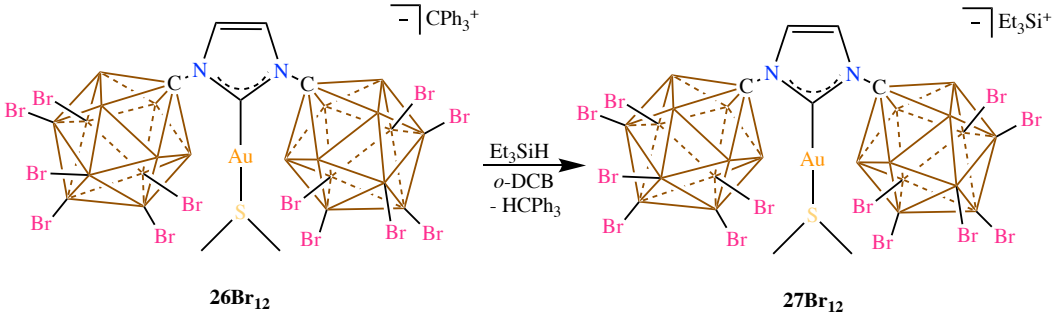

26Br12 **27Br12**

Scheme **2.17** Synthesis of **27Br12**

A glass scintillation vial was equipped with a stir bar and loaded with **26Br12** (0.500 g, 0.278 mmol) and triethylsilane (0.090 mL, 0.064 mg, 0.556 mmol). The heterogeneous mixture was suspended in *ortho*-dichlorobenzene (7 mL) and stirred for 30 minutes at room temperature. The reaction mixture was filtered and the filtrate added to a stirring solution of pentane causing a white precipitate to form. The precipitate was washed with pentane (4 x 5 mL). Upon removal of the last pentane wash, the white solid was pumped down to dryness giving **27Br12** 87% yield (404 mg, 242 mmol). *Note: if the white solid begins to form a brown residue upon vacuum the ortho-dichlorobenzene was not removed completely.* ^{1}H NMR (600 MHz, ODCB-d$_4$, 25°C): δ = 7.49 & 7.48 (2H, s), 2.89 & 2.89 (6H, s), 1.30-1.10 (15H, m), 4.45-3.20 (10H, bs, B-H), ppm. ^{1}H[^{11}B]-NMR spectrum (600 MHz, ODCB-d$_4$, 25°C): δ = 7.47 & 7.47 (2H, s), 3.78 (10H, s, B-H), 2.87 & 2.87 (6H, s), 1.30-1.10 (15H, m) ppm. ^{11}B[^{1}H] NMR (192 MHz, ODCB-d$_4$, 25 °C): δ = 1.0, -8.1, -15.9 ppm. ^{11}B NMR (192 MHz, ODCB-d$_4$, 25 °C): δ = -1.0, -8.1, -15.9 ppm. ^{13}C[^{1}H] NMR (151 MHz, ODCB-d$_4$, 25 °C): δ = 178.0, 124.5, 73.0, 25.6, 7.2, 7.0, 6.9, 6.1 ppm.

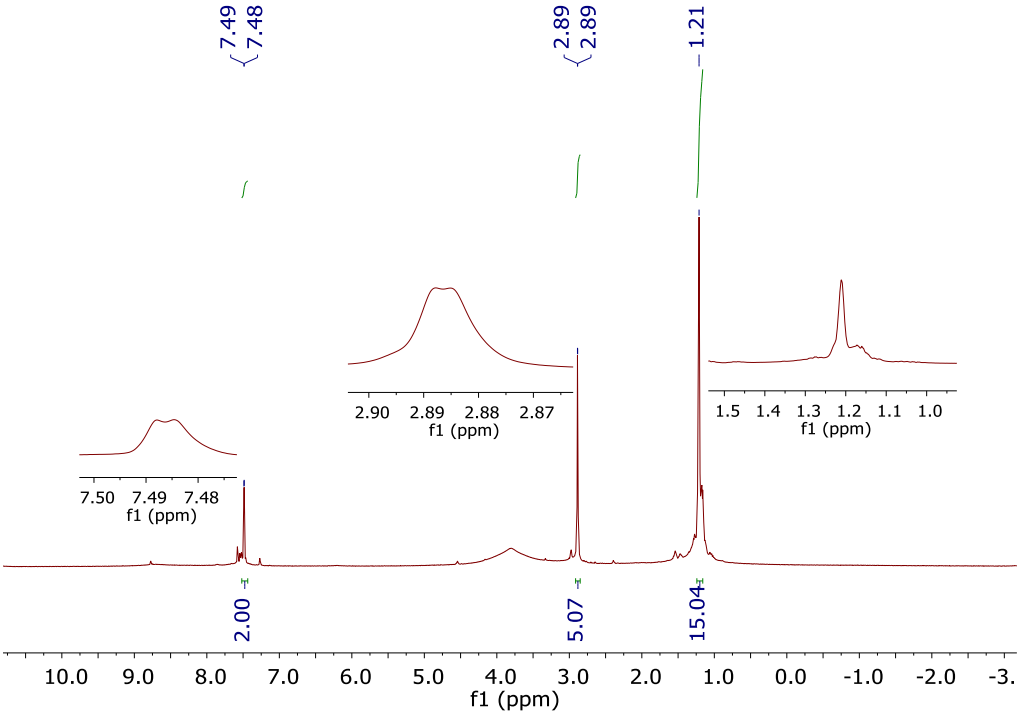

Fig. **2.46** ^{1}H-NMR spectrum of **27Br$_{12}$** in ortho-dichlorobenzene-d$_4$. The inserts show an expansion of each peak. *Note: The broad peak at 3.7 ppm is caused by the B-H protons.*

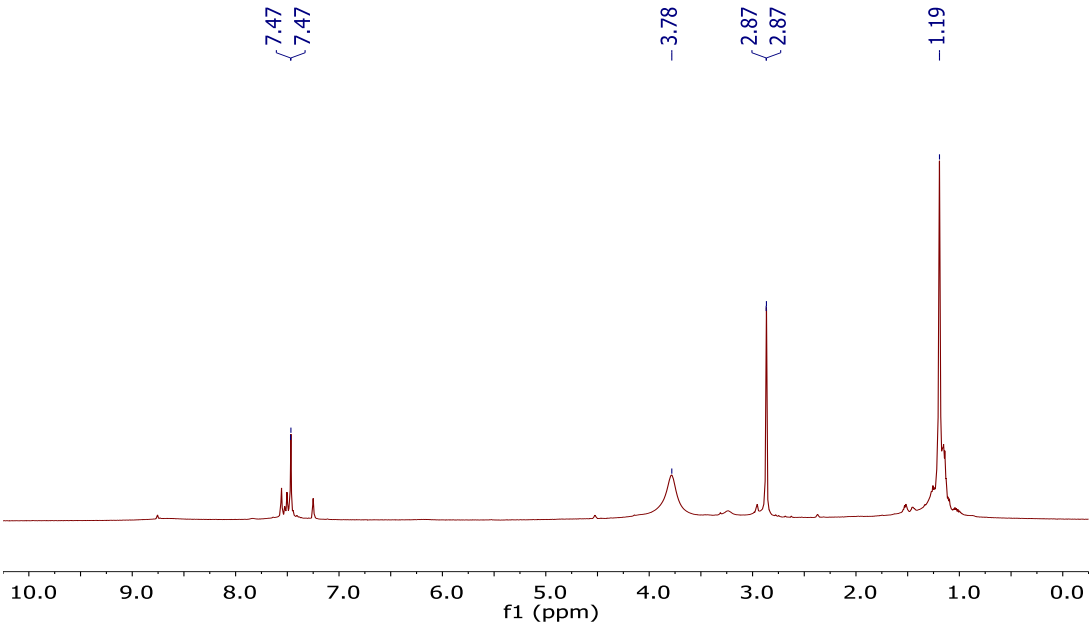

Fig. **2.47** ^{1}H[^{11}B]-NMR spectrum of **27Br$_{12}$** in ortho-dichlorobenzene-d$_4$. *Note: The B-H protons appear at 3.78 ppm.*

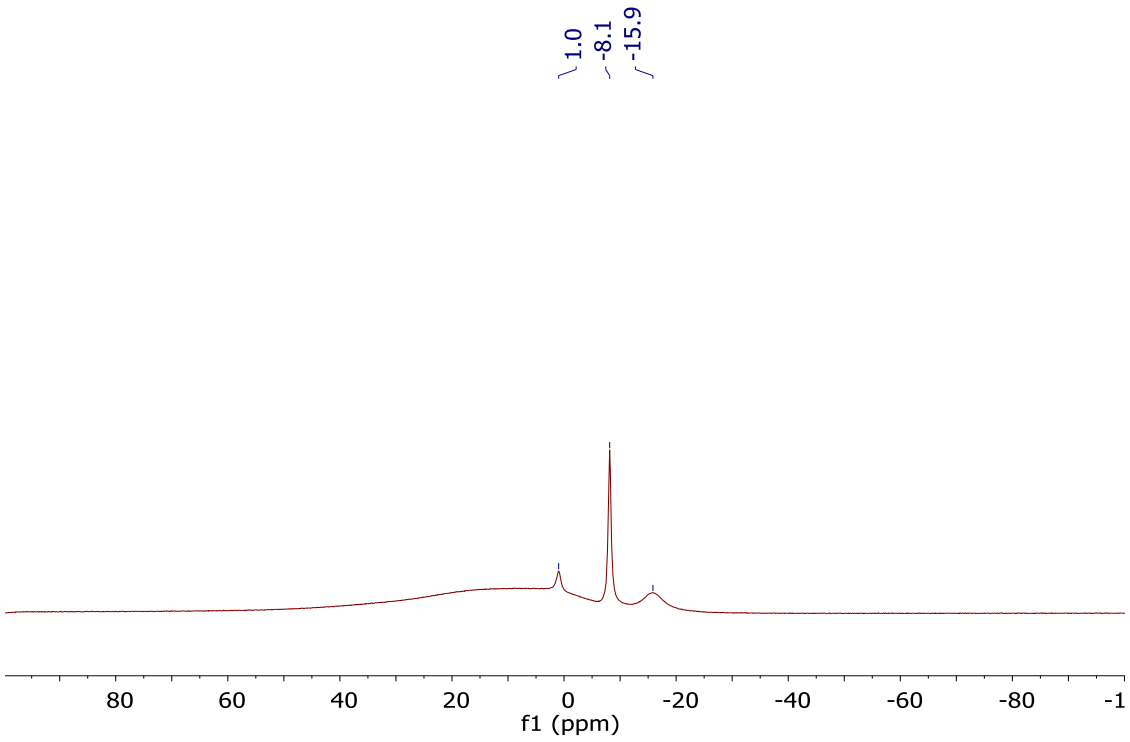

Fig. **2.48** $^{11}B[^{1}H]$-NMR spectrum of **27Br$_{12}$** in ortho-dichlorobenzene-d$_4$.

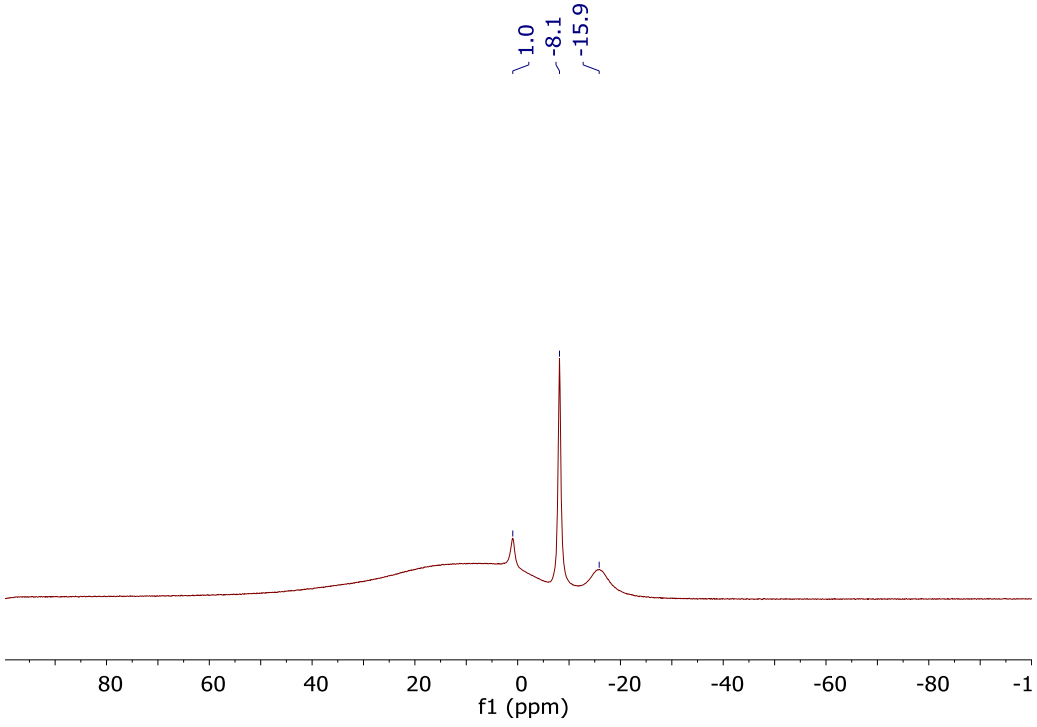

Fig. **2.49** ^{11}B-NMR spectrum of **27Br$_{12}$** in ortho-dichlorobenzene-d$_4$.

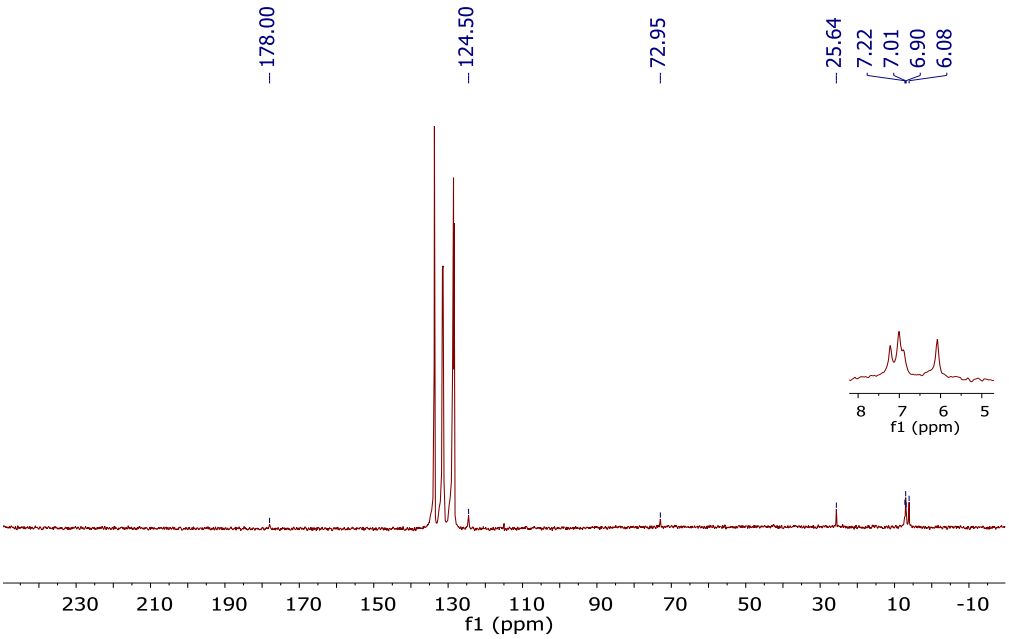

Fig. **2.50** $^{13}C[^{1}H]$-NMR spectrum of **27Br$_{12}$** in ortho-dichlorobenzene-d$_4$. The insert shows an expansion of the four upfield peaks.

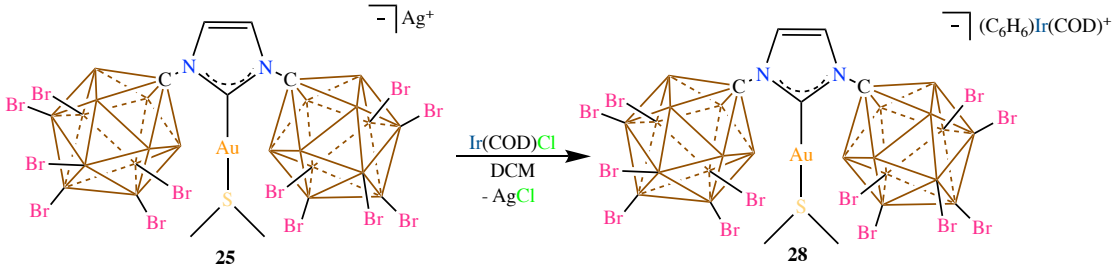

Scheme **2.18** Synthesis of the ion-pair **28**

A glass scintillation vial equipped with a stir bar was loaded with **25Br$_{12}$** (300 mg, 0.18 mmol) and suspended in DCM (10 mL). A solution of (ClIrCOD)$_2$ (COD=1,5-cyclooctadiene) (60.45 mg, 0.09 mmol) in DCM (5 mL) was added to the suspension containing **25Br$_{12}$**. A drop of benzene was added to the reaction mixture and stirred for 1 hour at room temperature. Subsequently the suspension was filtered, and the supernatant containing **28** pumped down to dryness. The solid residue, which is a mixture of AgCl and **28**, was washed with DCM and the DCM saved. The solid was washed repeatedly, and the DCM saved, until ^{11}B NMR analysis of the precipitate showed no more carborane

resonances. The DCM wash was combined with the initial dried supernatant and pumped to dryness to afford **28Br$_{12}$** in 90% yield. ^{1}H NMR (600 MHz, methylene chloride-d$_2$, 25°C): δ = 7.37 (2H, s), 6.72 (6H, s), 4.76 (4H, m), 2.93 (6H, s), 2.27 (2H, m), 2.15 (2H, m), 3.2 – 1.9 (bs, 10H, B-H) ppm. ^{1}H[^{11}B]-NMR spectrum (600 MHz, methylene chloride-d$_2$, 25°C): δ = 7.37 (2H, s), 6.72 (6H, s), 4.75 (4H, m), 3.30 (10H, bs), 2.93 (6H, s), 2.27 (2H, m), 2.15(2H, m) ppm. ^{11}B[^{1}H] NMR (192 MHz, methylene chloride-d$_2$, 25 °C): δ = -1.3, -10.3, -17.8 ppm. ^{11}B NMR (192 MHz, methylene chloride-d$_2$, 25 °C): δ = -1.3, -10.3, -17.8 ppm. ^{13}C[^{1}H] NMR (151 MHz, methylene chloride-d$_2$, 25 °C): δ = 123.7, 98.4, 64.5, 32.9, 25.0 ppm. HRMS (positive mode ESI/APCI) [M*$^{+}$] m/z Calc: $C_7H_{18}N_2Br_{12}B_{22}AuS$ = 1556.3126 : Found = 1556.3063, [M^{-}] m/z Calc: 379.1038 : Found = 379.1027. IR (Solid, ATR, 25°C) = 2594.6cm^{-1} (B-H). Melting Point: 271 °C.

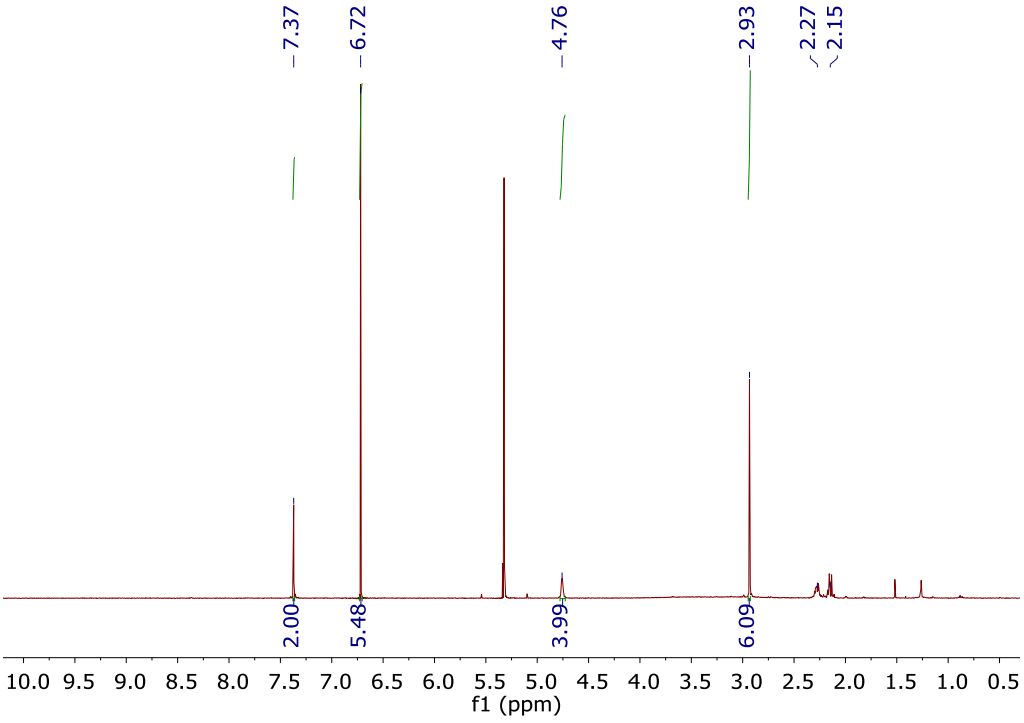

Fig. **2.51** ^{1}H NMR spectrum of **28** in methylene chloride-d$_2$.

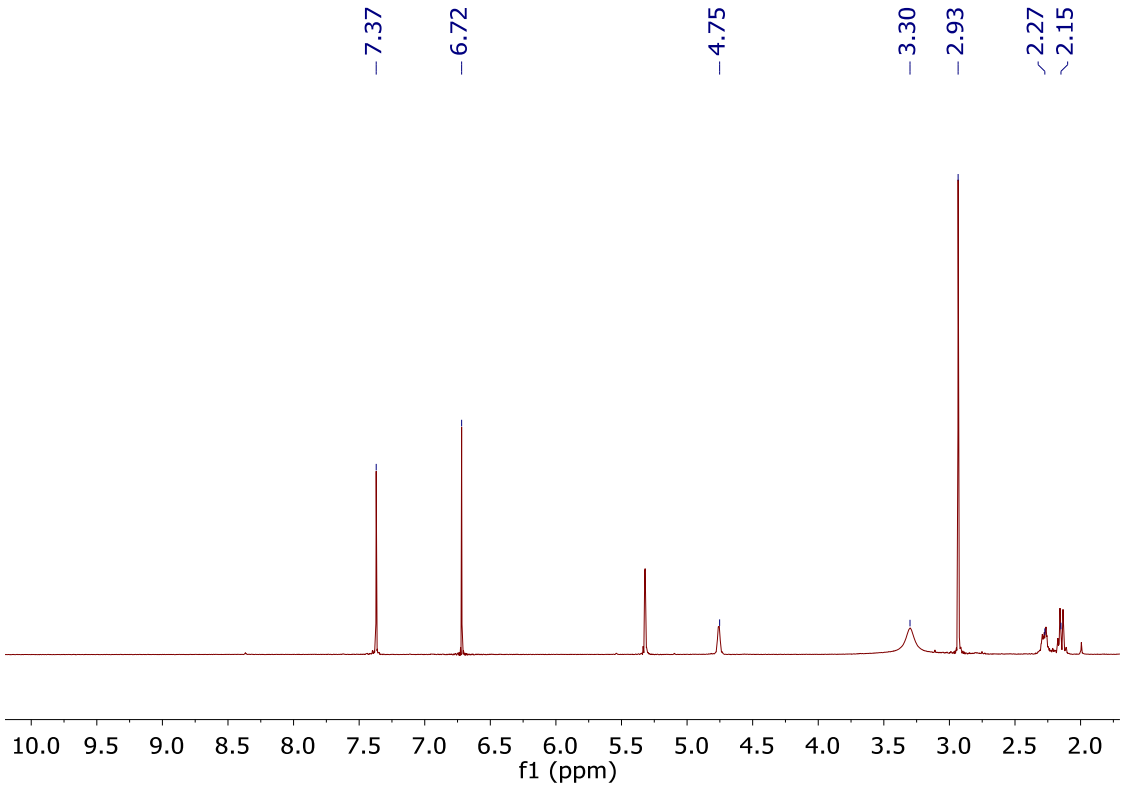

Fig. **2.52** $^{1}H[^{11}B]$ NMR spectrum of **28** in methylene chloride-d_2.

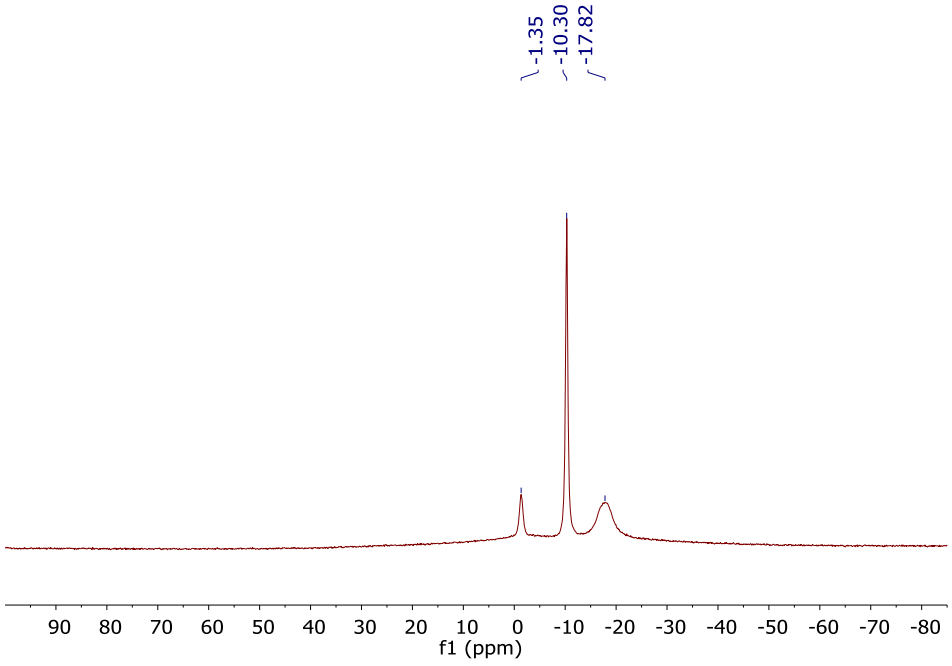

Fig. **2.53** ^{11}B NMR spectrum of **28** in methylene chloride-d_2.

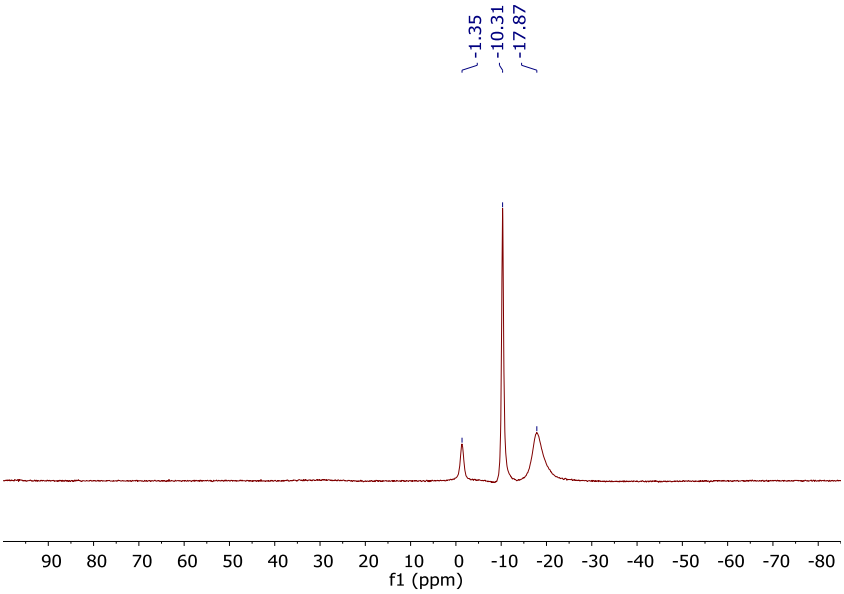

Fig. **2.54** $^{11}B[^{1}H]$ NMR spectrum of **28** in methylene chloride-d_2.

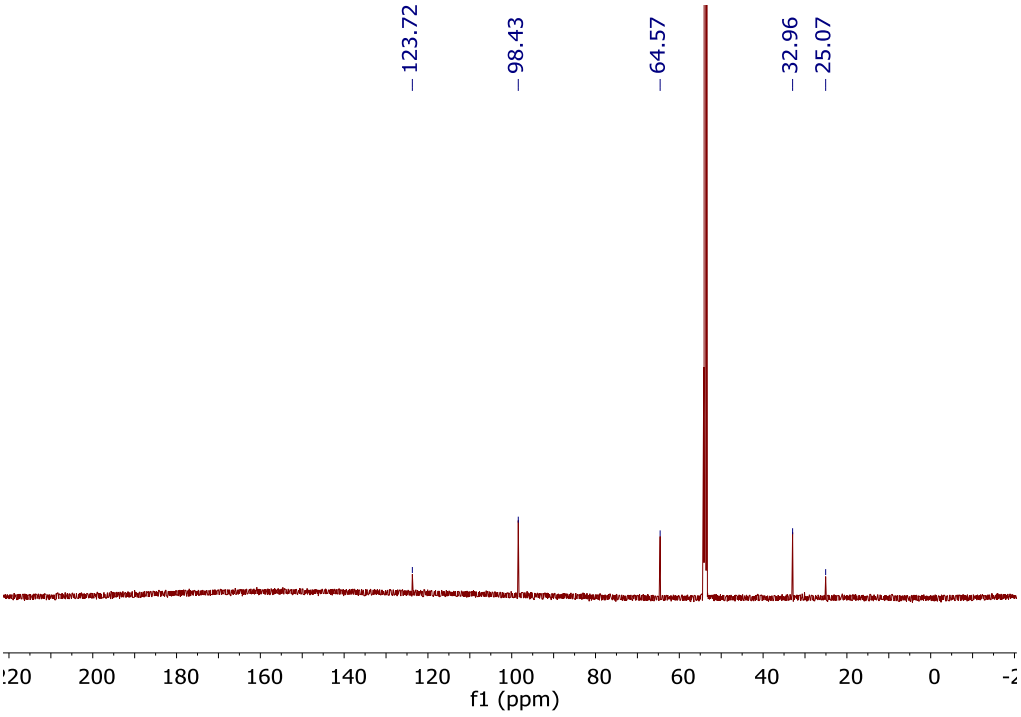

Fig. **2.55** $^{13}C[^{1}H]$ NMR spectrum of **28** in methylene chloride-d_2.

Note: The carbene carbon and the carborane carbon peaks do not show up even after running 20000 scans on a 700MHz spectrometer.

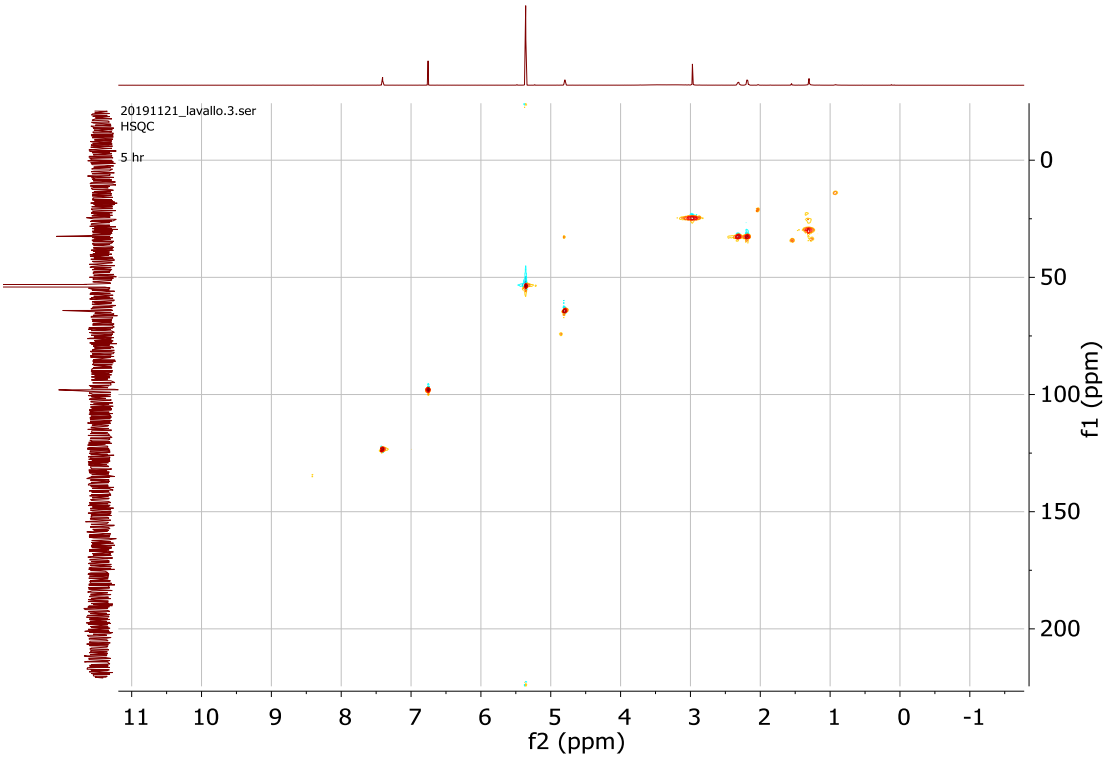

Fig. **2.56** HSQC NMR spectrum of **28** in methylene chloride-d_2.

General Procedure for Catalysis: A standard solution of the appropriate catalyst was prepared in methylene chloride. The desired amount of catalyst was transferred via a micropipette to a PTFE screw cap vial loaded with a stir bar. The methylene chloride solvent was evaporated from the open vial at 50°C. Using a micropipette, the designated alkyne substrate was added followed by the amine substrate and the vial sealed and heated at the indicated temperature for the allotted time. Yields were calculated by direct comparison of the integrals of the imine product to either the amine or imine starting material (uses an unobstructed resonance). The validity of this approach was confirmed by obtaining isolated yields of several products. Isolated yields were obtained by short path distillation (*N*-(2,6-diisopropylphenyl)-1-(4-fluorophenyl)ethan-1-imine), sublimation (*N*-(2,6-diisopropylphenyl)-1-(4-methoxyphenyl)ethan-1-imine) or filtration from pentane

followed by crystallization (1-(4-fluorophenyl)-*N*-mesitylethan-1-imine and *N*-mesityl-1-phenylethan-1-imine). All products spectroscopically matched those reported by Lavallo and coworkers.[13]

X-Ray Structure Determination:

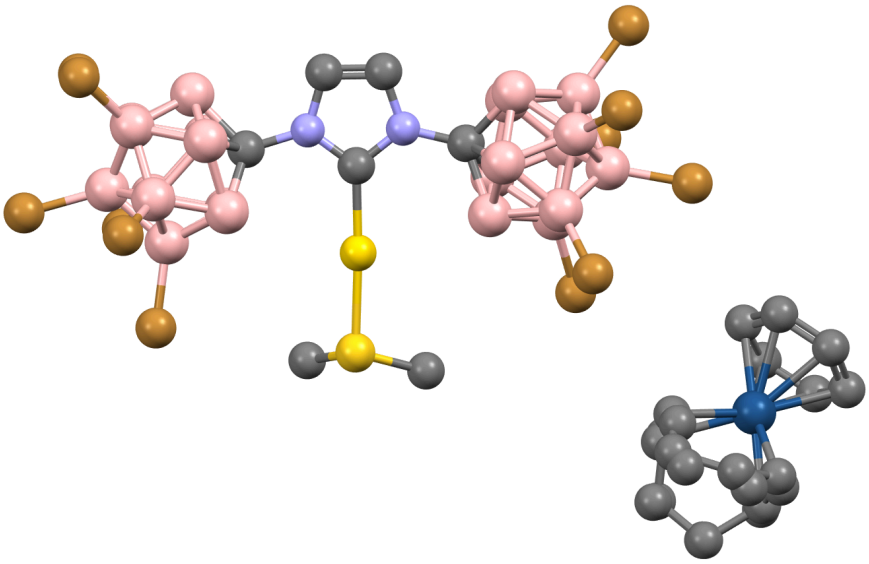

Fig. **2.3** Solid-State Structure of **28.** Hydrogen atoms omitted for clarity. N=Blue, B=pink, Au=gold, S=yellow, Br=brown, Ir= ocean blue

Diffraction data were collected on a Bruker-AXS Apex II diffractometer with an Apex II CCD detector using Mo K_α radiation ($\lambda = 0.71073$ Å) from a fine-focus sealed tube source. Data were collected at 100 K by performing 0.5° ω-scans, integrated using SAINT[1], and absorption corrected using SADABS[2]. The structure was solved by direct methods using SHELXT[3] and refined against F^2 on all data by full-matrix least squares with SHELXL-2018/3[4] following established refinement strategies[5]. All non-hydrogen atoms were refined anisotropically. All hydrogen atoms were included into the model at geometrically calculated positions and refined using a riding model. The isotropic displacement parameters of all hydrogen atoms were fixed to 1.2 times the *U* value of the atoms they are linked to. Crystal and data quality details, as well as a summary of the residual refinement values, are listed in the accompanying table.

Compound **vl338vl** crystallizes in the triclinic centrosymmetric space group *P-1* with one molecule of **vl338vl** and one molecule of dichloromethane per asymmetric unit.

The cyclooctadiene ligand on the cationic iridium moiety and the dichloromethane solvent molecule each exhibit disorder that was modeled over two positions; the disorder ratios were refined freely and converged at 68:32 and 53:47, respectively. These disorders were refined with the help of similarity restraints on 1,2- and 1,3- distances as well as similarity and rigid-bond restraints on anisotropic displacement parameters. The anisotropic displacement parameters of two sets of nearly-overlapping positions of disordered cyclooctadiene carbon atoms were constrained to be equivalent.

Table 2.2 Crystal data and structure refinement for **$10Br_{12}[Ir^{+}]$**

Identification code Empirical formula Formula weight Temperature Wavelength Crystal system Space group

Unit cell dimensions

vl358vl

C22 H38 Au B22 Br12 Cl2 Ir N2 S 2019.41

100(2) K

0.71073 Å

Triclinic

P-1

a = 9.7936(2) Å

b = 16.2715(4) Å

c = 17.0758(4) Å

2675.58(11) $Å^3$

2.507 Mg/m^3

14.348 mm^{-1}

1840

colourless

0.205 x 0.090 x 0.047 mm^3 1.876 to 29.130°

-13 <= *h* <= 13, -22 <= *k* <= 22, -23 <= *l* <=

63194

14381 [R(int) = 0.0445]

100.0 %

Semi-empirical from equivalents Full-matrix least-squares on F^2 14381 / 423 / 659

1.017

R1 = 0.0239, wR2 = 0.0494

R1 = 0.0323, wR2 = 0.0519 1.560 and -1.023 $e.Å^{-3}$

Volume Z2

Density (calculated) Absorption coefficient F(000)

Crystal color

Crystal size

Theta range for data collection

Index ranges

23

Reflections collected

Independent reflections

Completeness to theta = 25.242° Absorption correction

Refinement method

Data / restraints / parameters Goodness-of-fit on F^2

Final R indices [I>2sigma(I) = 12347 data] R indices (all data, 0.73 Å)

Largest diff. peak and hole

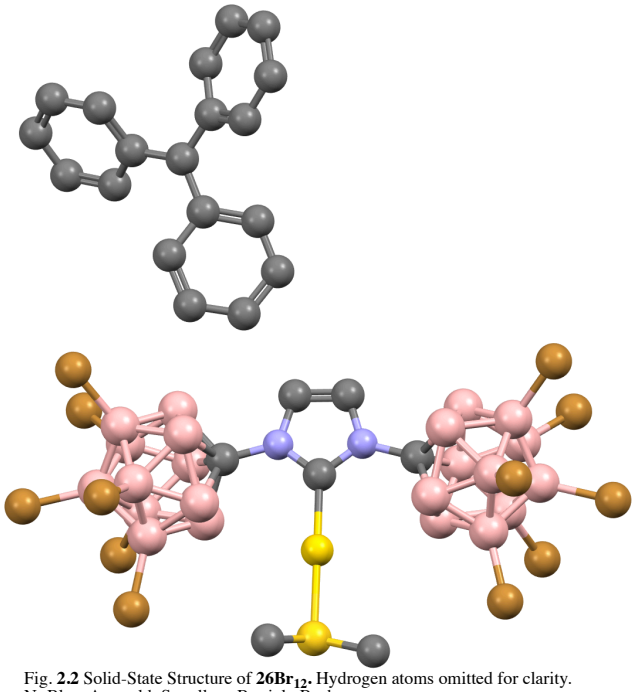

Fig. **2.2** Solid-State Structure of **26Br$_{12}$.** Hydrogen atoms omitted for clarity. N=Blue, Au=gold, S=yellow, B=pink, Br=brown

Diffraction data were collected on a Bruker-AXS Apex II diffractometer with an Apex II CCD detector using Mo K_α radiation (λ = 0.71073 Å) from a fine-focus sealed tube source. Data were collected at 100 K by performing 0.5° ω-scans, integrated using SAINT[1], and absorption corrected using SADABS[2]. The structure was solved by direct methods using SHELXT[3] and refined against F^2 on all data by full-matrix least squares with SHELXL-

2018/3[4] following established refinement strategies[5]. All non-hydrogen atoms were refined anisotropically. All hydrogen atoms were included into the model at geometrically calculated positions and refined using a riding model. The isotropic displacement parameters of all hydrogen atoms were fixed to 1.2 times the *U* value of the atoms they are linked to. Crystal and data quality details, as well as a summary of the residual refinement values, are listed in the accompanying table.

Compound **vl352sf** crystallizes in the triclinic centrosymmetric space group *P-1* with one molecule of **vl352sf**, one full molecule and two half-molecules of cationic $Li(THF)_4$, and two half-molecules of tetrahydrofuran (THF) per asymmetric unit.

One carborane cage and one $Li(THF)_4$ moiety each exhibited disorder that was modeled over two positions; the disorder ratios were refined freely and converged at 76:24 and 64:36, respectively. These disorders were refined with the help of similarity restraints on 1,2- and 1,3- distances as well as rigid-bond restraints on anisotropic displacement parameters.

A pocket of two $Li(THF)_4$ moieties and two THF solvent molecules resides on an inversion center whose symmetry is not fulfilled by the arrangement of molecules; these molecules were refined with the help of rigid-bond restraints on anisotropic displacement parameters.

All THF molecules were restrained to have similar geometries with the help of 1,2- and 1,3- distance restraints. The geometries of each $Li(THF)_4$ moiety were also restrained to be similar to each other by restraining equivalent 1,2- and 1,3- distances to refined free variables. Isotropic approximation restraints were applied to the anisotropic displacement parameters of seven poorly-behaved atoms within THF molecules.

References

[1] SAINT, version 8.34A, Bruker (2012), Bruker AXS Inc., Madison, Wisconsin, USA.

[2] SADABS, version 2012/1, Bruker (2012), Bruker AXS Inc., Madison, Wisconsin, USA.

[3] Sheldrick, G. M., *Acta Cryst.* **2015**, *A71*, 3-8.

[4] Sheldrick, G. M., *Acta Cryst.* **2015**, *C71*, 3-8.

[5] Müller, P. *Crystallography Reviews* **2009**, *15*, 57-83.

Table 2.3 Crystal data and structure refinement for **26Br$_{12}$**

Identification code	vl352sf_r
Empirical formula	C41 H84 B22 Br12 Li2 N2 O9
Formula weight	1959.72
Temperature	100(2) K
Wavelength	0.71073 Å
Crystal system	Triclinic
Space group	P-1
Unit cell dimensions	a = 9.7131(2) Å α = 76.8876(10)°.
	b = 18.7553(4) Å β = 86.5377(12)°.
	c = 21.2697(5) Å γ = 78.5050(11)°.
Volume	3697.56(14) Å3
Z	2
Density (calculated)	1.760 Mg/m3

Absorption coefficient 6.545 mm-1

F(000) 1904

Crystal color colourless

Crystal size 0.325 x 0.213 x 0.177 mm3

Theta range for data collection 1.136 to 28.700°

Index ranges -13 <= *h* <= 13, -25 <= *k* <= 25, -28 <= *l* <= 28

Reflections collected 127980

Independent reflections 19106 [R(int) = 0.0483]

Completeness to theta = 25.242° 99.9 %

Absorption correction Semi-empirical from equivalents

Refinement method Full-matrix least-squares on F2

Data / restraints / parameters 19106 / 3380 / 1383

Goodness-of-fit on F2 1.349

Final R indices [I>2sigma(I) = 16176 data] R1 = 0.0686, wR2 = 0.1514

R indices (all data, 0.74 Å) R1 = 0.0814, wR2 = 0.1551

Largest diff. peak and hole 0.898 and -1.011 e.Å-3

2.7 References

1. Reed, C. A., H+, CH3+, and R3Si+ Carborane Reagents: When Triflates Fail. *Accounts of Chemical Research* **2010,** *43* (1), 121-128.

2. Hoffmann, S. P.; Kato, T.; Tham, F. S.; Reed, C. A., Novel weak coordination to silylium ions: formation of nearly linear Si–H–Si bonds. *Chemical Communications* **2006,** (7), 767-769.

3. Xie, Z.; Bau, R.; Benesi, A.; Reed, C. A., The Silylium Ion (R3Si+) Problem: Effect of Alkyl Substituents R. *Organometallics* **1995,** *14* (8), 3933-3941.

4. Kato, T.; Stoyanov, E.; Geier, J.; Grützmacher, H.; Reed, C. A., Alkylating Agents Stronger than Alkyl Triflates. *Journal of the American Chemical Society* **2004,** *126* (39), 12451-12457.

5. Rohde, V. H. G.; Pommerening, P.; Klare, H. F. T.; Oestreich, M., Intramolecularly Sulfur-Stabilized Silicon Cations as Lewis Acid Catalysts. *Organometallics* **2014,** *33* (13), 3618-3628.

6. Prakash, G. K. S.; Bae, C.; Wang, Q.; Rasul, G.; Olah, G. A., Tris(trimethylsilyl)sulfonium and Methylbis(trimethylsilyl)sulfonium Ions: Preparation, NMR Spectroscopy, and Theoretical Studies1. *The Journal of Organic Chemistry* **2000,** *65* (22), 7646-7649.

7. Muetterties, E. L.; Bleeke, J. R.; Sievert, A. C., Arene transition metal chemistry: III. Arene exchange phenomena. *Journal of Organometallic Chemistry* **1979,** *178* (1), 197-216.

8. Sievert, A. C.; Muetterties, E. L., Arene transition-metal chemistry. 5. Arene ligand exchange and reactivity in .eta.6-arene iridium(I) complexes. *Inorganic Chemistry* **1981,** *20* (2), 489-501.

9. Widenhoefer, R. A.; Han, X., Gold-Catalyzed Hydroamination of C–C Multiple Bonds. *European Journal of Organic Chemistry* **2006,** *2006* (20), 4555-4563.

10. Mizushima, E.; Hayashi, T.; Tanaka, M., Au(I)-Catalyzed Highly Efficient Intermolecular Hydroamination of Alkynes. *Organic Letters* **2003,** *5* (18), 3349-3352.

11. Duan, H.; Yan, W.; Sengupta, S.; Shi, X., Highly efficient synthesis of vinyl substituted triazoles by Au(I) catalyzed alkyne activation. *Bioorganic & Medicinal Chemistry Letters* **2009,** *19* (14), 3899-3902.

12. Gorin, D. J.; Sherry, B. D.; Toste, F. D., Ligand Effects in Homogeneous Au Catalysis. *Chemical Reviews* **2008,** *108* (8), 3351-3378.

13. Lavallo, V.; Wright Ii, J. H.; Tham, F. S.; Quinlivan, S., Perhalogenated Carba-closo-dodecaborate Anions as Ligand Substituents: Applications in Gold Catalysis. *Angewandte Chemie International Edition* **2013,** *52* (11), 3172-3176.

14. El-Hellani, A.; Lavallo, V., Fusing N-Heterocyclic Carbenes with Carborane Anions. *Angewandte Chemie International Edition* **2014,** *53* (17), 4489-4493.

Chapter 3: Electrostatically Tethered Ion-Pairs in Tandem Catalysis

3.1 Introduction

In the previous chapter, we established that the NHC-Au(I) complex **24** can act as a weakly coordinating anion thus allowing to pair up reactive cations exemplified by compound **28**. Ideally, it's possible to pair up different transition metal and main group cations across the periodic table with this anion. Further, since the anion is a powerful catalyst, incorporation of a catalytically active cation could result in electrostatically tethered ion-pairs that can potentially perform tandem catalysis. The term tandem catalysis has been used in the literature to define a sequence of synthetic catalytic reactions that require minimal work up and isolation of the intermediate products.[1-3] This is advantageous in that the different reaction components can be added together in a single vessel to react and isolate the final product. Not having to isolate the intermediate products is beneficial in cutting down the usage of carcinogenic solvents and reagents for chromatographic purification.

However, the major challenges involve the compatibility of the two catalysts and the reaction conditions. For instance, the product of a first catalytic reaction could potentially react with the other catalyst leading to catalyst poisoning. In some cases, the reaction conditions of a first catalytic cycle could lead to the decomposition of the other catalyst. Other problems include the incompatibility of the reaction solvent with certain classes of substrates or one of the catalysts being too reactive thus generating too many undesired products that might be hard to separate.

However, in ion-pairs like **28**, since both the ions are strongly bound together by electrostatic attraction forces, they are always in close proximity to each other. We

envisioned using such ion-pairs in tandem catalysis would enhance the reaction rates since the product of the reaction catalyzed by the anion is in the vicinity of the cation or vice-versa. The tight ion-pairing should be more pronounced in weakly coordinating solvents like $CDCl_3$ or CD_2Cl_2 much more than coordinating solvents like THF or acetonitrile. This kinetically coupled tandem catalysis is expected to be significantly faster than performing both the catalytic reactions in different pots. Before we screen different ion-pairs for tandem catalysis, we wanted to investigate the versatility of this ion-pairing technique and develop a pool of cations with transition metals and main group compounds that can be paired with the anion **24**.

3.2 Organometallic Ion-Pairs

Initially, we targeted simple transition metal complexes with halides that can be abstracted using the silver salt **25** or the Li^+ salt **24** to generate the corresponding coordinatively saturated 16 or 18 electron cations. Treating **25** with half equivalent of $[Pd(allyl)Cl]_2$ in acetonitrile produced the Pd(allyl) cation with two coordinated acetonitrile molecules at the Pd (II) center (Scheme **3.1**).[4]

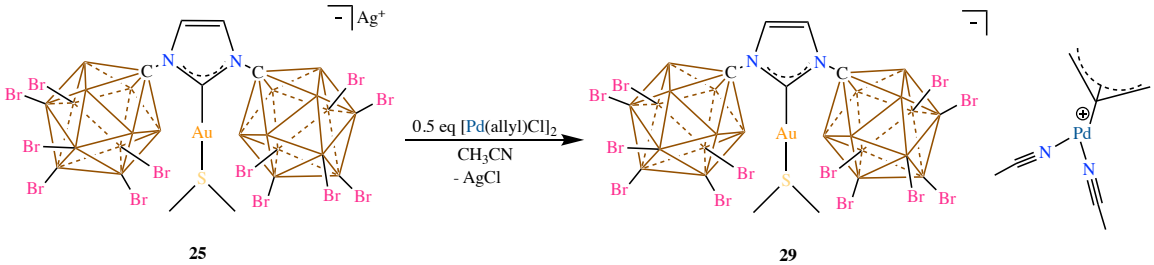

25 **29**

Scheme **3.1** Synthesis of the Pd(allyl) ion-pair **29** from **25**

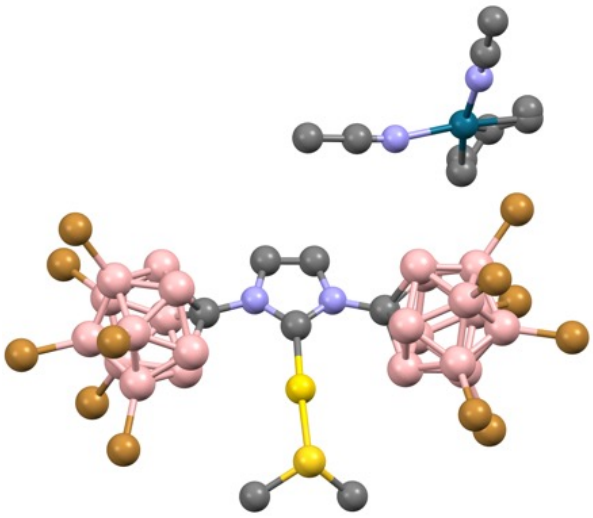

Fig. **3.1** X-Ray Structure of the ion-pair **29**. Hydrogen atoms omitted for clarity. N=Blue, C=grey, B=pink, Br=brown, Au=gold, S=yellow, Pd=ocean blue

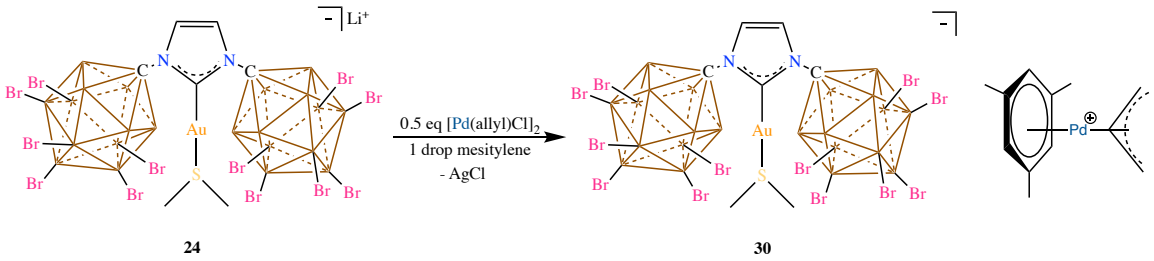

Scheme **3.2** Synthesis of the Pd(allyl) ion-pair **30** from **24**

Similarly, when **25** or **24** was treated with $[Pd(allyl)Cl]_2$ in DCM with a drop of η^6 coordinating arene like mesitylene at -78°C, the mesitylene coordinated 18 electron Pd(allyl) cation was produced (Scheme **3.2**).[5] The formation of the ion-pairs **29** and **30** was confirmed by multinuclear NMR spectroscopy, mass spectrometry, and with X-Ray crystal structure in case of **29**.

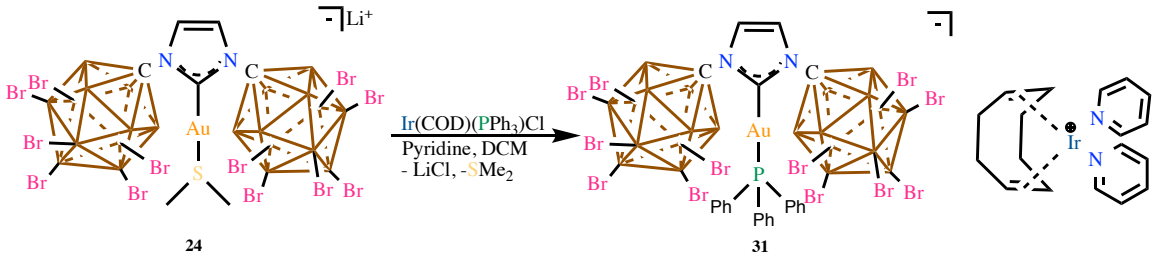

Scheme **3.3** Synthesis of PPh_3 bound Au complex **31** from **24**

Moving to the next group on the periodic table, we started synthesizing ion-pairs with Ir other than the previously reported **28**. Initially, we targeted pairing the Crabtree's Ir hydrogenation catalyst $[(COD)Ir(PPh_3)(pyridine)]^+$ with the Au(I) complex **24**.[6] To make the ion-pair, $[Ir(COD)Cl]_2$ was first treated with triphenyl phosphine in dichloromethane to make $[Ir(COD)(PPh_3)_2]$ using the literature protocol. In the next step, this compound was reacted with the **24Br12** in the presence of excess pyridine attempting to make the desired ion-pair. However, the ^1H NMR of the crude reaction mixture showed the absence of the dimethyl sulfide protons of the Au complex. Further, the integrations compared to the NHC backbone revealed the presence of two pyridine molecules for one molecule of the anion. This was presumably due to the displacement of SMe_2 by the stronger PPh_3 ligand producing the unexpected ion-pair **31**. The structure of **31** was further determined by single crystal X-Ray diffraction. The reaction was not attempted with stoichiometric amount of pyridine since we predicted that would still lead to the transmetalation of SMe_2 by the triphenyl phosphine.

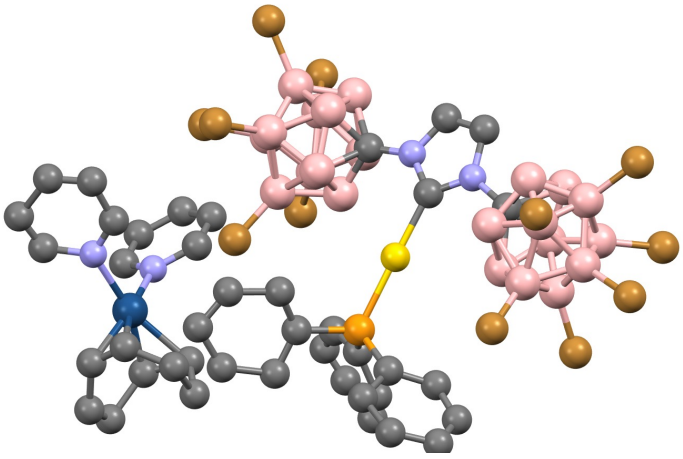

Fig. **3.2** X-Ray Structure of ion-pair **31**. Hydrogen atoms omitted for clarity. N=Blue, C=grey, Au=gold, P=orange, Ir=ocean blue, B=pink, Br=brown

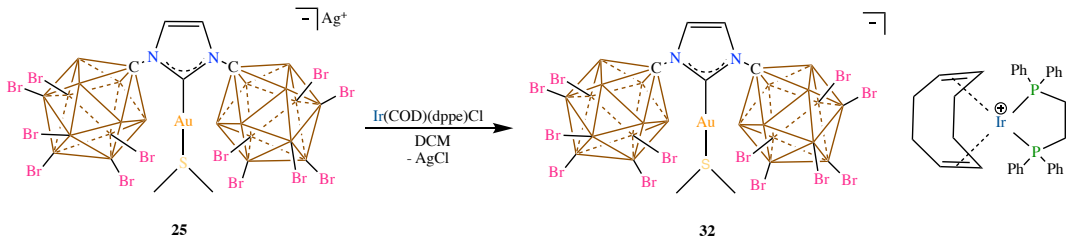

25 32

Scheme **3.5** Synthesis of the ion-pair **32** from **25**

While the monodentate phosphines could cause the transmetalation, the bidentate phosphine ligands would likely be compatible with **24** since they are chelated at the metal center and have less tendency to displace labile ligands like SMe_2. To test our hypothesis, we treated [Ir(COD)(dppe)]Cl (dppe= 1,2 diphenyl phosphinoethane) with **25** in DCM (Scheme **3.4**). As expected, the reaction yielded the clean ion-pair **32**[7] as a dark green oil showing the compatibility of chelated bis(phosphines) with **24** as confirmed by multinuclear NMR spectroscopy and High Resolution Mass Spectrometry.

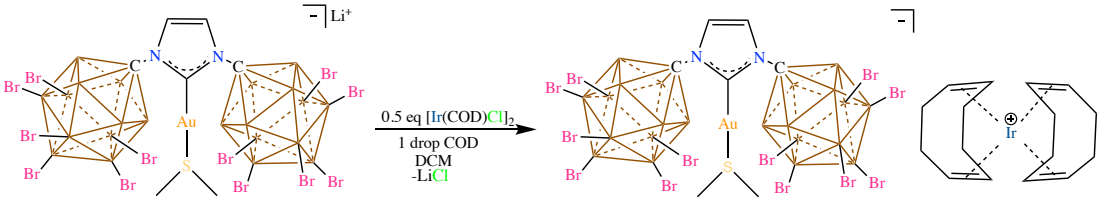

24 33

Scheme **3.4** Synthesis of the ion-pair **33** from **24**

Since the crabtree's cation was not compatible with the anion **24**, we targeted other cationic olefin hydrogenation catalysts in the literature. Subsequently, we treated the anion **24** with $[Ir(COD)Cl]_2$ in the presence of a drop of the free COD ligand. The reaction followed by work up produced the ion-pair **33** (Scheme **3.5**).[8] A similar protocol was adapted for the

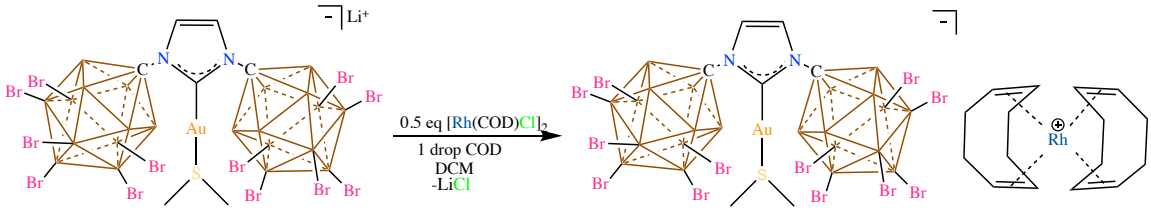

Scheme **3.6** Synthesis of the ion-pair **34** from **24**

Rh version of the same cation **34**. The identity of these ion -pairs was confirmed using NMR and mass spectrometry (Scheme **3.6**).

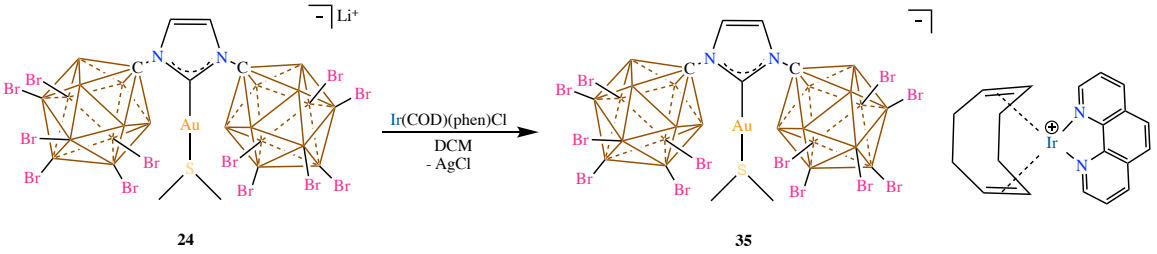

Scheme **3.7** Synthesis of the ion-pair **35** from **24**

Further expanding the scope of Ir(I) cations, we made the [(COD)Ir(phen)] (phen: 1,10 phenanthroline) cation paired Au(I) by treating a fluorobenzene solution of [(COD)Ir(phen)Cl] with **24**, as seen by NMR and mass spectrometry (Scheme **3.7**).[9]

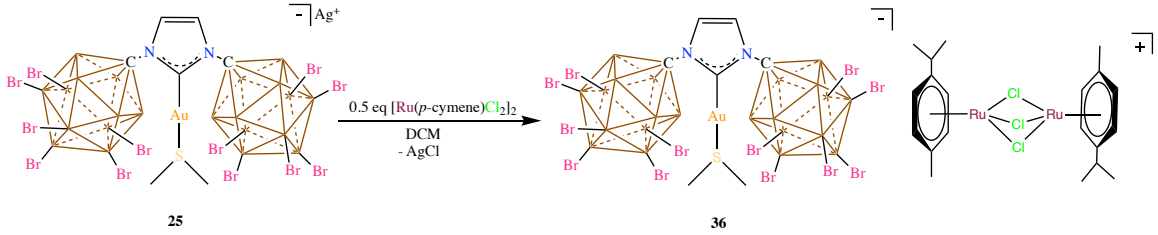

Scheme **3.8** Synthesis of the ion-pair **36** from **25**

Moving to the next group, we reacted **25** with Ru(p-cymene)Cl_2 dimer. Instead of the expected [(p-cymene)RuCl] cation, the reaction yielded a trichlorobridged diruthenium cation paired with **24** (Scheme **3.8**) as confirmed by X-Ray diffraction of the crystals grown by layering a chloroform solution of the compound with hexanes. The product was further confirmed by ^{1}H NMR spectroscopy. This indicates the tendency of organometallic complexes bearing two halogens to dimerize unlike those having one halogen.

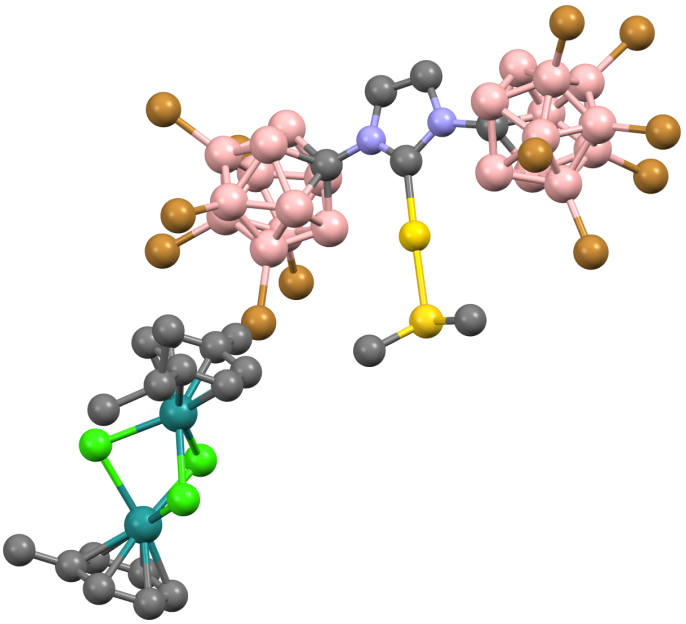

Fig. **3.3** X-Ray Structure of ion-pair **36**. Hydrogen atoms omitted for clarity. N=Blue, C=grey, Au=gold, S=yellow, B=pink, Br=brown, Ru=teal, Cl=green

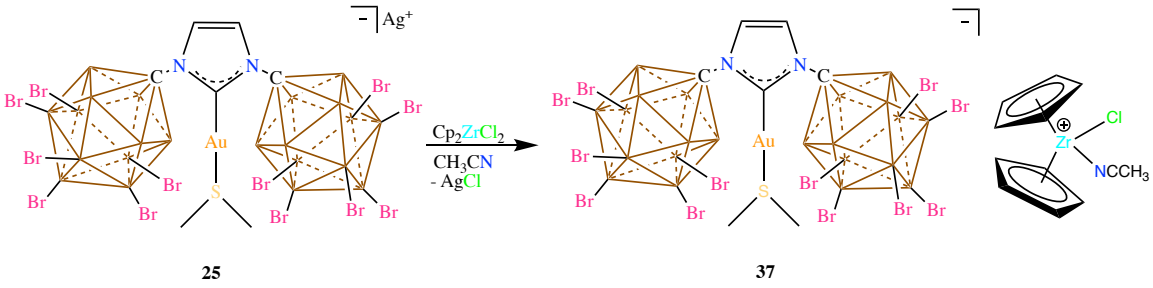

25 **37**

Scheme **3.9** Synthesis of the ion-pair **37** from **25**

We then wanted to check the compatibility of the anion **24** with early transition metal cations. Treating an acetonitrile solution of **25** with Cp_2ZrCl_2 produced the ion-pair with the $[Cp_2ZrCl(NCCH_3)]$ cation by precipitating AgCl, as confirmed by ^1H NMR and X-Ray crystallography. Interestingly, despite having two chlorines, stoichiometric reaction with **25** did not yield any dimeric halogen bridged cations here as seen in the ion-pair **36**.

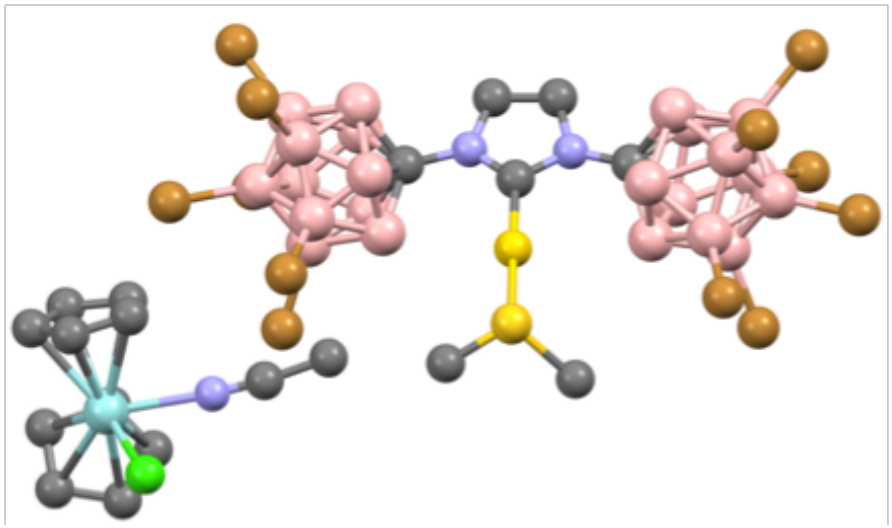

Fig. **3.4.** Solid-State structure of ion-pair **37**. Hydrogen atoms omitted for clarity. N=Blue, Au=gold, S=yellow, B=pink, B=brown, Cl=green, Zr=torquoise

After synthesizing the above ion-pairs, we sought to investigate the tandem reactions they could catalyze. Initially, we investigated different reactions our complex **24** could catalyze. Eventually, these catalytic reactions would be coupled with another reaction catalyzed by the counter cation to perform tandem catalysis. Since, Au(I) behaves as a π acid and activates alkynes,[10] we investigated reactions that use activation of alkynes to functionalize different organic molecules. Some of those reactions are outlined here.

*3.3 Organic Transformations Catalyzed by NHC Au(I) Complex **24***

a. *C-2 Functionalization of Indoles*:

Synthetic methods to access indole derivatives have been an area of interest in organic chemistry owing to their importance in medicinal and pharmaceutical industry.[11] Several transition metal complexes were found to catalyze the functionalization of indole selectively at different positions on the ring.[12-13] Based on the literature precedence of Au(I) complexes functionalizing indoles with alkynes,[14] we were curious if complex **24** could perform similar catalysis. When C-1 substituted indoles were treated with alkynes in the

presence of **24**, C-2 olefin functionalized indoles were produced as shown in Scheme **3.10**. The Au(I) center activates the alkyne generating the carbocation onto which the ring undergoes an electrophilic aromatic substitution like reaction. Subsequent protonation of the olefin carbon regenerates the catalyst and the C-2 olefin substituted indole product.

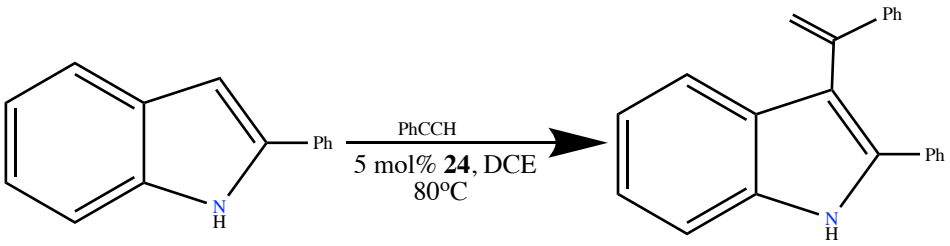

Scheme **3.10** Catalytic functionalization of 2-phenyl indole

The reaction was performed by treating indole with phenyl acetylene and 5 mol% **24** in 1,2 dichloroethane. The starting material was found completely consumed after heating for about 12h at 80°C based on the relative integrals on the ^{1}H NMR of the starting materials and the final product.

b. *Cyclization of Propargyl Amides*:

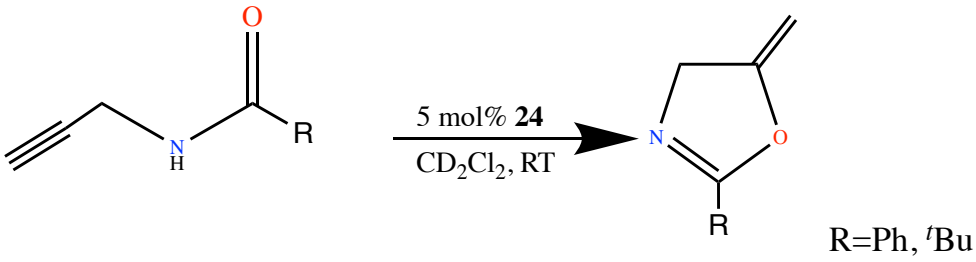

Scheme **3.11** Catalytic Cyclization of Propargyl Amides

Propargyl amides are known to undergo an intramolecular hydroamination reaction to produce oxazoles.[15] This reaction is a convenient way to synthesize N-Heterocycles and can be catalyzed by a variety of transition metals and bronsted acids. Au complexes are well documented in the literature to catalyze this rection.[16-17] Subsequently when a catalytic

amount of **24** was treated with the propargyl amide shown in Scheme **3.11**, the rapid conversion to the oxazole was observed at room temperature. With 5 mol% of **24** added to the propargyl amide in CD_2Cl_2 in an NMR tube, the cyclization reaction went to about 99% completion in less than 45 minutes at room temperature. 1 mol% catalyst needed about 4-6 hours to reach the same conversion at room temperature.

Since the products of the two reactions discussed above are olefins, we envisioned the above reactions could potentially be coupled with another reaction functionalizing the olefin in the presence of a catalytic cation. The ion-pairs we had would thus be able to catalyze the two reactions in parallel in a tandem catalytic fashion. Specifically, we targeted using the ion-pairs **33** and **34** to perform hydroboration and hydrosilylation on the olefins. However, before proceeding to the one-pot reactions, we wanted to check the compatibility of the ion-pair catalysts towards the above-mentioned reactions.

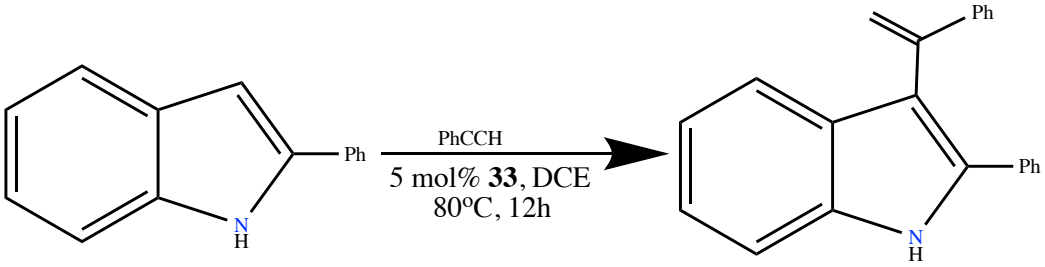

Scheme **3.12** Catalytic functionalization of 2-phenyl indole

When the reaction in Scheme **3.12** was attempted with 5 mol% of the ion-pairs **33** and **34**, no product formation was observed. We assumed this was due to the cation interfering with the catalytic cycle, since we know the anion is compatible with the reaction conditions. Moreover, we observed these ion-pairs rapidly producing a plate of metal in the reaction vessel indicating the decomposition of the ion-pair under the reaction conditions. We then attempted the hydroboration and hydrosilylation reactions on the olefin produced in Scheme **3.11**, discussed below.

3.4 Tandem Cyclization and Hydrofunctionalization of Propargyl Amides

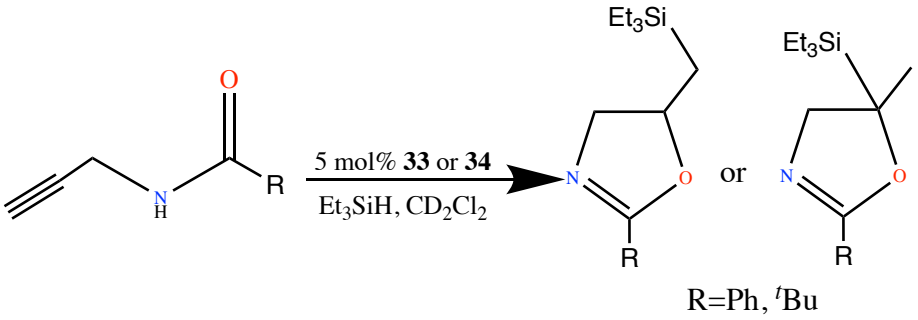

Scheme **3.13** Tandem Cyclization and Hydrosilylation of Propargyl Amides

Using the ion-pair **33** or **34**, we attempted the reaction in Scheme **3.13** together with triethylsilane expecting to achieve the hydrosilylated olefin produced as shown in Scheme **3.13**. A 5 mol% of the ion-pair catalyst, the propargyl amide and triethylsilane were added to the NMR tube in CD_2Cl_2 and heated at 60°C overnight. While the ^1H NMR spectrum displayed new silyl resonances suggesting a silylated product, the olefin produced from gold catalyzed cyclization was not consumed, indicating the olefin not undergoing hydrosilylation.

We then attempted a tandem hydroboration reaction with a 5 mol% catalyst, the propargyl amide and HBPin (Scheme **3.14**). The crude ^1H NMR spectrum shows the olefin produced by cyclization mostly consumed; however, it wasn't clear if the conversion was to the

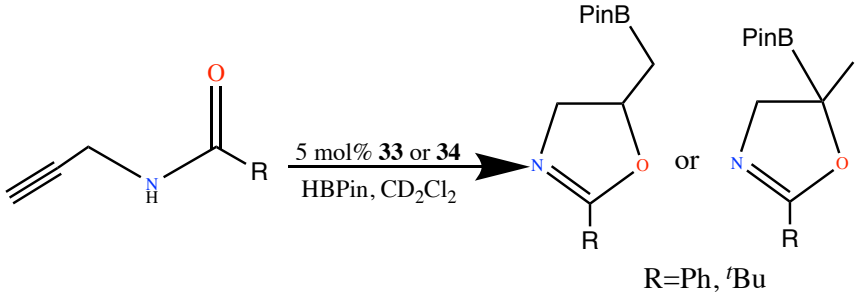

Scheme **3.14** Tandem Cyclization and Hydroboration of Propargyl Amides

hydroboration product. The mass spectrum of the crude reaction mixture didn't display the hydroboration product too, which led us to conclude the reaction failed.

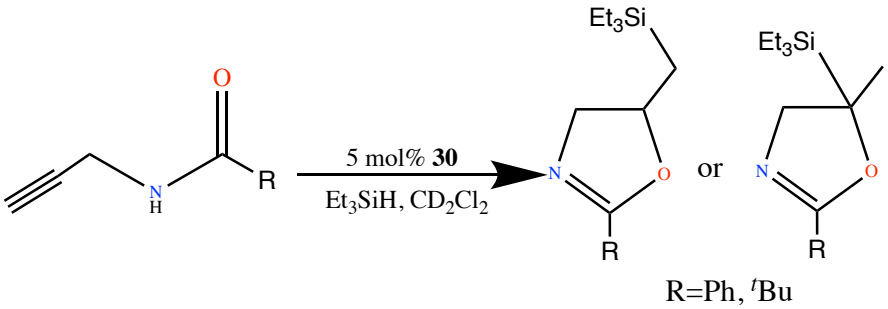

Scheme **3.15** Tandem Cyclization and Hydrosilylation of Propargyl Amides

To check if the other ion-pairs were active towards similar transformations, we employed the ion-pair **30** to the hydrosilylation conditions as shown in Scheme **3.15**. Similar to the previous reaction (Scheme **3.13**), the ^{1}H NMR shows new silyl resonances, but the olefin not consumed. The crude mass spectrum didn't show the peak for the expected hydrosilylation product, and we concluded the ion-pair **30** failed in achieving the expected transformation as well.

3.5 Ion-Pairs with Main Group Cations

Since the organometallic ion-pairs were either too reactive or not producing the desired product, we moved to pairing **24** with the main group cations. Specifically, we targeted the main group Lewis acids that are active towards hydrosilylation reactions. The N-methyl benzothiazolium cation (Fig. **3.5**, **38**) reported by Ingleson has a strong Hydride Ion Affinity (HIA) and thus activates the H-H and Si-H bonds.[18] Further, they reported the use of this cation as a catalyst for the hydrosilylation of imines. This was relevant for our cause since the

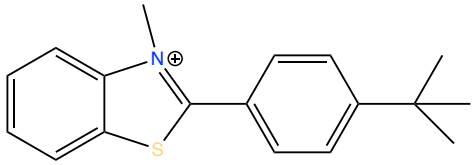

38

Fig. **3.5** N-methyl benzothiazolium cation

imines can potentially be produced by the gold catalyzed hydroamination of alkynes and then could be reduced by silanes using this cation in one-pot.

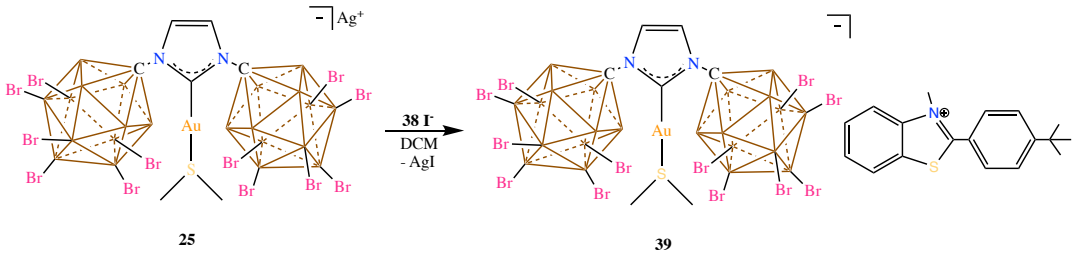

25 39

Scheme **3.16** Synthesis of the ion-pair **39** from **25**

Subsequently, treating the N-methyl benzothiazolium iodide with **25** in dichloromethane cleanly afforded the desired ion-pair **29** (Scheme **3.16**). Similarly, another main group Lewis acid N-methyl acridinium has a HIA of -53.3 Kcal, indicating its strong hydride affinity. This cation was found to be an active imine hydrosilylation catalyst by Ingleson, which motivated us to pair up it with **24**.[19] Thus, the iodide salt of the cation was treated **25** to cleanly afford the ion-pair **40** (Scheme **3.17**). The ion-pair **40** showed a strong yellow

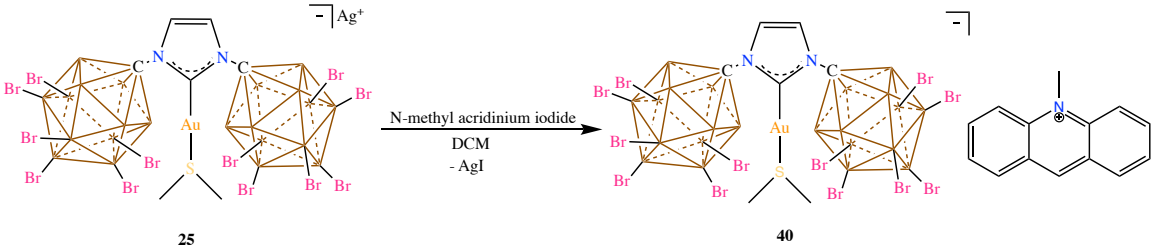

25 40

Scheme **3.17** Synthesis of the ion-pair **40** from **25**

green color arising due to the resonance stabilized carbocation and the highly conjugated acridinium salt. These cations partially activate the H-Si bonds in an FLP fashion and deliver the silylium to the imine nitrogen. Subsequent delivery of hydride to the imine carbon reduces the imines to N-silylated products.

The ion-pairs **39** and **40** are structurally characterized using multinuclear NMR spectroscopy, mass spectrometry and using X-Ray Crystallography in case of **40**. With these main group cation-based ion-pairs in hand, we proceeded to employ them as catalysts for gold catalyzed hydroamination followed by the hydrosilylation of imines in tandem.

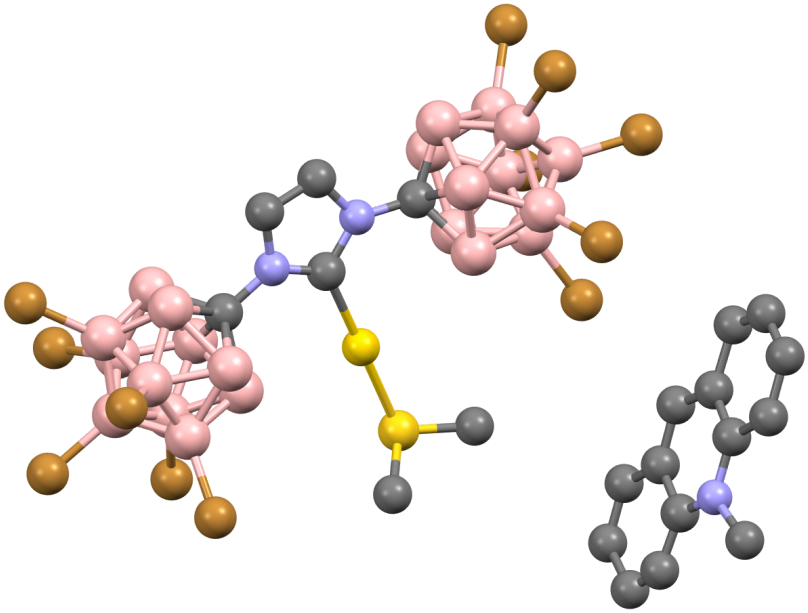

Fig. **3.6** X-Ray structure of ion-pair **40**. Hydrogen atoms omitted for clarity. N=Blue, C=grey, Au=gold, S=yellow, B=pink, Br=brown

3.6 Tandem Hydroamination of Alkynes and Hydrosilylation of Imines

Initially, the Au complex **14** was treated with a mixture of aniline and phenyl acetylene in $CDCl_3$ to check the progress of the hydroamination reaction. The formation of imine from the Au catalyzed hydroamination was evident by the ^1H NMR in a few minutes.

Taking a step further, 5 mol% of complex **14** was added to an NMR tube with aniline, phenyl acetylene and triethylsilane in $CDCl_3$. As expected, the imine formation was seen by the crude ^1H NMR. Concomitant hydrosilylated product was observed as well albeit in a smaller quantity indicating the Au complex catalyzed the imine hydrosilylation reaction

acting as a bifunctional catalyst. Heating the reaction mixture to 80°C achieved almost complete conversion of the starting materials to the final hydrosilylated product in 18h, with an overall yield of about 92%. So far, there are not many reports of Au catalyzed tandem hydroamination and hydrosilylation in the literature. Moreover, since it was not obvious if the Li^+ counter-cation had any role in the catalysis, we investigated the role of cations by performing the catalysis with Na^+ and K^+ salts of the Au complex. The conversions were estimated by a adding a known quantity of the internal standard durene to the reaction mixture and recording the crude ^1H NMR of the reaction mixture.

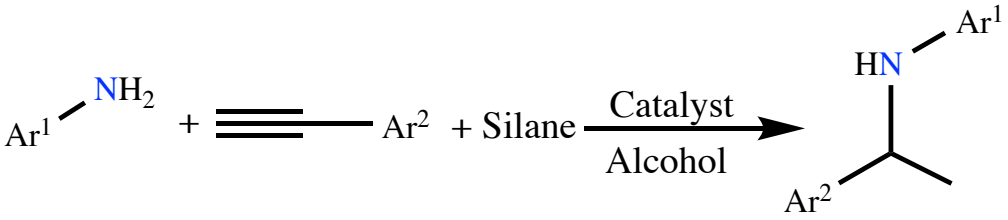

Scheme **3.18** Tandem Hydroamination followed by hydrosilylation

Further, we observed the N-silylated products could be hydrolyzed when the reaction was performed in alcoholic solvents. This was useful since the final product could be isolated as a secondary amine and the NMR shifts for the expected products could be compared with those reported in the literature already. Table **3.1** shows the results obtained when the reactions were performed with 1 mol% of Li^+, Na^+, K^+ salts of the Au complex.

Table **3.1** NMR Yields of the tandem catalytic reaction with different counter-cations

	Catalyst	Amine (Ar^1)	Alkyne (Ar^2)	Silane	Solvent	Temp (^0C)	Time (h)	Imine	Final Product
1	**39** (5 mol%)	Ph	*p*-F Ph	Et_3SiH	MeOH	70	18	4	96
2	**39** (5 mol%)	Ph	*p*-F Ph	Et_3SiH	EtOH	90	18	4	96
3	**39** (5 mol%)	Ph	*p*-F Ph	$PhMe_2SiH$	MeOH	70	18	50	50
4	**39** (5 mol%)	Ph	*p*-F Ph	$PhMe_2SiH$	EtOH	90	18	32	68
5	**39** (5 mol%)	Ph	*p*-F Ph	$PhMe_2SiH$	^{i}PrOH	100	18	12	88

6	**39** (5 mol%)	Ph	Ph	Et_3SiH	^{i}PrOH	100	18	4	96
7	**40** (5 mol%)	Ph	*p*-F Ph	Et_3SiH	^{i}PrOH	100	18	8	92

From the table, we see the reactions performed with 1 mol% Li^+ salt had conversions in the range of 50-60%, while the reactions performed with 1 mol% Na^+ had conversions in the range of 30-40%. We hypothesized the higher yields obtained with Li^+ salts are due to its higher extent of lewis acidity enabling its coordination to the imine nitrogen lone-pair and thus activating it for hydrosilylation. On the other hand, the Na^+ and K^+ are not stronger Lewis acidic cations due to their larger size compared to Li^+. Further, if this were true, using a 1 mol% of the ion-pair **39** should produce conversions of about the same or higher range since the benzothaizolium counter-cation is an example of a mild Lewis acid.

3.7 Conclusion

3.8 Experimental

General Considerations:

All manipulations were carried out using standard Schlenk or glovebox techniques under a dinitrogen atmosphere (industrial grade, glovebox) or purified elemental argon (99.995%, Schlenk line) unless otherwise stated. Dry solvents were obtained via distillation under argon from calcium hydride (acetonitrile, fluorobenzene, methylene chloride), sodium-potassium alloy (diethyl ether), potassium (benzene), sodium (toluene) or potassium using benzophenone ketyl radical as an indicator (tetrahydrofuran). Pentane was collected from a solvent purification system by SG Waters USA, LLC utilizing a fifteen minute argon sparge followed by passage though activated aluminum. The compounds **24**, **25**,[20] the propargyl amides and the reagents Ir(COD)(phen)Cl,[9] Ir(COD)(dppe)Cl[7] were

prepared using the literature methods. A slightly modified procedure from the literature was used for the synthesis of N-methyl benzothiazolium iodide[18] and N-methyl acridinium iodide.[19] All the other reagents were purchased from commercial sources and used without further purification. Nuclear magnetic resonance (NMR) spectroscopy was carried out using: Bruker Avance 600 MHz, and Bruker NEO 400 MHz (Prodigy LN2 cryoprobe). NMR chemical shifts are reported in parts per million (ppm) with ^{1}H and ^{13}C chemical shifts referenced to the residual non-deuterated solvent. Infrared spectroscopy was recorded on a Bruker ALPHA FTIR Spectrometer or Thermo Fisher Nicolet FTIR Spectrometer. High-resolution mass spectrometry (HRMS) was collected on an Agilent Technologies 6210 (TOF LC/MS) featuring a direct injection with multimode electrospray ionization/atmospheric-pressure chemical ionization (ESI/APCI).

Synthesis of 29:

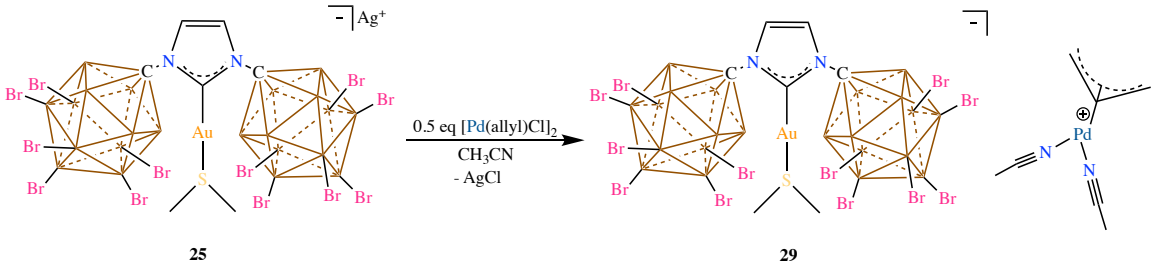

Scheme **3.1** Synthesis of the Pd(allyl) ion-pair **29** from **25**

In a nitrogen filled glove box, a glass vial was loaded with a stir bar and 50mg (0.03 mmol) of **25**. The solid was dissolved in 3 mL acetonitrile. In another vial, 5.48mg (0.015 mmol) of $[Pd(allyl)Cl]_2$ dimer was loaded and dissolved in 2 mL acetonitrile. The solution was then transferred to the vial containing **25** by a pipette and stirred for an hour. The suspension was then filtered over celite and pumped down to dryness under vacuum to furnish the ion-pair **29** as a yellow solid in 93% yield (50 mg, 0.028 mmol). ^{1}H NMR (400

MHz, CD_2Cl_2, 25°C): 7.37 (s, 2H, CH), 5.71 (m, 1H, allyl CH), 4.38 (d, 2H, allyl CH_2), 3.24 (d, 2H, allyl CH_2), 2.92 (s, 6H, SMe_2), 2.18 (s, 6H, coordinated CH_3CN); $^{11}B[^1H]$ NMR (128 MHz, CD_2Cl_2, 25°C): $^{13}C[^1H]$ NMR (100 MHz, CD_2Cl_2, 25°C): 172.31, 123.46, 120.18, 115.52, 71.75, 64.78, 24.76, 3.30 ppm. HRMS observed: calculated:

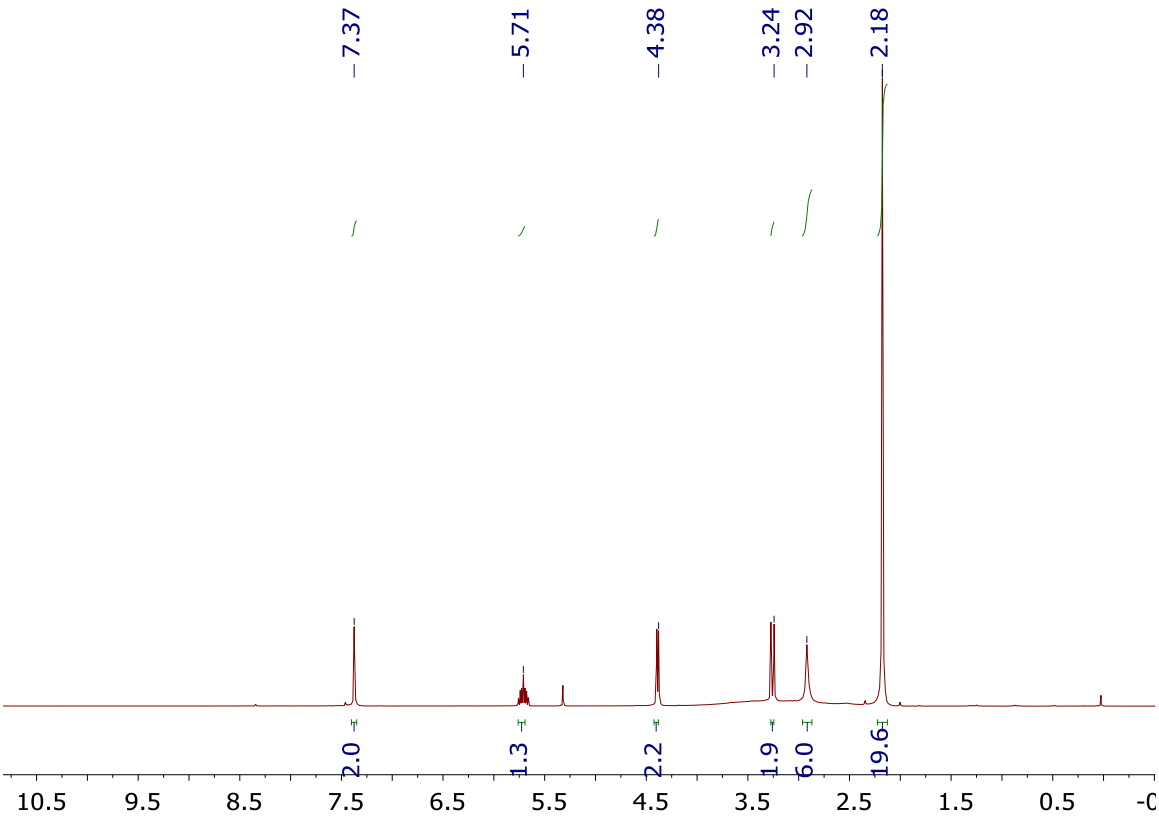

Fig. **3.7** ^1H NMR of **29** in DCM-d_2

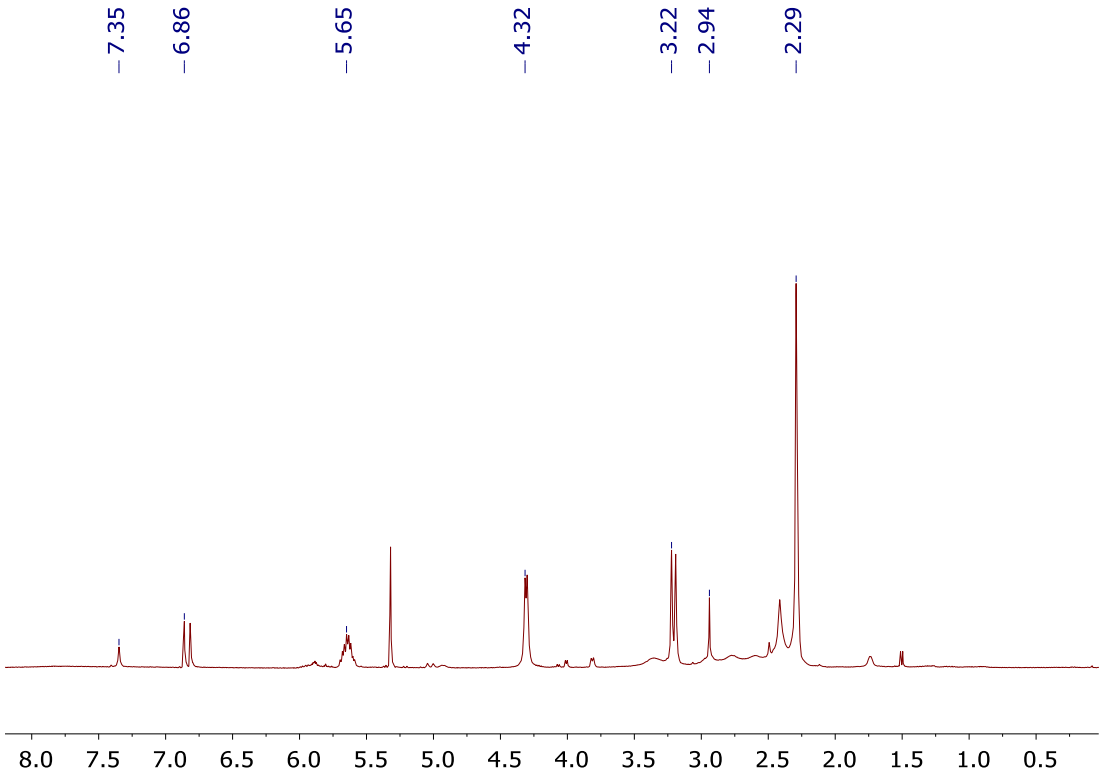

Fig. **3.8** $^{1}H[^{11}B]$ NMR of **29** in CD_2Cl_2

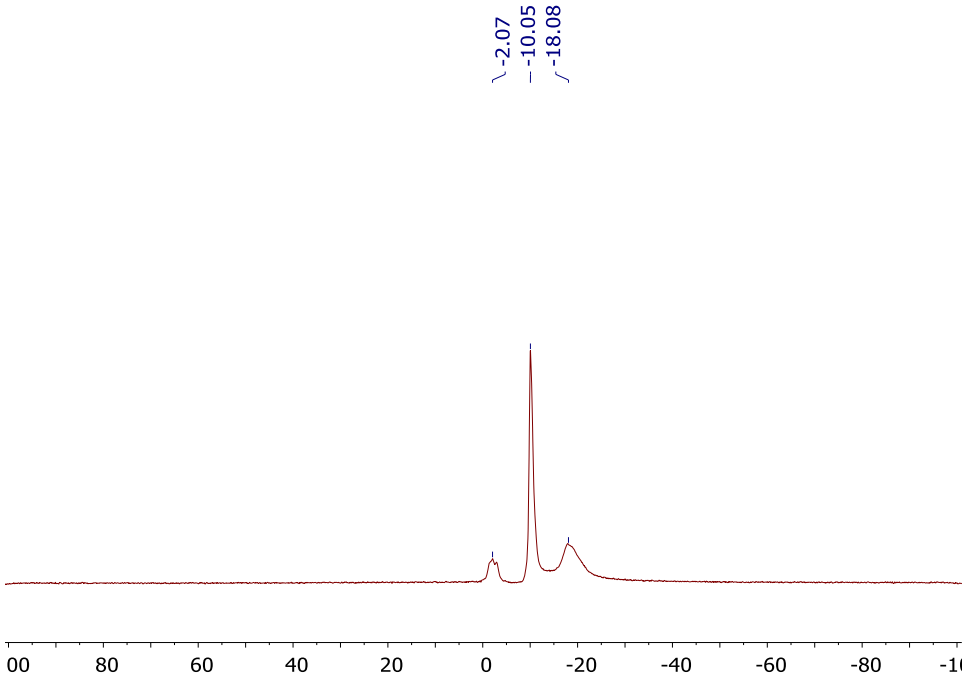

Fig. **3.9** ^{11}B NMR of **29** in CD_2Cl_2

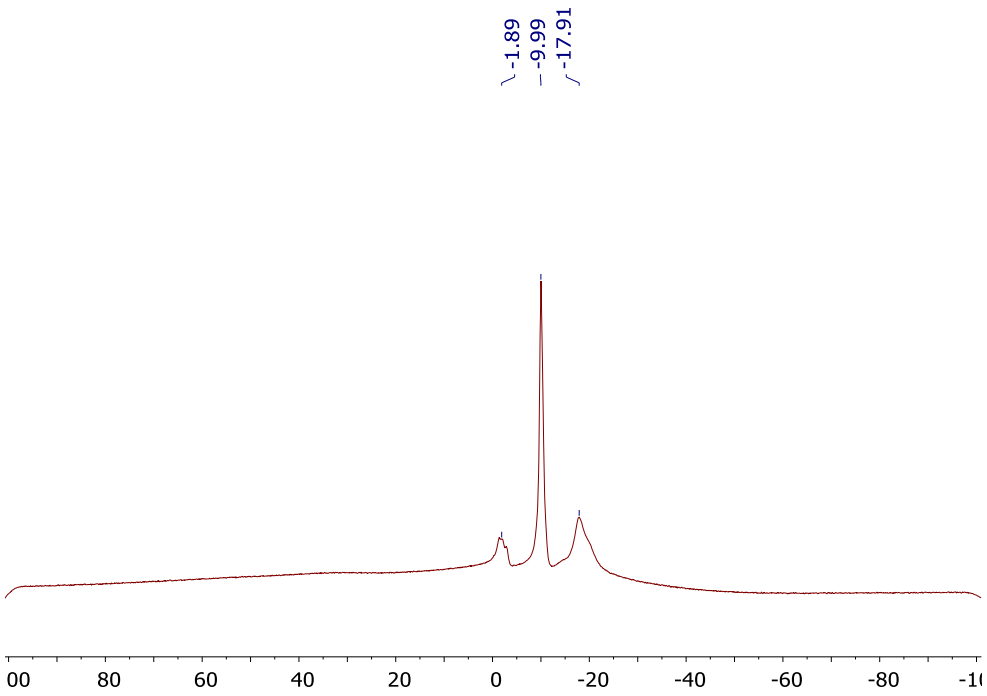

Fig. **3.10** $^{11}B[^{1}H]$ NMR of **29** in CD_2Cl_2

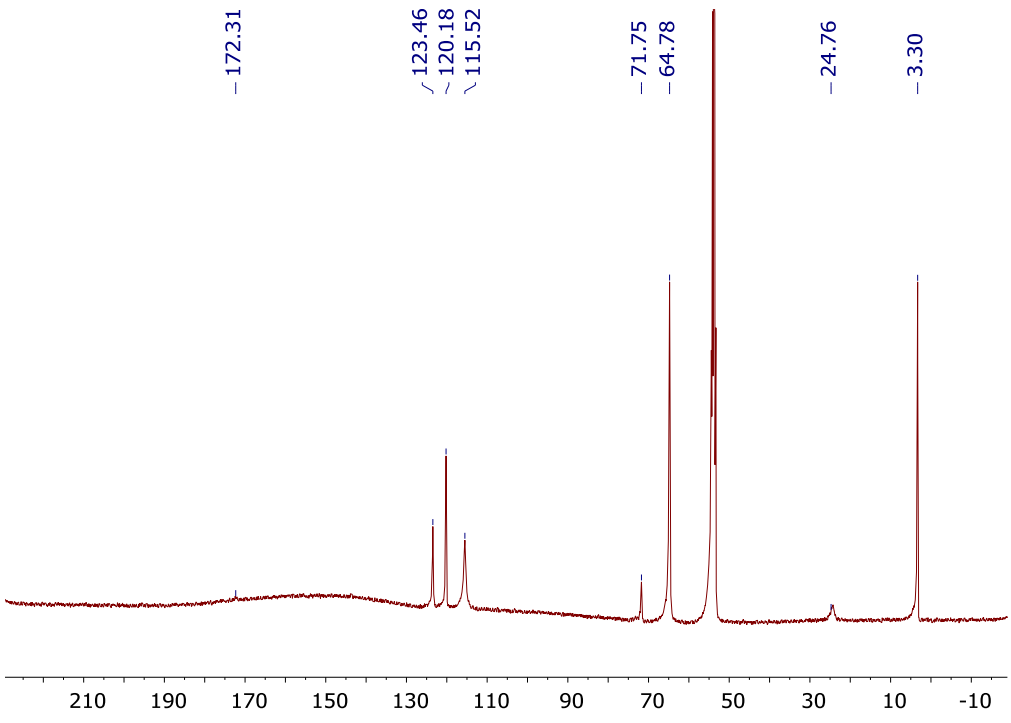

Fig. **3.11** $^{13}C[^{1}H]$ NMR of **29** in CD_2Cl_2

Synthesis of 30:

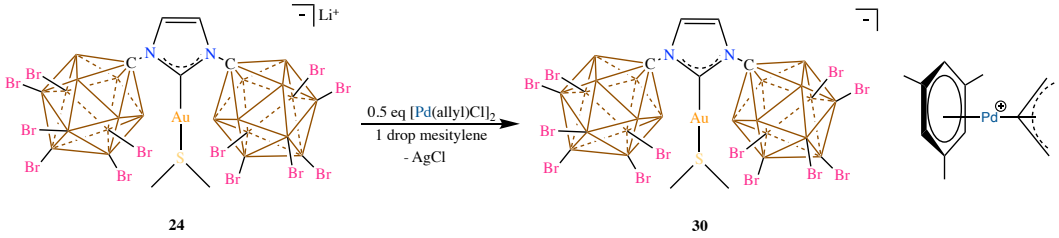

24 **30**

Scheme **3.2** Synthesis of the Pd(allyl) ion-pair **30** from **24**

In an oven dried schlenk flask, 10.3mg of $[Pd(allyl)Cl]_2$ dimer (0.028 mmol) was loaded and dissolved in 4 mL dichloromethane and cooled down to -80°C in a dry ice/acetone bath under argon. In another schlenk flask, 100mg of **24** (0.056 mmol) was loaded and dissolved in 10mL dichloromethane. This solution was then slowly transferred to the other Schlenk flask via an oven dried canula. The suspension was stirred at -80°C for a few minutes before slowly warming it to room temperature while continuing the stirring. The solution was then filtered over celite and pumped down to dryness under high vacuum to afford **30** as a grey solid. The compound readily decomposed by plating Pd metal when left in solution. ^{1}H NMR (600 MHz, 25°C, CD_2Cl_2): 7.37 (s, 2H, CH), 6.78 (s, 3H, mesitylene), 5.48 (m, 2H, allyl), 4.08 (m, 1H, allyl), 3.04 (m, 2H, allyl), 2.93 (s, 6H, SMe_2), 2.26 (s, 9H, mesitylene); ^{11}B NMR (192 MHz, 25°C, CD_2Cl_2): -0.87, -10.18, -18.01 ppm; $^{13}C[^{1}H]$ NMR (150 MHz, 25°C, CD_2Cl_2): 138.00, 127.17, 114.70, 70.66, 67.77, 21.32 ppm.

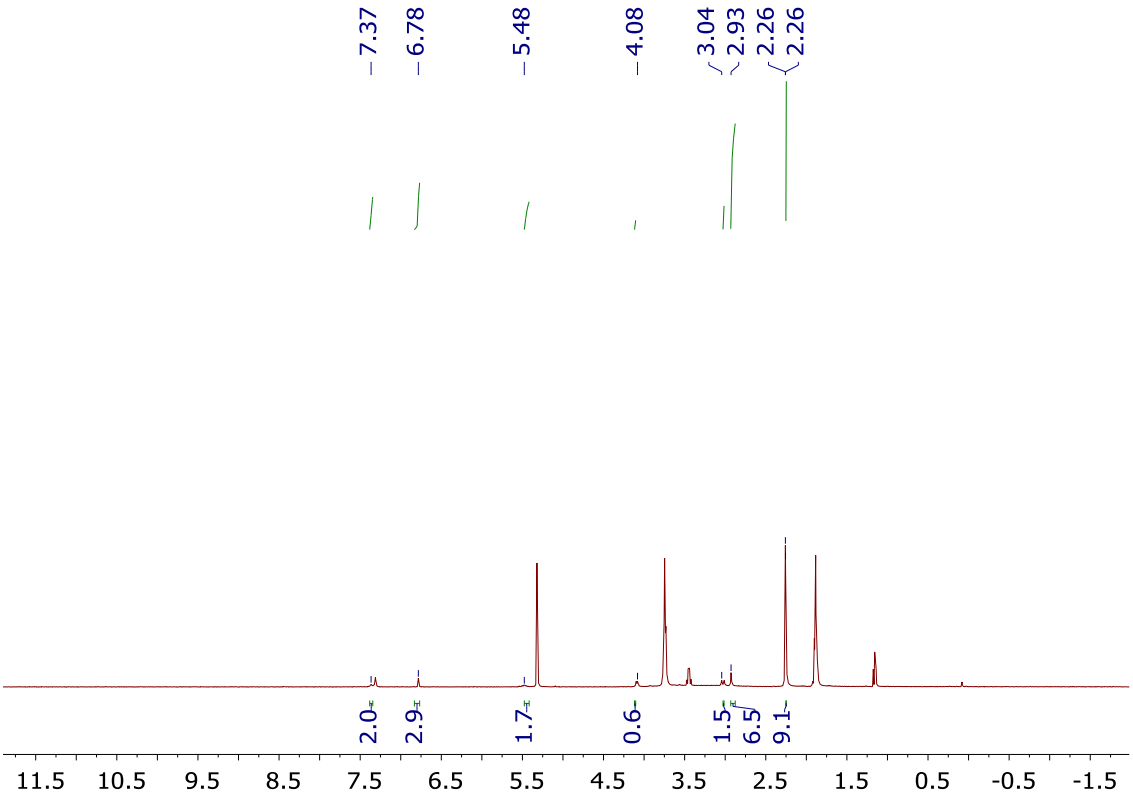

Fig. **3.12** ^{1}H NMR of **30** in CD_2Cl_2

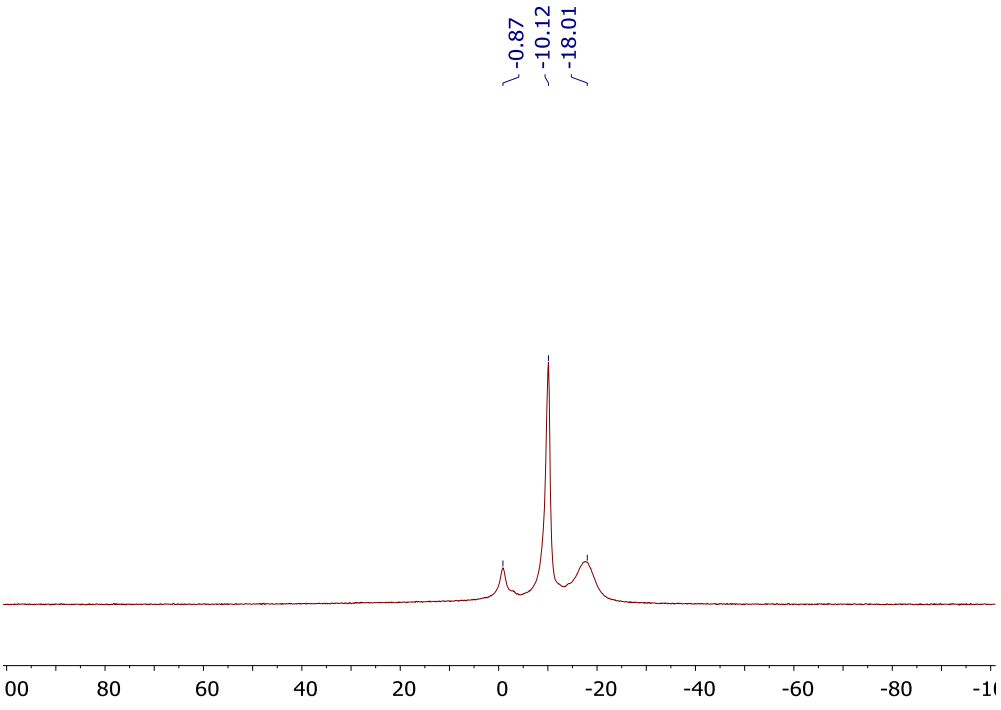

Fig. **3.13** ^{11}B NMR of **30** in CD_2Cl_2.

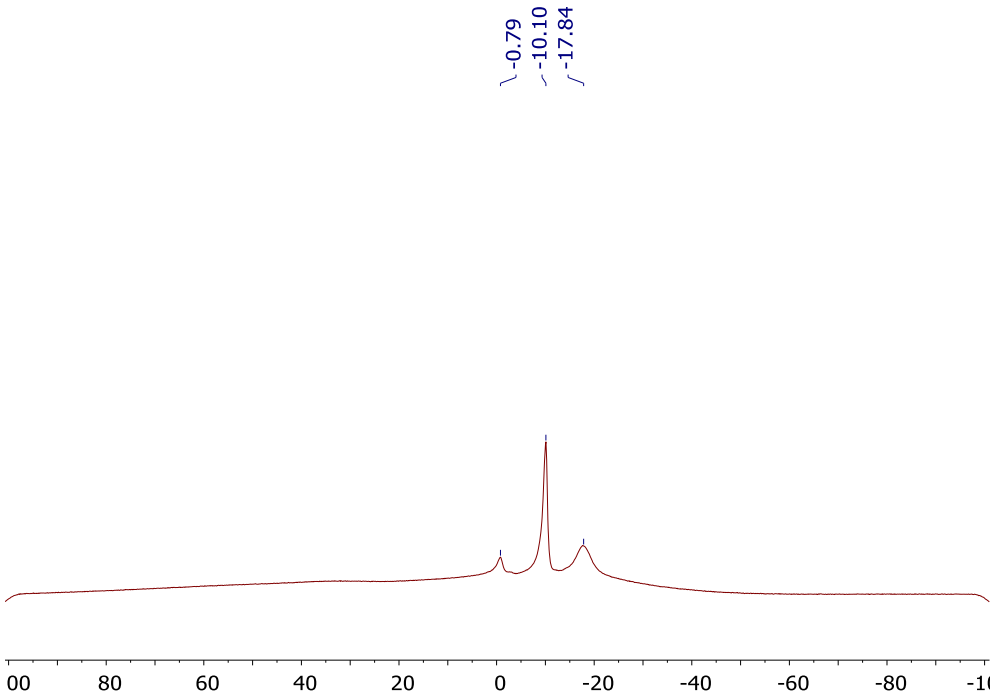

Fig. **3.14** $^{11}B[^{1}H]$ NMR of **30** in CD_2Cl_2

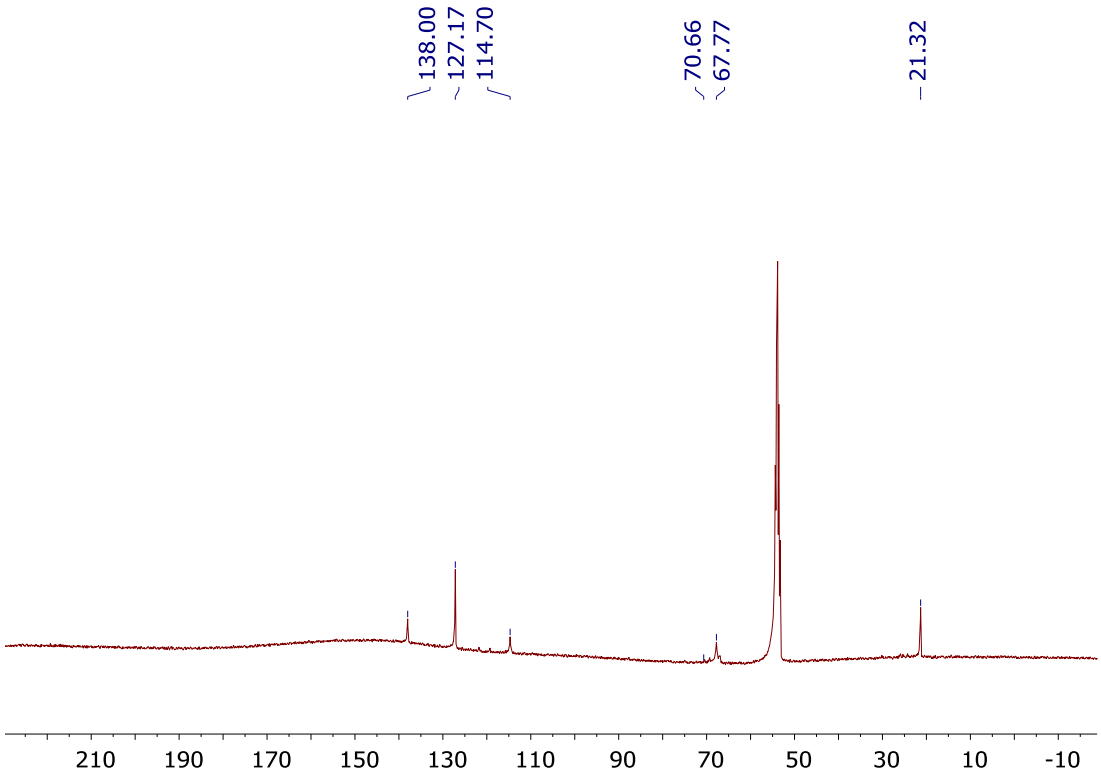

Fig. **3.15** $^{13}C[^{1}H]$ NMR of **30** in CD_2Cl_2

Synthesis of 31:

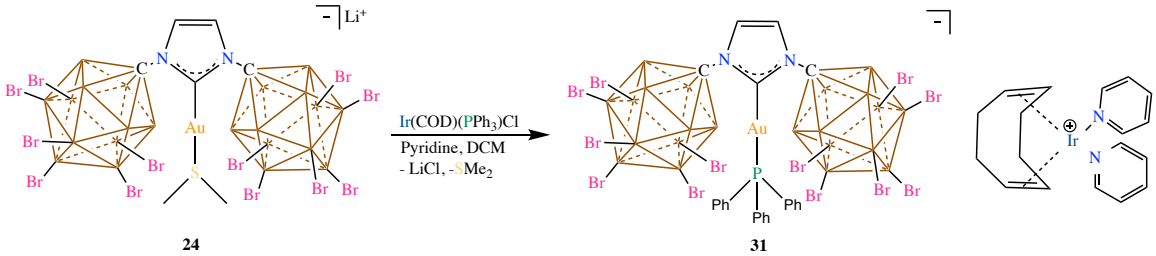

Scheme **3.3** Synthesis of PPh_3 bound Au complex **31** from **24**

To an oven dried glass vial, **24** was loaded with a stir bar and dissolved in dichloromethane. To this, a solution of Ir(COD)(PPh_3)Cl in dichloromethane was added. A drop of dry distilled pyridine was then added to the reaction mixture and stirring continued for an hour. The solution was then filtered and pumped down to dryness producing **31** in 95% yield. ^{1}H NMR (400 MHz, CD_2Cl_2, 25°C): 8.62 (d, 4H, CH), 7.82 (t, 2H, CH), 7.63-7.50 (m, 19H, CH), 7.40 (s, 2H, CH), 3.87 (m, 4H, olefin CH), 2.46 (m, 4H, olefin CH_2), 1.87 (m, 4H, olefin CH_2); $^{11}B[^{1}H]$ NMR (128 MHz, CD_2Cl_2, 25°C): -1.34, -10.29, -17.83 ppm.

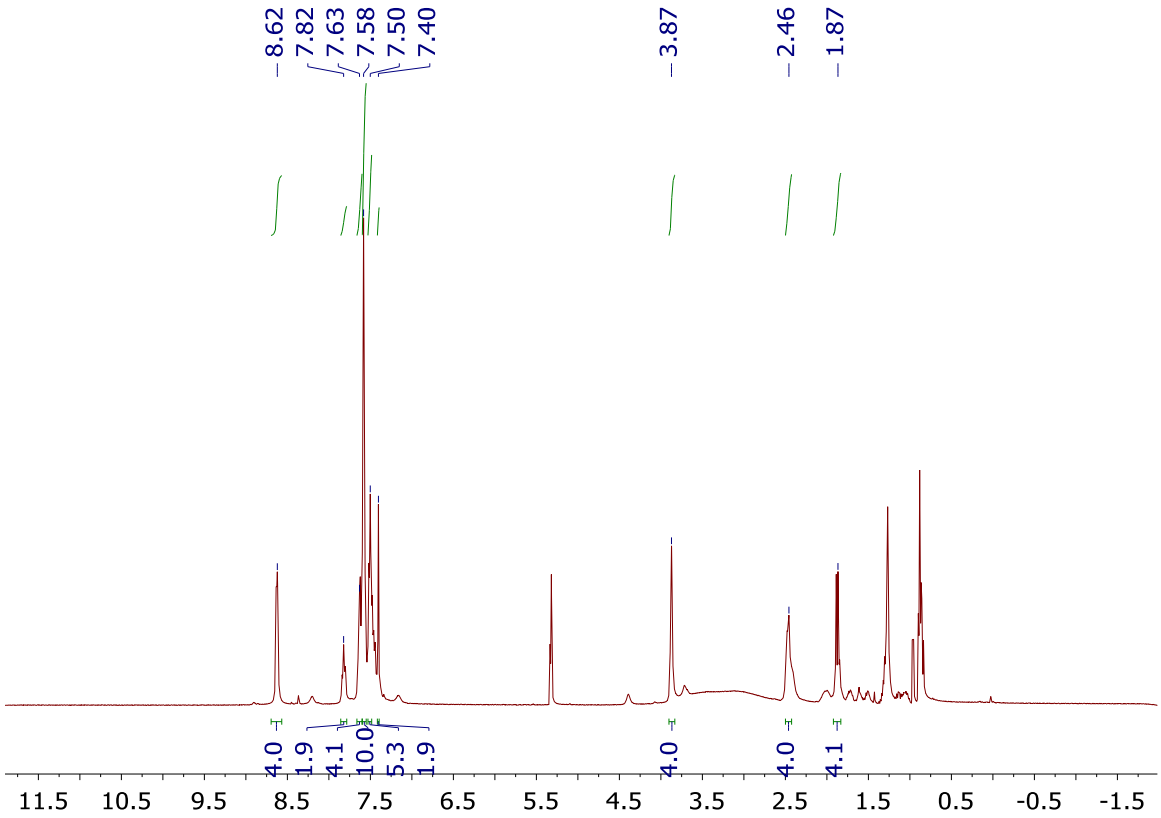

Fig. **3.16** ^{1}H NMR of **31** in CD_2Cl_2

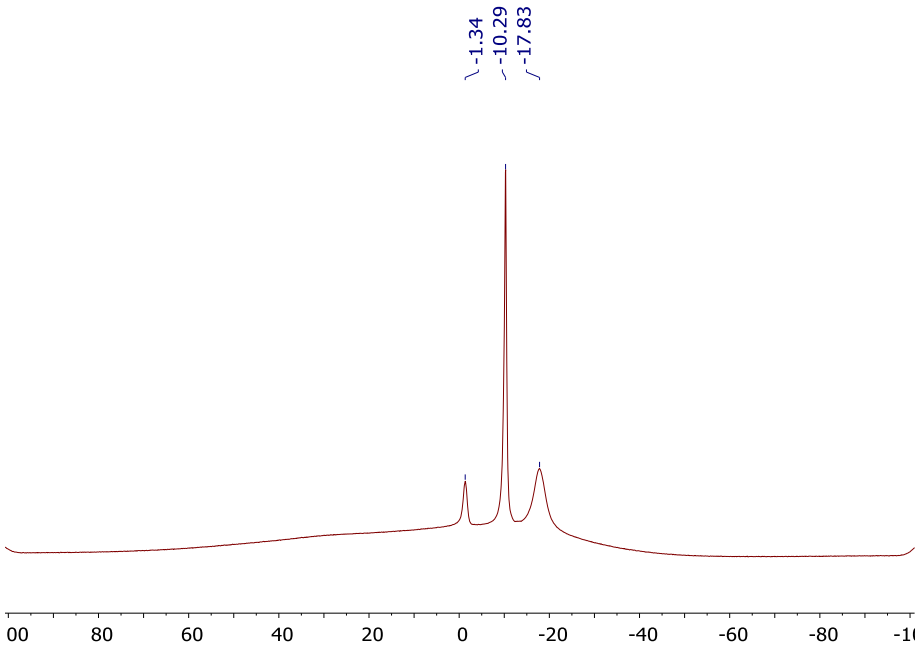

Fig. **3.17** $^{11}B[^{1}H]$ NMR of **31** in CD_2Cl_2

Synthesis of 32:

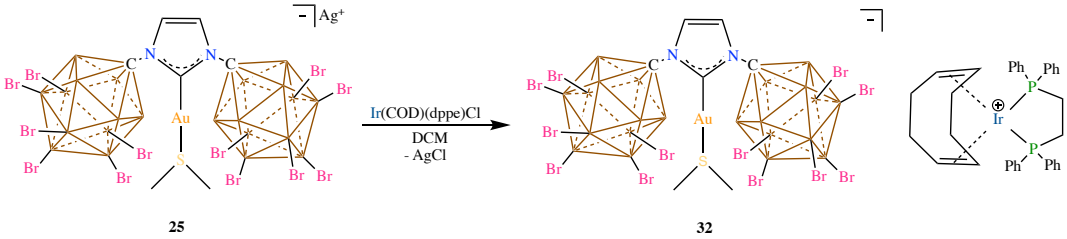

25 **32**

Scheme **3.4** Synthesis of the ion-pair **32** from **25**

In a vial, 50mg (0.028 mmol) of **25** was weighed and suspended in 3 mL dichloromethane. To this, a solution of Ir(COD)(dppe)Cl (20.5mg, 0.028 mmol) in dichloromethane (3 mL) was added and the dark green suspension was stirred for an hour. The suspension was then filtered over celite and pumped to dryness under vacuum to afford **32** in 95% yield as a green solid. ^{1}H NMR (600 MHz, CD_2Cl_2, 25°C): 7.61-7.59 (m, 20H, aromatic CH), 7.36 (s, 2H, CH), 4.60 (m, 4H, COD CH), 2.93 (s, 6H, SMe_2), 2.31 (t, 2H, CH_2), 2.27 (t, 2H, CH_2), 2.23 (m, 8H, COD CH_2); ^{11}B[^{1}H] NMR (192 MHz, CD_2Cl_2, 25°C): -1.14, -10.12, -17.23; ^{31}P[^{1}H] NMR (242 MHz, CD_2Cl_2, 25°C): 46.51 ^{13}C[^{1}H] NMR (150 MHz, CD_2Cl_2, 25°C): 176.88, 133.29, 132.63, 130.08, 129.57, 123.68, 90.24, 71.48, 31.25, 27.23, 24.72 ppm.

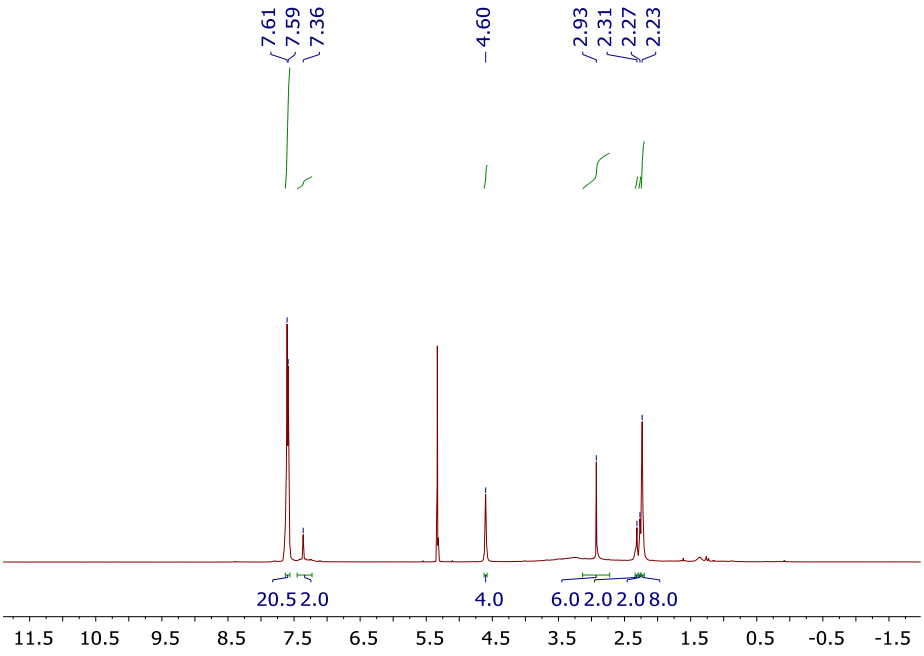

Fig. **3.18** ^{1}H NMR of **32** in CD_2Cl_2

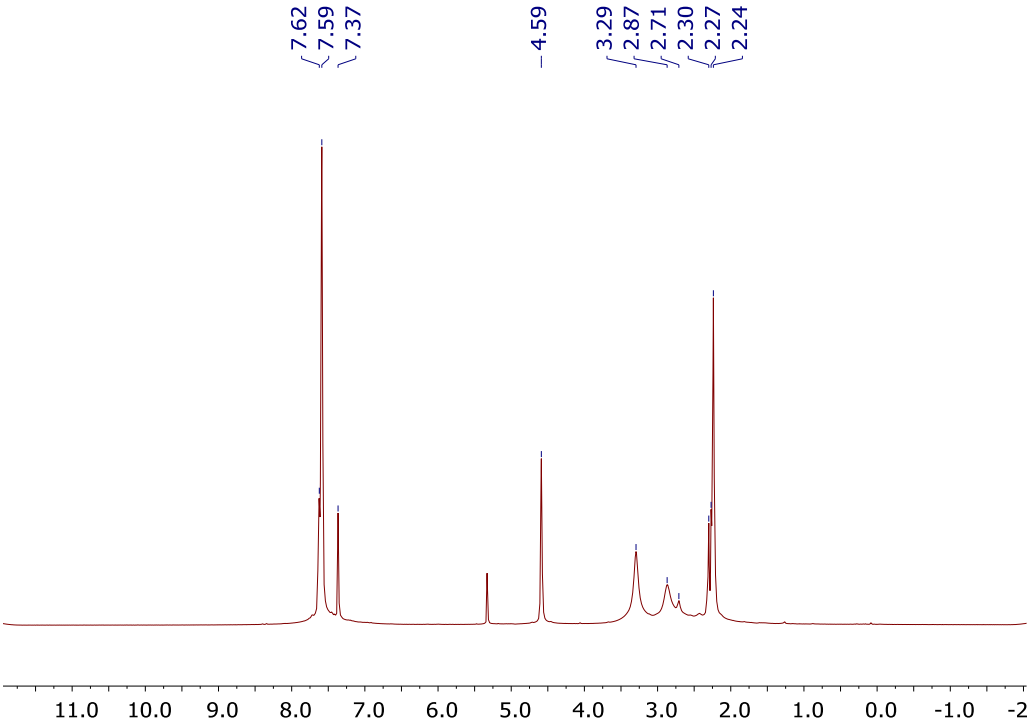

Fig. **3.19** $^{1}H[^{11}B]$ NMR of **32** in CD_2Cl_2

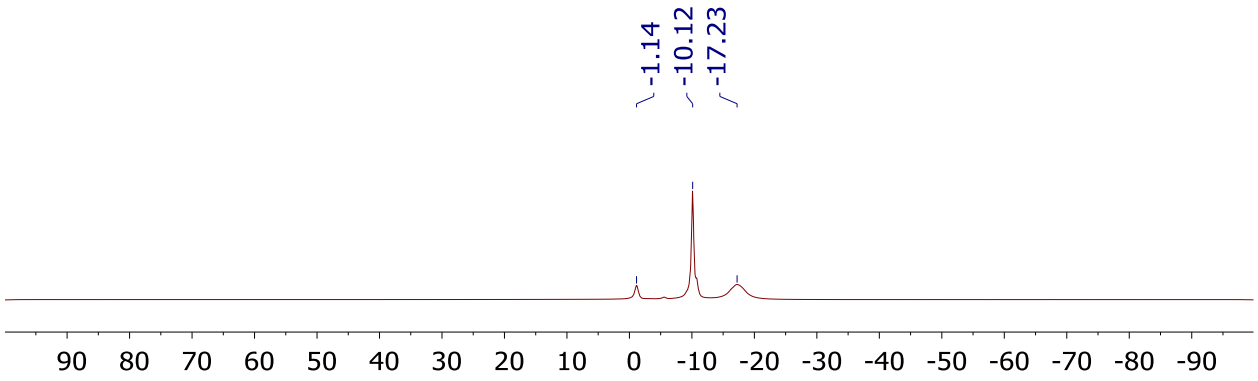

Fig. **3.20** ^{11}B NMR of **32** in CD_2Cl_2

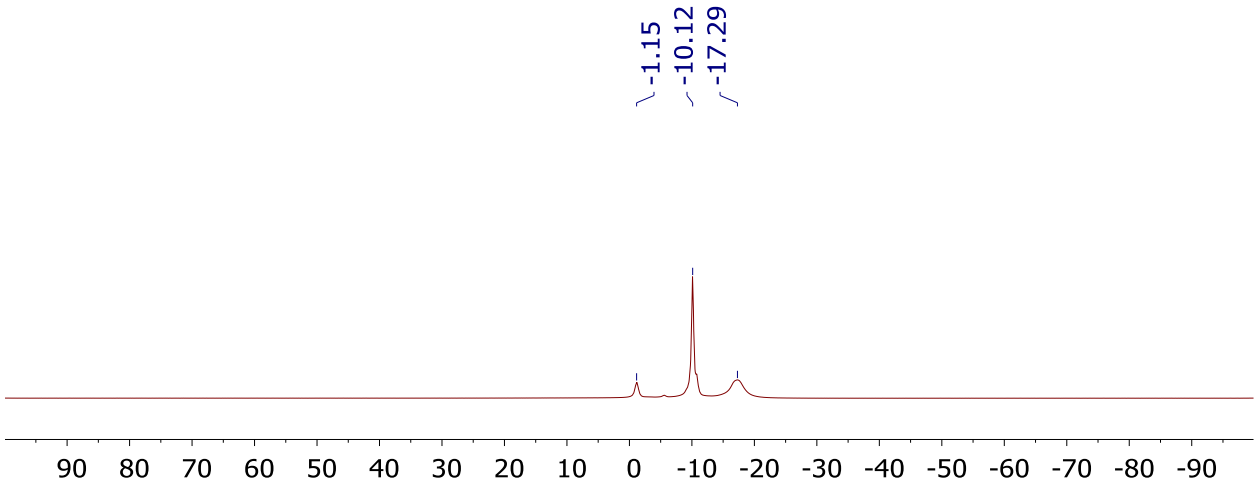

Fig. **3.21** $^{11}B[^{1}H]$ NMR of **32** in CD_2Cl_2

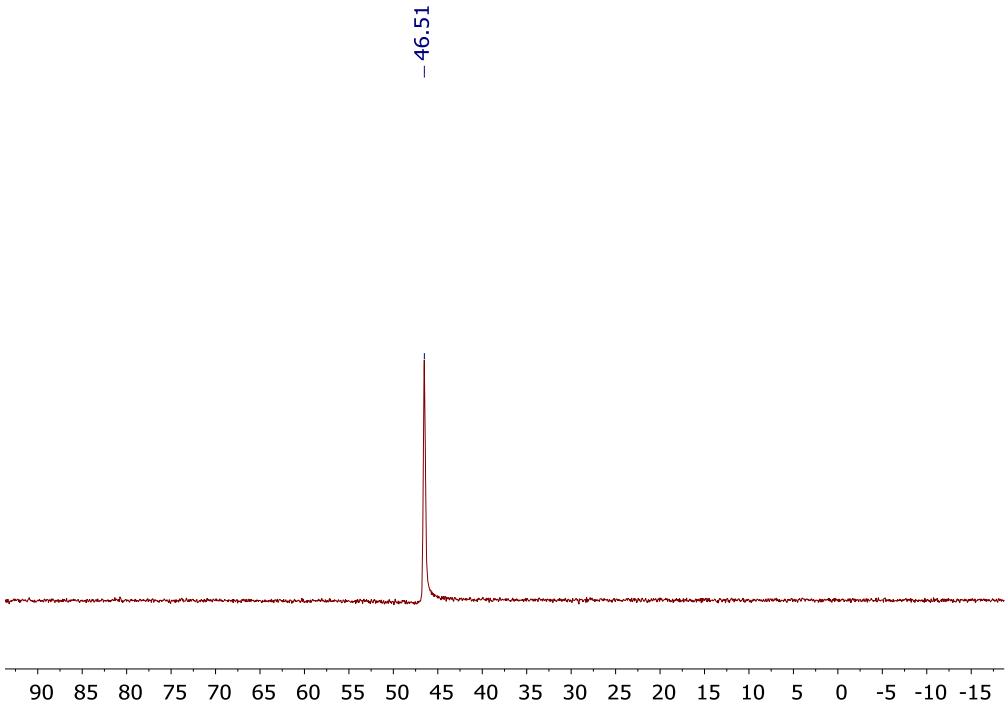

Fig. **3.22** ^{31}P NMR of **32** in CD_2Cl_2

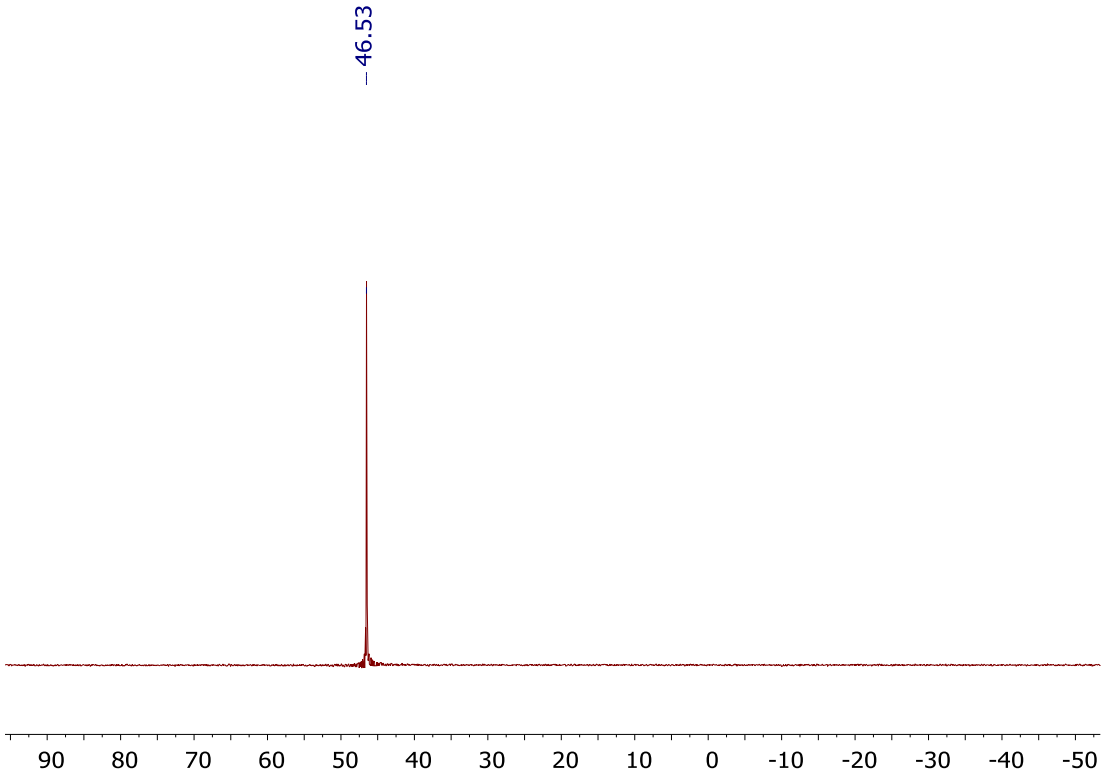

Fig. **3.23** $^{31}P[^{1}H]$ NMR of **32** in CD_2Cl_2

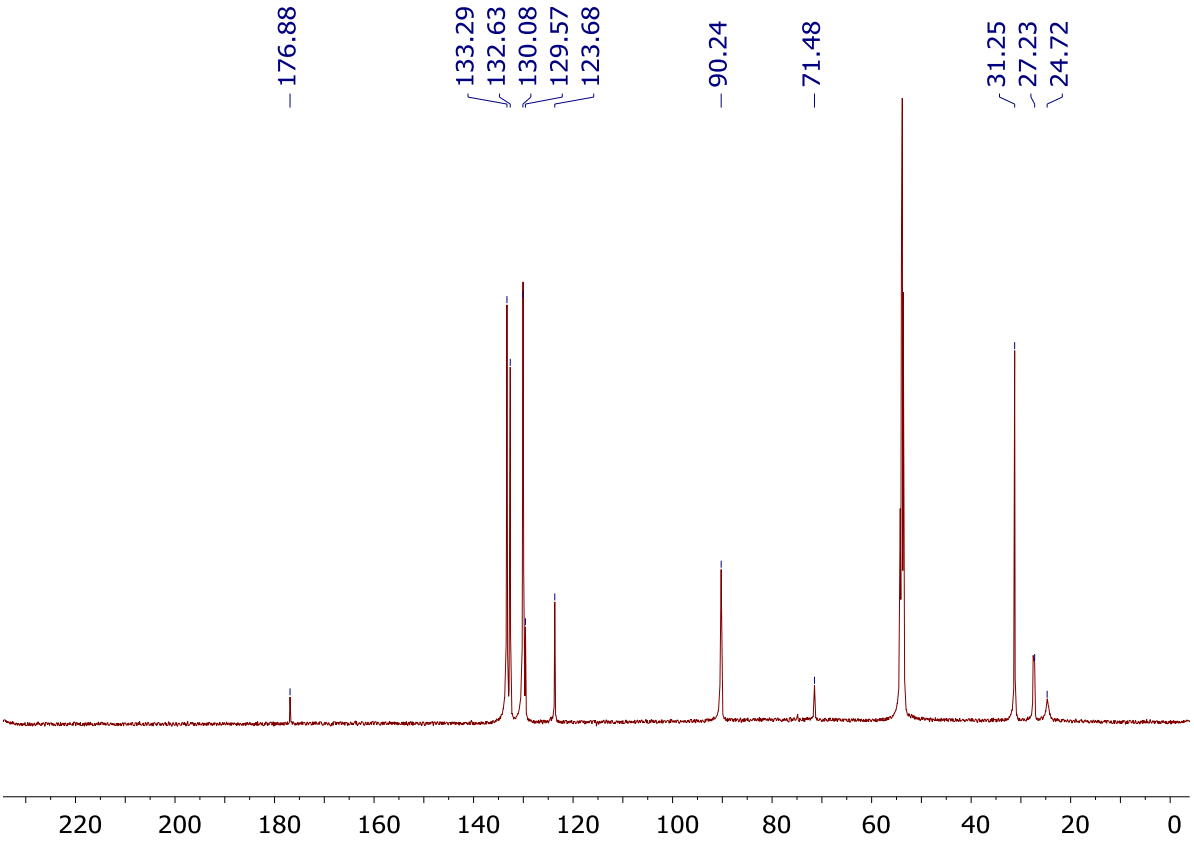

Fig. **3.24** $^{13}C[^{1}H]$ NMR of **32** in CD_2Cl_2

Synthesis of 33:

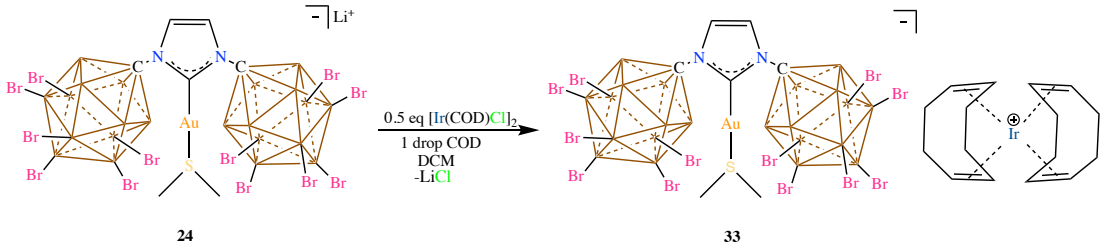

Scheme **3.5** Synthesis of the ion-pair **33** from **24**

In a vial, 50mg (0.028 mmol) of **24** was weighed and dissolved in 3 mL dichloromethane. To this solution, 9.4mg (0.014 mmol) of $[Ir(COD)Cl]_2$ dimer dissolved in dichloromethane (3 mL) was added. After adding a drop of COD, the solution was stirred for an hour and the solution concentrated down to 2 mL under vacuum. At this point, 8 mL of diethyl ether was added to precipitate the compound and decanted after stirring for 10 minutes. The ether wash was repeated once more, and the red solid obtained was then pumped down to dryness

under vacuum to produce **33** in 85% yield as a dark solid. ^{1}H NMR (600 MHz, CD_2Cl_2, 25°C): 7.37 (s, 2H, CH), 5.13 (m, 8H, COD CH), 2.93 (s, 6H, SMe_2), 2.49 (m, 16H, COD CH_2), ^{11}B[^{1}H] NMR (192 MHz, CD_2Cl_2, 25°C): -1.32, -10.28, -16.85; ^{13}C[^{1}H] NMR (150 MHz, CD_2Cl_2, 25°C): 177.27, 123.74, 100.83, 71.07, 31.10 ppm. HRMS observed: calculated:

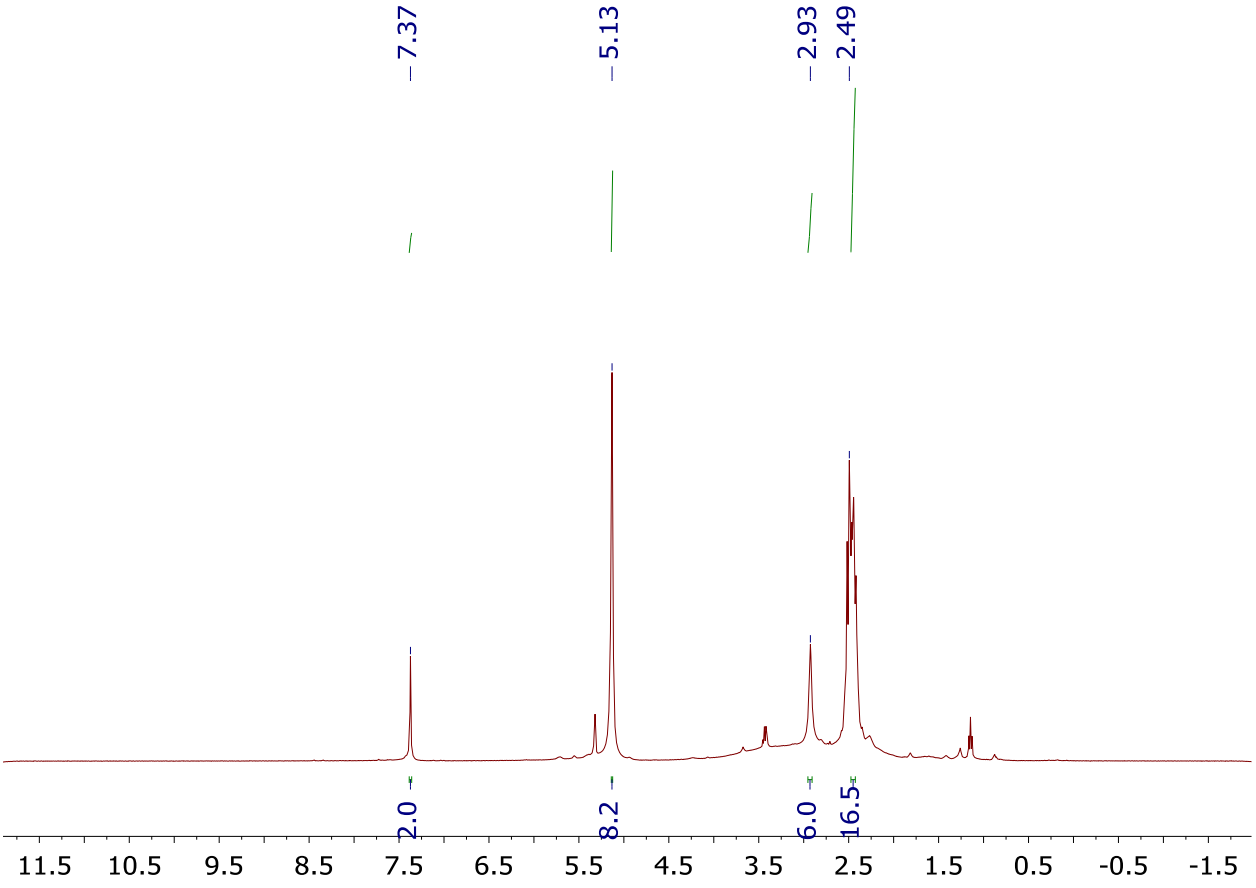

Fig. **3.25** ^{1}H NMR of **33** in CD_2Cl_2

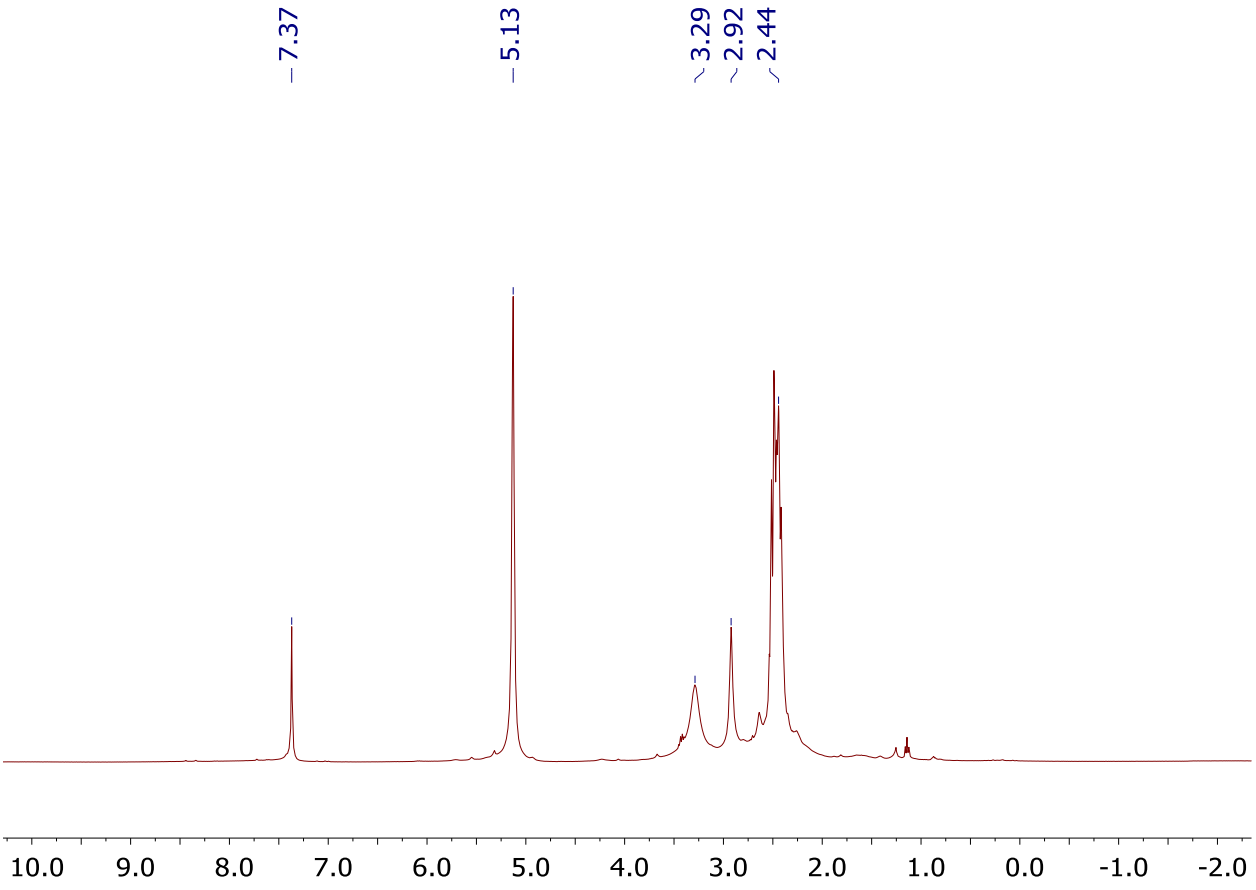

Fig. **3.26** $^{1}H[^{11}B]$ NMR of **33** in CD_2Cl_2

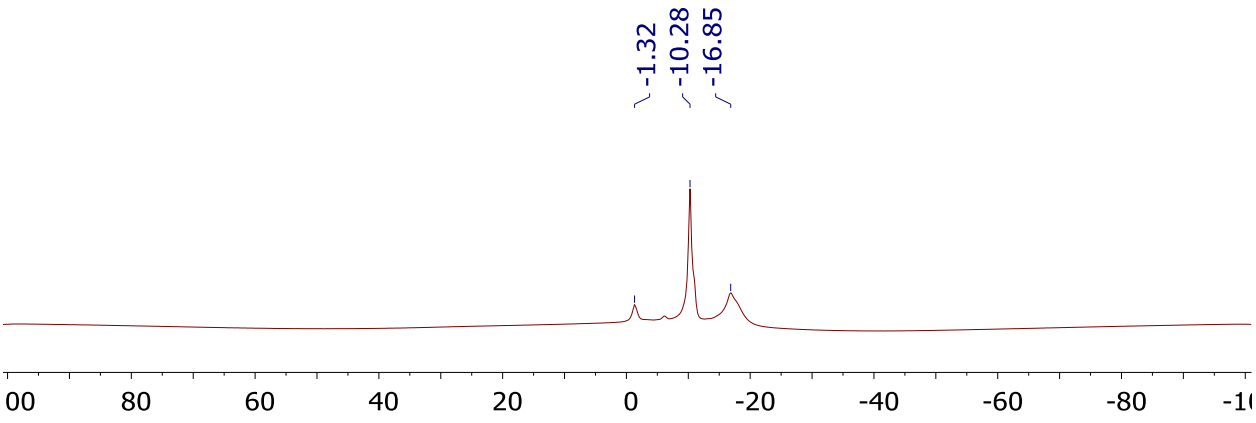

Fig. **3.27** $^{11}B[^{1}H]$ NMR of **33** in CD_2Cl_2

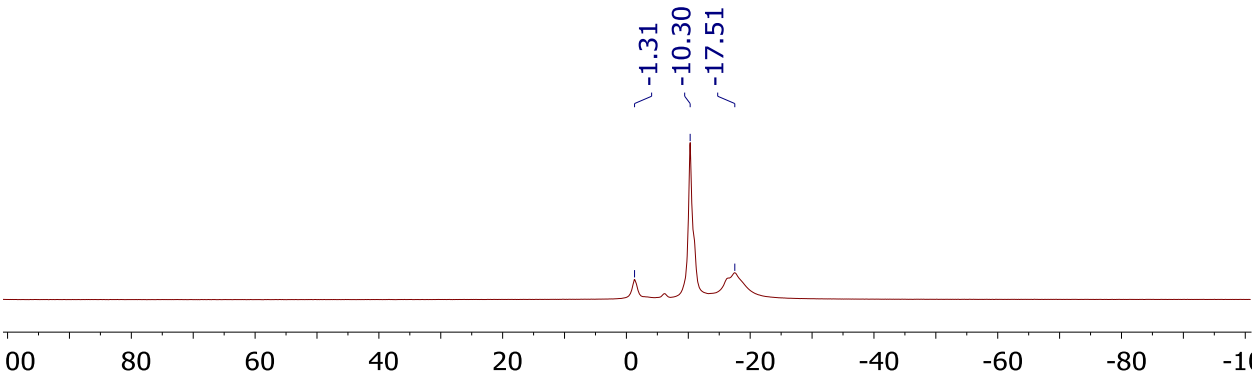

Fig. **3.28** ^{11}B NMR of **33** in CD_2Cl_2

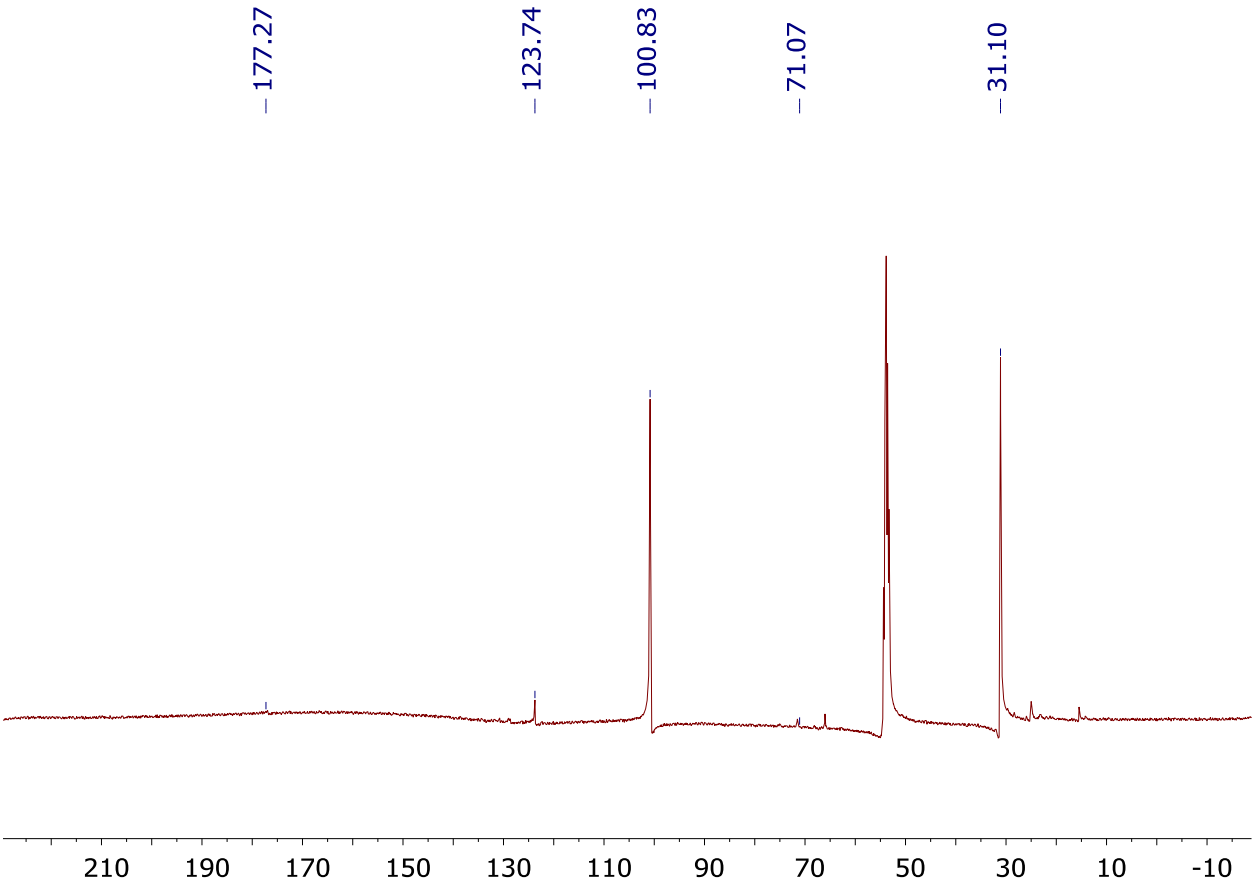

Fig. **3.29** $^{13}C[^1H]$ NMR of **33** in CD_2Cl_2

Synthesis of 34:

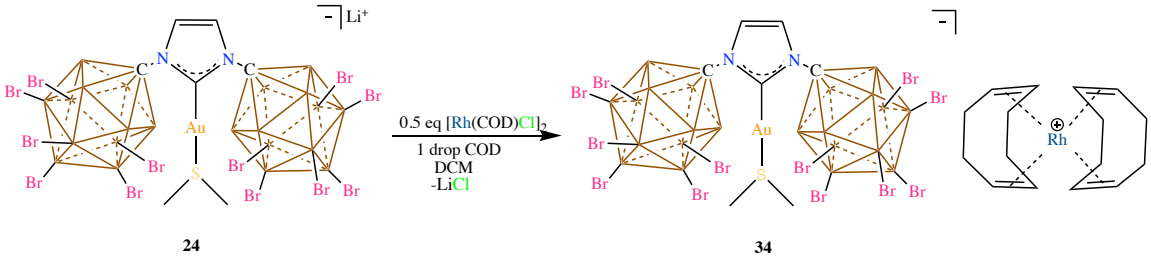

24 **34**

Scheme **3.6** Synthesis of the ion-pair **34** from **24**

In a vial, 50mg (0.028 mmol) of **24** was weighed and dissolved in 3 mL dichloromethane. To this solution, 6.9mg (0.014 mmol) of $[Rh(COD)Cl]_2$ dimer dissolved in dichloromethane (3 mL) was added. After adding a drop of COD, the solution was stirred for an hour and the solution concentrated down to 2 mL under vacuum. At this point, 8 mL of diethyl ether was added to precipitate the compound and decanted after stirring for 10 minutes. The ether wash was repeated once more, and the red solid obtained was then pumped down to dryness under vacuum to produce **34** in 81% yield as a brick red solid. ^{1}H NMR (600 MHz, CD_2Cl_2, 25°C): 7.37 (s, 2H, CH), 5.29 (m, 8H, COD CH), 2.93 (s, 6H, SMe_2), 2.56 (m, 16H, COD CH_2); $^{11}B[^{1}H]$ NMR (192 MHz, CD_2Cl_2, 25°C): -1.28, -10.29, -17.84; $^{13}C[^{1}H]$ NMR (150 MHz, CD_2Cl_2, 25°C): 176.89, 123.72, 108.10, 71.53, 59.83, 38.46, 31.46, 30.23, 25.03 ppm. HRMS calculated: observed:

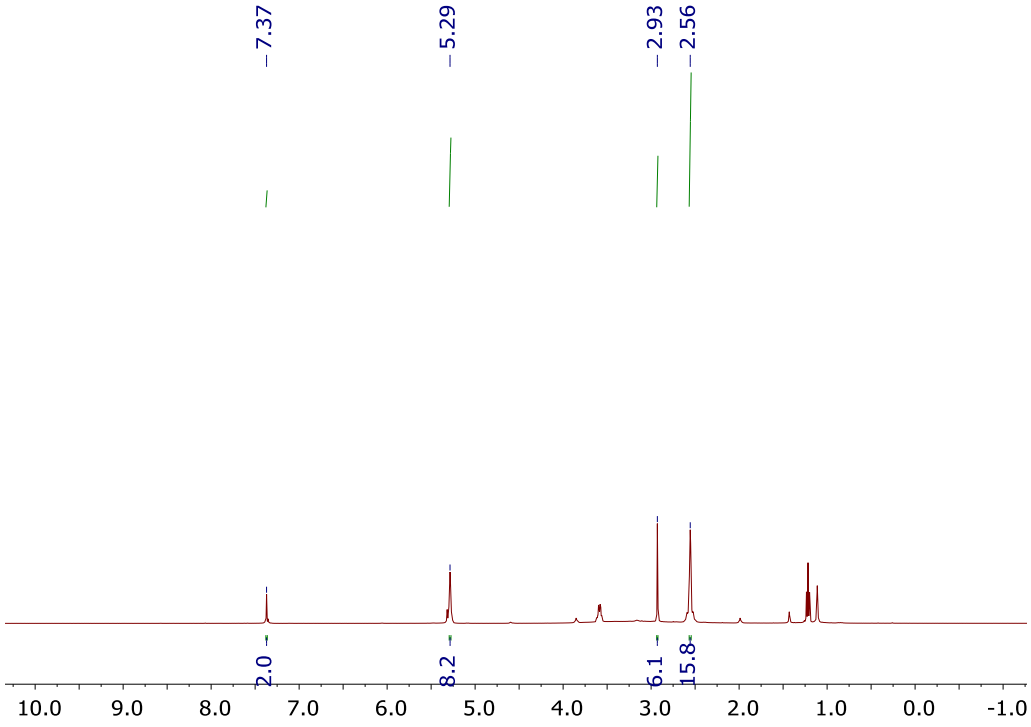

Fig. **3.30** ^{1}H NMR of **34** in CD_2Cl_2

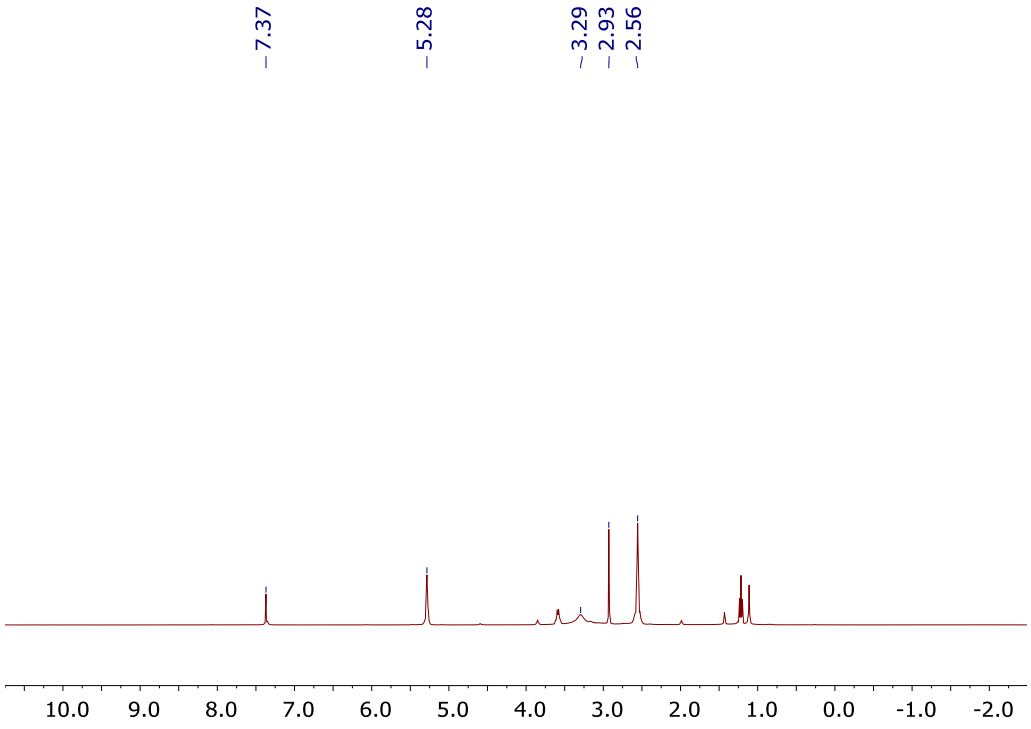

Fig. **3.31** $^{1}H[^{11}B]$ NMR of **34** in CD_2Cl_2

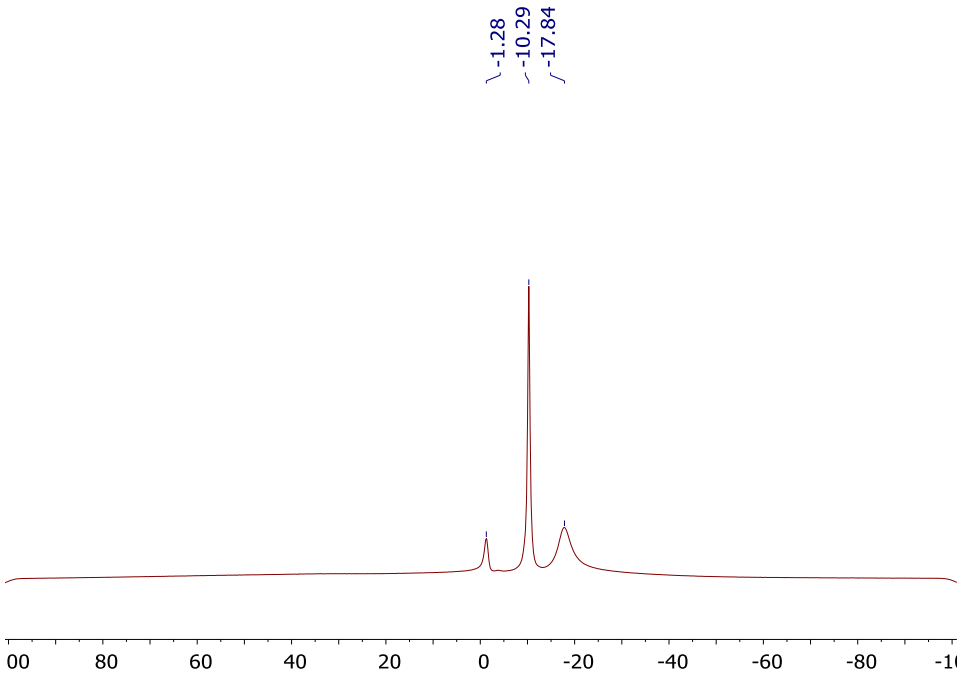

Fig. **3.32** $^{11}B[^{1}H]$ NMR of **34** in CD_2Cl_2

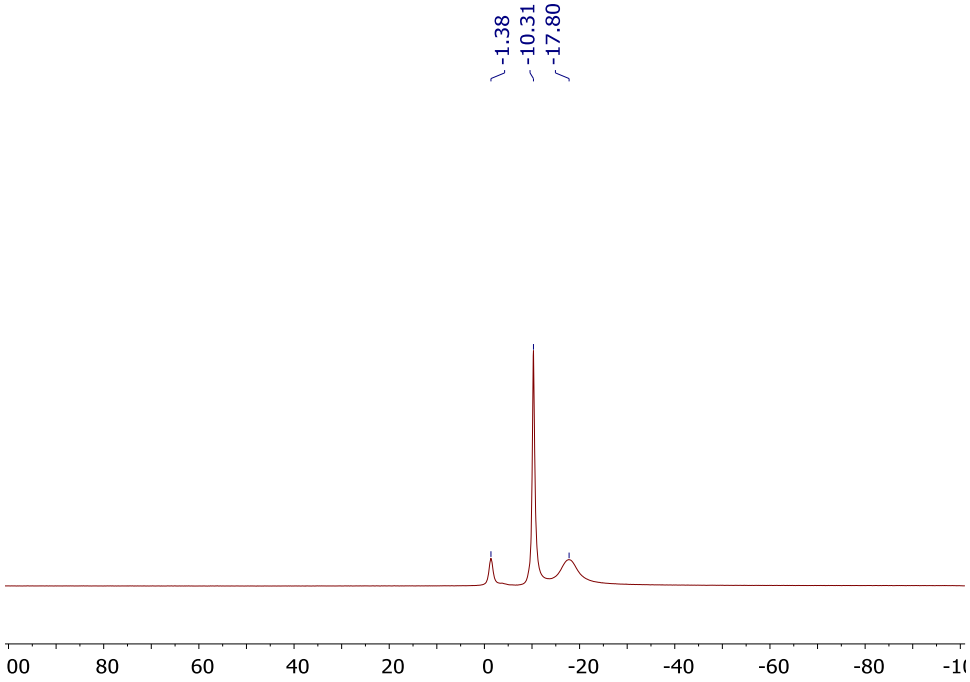

Fig. **3.33** ^{11}B NMR of **34** in CD_2Cl_2

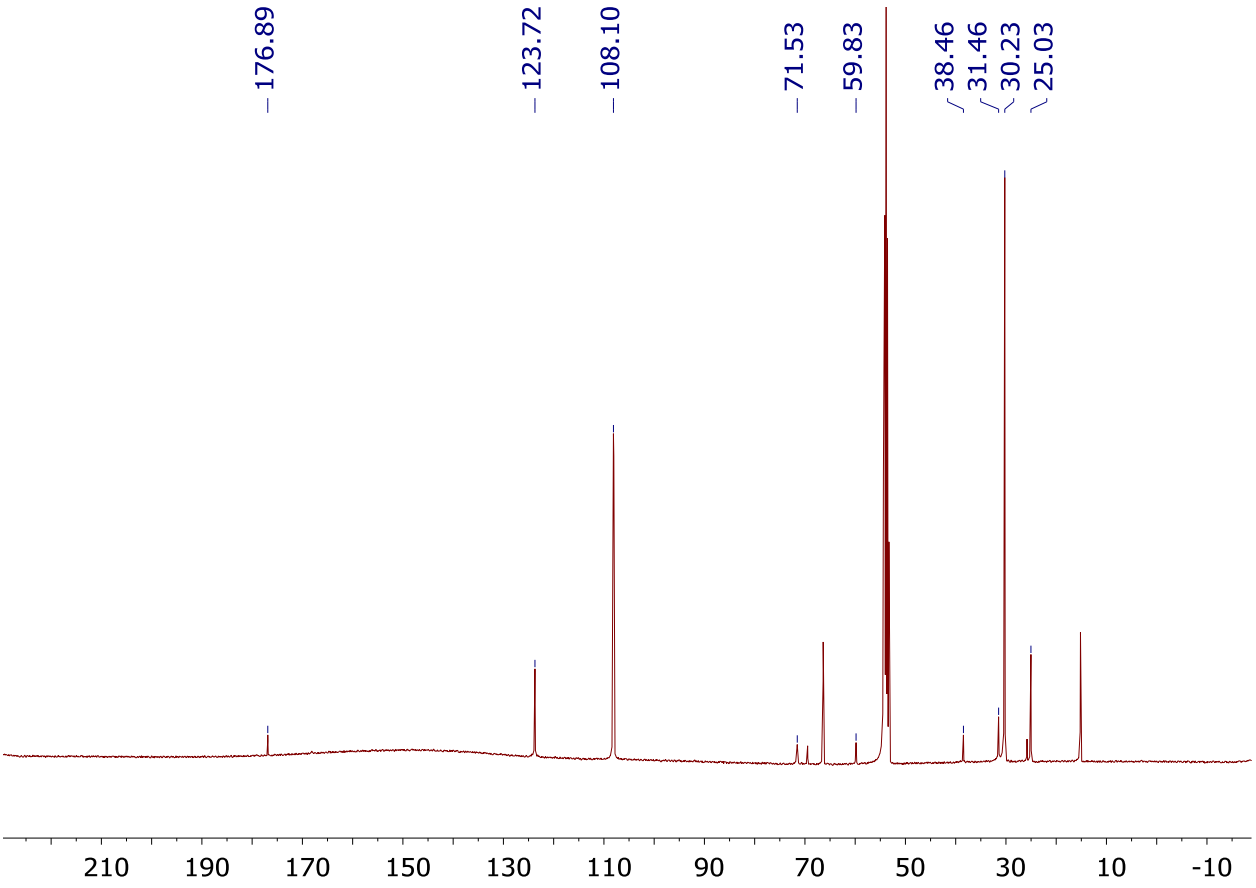

Fig. **3.34** $^{13}C[^{1}H]$ NMR of **34** in CD_2Cl_2

Synthesis of 35:

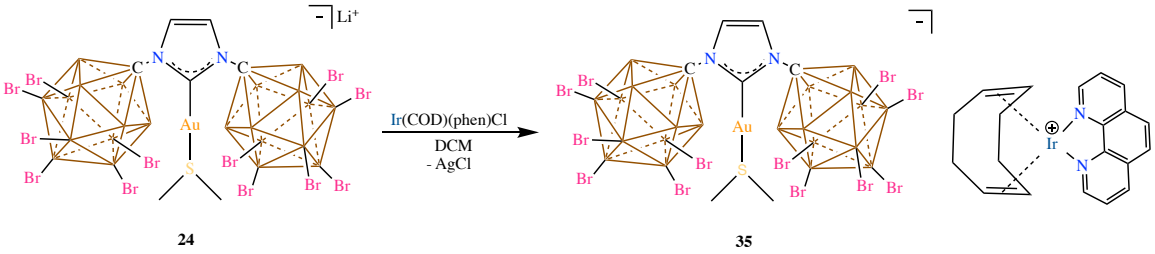

24 **35**

Scheme **3.7** Synthesis of the ion-pair **35** from **24**

In a glass vial, 50mg (0.03 mmol) of **24** was weighed and suspended in fluorobenzene (4 mL). To this, a solution of Ir(COD)(phen)Cl (15.1mg, 0.03 mmol) in fluorobenzene (4 mL) was added and the dark solution stirred for an hour. It was then filtered over celite and pumped to dryness producing **35** in 90% yield as a dark green solid. ^{1}H NMR (600 MHz, CD_2Cl_2, 25°C): 8.81 (d, 2H, CH), 8.55 (d, 2H, CH), 8.16 (s, 2H, CH), 8.08 (d, 2H, CH),

7.36 (s, 2H, CH), 4.64 (m, 4H, COD CH), 2.92 (s, 6H, SMe_2), 2.48 (m, 4H, COD CH_2), 2.10 (m, 4H, COD CH_2); $^{11}B[^1H]$ NMR (192 MHz, CD_2Cl_2, 25°C): -1.32, -10.31, -17.13; $^{13}C[^1H]$ NMR (150 MHz, CD_2Cl_2, 25°C): 176.83, 149.92, 149.36, 141.56, 131.17, 130.31, 128.59, 126.98, 124.43, 123.69, 115.37, 71.44, 25.84, 24.99 ppm.

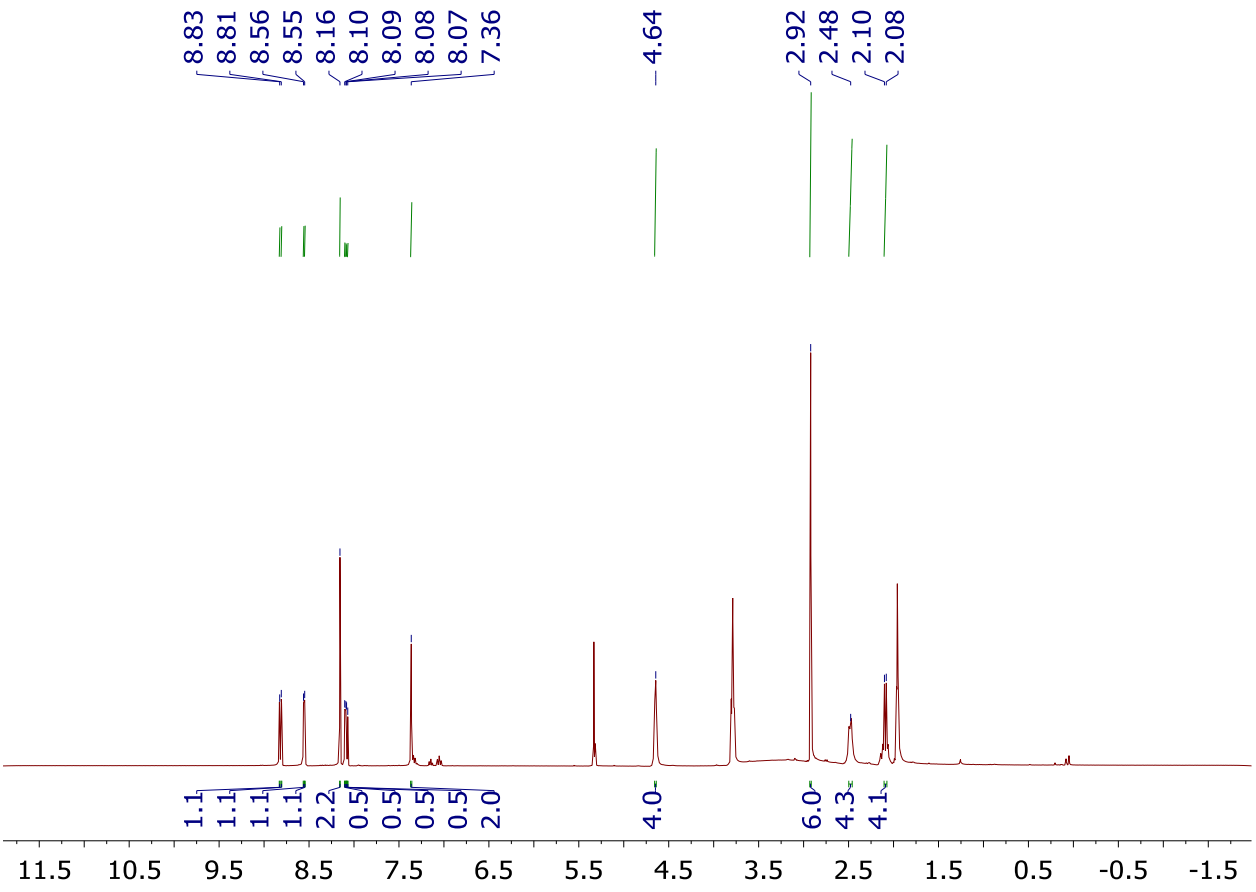

Fig. **3.35** ^1H NMR of **35** in CD_2Cl_2

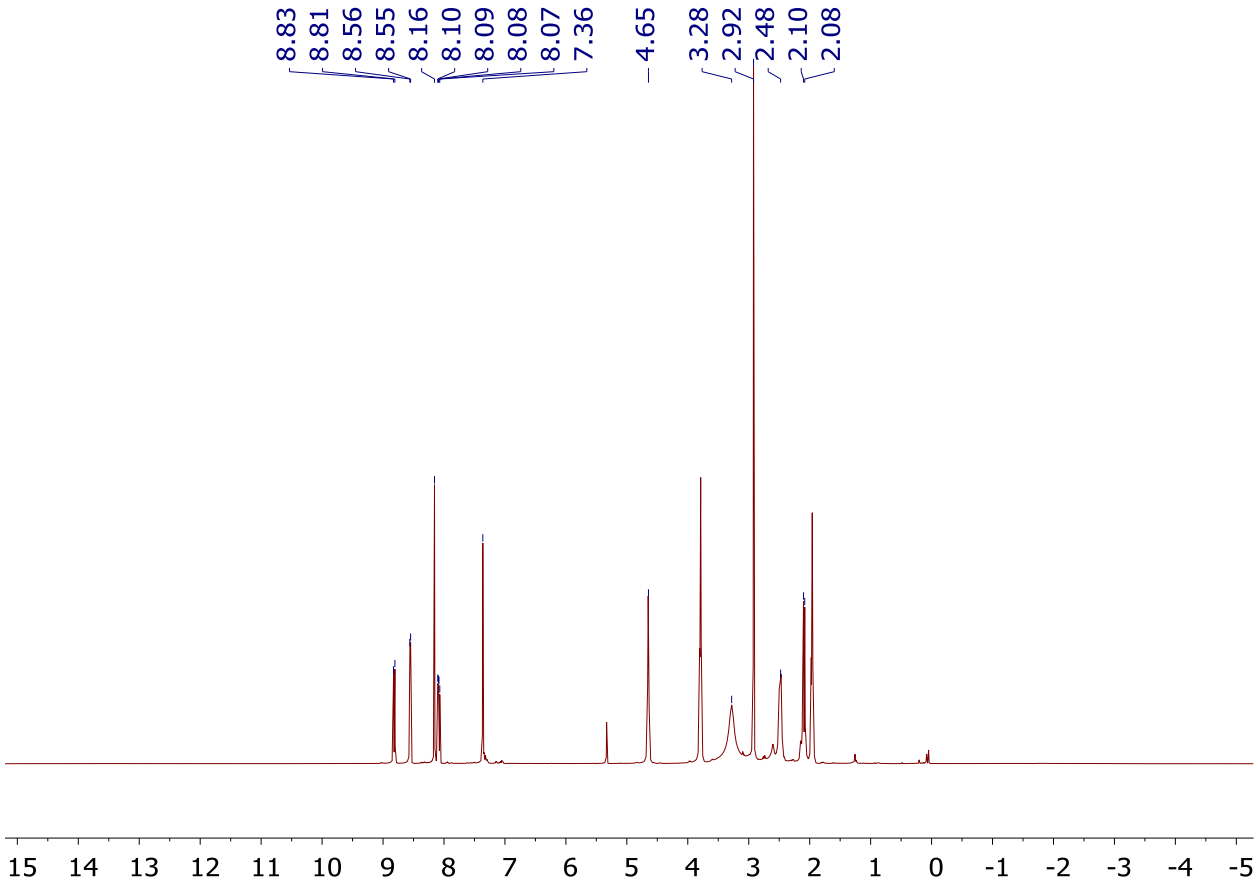

Fig. **3.36** $^{1}H[^{11}B]$ NMR of **35** in CD_2Cl_2

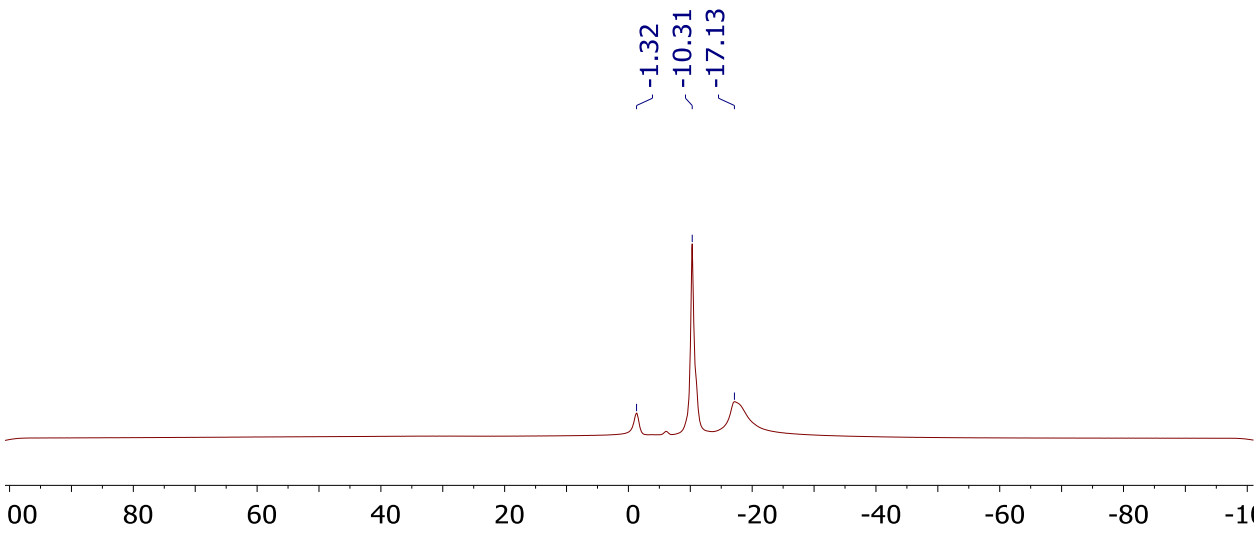

Fig. **3.37** $^{11}B[^{1}H]$ NMR of **35** in CD_2Cl_2

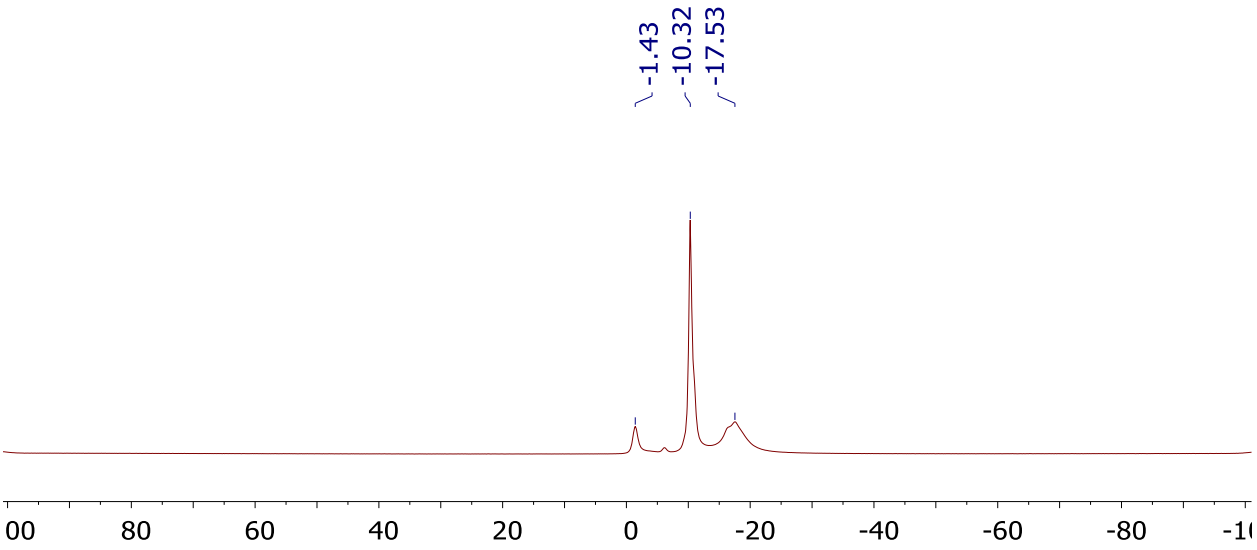

Fig. **3.38** ^{11}B NMR of **35** in CD_2Cl_2

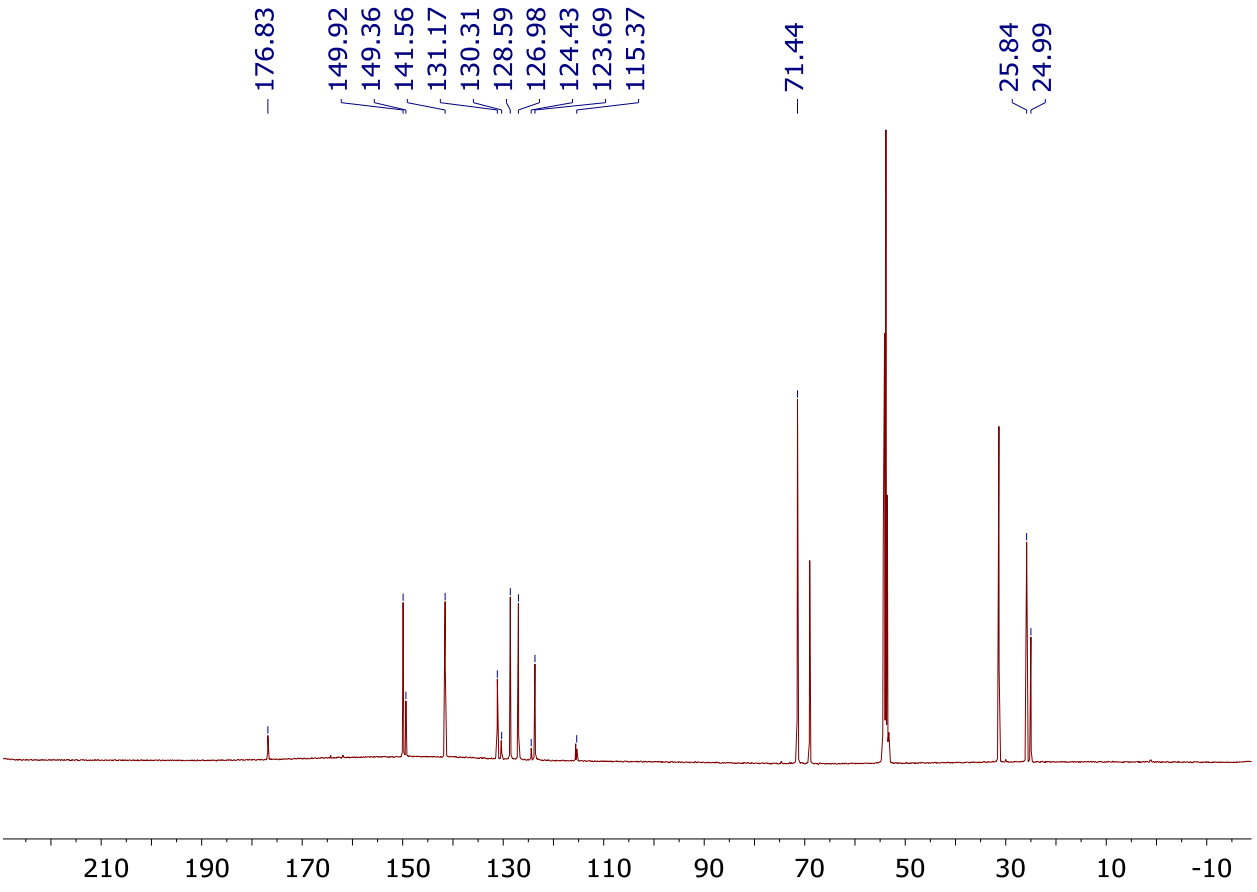

Fig. **3.39** $^{13}C[^1H]$ NMR of **35** in CD_2Cl_2

Synthesis of 36:

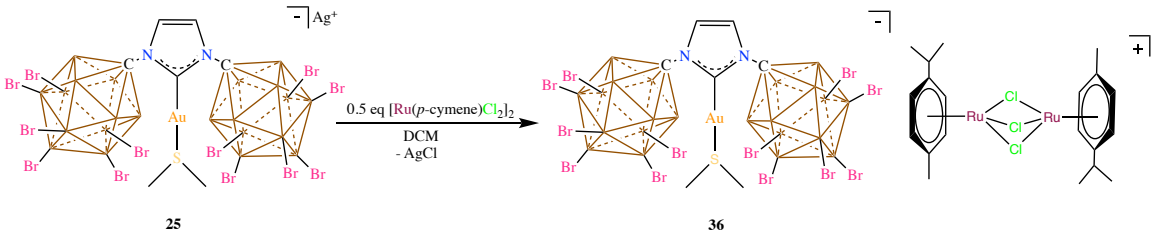

Scheme **3.8** Synthesis of the ion-pair **36** from **25**

In a vial, 50mg (0.03 mmol) of **25** was weighed and suspended in dichloromethane (3 mL). To this, a suspension of Ru(*p*-cymene)Cl_2 dimer (9.18mg, 0.015 mmol) in dichloromethane (6 mL) was added and stirred for an hour. The suspension was then filtered over celite and pumped to dryness to produce **36** as a red solid. ^{1}H NMR (600 MHz, $CDCl_3$, 25°C): 7.39 (s, 2H, CH), 5.66 (d, 4H, CH), 5.51 (d, 4H, CH), 2.97 (s, 6H, SMe_2), 2.82 (m, 2H, ^{i}Pr), 2.29 (s, 6H, methyl), 1.36 (d, 12H, ^{i}Pr); ^{11}B[^{1}H] NMR (192 MHz, $CDCl_3$, 25°C): -0.98, -10.16, -18.33 ppm. ^{13}C[^{1}H] NMR (150 MHz, $CDCl_3$, 25°C): 176.47, 123.35, 102.27, 97.32, 78.95, 31.62, 22.40, 19.28, 15.41 ppm.

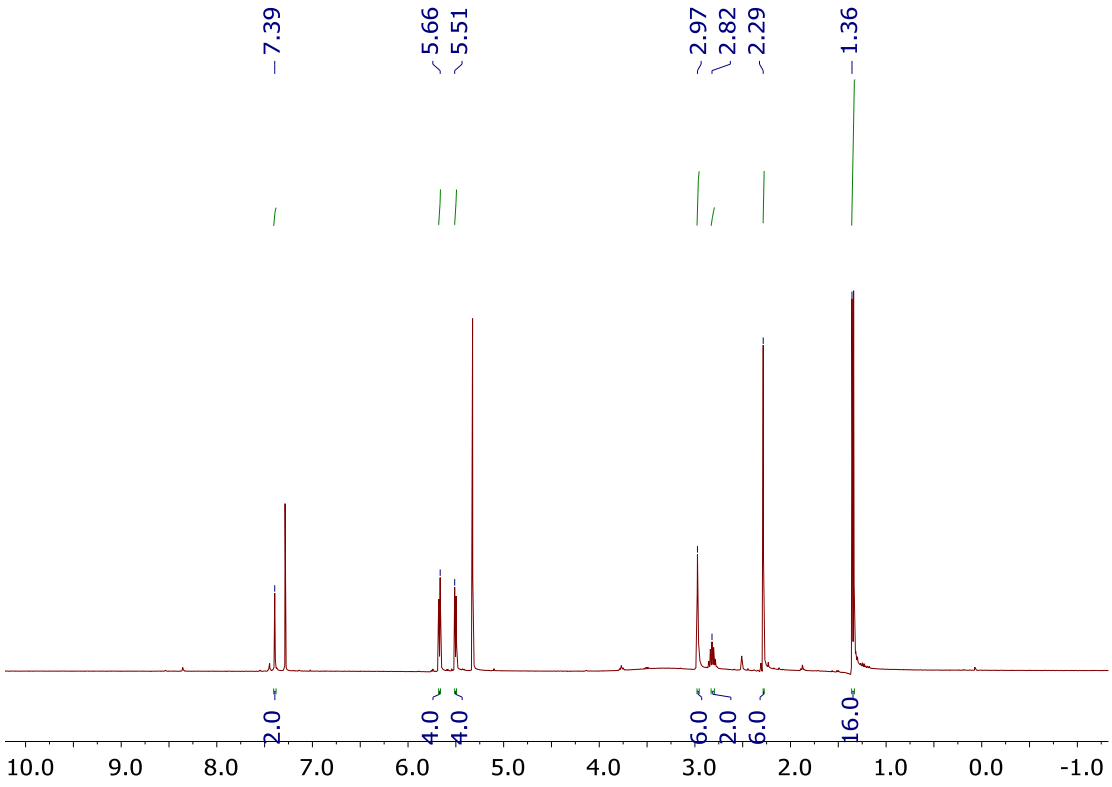

Fig. **3.40** ^{1}H NMR of **36** in $CDCl_3$

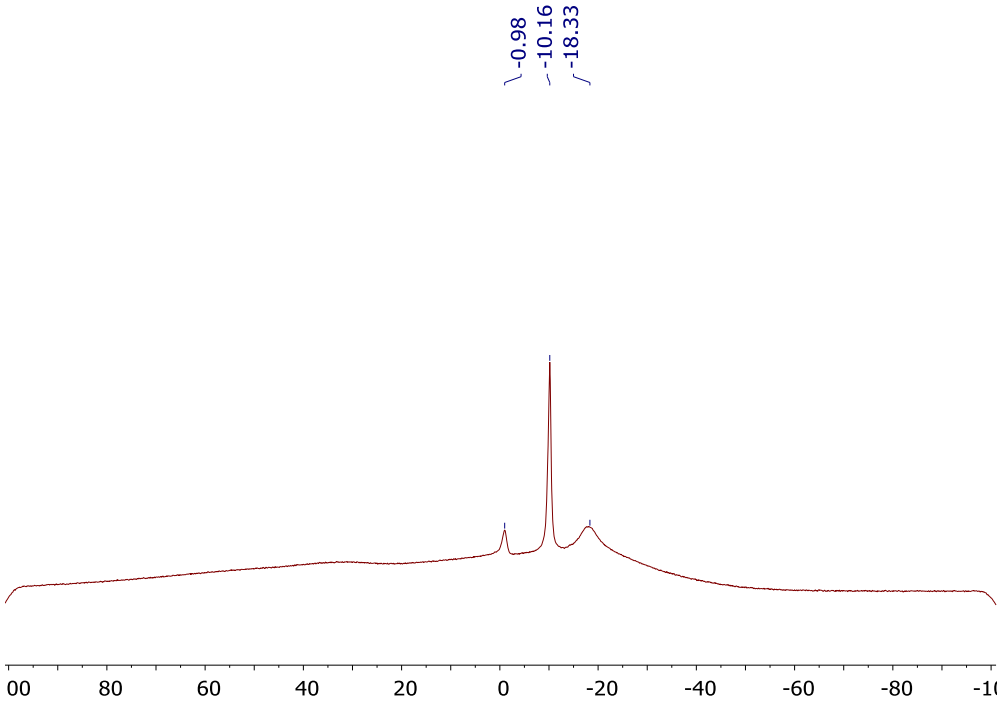

Fig. **3.41** $^{11}B[^{1}H]$ NMR of **36** in $CDCl_3$

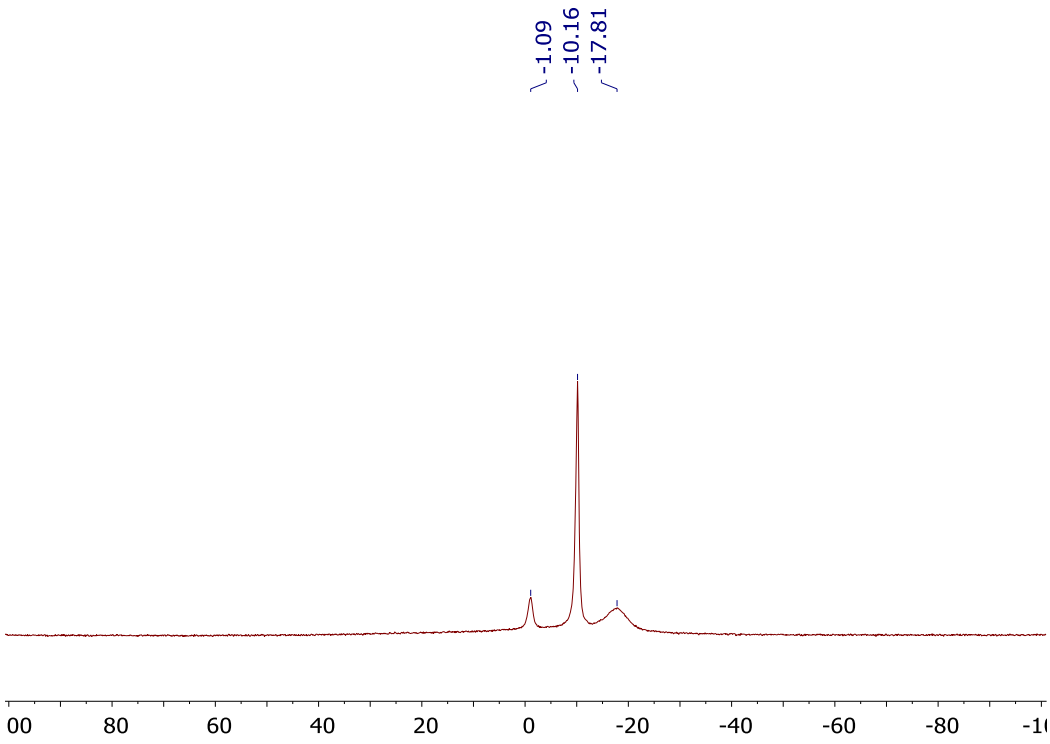

Fig. **3.42** ^{11}B NMR of **36** in $CDCl_3$

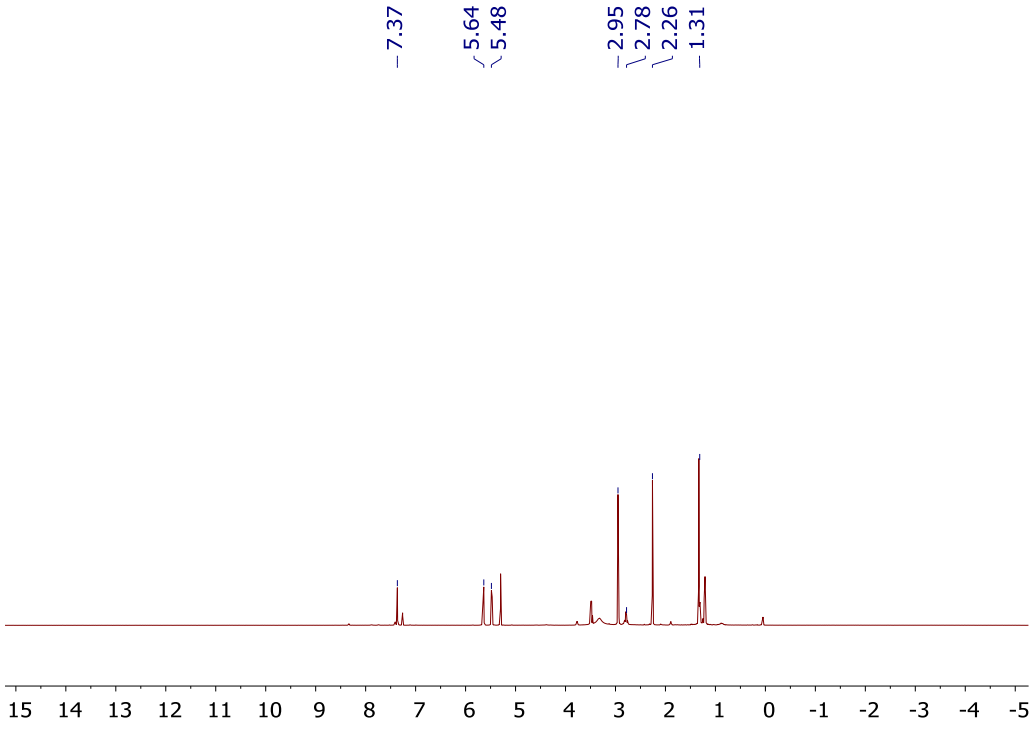

Fig. **3.43** $^{1}H[^{11}B]$ NMR of **36** in $CDCl_3$

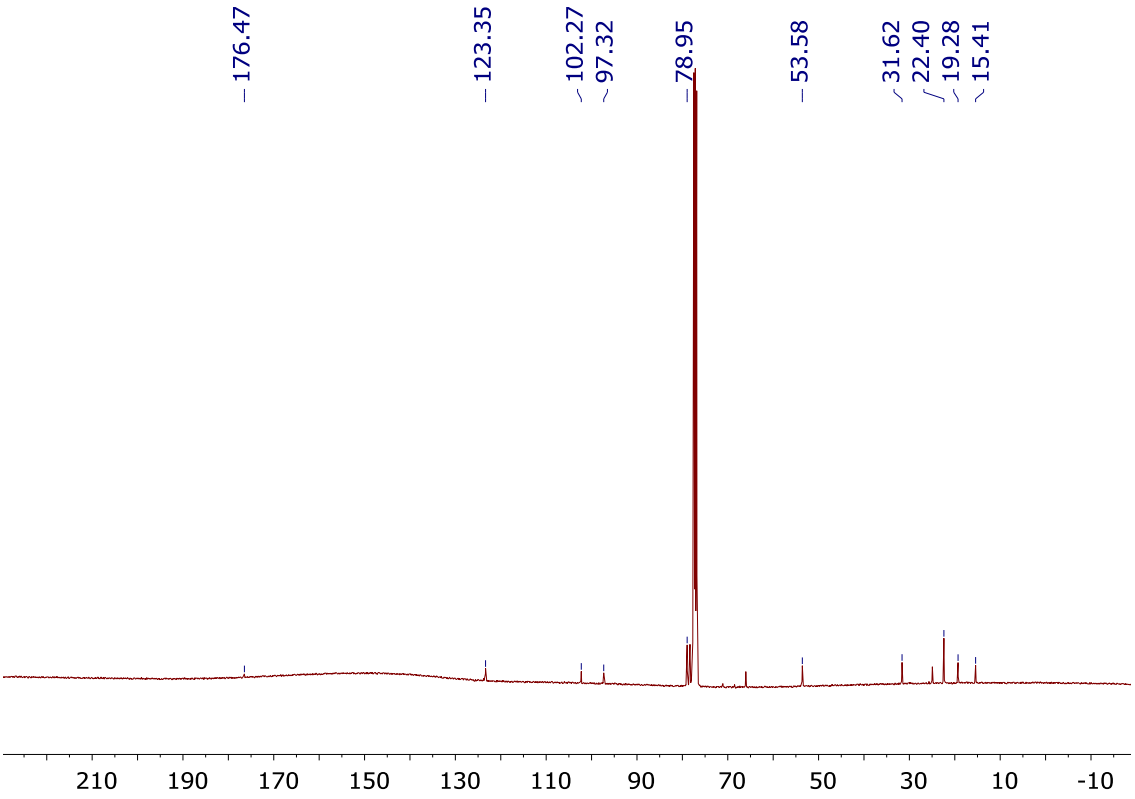

Fig. **3.44** $^{13}C[^{1}H]$ NMR of **36** in $CDCl_3$

Synthesis of 37:

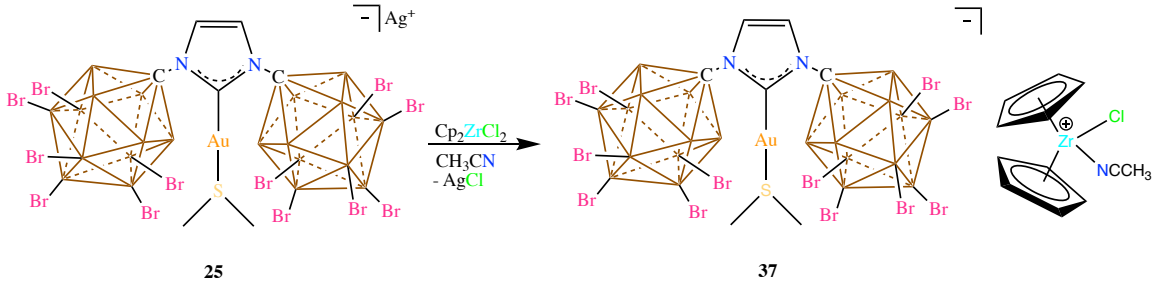

Scheme **3.9** Synthesis of the ion-pair **37** from **25**

In a vial, 50mg (0.03 mmol) of **25** was loaded and dissolved in acetonitrile (3 mL). To this, a solution of Cp_2ZrCl_2 (8.77mg, 0.03 mmol) in acetonitrile (3 mL) was added and stirred for an hour. The solution was then filtered over celite and pumped to dryness under vacuum affording **37** as a bright yellow solid in 90% yield. ^{1}H NMR (400 MHz, CD_2Cl_2, 25°C): 7.37 (s, 2H, CH), 6.48 (s, 10H, Cp), 2.92 (s, 6H, SMe_2), 2.02 (s, 3H, CH_3CN); $^{11}B[^{1}H]$

NMR (128 MHz, CD_2Cl_2, 25°C): -1.33, -10.27, -17.81; $^{13}C[^1H]$ NMR (100 MHz, CD_2Cl_2, 25°C): 176.92, 123.72, 117.59, 116.46, 71.92, 25.01, 2.26 ppm.

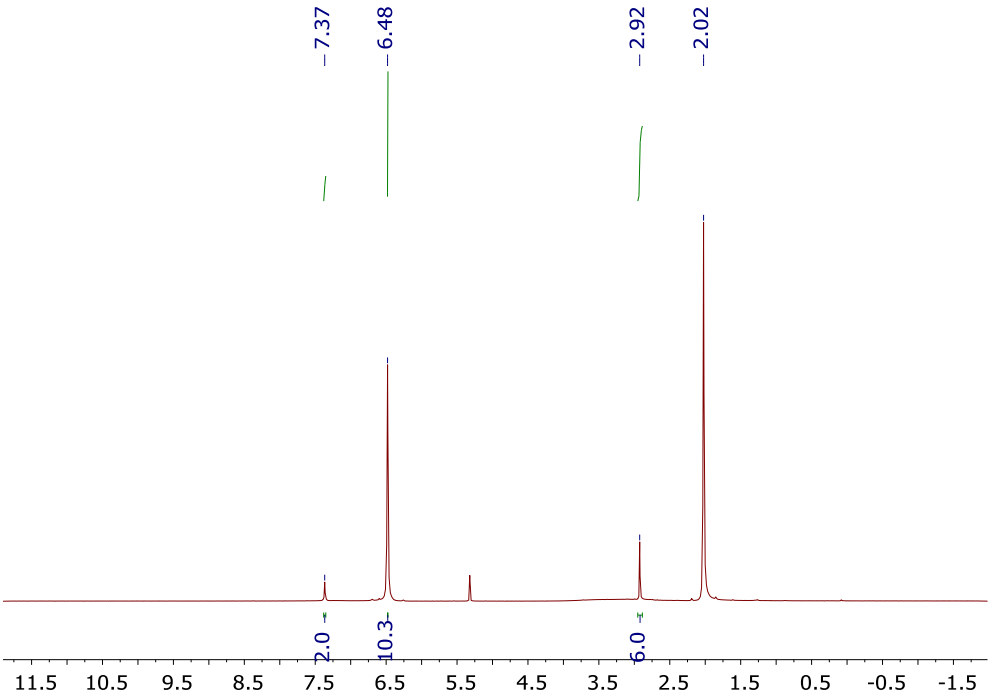

Fig. **3.45** ^1H NMR of **37** in CD_2Cl_2

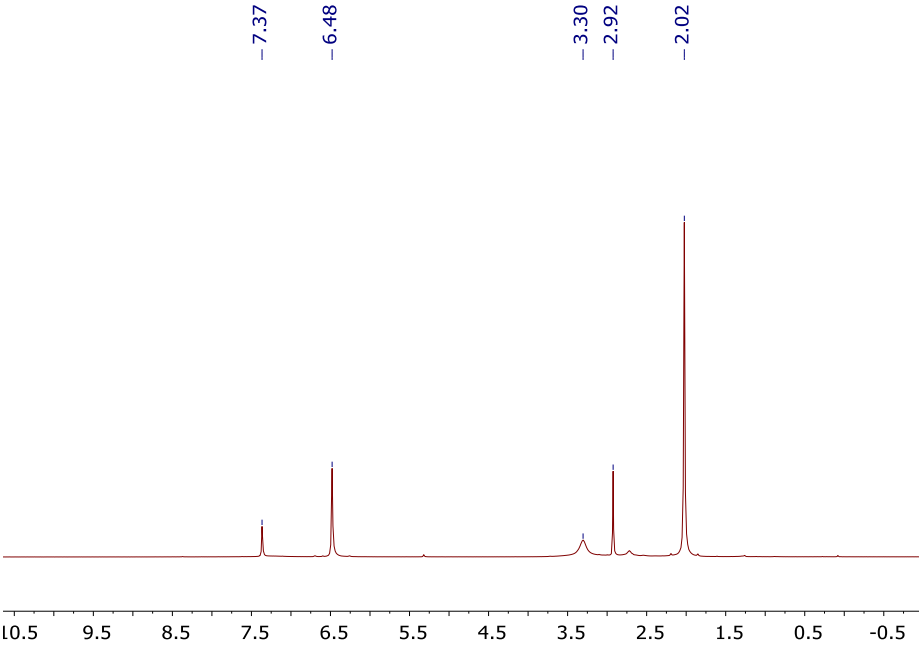

Fig. **3.46** $^1H[^{11}B]$ NMR of **37** in CD_2Cl_2

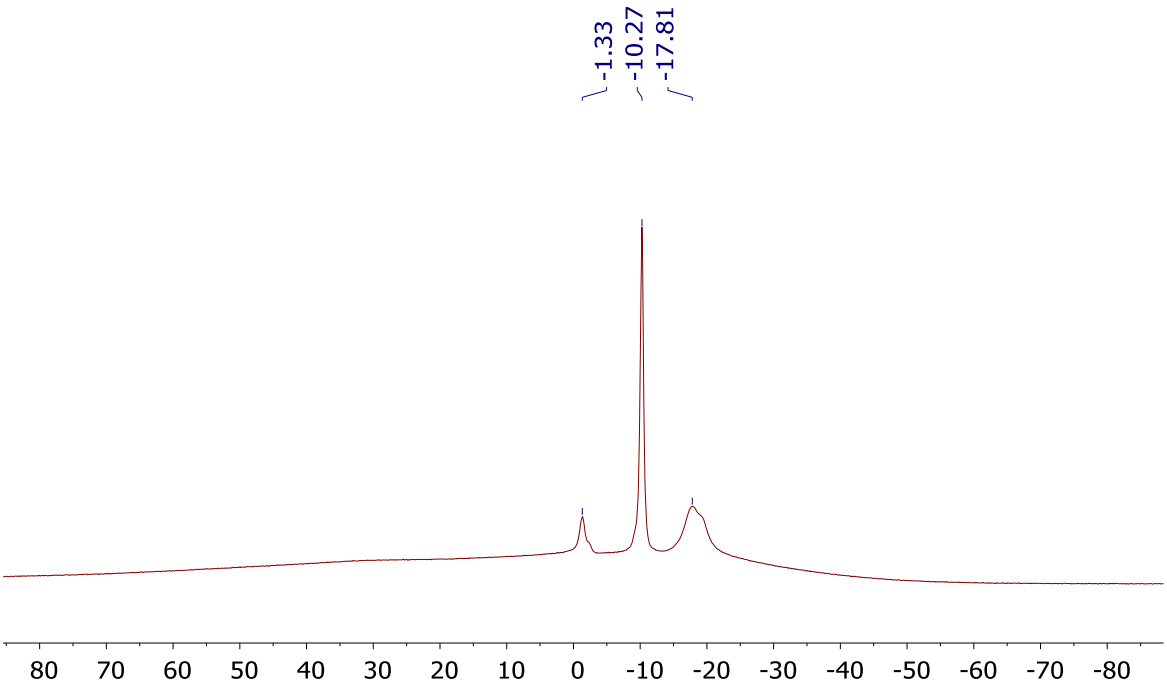

Fig. **3.47** $^{11}B[^{1}H]$ NMR of **37** in CD_2Cl_2

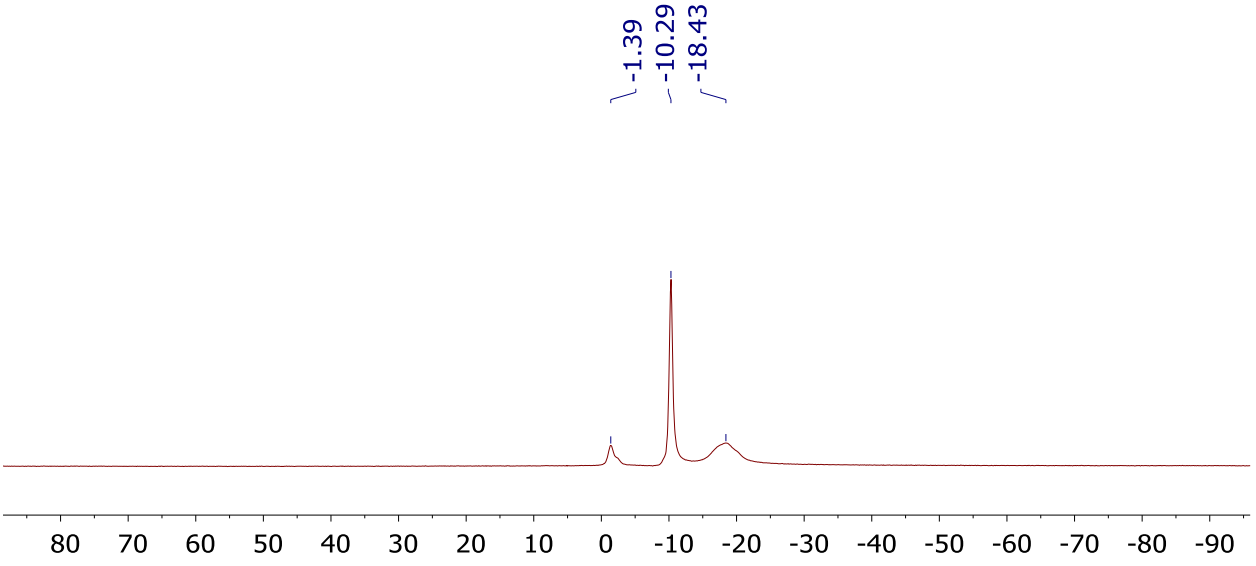

Fig. **3.48** ^{11}B NMR of **37** in CD_2Cl_2

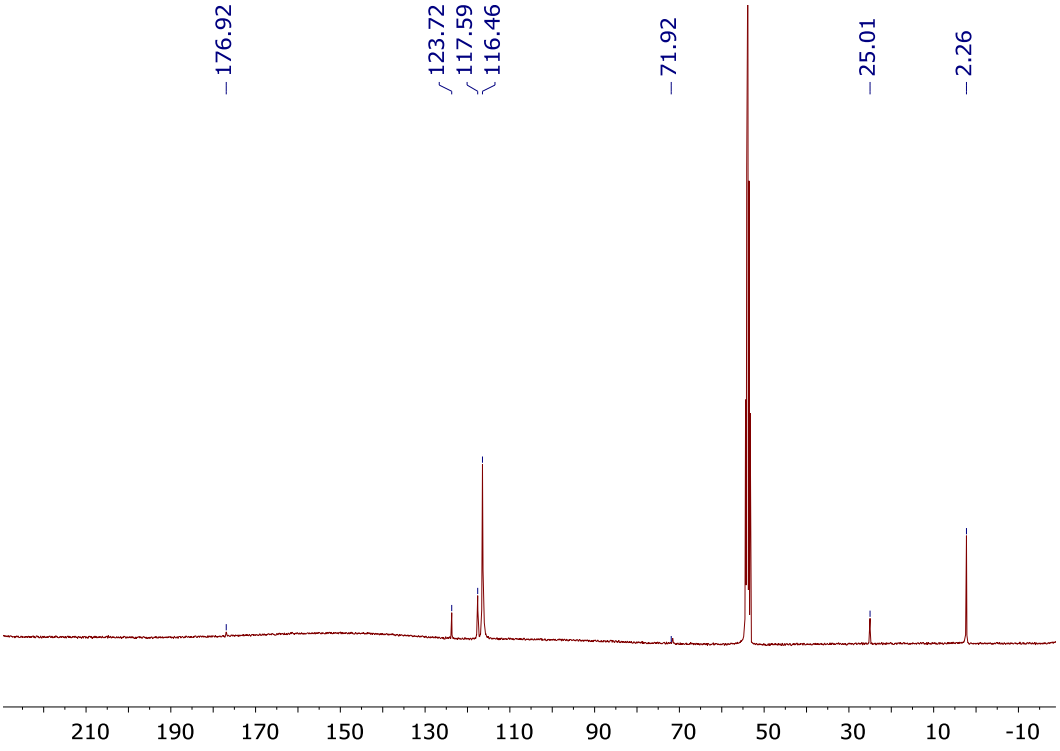

Fig. **3.49** $^{13}C[^{1}H]$ NMR of **37** in CD_2Cl_2

Synthesis of 39:

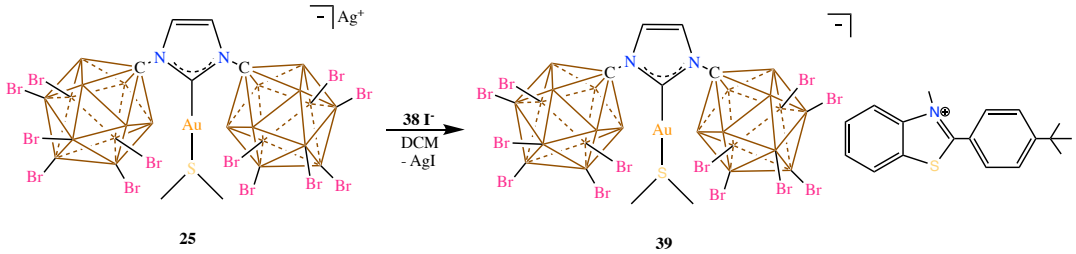

Scheme **3.16** Synthesis of the ion-pair **39** from **25**

The N-methyl benzothiazolium iodide precursor was synthesized as mentioned in the literature using 2-aminothiophenol and p-*t* butyl benzaldehyde. The crude reaction mixture after stirring for 2 days was dissolved in hot ethanol and allowed to cool to recrystallize the product. The obtained clean product was then vacuum dried at 60°C overnight and brought into the glove box. 11.45mg (0.028 mmol) was then weighed in a glass vial and dissolved in 3 mL dichloromethane. This was then transferred to a vial containing 50mg (0.028 mmol) of **25** suspended in 5 mL dichloromethane. The suspension was then stirred

for an hour and filtered over celite. The solution was then pumped under vacuum to afford clean **39** as a pale brown powder in 95% yield. ^{1}H NMR (600 MHz, CD_2Cl_2, 25°C): 8.26 (d, 1H, CH), 8.14 (d, 1H, CH), 8.03 (m, 1H, CH), 7.92 (m, 1H, CH), 7.78 (m, 4H, CH), 7.36 (s, 2H, CH), 4.41 (s, 3H, methyl), 2.92 (s, 6H, SMe_2), 1.42 (s, 9H, *t*-butyl); ^{11}B[^{1}H] NMR (192 MHz, CD_2Cl_2, 25°C): -1.24, -10.16, -17.58; ^{13}C[^{1}H] NMR (150 MHz, CD_2Cl_2, 25°C): 176.89, 160.08, 142.46, 131.55, 130.56, 130.32, 129.60, 128.10, 124.43, 123.71, 121.72, 117.53, 71.52, 39.04, 35.96, 31.09, 24.99 ppm.

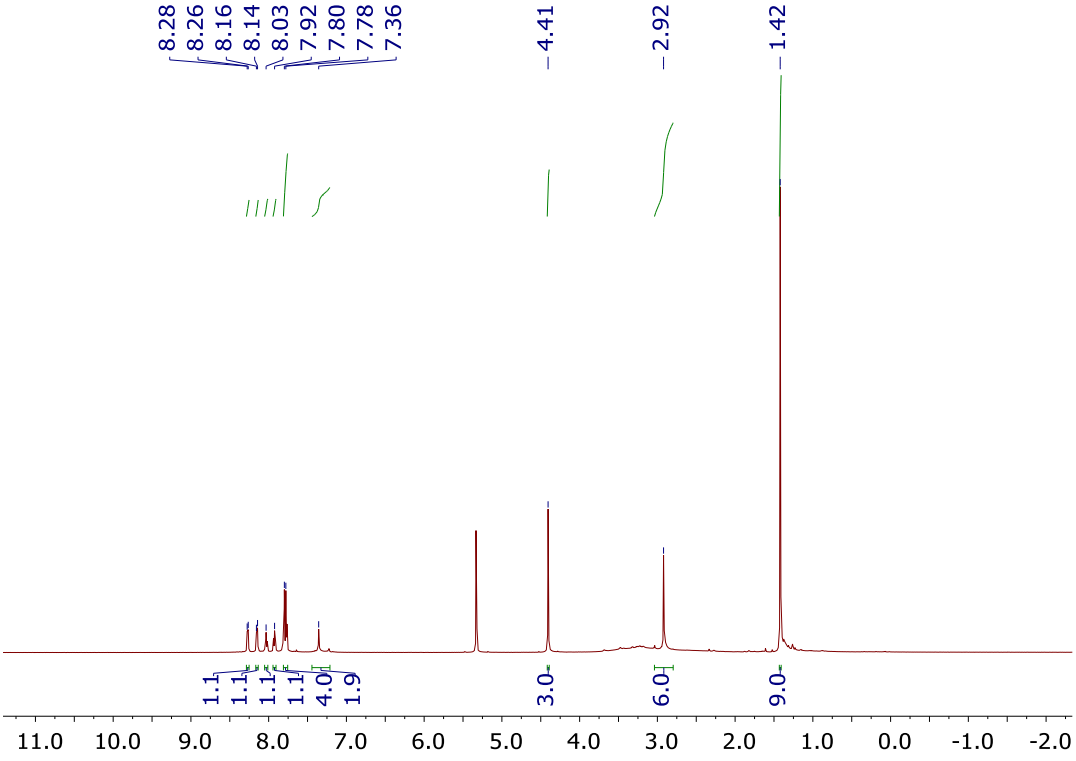

Fig. **3.50** ^{1}H NMR of **39** in CD_2Cl_2

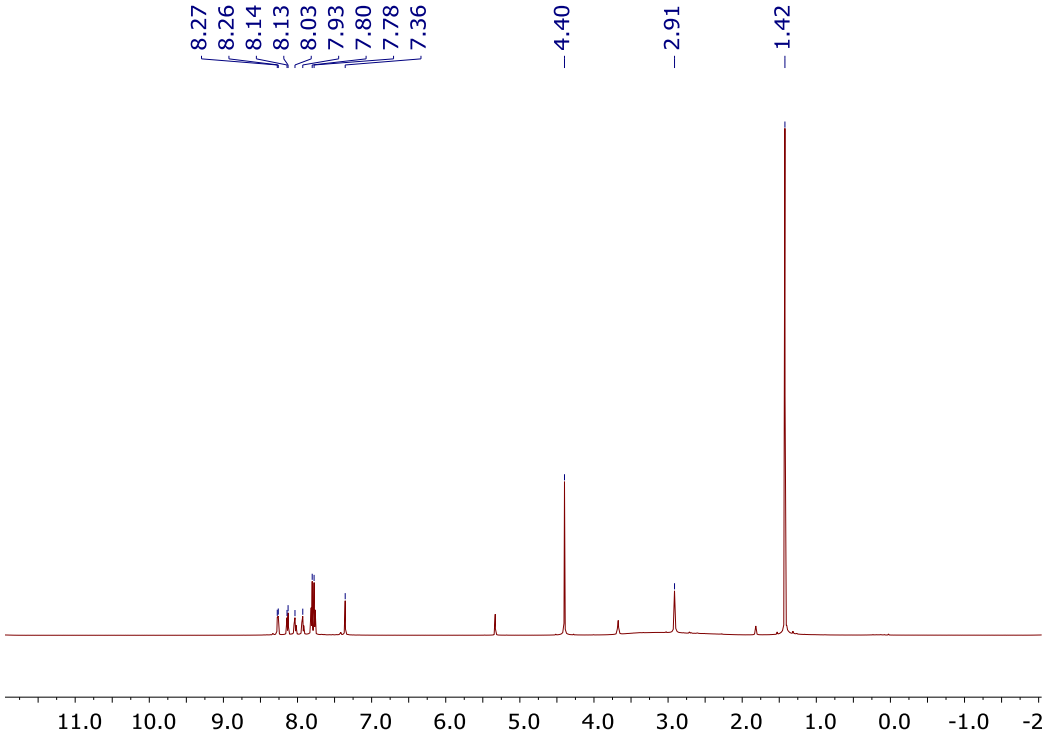

Fig. **3.51** $^{1}H[^{11}B]$ NMR of **39** in CD_2Cl_2

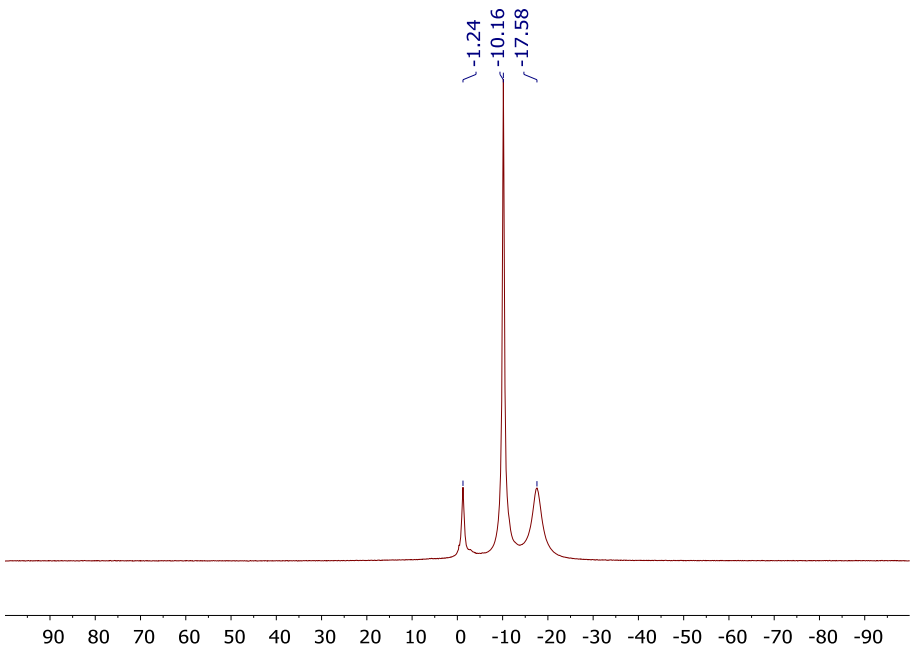

Fig. **3.52** $^{11}B[^{1}H]$ NMR of **39** in CD_2Cl_2

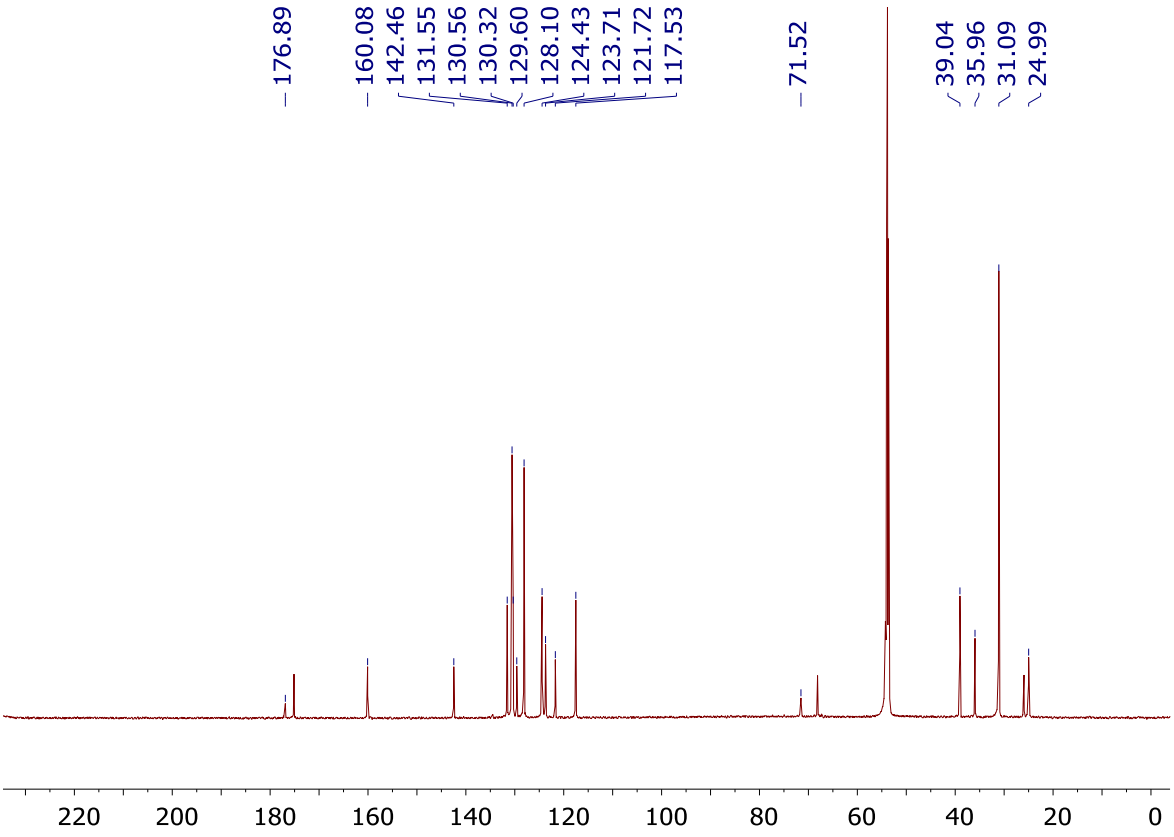

Fig. **3.53** $^{13}C[^{1}H]$ NMR of **39** in CD_2Cl_2

Synthesis of 40:

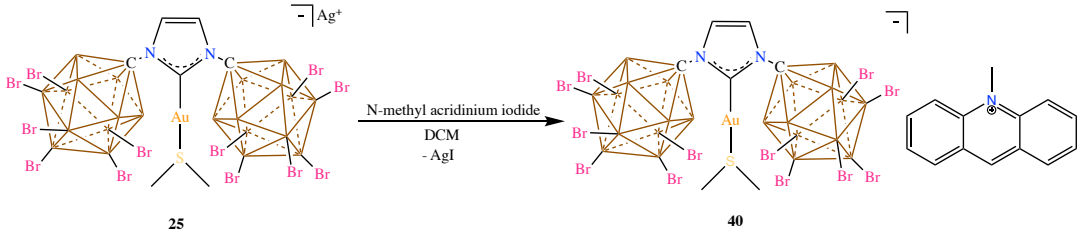

Scheme **3.17** Synthesis of the ion-pair **40** from **25**

The N-methyl acridinium iodide precursor was synthesized as per literature method by treating acridine with methyl iodide and filtering the crude. The crude product was then dissolved in hot ethanol and allowed to cool to produce the clean product as dark red crystals. This product was heated at 60°C overnight under vacuum and brought inside the glove box. 17.98mg (0.056 mmol) of the compound was then weighed in a glass vial and suspended in 7 mL dichloromethane. This was then transferred to a vial containing 100mg

(0.056 mmol) of **25** and stirred for an hour. The suspension was then filtered and pumped down to dryness under vacuum to afford clean **40** as a bright yellow powder in 90% yield. ^{1}H NMR (600 MHz, CD_2Cl_2, 25°C): 9.76 (s, 1H, CH), 8.54 (d, 2H, CH), 8.48 (s, 4H, CH), 8.06 (t, 2H, CH), 7.36 (s, 2H, CH), 4.87 (s, 3H, methyl), 2.88 (s, 6H, SMe_2); ^{11}B[^{1}H] NMR (192 MHz, CD_2Cl_2, 25°C): -1.21, -10.30, -17.50; ^{13}C[^{1}H] NMR (150 MHz, CD_2Cl_2, 25°C): 176.93, 151.14, 141.93, 140.86, 132.58, 129.07, 126.99, 123.71, 118.04, 71.56, 39.07 ppm.

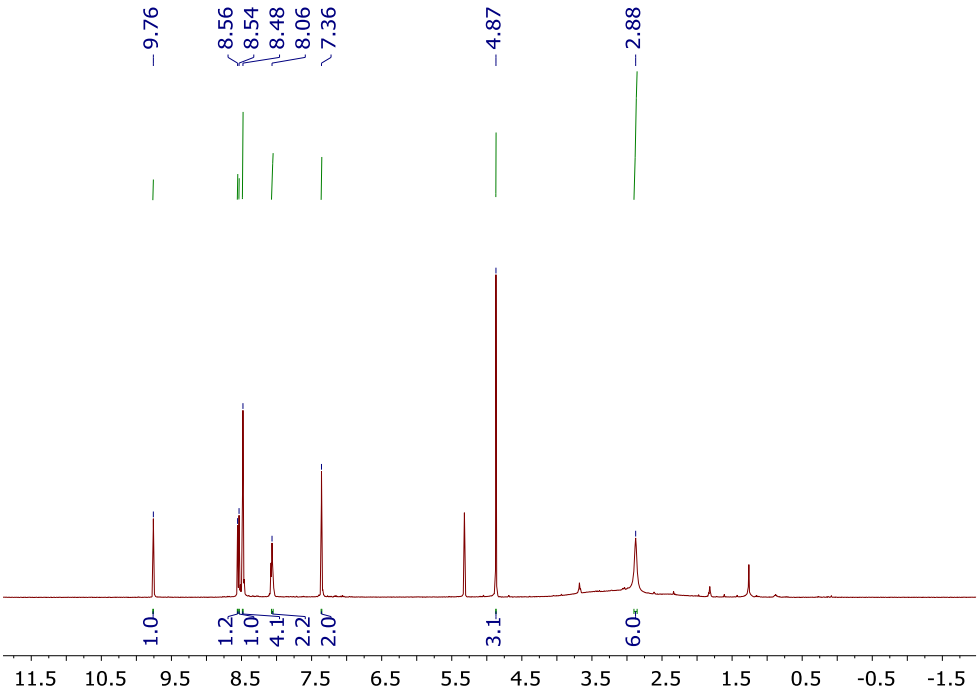

Fig. **3.54** ^{1}H NMR of **40** in CD_2Cl_2

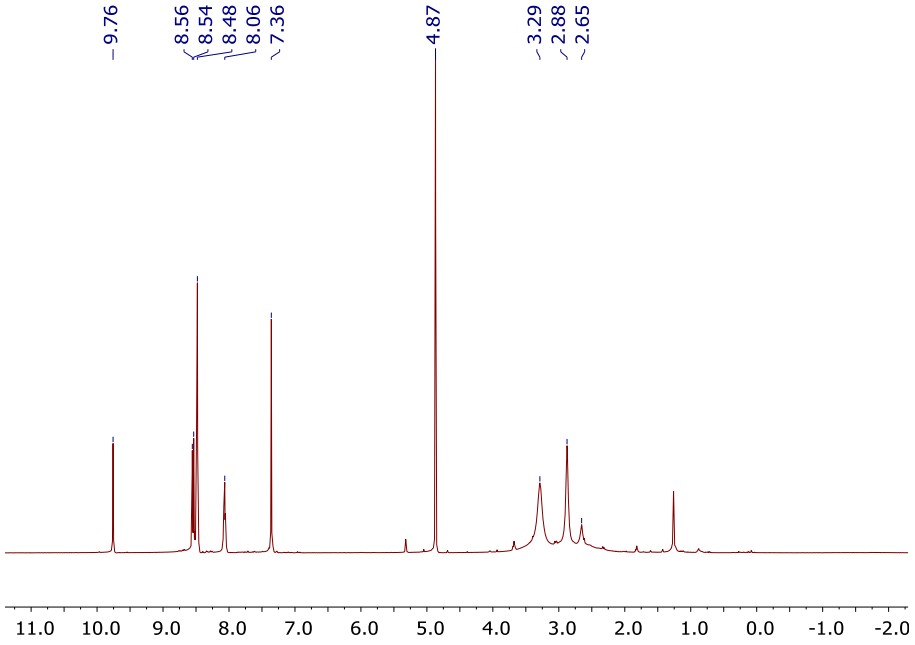

Fig. **3.55** $^{1}H[^{11}B]$ NMR of **40** in CD_2Cl_2

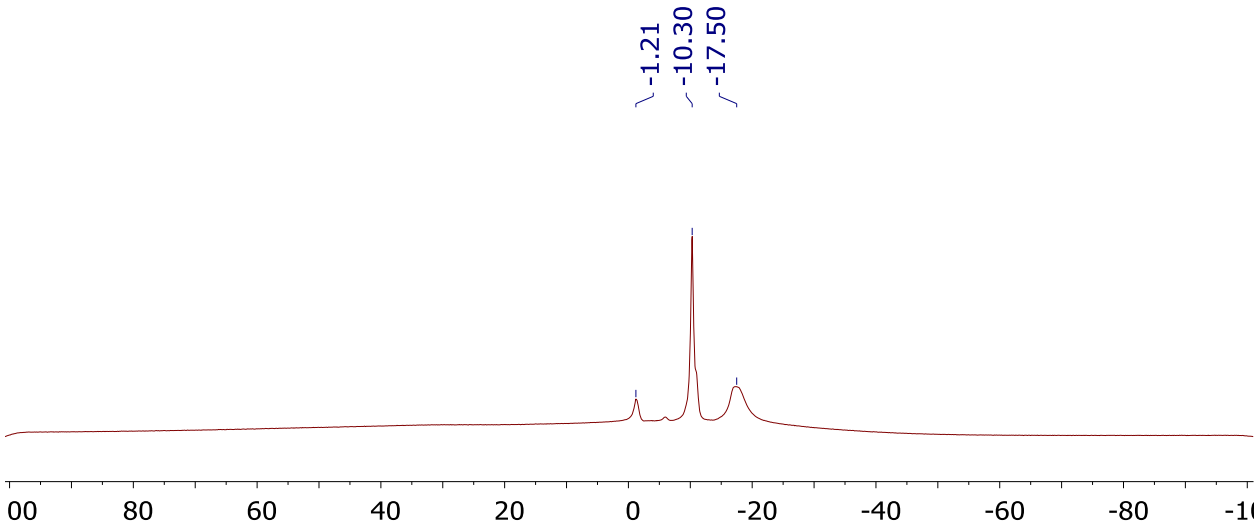

Fig. **3.56** $^{11}B[^{1}H]$ NMR of **40** in CD_2Cl_2

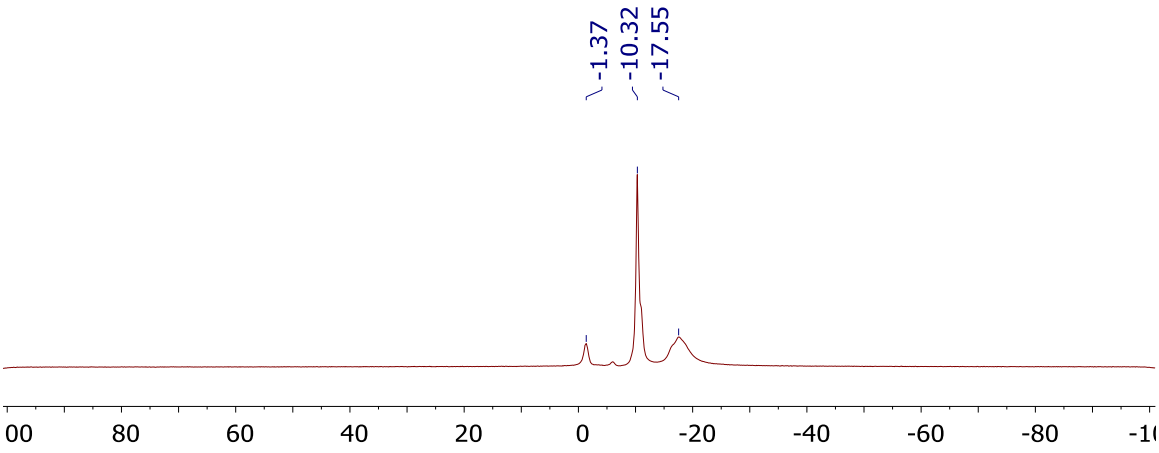

Fig. **3.57** ^{11}B NMR of **40** in CD_2Cl_2

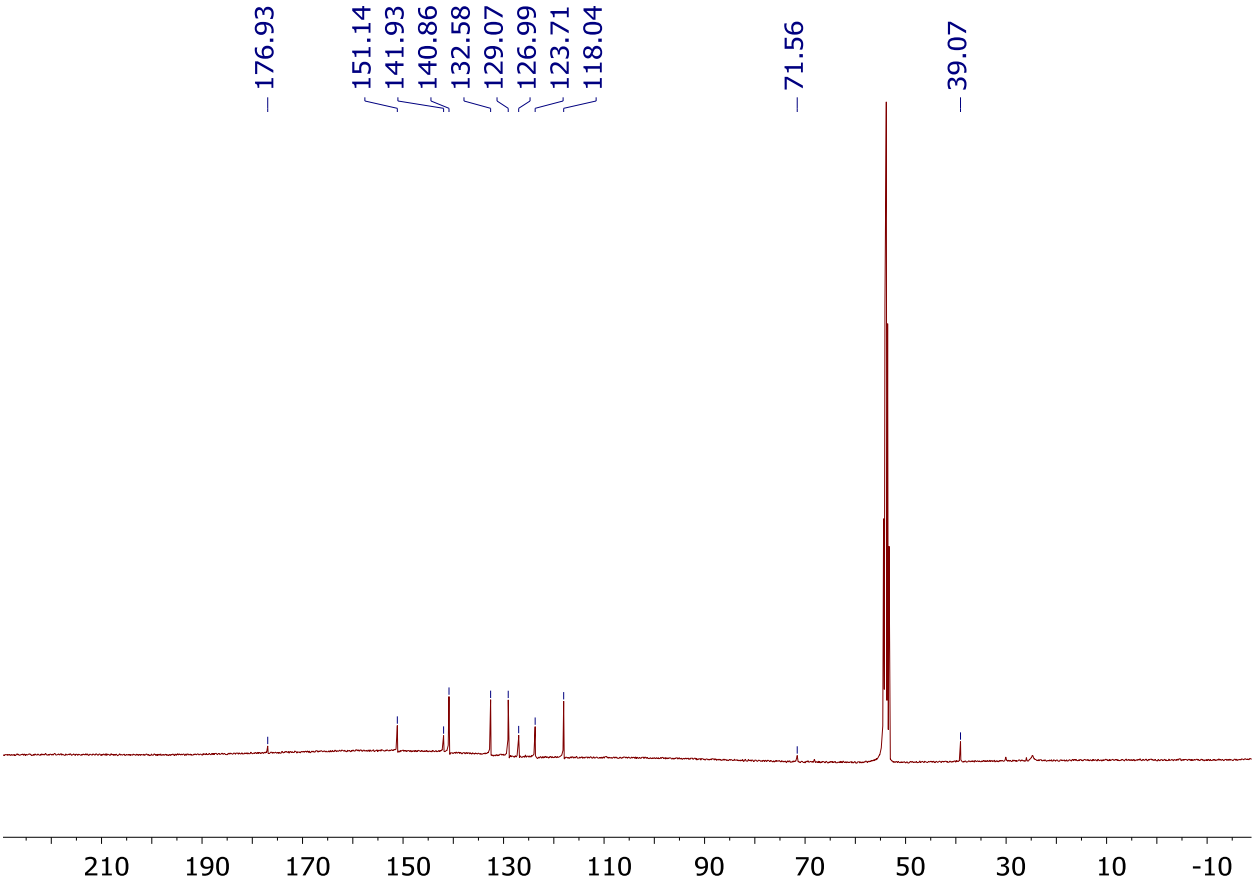

Fig. **3.58** $^{13}C[^1H]$ NMR of **40** in CD_2Cl_2

General Protocol for Tandem Catalysis:

The required amount of the catalyst was weighed in a vial inside the glovebox. The vial was then brought outside; to this, 0.165 mmol (1 eq) of the amine, 0.21 mmol (1.3 eq) alkyne and 0.33 mmol (2 eq) triethylsilane were added. The mixture was then dissolved in ethanol and transferred to a 10 mL Teflon Schlenk and heated at 80°C in an oil bath for about 24h. The volatiles were then evaporated under vacuum and the oily crude was dissolved in $CDCl_3$ with 0.5mg durene as an internal standard for ^1H NMR analysis. The percent yield of the final secondary amine product was calculated from the relative integrals on the ^1H NMR.

Indole Functionalization Catalysis:

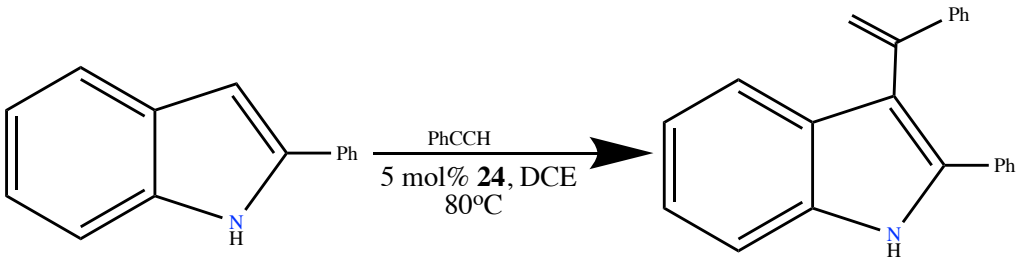

Scheme **3.10** Catalytic functionalisation of 2-phenyl indole

11.5mg (0.00645 mmol) of **24** was weighed in a glass vial inside the glove box and dissolved in dry 1,2-dichloroethane (3 mL). To the solution, 25mg of 2-phenyl indole (0.129 mmol) and 0.043 mL phenylacetylene were added. The solution was then transferred to a 10 mL Teflon schlenk flask and heated to 80°C overnight in an oil bath. The reaction was then cooled to room temperature and the volatiles were pumped down under vacuum. The reaction conversion was then measured based on the relative integrals on the ^1H NMR spectrum in $CDCl_3$.

Propargyl Amide Cyclization Catalysis:

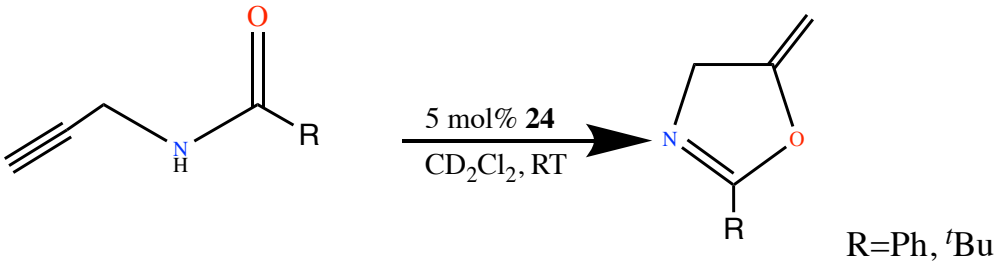

Scheme **3.11** Catalytic Cyclization of Propargyl Amides

25mg (0.17 mmol) of the propargyl amide shown in the scheme (R= ^{t}Bu) was weighed in a glass vial. To this, 15.1mg (0.0085 mmol) of **24** was added and the solids were dissolved in CD_2Cl_2. The solution was then transferred to an NMR tube and the reaction was monitored periodically using ^{1}H NMR. The percent conversion was calculated using relative integrals of the product vs the reactants on the ^{1}H NMR.

Crystal Structure Determination

X-Ray Structure of **29**:

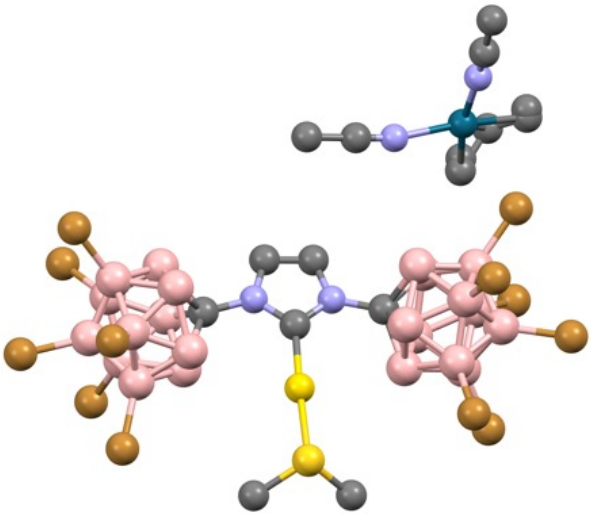

Fig. **3.1** X-Ray Structure of ion-pair **29.** Hydrogen atoms omitted for clarity. N=Blue, C=grey, B=pink, Br=Brown, Au=gold, S=yellow, Pd=ocean blue

Diffraction data were collected on a Bruker D8 Venture Duo diffractometer with a Bruker Photon III CPAD detector using Mo K_α radiation (λ = 0.71073 Å) from an IμS micro-source. Data were collected at 100 K by performing 0.5° φ- and ω-scans, integrated using SAINT[1], and scaled using SADABS[2]. The structure was solved by dual-space methods using SHELXT[3] and refined against F^2 on all data by full-matrix least squares with SHELXL-2018/3[4] following established refinement strategies[5]. All non-hydrogen atoms were refined anisotropically, and all hydrogen atoms were included into the model at geometrically calculated positions and refined using a riding model. The isotropic displacement parameters of all hydrogen atoms were fixed to 1.2 times the U value of the atoms they are linked to (1.5 times for methyl groups). Crystal and data quality details, as well as a summary of the residual refinement values, are listed in the accompanying table.

Compound **vl360vt** crystallizes in the triclinic centrosymmetric space group *P-1* with one molecule of **vl360vt**, which consists of a cationic palladium moiety and an anionic gold moiety, and one molecule of dichloromethane per asymmetric unit.

The palladium-bound allyl ligand exhibited positional disorder that was modeled over two positions; the disorder ratio was refined freely and converged at 89:11. This disorder was modeled with the help of similarity restraints on 1,2- and 1,3- distances as well as similarity and rigid bond restraints for anisotropic displacement parameters. The anisotropic displacement parameters of the major and minor disorder components were constrained to be equivalent for two nearly-overlapping major/minor carbon positions of the disordered allyl group.

The SQUEEZE[6] program within the PLATON[7] suite was used to address a solvent channel containing heavily disordered molecules of dichloromethane; a model that includes two positions of this dichloromethane molecule (vl360vt_dichloromethane) is available for perusal.

References

[1] SAINT, version 8.40, Bruker (2019), Bruker AXS Inc., Madison, Wisconsin, USA.

[2] SADABS, version 2016/2, Bruker (2016), Bruker AXS Inc., Madison, Wisconsin, USA.

[3] Sheldrick, G. M., *Acta Cryst.* **2015**, *A71*, 3-8.

[4] Sheldrick, G. M., *Acta Cryst.* **2015**, *C71*, 3-8.

[5] Müller, P. *Crystallography Reviews* **2009**, *15*, 57-83.

[6] van der Sluis, P. & Spek, A. L., *Acta Cryst.* **1990**, *A46*, 194-201.

[7] Spek, A. L. *Acta Cryst.* **2009**, *D65*, 148-155.

Table 3.2 Crystal data and structure refinement for ion-pair **29**

Identification code	vl360vt_sq
Empirical formula	C15 H31 Au B22 Br12 Cl2 N4 Pd S
Formula weight	1870.50
Temperature	100(2) K
Wavelength	0.71073 Å
Crystal system	Triclinic
Space group	P-1
Unit cell dimensions	a = 9.8721(4) Å α = 70.9905(14)°.
	b = 16.1769(6) Å β = 84.6499(17)°.
	c = 17.6763(7) Å γ = 85.7517(14)°.

Volume 2654.46(18) Å3

Z 2

Density (calculated) 2.340 Mg/m3

Absorption coefficient 12.294 mm-1

F(000) 1708

Crystal color colourless

Crystal size 0.172 x 0.160 x 0.059 mm3

Theta range for data collection 2.074 to 32.032°

Index ranges -14 <= *h* <= 14, -24 <= *k* <= 24, -26 <= *l* <= 26

Reflections collected 215930

Independent reflections 18487 [R(int) = 0.0418]

Completeness to theta = 25.242° 100.0 %

Absorption correction Semi-empirical from equivalents

Refinement method Full-matrix least-squares on F2

Data / restraints / parameters 18487 / 90 / 543

Goodness-of-fit on F2 1.028

Final R indices [I>2sigma(I) = 16712 data] R1 = 0.0177, wR2 = 0.0379

R indices (all data, 0.67 Å) R1 = 0.0218, wR2 = 0.0387

Largest diff. peak and hole 1.244 and -1.197 e.Å-3

X-Ray Structure of **30**:

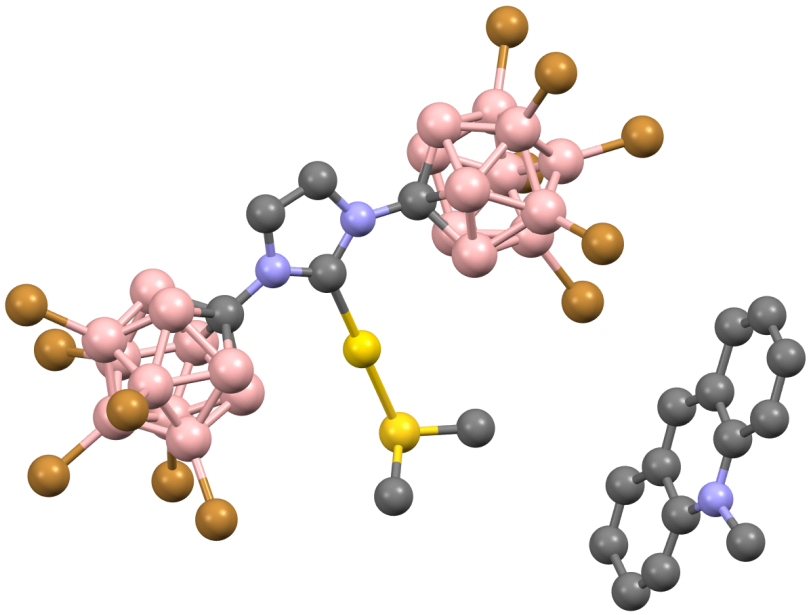

Fig. **3.6** X-Ray Structure of ion-pair **40**. Hydrogen atoms omitted for clarity. N=Blue, C=grey, Au=gold, S=yellow, B=pink, Br=brown

The sample was submitted by Varun Tej (research group of Professor Vincent Lavallo, Department of Chemistry, University of California, Riverside). The report was prepared by Dr. Veronica Carta.

Data collection

Single crystals suitable for X-ray diffraction were grown by slow evaporation of dichloromethane. A yellow crystal (plate, approximate dimensions 0.13 × 0.04 × 0.01 mm^3) was placed onto the tip of a MiTeGen pin and mounted on a Bruker Venture D8 diffractometer equipped with a PhotonIII detector at 180.00 K. The data collection was carried out using Cu Kα radiation (λ = 1.54178 Å, IμS micro-source) with a frame time of 7 seconds and a detector distance of 40 mm. A collection strategy was calculated and

complete data to a resolution of 0.82 Å were collected. The frames were integrated with the Bruker SAINT[1] software package using a narrow-frame algorithm to 0.84 Å resolution. Data were corrected for absorption effects using the multi-scan method (SADABS).[2] Please refer to Table 1 for additional crystal and refinement information.

Structure solution and refinement

The space group P $2_1/c$ was determined based on intensity statistics and systematic absences. The structure was solved using the SHELX suite of programs[3] and refined using full-matrix least-squares on F^2 within the OLEX2 suite.[4] A direct-methods solution was calculated, which provided most non-hydrogen atoms from the E-map. Full-matrix least squares / difference Fourier cycles were performed, which located the remaining non-hydrogen atoms. All non-hydrogen atoms were refined with anisotropic displacement parameters. The hydrogen atoms were placed in ideal positions and refined as riding atoms with relative isotropic displacement parameters. The final full matrix least squares refinement converged to R1 = 0.1458 and wR2 = 0.4466 (F^2, all data). The goodness-of-fit was 1.932. On the basis of the final model, the calculated density was 2.373 g/cm^3 and F(000), 3430 e^-. The structure suffers from poor data quality, low resolution and high mosaicity. Non merohedral twinning is present (twin law 1 0 0.77, 0 -1 0, 0 0 -1). An impurity co-crystalized with the target molecule. Likely the impurity is the result of excessive bromination.

[1]SAINT, V8.30A, Bruker Analytical X-Ray Systems, Madison, WI, 2012.

[2]SADABS, 2.03, Bruker Analytical X-Ray Systems, Madison, WI, 2016.

[3]G. M. Sheldrick, Acta Cryst. A64, 112 - 122 (2008). Sheldrick, G.M. (2015). Acta Cryst. A71, 3-8.

[4]O. V. Dolomanov, L. J. Bourhis, R. J. Gildea, J. A. K. Howard and H. Puschmann, J. Appl. Crystallogr., 2009, 42, 339–341.

Table 3.3 Crystal data and structure refinement for ion-pair **40**

Empirical formula	C22 H31.60 Au B22 Br12.40 Cl2 N3 S
Formula weight	1866.73
Crystal color, shape, size	yellow plate, 0.13 × 0.04 × 0.01 mm^3
Temperature	180.00 K
Wavelength	1.54178 Å
Crystal system, space group	Monoclinic, P 1 21/c 1
Unit cell dimensions	a = 20.101(3) Å α = 90°.
	b = 17.102(2) Å β = 107.802(8)°.
	c = 15.9651(19) Å γ = 90°.
Volume	5225.6(11) $Å^3$
Z	4
Density (calculated)	2.373 g/cm^3
Absorption coefficient	17.920 mm^{-1}
F(000)	3430

Data collection

Diffractometer	Bruker D8 Venture
Theta range for data collection	2.308 to 67.159°.
Index ranges	-23<=h<=23, -20<=k<=20, -19<=l<=19
Reflections collected	93250

Independent reflections 9273 [Rint = 0.1475]

Observed Reflections 7182

Completeness to theta = 67.159° 99.2 %

Solution and Refinement

Absorption correction Semi-empirical from equivalents

Max. and min. transmission 0.7528 and 0.4304

Solution Intrinsic methods

Refinement method Full-matrix least-squares on F^2

Weighting scheme $w = [\sigma^2 Fo^2 + AP^2 + BP]^{-1}$, with

$P = (Fo^2 + 2\,Fc^2)/3$, A = 0.2, B = 0.0

Data / restraints / parameters 9273 / 778 / 601

Goodness-of-fit on F^2 1.932

Final R indices [I>2σ(I)] R1 = 0.1458, wR2 = 0.3983

R indices (all data) R1 = 0.1787, wR2 = 0.4466

Largest diff. peak and hole 3.778 and -4.156 e.$Å^{-3}$

Twin Details

Type, twin law non merohedral (1 0 0.77, 0 -1 0, 0 0 -1)

Twin element, domain ratio 180˚ rotation around a* 85:15

3.9 References

1. Balema, V. P.; Hey-Hawkins, E., Die CuCl-katalysierte Reaktion von Trimethylsilyl(t-butyl)chlorphosphan mit Dimethylzirconocen: Ein Beispiel der Tandem-Katalyse. *Zeitschrift für anorganische und allgemeine Chemie* **1996,** *622* (12), 2053-2056.

2. Burk, M. J.; Lee, J. R.; Martinez, J. P., A Versatile Tandem Catalysis Procedure for the Preparation of Novel Amino Acids and Peptides. *Journal of the American Chemical Society* **1994,** *116* (23), 10847-10848.

3. Wasilke, J.-C.; Obrey, S. J.; Baker, R. T.; Bazan, G. C., Concurrent Tandem Catalysis. *Chemical Reviews* **2005,** *105* (3), 1001-1020.

4. Sen, A.; Lai, T. W., Oligomerization and isomerization of olefins by .eta.3-allyl complexes of palladium. The role of the allyl group. *Organometallics* **1983,** *2* (8), 1059-1060.

5. O'Connor, A. R.; Urbin, S. A.; Moorhouse, R. A.; White, P. S.; Brookhart, M., Synthesis and Reactivity of Cationic (Allyl)(arene)nickel(II) and (Allyl)(arene)palladium(II) Complexes. *Organometallics* **2009,** *28* (8), 2372-2384.

6. Crabtree, R. H.; Felkin, H.; Morris, G. E., Cationic iridium diolefin complexes as alkene hydrogenation catalysts and the isolation of some related hydrido complexes. *Journal of Organometallic Chemistry* **1977,** *141* (2), 205-215.

7. Fordyce, W. A.; Crosby, G. A., Electron spectroscopy of diphosphine and diarsine complexes of rhodium(I) and iridium(I). *Inorganic Chemistry* **1982,** *21* (4), 1455-1461.

8. Green, M.; Kuc, T. A.; Taylor, S. H., Cationic transition-metal complexes. Part I. Synthesis and reactions of bis(diene)-rhodium and -iridium tetrafluoroborates. *Journal of the Chemical Society A: Inorganic, Physical, Theoretical* **1971,** (0), 2334-2337.

9. Mestroni, G.; Camus, A.; Zassinovich, G., Complexes of iridium(I) with 2,2′-bipyridine and 1,10-phenanthroline: Synthesis and reactions of cationic complexes with diolefins. *Journal of Organometallic Chemistry* **1974,** *73* (1), 119-127.

10. Widenhoefer, R. A.; Han, X., Gold-Catalyzed Hydroamination of C–C Multiple Bonds. *European Journal of Organic Chemistry* **2006,** *2006* (20), 4555-4563.

11. Kumari, A.; Singh, R. K., Medicinal chemistry of indole derivatives: Current to future therapeutic prospectives. *Bioorganic Chemistry* **2019,** *89*, 103021.

12. Guo, T.; Huang, F.; Yu, L.; Yu, Z., Indole synthesis through transition metal-catalyzed C–H activation. *Tetrahedron Letters* **2015,** *56* (2), 296-302.

13. Shah, T. A.; De, P. B.; Pradhan, S.; Punniyamurthy, T., Transition-metal-catalyzed site-selective C7-functionalization of indoles: advancement and future prospects. *Chemical Communications* **2019,** *55* (5), 572-587.

14. Pirovano, V., Gold-Catalyzed Functionalization Reactions of Indole. *European Journal of Organic Chemistry* **2018,** *2018* (17), 1925-1945.

15. Hu, Y.; Xin, X.; Wan, B., Cyclization reactions of propargylic amides: mild access to N-heterocycles. *Tetrahedron Letters* **2015,** *56* (1), 32-52.

16. Mai, S.; Rao, C.; Chen, M.; Su, J.; Du, J.; Song, Q., Merging gold catalysis, organocatalytic oxidation, and Lewis acid catalysis for chemodivergent synthesis of functionalized oxazoles from N-propargylamides. *Chemical Communications* **2017,** *53* (75), 10366-10369.

17. Litle, E. D.; Wilkins, L. C.; Gabbaï, F. P., Ligand-enforced intimacy between a gold cation and a carbenium ion: impact on stability and reactivity. *Chemical Science* **2021,** *12* (11), 3929-3936.

18. Fasano, V.; Radcliffe, J. E.; Curless, L. D.; Ingleson, M. J., N-Methyl-Benzothiazolium Salts as Carbon Lewis Acids for Si−H σ-Bond Activation and Catalytic (De)hydrosilylation. *Chemistry – A European Journal* **2017,** *23* (1), 187-193.

19. Clark, E. R.; Ingleson, M. J., N-Methylacridinium Salts: Carbon Lewis Acids in Frustrated Lewis Pairs for σ-Bond Activation and Catalytic Reductions. *Angewandte Chemie International Edition* **2014,** *53* (42), 11306-11309.

20. Fisher, S. P.; McArthur, S. G.; Tej, V.; Lee, S. E.; Chan, A. L.; Banda, I.; Gregory, A.; Berkley, K.; Tsay, C.; Rheingold, A. L.; Guisado-Barrios, G.; Lavallo, V., Strongly Coordinating Ligands To Form Weakly Coordinating Yet Functional Organometallic Anions. *Journal of the American Chemical Society* **2020,** *142* (1), 251-256.

Chapter 4: Fusing 10-vertex *closo*-Carborane Anions with N-Heterocyclic Carbenes

4.1 Introduction

In Chapters **2** and **3**, we have established the icosahedral carborane anion $[HCB_{11}H_{11}^{1-}]$ **2** and its derivatives as an elite set of weakly coordinating anions that feature unmatched chemical robustness. Polyhalogenation of the B-H vertices of this cluster amplifies its robustness and also enhances the weak coordinative ability of the cluster as a whole.[1-2] These properties have allowed for the isolation of a variety of super reactive cations as well as the design of main group catalysts capable of C-F and C-H functionalization.[3-6] Moreover, we have seen how these clusters can be utilized as substituents for ligands in catalyst design, which in some cases have led to superior catalysts compared to the systems containing ligands with pure aryl groups.[7]

There has been growing interest in anionic NHC ligands, since they offer the possibility of preparing distinct coordination environments as well as allowing the formation of zwitterionic transition metal complexes with enhanced solubility in hydrocarbons compared to standard cationic catalysts.[8] Tamm has elegantly demonstrated the advantages of such systems and recently reviewed the topic.[9-10]

Compared to the icosahedral carborane anion **2**, the smaller ten-vertex bicapped square antiprism $[HCB_9H_9^{1-}]$ **3** (Fig. **4.1**), which was discovered by Knöth in 1967, has been far less investigated.[11] A survey of the literature indicates that this anion is compatible with strong acids/bases and studies from our lab have shown it is very

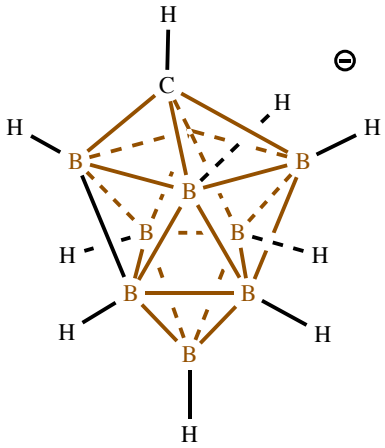

Fig. **4.1** The 10-vertex *closo*-carborane

stable towards redox chemistry.[12-13] In addition, similar to **2, 3** can undergo selective B-H halogenation to form more weakly coordinating derivatives.[14] We therefore became interested in the use of **3** as a less sterically demanding surrogate of **2** in ligand design. Recently we reported the first phosphine ligands containing this smaller cluster and showed that the [-$CB_9H_9^{1-}$] group is not only less sterically demanding than **2**, but also a significantly stronger σ-inductive donor.[15] Subsequently, we became curious if it were possible to prepare N-carboranyl NHCs, featuring **3** as a ligand substituent. Here we report the isolation of the first 10-vertex N-carboranyl carbenoids.

To synthesize the 10-vertex N-carboranyl carbenoids, we had to synthesize the corresponding imidazolium which produces the carbenoid upon deprotonation analogous to their 12-vertex

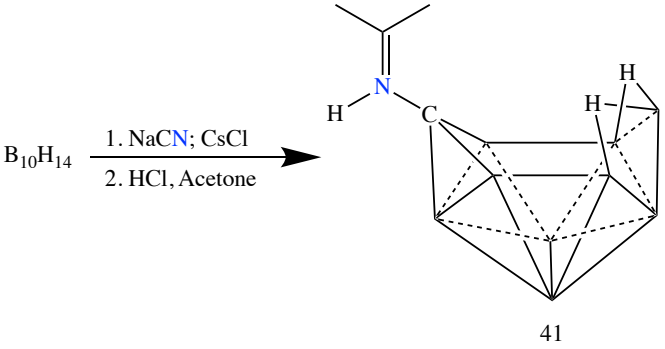

41

Scheme **4.1** Synthesis of zwitterionic iminium from decaborane

counterparts discussed in Chapter-1. This is done in two steps: treating the 10-vertex amine with glyoxal to form the dianionic diimine which closes into imidazolium upon treatment with *p*-formaldehyde and HCl/ether. However, a clean and reliable synthesis of the 10-vertex amine was not available in the literature.

4.2 Synthesis of the 10-vertex Amine

Jelinek and co-workers reported the synthesis of the iminium **41** as shown in Scheme **4.1**.[16] Our lab envisioned oxidatively closing this iminium should produce the 2-isomer of the

carboranyl amine which isomerizes to the 1-amine upon heating. Our lab predecessors oxidized this iminium with iodine in water to produce the 2-amine which was then heated to form the 1-amine. However, this procedure was not reproducible and even during the times it worked, the yields were as little as 5-10%, making the further synthesis with the precursor impossible.

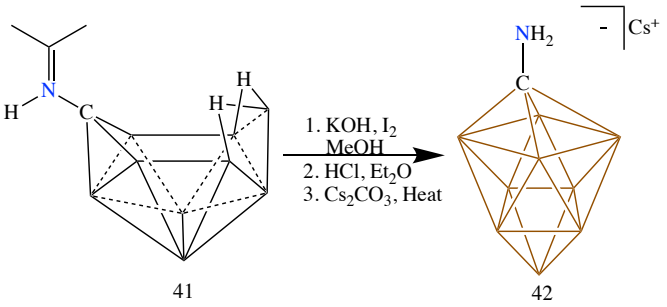

Scheme **4.2** Oxidative Closure of iminium to 10-vertex closo amine **42**

By optimizing the reaction conditions with the help of my lab mates, I found the clean iminium can be produced in about 40% yield. Any impurities could be washed away with diethyl ether. I found the oxidative cluster closure reaction works best in cold methanol unlike the previous procedure done in cold water, where 90% of the iminium decomposes to boric acid in less than 10 minutes. Further, the reaction rate and yield were greatly improved by using 1.5M KOH solution and one addition of iodine. Under these conditions, the reaction was found to go to completion in about 20 min producing clean 2-amine (Scheme **4.2**).

The 2-isomer was then extracted as zwitterionic ammonium in ether and heated in water to isomerize. The previous protocol involved addition of NaOH for deprotonation of the ammonium and CsCl to produce the corresponding Cs salt. However, this procedure involved too many Na and Cs salts co-crystallizing with the amine and involved multiple tedious extractions with acetonitrile to remove them. This resulted in a great loss of yield

and time. To avoid this issue, cesium carbonate was added; it acts as a base and deprotonates the ammonium making the cesium salt of the amine, cleanly isolated upon recrystallization (Scheme **4.2**). This procedure is quite reliable and reproducible on multigram scale.

4.3 Synthesis of 10-vertex Imidazolium

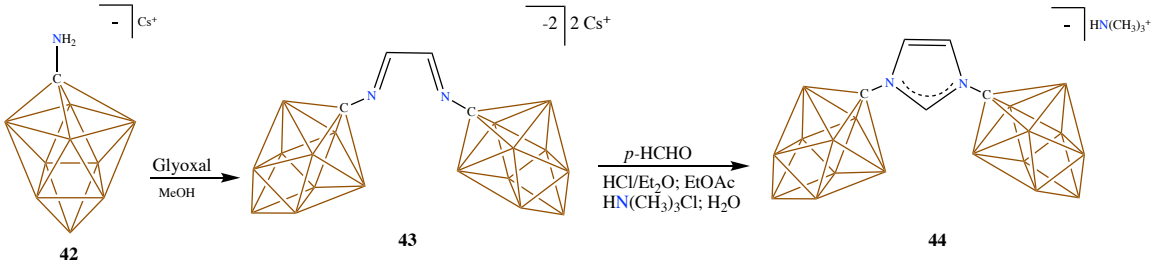

42 **43** **44**

Scheme **4.3** Synthesis of the dianionic diimine **43** and the imidazolium **44**

With the 10-vertex amine in hand, we reacted two equivalents of the anionic amine **42** with glyoxal and observed the formation of the corresponding dianionic carboranyl diimine **43**, as indicated by the ^{1}H NMR spectroscopy. Subsequent ring closure with *para*-formaldehyde in the presence of HCl/ether cleanly afforded the desired anionic imidazolium. It should be noted here that the order of addition of the diimine and the mixture of *p*-formaldehyde, HCl/ether makes a drastic difference in the reaction outcome. Unlike with the 12-vertex symmetric imidazolium synthesis, addition of an ethyl acetate solution of diimine to the mixture of *p*-formaldehyde in HCl/ether produced the desired imidazolium **44** cleanly.[17] Subsequent cation exchange with trimethylammonium chloride afforded the trimethylammonium salt of the imidazolium **44** in 76% yield (Scheme **4.3**). Cation exchange for trimethylammonium is advantageous, *vide infra*, since in subsequent imidazolium anion deprotonations one can choose the counter cation the ensuing NHCs will have, depending on the nature of the base employed.

4.4 The 10-vertex Carboranyl Carbenes

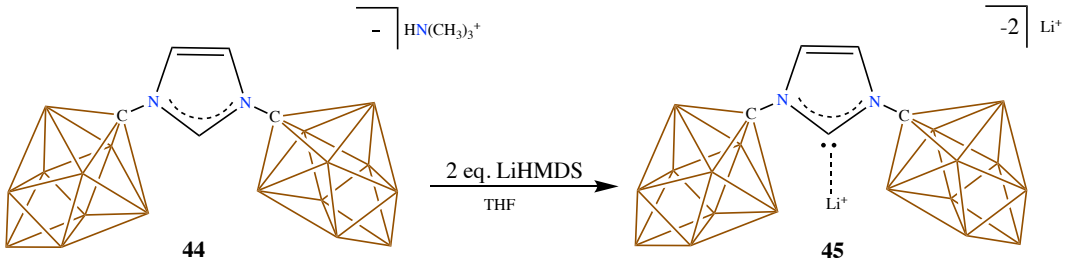

Scheme **4.4** Synthesis of the 10-veretx fused N-Heterocyclic Carbene **45**

We next turned our attention to the possibility of preparing the corresponding normal C-2 deprotonated NHC **45[Li$^+$]** (Scheme **4.4**). Imidazolium anion **44** was thus reacted with two equivalents of lithium hexamethyl disilazide (LiHMDS) and the reaction was monitored

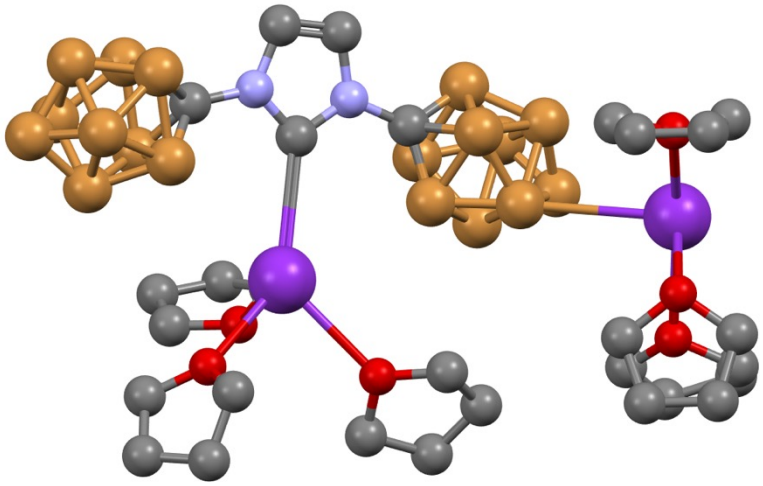

Fig. **4.2** Solid-State Structure of the NHC **45[K$^+$]**. Hydrogen atoms omitted for clarity. N=Blue, B=Brown, O=red, K=violet

by multinuclear NMR spectroscopy. The ^{1}H NMR spectrum shows the disappearance of the characteristic triplet/doublet pattern (10.26; 8.45 ppm, respectively) of the imidazolium ring and the formation of a new upfield singlet resonance at 7.75 ppm, which is consistent with the formation of **45[Li$^+$]**. The ^{11}B NMR spectrum shows a set of three resonances (31.4; -12.8; -22.2 ppm) in 1:4:4 ratio, indicating that the new species retains the local C_{4v} symmetry of the cluster. Analysis of the ^{13}C NMR spectrum shows the appearance of a

new resonance at 197.7 ppm, which is also consistent with the generation of the carbenoid **45[Li$^+$]**. All attempts to grow single crystals of **45[Li$^+$]** for X-ray diffraction studies were unsuccessful. However, utilizing KHMDS in lieu of LiHMDS afforded **45[K$^+$]**, which readily crystalized (Fig. **4.2**). Although the structure is too disordered to have a meaningful discussion of bond lengths and angles, the connectivity of the square pyramidal structure is unambiguous.

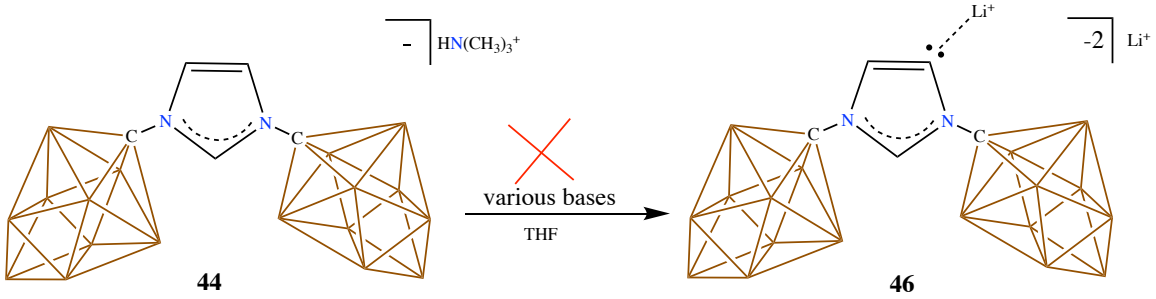

Scheme **4.5** Attempted synthesis of the 10-veretx fused abnormal N-Heterocyclic Carbene **46**

We next sought to investigate if these small 10-vertex carborane anions would allow for the selective formation of the abnormal C-5 deprotonated NHC Li$^+$ adduct **46**. Regardless of the conditions or bases employed we did not observe any evidence for the formation of **46** (Scheme **4.5**), which is in stark contrast to the exquisite selectivity previously reported

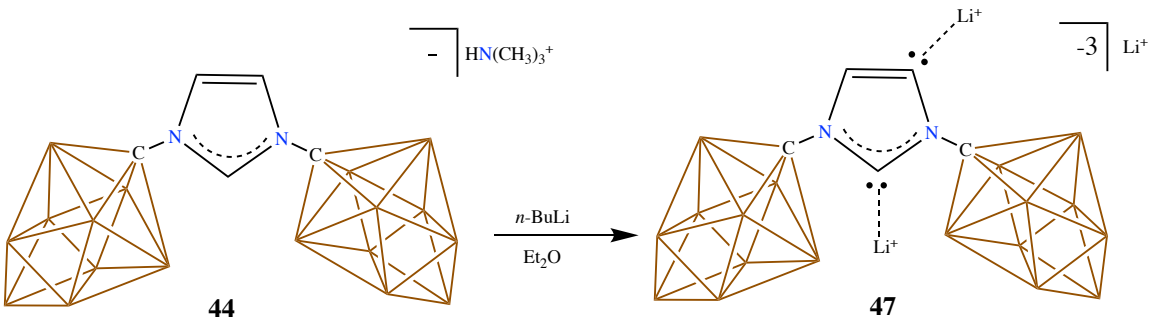

Scheme **4.6** Synthesis of the 10-veretx fused paranormal N-Heterocyclic Carbene **47**

for formation of **6** (**Figure 1**).[17] Therefore, the selectivity induced by the bulkier anionic icosahedral carborane substituents is likely a steric effect and not related to the charge of such anions.

While we were unable to prepare **46**, the trianionic doubly deprotonated species **47** was readily accessible by reacting **44** with three equivalents of *n*-BuLi. The formation of **47** was corroborated by ^{1}H NMR spectroscopy, which shows an upfield shift of the carbenoid backbone proton to 7.0 ppm. In addition, the ^{13}C spectrum shows two distinct downfield carbon resonances at 197.6 and 169.3 ppm, which is consistent with C-2 and C-5 imidazolium deprotonation, respectively. In the ^{11}B NMR spectrum the two sets of resonances for the inequivalent carborane clusters are superimposed by coincidence. The carbenoid structure of **47** was unambiguously determined by a single crystal X-ray diffraction study, but the data is not of sufficient quality to discuss structural parameters (Fig. **4.3**). What we can say is that similar to its 12-vertex homolog, in the solid state **47**

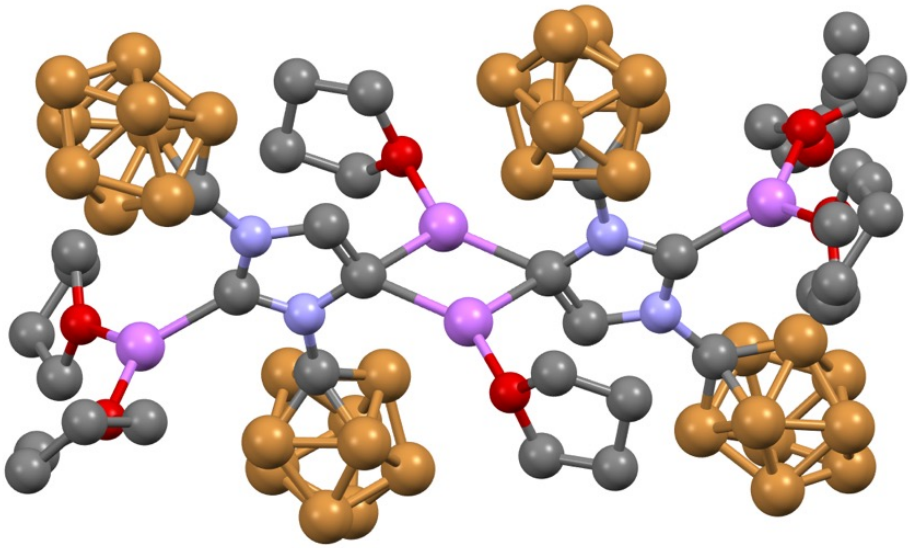

Fig. **4.3** Solid-State Structure of **47**. Hydrogen atoms omitted for clarity.
N=blue, O=red, B=brown, Li=purple

adopts a dimeric structure with terminal Li^+ cations coordinated to the C-2 positions and two bridging Li^+ cations gluing the dimer together via the C-5 positions.

4.5 Conclusion

In conclusion, over 50 years after Knöth's discovery of the $[HCB_9H_9]^{1-}$ anion and 30 years after Arduengo's seminal discovery of the first stable NHC, we show that these two families of molecules can be fused to form unusual charged carbenoids. We are currently investigating the possibility of utilizing these ligands in catalysis as well as for the formation of functional weakly coordinating anions.

4.6 Experimental

General Considerations:

Unless otherwise stated, all manipulations were carried out using standard Schlenk or glovebox techniques (O_2, H_2O < 1ppm) under a dinitrogen or argon atmosphere. Solvents were dried on sodium-potassium alloy or potassium benzophenone ketyl and distilled under argon before use. Imine **41** was prepared according to literature methods.[16] Reagents were purchased from commercial vendors and used without further purification. NMR spectra were recorded on Bruker Avance 300 MHz, Bruker Avance Neo 400 MHz, Bruker Avance 600 MHz, Bruker Avance III 700 MHz, Varian Inova 300 MHz, or Varian Inova 400 MHz spectrometers. NMR chemical shifts are reported in parts per million (ppm). ^1H NMR and ^{13}C NMR chemical shifts were referenced to residual solvent. ^{11}B NMR chemical shifts were externally referenced to $BF_3{\cdot}OEt_2$. High-resolution mass spectrometry (HRMS) was recorded on Agilent Technologies 6210 (time of flight LC/MS) using ESI technique. Complete crystallographic data for compounds **45[K^+]**, and **47** are available free of charge

from the Cambridge Crystallographic Data Center under the reference numbers 848686 and 1848697 respectively**.** The crystallographic data of these structures can be accessed via the ccdc website: http://www.ccdc.cam.ac.uk/Community/Requestastructure/Pages/DataRequest.aspx.

Synthesis of 10-vertex Carborane Amine:

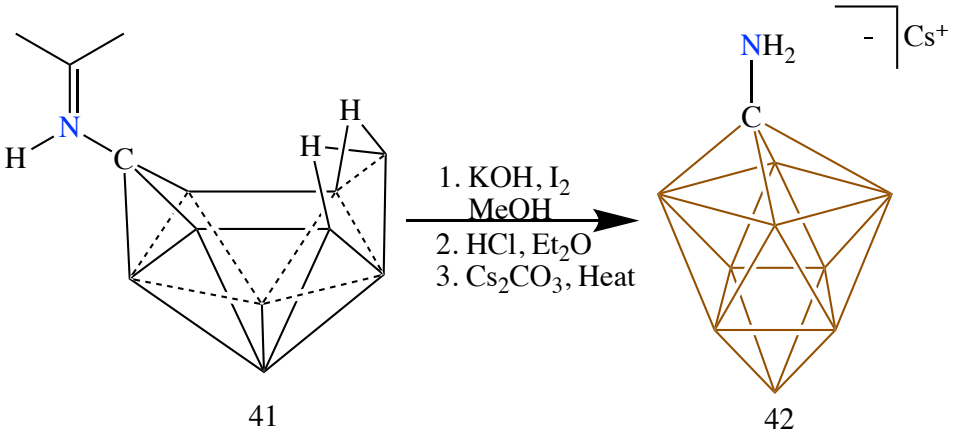

41 42

Scheme 4.2 Oxidative Closure of Iminium to 10-vertex closo Amine 42

In a 500 mL round bottom, 2.00 grams of the zwitterion **41** (11.3 mmol) was added to 260 mL of a 1.5 M solution of KOH in MeOH pre-cooled in an ice bath. To the stirring solution, 6.5 grams (17.7 mmol) of I_2 was added and allowed to stir for 1 hour. The MeOH was removed via reduced pressure and the resulting solid was resuspended in 100 mL of H_2O, and the excess base was quenched by slowly acidifying with 27 mL of concentrated HCl (checked by litmus). The aqueous solution is then extracted with diethyl ether (3 x 20mL) and the combined organic layers were pumped down on a rotary evaporator, resulting in a light brown oil. *The crude ^{11}B NMR should be checked at this point to see if there was any spontaneous isomerization*. If the isomerization is not complete, 30 mL of H_2O and 3.68 grams of Cs_2CO_3 (11.3 mmol) were added to this oil and the solution was refluxed (usually

overnight-24 hours) to fully isomerize to the *closo* amine. The desired product **42** then crystallized out of the aqueous solution as off white crystals in about 60% yield. (1.81 g, 6.77 mmol). ^{1}H NMR (400 MHz, acetonitrile-d_3, 25 °C): 3.21 (s, 2H, N-H), 5.5-0.0 (bm, 9H, B-H); ^{1}H (^{11}B-dec) NMR (300 MHz, acetonitrile-d_3, 25 °C): 3.20 (s, 2H, N-H), 1.50 (s, 5H, B-H), 0.47 (s, 4H, B-H); ^{11}B (^{1}H-dec) NMR (96 MHz, acetonitrile-d_3, 25 °C): δ = 19.8, -16.6, -25.9; ^{11}B NMR (96 MHz, acetonitrile-d_{63}, 25 °C): δ = 19.2, -17.2, -26.5; ^{13}C-(^{1}H-dec) NMR (124 MHz, acetonitrile-d_6, 25°C): δ = 85.1 ppm.

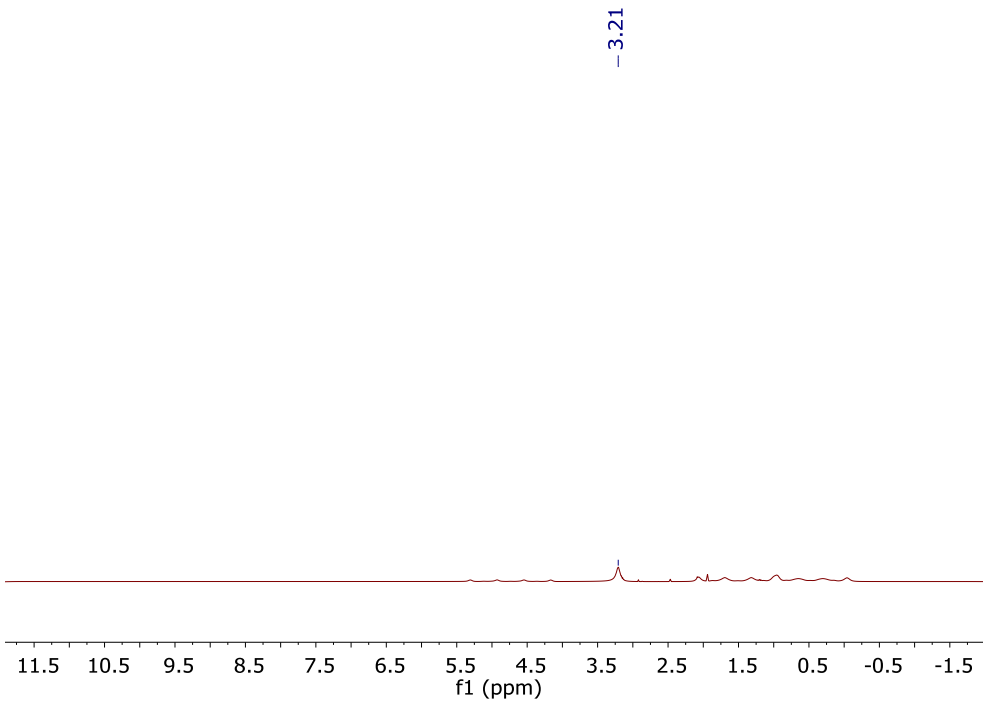

Fig. **4.1** ^{1}H NMR of **42** in CD_3CN

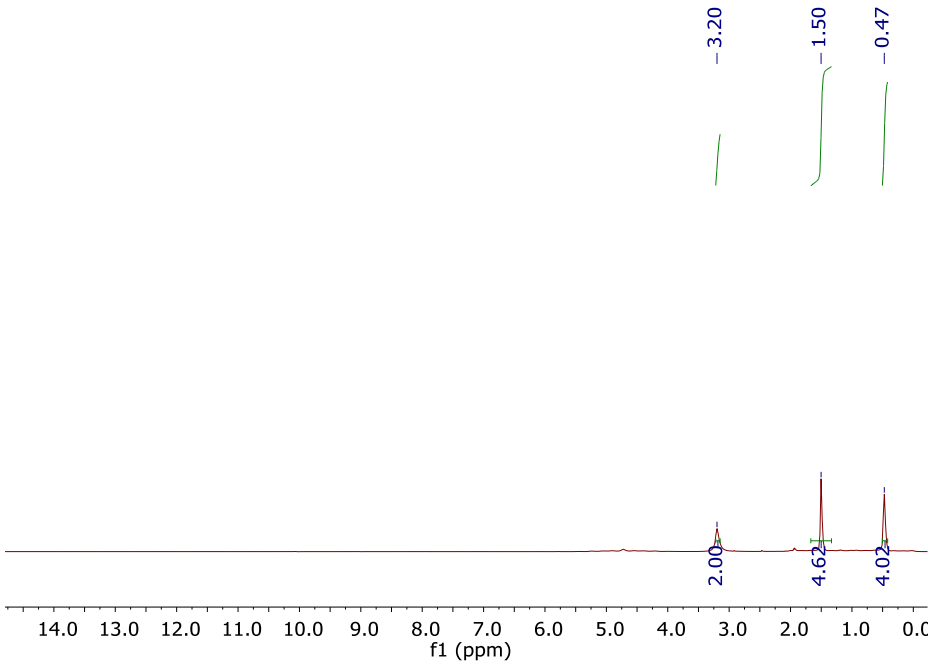

Fig. **4.2** $^{1}H[^{11}B]$ NMR of **42** in CD_3CN

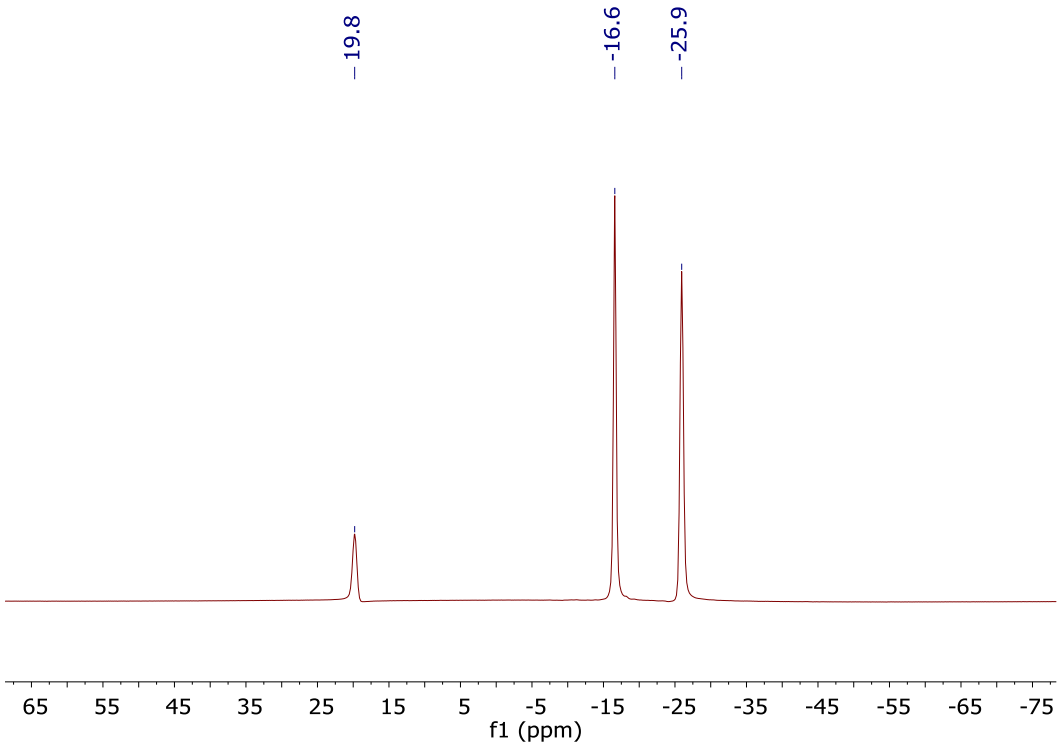

Fig. **4.3** $^{11}B[^{1}H]$ NMR of **42** in CD_3CN

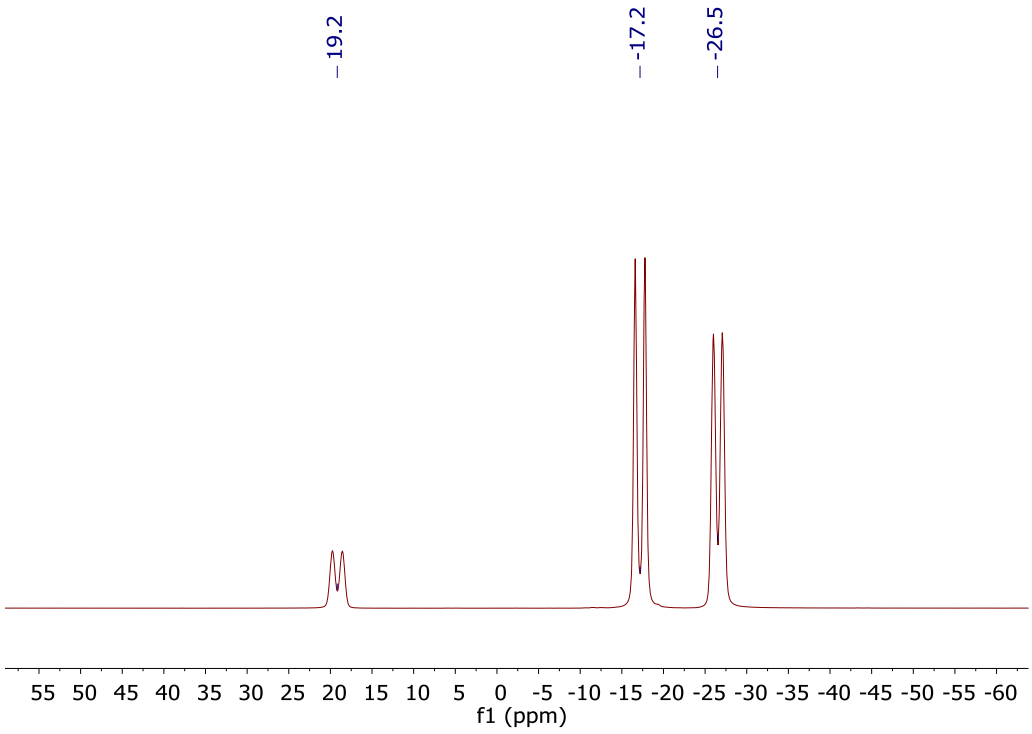

Fig. **4.4** ^{11}B NMR of **42** in CD_3CN

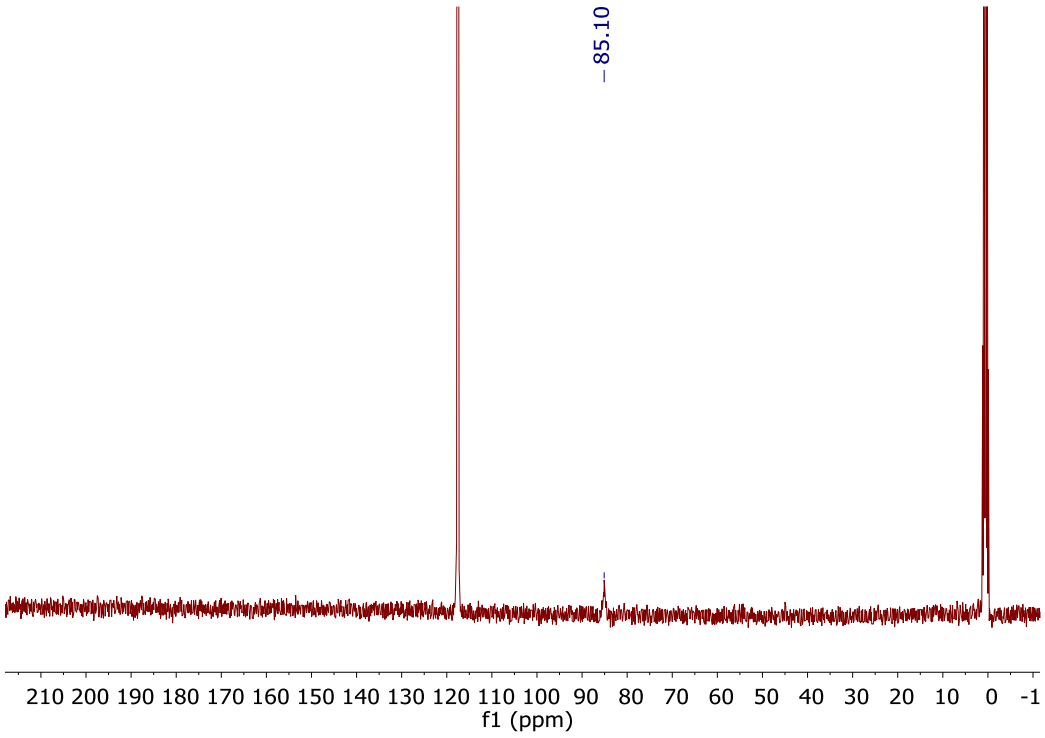

Fig. **4.5** $^{13}C[^1H]$ NMR of **42** in CD_3CN

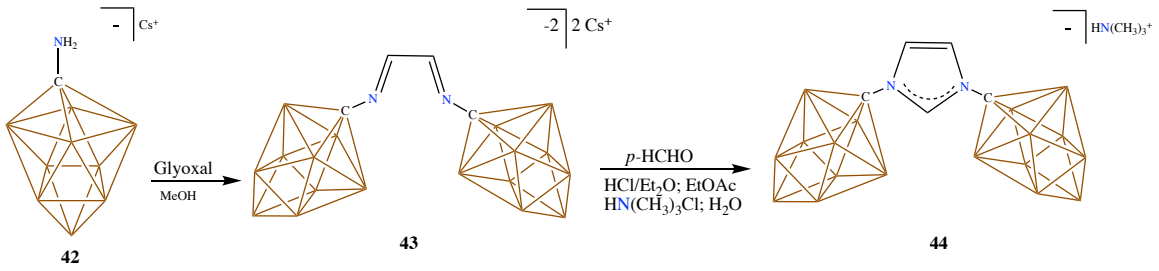

Scheme **4.3** Synthesis of the dianionic diimine **43** and the imidazolium **44**

Glyoxal ($O_2C_2H_2$) aqueous solution (40 % w/w, 325 mg, 2.2 mmol) was added to a solution of **42** (1.20 g, 4.4 mmol) dissolved in methanol (15 mL) and the reaction mixture stirred for 24 hours. Volatiles were removed under vacuum to afford the crude diimine as a light brown powder. The resulting yield of the Cs^+ diimine salt **43** was 98% (1.22 g, 2.2 mmol) ^{1}H NMR (400 MHz, acetonitrile-d_3, 25 °C): δ = 8.94 (s, 2H), 2.70-0.0 (bm, 18H, B-H); ^{13}C-(^{1}H-dec) NMR (125 MHz, acetonitrile-d_3, 25 °C): δ = 165.2; ^{11}B-(^{1}H-dec) NMR (96 MHz, acetonitrile-d_3, 25 °C): δ = 26.2, -17.4, -25.2 ppm.

Without further purification, the crude diimine (1.22 g, 2.2 mmol) was dissolved in a solution of ethyl acetate (10 mL). A second solution of 2M HCl/diethyl ether (4 mL) was added to paraformaldehyde (79 mg, 2.6 mmol) and stirred for 30 minutes. To this mixture of paraformaldehyde and HCl/diethyl ether, the ethyl acetate solution of diimine was transferred via a canula and stirred for three hours. Subsequent removal of all volatiles under high vacuum afforded **44Cs**$^+$ as a crude mixture. The corresponding $HNMe_3^+$ salt was made by the addition of 1.3 equivalents of trimethylammonium hydrochloride to a suspension of the compound in water and stirring overnight. The resulting suspension was then vacuum filtered to produce the trimethyl ammonium salt of the imidazolium **44** in 76% (473 mg, 1.70 mmol) yield. ^{1}H NMR (300 MHz, acetone-d_6, 25 °C): δ = 10.26 (t, $^4J(H,H)$

= 1.72 Hz, 1H), 8.45 (d, $^{4}J(H,H)$ = 1.72 Hz, 2H), 3.25-0.0 (bm, 18H, B-H); ^{13}C-(^{1}H-dec) NMR (125 MHz, acetone-d_6, 25 °C): δ = 139.27, 125.94, 73.71; ^{11}B-(^{1}H-dec) NMR (96 MHz, acetone-d_6, 25 °C): δ = 31.0, -15.4, -25.2 ppm. HRMS (negative mode ESI/APCI) [M]- m/z calc'd for $N_2C_5B_{18}H_{21}^-$ = 304.3498; Found = 304.3491.

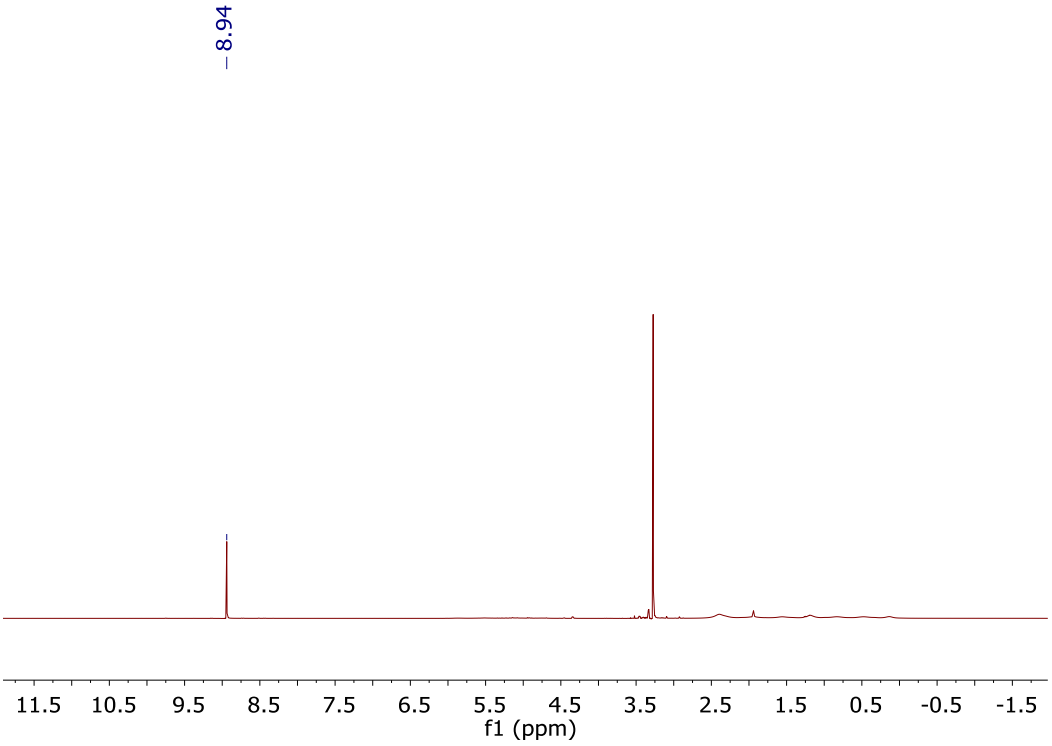

Fig. **4.6** ^{1}H NMR of **43** in CD_3CN. *The peak at 3.27 ppm is due to MeOH.*

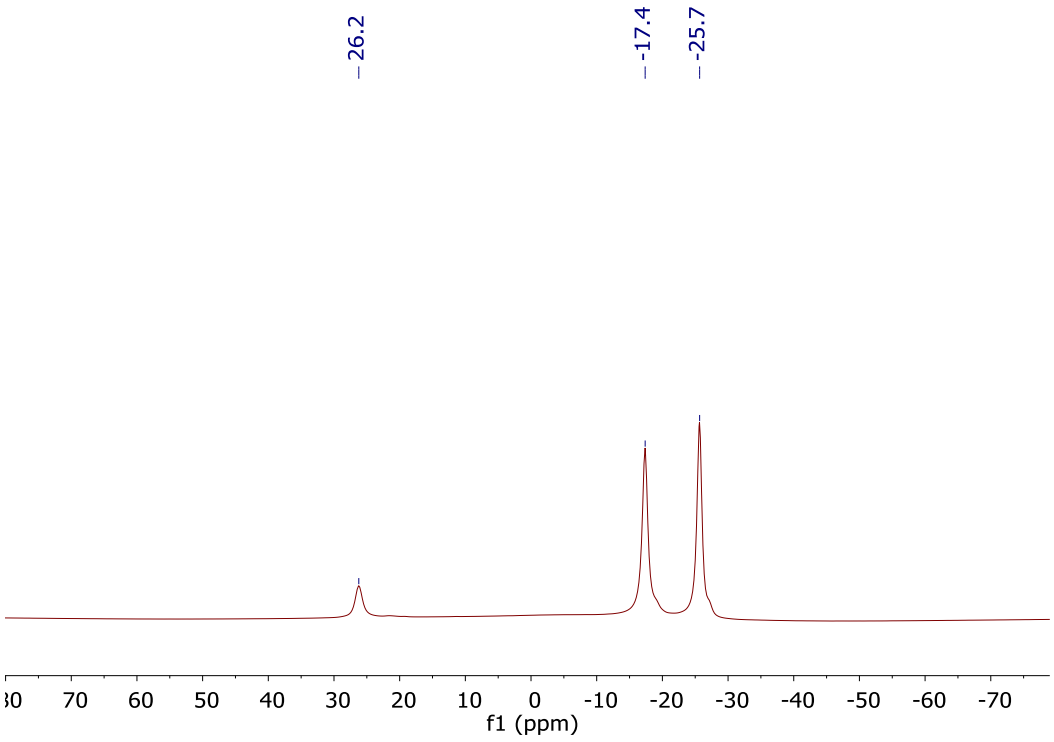

Fig. **4.7** $^{11}B[^{1}H]$ NMR of **43** in CD_3CN

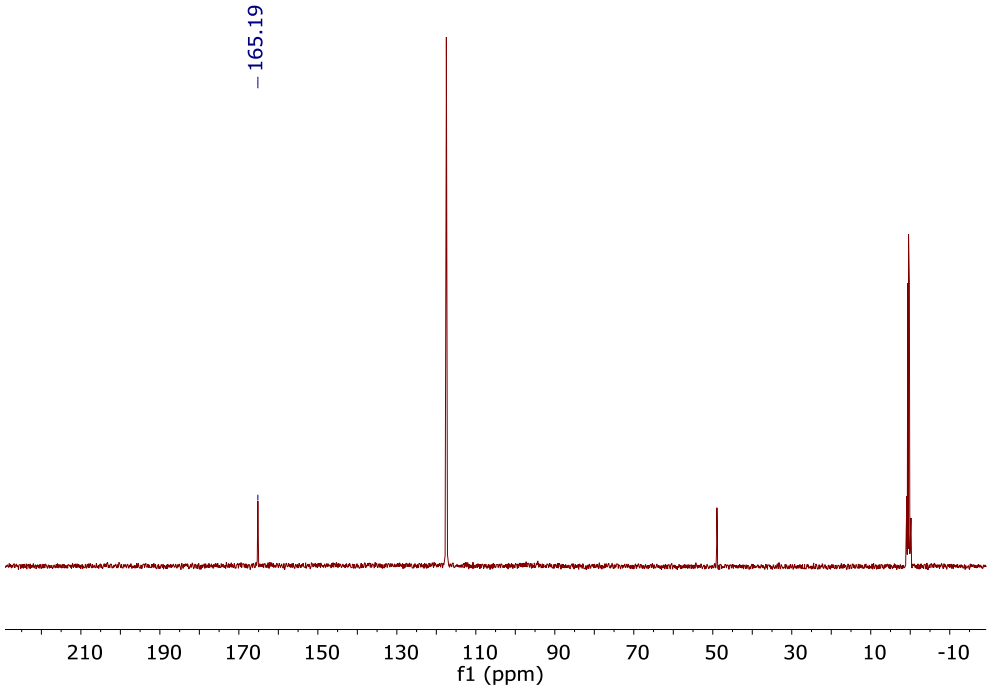

Fig. **4.8** $^{13}C[^{1}H]$ NMR of **43** in CD_3CN. The peak at 48.9 ppm is due to MeOH.

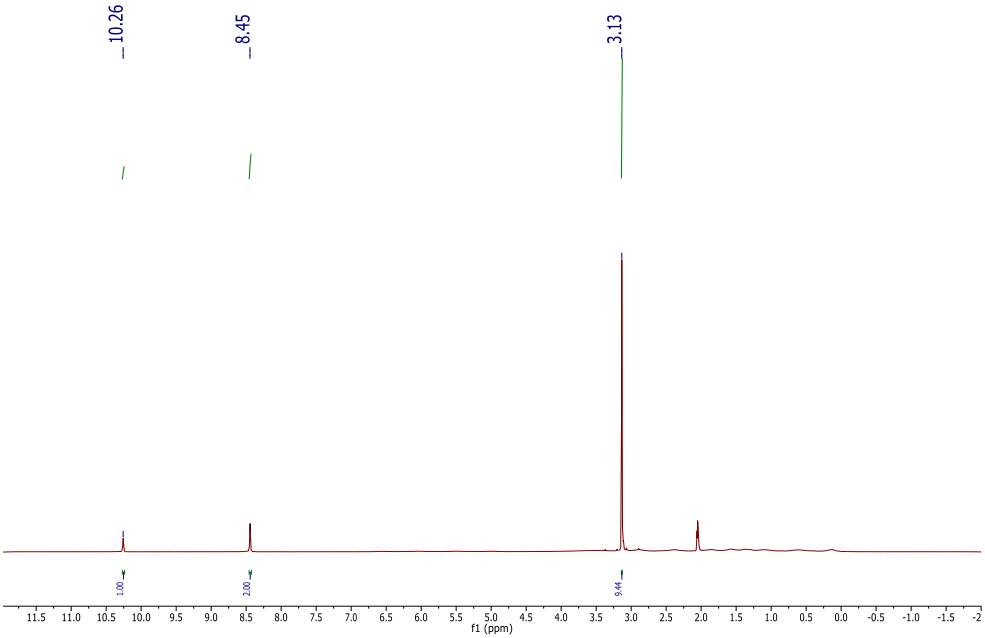

Fig. **4.9** ^{1}H NMR of **44** in acetone-d_6.

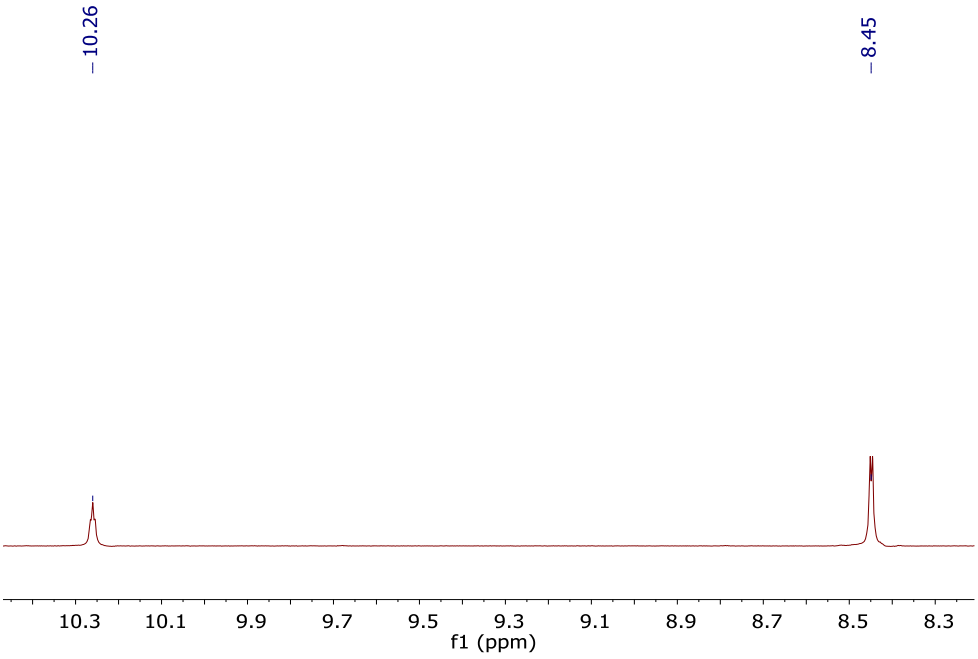

Fig. **4.10** An expanded view of the aromatic region of the ^{1}H-NMR of **44** in acetone-d_6, showing the small 4J(H,H) coupling through the imidazolium ring.

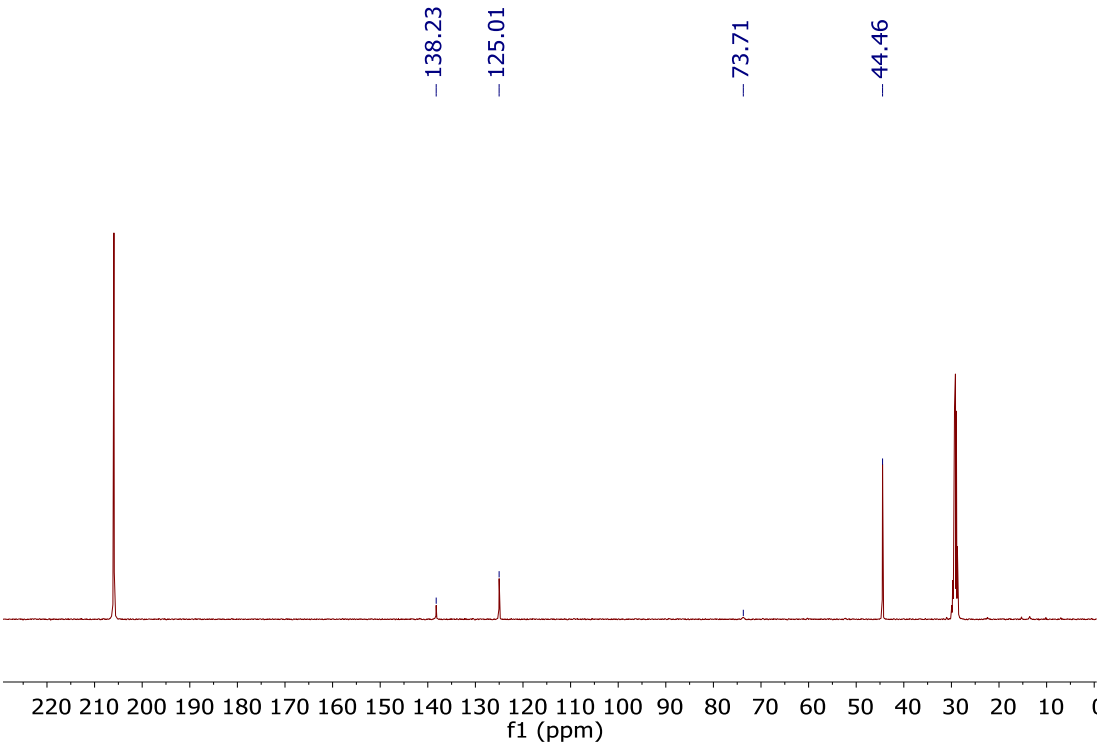

Fig. **4.11** $^{13}C[^{1}H]$ NMR of **44** in acetone-d_6.

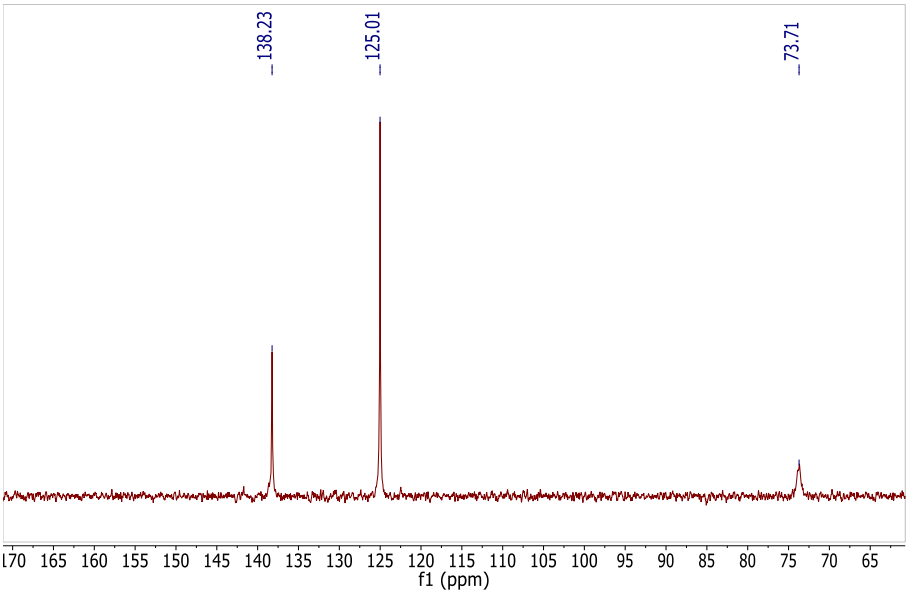

Fig. **4.12** The expanded view of the $^{13}C[^{1}H]$ NMR of **44** in acetone-d_6 showing the resonance of the carborane carbon at 73.71, as well as the carbon resonances of the imidazolium ring.

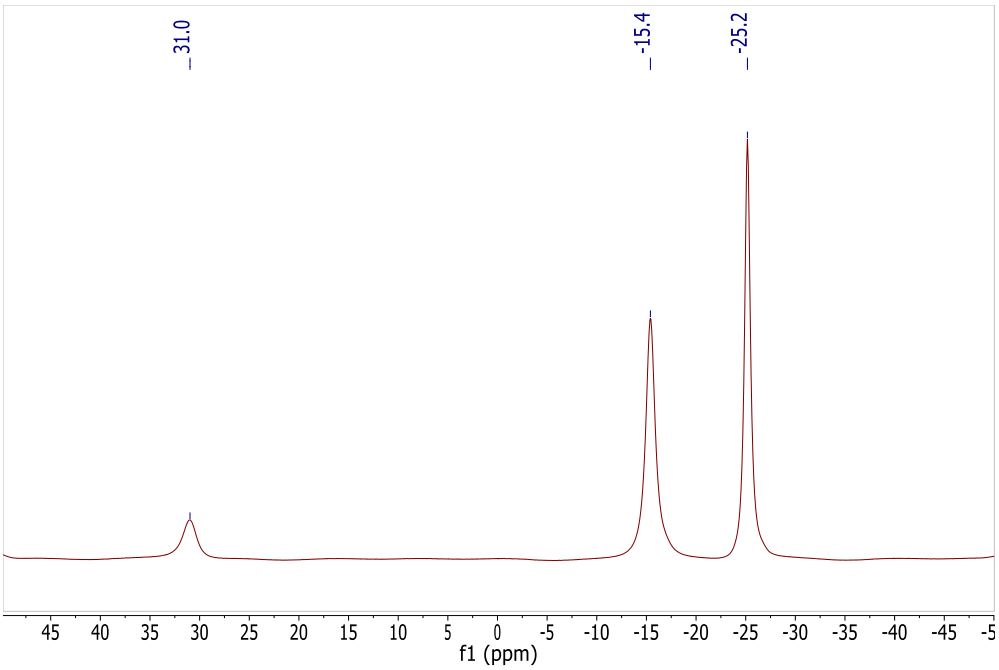

Fig. **4.13** $^{11}B[^{1}H]$ NMR of **44** in acetone-d_6.

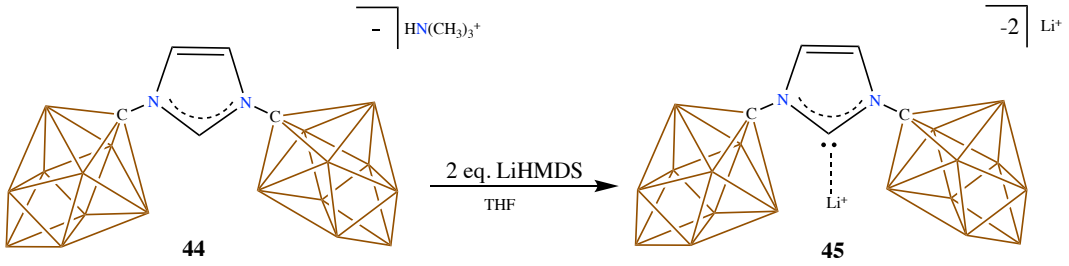

Scheme **4.4** Synthesis of the 10-vertex fused N-Heterocyclic Carbene **45**

A vial equipped with a stir bar was loaded with 310 mg (0.83 mmol) of **44** and 3 mL of tetrahydrofuran. In a second vial, 2.3 equivalents (321.6 mg, 1.92 mmol) of LiHMDS was added and dissolved in tetrahydrofuran (3 mL). The two tetrahydrofuran solutions were combined, the vial capped, and the mixture stirred for 1 hour. The tetrahydrofuran solution was added dropwise to a stirring vial of diethyl ether (20 mL), precipitating a light brown powder. The precipitate was left stirring in diethyl ether for 30 minutes. The solvent was decanted off the precipitate, and the remaining volatiles were removed under vacuum,

affording the product **45[Li$^+$]** in 92% yield (454 mg, 0.75 mmol) (Note: Li^+ countercations contain 4 coordinated tetrahydrofuran molecules). ^{1}H NMR (400 MHz, tetrahydrofuran-d_8, 25 °C): δ = 7.75 (s, 2H), 0.01-2.75 (bm, 18H, B-H); ^{13}C-(^{1}H-dec) NMR (125 MHz, tetrahydrofuran-d_8, 25 °C): δ = 197.72, 121.58, 79.34; ^{11}B-(^{1}H-dec) NMR (96 MHz, tetrahydrofuran-d_8, 25 °C): δ = 31.4, -21.8, -22.2 ppm.

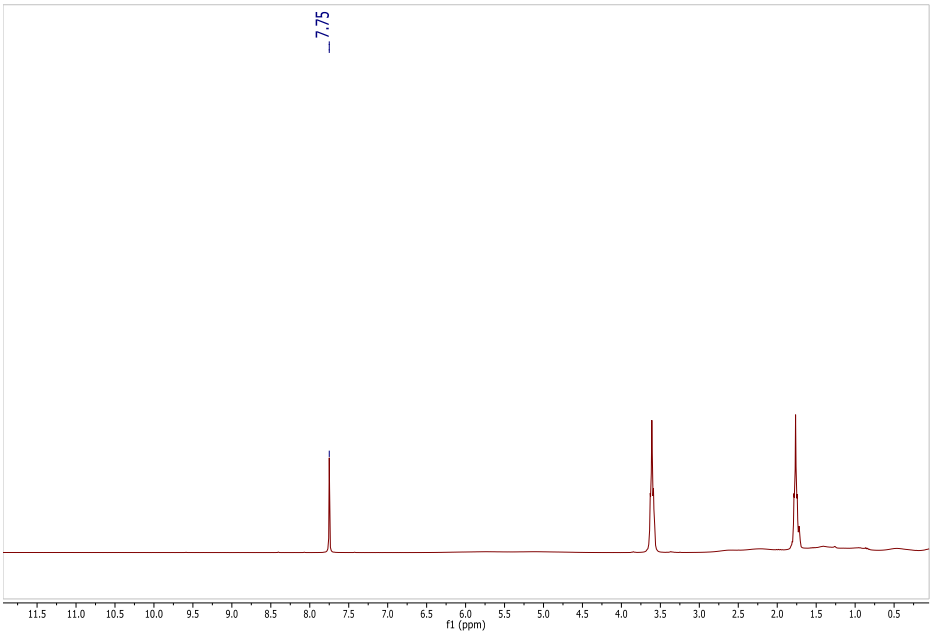

Fig. **4.14** ^{1}H NMR spectrum of **45[Li$^+$]** in THF-d_8.

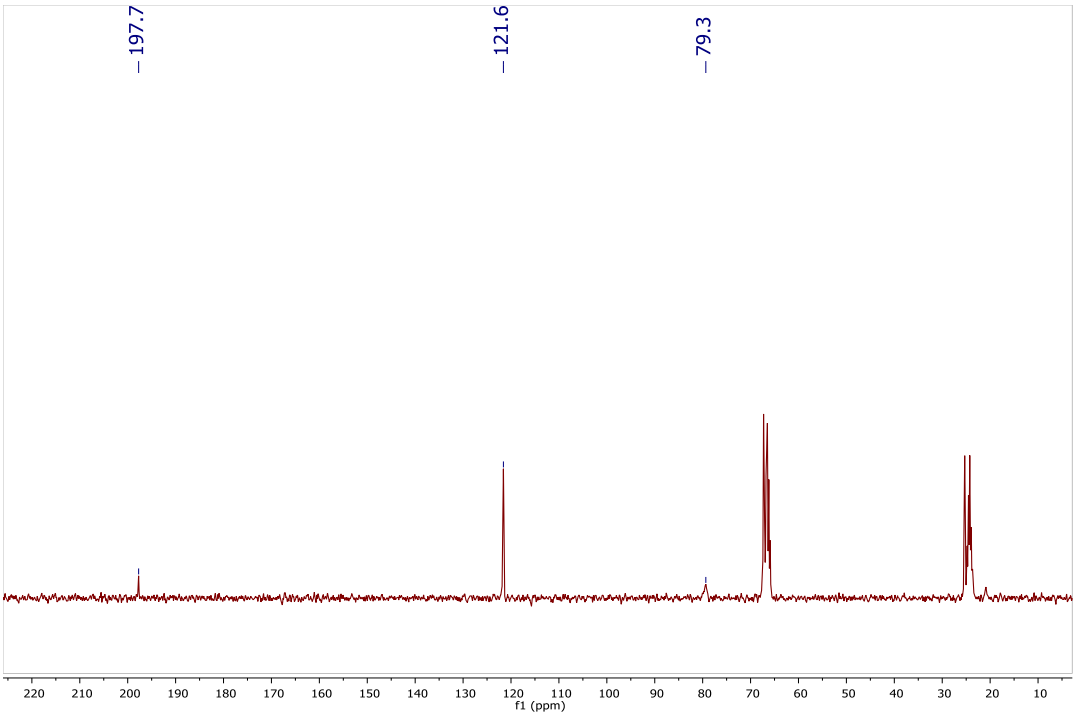

Fig. **4.15** $^{13}C[^{1}H]$ NMR spectrum of **45[Li^{+}]** in THF-d_8.

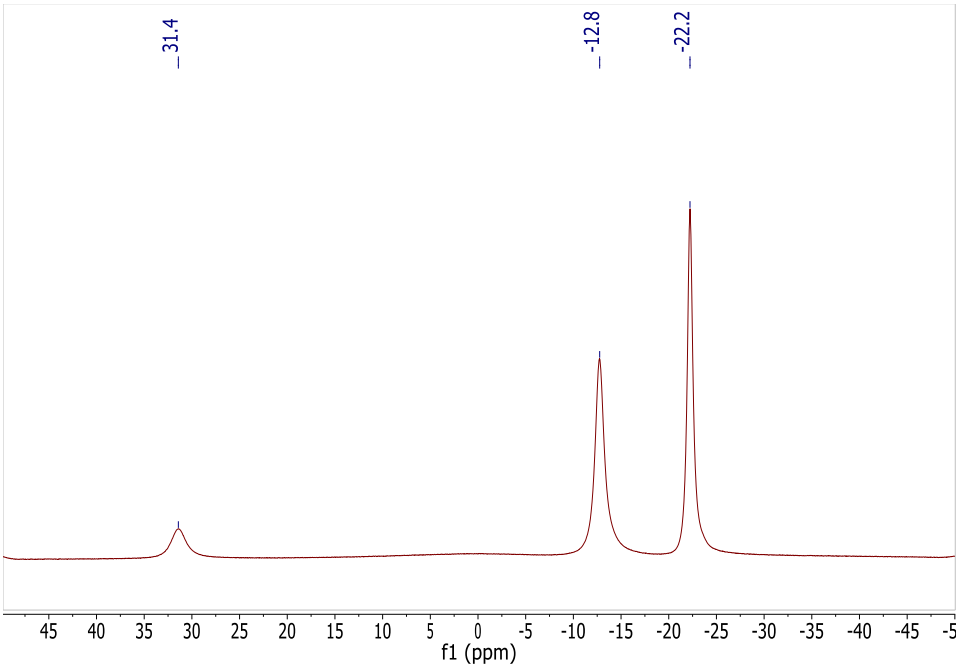

Fig. **4.16** $^{11}B[^{1}H]$ NMR spectrum of **45[Li^{+}]** in THF-d_8.

Synthesis of **45[K$^+$]**:

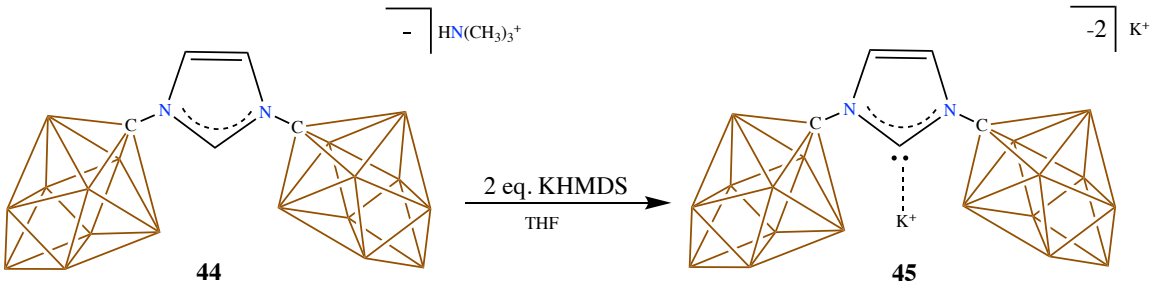

Scheme **4.7** Synthesis of the 10-vertex fused N-Heterocyclic Carbene **45[K$^+$]**

A vial equipped with a stir bar was loaded with 260 mg (0.7 mmol) of **44** dissolved in tetrahydrofuran (3 mL). In a second vial, 2.3 equivalents (320.3 mg, 1.61 mmol) of KHMDS was dissolved in tetrahydrofuran (3 mL) and added to the fist vial containing **44**. The vial was capped and the mixture was stirred for 1 hour. The tetrahydrofuran reaction solution was added dropwise to a stirring vial of diethyl ether, precipitating a brown powder. The precipitate was left stirring in diethyl ether for 30 minutes. The solvent was decanted from the precipitate, and the remaining volatiles were removed under vacuum, affording the product **45[K$^+$]** in 89% yield (459 mg, 0.61 mmol). (Note: K^+ countercations contain 3 coordinated THF molecules). Crystals suitable for a single crystal X-ray diffraction study were grown at -30 °C by layering a tetrahydrofuran solution of **45[K$^+$]** with diethyl ether. ^{1}H NMR (500 MHz, tetrahydrofuran -d_8, 25 °C): δ = 7.72 (s, 2H), 2.50-0.0 (bm, 22H, B-H); ^{11}B-(^{1}H-dec) NMR (96 MHz, tetrahydrofuran -d8, 25 °C): δ = 30.5, -12.7, -22.1 ppm.

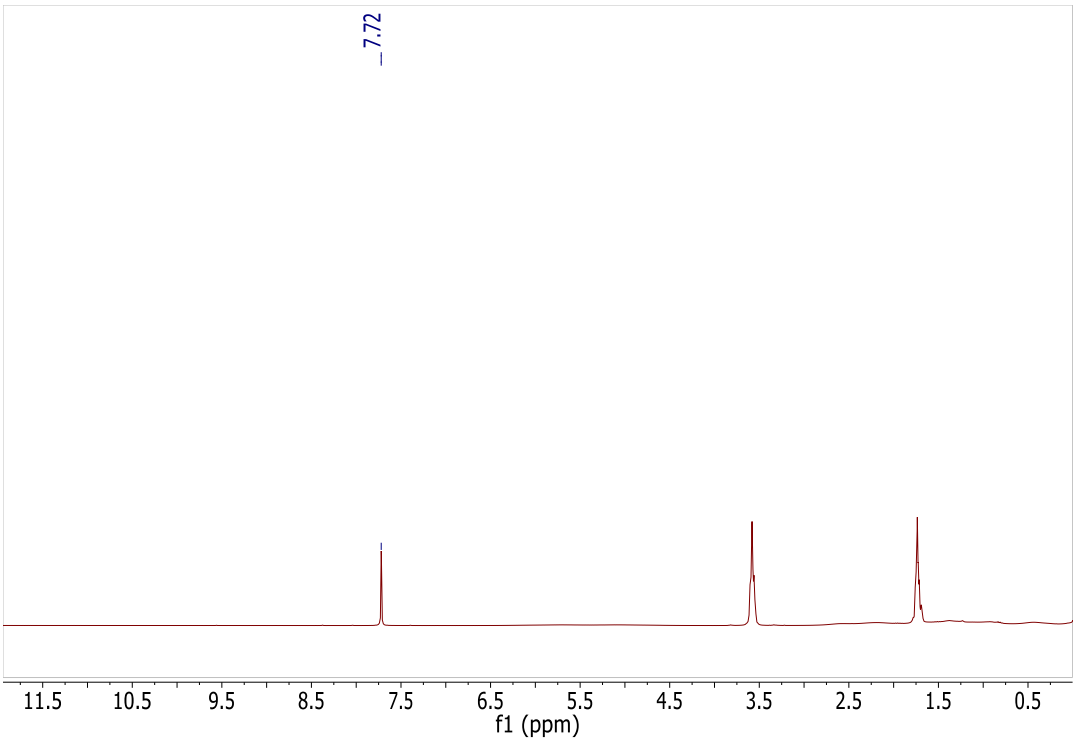

Fig. **4.17** ^{1}H NMR spectrum of **45[K^{+}]** in THF-d$_{8}$.

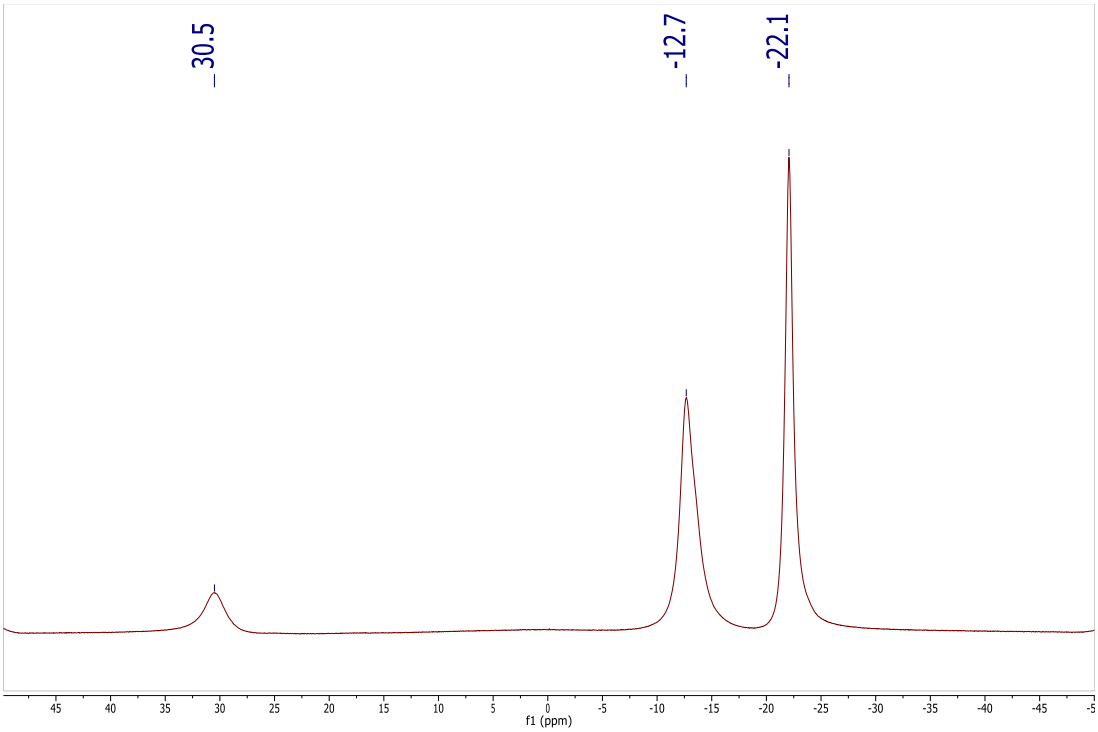

Fig. **4.18** ^{11}B[^{1}H] NMR spectrum of **45[K^{+}]** in THF-d$_{8}$

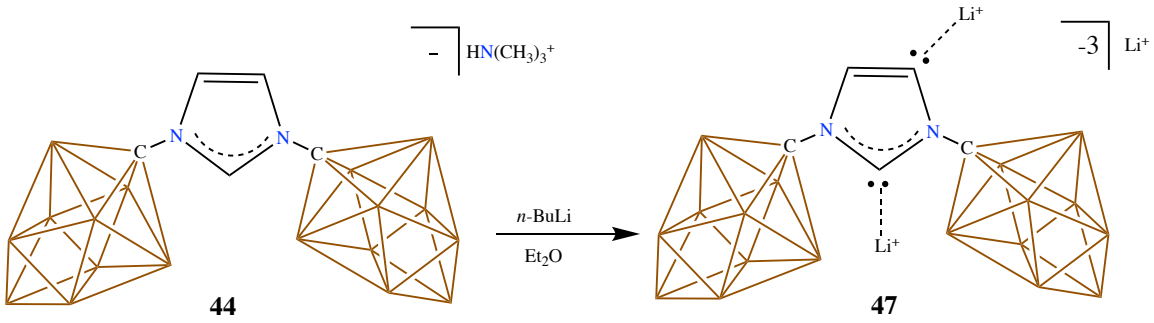

Scheme **4.6** Synthesis of the 10-vertex fused Paranormal N-Heterocyclic Carbene **47**

A vial equipped with a stir bar was loaded with 190 mg (0.51 mmol) of **44**. In a second vial, 3.1 equivalents (102 mg, 0.15 mL, 1.6 mmol) of neat *n*-butyllithium was dissolved in diethyl ether (7 mL) and added to the vial containing **44**. The vial was capped, and the mixture stirred. Upon initial addition of the Et_2O mixture to **44**, an oil formed. After vigorous stirring for 3 hours, the oil developed into a white precipitate. The solvent was decanted from the precipitate, and the remaining volatiles were removed under vacuum, affording the product **47** in 97% yield (370 mg, 0.49 mmol) (Note: Li^+ countercations contain 10 coordinated THF molecules). ^{1}H NMR (700 MHz, tetrahydrofuran-d_8, 25 °C): δ = 7.00 (s, 2H), 0.01-2.65 (bm, 18H, B-H); ^{13}C-(^{1}H-dec) NMR (125 MHz, tetrahydrofuran-d_8, 25 °C): δ = 197.6, 169.3, 128.8, 90.0, 83.3; ^{11}B-(^{1}H-dec) NMR (96 MHz, tetrahydrofuran-d_8, 25 °C): δ = 31.4, -21.8, -22.2 ppm.

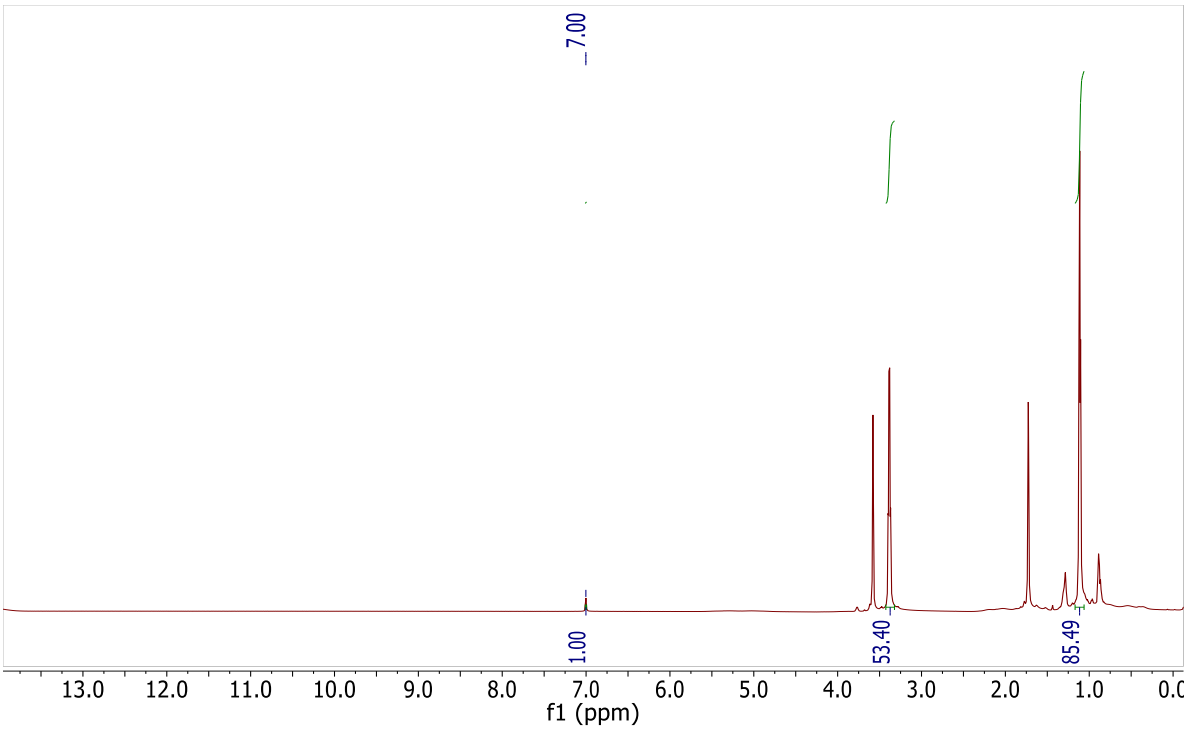

Fig. **4.19** ^{1}H NMR spectrum of **47** in THF-d_8.

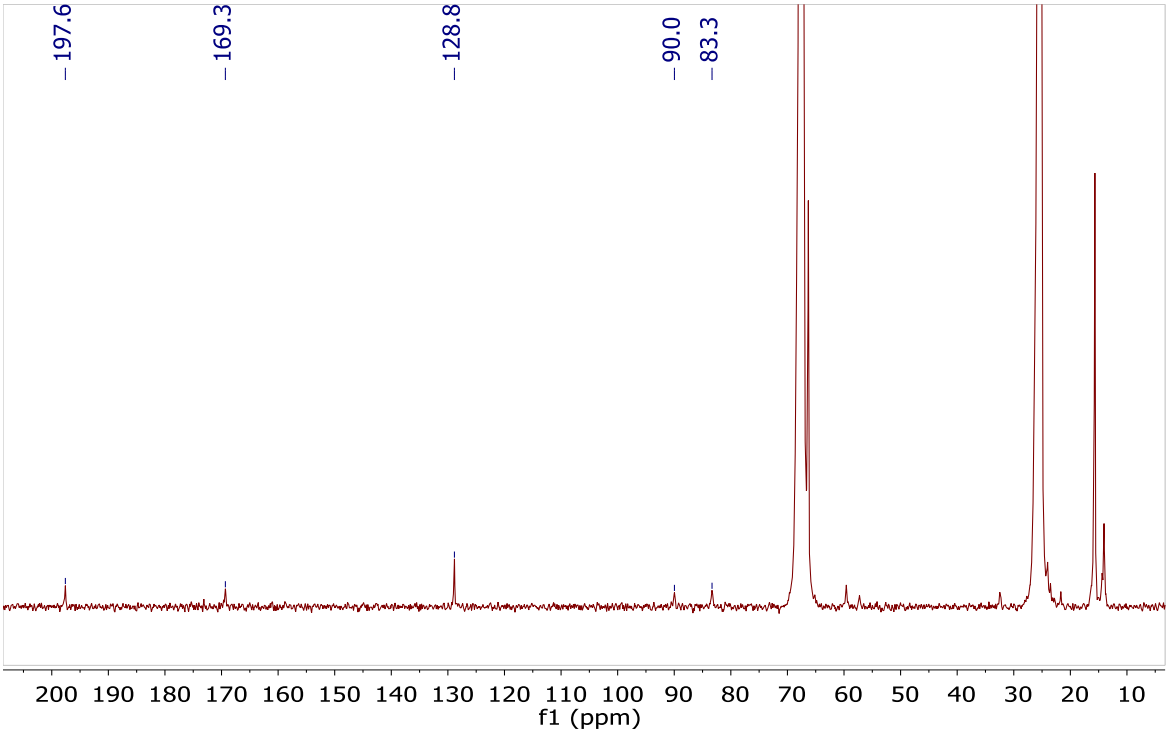

Fig. **4.20** ^{13}C[^{1}H] NMR spectrum of **47** in THF-d_8. Trace n-butyllithium is seen at 14.0, 21.7, and 32.5 ppm.

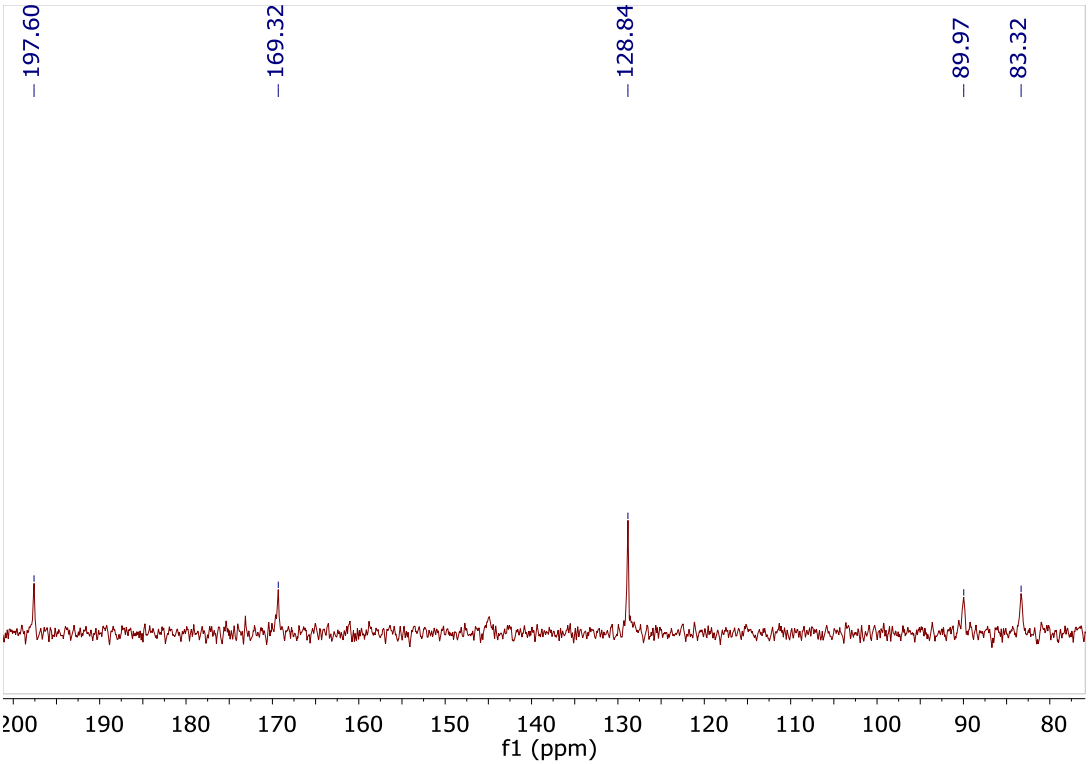

Fig. **4.21** An expanded view of the $^{13}C[^{1}H]$ NMR spectrum of **47** in THF-d_8.

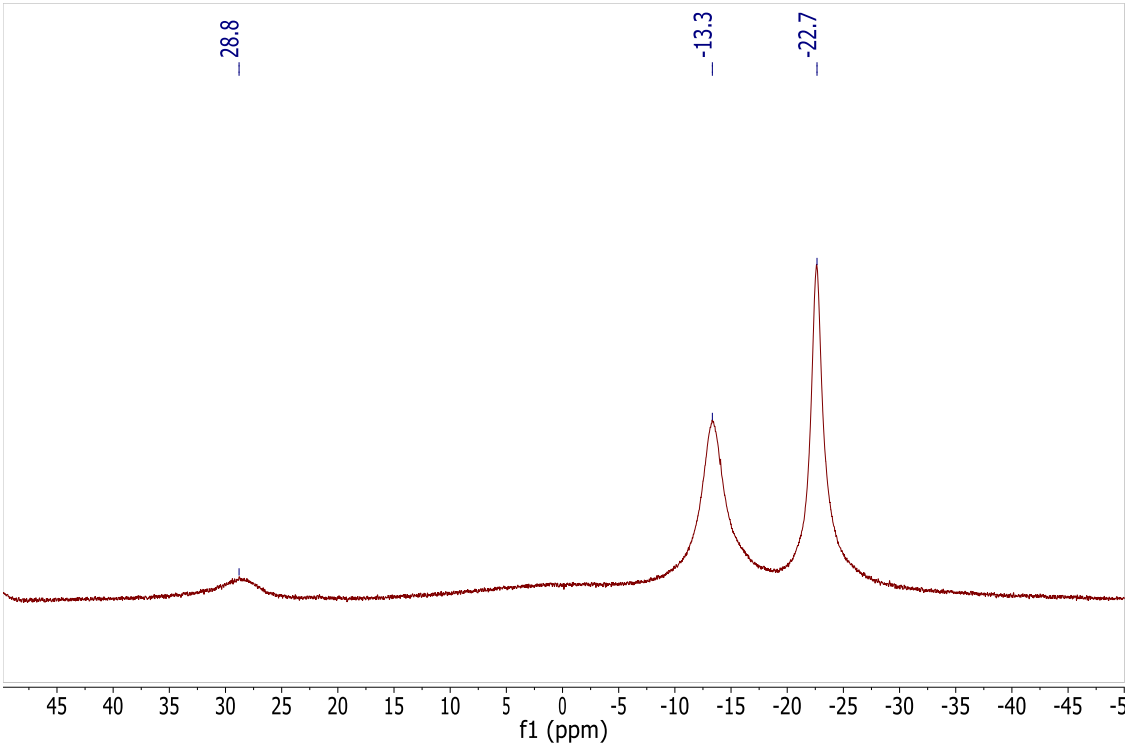

Fig. **4.22** $^{11}B[^{1}H]$ NMR spectrum of **47** in THF-d_8.

X-Ray Structure Determination

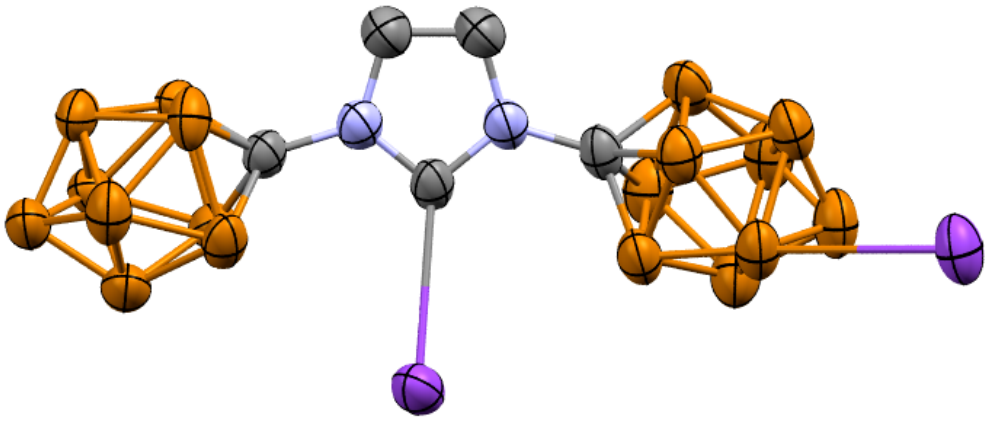

Fig. **4.26**. Solid-state structure of the 10-Vertex NHC dianion **45[K$^+$]**. Boron = brown, carbon= gray, nitrogen= blue, potassium= purple.

For clarity, hydrogen atoms and tetrahydrofuran molecules coordinated to the potassium cations are omitted. One potassium cation is bound to the deprotonated position of the N-heterocyclic carbene, while the other potassium cation is coordinated to the carborane cluster. The line drawn between the potassium cation and the cluster does not represent a sigma bond. The potassium atom bound to the NHC has three THF molecules coordinated to it, while the potassium coordinated to the carborane cluster is also coordinating to the cluster of another NHC molecule and possesses two THF molecules.

A colorless prism fragment (0.589 x 0.559 x 0.478 mm^3) was used for the single crystal x-ray diffraction study of $[C_5H_{20}B_{18}N_2K_2].[C_4H_8O]_7$ (sample vL157SL_70A_0m). The crystal was coated with paratone oil and mounted on to a cryo-loop glass fiber. X-ray intensity data were collected at 200(2) K on a Bruker APEX2 platform-CCD x-ray diffractometer system (fine focus Mo-radiation, λ = 0.71073 Å, 50KV/30mA power). The CCD detector was placed at a distance of 7.0900 cm from the crystal.

A total of 6600 frames were collected for a sphere of reflections (with scan width of 0.3° in ω, starting $\omega/2\theta$ angles at –24°/–24° with ϕ angles of 0°, 90°, 120°, 225°, and starting ω/2θ angles at –29°/–29° with ϕ angles of 0°, 30°, 60°, 90°, 180°, 240°, 270° for every 600 frames, 60 sec/frame exposure time). The frames were integrated using the Bruker SAINT software package and using a narrow-frame integration algorithm. Based on an orthorhombic crystal system, the integrated frames yielded a total of 129683 reflections at a maximum 2θ angle of 52.044° (0.81 Å resolution), of which 10591 were independent reflections (R_{int} = 0.0275, R_{sig} = 0.0132, redundancy = 12.2, completeness = 99.9%) and 9804 (92.6%) reflections were greater than 2σ(I). The unit cell parameters were, **a** = 60.9506(58) Å, **b** = 17.6644 (17) Å, **c** = 9.8809(10) Å, **α** = **β** = γ = 90°**,** V = 10638.3(18) $Å^3$, Z = 8, calculated density D_c = 1.106 g/cm^3. Absorption corrections were applied (absorption coefficient μ = 0.219 mm^{-1}; max/min transmission = 0.903/0.882) to the raw intensity data using the SADABS program.

The Bruker SHELXTL software package was used for phase determination and structure refinement. The distribution of intensities (E^2-1 = 0.721) and systematic absent reflections indicated three possible space groups, Cmc2(1), Cmcm, and Ama2. The space group Ama2 (#40) was later determined to be correct. Direct methods of phase determination followed by two Fourier cycles of refinement led to an electron density map from which most of the non-hydrogen atoms were identified in the asymmetric unit of the unit cell. With subsequent isotropic refinement, all of the non-hydrogen atoms were identified. There was one polymeric structure of $C_5H_{20}B_{18}N_2K_3$ and seven C_4H_8O solvent molecules present in the asymmetric unit of the unit cell. Five of the seven THF molecules were modeled with disorder (disordered site occupancy ratios were 75%/25%, 70%/30%, 58%/42%, 53%/47%

and 50%/50%). The K2 atom and three disordered-THF molecules were located at the mirror plane perpendicular to the a-axis. The K3 atom and two disordered-THF molecule were located at the 2-fold rotation axis parallel to the c-axis. The polymeric chain is propagated along the a-axis. The level B-alerts are probably due to the poor crystal quality and the five highly disordered THF molecules where rigid model restraints were used. The crystal cracks at 100K due to low temperature phase transition and data was collected at 200K.

Atomic coordinates, isotropic and anisotropic displacement parameters of all the non-hydrogen atoms were refined by means of a full matrix least-squares procedure on F^2. The H-atoms were included in the refinement in calculated positions riding on the atoms to which they were attached. The absolute structure Flack's parameter x = 0.038(5). The refinement converged at R1 = 0.0590, wR2 = 0.1698, with intensity, I>2σ(I). The largest peak/hole in the final difference map was 0.589/-0.311 e/Å^3.

Table 4.1 Crystal data and structure refinement for **45[K^+]**

Identification code	vL157SL_70A_0m	
Empirical formula	C33 H76 B18 K2 N2 O7	
Formula weight	885.73	
Temperature	200(2) K	
Wavelength	0.71073 Å	
Crystal system	Orthorhombic	
Space group	A m a 2	
Unit cell dimensions	a = 60.951(6) Å	α= 90°.
	b = 17.6644(17) Å	β= 90°.

	c = 9.8809(10) Å γ = 90°.
Volume	10638.3(18) $Å^3$
Z	8
Density (calculated)	1.106 Mg/m^3
Absorption coefficient	0.219 mm^{-1}
F(000)	3776
Crystal size	0.589 x 0.559 x 0.478 mm^3
Theta range for data collection	2.005 to 26.022°.
Index ranges	-75<=h<=75, -21<=k<=21, -12<=l<=12
Reflections collected	129683
Independent reflections	10591 [R(int) = 0.0275]
Completeness to theta = 25.242°	99.9 %
Absorption correction	Semi-empirical from equivalents
Refinement method	Full-matrix least-squares on F^2
Data / restraints / parameters	10591 / 971 / 775
Goodness-of-fit on F^2	1.100
Final R indices [I>2sigma(I)]	R1 = 0.0590, wR2 = 0.1698
R indices (all data)	R1 = 0.0630, wR2 = 0.1747
Absolute structure parameter	0.038(5)
Extinction coefficient	n/a
Largest diff. peak and hole	0.589 and -0.311 $e.Å^{-3}$

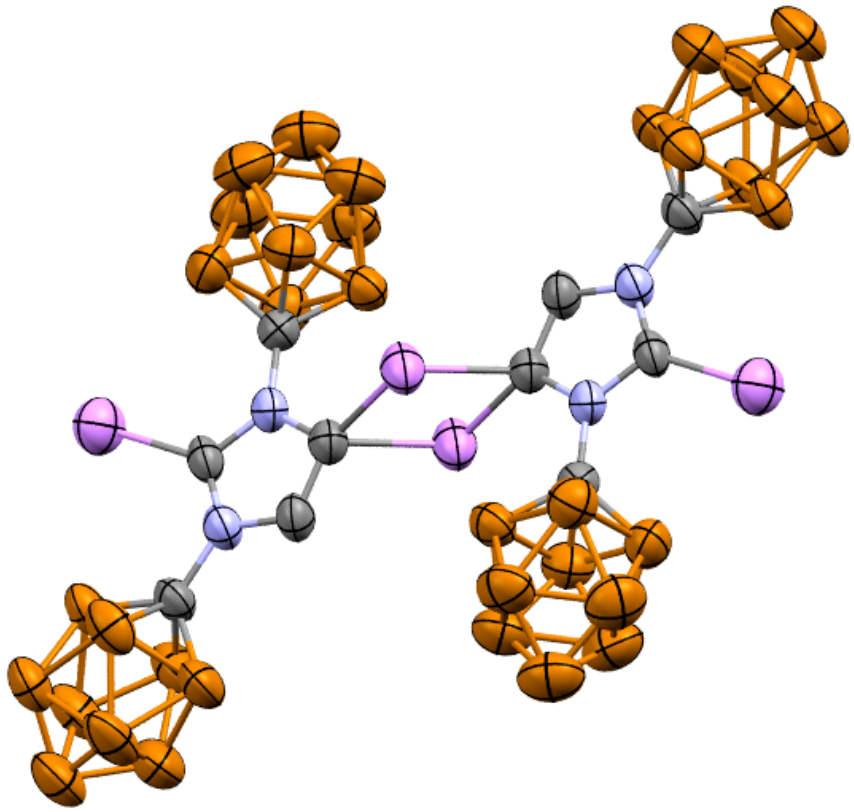

Fig. **4.27**. Solid-state structure of the dimeric 10-vertex tri-anionic doubly deprotonated NHC **47**. Boron = brown, carbon= gray, nitrogen= blue, lithium= purple.

For clarity, hydrogen atoms and six molecules of coordinated THF have been omitted from the lithium countercations shown, as well as two additional Li^+ cations. The crystal structure is dimeric with the C-2 center bound to a single lithium cation and the C-5 center bridging two other lithium cations. This dimeric structure is analogous to the X-ray diffraction study of the trianionic doubly deprotonated C-2/C-5 species possessing 12-vertex carborane clusters.

A colorless needle fragment (0.531 x 0.211 x 0.066 mm^3) was used for the single crystal x-ray diffraction study of $[Li[C_4H_8O]_4]^+.[[C_5H_{19}B_{18}]Li_2[C_4H_8O]_3]^-.[C_4H_8O]$ (sample vL275SL_0m-5). The crystal was coated with paratone oil and mounted on to a cryo-loop

glass fiber. X-ray intensity data were collected at 190(2) K on a Bruker APEX2 platform-CCD x-ray diffractometer system (fine focus Mo-radiation, λ = 0.71073 Å, 50KV/30mA power). The CCD detector was placed at a distance of 5.0600 cm from the crystal.

A total of 3600 frames were collected for a sphere of reflections (with scan width of 0.3^o in ω, starting ω and 2θ angles of –30^o, and ϕ angles of 0^o, 90^o, 120^o, 180^o, 240^o, and 270^o for every 600 frames, 120 sec/frame exposure time). The Bruker Cell_Now program was used to obtain the two different orientation matrices of the rotational twin components (Twin law is 180^o rotation about the 0 0 1 reciprocal axis). These matrices were imported into the APEX2 program for Bravais lattice determination and initial unit cell refinement. The frames were integrated using the Bruker SAINT software package and using a narrow-frame integration algorithm. Based on a triclinic crystal system, the integrated frames yielded a total of 14348 reflections at a maximum 2θ angle of 39.174^o (1.06 Å resolution), of which 4819 were independent reflections (R_{int} = 0.0308, R_{sig} = 0.0370, redundancy = 3.0, completeness = 48.5%) and 3759 (78.0%) reflections were greater than 2σ(I). The unit cell parameters were, **a** = 9.5622(10) Å, **b** = 18.2827(19) Å, **c** = 18.5319(19) Å, α = 114.0568(16) β = 100.8752(17)^o, γ = 102.6755(17) V = 2742.0(5) Å^3, Z = 2, calculated density D_c = 1.086 g/cm^3. Absorption corrections were applied (absorption coefficient μ = 0.066 mm^{-1}; max/min transmission = 0.996/0.966) to the raw intensity data using the TWINABS program.

The Bruker SHELXTL software package was used for phase determination and structure refinement. The distribution of intensities (E^2-1 = 0.854) and no systematic absent reflections indicated two possible space groups, P-1and P1. The space group P-1 (#2) was

later determined to be correct. Direct methods of phase determination followed by two Fourier cycles of refinement led to an electron density map from which most of the non-hydrogen atoms were identified in the asymmetric unit of the unit cell. With subsequent isotropic refinement, all of the non-hydrogen atoms were identified. The combined (major and minor components) HKLF 5 intensity dataset was used in the final structure refinement. There were one disordered cation of $Li[C_4H_8O]_4$, one anion of $[C_5H_{19}B_{18}]Li_2[C_4H_8O]_3$, and one partially occupied (96% occupied) THF solvent molecule present in the asymmetric unit of the unit cell. The dimer-anion was located at the inversion center. Six of the eight THF molecules were modeled with disordered (disordered site occupancy ratios were 70%/30%, 61%/39%, 59%/41%, 59%/41%, 56%/44% and 50%/50%). The rotational twin law was 180° rotation about the 0 0 1 reciprocal axis. The major/minor component twin ratio was 59%/41%. The crystal cracks at 100K due to low temperature phase transition and data was collected at 190K. The A and B-level alerts are due to the poor crystal quality, incomplete data set, and the six highly disordered THF molecules where rigid model restraints were used. Because of the twinning/disorder issues, only about 49% of the triclinic data were collected at long exposure time of 120 second/frame.

Atomic coordinates, isotropic and anisotropic displacement parameters of all the non-hydrogen atoms were refined by means of a full matrix least-squares procedure on F^2. The H-atoms were included in the refinement in calculated positions riding on the atoms to which they were attached. The refinement converged at R1 = 0.0703, wR2 = 0.1722, with intensity $I>2\sigma$ (I). The largest peak/hole in the final difference map was 0.228/-0.217 e/Å^3.

Table 4.2 Crystal data and structure refinement for **47**

Identification code	vL275SL_0m-5	
Empirical formula	C36.83 H82.67 B18 Li3 N2 O7.96	
Formula weight	896.49	
Temperature	190(2) K	
Wavelength	0.71073 Å	
Crystal system	Triclinic	
Space group	P -1	
Unit cell dimensions	a = 9.5622(10) Å	α= 114.0568(16)°.
	b = 18.2827(19) Å	β= 100.8752(17)°.
	c = 18.5319(19) Å	γ = 102.6755(17)°.
Volume	2742.0(5) $Å^3$	
Z	2	
Density (calculated)	1.086 Mg/m^3	
Absorption coefficient	0.066 mm^{-1}	
F(000)	961	
Crystal size	0.531 x 0.211 x 0.066 mm^3	
Theta range for data collection	2.193 to 19.587°.	
Index ranges	-9<=h<=8, -17<=k<=15, 0<=l<=17	
Reflections collected	14348	
Independent reflections	4819 [R(int) = 0.0308]	
Completeness to theta = 25.242°	48.5 %	
Absorption correction	Semi-empirical from equivalents	

Refinement method	Full-matrix least-squares on F^2
Data / restraints / parameters	4819 / 1104 / 797
Goodness-of-fit on F^2	1.060
Final R indices [I>2sigma(I)]	R1 = 0.0703, wR2 = 0.1722
R indices (all data)	R1 = 0.0949, wR2 = 0.1904
Extinction coefficient	n/a
Largest diff. peak and hole	0.228 and -0.217 e.$Å^{-3}$

References

1. Reed, C. A., H+, CH3+, and R3Si+ Carborane Reagents: When Triflates Fail. *Accounts of Chemical Research* **2010,** *43* (1), 121-128.

2. Jelinek, T.; Baldwin, P.; Scheidt, W. R.; Reed, C. A., New weakly coordinating anions. 2. Derivatization of the carborane anion CB11H12. *Inorganic Chemistry* **1993,** *32* (10), 1982-1990.

3. Douvris, C.; Nagaraja, C. M.; Chen, C.-H.; Foxman, B. M.; Ozerov, O. V., Hydrodefluorination and Other Hydrodehalogenation of Aliphatic Carbon−Halogen Bonds Using Silylium Catalysis. *Journal of the American Chemical Society* **2010,** *132* (13), 4946-4953.

4. Douvris, C.; Ozerov, O. V., Hydrodefluorination of Perfluoroalkyl Groups Using Silylium-Carborane Catalysts. *Science* **2008,** *321* (5893), 1188-1190.

5. Shao, B.; Bagdasarian, A. L.; Popov, S.; Nelson, H. M., Arylation of hydrocarbons enabled by organosilicon reagents and weakly coordinating anions. *Science* **2017,** *355* (6332), 1403-1407.

6. Khandelwal, M.; Wehmschulte, R. J., Deoxygenative Reduction of Carbon Dioxide to Methane, Toluene, and Diphenylmethane with [Et2Al]+ as Catalyst. *Angewandte Chemie International Edition* **2012,** *51* (29), 7323-7326.

7. Lavallo, V.; Wright Ii, J. H.; Tham, F. S.; Quinlivan, S., Perhalogenated Carba-closo-dodecaborate Anions as Ligand Substituents: Applications in Gold Catalysis. *Angewandte Chemie International Edition* **2013,** *52* (11), 3172-3176.

8. Kolychev, E. L.; Kronig, S.; Brandhorst, K.; Freytag, M.; Jones, P. G.; Tamm, M., Iridium(I) Complexes with Anionic N-Heterocyclic Carbene Ligands as Catalysts for the Hydrogenation of Alkenes in Nonpolar Media. *Journal of the American Chemical Society* **2013,** *135* (33), 12448-12459.

9. Kronig, S.; Theuergarten, E.; Daniliuc, C. G.; Jones, P. G.; Tamm, M., Anionic N-Heterocyclic Carbenes That Contain a Weakly Coordinating Borate Moiety. *Angewandte Chemie International Edition* **2012,** *51* (13), 3240-3244.

10. Nasr, A.; Winkler, A.; Tamm, M., Anionic N-heterocyclic carbenes: Synthesis, coordination chemistry and applications in homogeneous catalysis. *Coordination Chemistry Reviews* **2016,** *316*, 68-124.

11. Knoth, W. H., 1-B9H9CH- and B11H11CH. *Journal of the American Chemical Society* **1967,** *89* (5), 1274-1275.

12. Wiersema, R. J.; Hawthorne, M. F., Electrochemistry and boron-11 nuclear magnetic resonance spectra of monocarbon carboranes. *Inorganic Chemistry* **1973,** *12* (4), 785-788.

13. McArthur, S. G.; Jay, R.; Geng, L.; Guo, J.; Lavallo, V., Below the 12-vertex: 10-vertex carborane anions as non-corrosive, halide free, electrolytes for rechargeable Mg batteries. *Chemical Communications* **2017,** *53* (32), 4453-4456.

14. Tsang, C.-W.; Yang, Q.; Sze, E. T.-P.; Mak, T. C. W.; Chan, D. T. W.; Xie, Z., Synthesis and Structural Characterization of Highly Chlorinated, Brominated, Iodinated, and Methylated Carborane Anions, 1-H-CB9X9-, 1-NH2-CB9X9- (X = Cl, Br, I), and 1-H-CB9(CH3)9-. *Inorganic Chemistry* **2000,** *39* (16), 3582-3589.

15. Estrada, J.; Lugo, C. A.; McArthur, S. G.; Lavallo, V., Inductive effects of 10 and 12-vertex closo-carborane anions: cluster size and charge make a difference. *Chemical Communications* **2016,** *52* (9), 1824-1826.

16. Jelinek, T.; Plešek, B.; Heřmánek, S., Isolation and reactions of 6-H3N-6-CB9H11. *Journal of Organometallic Chemistry* **1986,** *307* (2), C13-C15.

17. El-Hellani, A.; Lavallo, V., Fusing N-Heterocyclic Carbenes with Carborane Anions. *Angewandte Chemie International Edition* **2014,** *53* (17), 4489-4493.

Chapter 5: Isolation of a Water Stable Carbene

5.1 Introduction

Thiamine **48**, more commonly known as vitamin B1, is an essential micronutrient for human life.[1] Phosphorylated forms of thiamine are essential for certain metabolic pathways. For example, in the form of its pyrophosphate cocarboxylase, it is the coenzyme for a number of important aqueous biochemical pathways, such as the decarboxylation of pyruvic acid to acetaldehyde, and the conversion of pyruvic acid to acetoin.[2] Thiamine and its derivatives have also been shown to catalyze a variety of interesting umpolung reactions in the presence of base, such as the classical benzoin and acyloin condensation reactions.[3] Although initially poorly understood, in 1958, based on deuterium labeling experiments in D_2O, Breslow proposed that the active species generated from the thiamine residue was an N-Heterocyclic Carbene (NHC), thiazolylidene (Scheme **5.1**).[4] The proposition that a carbene, a typically exceedingly reactive molecule featuring a divalent carbon atom and a nonbonding pair of electrons could be persistent long enough to engage in controlled chemical reactivity, let alone in water, was a visionary hypothesis. Although there has never been any spectroscopic evidence for the formation of a carbene in water, Breslow's hypothesis has been accepted by the scientific community to be correct.

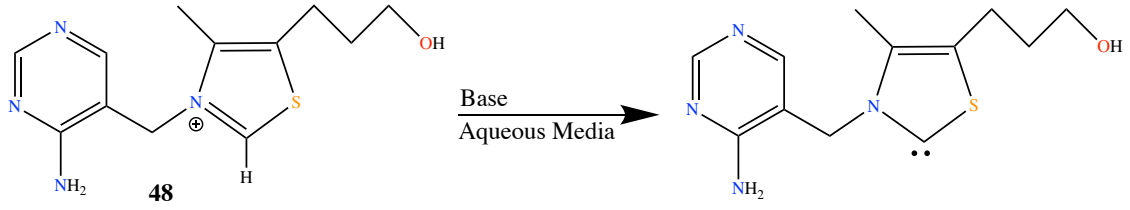

Scheme **5.1** Breslow's proposed carbene generation in water

Subsequently, in 1968 Wanzlick and Ofele independently showed that the N-Heterocyclic Carbene (NHC) metal complexes could be formed by contact of an imidazolium salt with

basic transition metal precursors, implying the complexes might be generated via the formation of transient metal free NHCs.[5] For years, Wanzlick went on to attempt to isolate these so-called imidazolylidenes but was not successful. These pioneering works paved the way for the seminal discoveries of Bertrand (1988)[6] and Arduengo (1991)[7] of the first bottleable carbene and NHC, namely the liquid phosphinosilylcarbene and solid N,N-diadamantylimidazolylidene, respectively.

5.2 Air-Stable Carbenes

Neither of these carbenes are air stable, presumably because of gaseous water in our atmosphere. However, Arduengo took carbene stability to a new level with his report of the only known "air-stable" NHC **49** (Fig. **5.1**)[8], which features a doubly chlorinated imidazolylidene backbone and the carbene center flanked by two N-mesityl groups. The double chlorination of the backbone is thought to be key as it stabilizes the NHC lone pair via σ-inductive effects. In the manuscript, Arduengo claimed that stirred benzene solutions of this molecule open to air showed no decomposition after several days, meaning that in principle this carbene should be bench-top stable. It was not reported if this NHC was actually stable towards contact with water or perhaps there may be some sort of shielding effect from the water in the atmosphere because of the hydrophobic nature of benzene. Subsequently, Denk and coworkers showed that a THF solution of the *t*-butyl substituted NHC **50** (Fig. **5.2**) undergoes slow hydrolysis over 3 months when it is reacted with one equivalent of water.[9]

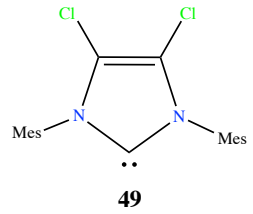

49

Fig. **5.1** Arduengo's Air-Stable Carbene

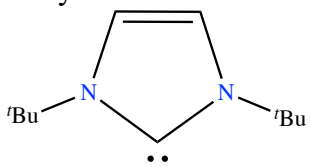

50

Fig. **5.2** t-butyl substituted NHC

Here we report the first truly water stable carbene. This molecule appears to exist indefinitely in liquid water solutions, and we present spectroscopic proof that this carbene is not only stable towards water but can also be generated in water. Thus, this study unambiguously confirms Breslow's hypothesis that under the right circumstances it is possible to generate persistent carbenes in an aqueous environment.

*5.3 Perchlorination of Imidazolium **44***

Over the last decade we have been developing ligands bearing functionalized carborane clusters for various applications.[10] In the previous chapter, we showed that it is possible to prepare anionic imidazolium salts **44** and the corresponding dianionic carbenoid **45** appended with the ten 10-vertex *closo*-carborane anions (CB_9^{1-}).[11] Similar to what we have shown is possible with polyhalogenated carboranyl NHCs bearing 12-vertex N-carboranyl groups (CB_{11}^{1-}), we are interested in developing analogues of these ligands with the smaller 10-vertex cluster to implement in studies of weakly coordinating yet reactive organometallic and main group ion-pairs.

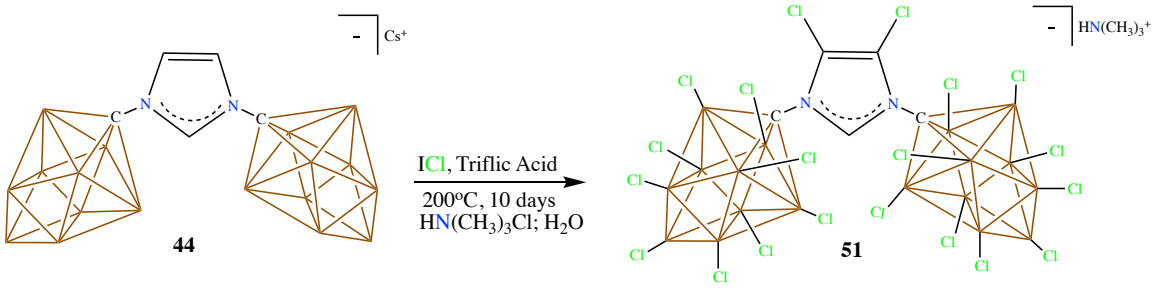

Scheme **5.2** Synthesis of the perchlorinated 10-veretx imidazolium **51**

We have learned that perchlorination of NHCs bearing anionic 12-vertex N-hydrido carboranyl clusters is not possible (the reaction never goes to completion probably for steric reasons), however, we have discovered that the imidazolium anion **44** can be completely

chlorinated, including the backbone by heating with ICl and triflic acid in a Teflon bomb over a period of 10-15 days to produce **51**.

5.4 Perchlorinated 10-vertex Carbene

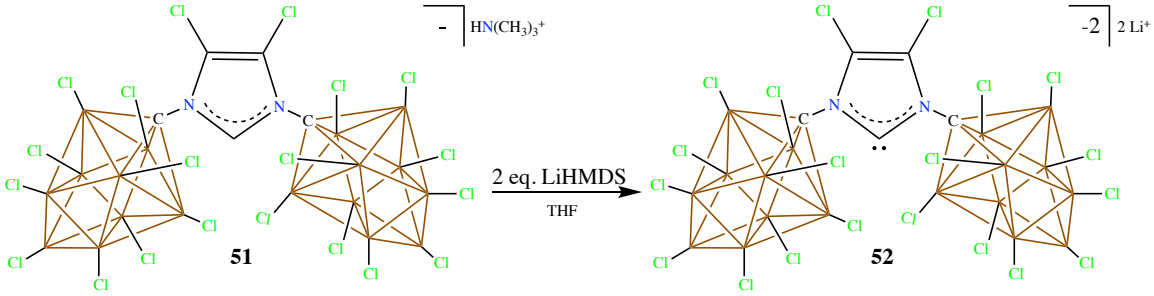

Scheme **5.3** Synthesis of the perchlorinated NHC **52**

The corresponding carbene **52** can be easily formed in quantitative yield by deprotonation with two equivalents of LiHMDS. Analysis of the ^{1}H NMR of **52** showed the expected absence of the single imidazolium proton and the ^{11}B NMR shows movement of the resonances but retention of the local C_{4v} symmetry, which is consistent with the formation of a new single compound. The ^{13}C NMR spectrum is most instructive as it shows a carbene

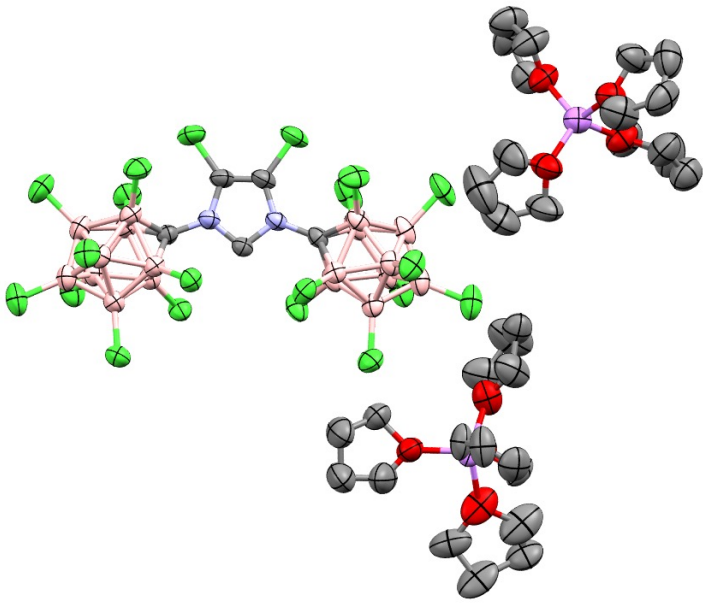

Fig. **5.1** Solid-State Structure of the NHC **52**. Hydrogen atoms omitted for clarity. N=Blue, Cl=green, B=pink, Li=purple, O=red, C=grey

carbon resonance significantly shifted downfield (240 ppm for **52**) relative to the carbenoid **45** (200 ppm), which is consistent with a deshielding effect from all of the electron withdrawing Cl groups. Analysis of the ^{7}Li NMR shows a single Li peak that corresponding to $Li^{+}(THF)_4$ suggesting that in contrast to **45**, **52** is a free carbene in solution. The structure of **52** was unambiguously determined via single crystal X-ray diffraction, which shows that indeed this species is a free dianionic carbene and not a carbenoid in the solid-state (Fig. **5.3**).

5.5 Water Stability Studies

The NMR samples were prepared in normal NMR tubes in the glove box, with the caps wrapped with electrical tape to slow down the diffusion of air into the samples in lieu of the more expensive J-Young tubes. We noticed that when the samples were left on the bench for several days, the NMR spectra remained completely unchanged showing no signs of decomposition via hydrolysis. This is rather unusual for most NHCs, save for the reports mentioned above and this observation piqued our curiosity into the potential water stability of this compound. Adding tap water to the THF solutions of the carbene to the point of water saturation (a monophasic solution), we noticed immediate protonation of the carbene and reformation of the starting material **51** but no hydrolysis. We hypothesized that perhaps impurities, such as carbonic acid from CO_2 dissolution in the tap water, were leading to the observed protonation. Thus, we carefully distilled water under argon and repeated the experiment in a J-Young tube and amazingly the NHC was completely intact with no signs of protonation or decomposition of any kind even in massive excess of water. Monitoring this sample and a few others over 6 months via NMR spectroscopy showed absolutely no decomposition of the carbene, thus it is truly the first water stable carbene.

We next attempted to generate the carbene in pure water with LiOH but learned that the reaction did not proceed due to the insolubility of **51** in water. Thus, we added enough THF to the water suspension to solubilize **51** and found that **52** indeed formed under these aqueous conditions. However, when **52** is formed in this manner it is the minor product and the major product is the ring opened amide **53**. As the carbene **52** and amide **53** are both persistent in the water/THF solution and no interconversion from carbene to ring opened product is observed, one can conclude that the formation of **53** is the result of competitive nucleophilic attack by hydroxide and not from the reaction of the carbene with water itself.

To confirm that the carbene **52** possess special water stability compared to the reported water-resistant species, we decided to synthesize these Arduengo-type NHCs and reinvestigate how they behaved in an excess of water. When a benzene or THF solution of compound **49**, Arduengo's so-called "air-stable" carbene[8], was treated with one equivalent of distilled H_2O they are completely consumed by the time the sample is loaded into the NMR spectrometer. The products consist of unidentified species as well resonances indicative of ring opening hydrolysis. When a THF solution of the NHC **50** is exposed to eleven equivalents of H_2O, it completely undergoes ring opening hydrolysis before an NMR spectrum can be recorded. If less than eleven equivalents were used, similar to Denk,[9] we observe the presence of NHC **50** as well as the hydrolysis product in the ^{1}H-NMR spectrum.

To gain insight into exactly why NHC **52** is stable in water, we calculated the pKa of imidazolium salt **51**. Using computational calculations, the pKa was found to be 11.94 iterating the significant electron withdrawing effect of the Cl groups. It further means the

compound is about 1000 times more acidic than water. Hence, we became curious to see if water can act as a base to deprotonate the precursor. Dissolving in a THF/water mixture with LiOH, the carbene was produced with the corresponding Li^+ counter-cation albeit in a small amount. The solution predominantly comprised of the precursor and a small quantity of the ring opened amide product probably form the nucleophilic attack of the hydroxide on the carbene carbon.

Given the indefinite stability of the compound in water, we tried growing single crystals of the compound suitable for X-Ray diffraction in water. This would prove the compound can exist in the presence of water beyond a doubt. However, this was limited by the insolubility of the compound in liquid water. Hence, we attempted growing single crystals from other water miscible solvents like methanol, ethanol, isopropanol, THF and DMSO with trace amounts of water added. Unfortunately, all our attempts to grow crystals from these solvent combinations failed. However, it's interesting to note that no protonation of the carbene was observed in any of these solvents, signifying the water stability of the compound.

5.6 Conclusion

In conclusion, 30 years after the first stable carbene was reported, the first example of a truly water stable carbene is presented here. This work demonstrates the functionalization of carborane clusters in imparting highly weakly coordinating properties to the ligands. It paves the way for future carbene design that can be employed as catalysts in aqueous media and help advance the realms of synthetic chemistry.

5.7 Experimental

General Considerations:

Unless otherwise stated, all manipulations were carried out using standard Schlenk or glovebox techniques (O_2, H_2O < 1ppm) under a dinitrogen or argon atmosphere. Solvents were dried on sodium-potassium alloy or potassium benzophenone ketyl and distilled under argon before use. Compound **44** was prepared according to literature methods.[11] Reagents were purchased from commercial vendors and used without further purification. NMR spectra were recorded on Bruker Avance 300 MHz, Bruker Avance Neo 400 MHz, Bruker Avance 600 MHz, Bruker Avance III 700 MHz, Varian Inova 300 MHz, or Varian Inova 400 MHz spectrometers. NMR chemical shifts are reported in parts per million (ppm). ^{1}H NMR and ^{13}C NMR chemical shifts were referenced to residual solvent. ^{11}B NMR chemical shifts were externally referenced to $BF_3.OEt_2$. High-resolution mass spectrometry (HRMS) was recorded on Agilent Technologies 6210 (time of flight LC/MS) using ESI technique. Complete crystallographic data for compound **52** is available free of charge from the Cambridge Crystallographic Data Center under the reference numbers 1848698, respectively**.** The crystallographic data of these structures can be accessed via the ccdc website:

http://www.ccdc.cam.ac.uk/Community/Requestastructure/Pages/DataRequest.aspx.

Synthesis of Perchlorinated Imidazolium Salt 51:

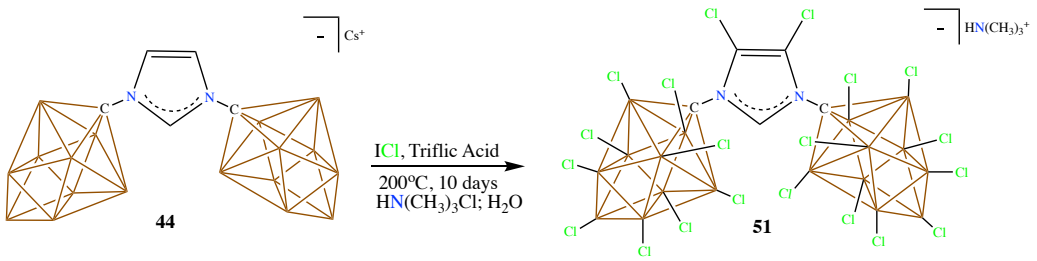

Scheme **5.2** Synthesis of the perchlorinated 10-vertex imidazolium **51**

A Teflon-lined bomb reactor (Berghof DAB-3) equipped with a stir bar was loaded with 1.12 grams (3.02 mmol) of **44[Cs^+]**. Iodine monochloride (68 g, 21mL) and triflic acid (50 mL) were slowly added under a blanket of dry argon. The reactor was sealed (use torque specs from the instruction manual, ca 30 NM), placed behind a blast shield and heated to 200°C for 10 days in a copper shot bath. Reaction progress was monitored via mass spectrometry. After 10 days, the reactor was allowed to cool to room temperature, opened and the solution was transferred into a round bottom flask. Excess ICl and triflic acid were removed via trap-to-trap distillation at 180°C. The remaining compound was dissolved in 150 mL of ethyl acetate and washed with 50 mL of 10% $NaHSO_3$ aqueous solution. The ethyl acetate was removed on a rotary evaporator and 1.5 equivalents of trimethylammonium hydrochloride in a 100 mL solution of water was added, affording the product **51** in 81% yield (2.78 g, 2.6 mmol). ^{1}H NMR (400 MHz, tetrahydrofuran -d_8, 25 °C): δ = 9.51 (s, 1H); ^{13}C[^{1}H] NMR (125 MHz, tetrahydrofuran -d_8, 25 °C): δ = 141.71, 124.83; ^{11}B[^{1}H] NMR (96 MHz, tetrahydrofuran -d_8, 25 °C): δ = 27.6, -0.05, -2.78 ppm. HRMS (negative mode ESI/APCI) [M]- m/z calc'd for $N_2C_5B_{18}Cl_{20}H^-$ = 992.5583; Found = 992.5597.

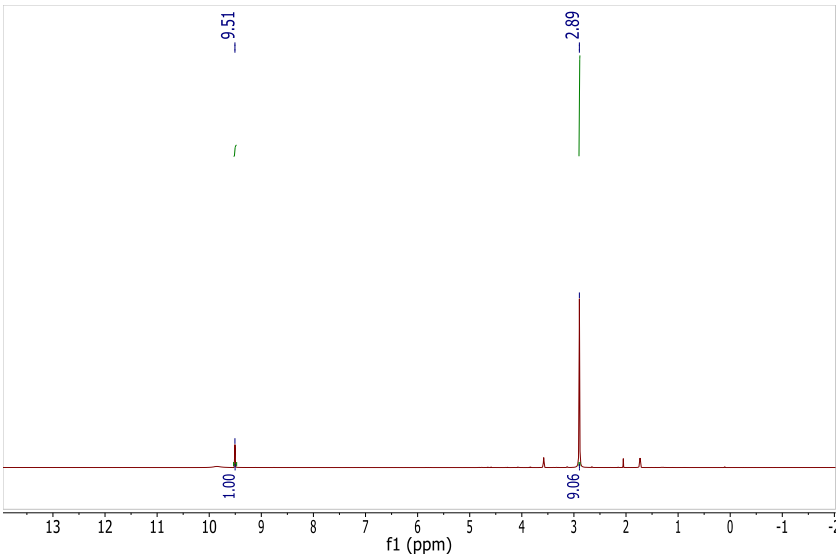

Fig. **5.2** ^{1}H NMR spectrum of **51** in THF-d_8.

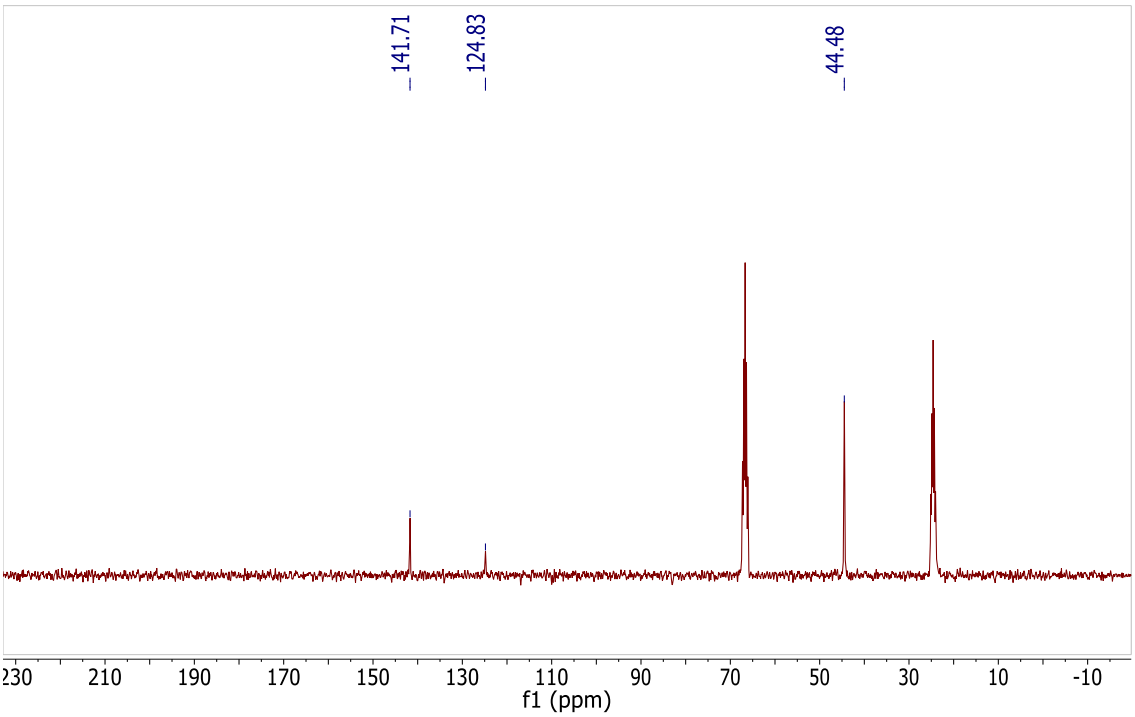

Fig. **5.3** ^{13}C[^{1}H] NMR spectrum of **51** in THF-d_8.

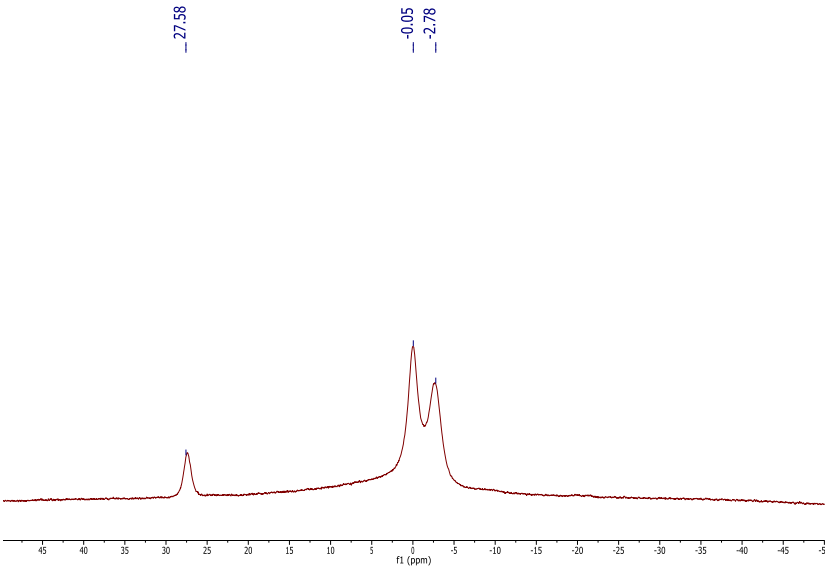

Fig. **5.4** $^{11}B[^{1}H]$ NMR of **51** in THF-d_8.

Synthesis of Perchlorinated Li^+ NHC 52:

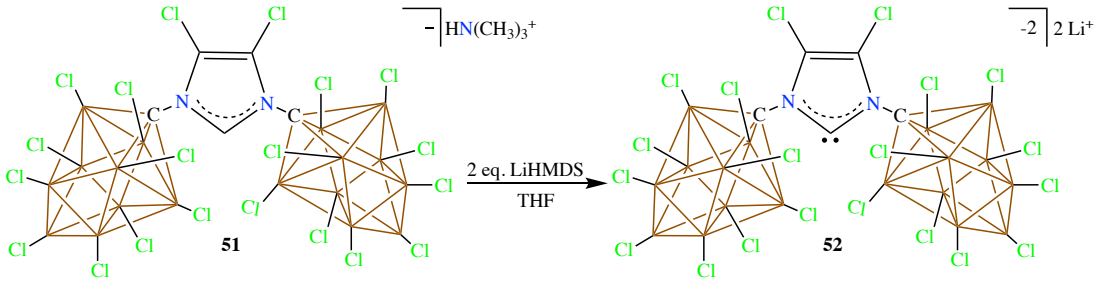

Scheme **5.3** Synthesis of the perchlorinated NHC **52**

A vial equipped with a stir bar was loaded with 200 mg (0.18 mmol) of **51** ($HNMe_3^+$) and 3 mL of tetrahydrofuran. In a second vial, 2.3 equivalents (69 mg, 0.41 mmol) of LiHMDS was added and dissolved in THF (3 mL). The two tetrahydrofuran solutions were combined, the vial capped, and the mixture was stirred for 15 minutes. The tetrahydrofuran solution was added dropwise to a stirring vial of diethyl ether (20 mL), precipitating a light

brown powder. The precipitate was left stirring in diethyl ether for 30 minutes. The solvent was decanted from the precipitate, and the remaining volatiles were removed under vacuum, affording the product **52** in 92% yield (253 mg, 0.16 mmol) (Note: Li^+ countercations contain 4 coordinated tetrahydrofuran molecules). Crystals suitable for a single crystal X-ray diffraction study were grown at -30 °C by layering a THF solution of **10** with diethyl ether. $^{13}C[^1H]$ NMR (125 MHz, tetrahydrofuran-d_8, 25 °C): δ = 238.9, 117.9; $^{11}B[^1H]$ NMR (96 MHz, tetrahydrofuran-d_8, 25 °C): δ = 22.6, -1.7, -4.1 ppm.

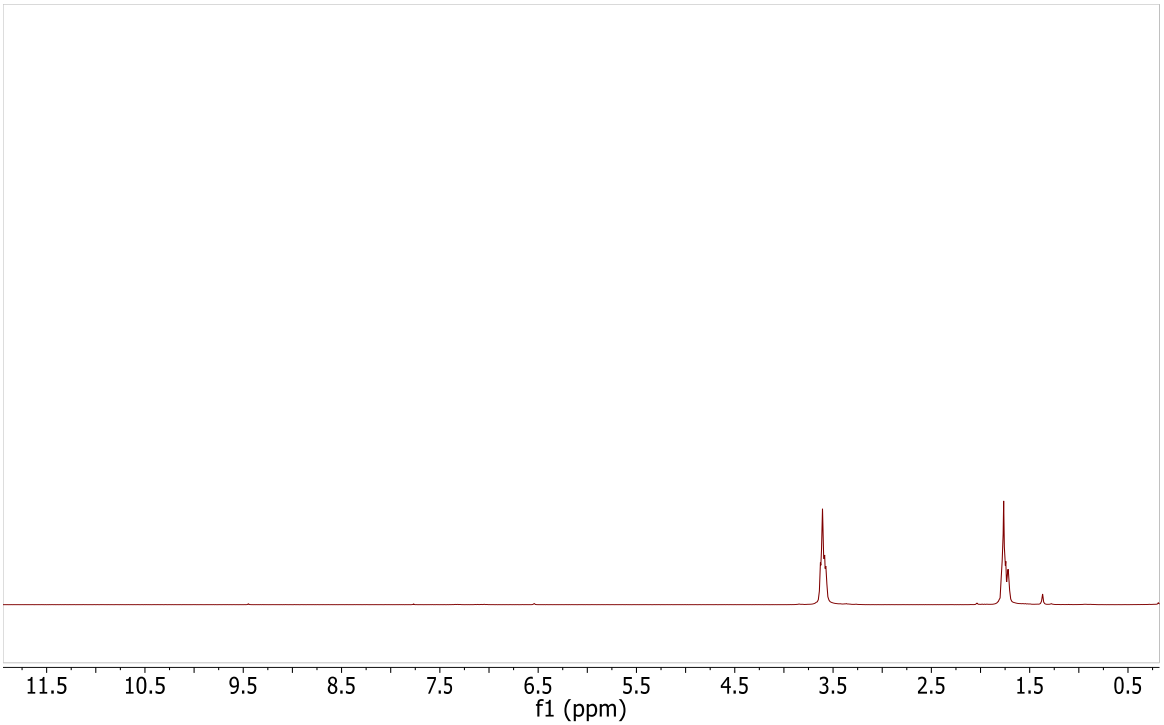

Fig. **5.5** ^1H NMR of **52** in THF-d_8. *Note: The disappearance of the C-2 proton after making the carbene.*

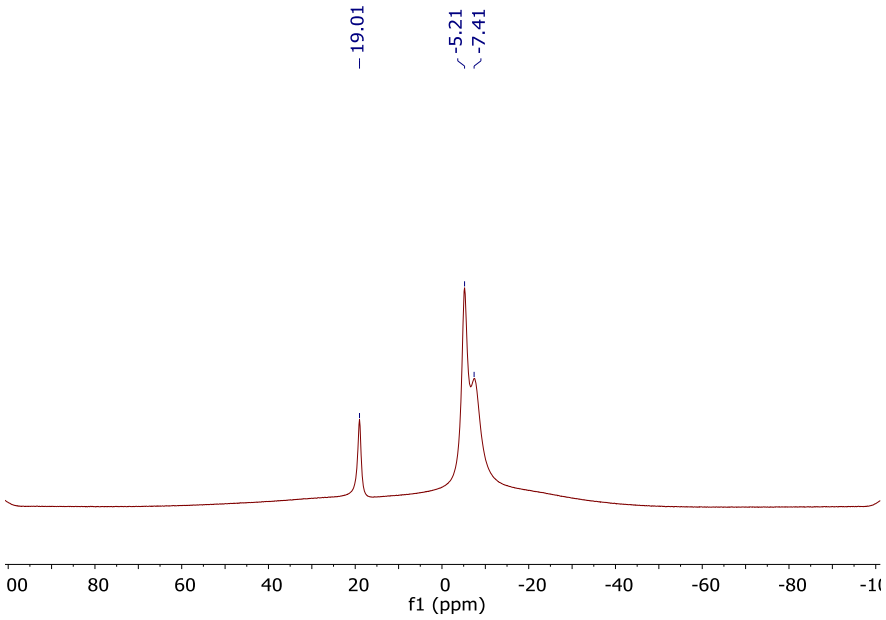

Fig. **5.6** $^{11}B[^{1}H]$ NMR of **52** in THF-d_8.

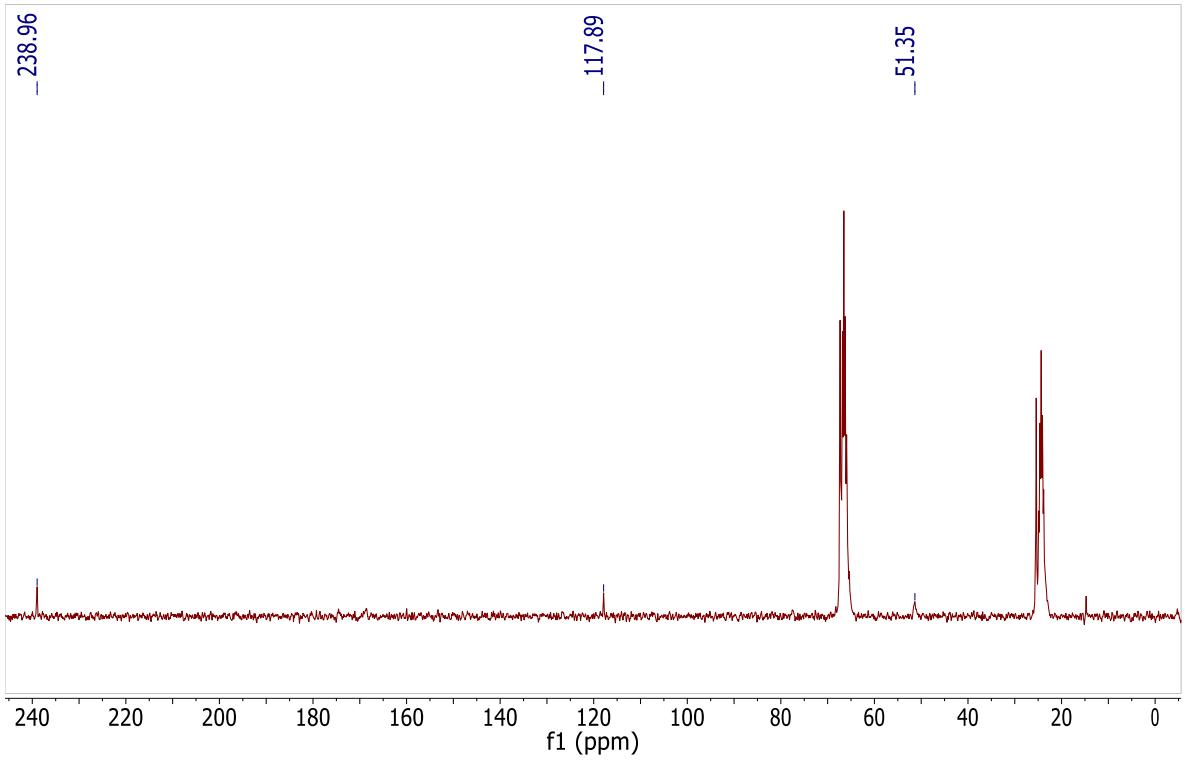

Fig. **5.7** $^{13}C[^{1}H]$ NMR of **52** in THF-d_8. *Note: The presence of carbene carbon peak at 238.96 ppm.*

Water Stability Observations of Li^+ NHC 52:

A) An NMR sample of **52** in 0.5 mL tetrahydrofuran-d_8 was prepared under a nitrogen atmosphere, and then exposed to air for 10 minutes. The sample was checked by ^1H, ^{11}B, and ^{13}C NMR, and upon seeing no protonation, distilled H_2O was added in increments of 0.025 mL, until 0.25 mL of H_2O total was added to the NMR tube. One drop (~0.01 mL) of 10% v/v HCl was added to the sample, protonating **52** and reforming **51**.

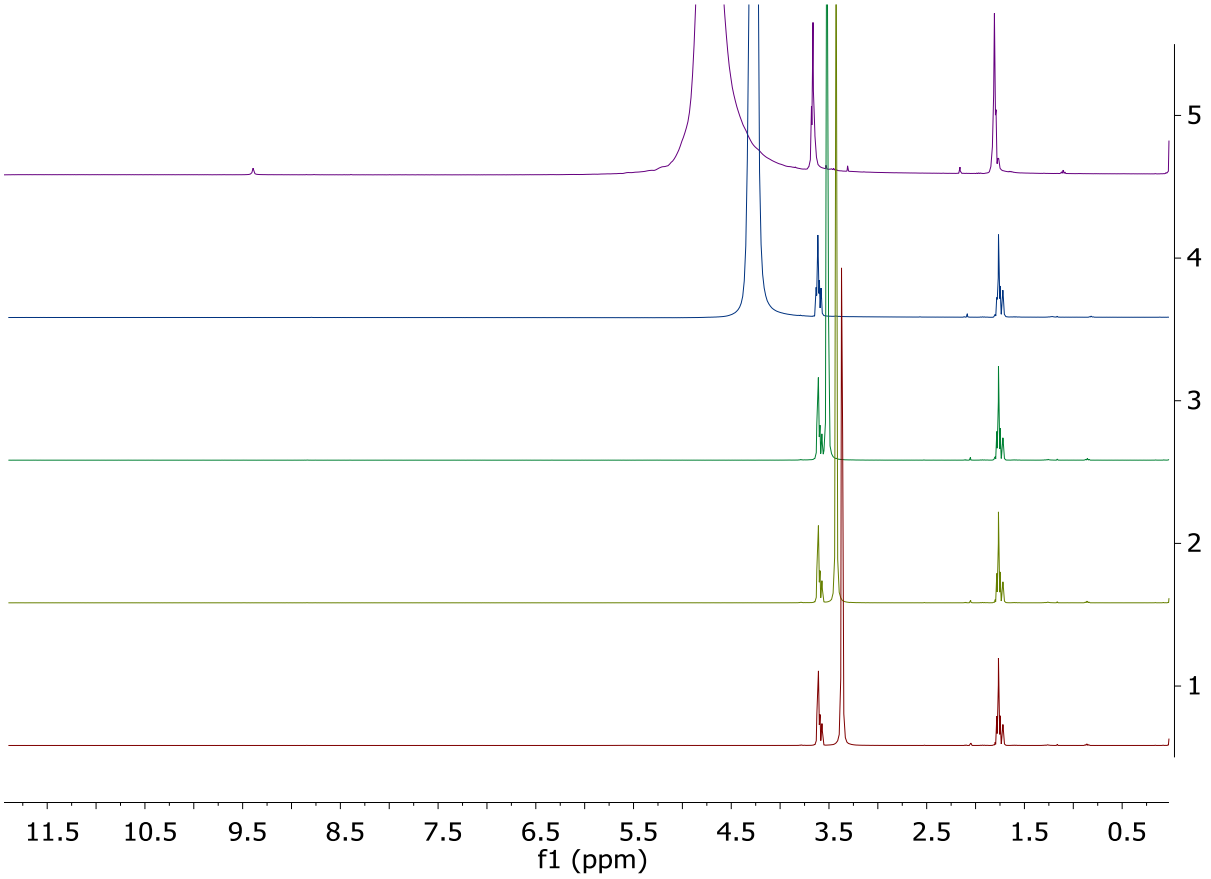

Fig. **5.8** ^1H NMR of **52** in tetrahydrofuran-d_8. 1.) 0.025 mL H_2O, 2.) 0.050 mL H_2O 3.) 0.075 mL H_2O 4.) 0.200 mL H_2O, 5.) 0.250 mL H_2O, 0.01 mL of 10% v/v HCl

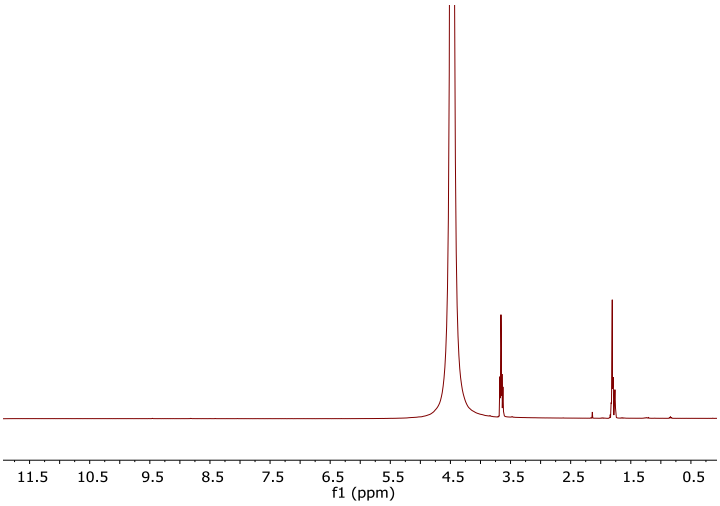

Fig. **5.9** ^{1}H NMR of **52** in THF-d_8 with 0.200 mL H_2O

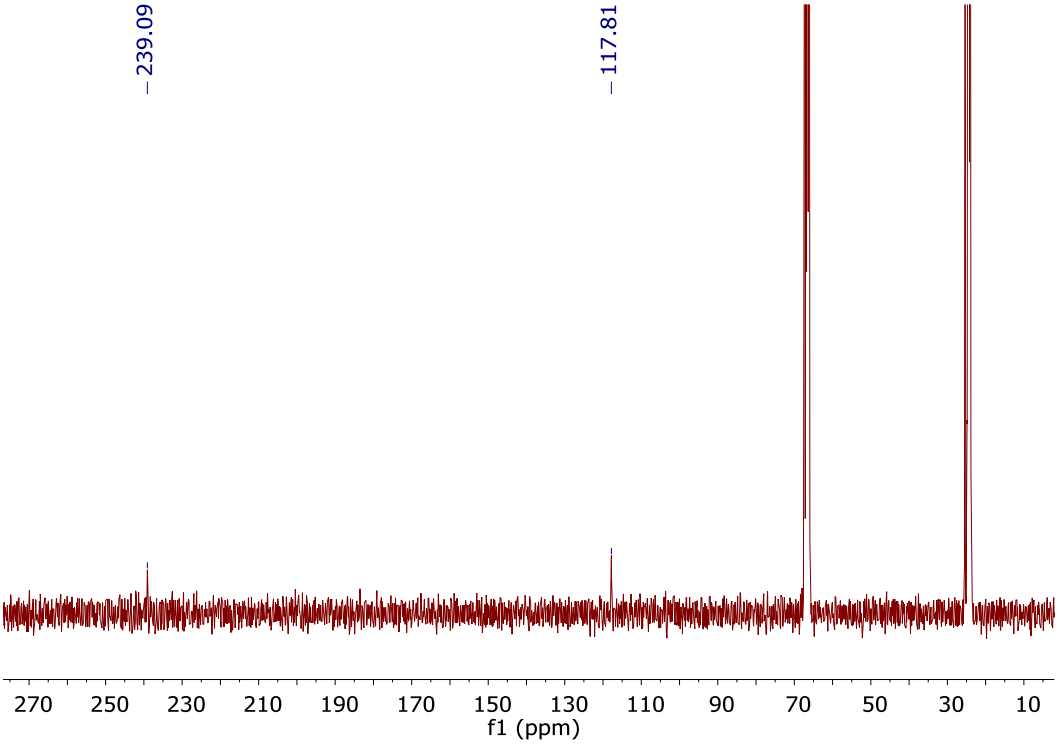

Fig. **5.10** $^{13}C[^{1}H]$ NMR of **52** in THF-d_8 with 0.200 mL H_2O

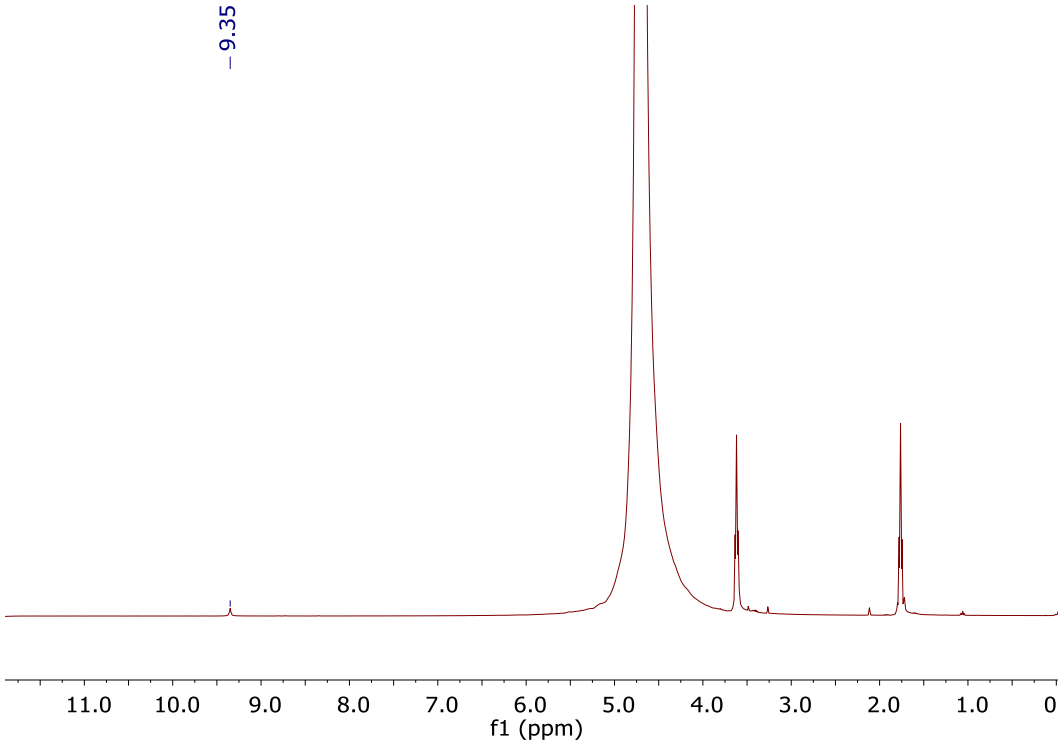

Fig. **5.11** ^{1}H NMR of **52** in THF-d_8 with 0.25 mL H_2O and 0.01 mL 10% v/v HCl

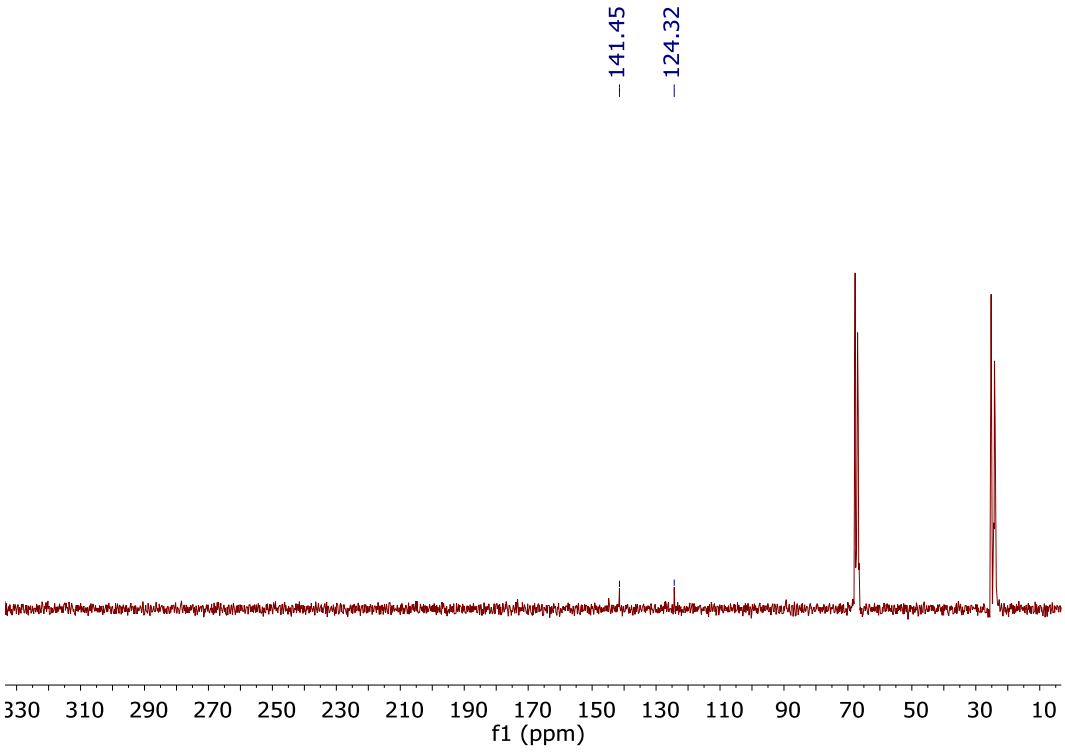

Fig. **5.12** $^{13}C[^{1}H]$ NMR of **52** in THF-d_8 with 0.25 mL H_2O and 0.01 mL 10% v/v HCl

B) A suspension of **52** in 0.30 mL H_2O was prepared in an NMR tube. Tetrahydrofuran was added dropwise, initially forming two layers, until **52** was detected by ^{13}C NMR. The NMR sample containing **52** was protonated with 0.01 mL of 10% v/v HCl added to the sample, reforming **51**.

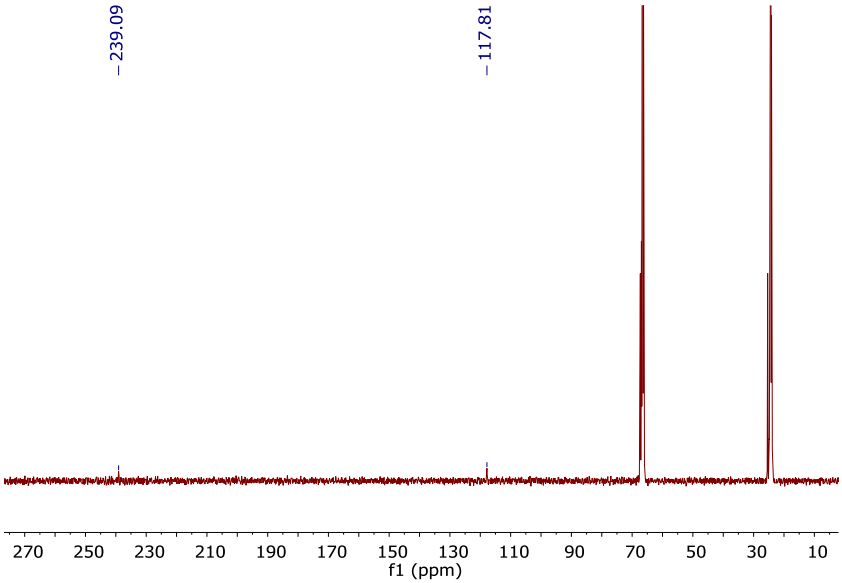

Fig. **5.13** $^{13}C[^1H]$ NMR of **52** in THF-d_8 with 0.30 mL H_2O

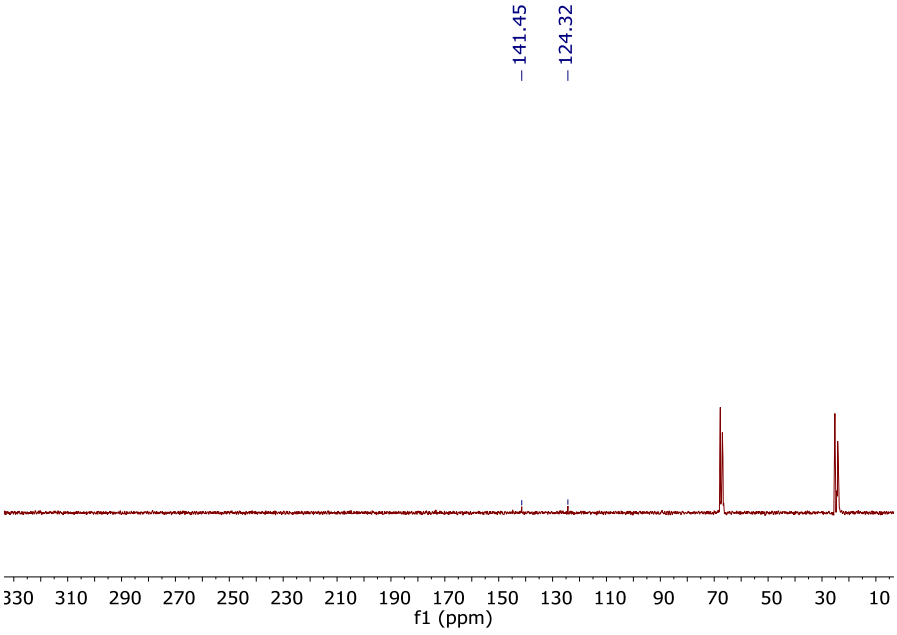

Fig. **5.14** $^{13}C[^1H]$ NMR of **52** in THF-d_8 with 0.30 mL H_2O and 0.01 mL 10% v/v HCl

Water Stability Observations of 49 in THF:

The carbene **49** was prepared according to literature methods.[8] An NMR sample of 1,3-dimesityl-4,5-dichloroimidazol-2-ylidene (0.124 g, 0.332 mmol) in 1.0 mL tetrahydrofuran-d_8 was prepared under a nitrogen atmosphere. Distilled H_2O (6 µL, 0.333 mmol) was added and the sample was checked by ^1H and ^{13}C NMR. A small amount of precipitate began to form. The solution was decanted, and the precipitate was dissolved with an additional 0.5 mL tetrahydrofuran-d_8 and checked by ^1H and ^{13}C NMR.

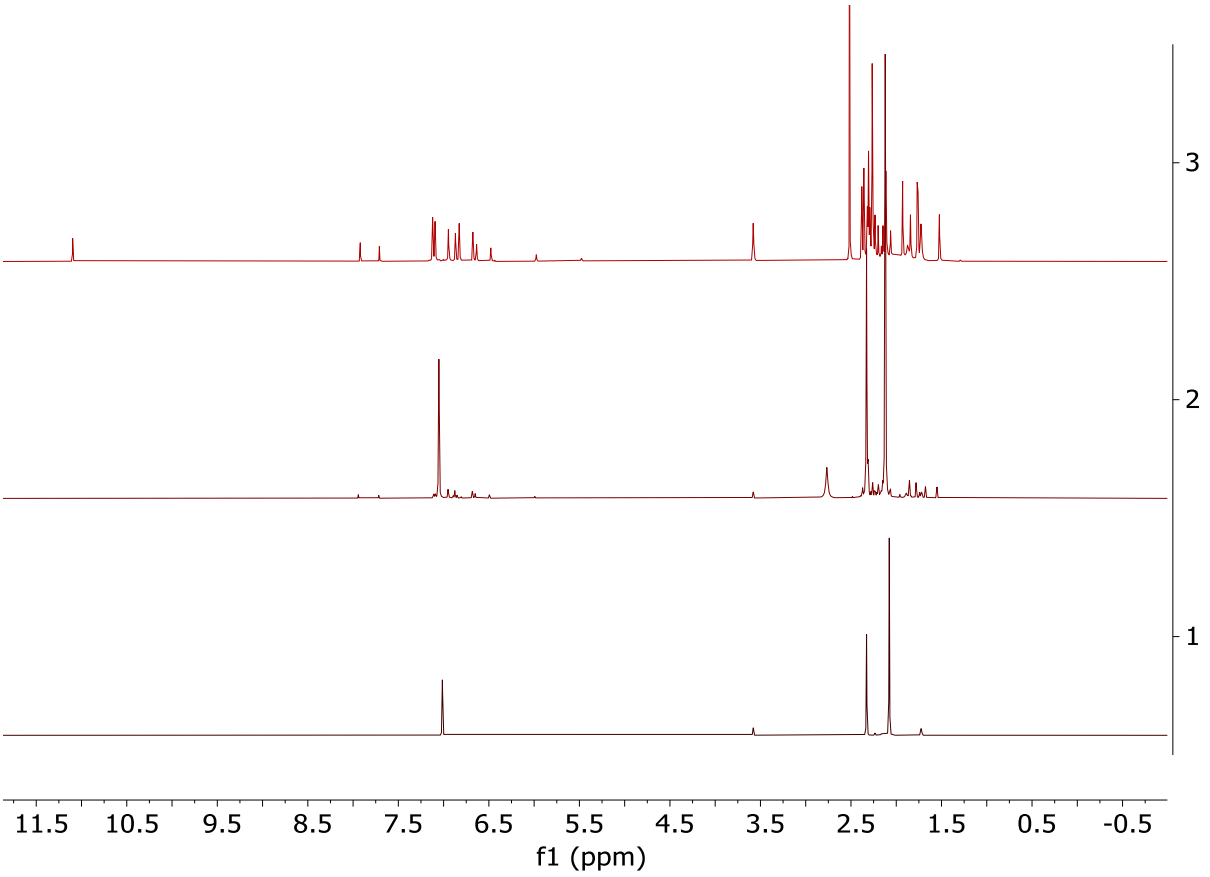

Fig. **5.15** ^1H NMR of **49** in THF-d_8. 1) no H_2O added 2) 1 equiv. H_2O added 3) sample decanted and precipitate dissolved with 0.5 mL THF-d_8.

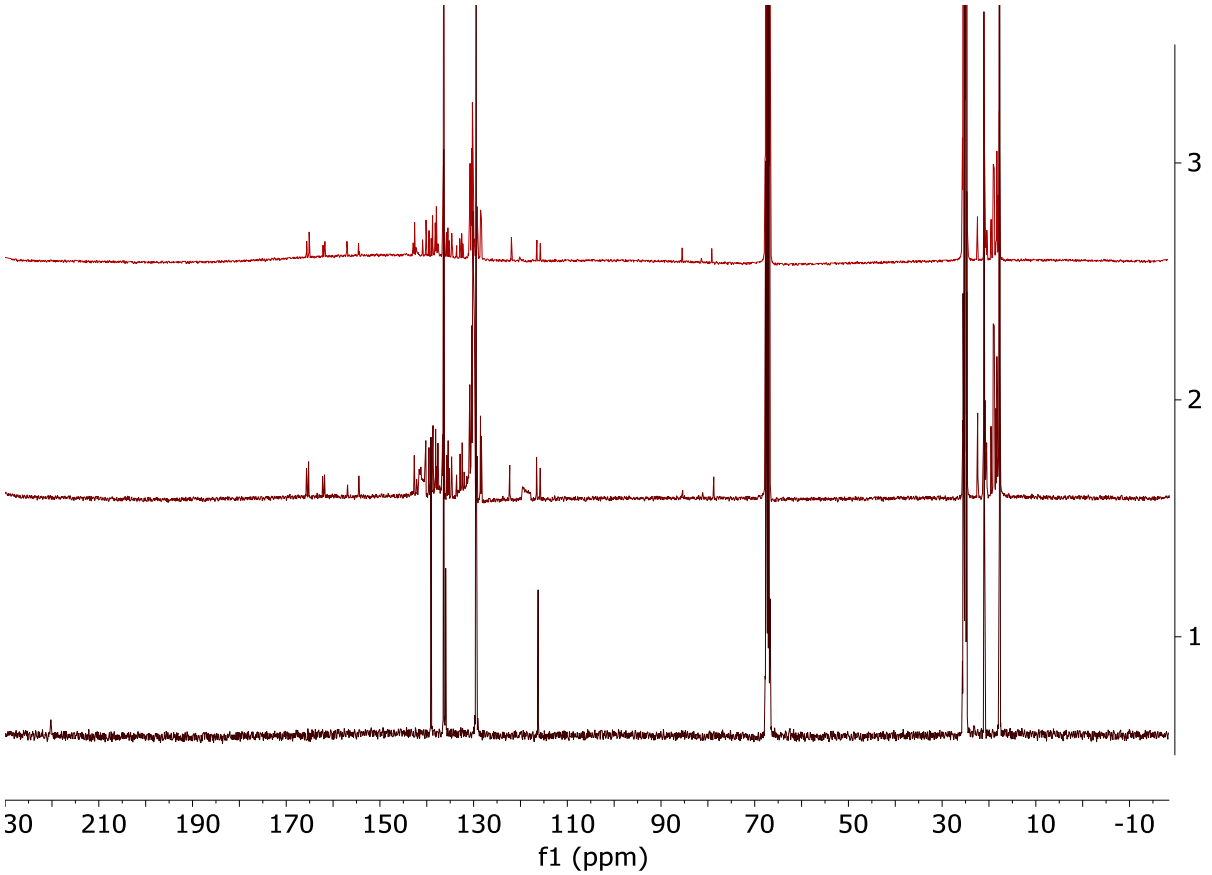

Fig. **5.16** ^{13}C NMR of **49** in THF-d_8. 1) no H_2O added 2) 1 equiv. H_2O added 3) sample decanted and precipitate dissolved with 0.5 mL tetrahydrofuran-d_8.

Water Stability Observations of 49 in C_6D_6:

The carbene **49** was prepared according to literature methods.[8] An NMR sample of 1,3-dimesityl-4,5-dichloroimidazol-2-ylidene (0.124 g, 0.332 mmol) in 1.0 mL C_6D_6 was prepared under a nitrogen atmosphere. Distilled H_2O (6 µL, 0.333 mmol) was added and the sample was checked by ^1H and ^{13}C NMR. The solution was checked by ^1H and ^{13}C NMR.

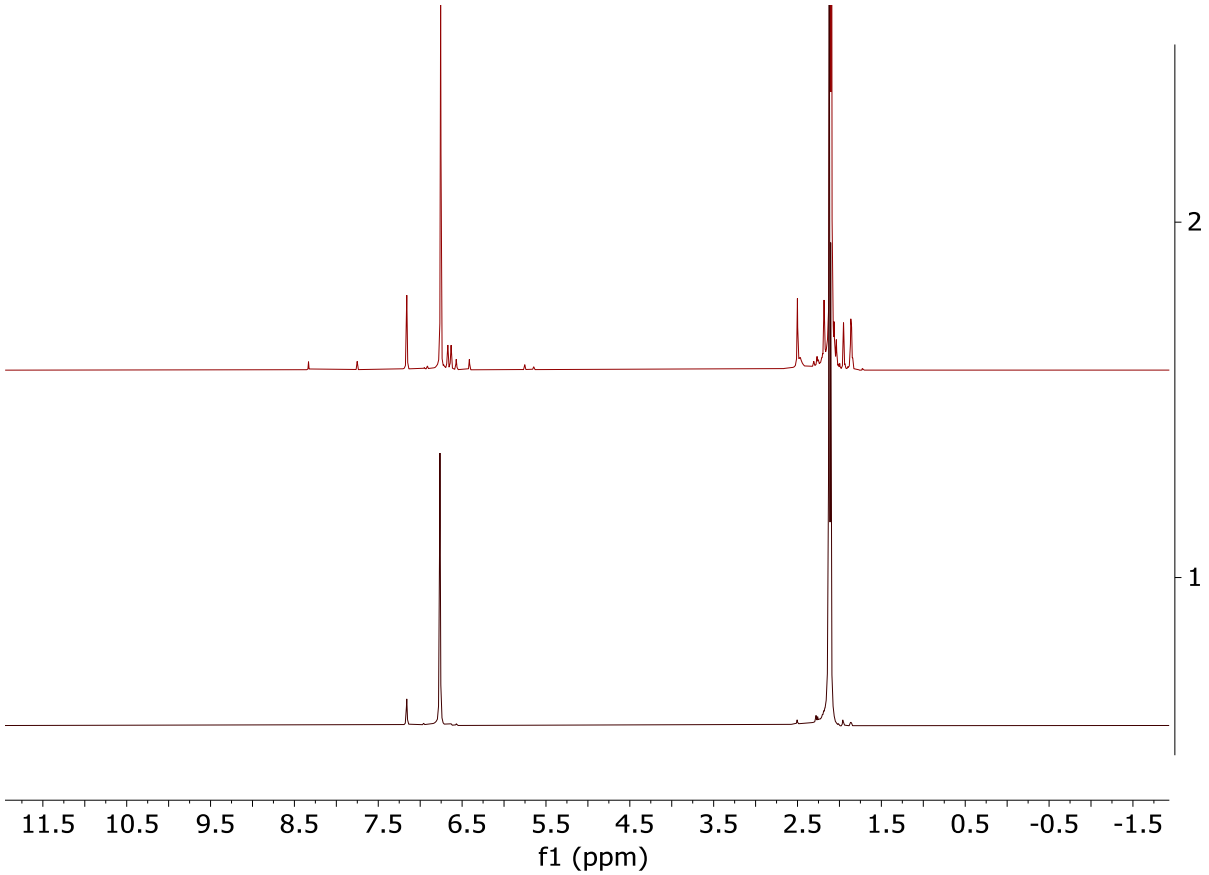

Fig. **5.17** ^{1}H NMR of **49** in C_6D_6. 1) no H_2O added 2) 1 equiv. H_2O added.

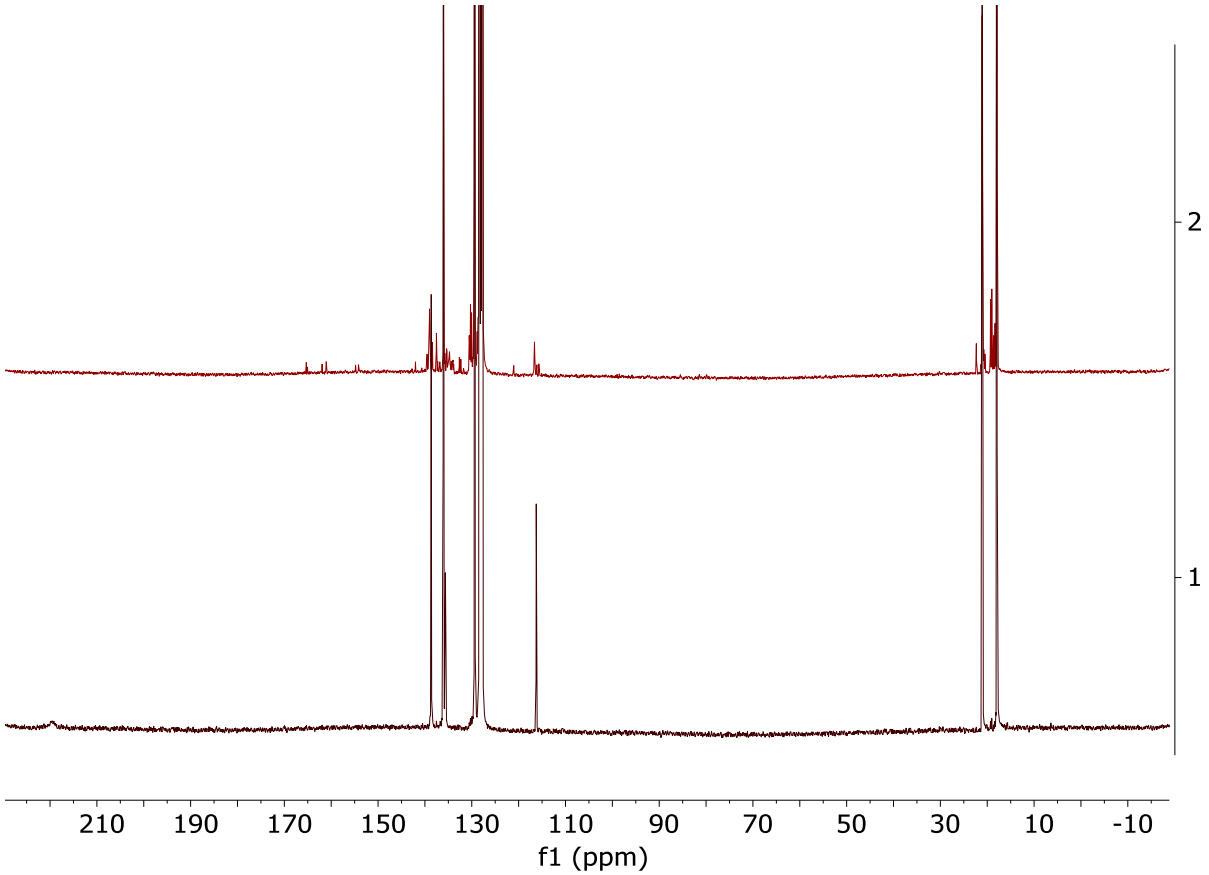

Fig. **5.18** ^{13}C NMR of **49** in C_6D_6. 1) no H_2O added 2) 1 equiv. H_2O added.

Water Stability of 50 in THF:

The carbene **50** was prepared according to literature methods.[9] An NMR sample of 1,3-di-*tert*-butylimidazol-2-ylidene (0.100 g, 0.555 mmol) in 2.0 mL tetrahydrofuran-d_8 was prepared under a nitrogen atmosphere. Distilled H_2O (10 µL, 0.555 mmol) was added and the sample was checked by ^1H and ^{13}C NMR. Distilled H_2O was then added in increments of 20 µL (1.11 mmol) until 0.110 mL of H_2O total (6.11 mmol) was added to the NMR tube.

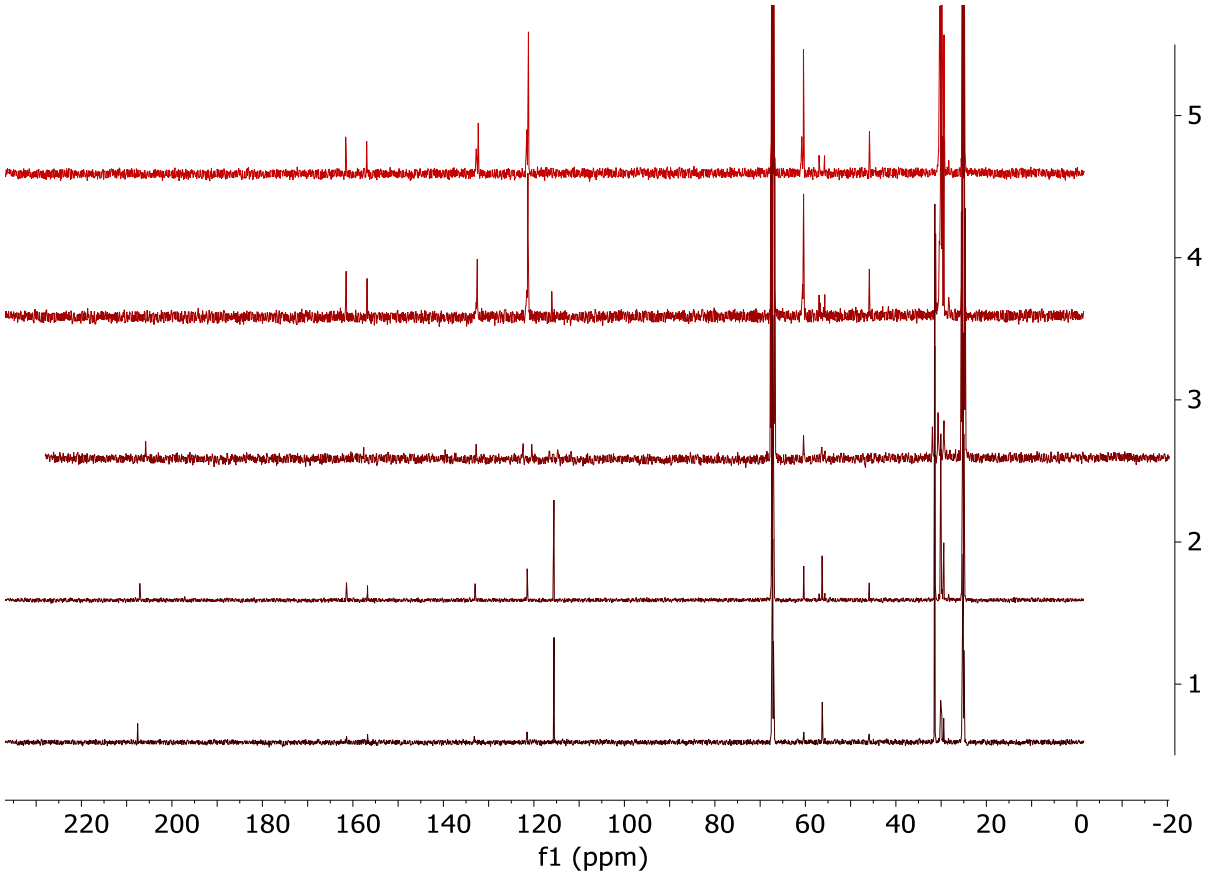

Fig. **5.19** ^{13}C NMR of **50** in THF-d_8. 1) 3 equiv. H_2O 2) 5 equiv. H_2O 3) 7 equiv. H_2O

Generation of the carbene 52 in water:

An NMR sample was made by dissolving 75 mg of the imidazolium **51** in 0.5 mL THF-d_8. To this, 0.5 mL distilled water and 2 equivalents of LiOH were added. The generation of carbene was confirmed by the presence of carbene carbon peak at 239 ppm on the $^{13}C[^1H]$ NMR.

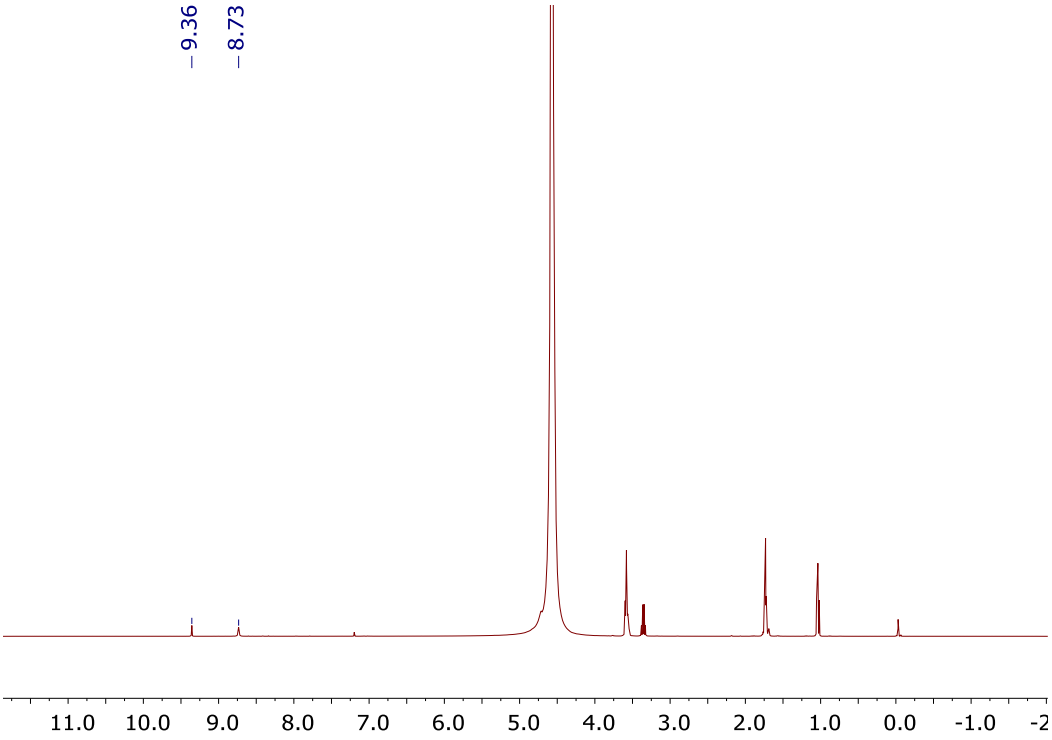

Fig. **5.20** ^{1}H NMR of the carbene **52** generated in water

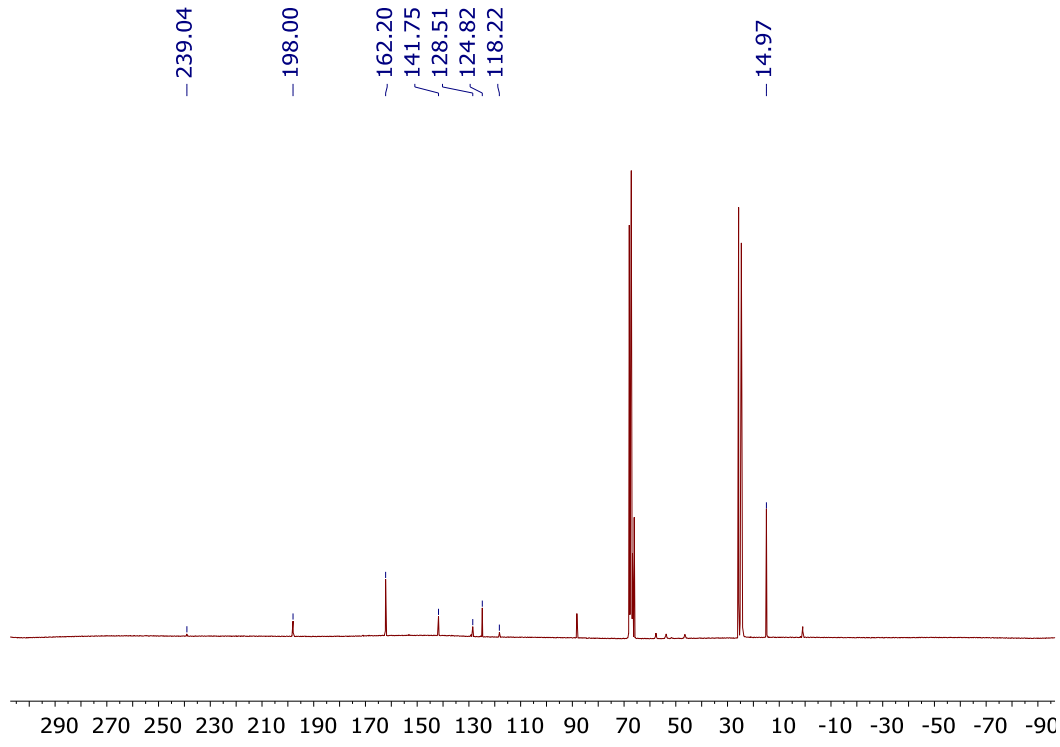

Fig. **5.21** ^{13}C NMR of carbene **52** generated in water. *The carbene carbon peak is seen at 239.04 ppm.*

X-Ray Structure Determination:

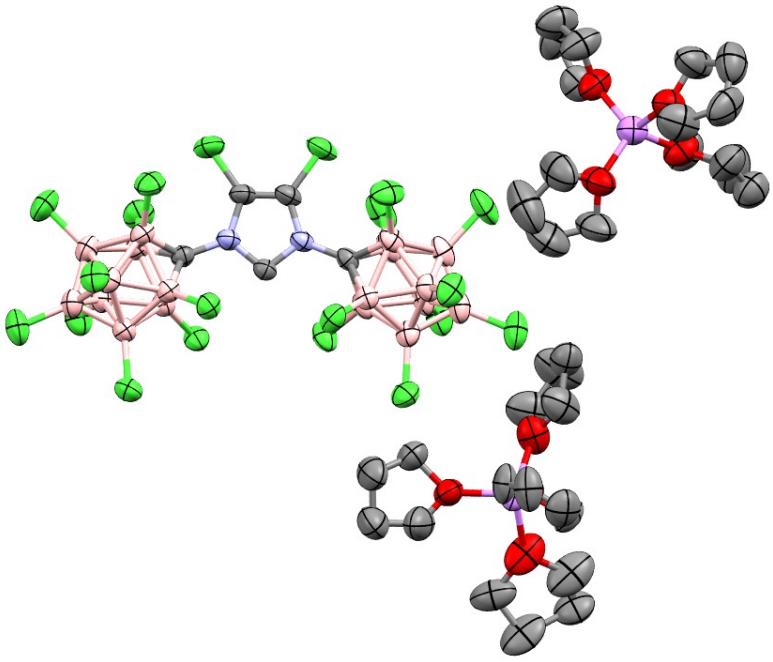

Fig. **5.3** Solid-State Structure of the NHC **52.** Hydrogen atoms omitted for clarity. N=Blue, Cl=green, B=pink, Li=purple, O=red, C=grey

A colorless prism fragment (0.327 x 0.172 x 0.135 mm^3) was used for the single crystal x-ray diffraction study of $[C_5B_{18}Cl_{20}N_2].[Li[C_4H_8O]_4]_2$ (sample vL180SL_0m). The crystal was coated with paratone oil and mounted on to a cryo-loop glass fiber. X-ray intensity data were collected at 200(2) K on a Bruker APEX2 platform-CCD x-ray diffractometer system (fine focus Mo-radiation, λ = 0.71073 Å, 50KV/30mA power). The CCD detector was placed at a distance of 5.0600 cm from the crystal.

A total of 4800 frames were collected for a sphere of reflections (with scan width of 0.3° in ω and ϕ, starting ω and 2θ angles of –30°, and ϕ angles of 0°, 90°, 120°, 180°, 240°, and 270° for every 600 frames, and 1200 frames with ϕ -scan from 0-360°, 120 sec/frame

exposure time). The frames were integrated using the Bruker SAINT software package and using a narrow-frame integration algorithm. Based on a triclinic crystal system, the integrated frames yielded a total of 86693 reflections at a maximum 2θ angle of 52.742 (0.80 Å resolution), of which 15766 were independent reflections (R_{int} = 0.0315, R_{sig} = 0.0218, redundancy = 5.5, completeness = 100%) and 12133 (77.0%) reflections were greater than 2σ(I). The unit cell parameters were, **a** = 13.9343(6) Å, **b** = 15.9345(7) Å, **c** = 17.9992(7) Å, **α** = 105.2353(7) **β** = 91.5694(7)°, **γ** = 90.0954(8) V = 3854.4(3) $Å^3$, Z = 2, calculated density D_c = 1.426 g/cm^3. Absorption corrections were applied (absorption coefficient μ = 0.754 mm^{-1}; max/min transmission = 0.905/0.791) to the raw intensity data using the SADABS program.

The Bruker SHELXTL software package was used for phase determination and structure refinement. The distribution of intensities (E^2-1 = 0.968) and no systematic absent reflections indicated two possible space groups, P-1and P1. The space group P-1 (#2) was later determined to be correct. Direct methods of phase determination followed by two Fourier cycles of refinement led to an electron density map from which most of the non-hydrogen atoms were identified in the asymmetric unit of the unit cell. With subsequent isotropic refinement, all of the non-hydrogen atoms were identified. There were two disordered cation of $[Li[C_4H_8O]_4]^+$ and one anion of $[C_5B_{18}Cl_{20}N_2]^{2-}$ present in the asymmetric unit of the unit cell. Seven out of the eight THF molecules of the two cations were modeled with disorder (THF disordered site occupancy ratios were 82%/18%, 65%/35%, 61%/39%, 59%/41%, 59%/41%, 55%/45%, and 53%/47%). The two solvents of crystallization were partially occupied THF (52%) and partially occupied diethylether (48%).

Atomic coordinates, isotropic and anisotropic displacement parameters of all the non-hydrogen atoms were refined by means of a full matrix least-squares procedure on F^2. The H-atoms were included in the refinement in calculated positions riding on the atoms to which they were attached. The refinement converged at R1 = 0.0460, wR2 = 0.1222, with intensity I>2σ (I). The largest peak/hole in the final difference map was 0.654/-0.415 e/Å^3.

Table 5.1 Crystal data and structure refinement for **52**

Identification code	vL180SL_0m	
Empirical formula	C41 H72.96 B18 Cl20 Li2 N2 O9	
Formula weight	1655.43	
Temperature	200(2) K	
Wavelength	0.71073 Å	
Crystal system	Triclinic	
Space group	P -1	
Unit cell dimensions	a = 13.9343(6) Å	α= 105.2353(7)°.
	b = 15.9345(7) Å	β= 91.5694(7)°.
	c = 17.9992(7) Å	γ = 90.0954(8)°.
Volume	3854.4(3) Å^3	
Z	2	
Density (calculated)	1.426 Mg/m^3	
Absorption coefficient	0.754 mm^{-1}	
F(000)	1682	
Crystal size	0.327 x 0.172 x 0.135 mm^3	
Theta range for data collection	1.521 to 26.372°.	

Index ranges	-17<=h<=17, -19<=k<=19, -22<=l<=22
Reflections collected	86693
Independent reflections	15766 [R(int) = 0.0315]
Completeness to theta = 25.242°	100.0 %
Absorption correction	Semi-empirical from equivalents
Refinement method	Full-matrix least-squares on F^2
Data / restraints / parameters	15766 / 1413 / 1163
Goodness-of-fit on F^2	1.032
Final R indices [I>2sigma(I)]	R1 = 0.0460, wR2 = 0.1222
R indices (all data)	R1 = 0.0624, wR2 = 0.1340
Extinction coefficient	n/a
Largest diff. peak and hole	0.654 and -0.415 e.$Å^{-3}$

5.8 References

1. Bettendorff, L., Chapter 10 - Thiamine. In *Present Knowledge in Nutrition (Eleventh Edition)*, Marriott, B. P.; Birt, D. F.; Stallings, V. A.; Yates, A. A., Eds. Academic Press: 2020; pp 171-188.

2. Begley, T. P.; Ealick, S. E., 7.15 - Thiamin Biosynthesis. In *Comprehensive Natural Products II*, Liu, H.-W.; Mander, L., Eds. Elsevier: Oxford, 2010; pp 547-559.

3. Das, T. K.; Biju, A. T., 1 - N-Heterocyclic Carbene (NHC)-Catalyzed Transformations for the Synthesis of Heterocycles. In *Progress in Heterocyclic Chemistry*, Gribble, G. W.; Joule, J. A., Eds. Elsevier: 2020; Vol. 31, pp 1-82.

4. Breslow, R., On the Mechanism of Thiamine Action. IV.1 Evidence from Studies on Model Systems. *Journal of the American Chemical Society* **1958,** *80* (14), 3719-3726.

5. Wanzlick, H. W.; Schönherr, H. J., Direct Synthesis of a Mercury Salt-Carbene Complex. *Angewandte Chemie International Edition in English* **1968,** *7* (2), 141-142.

6. Igau, A.; Grutzmacher, H.; Baceiredo, A.; Bertrand, G., Analogous .alpha.,.alpha.'-bis-carbenoid, triply bonded species: synthesis of a stable .lambda.3-phosphino carbene-.lambda.5-phosphaacetylene. *Journal of the American Chemical Society* **1988,** *110* (19), 6463-6466.

7. Arduengo, A. J., III; Harlow, R. L.; Kline, M., A stable crystalline carbene. *Journal of the American Chemical Society* **1991,** *113* (1), 361-363.

8. Arduengo, A. J.; Davidson, F.; Dias, H. V. R.; Goerlich, J. R.; Khasnis, D.; Marshall, W. J.; Prakasha, T. K., An Air Stable Carbene and Mixed Carbene "Dimers". *Journal of the American Chemical Society* **1997,** *119* (52), 12742-12749.

9. Denk, M. K.; Rodezno, J. M.; Gupta, S.; Lough, A. J., Synthesis and reactivity of subvalent compounds: Part 11. Oxidation, hydrogenation and hydrolysis of stable diamino carbenes. *Journal of Organometallic Chemistry* **2001,** *617-618*, 242-253.

10. Fisher, S. P.; Tomich, A. W.; Lovera, S. O.; Kleinsasser, J. F.; Guo, J.; Asay, M. J.; Nelson, H. M.; Lavallo, V., Nonclassical Applications of closo-Carborane Anions: From Main Group Chemistry and Catalysis to Energy Storage. *Chemical Reviews* **2019,** *119* (14), 8262-8290.

11. Tej Raviprolu, V.; McArthur, S. E.; Banda, I.; Gregory, A.; McArthur, S. G.; Fisher, S. P.; Lavallo, V., Fusing 10-vertex closo-carborane anions with N-heterocyclic carbenes. *Chemical Communications* **2022,** *58* (75), 10580-10582.

Chapter 6: Coinage Metal Complexes of the 10-vertex Carboranyl NHC

6.1 Introduction

Since the discovery of the N-Heterocyclic Carbenes in 1991, they have been widely employed as strong σ donating ancillary ligands for transition metals.[1-8] Their ease of synthesis further aided in producing the NHC complexes as most active catalysts for a myriad of organic transformations. Among transition metals, the coinage metals (Cu, Ag, Au) are catalytically active for various organic reactions including C-H bond functionalization, C-C coupling, cyclization, alkyne and olefin functionalization among others.[9-12] Their inexpensive sources and the stability of the NHC complexes makes them attractive choices for transition metal catalysis.[11, 13-15] The stability of coinage NHC complexes stems from the strong σ donation of the NHC to the metal and a minor contribution from the metal to NHC π back donation. The NHC-M (M=coinage metal) bond is primarily an electrostatic attraction force in case of Ag and is strongly covalent in case of Au as evidenced by the use of NHC-Ag complexes as transmetalating agents for other transition metal complexes.[12]

Over the last few years, we have developed NHCs flanked by the carborane anions on the ring nitrogens in our lab.[16] These NHCs are typically dianionic which renders the corresponding coinage metal complexes mono or dianionic depending on the other ligand on the metal.[17-18] The Au complexes of the 12-vertex carboranyl NHC and its hexahalogenated derivatives discussed in Chapters 2 and 3 are highly active catalysts towards hydroamination of alkynes. In chapter 4, we discussed the synthesis of the corresponding 10-vertex carboranyl NHC.[19] The 10-vertex carborane is sterically less bulky and more strongly donating compared to the 12-vertex analogue. Hence the

corresponding NHC has a different steric and electronic environment compared to the 12-veretx carboranyl NHC. We thus became interested in investigating the properties of the corresponding coinage metal complexes.

6.2 10-vertex Carboranyl NHC Cu(I) Complexes

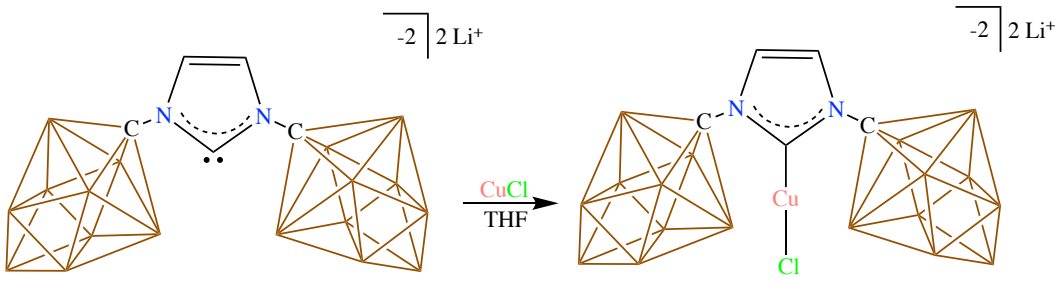

45 **53**

Scheme **6.1** Synthesis of 10-vertex NHC-CuCl complex **53**

The 10-vertex carboranyl NHC was synthesized as discussed in Chapter-4. When a suspension of CuCl in THF was added to this solid, a yellow brown suspension was obtained. Stirring the solution followed by filtration cleanly produced the dianionic NHC-CuCl complex in about 80% yield (Scheme **6.1**). The compound was characterized by multinuclear NMR spectroscopy and mass spectrometry. The imidazolylidene backbone proton resonance was shifted upfield to 7.77 ppm on the ^{1}H NMR suggesting the formation of a NHC-Cu complex. This was confirmed by the upfield shift of the carbene carbon resonance in the ^{13}C NMR from 200 ppm on to 179.8 ppm. The ^{11}B NMR displayed three resonances in 1:4:4 ratio indicating the clusters retain the local C_{4v} symmetry.

We then wanted to synthesize a three coordinate NHC-Cu complex with a N,N chelating ligand, since similar complexes have found numerous applications as Thermally Activated Delayed Flourescence (TADF) materials.[20-23] To do this, 1,10 phenanthroline was reacted with compound, anticipating the loss of LiCl, producing the three coordinate Cu complex (Scheme **6.2**).

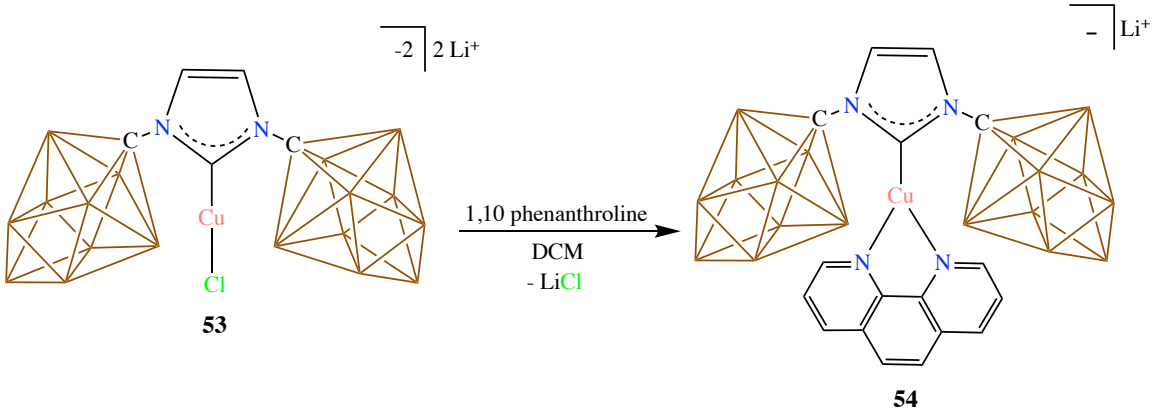

Scheme **6.2** Attempted synthesis of the NHC-Cu-phen complex **54**

However, the compound appeared to decompose rapidly in the solid state. The initial crude reaction mixture after filtering over celite was bright orange red and stayed the same color after the solvent was evaporated under vacuum. However, the solid started turning grey after removing from under vacuum and turned completely grey in less than a minute. The crude ^{1}H NMR looked like a mixture of multiple products most likely due to the decomposition. Performing the filtration and solvent evaporation in the absence of light proved better; however, there was still color change of the solid and a mixture of at least two products on the ^{1}H NMR.

Attempting to replace the Cl ligand by other L type ligands, **53** was reacted with triphenyl phosphine (PPh_3) (Scheme **6.3**). By the crude ^{1}H NMR of the reaction mixture, the triphenyl phosphine resonances were seen between 7.4 to 7.6 ppm. However, the reaction resulted in a huge protonation of the complex **53**, regenerating the imidazolium **44**.

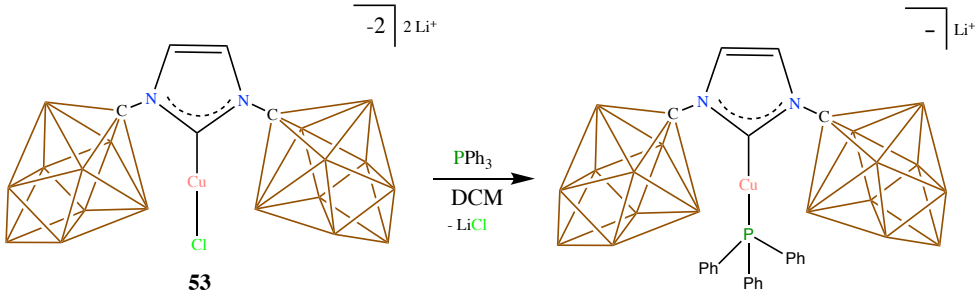

Scheme **6.3** Attempted synthesis of the NHC-Cu-PPh_3 complex **55**

Although the reaction produced the expected NHC-Cu- PPh_3 product **54**, the generation of imidazolium **44** in the reaction mixture made the isolation of clean product harder.

6.3 10-vertex Carboranyl NHC Au(I) Complexes

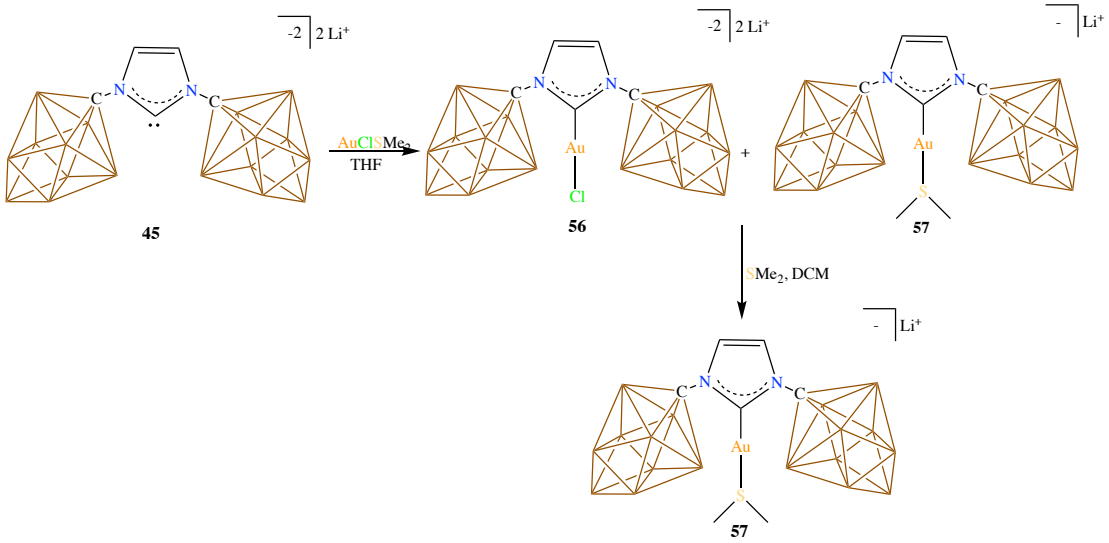

Scheme **6.4** Reaction of **45** with $ClAuSMe_2$ to produce **57**

To make the analogous Au(I) complexes, the NHC **45** was treated with the gold precursor $ClAuSMe_2$ (Scheme **6.4**). The crude ^1H NMR displayed two backbone imidazolylidene resonances very close to each other. Moreover, a small singlet was seen at 2.6 ppm, that integrated with one of the backbone peaks in 1:3 ratio. We understood the reaction generated a mixture of AuCl and $AuSMe_2$ complexes **56** and **57**. The crude reaction mixture was then treated with excess SMe_2 in dichloromethane to fully convert the mixture to **57**. After this step, the crude ^1H NMR showed a single imidazolylidene backbone peak at 7.79 ppm, indicating **57** as the only product. The SMe_2 peak was seen as a singlet at 2.6 ppm and integrating 1:3 with the backbone peak, corroborating the previous observation. The carbene carbon resonance in the ^{13}C NMR spectrum shifted upfield from 200 ppm to 176.88 ppm indicating the formation of a metal complex. The ^{11}B NMR displayed three peaks with relative intensities in 1:4:4 ratio indicating the carborane cluster retained its C_{4v}

symmetry.

6.4 Conclusion

In conclusion, we show that the recently reported 10-vertex carboranyl NHC is a strong ligand for forming coinage metal complexes. The synthesized complexes were characterized using NMR and mass spectrometry. The less steric and more donating properties of this ligand is expected to have its impact on the catalytic activity of the complexes. These works are currently underway in our laboratory.

6.5 Experimental

General Considerations:

Unless otherwise stated, all manipulations were carried out using standard Schlenk or glovebox techniques (O_2, H_2O < 1ppm) under a dinitrogen or argon atmosphere. Solvents were dried on sodium-potassium alloy (ether) or potassium benzophenone ketyl, (THF) or calcium hydride (acetonitrile, dichloromethane) and distilled under argon before use. The 10-Vertex carboranyl NHC was prepared according to literature methods.[19] Reagents were purchased from commercial vendors and used without further purification. NMR spectra were recorded on Bruker Avance 300 MHz, Bruker Avance Neo 400 MHz, Bruker Avance 600 MHz, Bruker Avance III 700 MHz, Varian Inova 300 MHz, or Varian Inova 400 MHz spectrometers. NMR chemical shifts are reported in parts per million (ppm). ^{1}H NMR and ^{13}C NMR chemical shifts were referenced to residual solvent. ^{11}B NMR chemical shifts were externally referenced to $BF_3{\cdot}OEt_2$. High-resolution mass spectrometry (HRMS) was recorded on Agilent Technologies 6210 (time of flight LC/MS) using ESI technique.

Synthesis of 53:

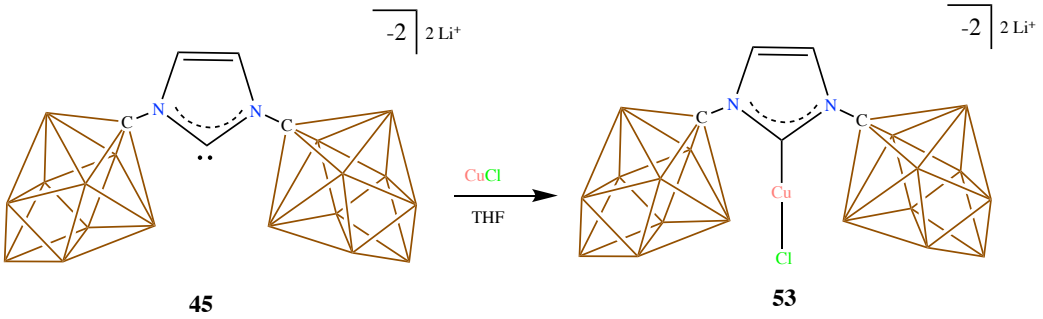

45 **53**

Scheme **6.1** Synthesis of 10 vertex NHC-CuCl complex **53**

In a glass vial, 600 mg (1.29 mmol) of **45** was weighed out and loaded with a stir bar. To this, a suspension of CuCl (127.75 mg, 1.29 mmol) in THF (5 mL) was added and stirred for an hour. The volatiles were then pumped down under vacuum and dichloromethane (15 mL) was added to the solid and stirred for a few minutes. The suspension was then filtered over a pad of celite and pumped down under vacuum to afford **53** as a yellow powder in 54% yield (370 mg). Loss of yield was due to the filtration in poorly soluble dichloromethane. ^{1}H NMR (600 MHz, CD_2Cl_2, 25°C): 7.77 (s, 2H, CH), 3.61 (m, 30H, THF), 1.88 (m, 30H, THF); ^{11}B NMR (192 MHz, CD_2Cl_2, 25°C): 25.93, -15.33, -25.17 ppm; ^{13}C NMR (150 MHz, CD_2Cl_2, 25°C): 179.86, 123.45, 68.85, 25.85 ppm.

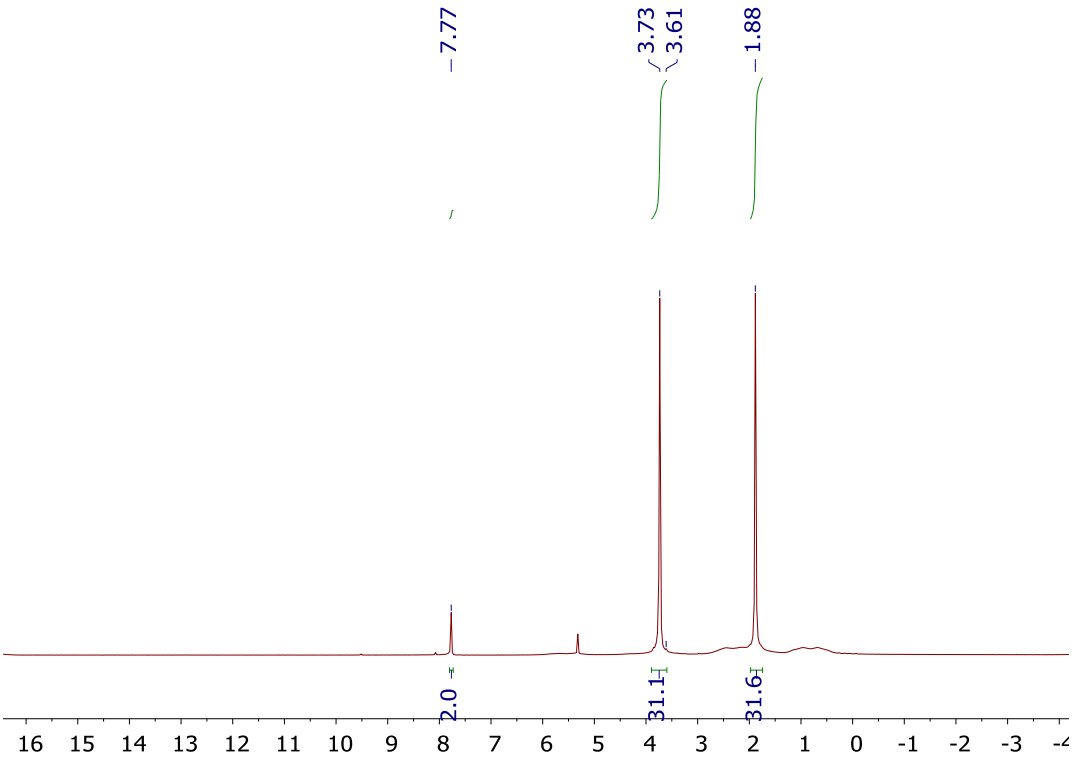

Fig. **6.1** ^{1}H NMR of **53** in CD_2Cl_2

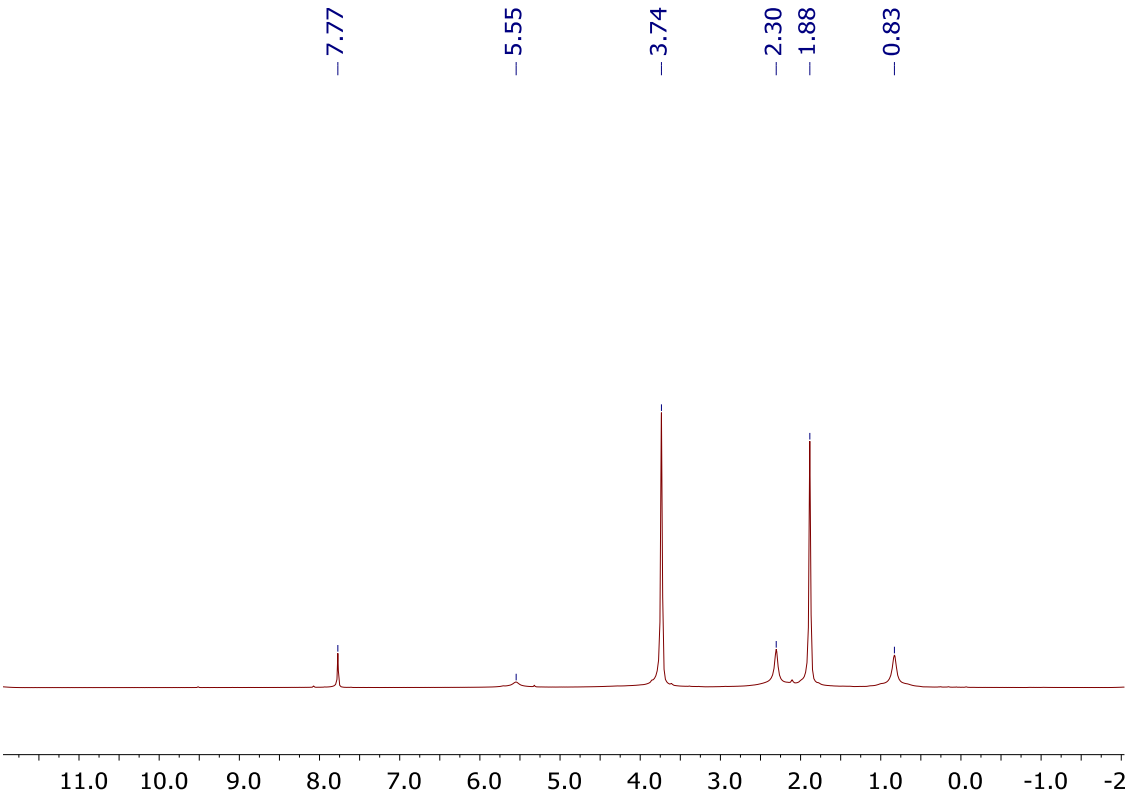

Fig. **6.2** $^{1}H[^{11}B]$ NMR of **53** in CD_2Cl_2

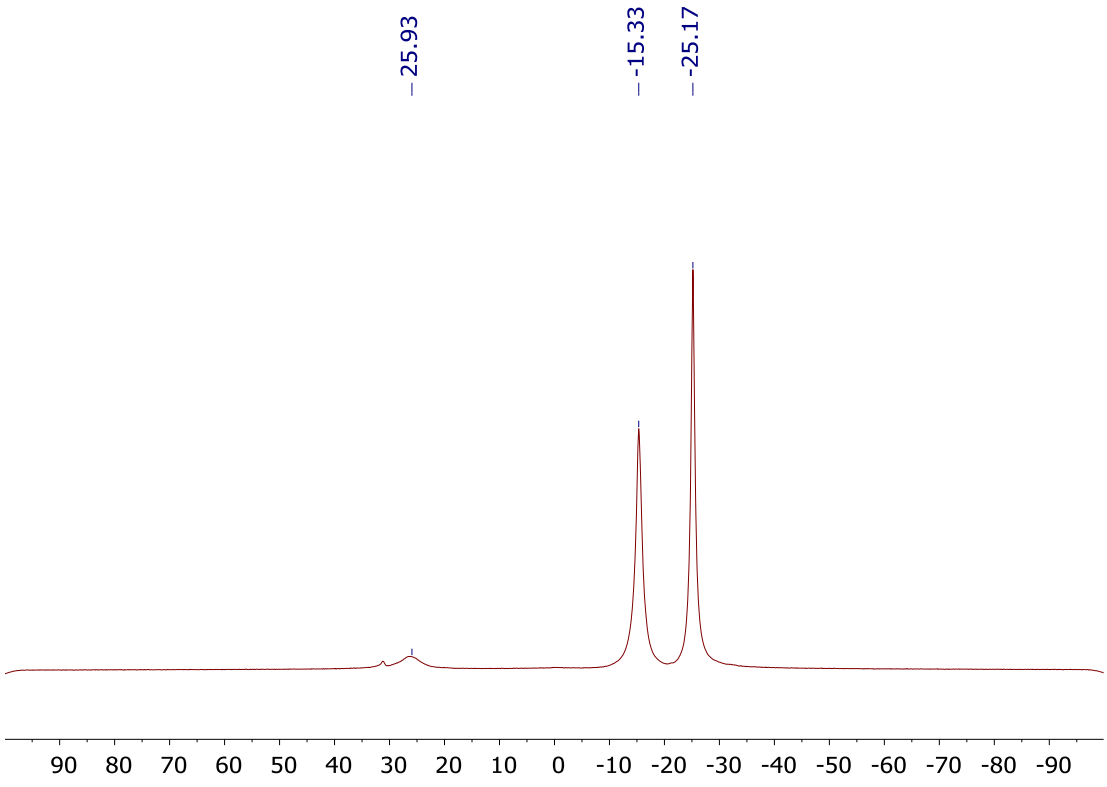

Fig. **6.3** $^{11}B[^{1}H]$ NMR of **53** in CD_2Cl_2

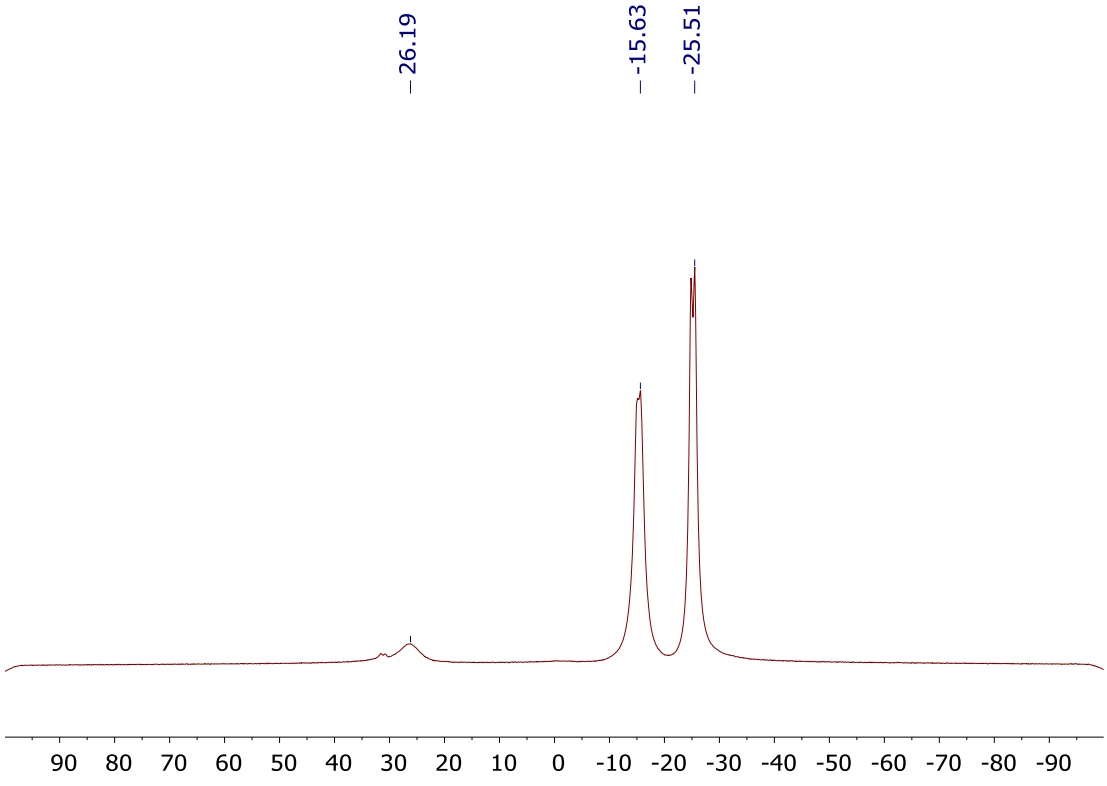

Fig. **6.4** ^{11}B NMR of **53** in CD_2Cl_2

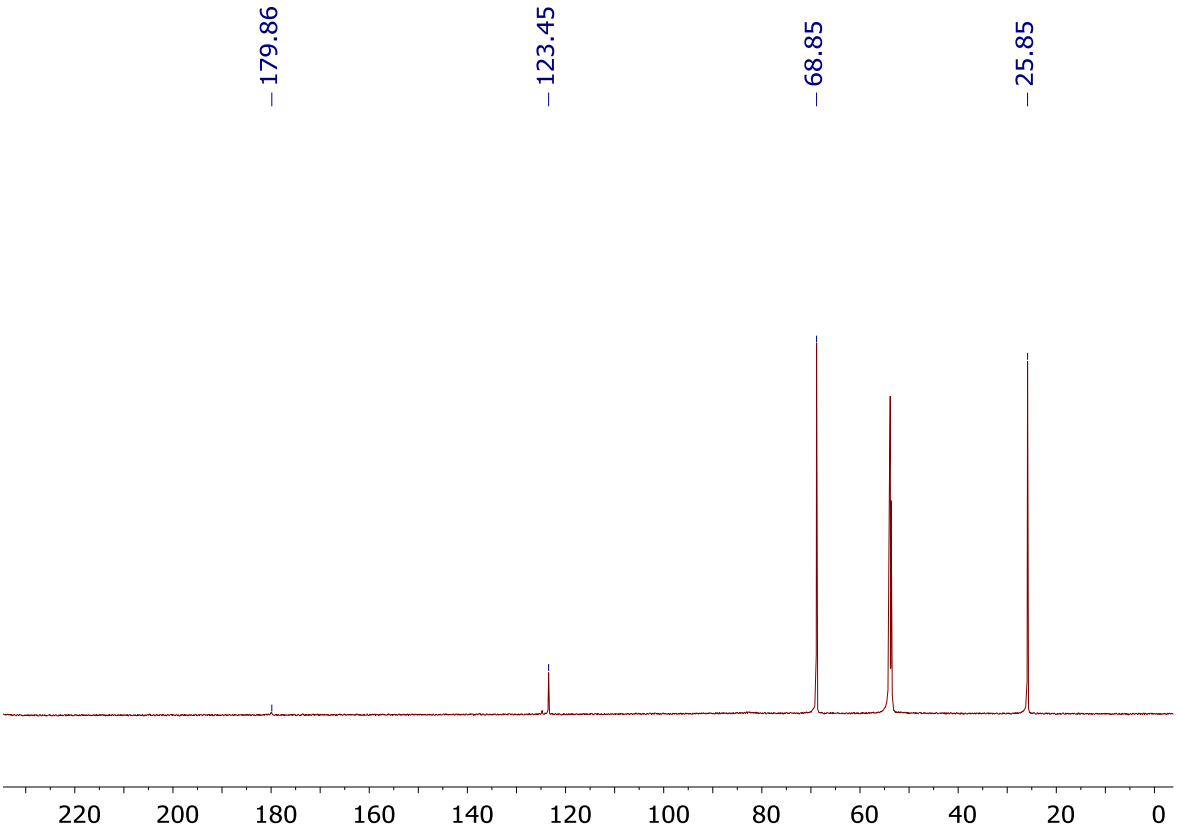

Fig. **6.5** $^{13}C[^{1}H]$ NMR of **53** in CD_2Cl_2

Attempted Synthesis of 54:

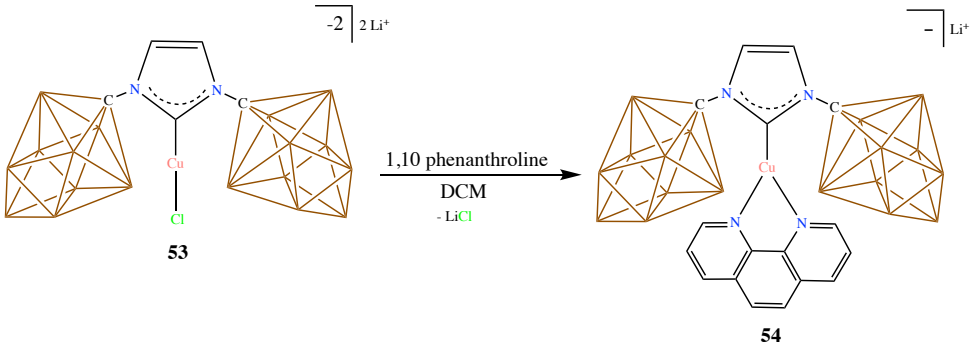

Scheme **6.2** Attempted Synthesis of the NHC-Cu-phen complex **54**

In a glass vial, 80 mg (0.15 mmol) of **53** was weighed, loaded with a stir bar and dissolved in dichloromethane (3 mL). To this, a solution of 1,10 phenanthroline monohydrate (27 mg, 0.15 mmol) in dichloromethane (3 mL) was added. The solution immediately changed

color from pale yellow to bright orange red. Stirring was continued overnight and the solution was then filtered to yield a bright red clear solution. During the evaporation of dichloromethane under vacuum, the orange solid that was forming started turning grey.

Attempted Synthesis of 55:

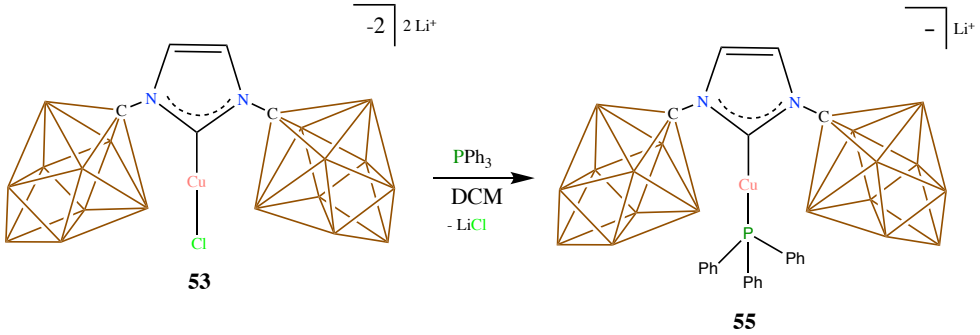

Scheme **6.3** Attempted Synthesis of the NHC-Cu-PPh_3 complex **55**

In a glass vial, 80 mg (0.15 mmol) of **53** was weighed and dissolved in dichloromethane (3 mL). To this, a solution of triphenylphosphine (39.34 mg, 0.15 mmol) in dichloromethane (3 mL) was added. A stir bar was added to the reaction mixture and the reaction stirred overnight. The yellow suspension was then filtered over celite, and the filtrate pumped down under vacuum to yield **55** and a small quantity of impurity **44**.

Synthesis of 57:

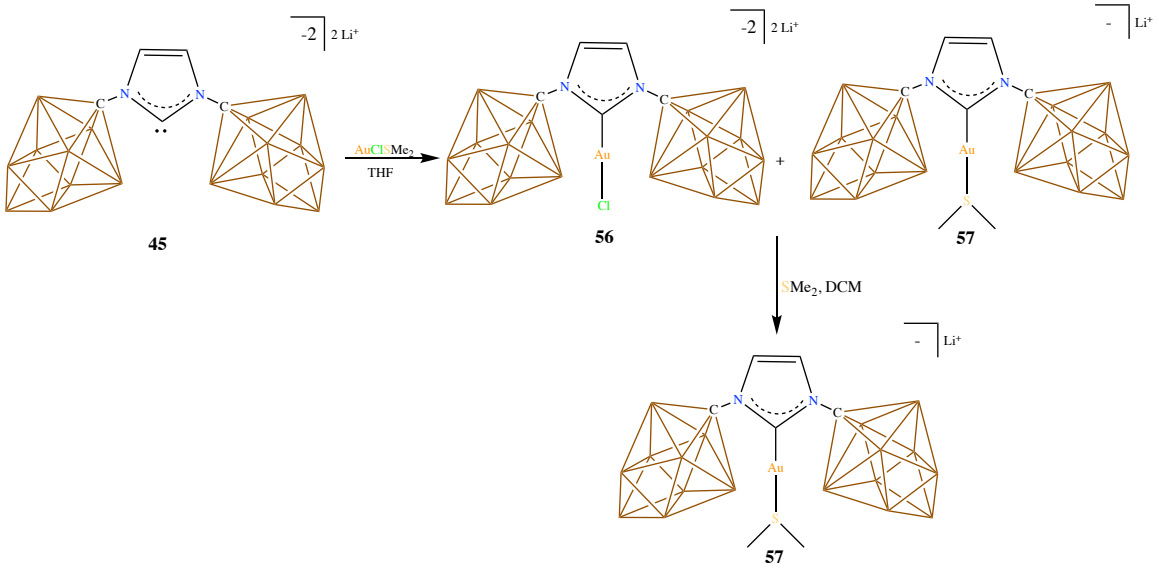

Scheme **6.4** Reaction of **45** with $ClAuSMe_2$ to produce **57**

In a glass vial, 200 mg (0.43 mmol) of **45** was weighed and loaded with a stir bar. In another vial, 126.65 mg (0.43 mmol) of $ClAuSMe_2$ was weighed in the absence of light and suspended in THF (4 mL). The THF suspension was then rinsed with the pipette for a few times and quickly transferred to the vial with **45** to form a dark suspension. The suspension was stirred for an hour after which the volatiles were pumped down under vacuum to produce a dark purple solid. The solid was then dissolved in dichloromethane (10 mL) and excess SMe_2 (2 mL) was added to the reaction mixture. The reaction was stirred overnight and filtered over a pad of celite. The filtrate was then evaporated under vacuum to afford **57** as a yellow solid in 85% yield. ^{1}H NMR (600 MHz, CD_2Cl_2, 25°C): 7.79 (s, 2H, CH), 3.79 (m, 20H, THF), 2.56 (s, 6H, SMe_2), 1.95 (m, 20H, THF); ^{11}B NMR (192 MHz, CD_2Cl_2, 25°C): 28.85, -15.32, -25.22 ppm. $^{13}C[^{1}H]$ NMR (150 MHz, CD_2Cl_2, 25°C): 176.88, 124.10, 78.39, 68.96, 25.83, 24.06 ppm.

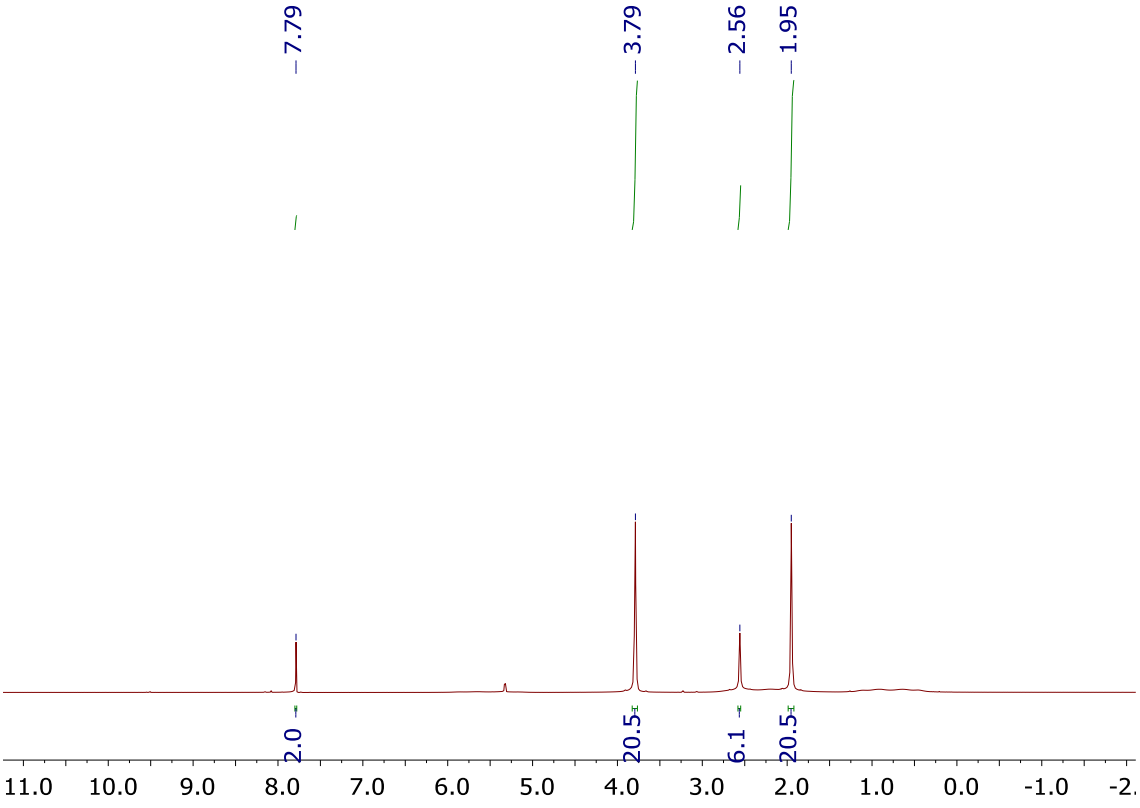

Fig. **6.6** ^{1}H NMR of **57** in CD_2Cl_2

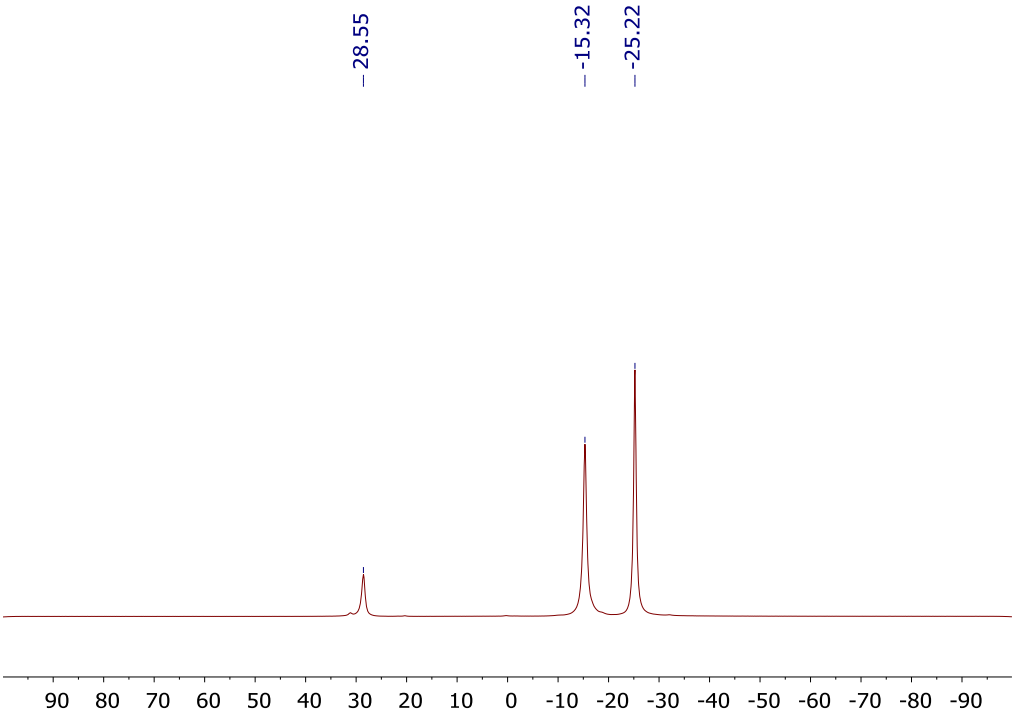

Fig. **6.7** $^{11}B[^{1}H]$ NMR of **57** in CD_2Cl_2

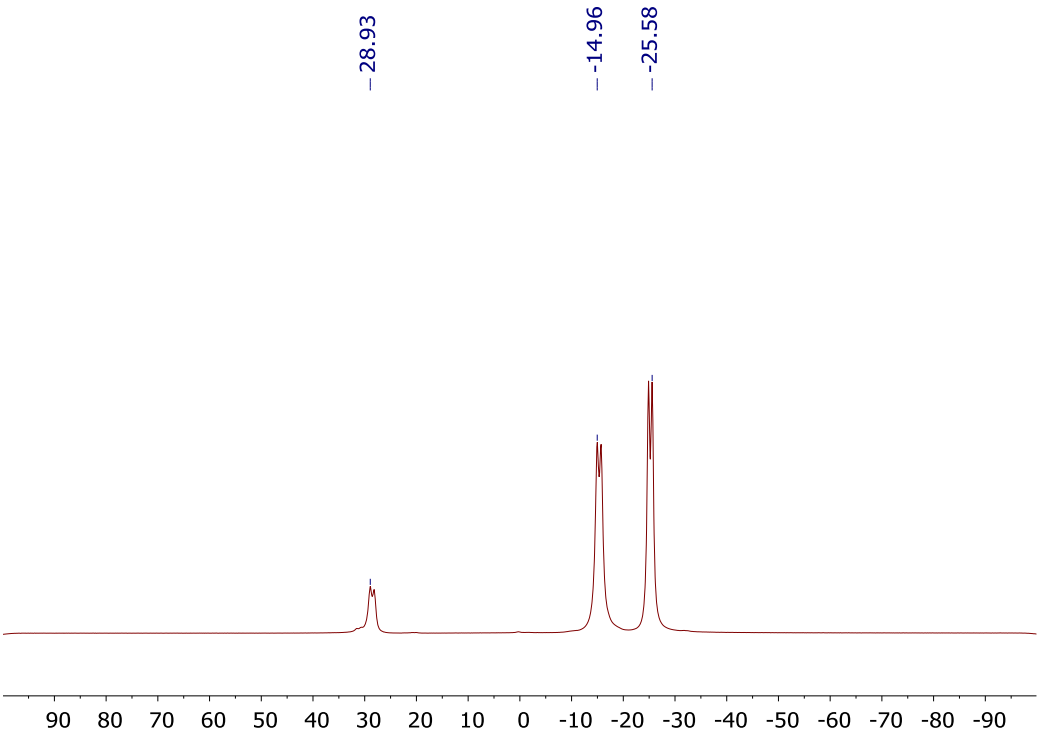

Fig. **6.8** ^{11}B NMR of **57** in CD_2Cl_2

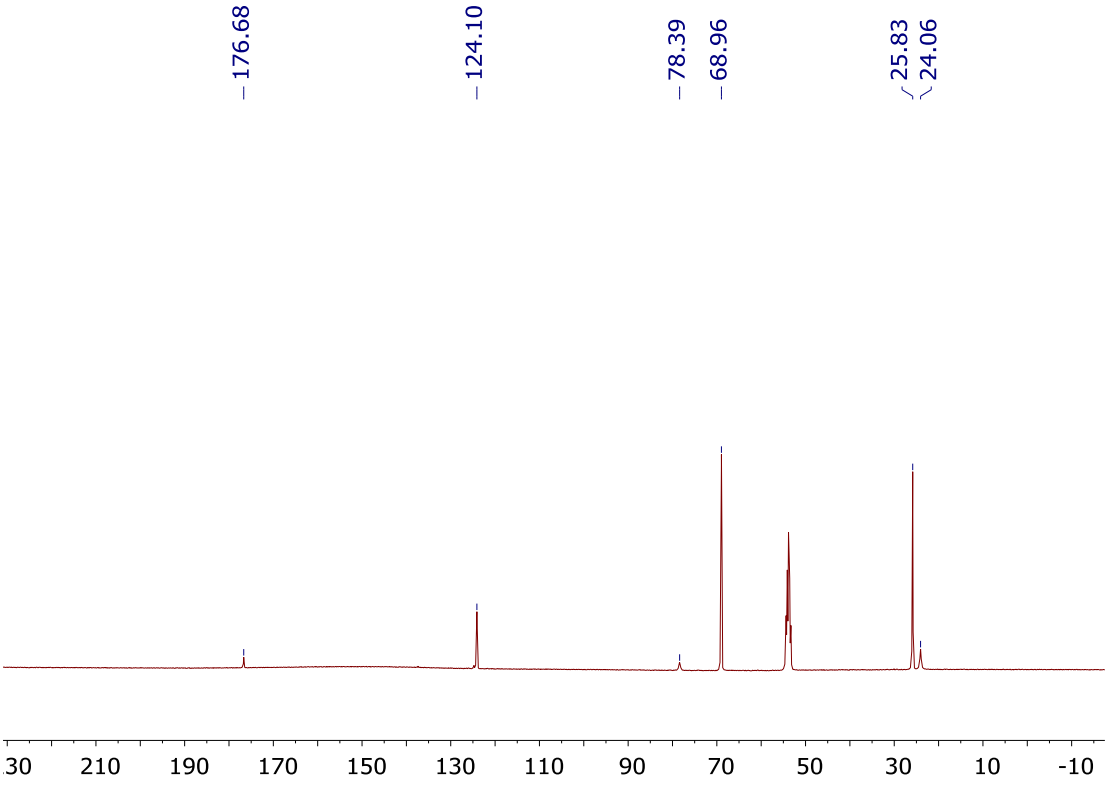

Fig. **6.9** $^{13}C[^1H]$ NMR of **57** in CD_2Cl_2

6.6 References

1. de Frémont, P.; Marion, N.; Nolan, S. P., Carbenes: Synthesis, properties, and organometallic chemistry. *Coordination Chemistry Reviews* **2009,** *253* (7), 862-892.

2. Kelly Iii, R. A.; Clavier, H.; Giudice, S.; Scott, N. M.; Stevens, E. D.; Bordner, J.; Samardjiev, I.; Hoff, C. D.; Cavallo, L.; Nolan, S. P., Determination of N-Heterocyclic Carbene (NHC) Steric and Electronic Parameters using the [(NHC)Ir(CO)2Cl] System. *Organometallics* **2008,** *27* (2), 202-210.

3. Marion, N.; Navarro, O.; Mei, J.; Stevens, E. D.; Scott, N. M.; Nolan, S. P., Modified (NHC)Pd(allyl)Cl (NHC = N-Heterocyclic Carbene) Complexes for Room-Temperature Suzuki−Miyaura and Buchwald−Hartwig Reactions. *Journal of the American Chemical Society* **2006,** *128* (12), 4101-4111.

4. Martin, A. R.; Makida, Y.; Meiries, S.; Slawin, A. M. Z.; Nolan, S. P., Enhanced Activity of [Ni(NHC)CpCl] Complexes in Arylamination Catalysis. *Organometallics* **2013,** *32* (21), 6265-6270.

5. Fortman, G. C.; Nolan, S. P., N-Heterocyclic carbene (NHC) ligands and palladium in homogeneous cross-coupling catalysis: a perfect union. *Chemical Society Reviews* **2011,** *40* (10), 5151-5169.

6. Zhao, Q.; Meng, G.; Nolan, S. P.; Szostak, M., N-Heterocyclic Carbene Complexes in C–H Activation Reactions. *Chemical Reviews* **2020,** *120* (4), 1981-2048.

7. Nelson, D. J.; Nolan, S. P., Quantifying and understanding the electronic properties of N-heterocyclic carbenes. *Chemical Society Reviews* **2013,** *42* (16), 6723-6753.

8. Izquierdo, F.; Manzini, S.; Nolan, S. P., The use of the sterically demanding IPr* and related ligands in catalysis. *Chemical Communications* **2014,** *50* (95), 14926-14937.

9. Lazreg, F.; Nahra, F.; Cazin, C. S. J., Copper–NHC complexes in catalysis. *Coordination Chemistry Reviews* **2015,** *293-294*, 48-79.

10. Marion, N.; Nolan, S. P., N-Heterocyclic carbenes in gold catalysis. *Chemical Society Reviews* **2008,** *37* (9), 1776-1782.

11. Kaur, H.; Zinn, F. K.; Stevens, E. D.; Nolan, S. P., (NHC)CuI (NHC = N-Heterocyclic Carbene) Complexes as Efficient Catalysts for the Reduction of Carbonyl Compounds. *Organometallics* **2004,** *23* (5), 1157-1160.

12. Lin, J. C. Y.; Huang, R. T. W.; Lee, C. S.; Bhattacharyya, A.; Hwang, W. S.; Lin, I. J. B., Coinage Metal−N-Heterocyclic Carbene Complexes. *Chemical Reviews* **2009,** *109* (8), 3561-3598.

13. Santoro, O.; Collado, A.; Slawin, A. M. Z.; Nolan, S. P.; Cazin, C. S. J., A general synthetic route to [Cu(X)(NHC)] (NHC = N-heterocyclic carbene, X = Cl, Br, I) complexes. *Chemical Communications* **2013,** *49* (89), 10483-10485.

14. Collado, A.; Gómez-Suárez, A.; Martin, A. R.; Slawin, A. M. Z.; Nolan, S. P., Straightforward synthesis of [Au(NHC)X] (NHC = N-heterocyclic carbene, X = Cl, Br, I) complexes. *Chemical Communications* **2013,** *49* (49), 5541-5543.

15. Díez-González, S.; Stevens, E. D.; Scott, N. M.; Petersen, J. L.; Nolan, S. P., Synthesis and Characterization of [Cu(NHC)2]X Complexes: Catalytic and Mechanistic Studies of Hydrosilylation Reactions. *Chemistry – A European Journal* **2008,** *14* (1), 158-168.

16. Fisher, S. P.; Tomich, A. W.; Lovera, S. O.; Kleinsasser, J. F.; Guo, J.; Asay, M. J.; Nelson, H. M.; Lavallo, V., Nonclassical Applications of closo-Carborane Anions: From Main Group Chemistry and Catalysis to Energy Storage. *Chemical Reviews* **2019,** *119* (14), 8262-8290.

17. Fisher, S. P.; McArthur, S. G.; Tej, V.; Lee, S. E.; Chan, A. L.; Banda, I.; Gregory, A.; Berkley, K.; Tsay, C.; Rheingold, A. L.; Guisado-Barrios, G.; Lavallo, V., Strongly Coordinating Ligands To Form Weakly Coordinating Yet Functional Organometallic Anions. *Journal of the American Chemical Society* **2020,** *142* (1), 251-256.

18. Fisher, S. P.; El-Hellani, A.; Tham, F. S.; Lavallo, V., Anionic and zwitterionic carboranyl N-heterocyclic carbene Au(i) complexes. *Dalton Transactions* **2016,** *45* (24), 9762-9765.

19. Tej Raviprolu, V.; McArthur, S. E.; Banda, I.; Gregory, A.; McArthur, S. G.; Fisher, S. P.; Lavallo, V., Fusing 10-vertex closo-carborane anions with N-heterocyclic carbenes. *Chemical Communications* **2022,** *58* (75), 10580-10582.

20. Krylova, V. A.; Djurovich, P. I.; Conley, B. L.; Haiges, R.; Whited, M. T.; Williams, T. J.; Thompson, M. E., Control of emission colour with N-heterocyclic carbene (NHC) ligands in phosphorescent three-coordinate Cu(i) complexes. *Chemical Communications* **2014,** *50* (54), 7176-7179.

21. Hamze, R.; Peltier, J. L.; Sylvinson, D.; Jung, M.; Cardenas, J.; Haiges, R.; Soleilhavoup, M.; Jazzar, R.; Djurovich, P. I.; Bertrand, G.; Thompson, M. E., Eliminating nonradiative decay in Cu(I) emitters: >99% quantum efficiency and microsecond lifetime. *Science* **2019,** *363* (6427), 601-606.

22. Krylova, V. A.; Djurovich, P. I.; Aronson, J. W.; Haiges, R.; Whited, M. T.; Thompson, M. E., Structural and Photophysical Studies of Phosphorescent Three-Coordinate Copper(I) Complexes Supported by an N-Heterocyclic Carbene Ligand. *Organometallics* **2012,** *31* (22), 7983-7993.

23. Krylova, V. A.; Djurovich, P. I.; Whited, M. T.; Thompson, M. E., Synthesis and characterization of phosphorescent three-coordinate Cu(i)–NHC complexes. *Chemical Communications* **2010,** *46* (36), 6696-6698.

Chapter 7: When the Ferrocene Analogy Breaks Down: Promiscuous Behavior of Dicarbollide Derivatives

7.1 Introduction

Ferrocene, which was first reported in 1951 by Pauson and Kealy, is the archetypical metallocene or sandwich-type complex (Fig **7.1**).[1] In their initial publication they note its extreme chemical and thermal stability, which perplexed these investigators as all prior claims of organo-iron compounds were as fleeting intermediates. While these investigators correctly identified it as a complex of formal Fe(II) with two cyclopentadienyl ligands they did not know it's true three dimensional structure. The following year Wilkinson and Fisher independently reported experimental evidence of ferrocene's classic metallocene structure, which ultimately resulted in their award of the 1973 Nobel Prize in chemistry.[2-3]

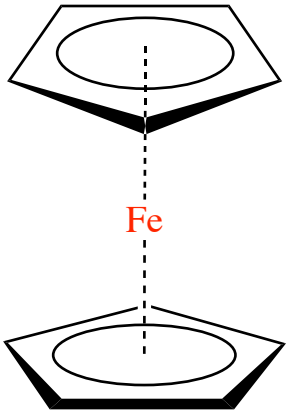

Fig. **7.1** Ferrocene

In 1965 Hawthorne reported the synthesis of the dicarbollide ion, a carborane that is isolobal with the cyclopentadienyl anion.[4] In this same manuscript he reported that this dianion could be used to access the first transition metal bisdicarbollide complex (Fig. **7.2**, **13**) (Scheme **1.8**) which is an analogue of ferrocene (Fig. **7.1**).[5] The metallic core of this so-called metallacarborane exhibits similar stability and redox properties to ferrocene. Additionally, it undergoes analogous derivatization chemistry, in that the B-H cluster substituents can be replaced in a manner similar to

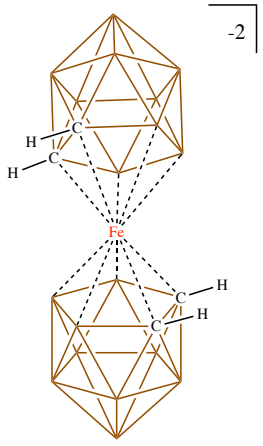

13

Fig. **7.2** Bis(dicarbollide)iron **13**

electrophilic aromatic substitution.[6] Furthermore, like ferrocene, the mildly acidic C-H bonds can be deprotonated and functionalized with various electrophiles.[6-12] It has long been accepted that like ferrocene, the metal center of **13** is substitutionally inert except under extremely harsh basic and acidic conditions that decompose the complex (a form of substitution). Although less explored than as a synthon for building molecules, **13** and its derivatives have thus far given no indication that they should display more promiscuous chemical reactivity than ferrocene.

A different class of compounds that also contain unusual carbon centers are N-heterocyclic Carbenes (NHCs).[13-19] These entities have found wide applications as organic catalysts and ligands for transition metals and main group elements.[20-23] Typically, NHCs are neutral species that are legendary for their ability to strongly bind metals. When appended with an anionic group the NHC as a whole becomes an anion that nearly always forms carbenoid complexes with the alkali metal counter cations of the employed base used to generate the carbene lone pair.[24-26] We became curious if it was possible to create an Fe bisdicarbollide imidazolium species **58** (Fig. **7.3**) that might act as a precursor for the corresponding dianionic bis NHC. The introduction chapter discusses the marriage of dicarbollide anions and NHCs via the synthesis of the imidazolium precursor **19** and its subsequent deprotonation to produce **20** and **21**.[27] Here we report an intriguing set of

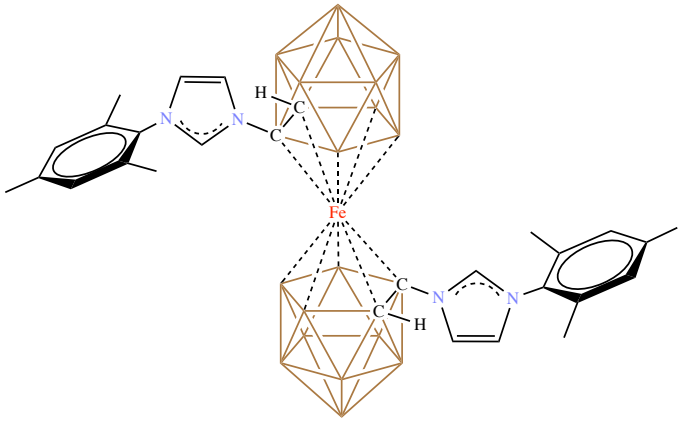

58

Fig. **7.3** Imidazolium appended bis(dicarbollide)iron **58**

reactions that demonstrate, unlike ferrocene and ferrocene "like" **13**, **58** is promiscuous and only resembles ferrocene in appearance. In the first set of reactions, we observe the unprecedented transmetalation from Fe to Ir, resulting in collapse of the ferrocene like core of **58** and formation of novel half sandwich complex of Ir. Cyclic voltammetry studies of **13** and **58** indicate that the charge compensated imidazolium species **58** is much harder to oxidize than **13**, suggesting the imidazolium ligand is a much weaker donor towards the Fe-center. In the second set of reactions, we demonstrate that a stable bis NHC carbenoid can be formed from **58** and this species is also similarly promiscuous, but with the added twist that in some cases the metallocene transmetalation occurs without concomitant carbene transmetalation.

7.2 Synthesis of Imidazolium Functionalized Bis(dicarbollide)iron

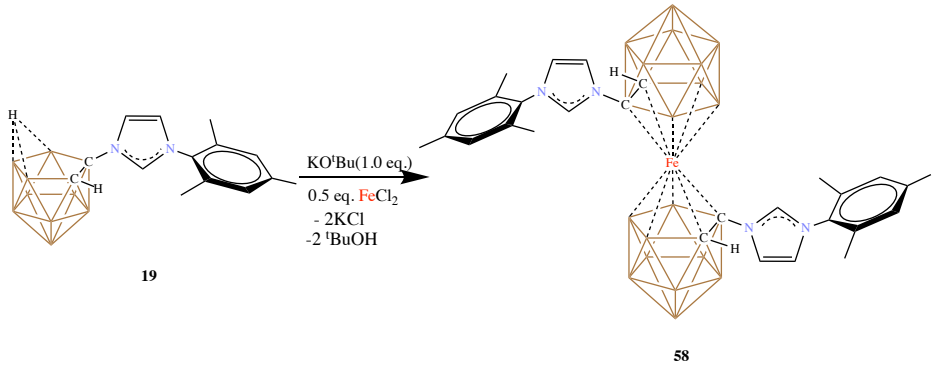

Scheme **7.1** Synthesis of the imidazolium functionalized bis(dicarbollide)iron **58**

To access **58**, we envisioned a strait forward reaction sequence starting from **20[K$^+$]** and reaction with $FeCl_2$. The imidazolium **19** was treated with KO^{t}Bu to produce **20[K$^+$]**. Addition of $FeCl_2$ insitu provided **58** as a purple solid (Scheme **7.1**). Indeed, this reaction is highly efficient and affords **58** in quantitative yield. The identity of diamagnetic **58** was confirmed by multinuclear NMR spectroscopy, high resolution mass spectrometry and single crystal X-Ray crystallography. Similar to **13**, **58** is sensitive to oxidation by

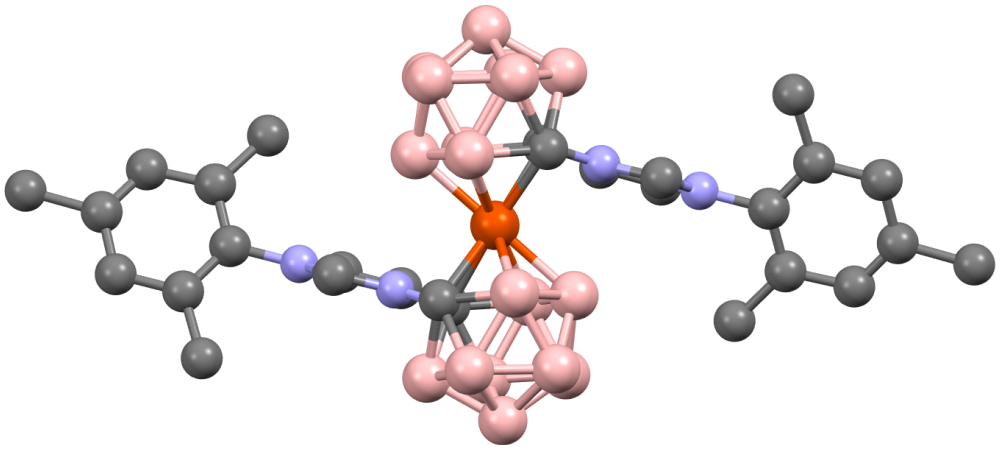

Fig. **7.4** Solid-State Structure of **58**. Hydrogen atoms omitted for clarity. N=Blue, Fe=maroon, B=pink, C=grey

molecular oxygen presumably forming the analogous Fe(III) species. However, unlike substitutionally inert **13**, we noticed that **58** appeared to react with different transition metal precursors to give mostly complex intractable mixtures. That being said, we did observe a clean reaction with $(ClIrCOD)_2$ discussed below.

7.3 Transmetalation Reactions of 58

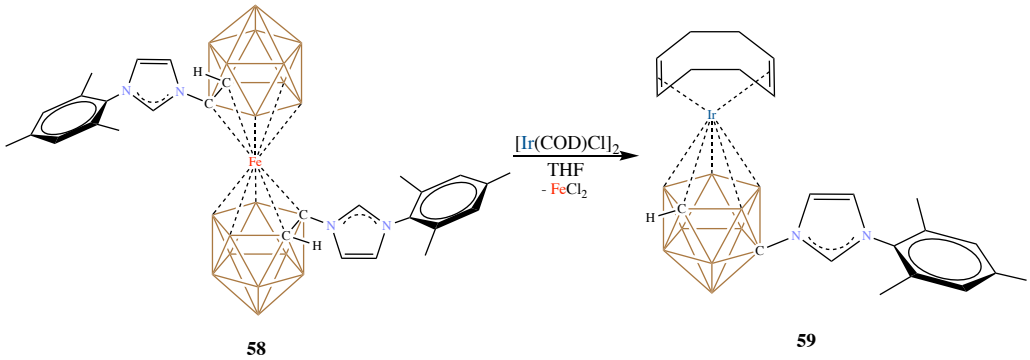

Scheme **7.2** Transmetalation of **58** to the Ir complex **59**

When **58** was treated with $(ClIrCOD)_2$ (1 eq), a rapid reaction occured resulting in the formation of a new compound as indicated by multinuclear NMR spectroscopy. To our surprise the new compound displayed resonances of both COD and the NHC dicarbollide ligand in a 1:1 ratio as well as a HRMS signature for a complex that contained only Ir and not Fe. This observation was perplexing until a single crystal X-ray diffraction study

revealed that an unprecedented transmetalation reaction had occurred between the metallocene-like **58** and $(ClIrCOD)_2$ to afford the novel half-sandwich Ir(I) imidazolium species **59**. Additionally, an *ortho* to *meta* isomerization had occurred at the carborane cage. While the transmetalation reaction has no precedence in the metallocene or bisdicarbollide transition metal chemistry, similar isomerizations have been observed a few

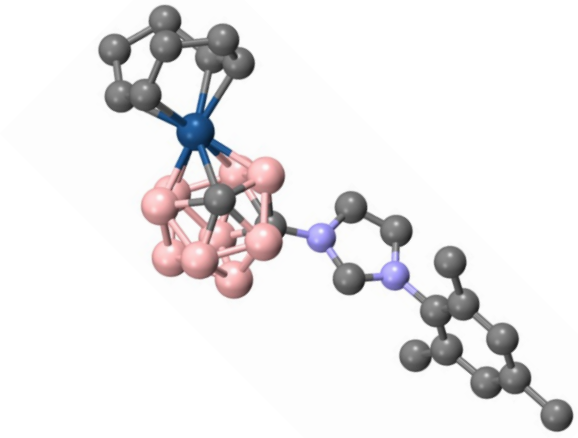

Fig. **7.5** Solid-State Structure of the Ir complex **59**. Hydrogen atoms omitted for clarity. N=Blue, B=pink, Ir=ocean blue, C=grey

times when complexing *o*-dicarbollide to heavier late metals like Rh and Ir.[7, 28-30]

In order to gain insight into the reactivity differences of **13** and **58**, we first examined their solid-state structures via single crystal X-ray diffraction studies to look for structural distortions/deviations. While a crystal structure of the homolog of **2** with Fe in the (III) oxidation state has been long known no such analysis has been performed of **2**

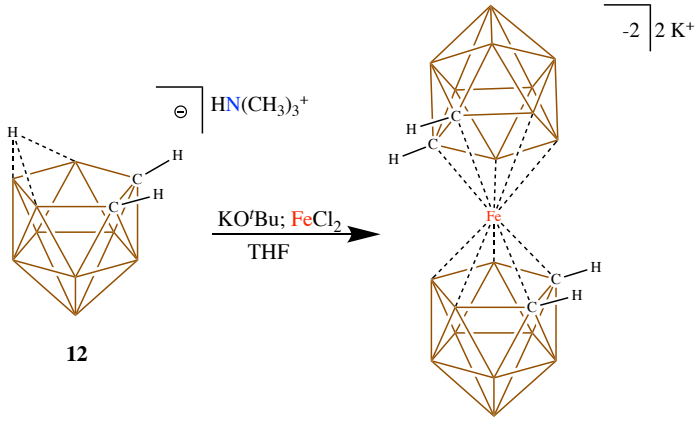

12 **13[K+]**

Scheme **7.3** Synthesis of bis(dicarbollide)iron **13[K+]**

itself. Thus, we synthesized **13[K$^+$]** by treating the *nido* carborane TMA salt with 2 eq of KO^{t}Bu and 0.5 eq of $FeCl_2$ (Scheme **7.3**).[4] Layering the THF solution of the compound with hexanes produced crystals suitable for X-Ray diffraction.

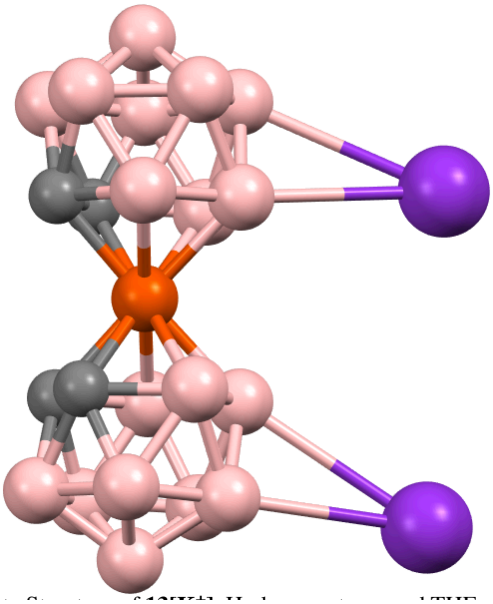

Fig. **7.6** Solid-State Structure of **13[K$^+$].** Hydrogen atoms and THF molecules coordinated to K$^+$ are omitted for clarity. B=pink, K=purple, Fe=maroon, C=grey

From the solid-state structures (Fig. **7.4** and **7.6**), the Fe-B bonds have an average bond length of about 2.09 Å in **13**, while the imidazolium derivative **58** has average bond length of 2.12 Å. Likewise, the Fe-C bond lengths are about 2.02 Å in **13**, while they are slightly elongated to about 2.04 Å in the imidazolium derivative **58**. This is likely due to the electron withdrawing effect of the imidazolium ring, elongating the bonds in the imidazolium derivative, making them weaker and thus facilitating the transmetalation. Further, the anionic charge on the ligand in the parent compound enforces stronger bonds, while the charge compensated neutral ligand in the imidazolium derivative makes them relatively weaker.

We then turned our attention to the differences in their redox chemistry as probed via cyclic voltammetry. Although both the compounds show reversible redox active behavior, they differ by the oxidation/reduction potentials significantly. The redox couple event for the parent compound **13** was at about -0.71 V and at 0.23 V for the imidazolium species **58** with reference to the ferrocene/ferrocenium redox couple (Fig. **7.7**). This is expected, as the ligand becomes poorer donating with charge compensation and due to the presence of a strong electron withdrawing imidazolium group. Hence the ensuing Fe(III) species becomes less stabilized by the ligand and requires higher positive potential to strip it off.

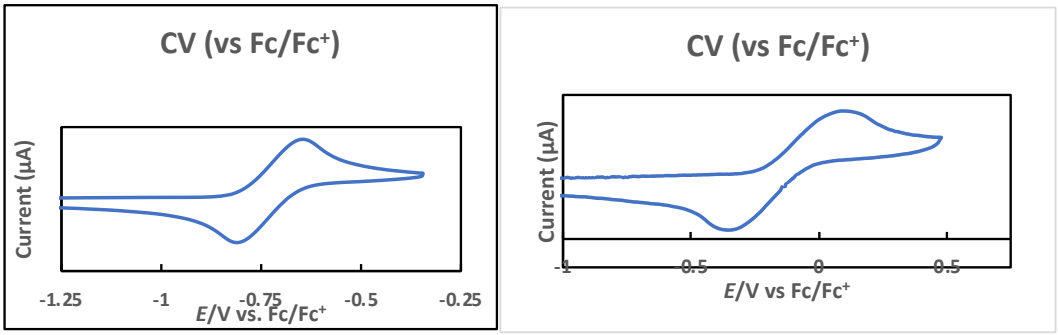

Fig. **7.7** Cyclic Voltammograms of **13[K$^+$]** (left) and **58** (right).

On the other hand, the ligand is still monoanionic and hence better donating to the ensuing Fe(III) in case of the parent compound.

7.4 Synthesis of bis(dicarbollide)iron appended NHCs:

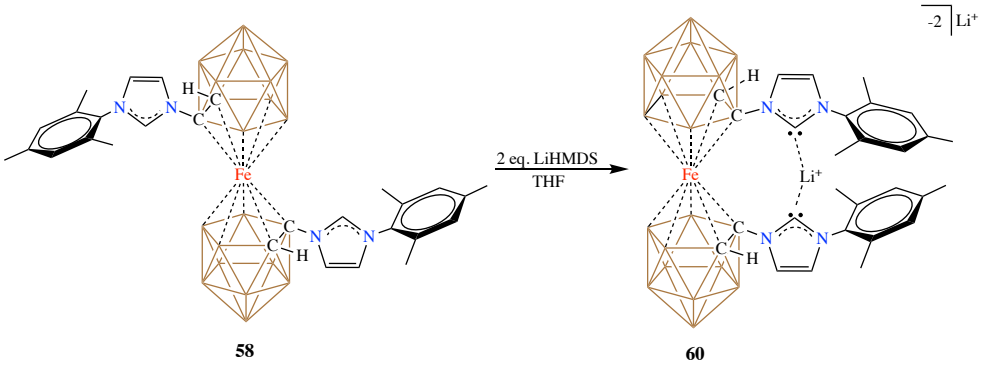

58 **60**

Scheme **7.5** Deprotonation of **58** to produce the NHC **60[Li$^+$]**

We next became curious if the corresponding NHC bis(dicarbollide) species could be generated from **58**. To do this, when **58** was reacted with two equivalents of a strong base like LiHMDS or NaHMDS (Scheme **7.4**), the reaction produced a mixture of paramagnetic compounds that were hard to separate and identify.

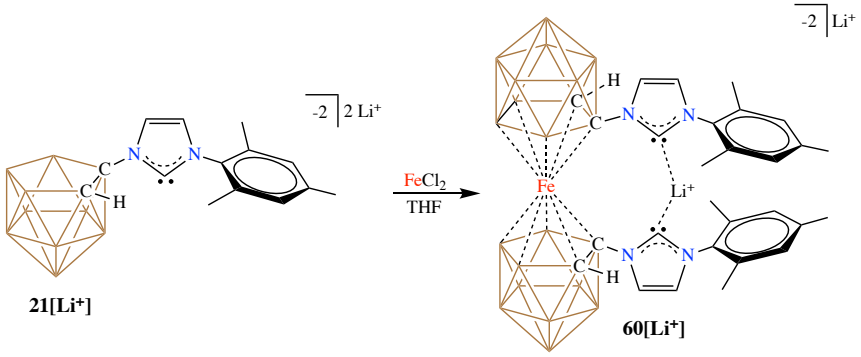

21[Li$^+$] **60[Li$^+$]**

Scheme **7.4** Synthesis of **60[Li$^+$]** from **21[Li$^+$]**

Although it seemed like the ensuing NHC species was paramagnetic, as seen in the crude ^{1}H NMR, we were later able to isolate the clean diamagnetic NHC species **60**, and

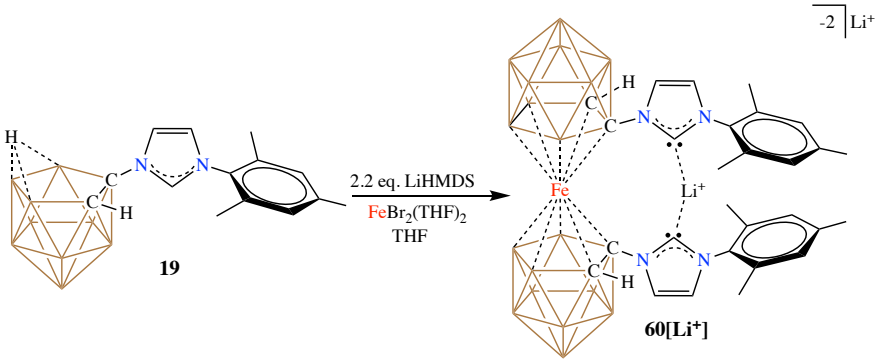

19 **60[Li$^+$]**

Scheme **7.6** Synthesis of **60[Li$^+$]** from **19**

concluded the broad peaks seen were due to the paramagnetic impurities generated in the reaction.

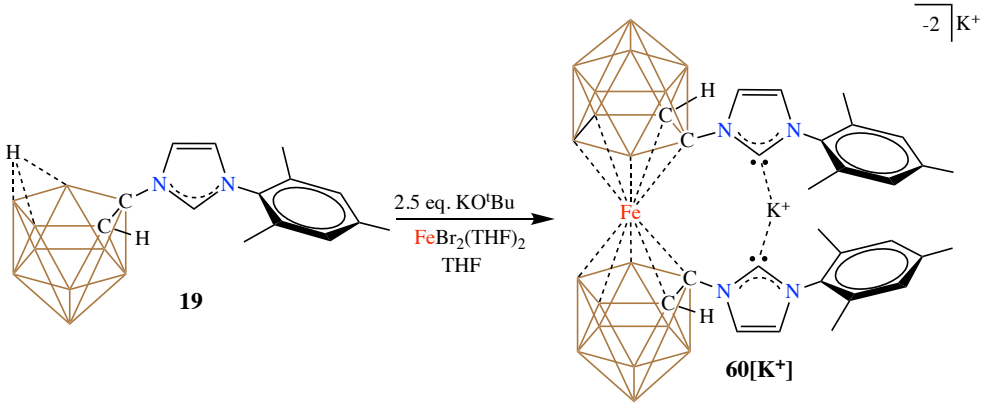

Scheme **7.7** Synthesis of **60[K$^+$]** from **19**

To avoid the formation of paramagnetic impurities, the pre-isolated NHC **21[Li$^+$]** was reacted with 0.5 eq. of $FeCl_2$, (Scheme **7.5**) and the reaction produced the NHC **60** with comparatively less paramagnetic impurities. Still, isolating the clean NHC decreased the yield of the reaction significantly. To mitigate these issues, we sought a way to produce this NHC with absolutely no paramagnetic impurities. $FeCl_2$ was replaced by a more soluble precursor, $FeBr_2(THF)_2$ added to **29[Li$^+$]** generated insitu by deprotonating **19** with LiHMDS (Scheme **7.6**). The change in the order of addition and the Fe precursor drastically improved the yield of the product and produced very little to no paramagnetic impurities.

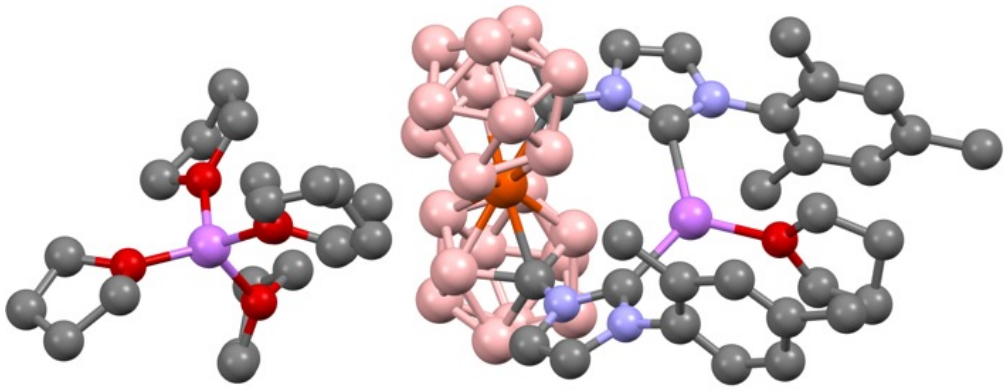

Fig. **7.8** Solid-State Structure of **60[Li$^+$].** Hydrogen atoms omitted for clarity. N=Blue, C=grey, B=pink, Fe=maroon, O=red, Li=purple

Further, the synthesis of the K^+ salt of the bis(dicarbollide) NHC **60[K^+]** could be done similarly starting from the imidazolium **19**, excess KO^{t}Bu and $FeBr_2(THF)_2$ producing the compound in about 80% yield.

The identity of the compound **60** was established by multinuclear NMR spectroscopy and single crystal X-Ray diffraction. The carbene carbon resonance on the ^{13}C NMR slightly shifted upfield to 207.99 ppm from 208.69 ppm in the parent NHC, indicating the increased electron withdrawing nature of the imidazolylidene ring upon coordination of Fe at the dicarbollide face. In the solid-state, the two carbenes are bridged by a lithium cation, hence technically this is an example of a carbenoid.

7.5 Transmetalation Reactions of 60

After discovering the transmetalation properties of **58**, we became curious how the corresponding NHC **60** would react with transition metals. When **60[Li^+]** was treated with $[Ir(COD)Cl]_2$, complete transmetalation to the corresponding Ir NHC **61** was observed as seen by the 1:1 ratio of the COD to NHC ligands on the ^1H NMR (Scheme **7.8**). To confirm if the compound **61** was a NHC complex, the crude ^{13}C NMR was taken; it displayed the carbene carbon resonance at 198.91 ppm indicating the transmetalation product **61** was still

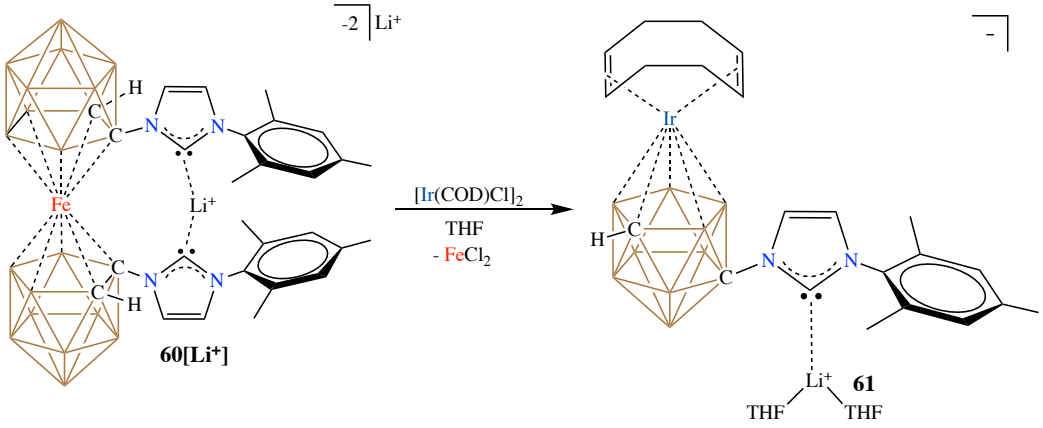

Scheme **7.8** transmetalation of **60[Li^+]** to **61**

a carbene. It was rather surprising to see the carbene Li^+ not transmetalating to Ir, instead the transmetalation was solely observed at the dicarbollide Fe center. The structure of the product unambiguously determined by single crystal X-Ray diffraction (Fig. **7.9**), revealed the compound **61** with no Fe present, confirming the transmetalation of Fe to Ir. Further, the NHC moiety was ring isomerized to the meta position of the dicarbollide from the

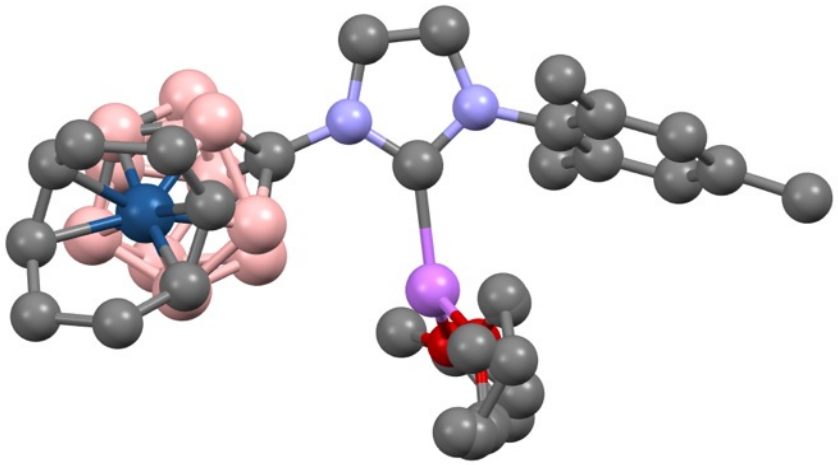

Fig. **7.9** Solid-State Structure of **61**. Hydrogen atoms omitted for clarity. N=blue, C=grey, Li=purple, B=pink, O=red, Ir=ocean blue

ortho, as seen in the previous transmetalation example. In solid-state, the Li^+ counter-cation was seen coordinating to the carbene lone-pair as seen in the case of other carbenoids. Another way of looking at this compound is a NHC attached to a mesityl group and a metallacarborane. This is the first example of a NHC directly attached to a metallacarborane unit.

Intrigued by this reaction, we reacted other transition metal precursors to react with the Fe NHC. When the NHC **60** was reacted with CuCl, it produced a mixture of two products, including the protonated precursor (Scheme **7.9**). The other product determined by single crystal X-Ray diffraction consisted of a trinuclear Cu core bound by the NHC ligands and stabilized additionally by the B-H…Cu interactions (Fig. **7.10**). This compound represents another example of transmetalation of Fe in Fe metallocene substituted NHCs. The carbene-Cu distances are in the range of about 1.9 Å which is expected for a NHC-Cu complex.

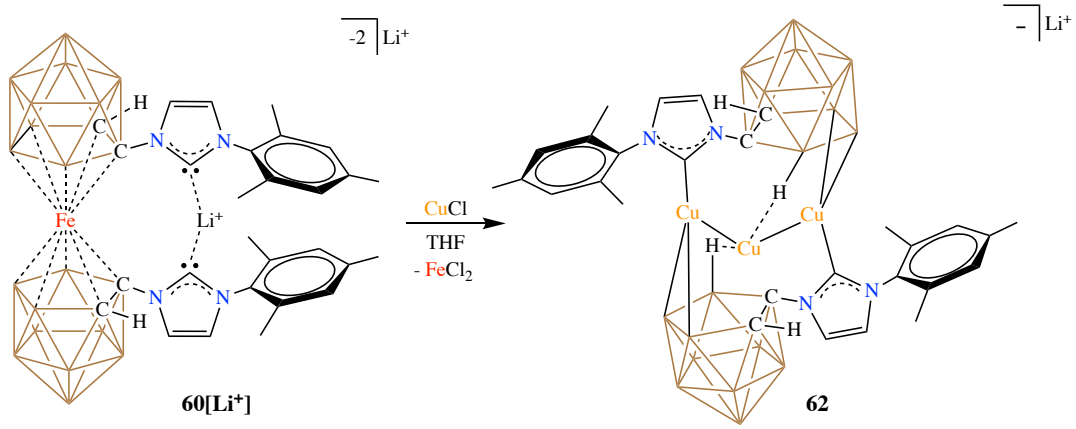

Scheme **7.9** Transmetalation of **60[Li$^+$]** to **62**

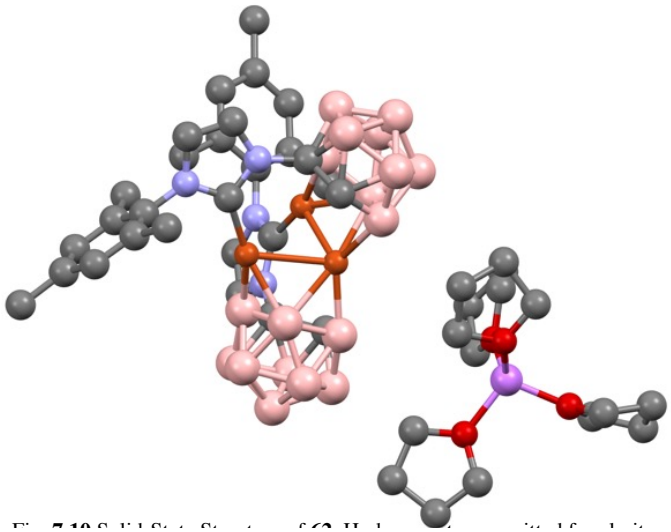

Fig. **7.10** Solid-State Structure of **62**. Hydrogen atoms omitted for clarity. N=blue, C=grey, O=red, Li=purple, B=pink, Cu=orange

7.6 Reactivity of 13 Towards Transition metals

At this point, we became curious to see how the parent Fe metallocene reacts with the above transition metal precursors. When **13** was reacted with $[Ir(COD)Cl]_2$ (Scheme **7.10**),

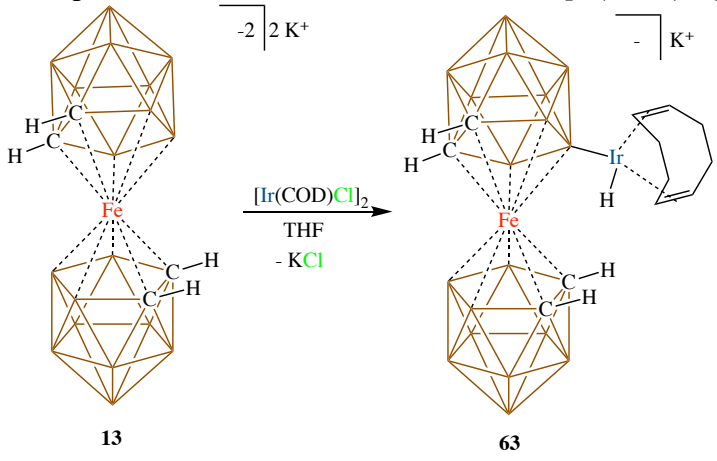

Scheme **7.10** B-H oxidative addition on **13** by $[Ir(COD)Cl]_2$

the crude $^{11}B[^{1}H]$ NMR spectrum displayed multiple peaks ranging from 50 ppm to -40 ppm. The peaks in the positive region of the ^{11}B NMR were previously seen in case of carborane Ir complexes formed by B-H oxidative addition onto the Ir(I) center. Suspecting it to be the case, a crude ^{1}H NMR was recorded on the sample to see any evidence for B-H oxidative addition. As expected, a couple of singlets were seen on the ^{1}H NMR at about -18 ppm suggesting the formation of Ir hydrides by B-H oxidative addition. Further, the high resolution mass spectrometry revealed the presence of a peak at m/z 600 confiriming the B-H oxidative addition product **63** among others. No transmetalation product was observed on the mass spec. Further, its interesting to note that no such oxidative addition product was observed upon transmetalation of **58** to **59**.

When **13** was reacted with CuCl, the crude ^{11}B NMR displayed multiple peaks indicating the compound was reacting with CuCl. However, the mass spec still displayed the m/z peak for the compound **13**; hence it's presumable that the reaction could be mere cation

exchange from K^+ to Cu^+. Further, the Cu^+ cations could be stabilized by B-H interactions as seen in other examples, causing the boron environment change on the ^{11}B NMR. No clean NMR data nor single crystal X-Ray structure could be obtained so far.

7.7 Metallacarboranes with Imidazolium Derivatives

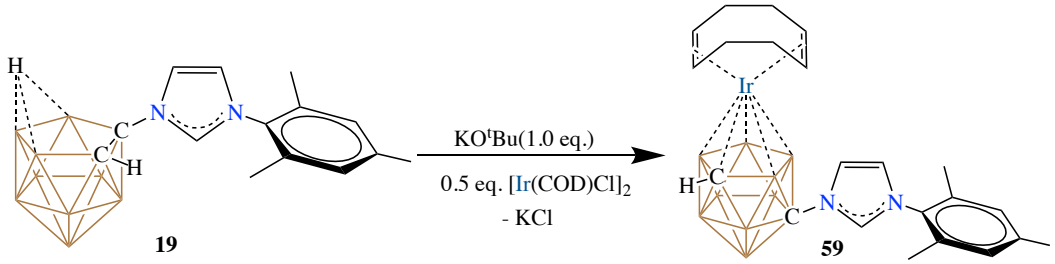

Scheme **7.11** Direct synthesis of **59** from **19**

After investigating the transmetalation reaction with imidazolium and NHC derivatives, we became curious about the carbon isomerization/polyhedral rearrangement in the dicarbollide cluster. Although this is precedent in the literature, it is not clear so far as to what conditions causes this rearrangement. To see if this was a consequence of transmetalating from Fe, we sought synthesizing these compounds directly from the imidazolium.

When the imidazolium **19** was treated with a mixture of KO^{t}Bu and [Ir(COD)Cl]$_2$ in THF, the reaction yielded **59** as the only product (Scheme **7.11**). The ^1H and ^{13}C NMR shifts completely matched with the compound obtained by transmetalating **58**. This proves, the transmetalation of Fe to Ir doesn't influence the reaction outcome; it yielded the more

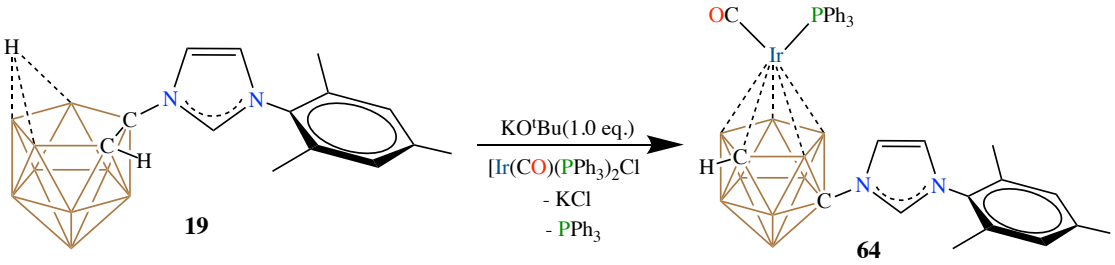

Scheme **7.12** Synthesis of the metallacarborane **64**

thermodynamically stable product. Surprisingly, when this reaction was performed at -78°C, **59** still ended up being the only product suggesting the formation of thermodynamic product. To investigate if the steric bulk of the COD ligand was responsible for the cage rearrangement, Ir precursors with less bulky ligands were reacted directly with the imidazolium.

Reacting the imidazolium with a mixture of KO^{t}Bu and the Vaska's complex $Ir(CO)(PPh_3)_2Cl$ produced the metallacarborane **64** (Scheme **7.12**) although with minor impurities. The cage isomerized structure of the product was confirmed by single crystal

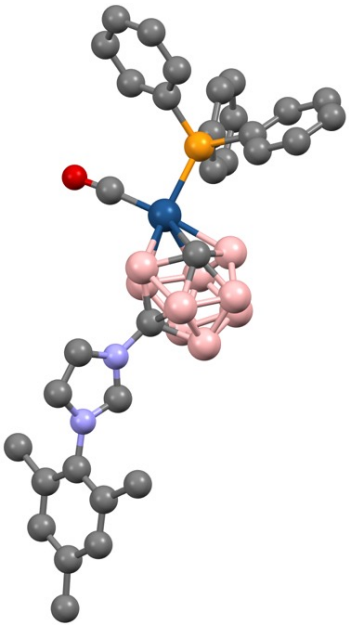

Fig. **7.11** Solid-State Structure of **64**. Hydrogen atoms omitted for clarity. N=Blue, B=pink, Ir=ocean blue, O=red, P=yellow, C=grey

X-Ray diffraction (Fig. **7.11**). Although PPh_3 is a bulky ligand, the presence of small ligand CO had no influence in the cage carbon rearrangement process.

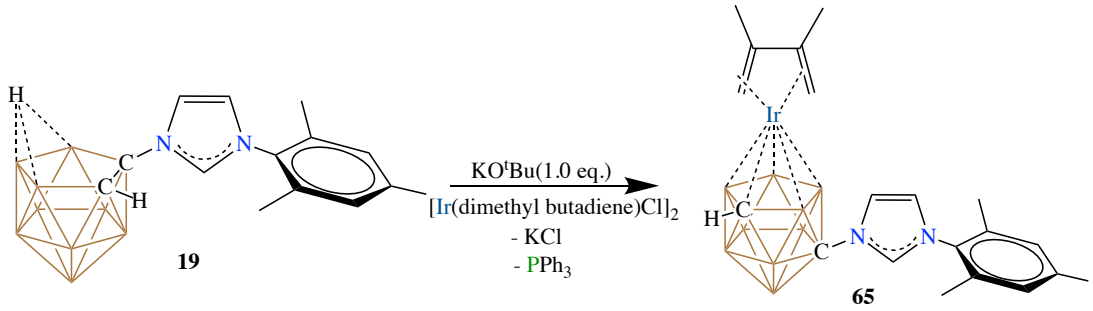

Scheme **7.13** Synthesis of the metallacarborane **65**

Further, in search of more sterically non-bulky ligands for Ir(I), we synthesized the Ir butadiene complex [Ir(2,3-Me$_2$ butadiene)Cl]$_2$.[31]This was reacted with the imidazolium **19** to see if the ligand causes cage rearrangement (Scheme **7.13**). The structure revealed by single crystal X-Ray diffraction, showed the complete rearrangement of the carbon bearing the imidazolium to the meta position (Fig. **7.12**). The structure revealed by single crystal X-Ray diffraction, showed the complete rearrangement of the carbon bearing the imidazolium to the meta position (Fig. **7.12**). From this we concluded, the steric bulk on the Ir(I) ligands has less influence on the cage carbon rearrangement. This process is more

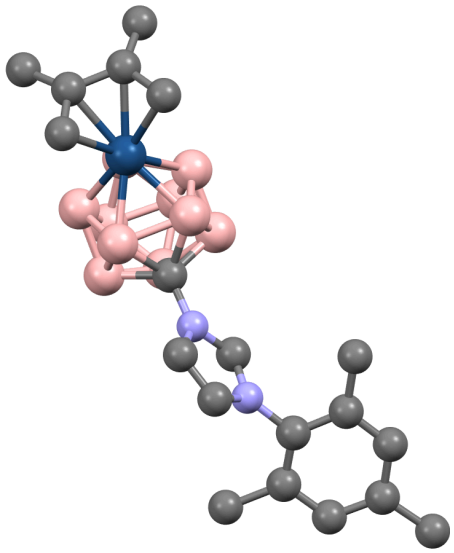

Fig. **7.12** Solid-State Structure of **65**. Hydrogen atoms omitted for clarity. N=blue, C=grey, B=pink, Ir=ocean blue

likely a result of the presence of bulky imidazolium group attached to the carbon; it favors to rearrange to the meta position, causing less steric bulk at the open *nido* Ir face.

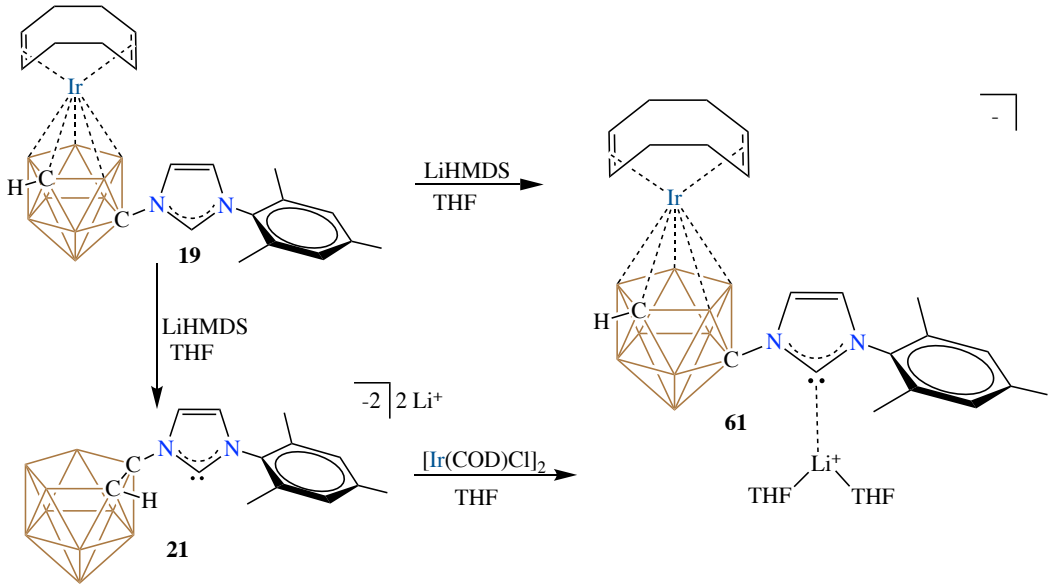

Scheme **7.14** Synthesis of the NHC **61** from **19** and **21**

The directly synthesized Ir metallacarborane **59** could then be deprotonated using LiHMDS in THF to produce the NHC **61**. The ^{1}H and the ^{13}C NMR data matched exactly with the data obtained by transmetalating the NHC **60** with Ir. Further, the pre-isolated dicarbollide-NHC was reacted with $[Ir(COD)Cl]_2$ anticipating a dicarbollide-NHC Ir(COD) complex. However, it only resulted in the Ir NHC **61** surprisingly (Scheme **7.14**). Its rather interesting to note that the NHC isomerizes to the lower belt as such without any reaction with the Ir; probably the only example where a strongly coordinating NHC ligand doesn't coordinate to a transition metal.

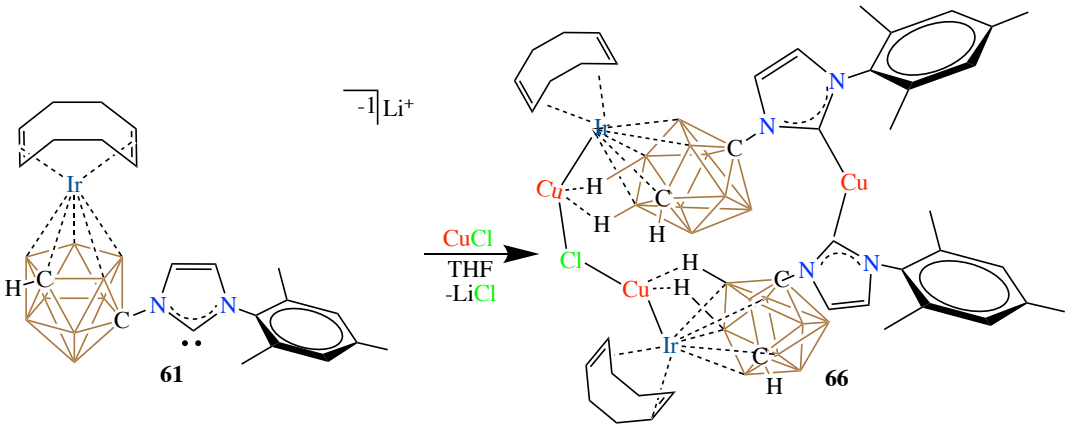

Scheme **7.15** Synthesis of the Ir-Cu bimetallic complex **66**

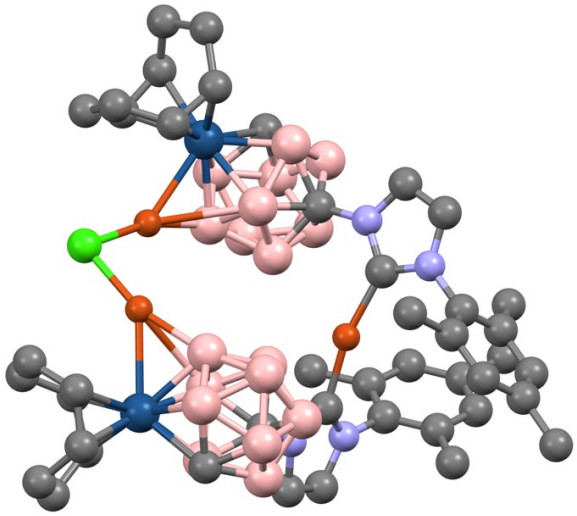

Fig. **7.13** Solid-State Structure of **66**. Hydrogen atoms omitted for clarity.
N=blue, C=grey, B=pink, Cu=brown, Cl=green, Ir=ocean blue

This led us to investigate if the Ir NHC **61** can coordinate to transition metals. The reaction between **61** and CuCl resulted in the formation of a bis(NHC) Cu complex **66** (Scheme **7.15**). Additionally, Cu behaves as a Z type ligand, forming covalent bonds with Ir. In a peculiar coordination, the two Ir-Cu units were bridged by the corresponding halogen (Cl, Br). As seen in the previous example, Cu(I) is stabilized by the B-H….Cu interactions in close proximity. Both the Cl and Br versions of this complex **66** and **67** were characterized by multinuclear NMR spectroscopy and single crystal X-Ray diffraction (Fig. **7.13**). The

NHC-Cu distances are at 1.9 Å, as expected for such complex.[21] The NHC-Cu-NHC bond angle is about 167º, largely deviating from the ideal linear bond angle of 180º. This might be due to the bending imposed by the bridging of the metallacarborane-Cu units by the halogen.

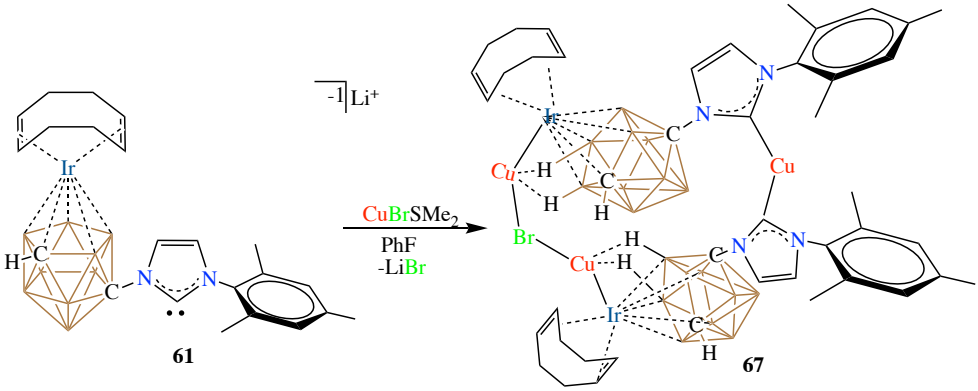

Scheme **7.16** Synthesisof Ir-Cu bimetallic complex **67**

The NHC was also treated with $BrCuSMe_2$, expecting a complex with NHC-Cu-SMe_2 bonding. However, the reaction still yielded the same product obtained by the reaction with CuBr. Although the carbene-Cu distances in **67** are about 1.9 Å, as seen in the case of **66**,

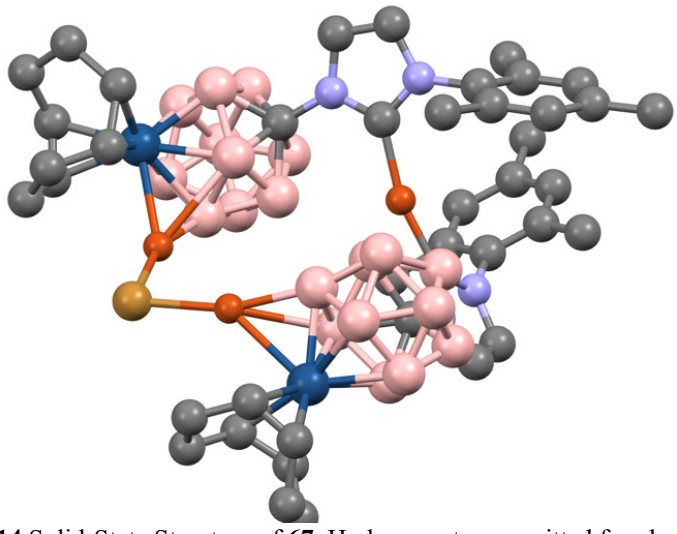

Fig. **7.14** Solid-State Structure of **67**. Hydrogen atoms omitted for clarity.
N=Blue, B=pink, Ir=ocean blue, Br=brown, Cu=orange, C=grey

the NHC-Cu-NHC bond angle is about 165°, slightly more bent than the corresponding chlorine analog. This is due to the relatively weaker Cu-Br-Cu bonds inducing more bending causing greater deviation in the NHC-Cu-NHC bond angle. This is further corroborated by the Cu-Cl bond length of 2.17 Å vs the longer Cu-Br bond length of 2.32 Å.

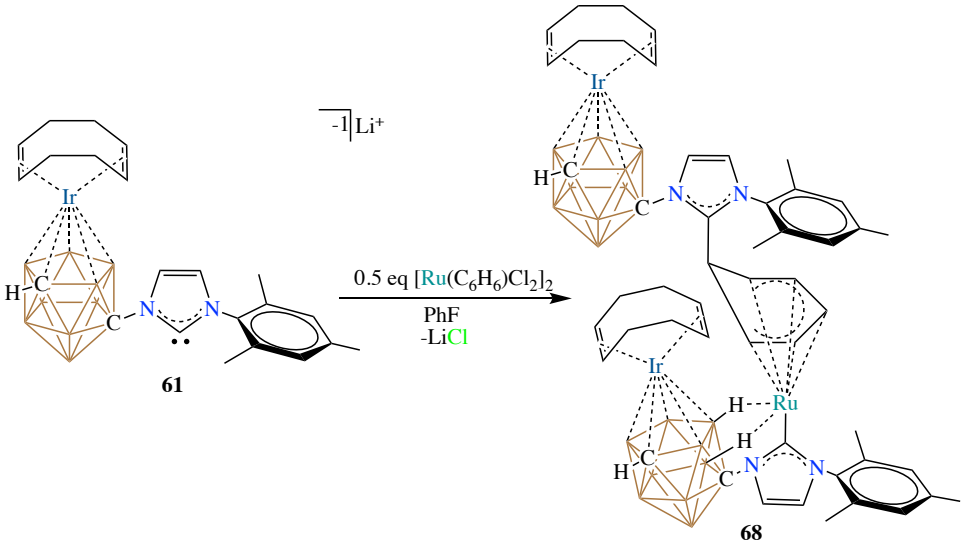

Scheme **7.17** Synthesis of the Ir-Ru complex **68**

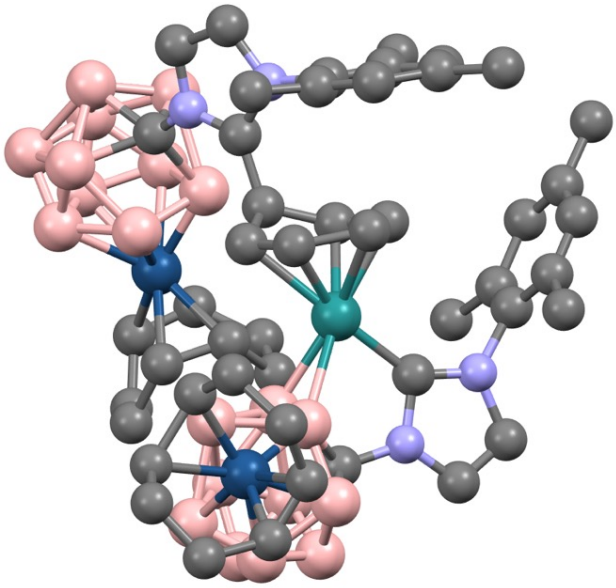

Fig. **7.15** Solid-State Structure of complex **68**. Hydrogen atoms omitted for clarity. N=blue, Ru=teal, Ir=ocean blue, C=grey, B=pink

Most other transition metal precursors protonated the NHC **61** back to the Ir metallacarborane **59**. The reaction with $[Ru(C_6H_6)Cl_2]_2$ yielded a complex mixture of products, out of which we could successfully isolate the single crystal of the major product. The product **65** featured a Ir NHC-Ru(η^5-C_6H_6)-NHC Ir complex (Scheme **7.17**). One of the carbons on the benzene ring undergoes nucleophilic attack by another molecule of carbene, resulting in a cyclohexadienyl ligand coordinated Ru complex. The sixth carbon on the ring coordinates to another NHC-Ir molecule. The NHC-Ru bond length was about 2.04 Å, as seen previously for such complexes. The NHC-Ru-B bond angle was found to be about 81.7°. All attempts to isolate and cleanly characterize this compound using NMR spectroscopy failed.

7.9 Conclusion

About 55 years after the discovery of bis(dicarbollide) metallocenes, their imidazolium and NHC substituted derivatives are shown to transmetalate Fe and produce other metallacarboranes. In some cases, the NHCs transmetalated without any reaction with the transition metal precursors. This sheds light on the synthetic utility of carborane anions in ligand design and tuning the properties of these anions to produce distinct reactivity hitherto unknown. Further, the first example of NHC directly attached to metallacarboranes has been discussed, producing organometallic complexes with peculiar coordination environments. This will potentially open the doors for design of bimetallic transition metal catalysts in the future.

7.10 Experimental

General Considerations:

Unless otherwise stated, all manipulations were performed inside a nitrogen filled glove box or under standard schlenk techniques (O_2, H_2O < 1 ppm). THF and diethyl ether were distilled under argon with K and NaK respectively. Dichloromethane, chloroform, fluorobenzene and acetonitrile were dried on CaH_2 and distilled under argon. Benzene and toluene were dried on K and Na and distilled under argon respectively. Hexanes was dried in a solvent purification system and collected under argon. The imidazolium,[27] the *nido* carborane,[4] $BrCuSMe_2$[32] were synthesized according to literature methods. All other reagents were purchased from commercial sources and used without any further purification. NMR spectra were recorded on Bruker Avance 300, Bruker Avance 600 and Varian Inova 400 MHz spectrometers. ^{1}H and ^{13}C NMRs are referenced to the residual solvents. ^{11}B NMRs were externally referenced to $BF_3.Et_2O$. ^{31}P NMRs were externally referenced to 80% H_3PO_4 in H_2O. High Resolution Mass Spectrometry data was recorded on Agilent Technologies 6210 (Time of Flight LC/MS) using ESI technique. CV experiments were performed using a Pine AFP1 potentiostat. The cell consisted of a glassy carbon working electrode, a Pt wire auxiliary electrode, and a Pt wire pseudoreference electrode. All potentials are referenced versus the ferrocene/ferrocenium couple measured as an internal standard.

Synthesis of **13[K$^+$]**:

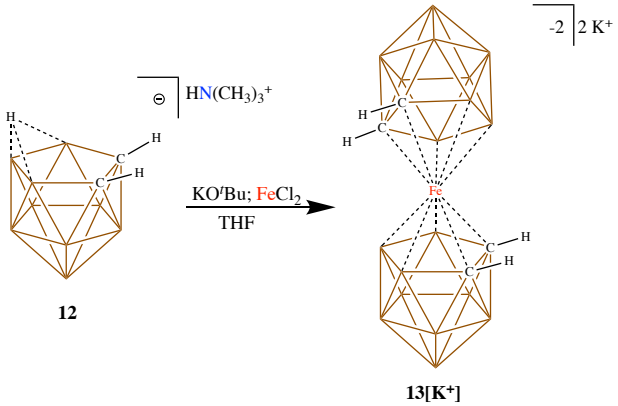

12 **13[K$^+$]**

Scheme **7.3** Synthesis of bis(dicarbollide)iron **13[K$^+$]**

In a glass vial, the trimethyl ammonium salt of the *nido* carborane **12** was loaded with a stir bar and dissolved in 3 mL THF. To this, a solution of KO^{t}Bu in THF was added and stirred for 15 minutes. The solution was then added to a suspension of anhydrous $FeCl_2$ in THF. The deep purple solution was stirred for 15 minutes and filtered over a pad of celite. The filtrate was concentrated to 2 mL under vacuum and precipitated by the addition of hexanes. The combined solvents were then decanted off leaving the purple solid in the vial. The solid was dried under vacuum to produce **13[K$^+$]** in about 80% yield. Crystals suitable for X-Ray diffraction were grown by layering a THF solution of the compound with hexanes.

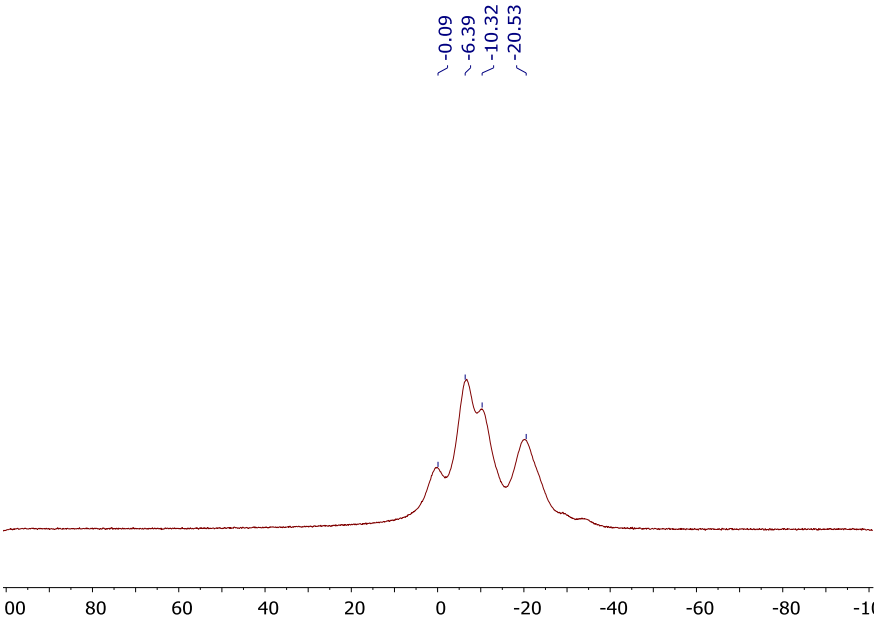

Fig. **7.16** $^{11}B[^{1}H]$ NMR of **13[K$^+$]** in THF

Synthesis of **58**:

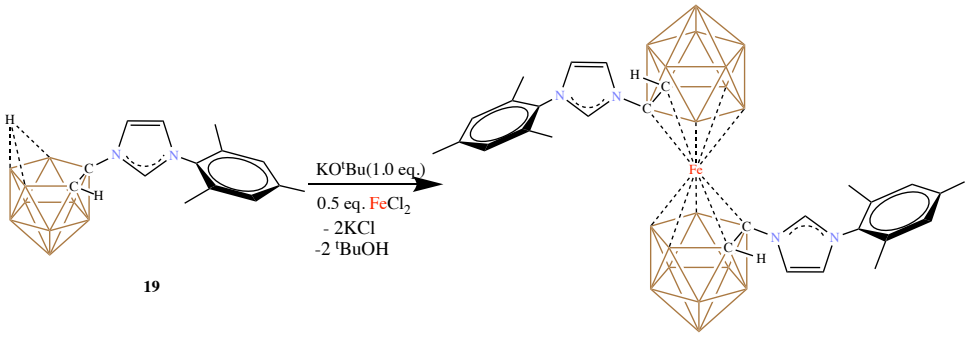

19 **58**

Scheme **7.1** Synthesis of the imidazolium functionalized bis(dicarbollide)iron **58**

In a vial, the imidazolium **19** (50 mg, 0.156 mmol) was weighed and dissolved in THF (2 mL). To this, a solution of KO^{t}Bu (22.4 mg, 0.19 mmol) in 2 mL THF was added and stirred for 10 minutes. The solution was then added to a suspension of anhydrous $FeCl_2$ (10 mg, 0.078 mmol) in THF (1 mL). The reaction mixture immediately turned purple after the addition of dicarbollide-imidazolium. The purple solution was stirred for 10 minutes after which the volatiles were pumped down under vacuum. The reaction mixture was then suspended in dichloromethane (10 mL) and filtered over a pad of celite. The DCM filtrate

was then pumped down under vacuum to afford **58** as a purple solid in 75% yield. X-Ray quality crystals were grown by vapor diffusing ether into a vial containing concentrated solution of the compound in THF in a -30°C freezer. ^{1}H NMR (600 MHz, THF-d_8, 25°C): 9.13 (dd, 1H, CH), 7.94 (dd, 1H, CH), 7.35 (dd, 1H, CH), 7.06 (s, 2H, *meta*-CH), 4.79 (bs, 1H, $CH_{carborane}$), 2.33 (s, 3H, *para*-CH_3), 2.08 (s, 6H, *ortho*-CH_3); ^{11}B[^{1}H] NMR (192.5 MHz, DCM-d_2, 25°C): -3.16, -8.17, -10.53, -13.32, -14.01, -14.90, -15.55, -20.56, -23.25 ppm; ^{13}C[^{1}H] NMR (150.9 MHz, THF-d_8, 25°C): 141.13, 136.07, 132.38, 129.93, 125.28, 120.65, 40.04, 20.87, 17.50 ppm. HRMS calculated: observed:

Note: The above reaction can be performed in DME in place of THF using similar procedure.

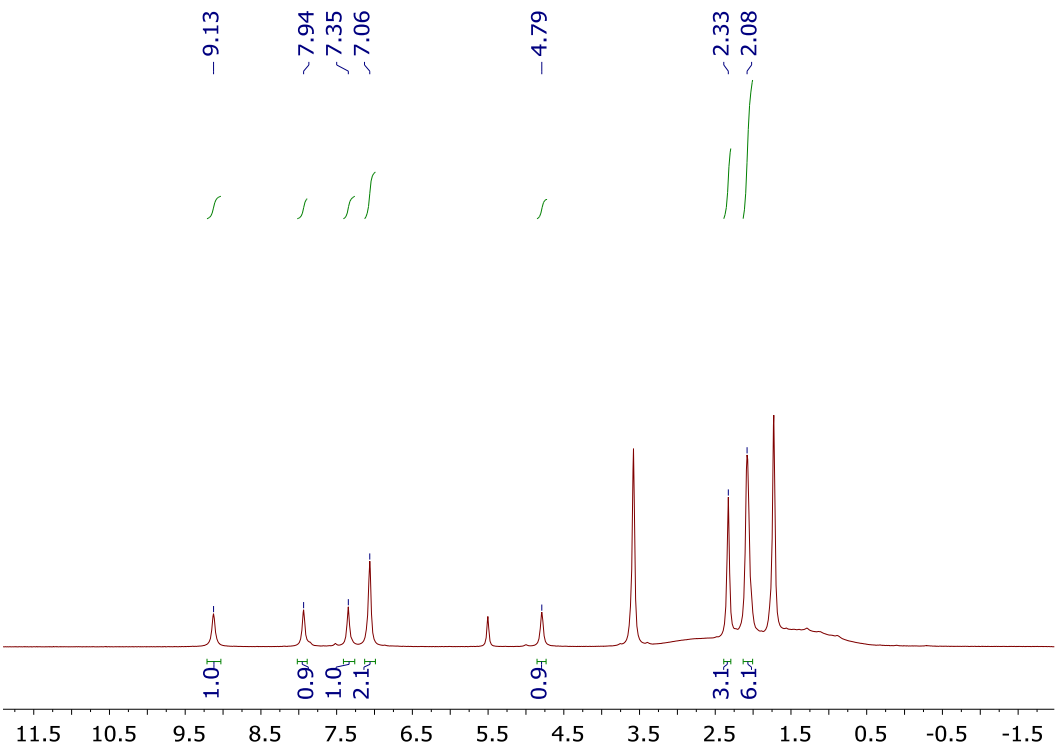

Fig. **7.17** ^{1}H NMR of **58** in THF-d_8

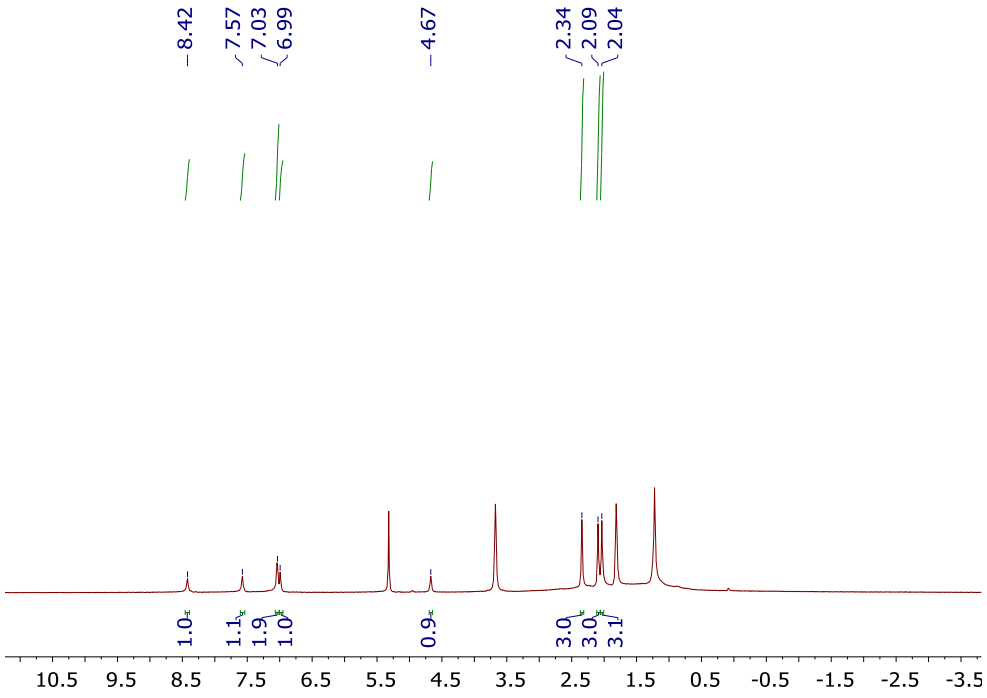

Fig. **7.18** ^{1}H NMR of **58** in CD_2Cl_2

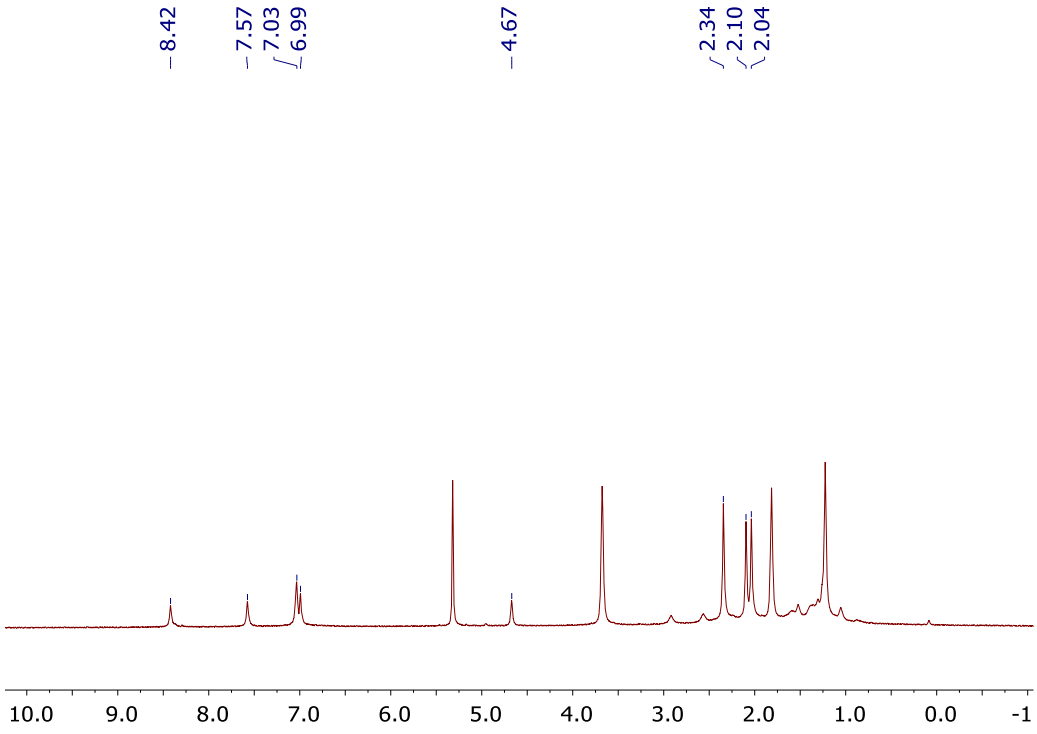

Fig. **7.19** $^{1}H[^{11}B]$ NMR of **58** in CD_2Cl_2

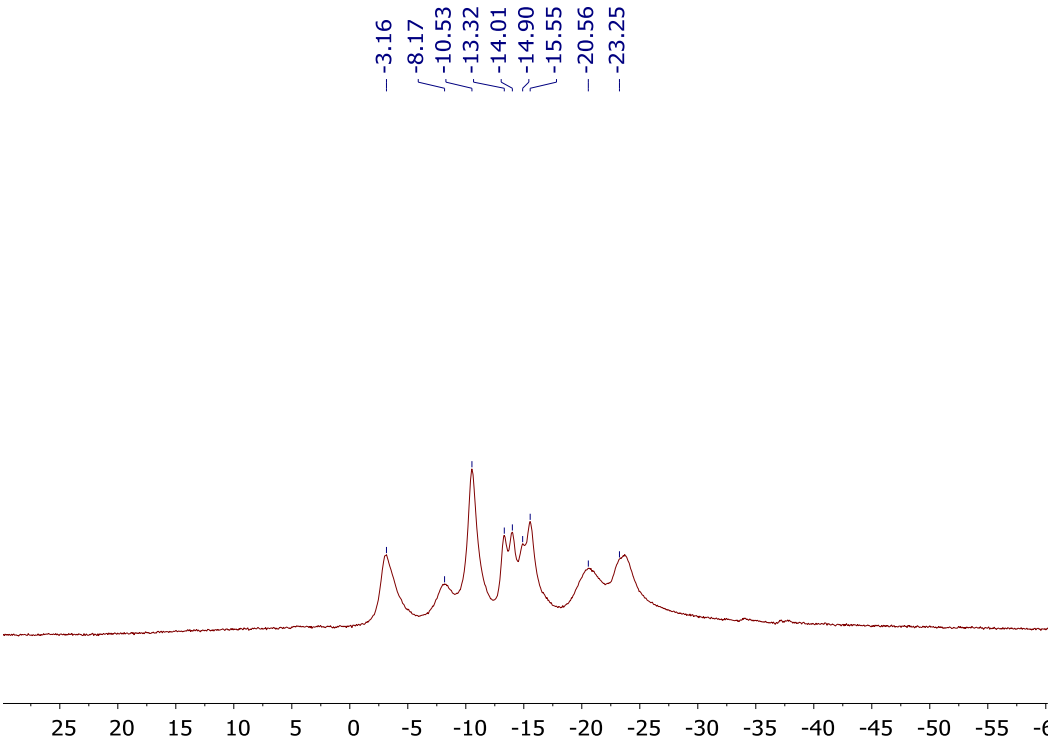

Fig. **7.20** $^{11}B[^{1}H]$ NMR of **58** in CD_2Cl_2

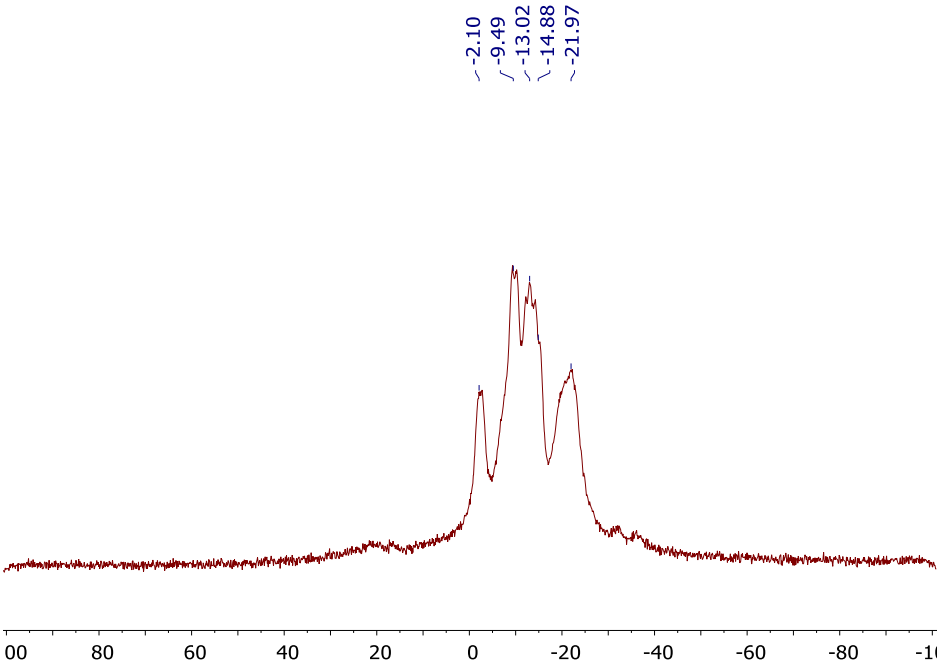

Fig. **7.21** ^{11}B NMR of **58** in CD_2Cl_2

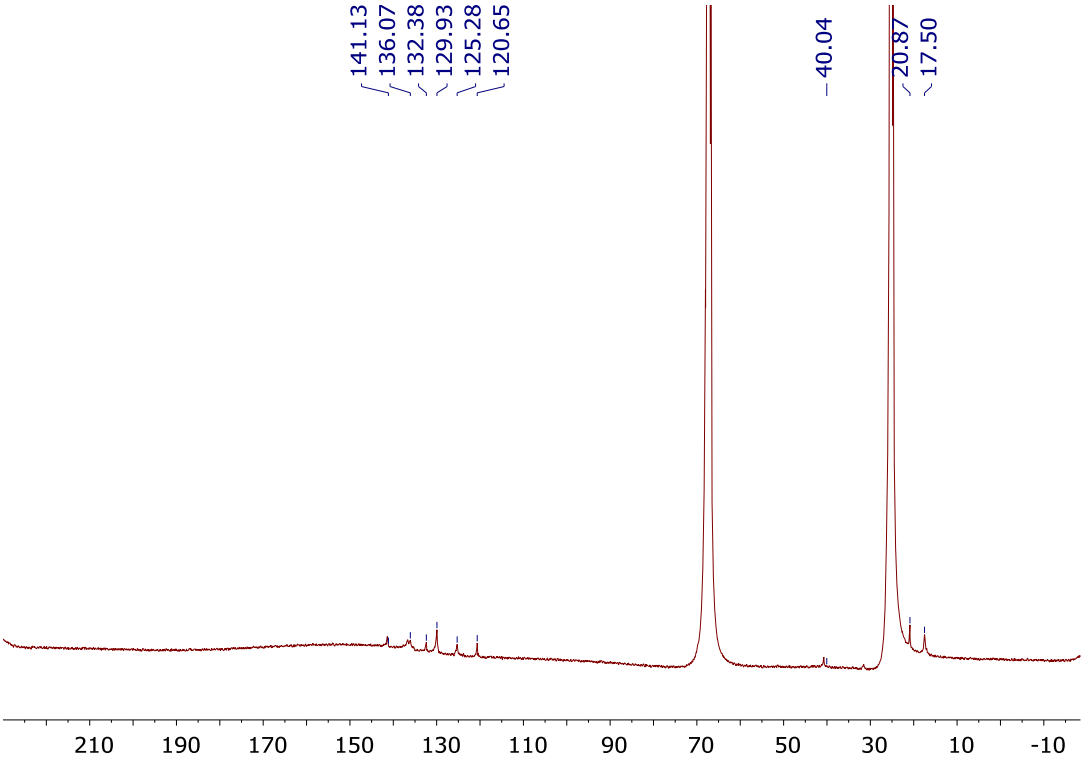

Fig. **7.22** $^{13}C[^{1}H]$ NMR of **58** in THF-d_8

Synthesis of **59**:

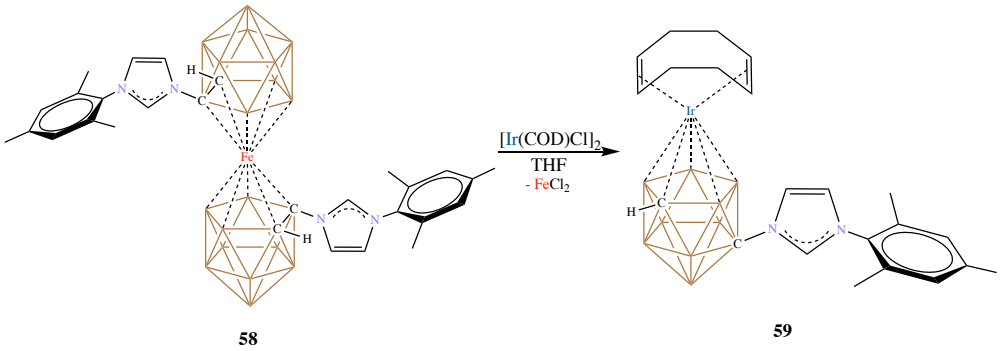

Scheme **7.2** Transmetalation of **58** to the Ir complex **59**

100 mg (0.144 mmol) of compound **58** was weighed in a vial containing a stir bar and dissolved in THF (4 mL). To this, $[Ir(COD)Cl]_2$ dimer (97.2 mg, 0.144 mmol) dissolved in 5 mL THF was added. The dark solution was then stirred for about 2 hours at room temperature. The volatiles were then pumped down under vacuum and the reaction mixture

was dissolved in dichloromethane (10 mL). The DCM solution was filtered over celite, and the filtrate was pumped down under vacuum. The obtained reddish brown solid was redissolved in minimal volume of THF (2 mL). Hexanes (10 mL) was then slowly added to layer the THF solution. The vial was then placed inside a -30ºC freezer overnight to produce brown red microcrystals. The crystals were collected by decanting off the combined solvents, followed by washing with cold hexanes (2x2 mL). Clean **59** was obtained in 90% yield. Crystals suitable for X-Ray diffraction were grown by slow evaporation of a concentrated solution of the compound in DCM in an NMR tube. ^{1}H NMR (400 MHz, $CDCl_3$, 25ºC): 8.27 (dd, 1H, CH), 7.75 (dd, 1H, CH), 7.05 (dd, 1H, CH), 6.99 (s, 2H, *meta*-CH), 4.03 (m, 2H, COD CH), 3.88 (m, 2H, COD CH), 2.60 (bs, 1H, $CH_{carborane}$), 2.43 (m, 8H, COD CH_2), 2.36 (s, 3H, *para*-CH_3), 2.00 (s, 6H, *ortho*-CH_3); ^{11}B[^{1}H] NMR (128 MHz, $CDCl_3$, 25ºC): -7.76, -11.40, -13.13, -22.25, -24.46 ppm. ^{13}C[^{1}H] NMR (100 MHz, THF-d_8, 25ºC):

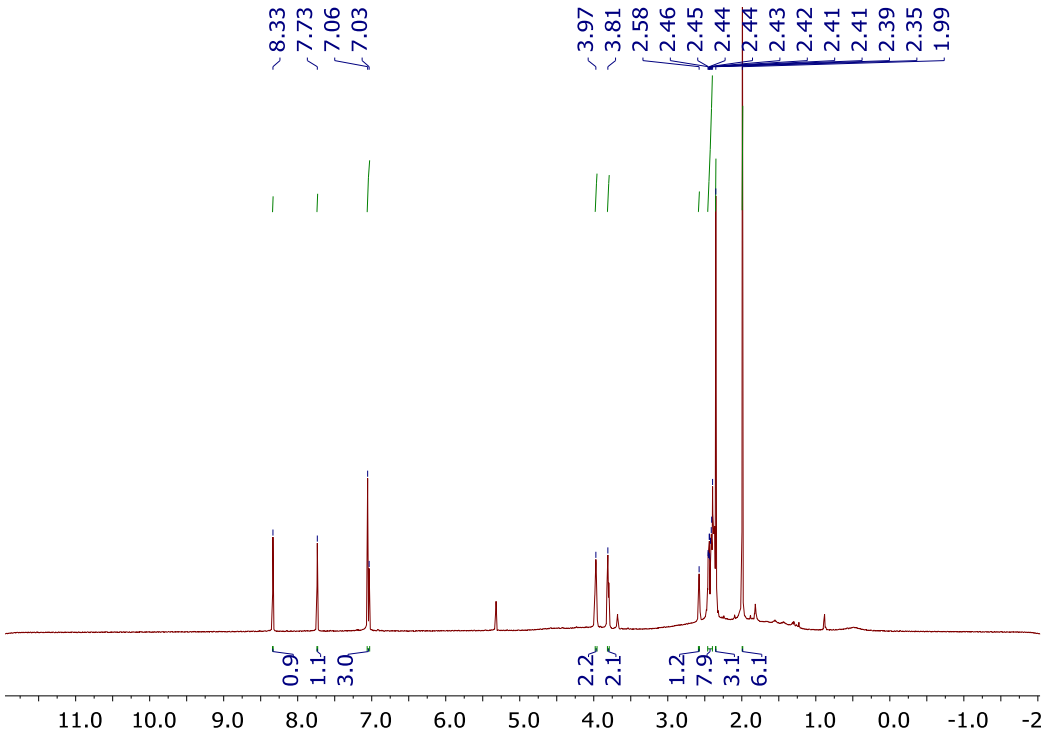

Fig. **7.23** ^{1}H NMR of **59** in CD_2Cl_2

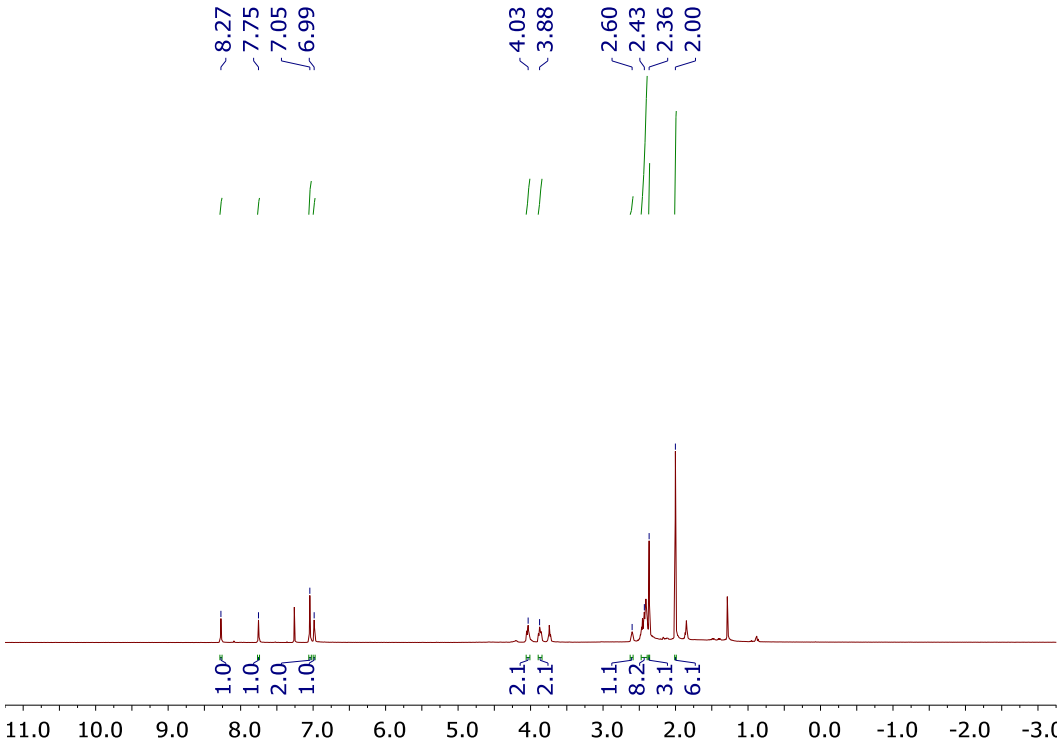

Fig. **7.24** ^{1}H NMR of **59** in $CDCl_3$

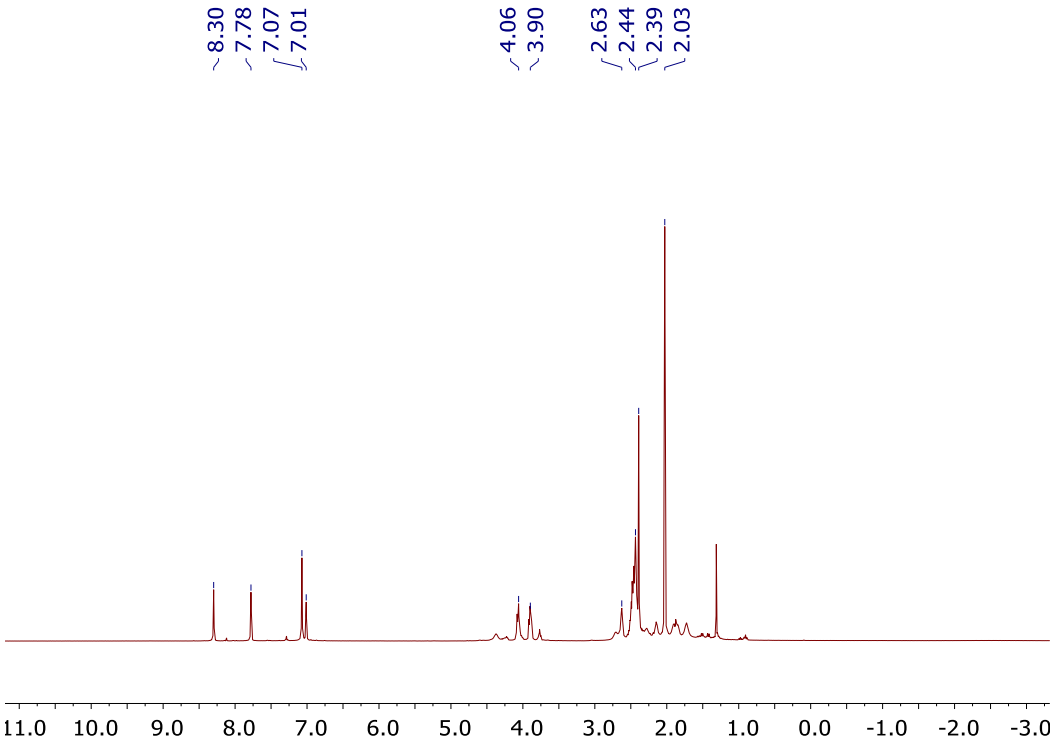

Fig. **7.25** $^{1}H[^{11}B]$ NMR of **59** in $CDCl_3$

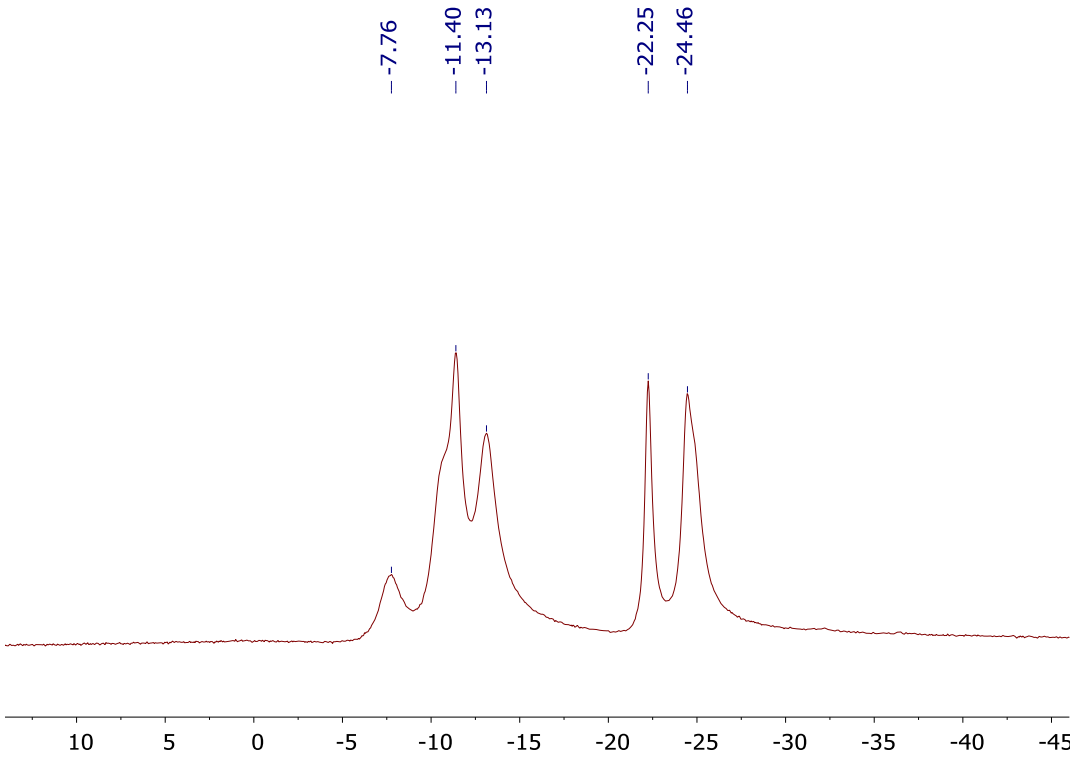

Fig. **7.26** $^{11}B[1H]$ NMR of **59** in $CDCl_3$

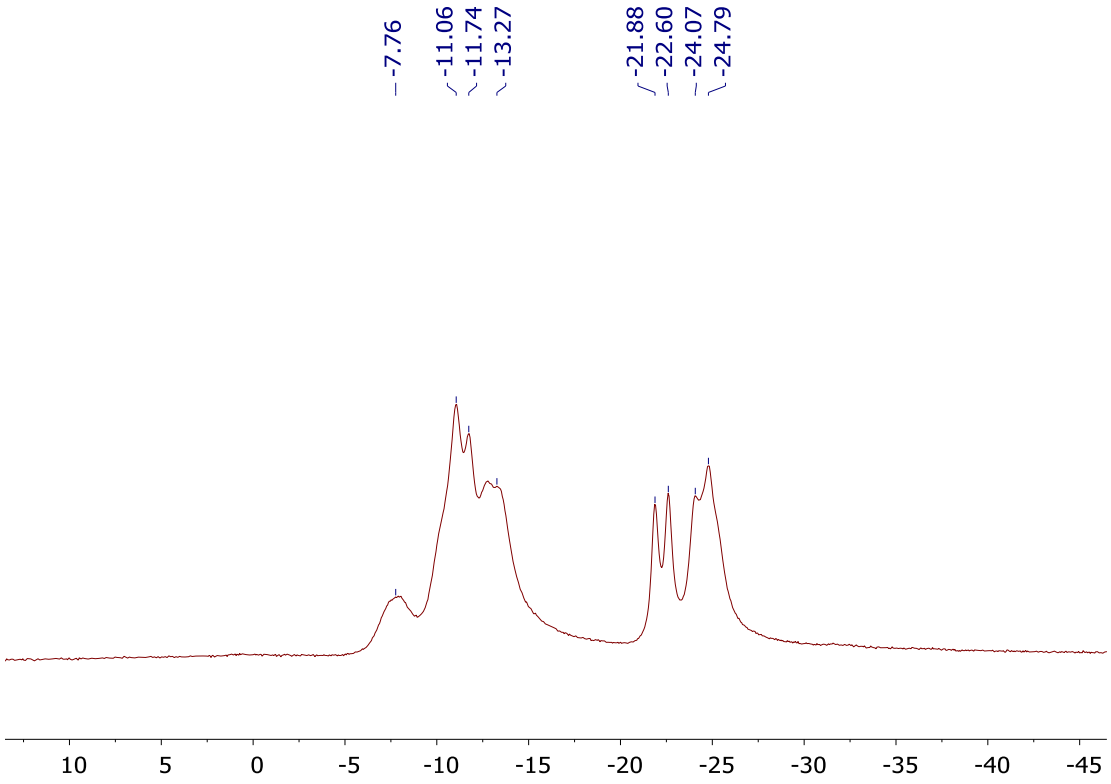

Fig. **7.27** ^{11}B NMR of **59** in $CDCl_3$

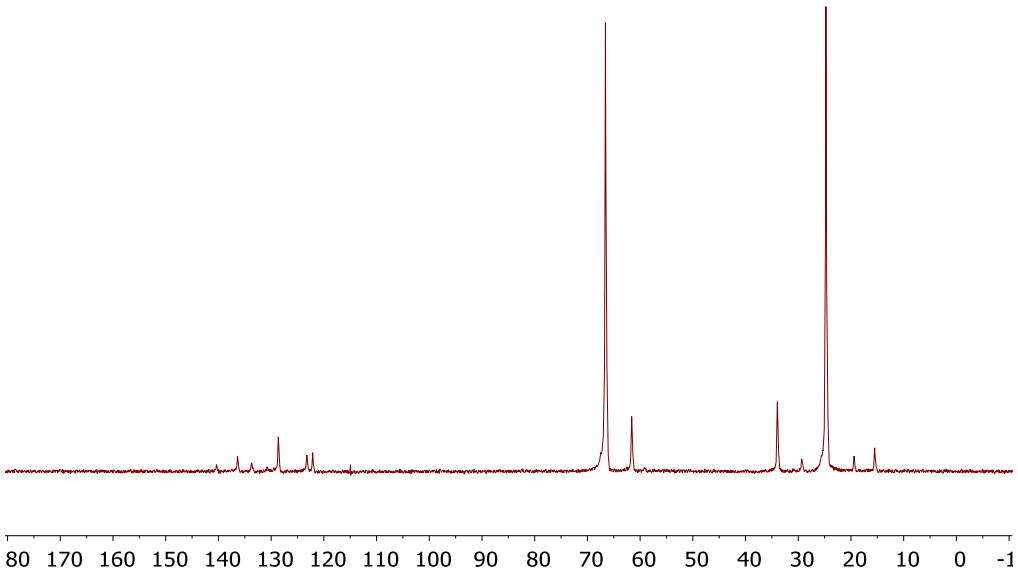

Fig. **7.28** $^{13}C[^{1}H]$ NMR of **59** in $CDCl_3$

Synthesis of Dicarbollide-NHC Li^+ 21:

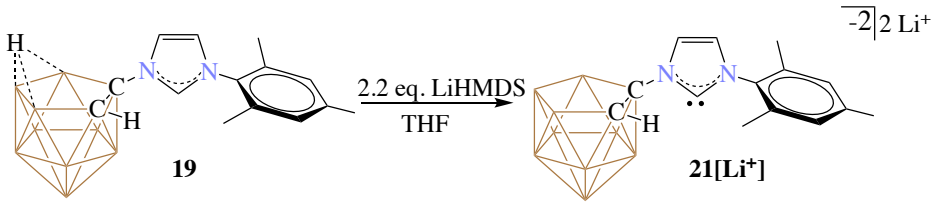

Scheme **7.18** Synthesis of the NHC **21[Li^+]** from **19**

In a glass vial, imidazolium **19** (200 mg, 0.627 mmol) was loaded with a stir bar and dissolved in THF (3 mL). A solution of LiHMDS (230.8 mg, 1.38 mmol) in THF (3 mL) was then added to the imidazolium and stirred for 15 minutes. The volatiles were then pumped down to dryness under vacuum and the resulting solid was washed with hexanes (2x15 mL). Decanting the hexane washes produced an off-white solid that was dried under vacuum to afford the title compound in 82% yield. ^{1}H NMR (400 MHz, THF-d_8, 25°C): 6.90 (s, 2H, *meta*-CH), 6.87 (d, 1H, CH), 6.47 (d, 1H, CH), 2.27 (s, 3H, *para*-CH_3), 1.96 (s, 3H, *ortho*-CH_3), 1.92 (s, 3H, *ortho*-CH_3); ^{11}B[^{1}H] NMR (128 MHz, THF-d_8, 25°C): -18.22, -20.52, -21.61, -22.46, -24.70, -27.14, -43.74 ppm. ^{13}C[^{1}H] NMR (100 MHz, THF-d_8, 25°C): 208.69, 139.06, 137.56, 135.49, 128.93, 119.07, 117.77, 39.17, 20.88, 17.62 ppm.

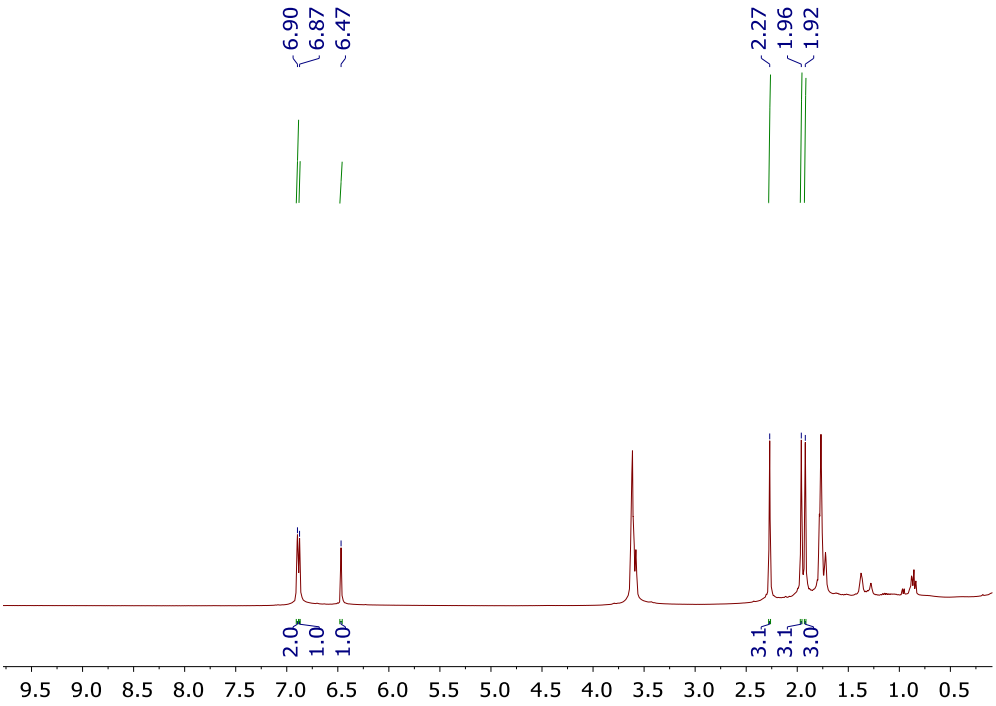

Fig. **7.29** ^{1}H NMR of **21[Li^{+}]** in THF-d$_8$

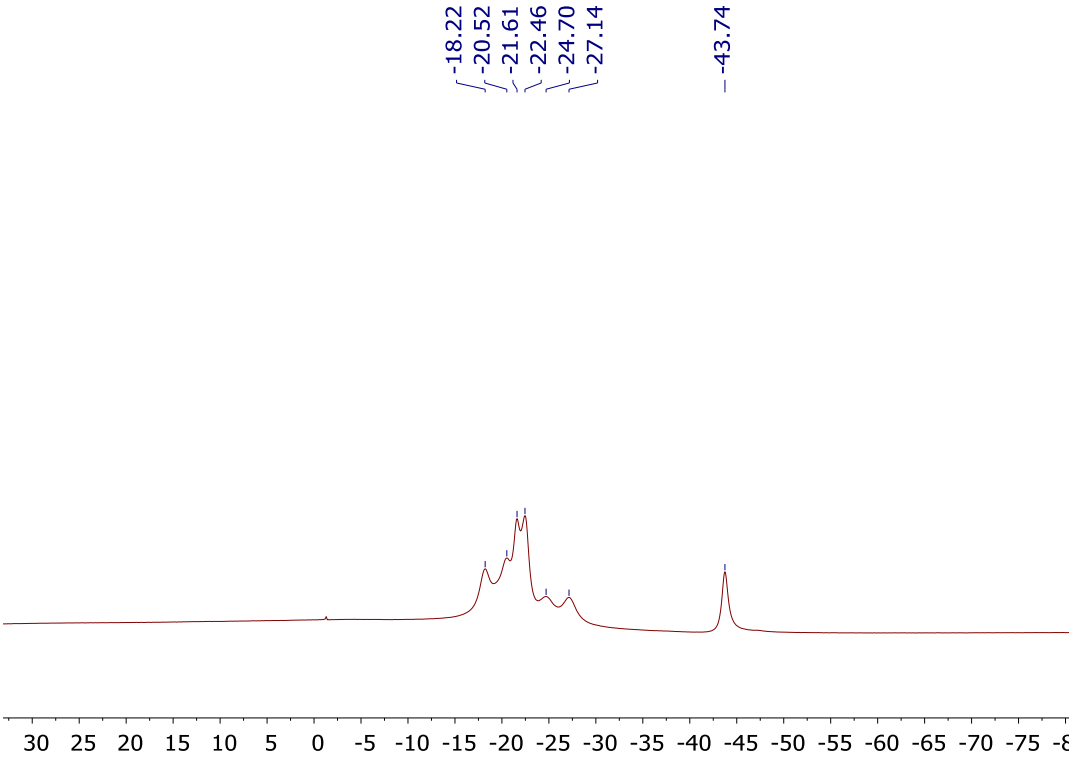

Fig. **7.30** ^{11}B[^{1}H] NMR of **21[Li^{+}]** in THF-d$_8$

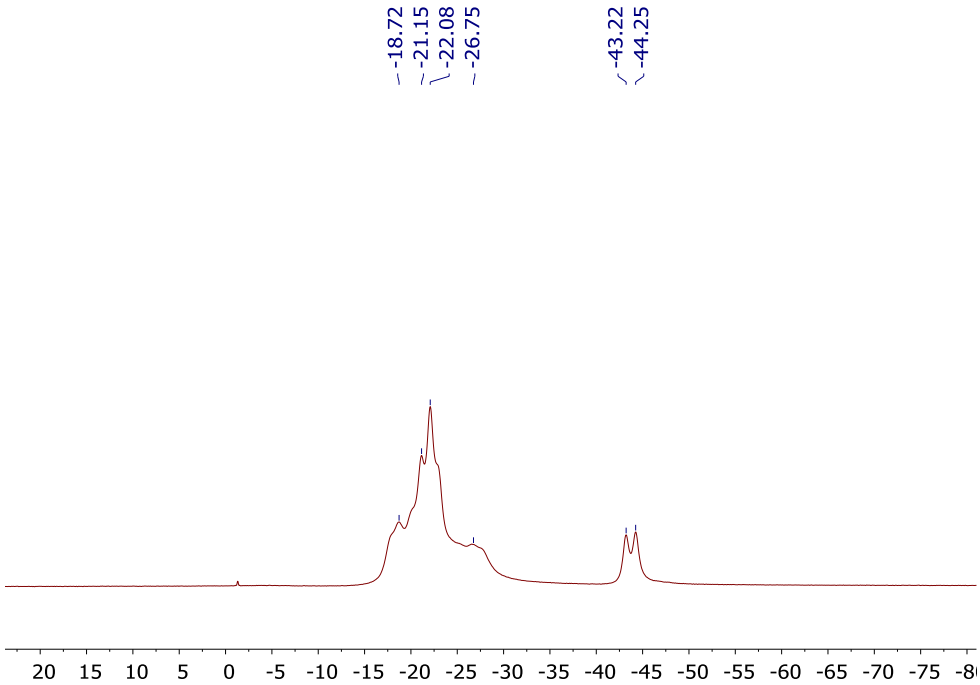

Fig. **7.31** ^{11}B NMR of **21[Li$^+$]** in THF-d$_8$

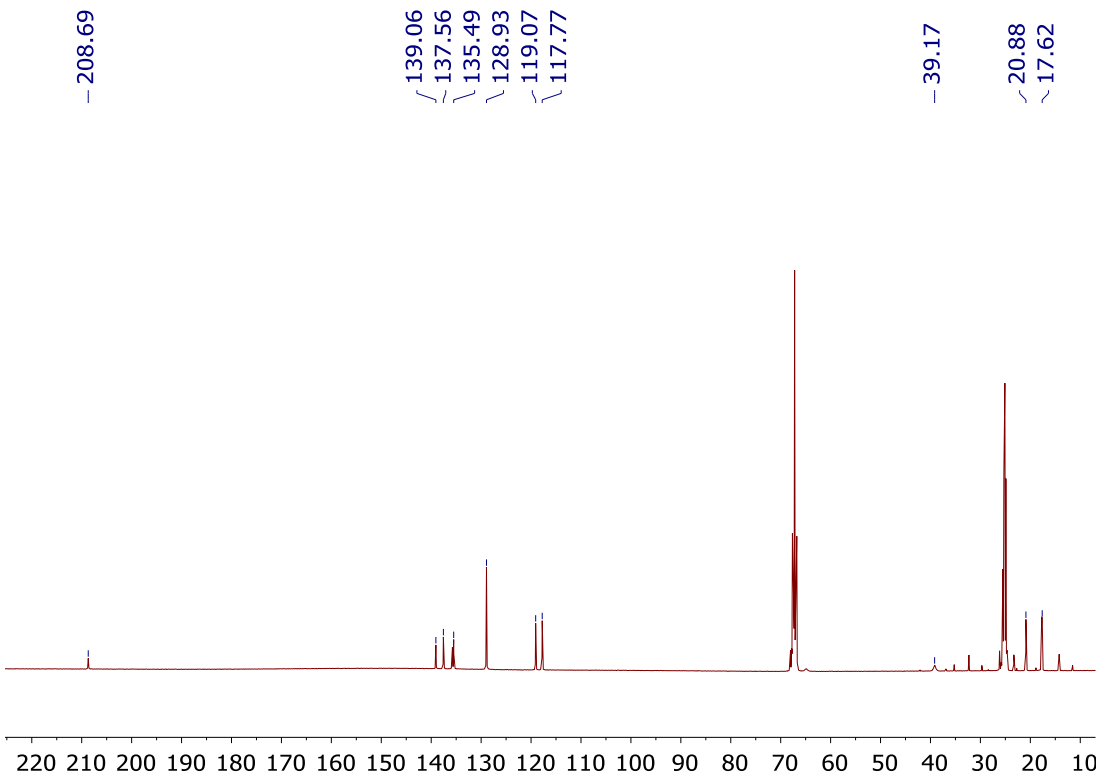

Fig. **7.32** ^{13}C[^{1}H] NMR of **21[Li$^+$]** in THF-d$_8$

Synthesis of **60[Li$^+$]**:

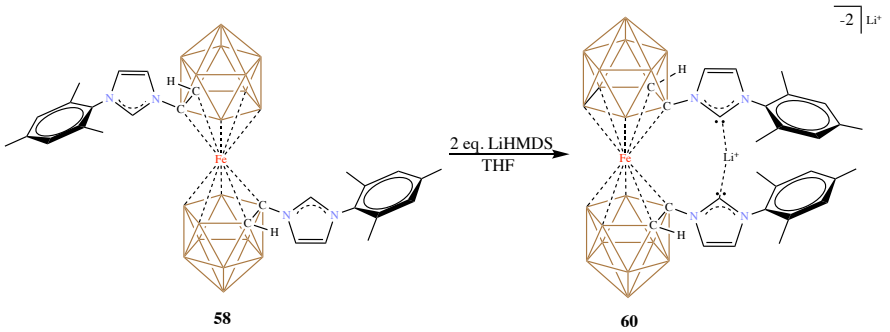

Scheme **7.4** Deprotonation of **58** to produce the NHC **60[Li$^+$]**

In a glass vial containing a stir bar, was added **58** (100 mg, 0.144 mmol) and dissolved in dry THF (3 mL). To this, a solution of LiHMDS (53.01 mg, 2.2 eq) in dry THF (3 mL) was added and stirred for 20 minutes at room temperature. The reaction mixture was then pumped down under vacuum to afford a sticky brown red solid. The solid was then thoroughly washed with dry hexanes (2x15 mL) and dried under vacuum to afford **60[Li$^+$]** in about 55% yield. X-Ray quality crystals were grown by layering a THF solution of the compound with hexanes. ^{1}H NMR (400 MHz, THF-d_8, 25^{o}C): 6.89 (s, 2H, *meta*-CH), 6.88 (d, 1H, CH), 6.47 (d, 1H, CH), 2.28 (s, 3H, *para*-CH_3), 1.97 (s, 3H, *ortho*-CH_3), 1.92 (s, 3H, *ortho*-CH_3). ^{11}B[^{1}H] NMR (128 MHz, THF-d_8, 25^{o}C): -18.19, -20.38, -21.45, -24.39, -26.64, -43.34 ppm. ^{13}C[^{1}H] NMR (100 MHz, THF-d_8, 25^{o}C): 207.99, 138.92, 137.51, 135.55, 128.87, 118.99, 117.76, 39.39, 20.89, 17.64 ppm. *Note: The above procedure is usually complicated by the reaction yielding too many unidentified paramagnetic impurities. Alternatively, the Fe source can be reacted directly with the NHC **21** to produce the compound cleaner in better yield. Moreover, we found replacing $FeCl_2$ by more soluble precursor $FeBr_2(THF)_2$ improved the yield. The procedures are described below.*

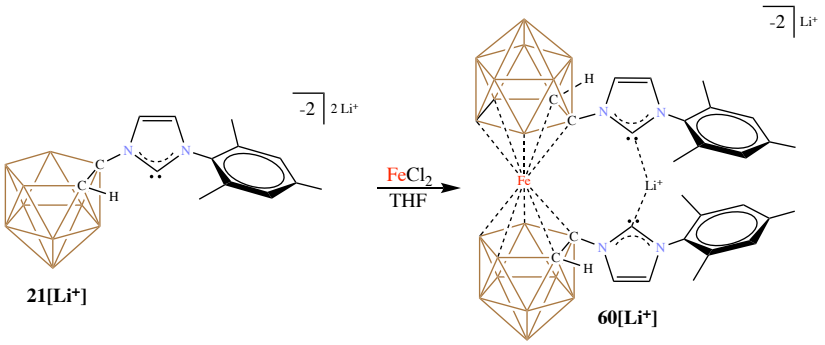

Scheme **7.5**. Synthesis of **60[Li$^+$]** from **21[Li$^+$]**

Alternatively, the pre-isolated NHC **21[Li$^+$]** (50 mg, 0.08 mmol) was taken in a vial with a stir bar and dissolved in THF (2 mL). The solution was then added to a suspension of $FeCl_2$ (5.1 mg, 0.04 mmol) stirring in THF (1 mL). The stirring was continued for 20 minutes after which the THF was evaporated under vacuum. The solid was then dissolved in diethyl ether (5 mL) and filtered over celite. The brownish pink filtrate was left inside a -30^{o}C freezer overnight. This deposited a purple precipitate which was separated by decanting off the ether layer. This decant was filtered over celite again and left in the freezer overnight. Decanting the ether layer and pumping down under vacuum then produced a light brown solid which was washed with hexanes (2x5 mL) to produce **60[Li$^+$]** in 45% yield. The spectroscopic data matched with that of the compound isolated in the previous procedure.

Improved Synthesis of **60[Li$^+$]**:

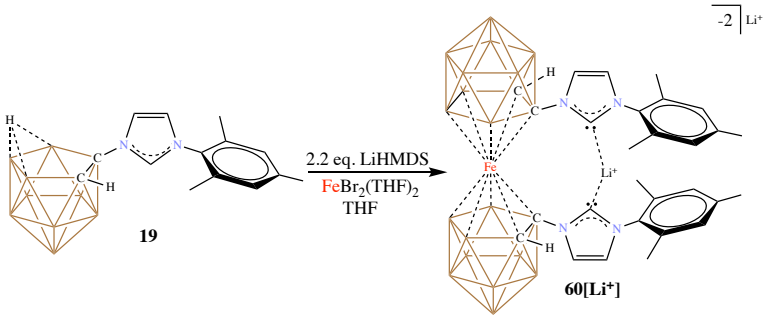

Scheme **7.6** Synthesis of **60[Li$^+$]** from **19**

In a glass vial with a stir bar, the imidazolium **19** (100 mg, 0.313 mmol) was dissolved in THF (3 mL). To this, was added 2.2 eq of LiHMDS (115.2 mg, 0.686 mmol) dissolved in THF (3 mL). The solution was stirred for 10 minutes to form the dicarbollide-NHC. To this solution, a suspension of $FeBr_2(THF)_2$ (56.9 mg, 0.156 mmol) in THF (5 mL) was added and stirred for 15 minutes. The solution was then dried under vacuum to form a dark brown solid. The solid was thoroughly washed with hexanes (2x15 mL) and decanted. The obtained solid was dried under vacuum to afford **60[Li$^+$]** in 90% yield. The spectroscopic data matched with that of the compounds isolated using previously mentioned procedures.

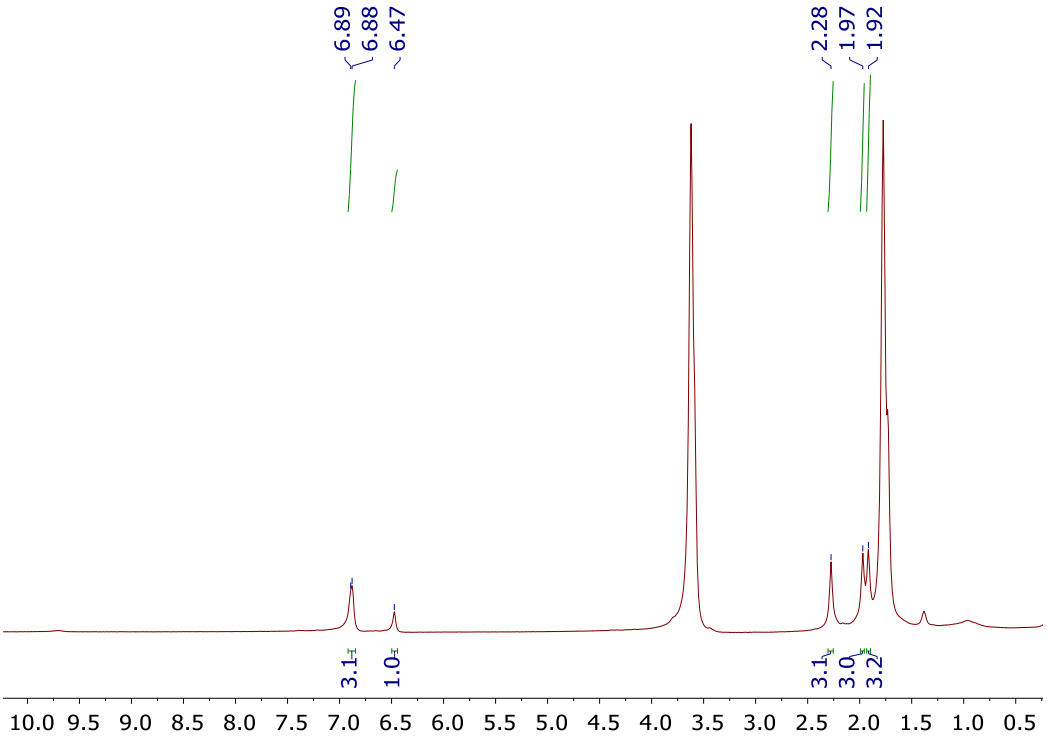

Fig. **7.33** ^{1}H NMR of **60[Li$^+$]** in THF-d_8

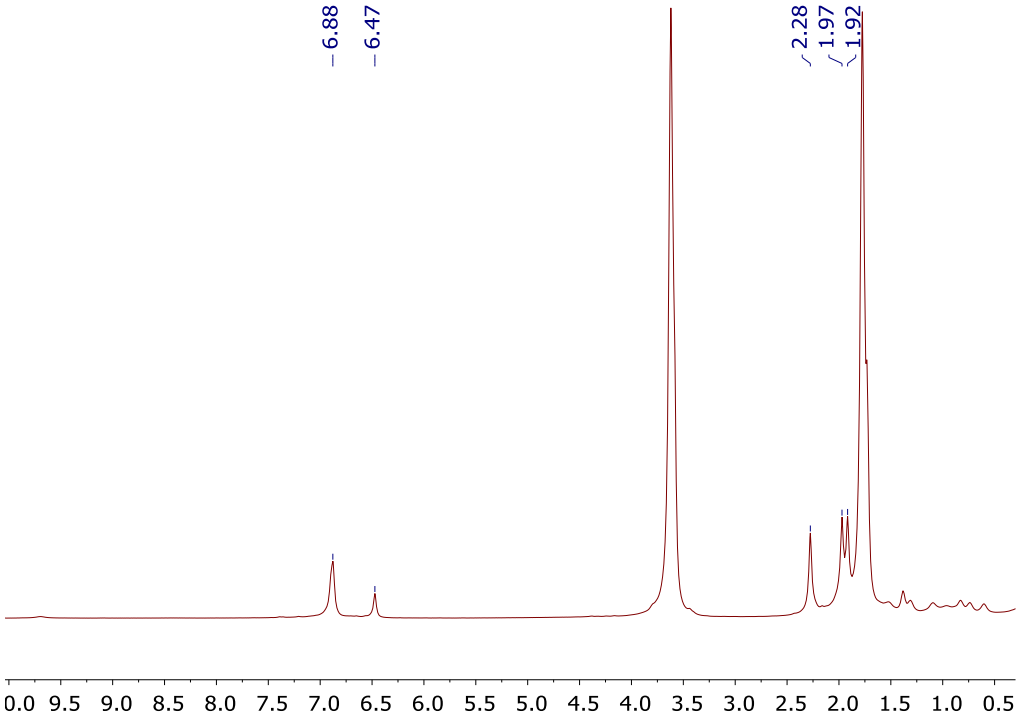

Fig. **7.34** $^{1}H[^{11}B]$ NMR of **60[Li^{+}]** in THF-d_8

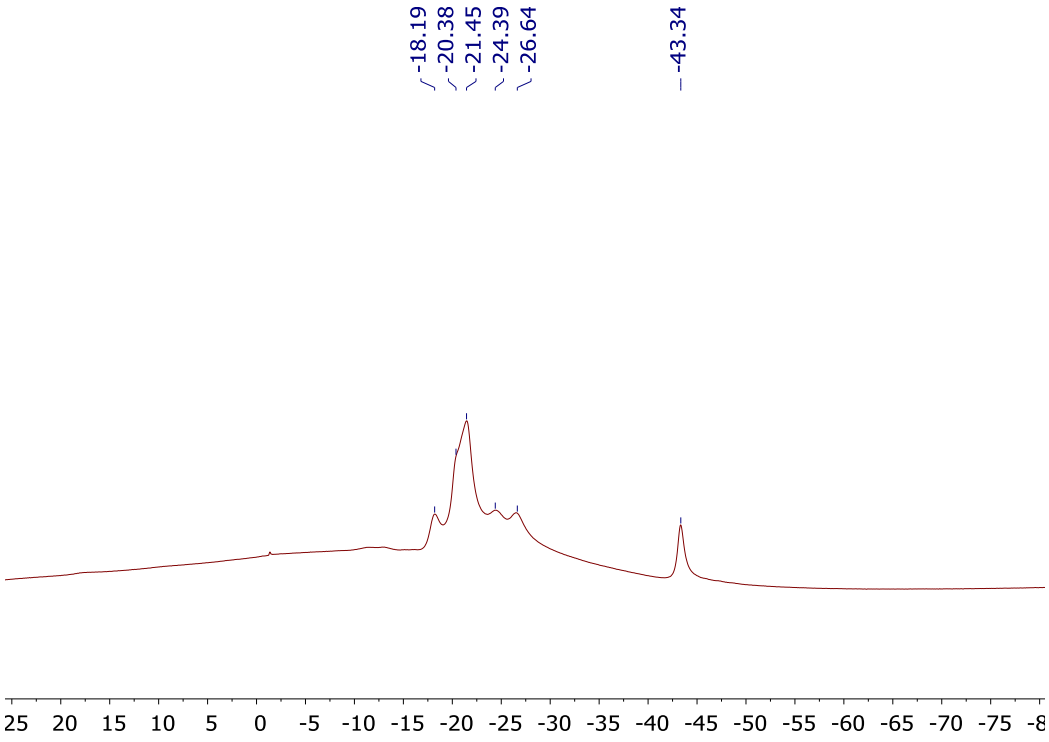

Fig. **7.35** $^{11}B[^{1}H]$ NMR of **60[Li^{+}]** in THF-d_8

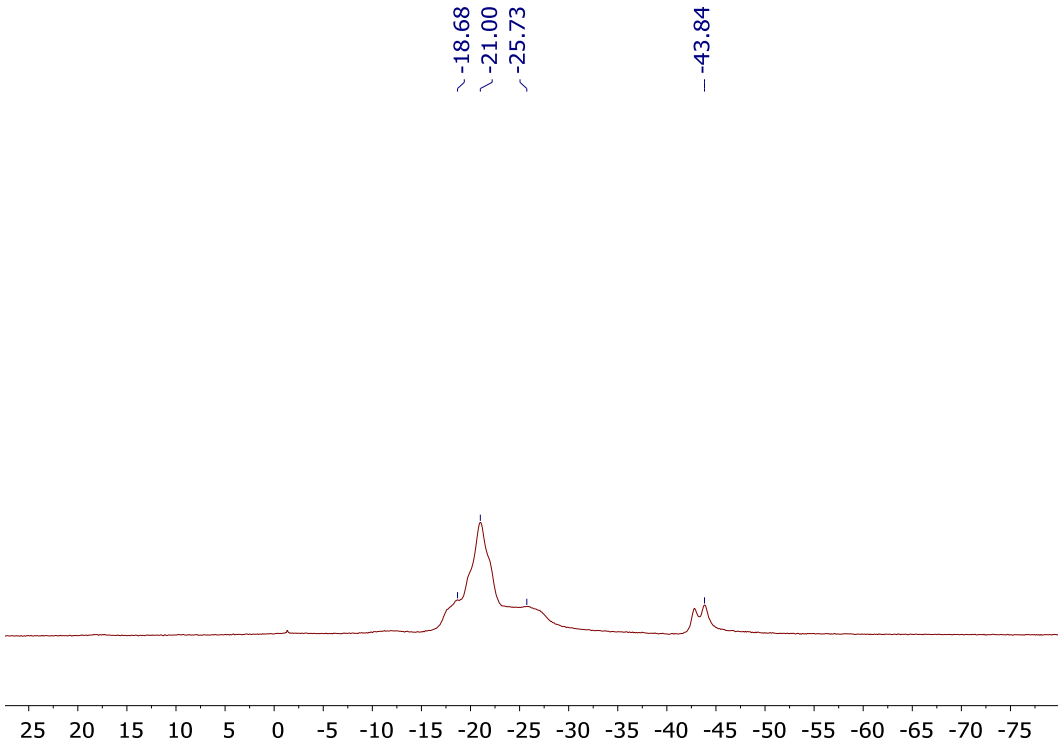

Fig. **7.36** ^{11}B NMR of **60[Li^{+}]** in THF-d_8

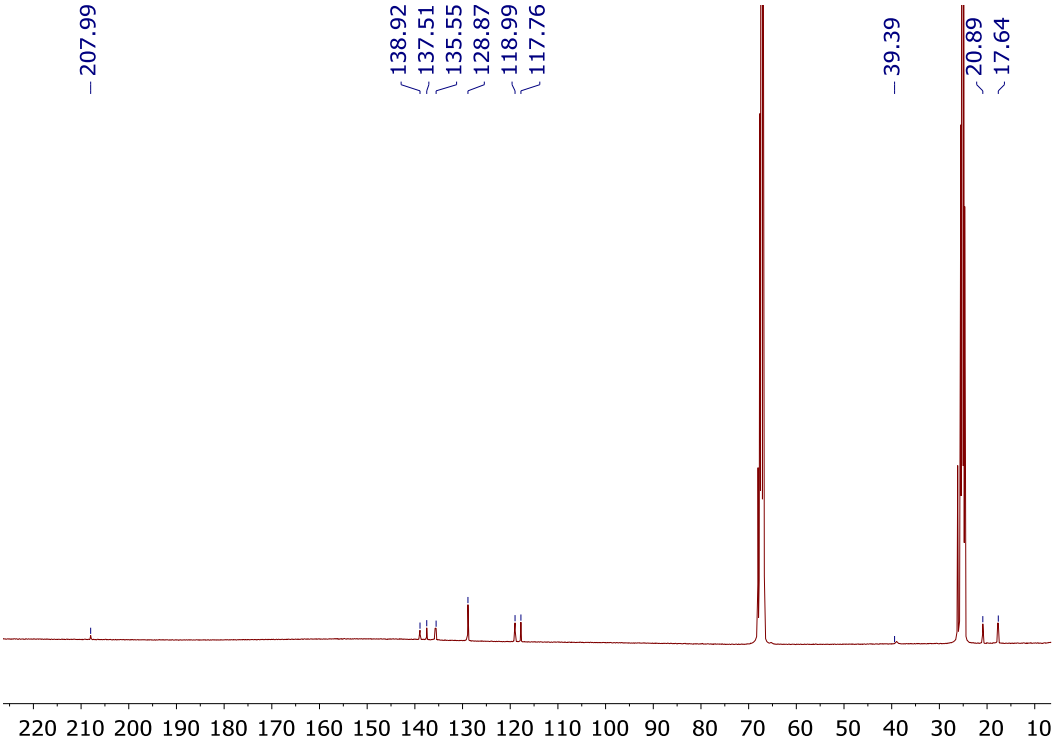

Fig. **7.37** $^{13}C[^{1}H]$ NMR of **60[Li$^+$]** in THF-d_8

Synthesis of **60[K$^+$]**:

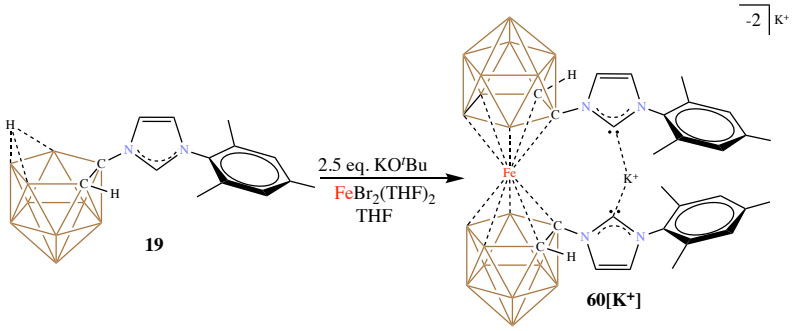

Scheme **7.7** Synthesis of **60[K$^+$]** from **19**

In a glass vial, imidazolium **19** (300 mg, 0.94 mmol) was taken with a stir bar and dissolved in THF (3 mL). To this, a solution of KO^{t}Bu (126.5 mg, 1.128 mmol) in THF (2 mL) was added and stirred for 5 minutes. A suspension of $FeBr_2(THF)_2$ (171 mg, 0.47 mmol) in THF (8 mL) was then added to the solution and stirred for 10 minutes. This was followed by the

addition of more KO^{t}Bu (137.12 mg, 1.22 mmol) and stirred for about 10 minutes till the suspension changed colors from purple to dark grey. The suspension was then pumped down dry under vacuum and suspended in warm toluene (15 mL) and stirred for about 10 minutes. The toluene suspension was then filtered over celite, and the filtrate pumped down dry under vacuum to afford **60[K$^+$]** as a greyish yellow solid in 73% yield. ^{1}H NMR (400 MHz, THF-d$_8$, 25^{o}C): 7.00 (d, 1H, CH), 6.86 (s, 2H, *meta*-CH), 6.41 (d, 1H, CH), 2.25 (s, 3H, *para*-CH$_3$), 1.93 (s, 3H, *ortho*-CH$_3$), 1.88 (s, 3H, *ortho*-CH$_3$); ^{11}B[^{1}H] NMR (128 MHz, THF-d$_8$, 25^{o}C): -18.32, -20.99, -25.02, -45.63 ppm; ^{13}C[^{1}H] NMR (100 MHz, THF-d$_8$, 25^{o}C): 212.38, 139.81, 138.03, 135.80, 128.81, 121.22, 116.56, 38.18, 24.72, 20.82, 17.73 ppm.

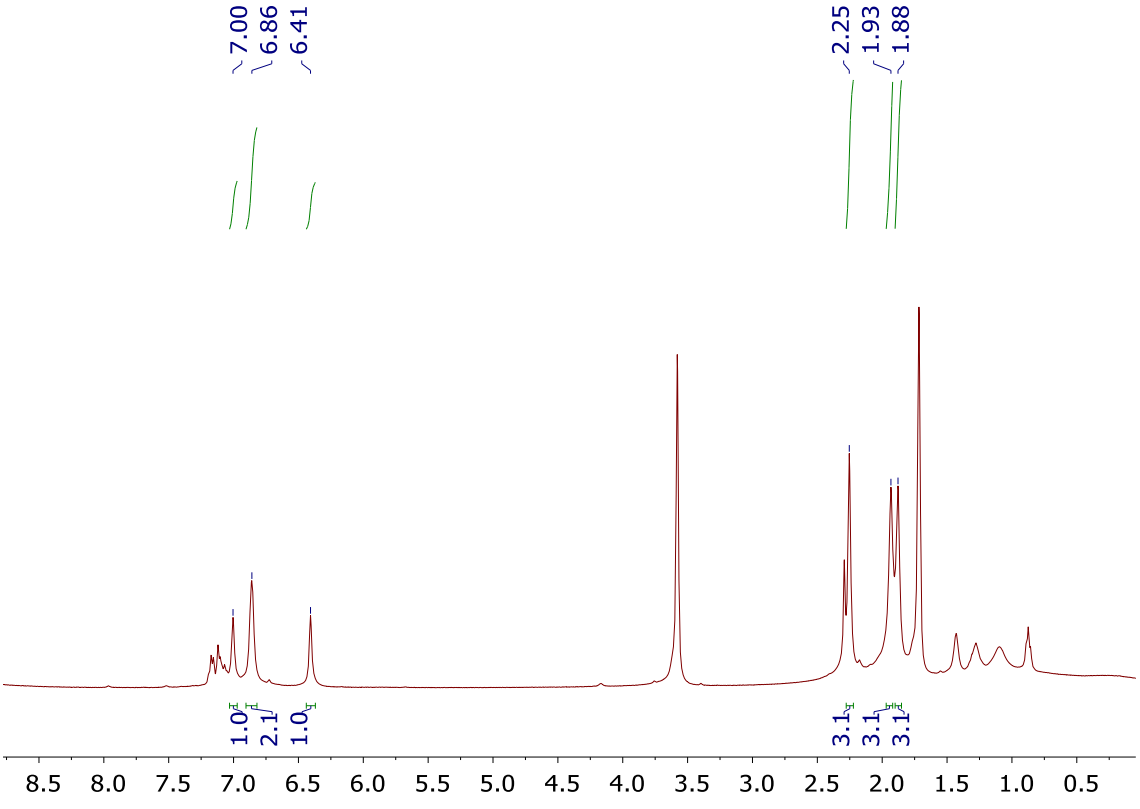

Fig. **7.38** ^{1}H NMR of **60[K$^+$]** in THF-d$_8$

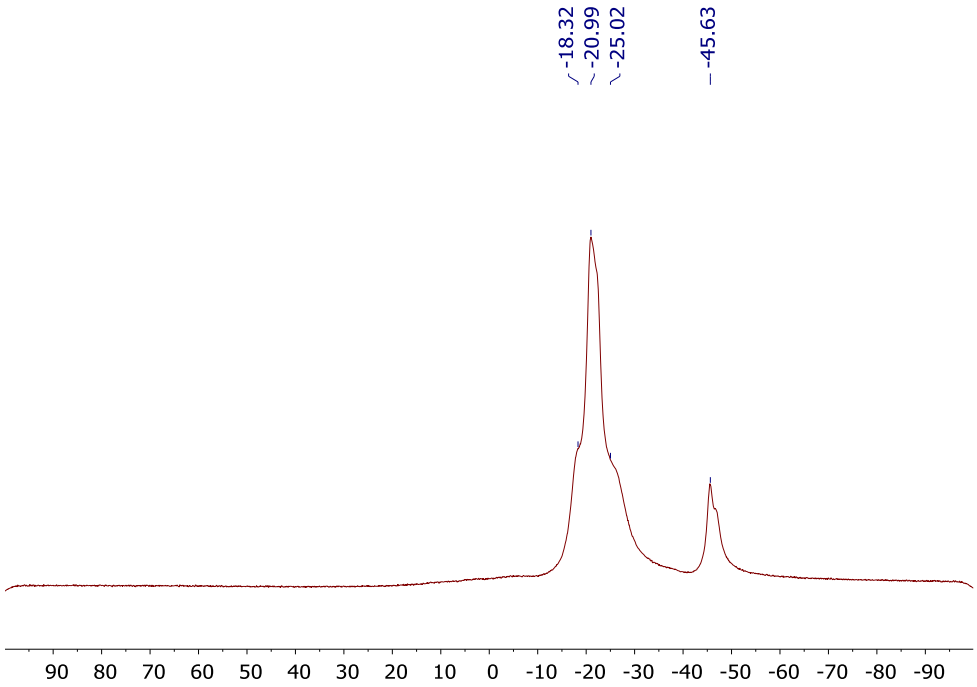

Fig. **7.39** ^{1}H NMR of **60[K^{+}]** in THF-d_8

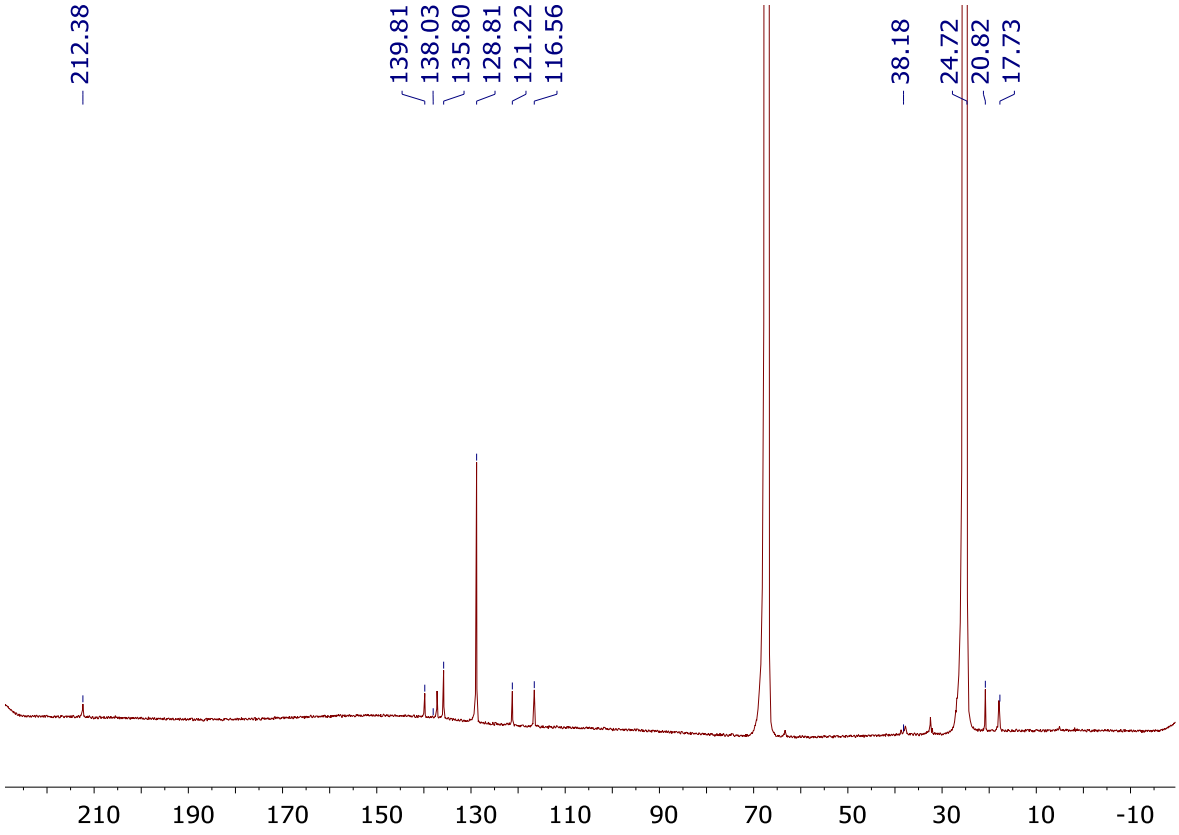

Fig. **7.40** $^{13}C[^{1}H]$ NMR of **60[K$^+$]** in THF-d_8

Synthesis of **61**:

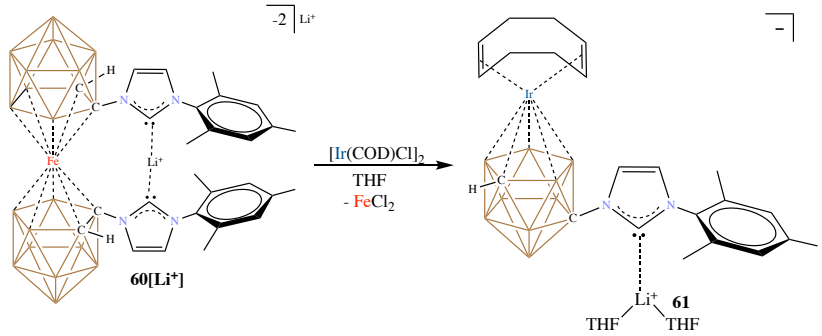

Scheme **7.8**. Transmetalation of **60[Li$^+$]** to **61**

In a glass vial, **60[Li$^+$]** (50 mg, 0.07 mmol) and a stir bar were loaded. To this, a solution of $[Ir(COD)Cl]_2$ (23.51 mg, 0.035 mmol) in THF (3 mL) was added while stirring and the stirring was continued for about 2 hours at room temperature. The solution was then filtered

over celite, and the filtrate dried under vacuum. The solid was then dissolved in benzene and filtered over celite, and the filtrate pumped down under vacuum. The brown solid obtained was then washed with hexanes (2x5 mL) and hexanes decanted. The residual solid was dried under vacuum to afford **61** in 87% yield. X-Ray quality crystals were grown by layering a THF solution of the compound with hexanes. ^{1}H NMR (400 MHz, THF-d_8, 25^{o}C): 7.45 (d, 1H, CH), 6.97 (d, 1H, CH), 6.80 (s, 2H, *meta*-CH), 3.80 (m, 2H, COD CH), 3.68 (m, 2H, COD CH), 2.41 (bs, 1H, $CH_{carborane}$), 2.33 (m, 8H, COD CH_2), 2.29 (s, 3H, *para*-CH_3), 1.95 (s, 3H, *ortho*-CH_3), 1.93 (s, 3H, *ortho*-CH_3); ^{11}B[^{1}H] NMR (128 MHz, THF-d_8, 25^{o}C): -7.73, -11.30, -13.06, -21.62, -24.66 ppm; ^{13}C[^{1}H] NMR (100 MHz, THF-d_8, 25^{o}C): 198.91, 138.78, 138.33, 135.72, 129.35, 122.54, 120.50, 61.59, 35.52, 20.83, 17.52 ppm.

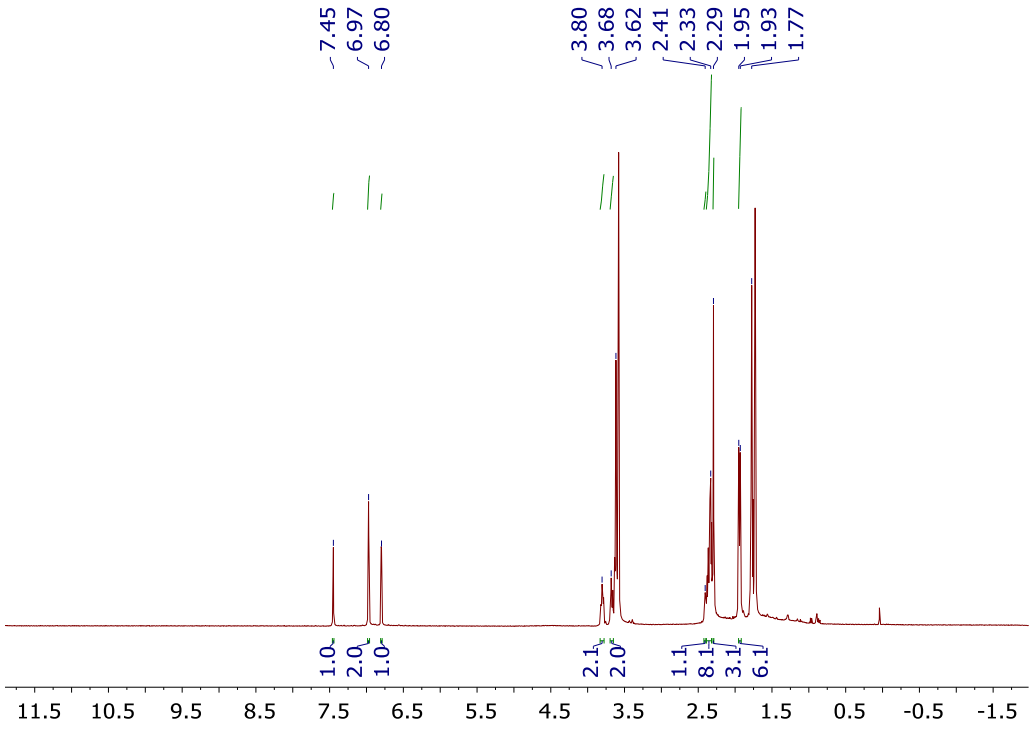

Fig. **7.41** ^{1}H NMR of **61** in THF-d_8

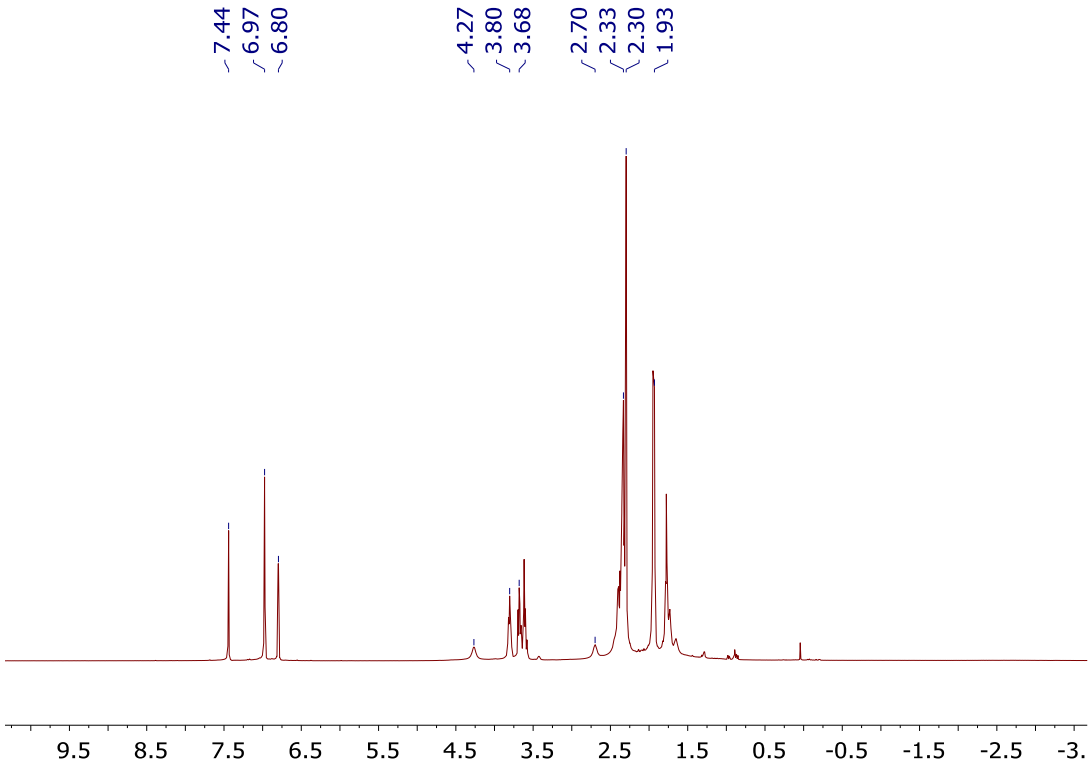

Fig. **7.42** $^{1}H[^{11}B]$ NMR of **61** in THF-d_8

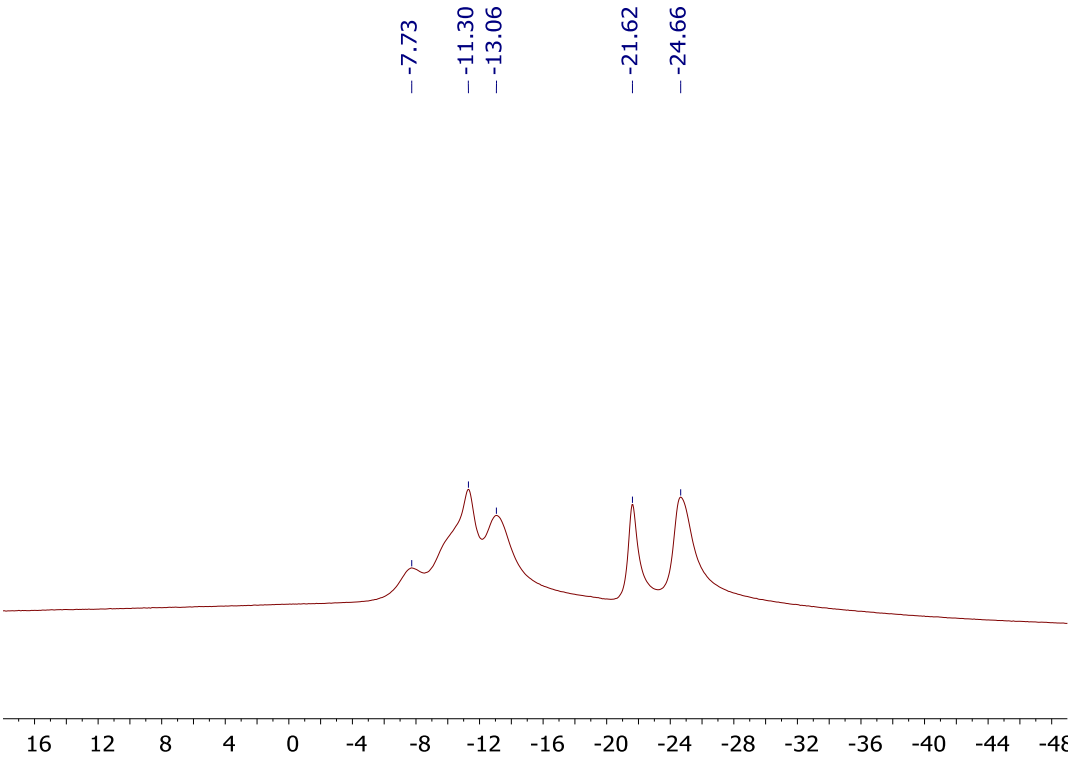

Fig. **7.43** $^{11}B[^{1}H]$ NMR of **61** in THF-d_8

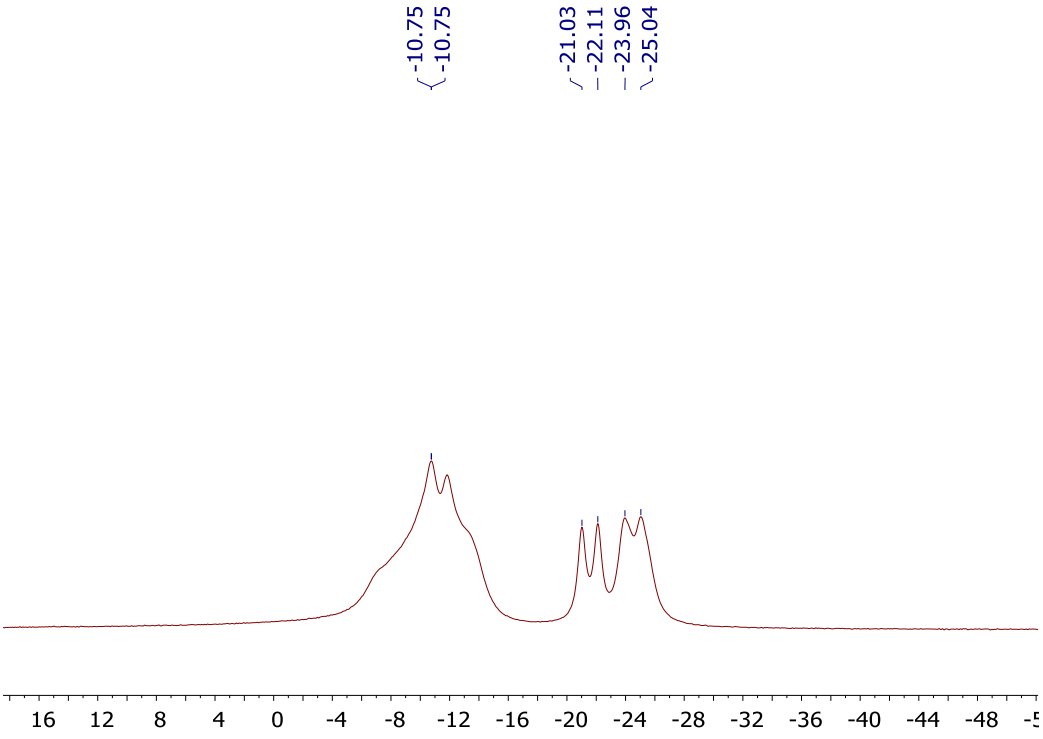

Fig. **7.44** ^{11}B NMR of **61** in THF-d_8

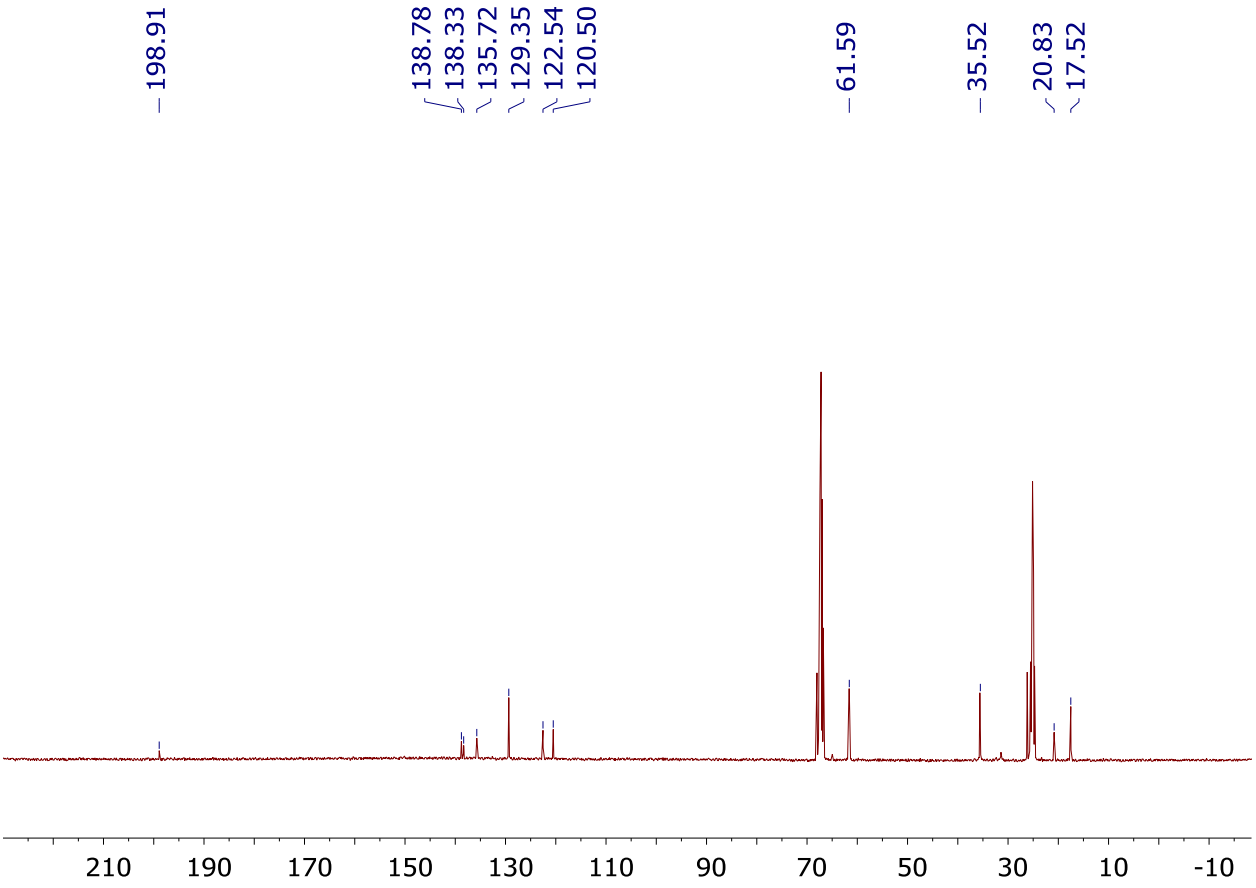

Fig. **7.45** $^{13}C[^{1}H]$ NMR of **61** in THF-d_8

Synthesis of **62**:

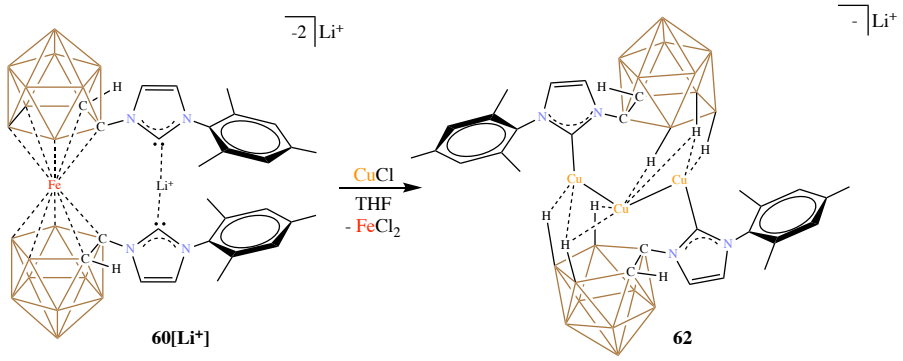

Scheme **7.9**. Transmetalation of **60[Li$^+$]** to **62**

In a glass vial, **60[Li$^+$]** (100 mg, 0.14 mmol) and a stir bar were loaded. To this, a suspension of CuCl (13.85 mg, 0.14 mmol) in THF (3 mL) was added while stirring, and

the stirring continued for about 2 hours at room temperature. The reaction mixture was then filtered over celite, and the filtrate pumped down to dryness under vacuum to afford an intractable mixture of compounds. The Fe transmetalation product was determined using X-Ray diffraction using crystals grown from a concentrated THF solution of the compound.

Direct Synthesis of **59**:

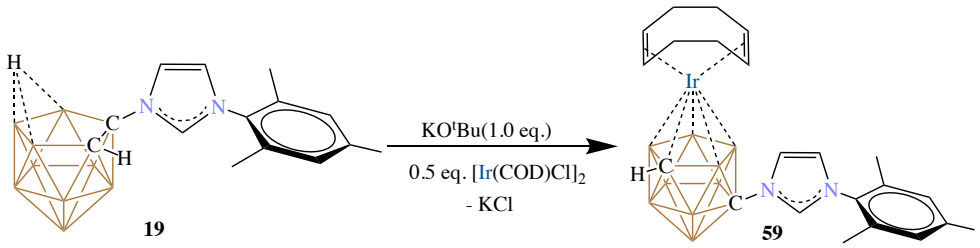

Scheme **7.11**. Direct Synthesis of **59** from **19**

In a glass vial, $[Ir(COD)Cl]_2$ and a stir bar were loaded and dissolved in THF (5 mL). To this, a solution of KO^{t}Bu in THF (3 mL) was added and stirred for 2 hours at room temperature. Imidazolium **19** was then added as a solid to the reaction mixture and stirring was continued overnight. The volatiles were then pumped down under vacuum and the crude reaction mixture was dissolved in dichloromethane and filtered over celite. The filtrate was pumped down to dryness and redissolved in a minimal volume of THF. Hexanes was then layered on the THF solution, and the vial was placed in a -30^{o}C freezer overnight. The THF/Hexane mixture was then decanted and the solid was washed with cold hexanes (2x5 mL). The residual solid was then pumped to dryness under vacuum yielding the title compound as a brown-red solid in 90% yield. The spectroscopic data matched with that of the compound made using the other procedure.

Direct Synthesis of **61**:

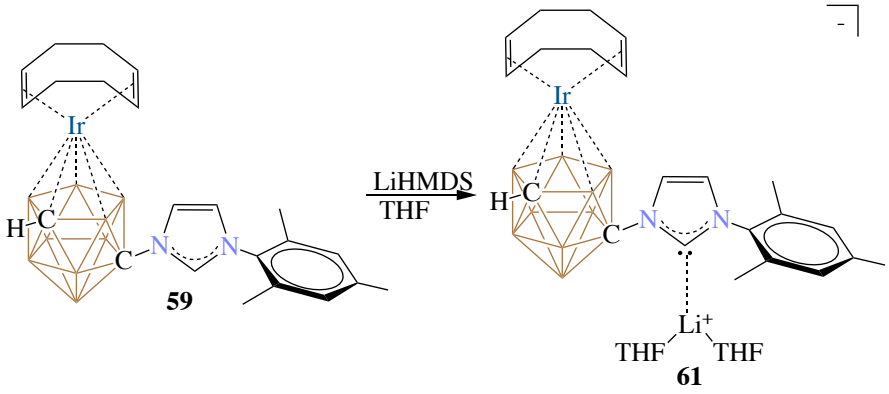

Scheme **7.19** Synthesis of **61** from deprotonation of **59**

In a glass vial, **59** and a stir bar were loaded and the solid dissolved in THF. To this, a solution of LiHMDS in THF was added while stirring and the stirring was continued for about 15 minutes. The volatiles were then pumped down to dryness under vacuum and the solid was washed with hexanes (2x15 mL). Decanting the hexane washes and leaving the residual solid under vacuum afforded **61** as a light brown solid in 90% yield.

Alternate Synthesis of **61**:

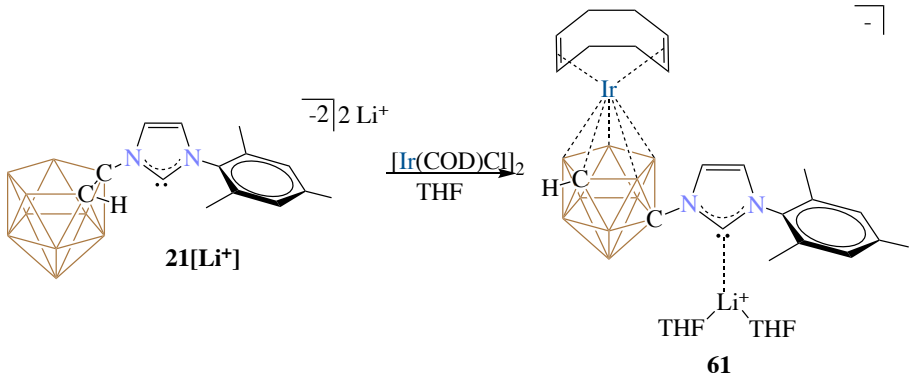

Scheme **7.20** Synthesis of **61** from **21[Li+]**

The dicarbollide-NHC **21[Li+]** was loaded in a glass vial with a stir bar. To this, a solution of $[Ir(COD)Cl]_2$ in THF was added and stirred for about 2 hours at room temperature. The THF was then pumped down dry under vacuum and the solid was dissolved in benzene. The benzene solution was filtered over celite, and the filtrate was pumped down to dryness

to afford the title compound in 64% yield. The spectroscopic data matched with the compound made using the previously discussed procedure.

Synthesis of **66**:

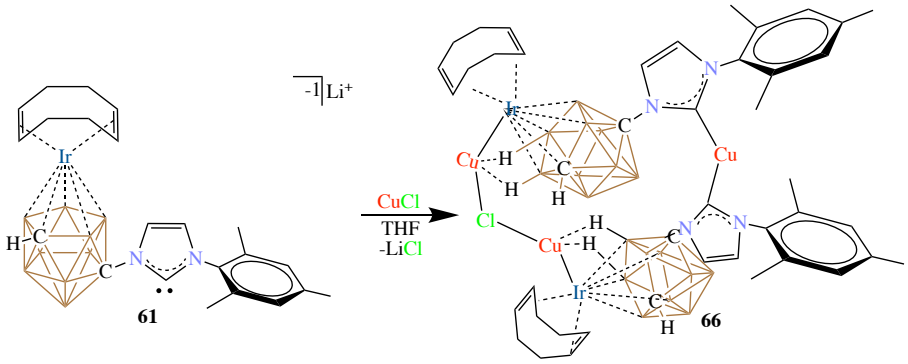

Scheme **7.15**. Synthesis of the Ir-Cu Bimetallic Complex **66**

In a vial, **61**and a stir bar were loaded. To this, a suspension of CuCl in THF was added while stirring and the suspension was continued stirring for about 2 hours at room temperature. The reaction mixture was then pumped down to dryness under vacuum. The solid was then suspended in dichloromethane and filtered over celite. The filtrate was then pumped down to dryness affording the title compound in about 46% yield. X-Ray quality crystals were grown by slow evaporation of concentrated THF solution of the compound in an NMR tube. ^{1}H NMR (400 MHz, $CDCl_3$, 25°C): 7.38 (d, 1H, CH), 6.95 (s, 1H, *meta*-CH), 6.80 (s, 1H, *meta*-CH), 6.57 (d, 1H, CH), 4.31 (m, 5H, COD CH), 3.74 (m, 2H, COD CH), 3.69-2.98 (m, 17H, COD CH_2), 2.31 (s, 3H, *para*-CH_3), 2.06 (s, 3H, *ortho*-CH_3), 1.33 (s, 3H, *ortho*-CH_3); ^{11}B[^{1}H] NMR (128 MHz, $CDCl_3$, 25°C): -4.97, -12.40, -19.74, -20.46, -23.89 ppm. ^{13}C[^{1}H] NMR (100 MHz, $CDCl_3$, 25°C): 180.45, 138.85, 136.39, 135.99, 134.54, 129.05, 128.76, 121.44, 120.45, 75.38, 68.91, 68.13, 61.07, 36.52, 35.21, 25.77, 21.27, 17.97, 17.51 ppm. HRMS calculated: observed:

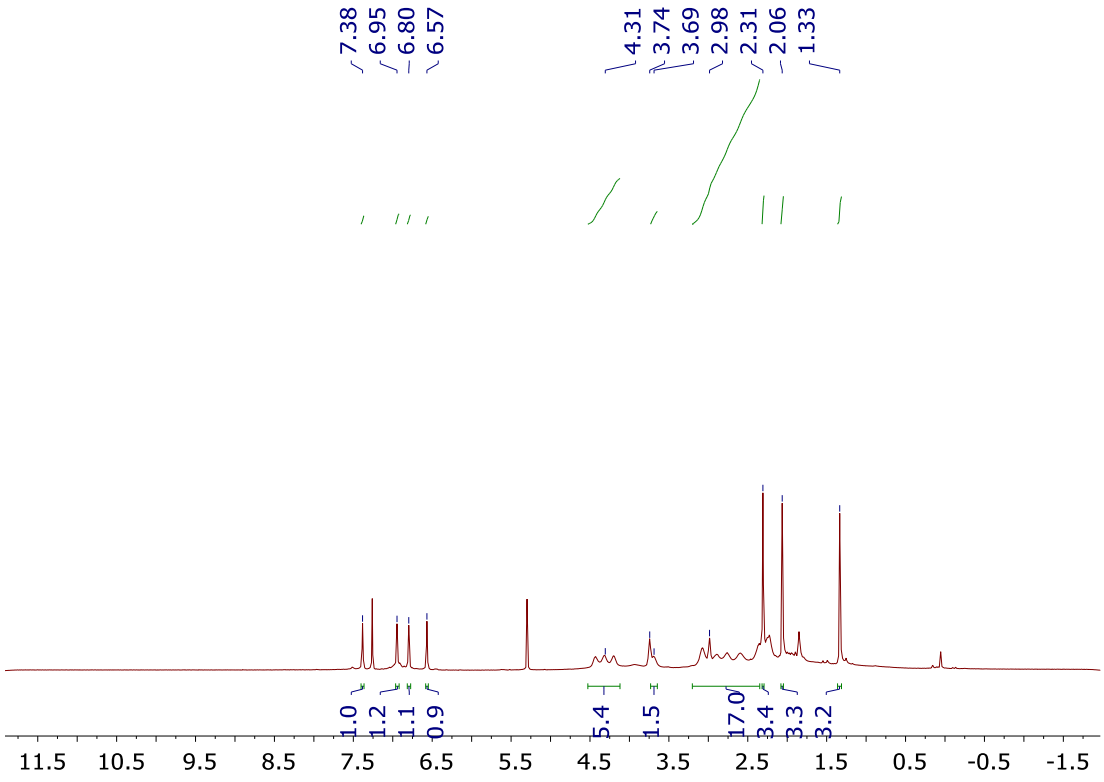

Fig. **7.46** ^{1}H NMR of **66** in $CDCl_3$

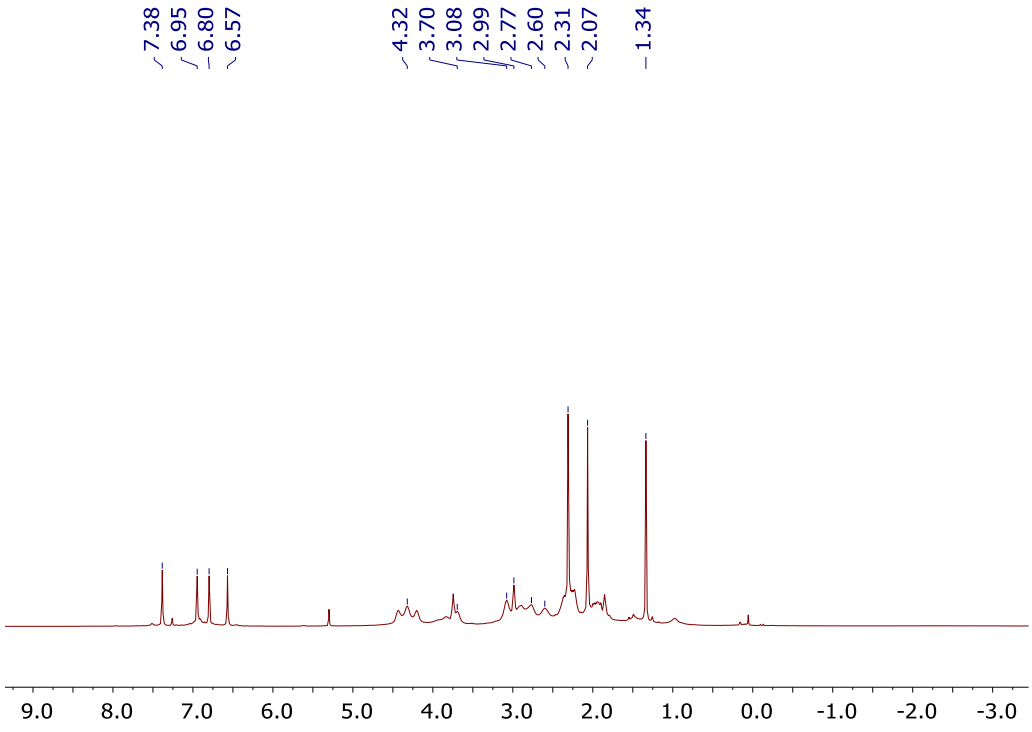

Fig. **7.47** $^{1}H[^{11}B]$ NMR of **66** in $CDCl_3$

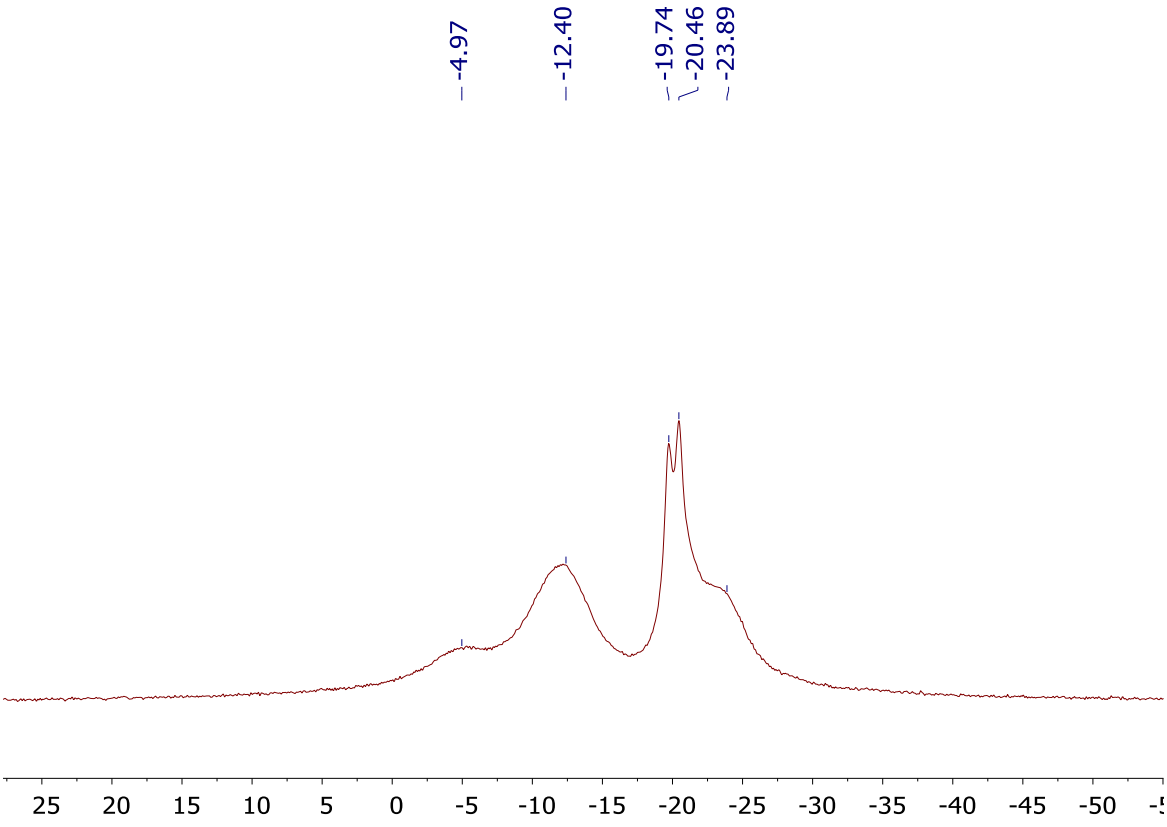

Fig. **7.48** ^{11}B NMR of **66** in $CDCl_3$

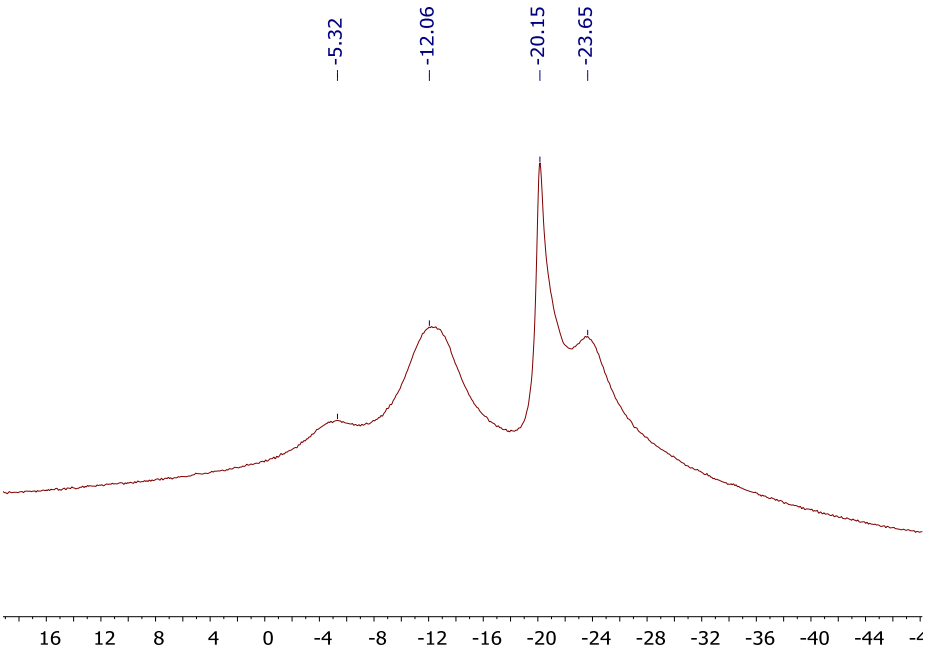

Fig. **7.49** $^{11}B[^{1}H]$ NMR of **66** in $CDCl_3$

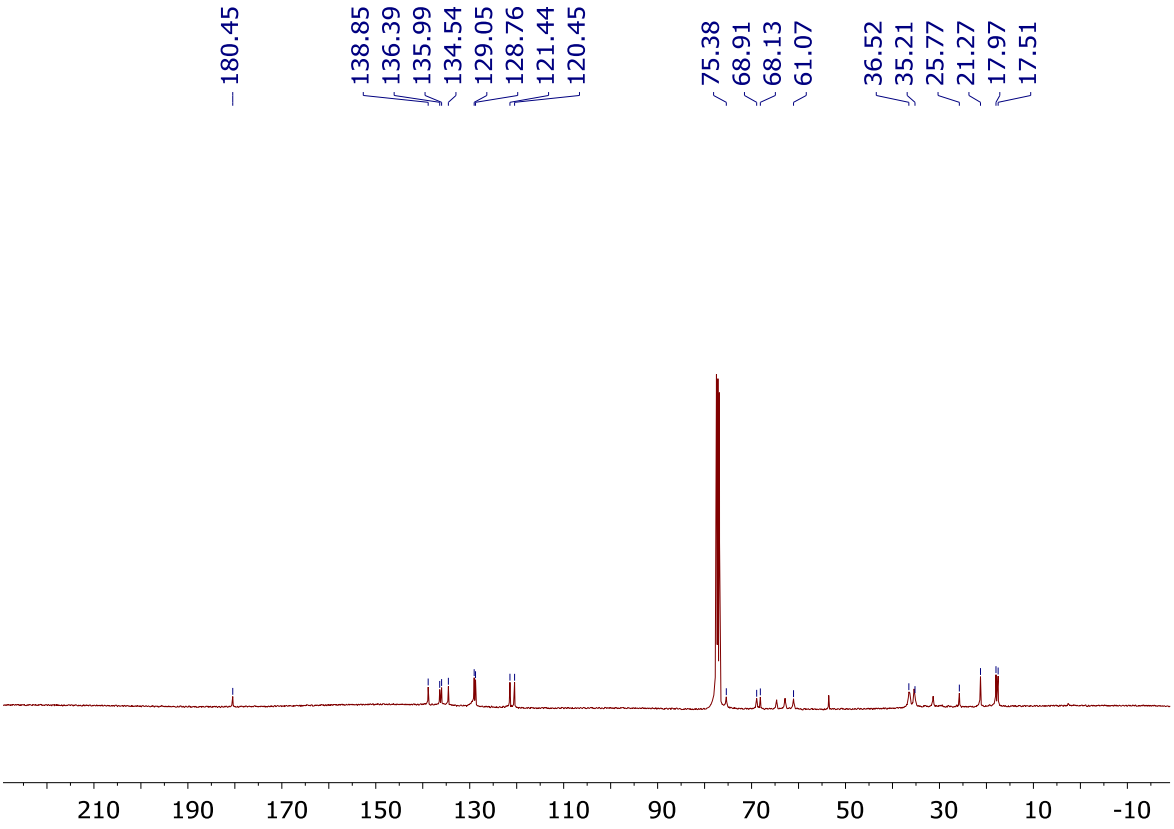

Fig. **7.50** $^{13}C[^{1}H]$ NMR of **66** in $CDCl_3$

Synthesis of **67**:

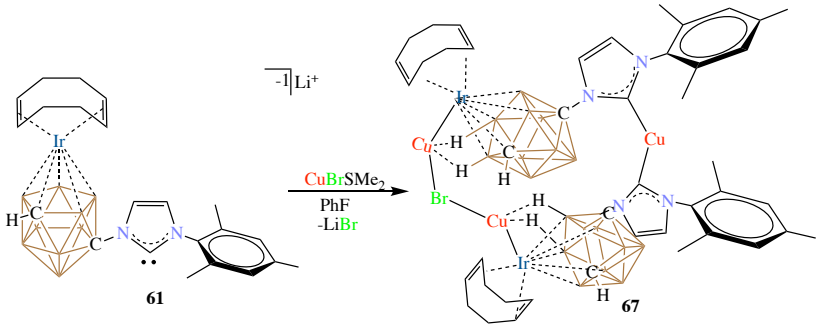

Scheme **7.16** Synthesis of Ir-Cu Bimetallic Complex **67**

A glass vial was loaded with a sit bar and **61**. To the solid, a suspension of $BrCuSMe_2$ in fluorobenzene was added while stirring and the stirring was continued for about two hours at room temperature. The fluorobenzene was then pumped down to dryness under vacuum

affording a pale grey solid that was suspended in dichloromethane and filtered over a pad of celite. The filtrate was pumped down to dryness affording the title compound in 37% yield. Crystals suitable for X-Ray diffraction were grown by layering a concentrated THF solution of the compound with hexanes.

Alternatively, the compound can be synthesized by reacting **61** with a suspension of CuBr in THF. The THF was then pumped down to dryness; the solid was suspended in dichloromethane and filtered over celite. The filtrate was then pumped down to dryness under vacuum to afford the title compound in 43% yield. ^{1}H NMR (400 MHz, $CDCl_3$, 25^{o}C): 7.38 (d, 1H, CH), 6.95 (s, 1H, *meta*-CH), 6.80 (s, 1H, *meta*-CH), 6.56 (d, 1H, CH), 4.43 (m, 5H, COD CH), 3.69 (m, 1H, COD CH), 3.11-2.31 (m, 18H, COD CH_2), 2.26 (s, 3H, *para*-CH_3), 2.06 (s, 3H, *ortho*-CH_3), 1.34 (s, 3H, *ortho*-CH_3); ^{11}B[^{1}H] NMR (128 MHz, $CDCl_3$, 25^{o}C): -4.80, -11.67, -18.96, -20.39, -23.21 ppm. ^{13}C[^{1}H] NMR (100 MHz, $CDCl_3$, 25^{o}C): 180.45, 138.86, 136.39, 135.98, 134.54, 129.08, 128.78, 121.42, 120.47, 68.80, 68.14, 64.72, 62.96, 61.08, 36.11, 35.41, 25.76, 21.27, 17.97, 17.53 ppm.

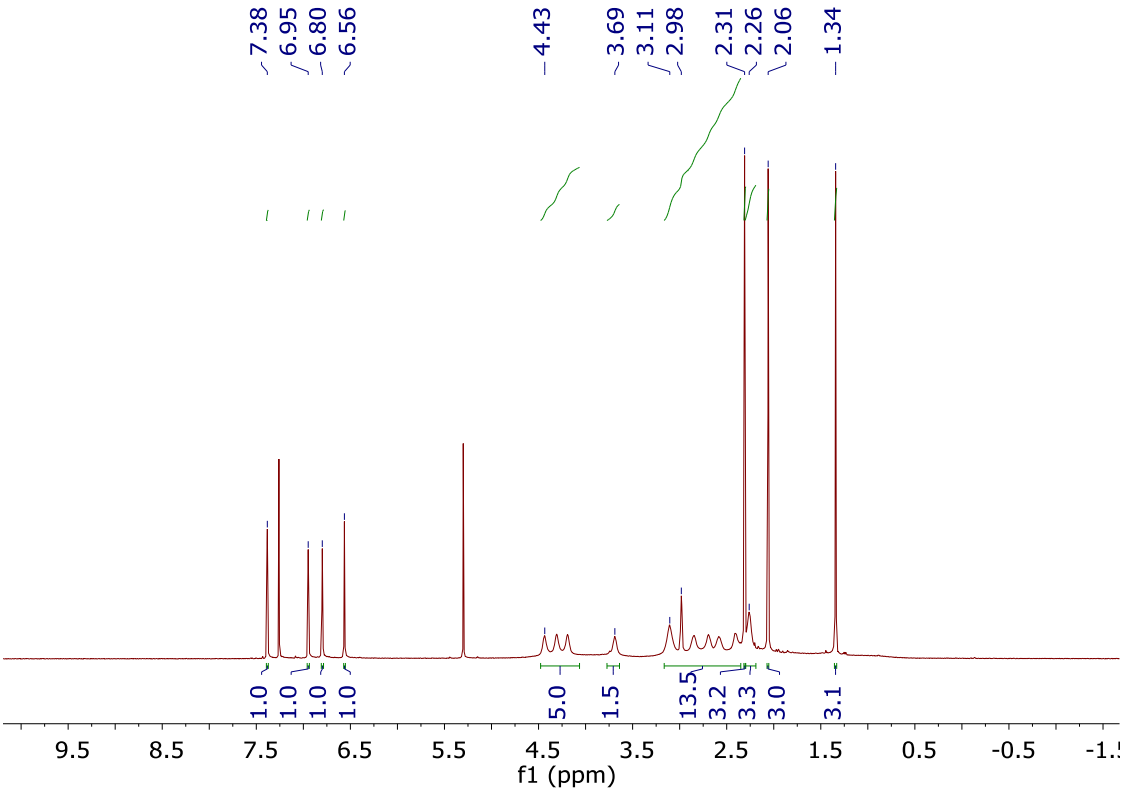

Fig. **7.51** ^{1}H NMR of **67** in $CDCl_3$

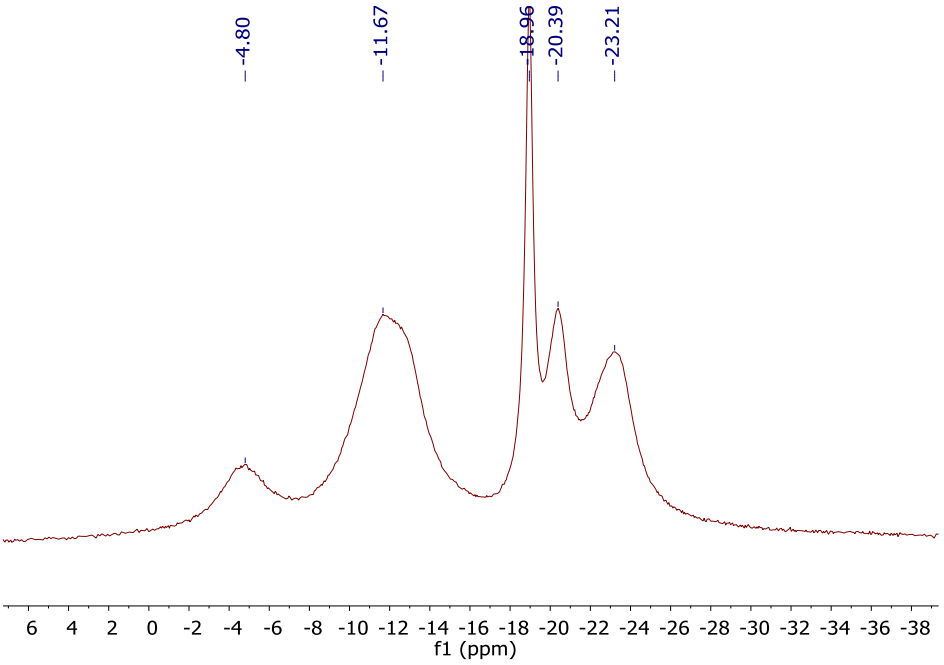

Fig. **7.52** $^{11}B[^{1}H]$ NMR of **67** in $CDCl_3$

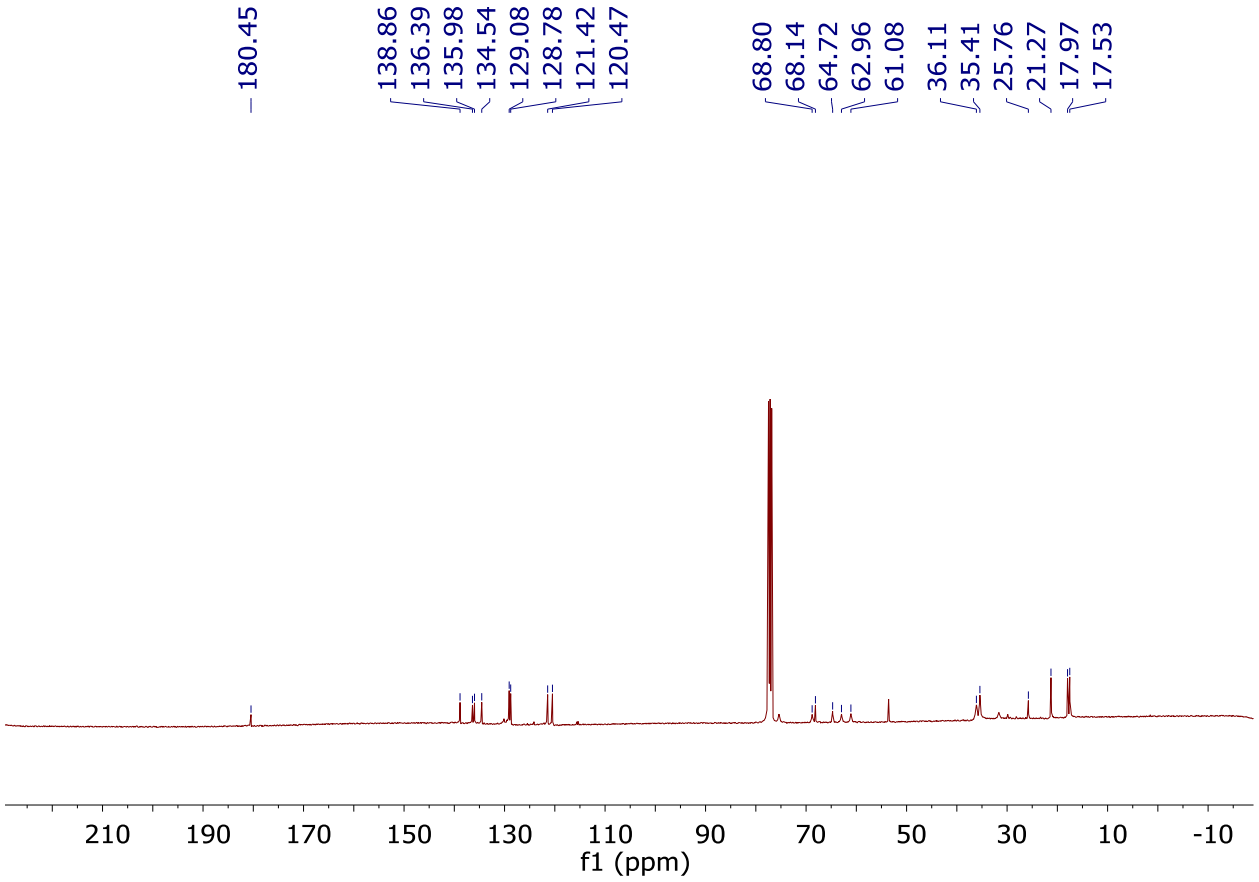

Fig. **7.53** $^{13}C[^{1}H]$ NMR of **67** in $CDCl_3$

Reaction of 13 with [Ir(COD)Cl]$_2$

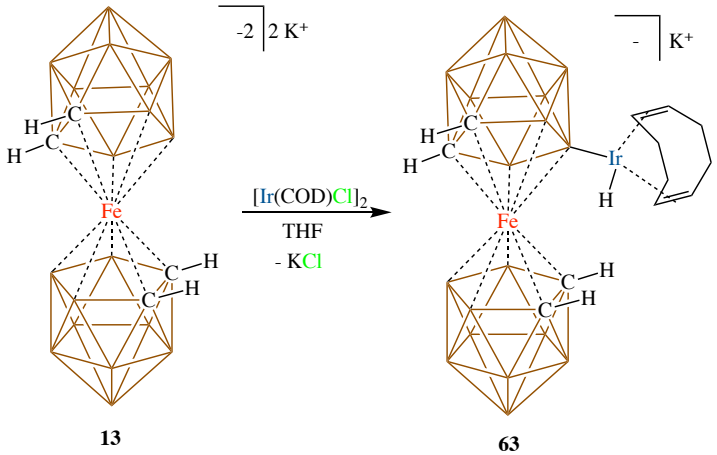

13 **63**

Scheme **7.10**. B-H Oxidative Addition on **13** by [Ir(COD)Cl]$_2$

In a glass vial, **13[K^+]** (100 mg, 0.25 mmol) was dissolved in THF (3 mL). To this, a solution of $[Ir(COD)Cl]_2$ (85.06 mg, 0.123 mmol) in THF (5 mL) was added and the dark solution was stirred at room temperature for about 2 hours. The solution was then filtered over celite and pumped down to produce a mixture of products. The product shown in Scheme **7.10** was identified by the hydrides on the ^1H NMR and the mass corroborated by HRMS.

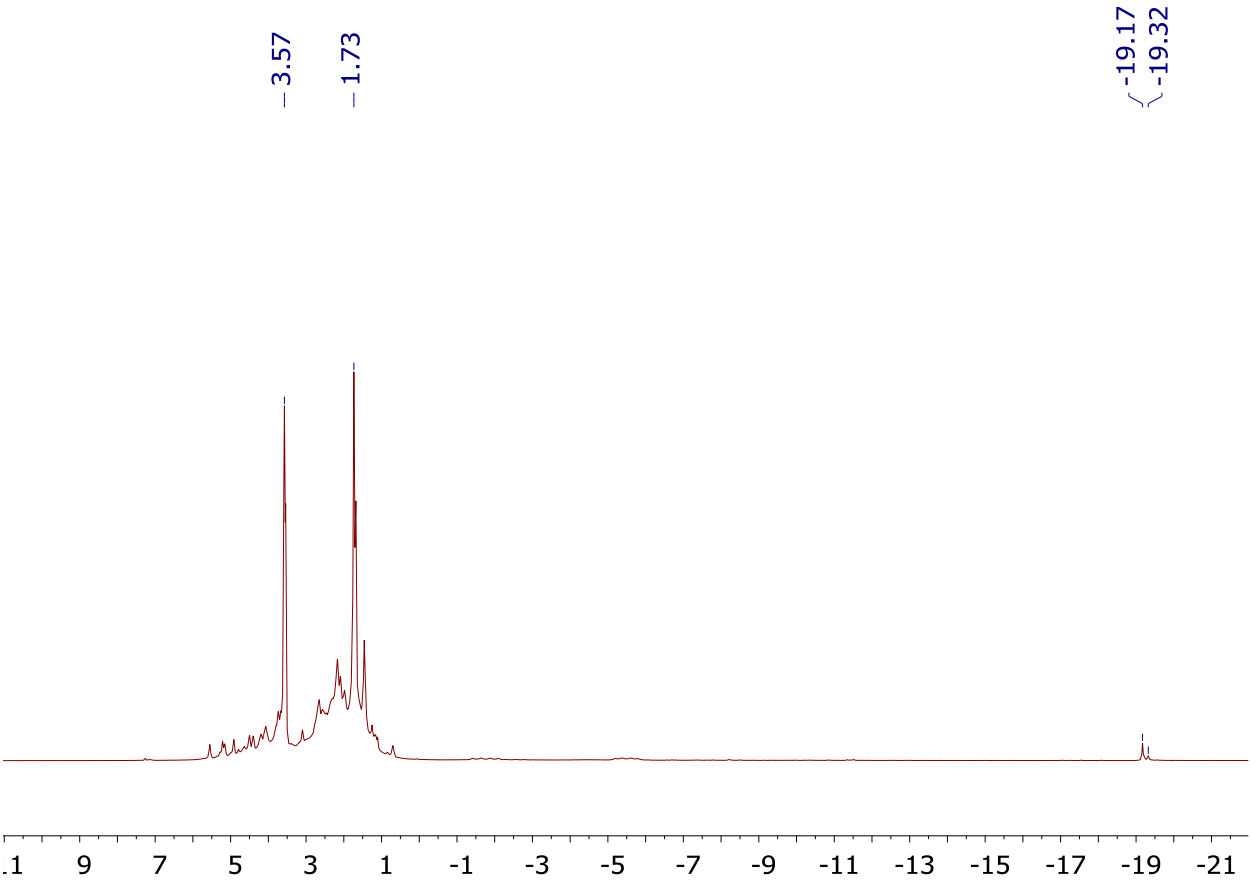

Fig. **7.54** The crude ^1H NMR spectrum of the reaction between **13** and $[Ir(COD)Cl]_2$ in THF-d_8. *The hydrides are seen at 19.17 and 19.32 ppm.*

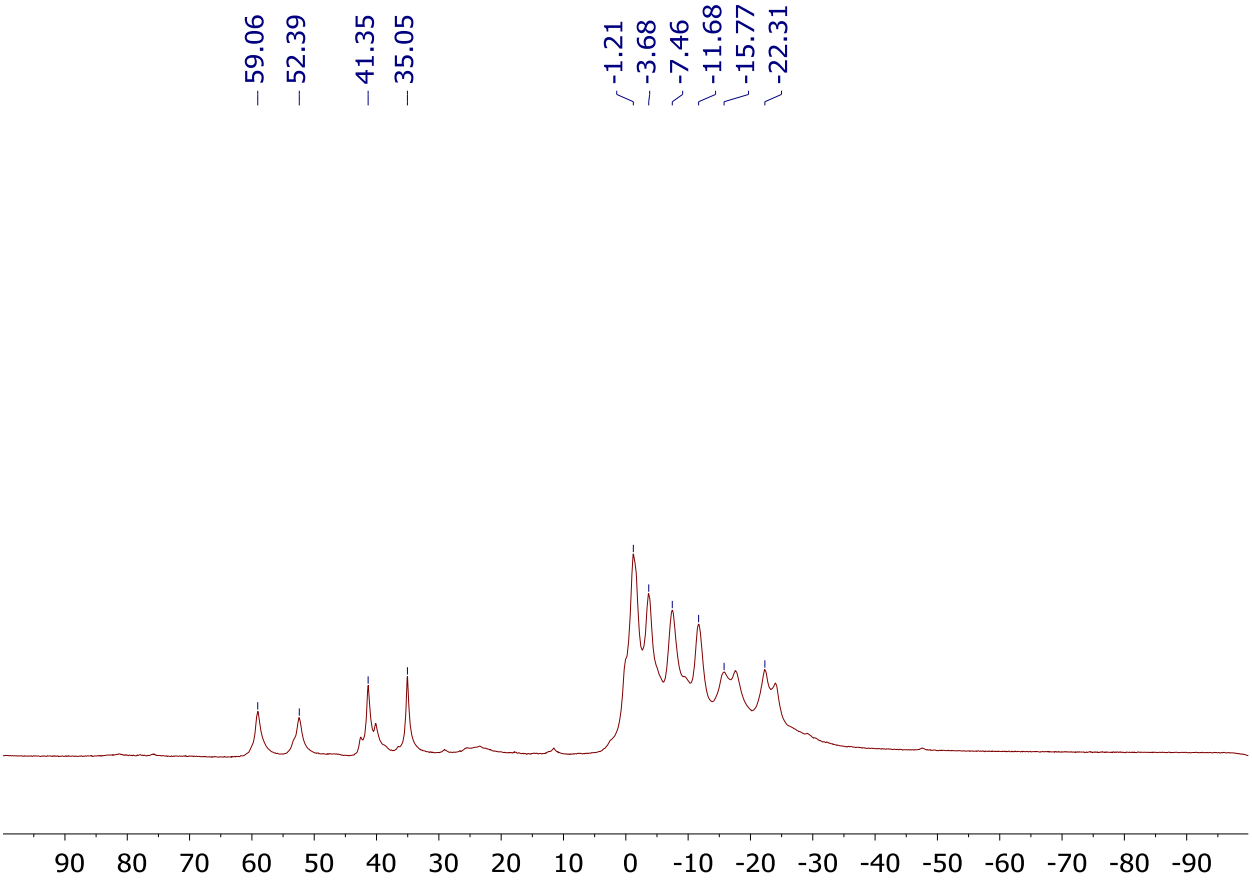

Fig. **7.55** The crude $^{11}B[^{1}H]$ NMR spectrum of the reaction of **13** with $[Ir(COD)Cl]_2$.

Synthesis of 64:

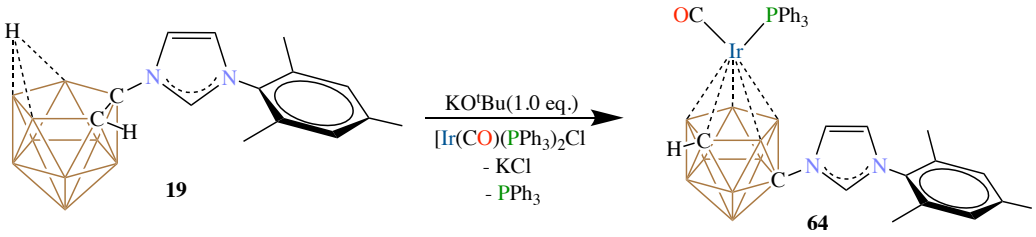

Scheme **7.12**. Synthesis of the Metallacarborane **64**

In a glass vial, the imidazolium **19** (100 mg, 0.31 mmol) was weighed and dissolved in THF (3 mL). To the solution, KO^{t}Bu (45.2 mg, 0.4 mmol) dissolved in THF (2 mL) was added and stirred for 10 minutes at room temperature. Vaska's complex $Ir(CO)(PPh_3)_2Cl$ (241.8 mg, 0.31 mmol) dissolved in THF (5 mL) was then added to the reaction mixture

and the orange red solution was stirred overnight. The volatiles were then removed under vacuum and the crude reaction mixture was dissolved in dichloromethane (15 mL), and the solution filtered over celite. The solution was then concentrated down to 3 mL under vacuum and hexanes (10 mL) was added to precipitate the compound **64**. The combined solvents were then decanted and the obtained solid was pumped down to dryness to produce **64** as an orange solid in 65% yield. ^{1}H NMR (600 MHz, 25°C, $CDCl_3$): 7.94 (t, 1H, CH), 7.67 (m, 7H, PPh_3), 7.24 (m, 9H, PPh_3), 7.04 (t, 1H, CH), 6.93 (t, 1H, CH), 2.37 (s, 3H, *p*-mesityl), 1.97 (s, 6H, *o*-mesityl); ^{31}P[^{1}H] NMR (243 MHz, 25°C, $CDCl_3$): -21.72 ppm; ^{11}B[^{1}H] NMR (192 MHz, 25°C, $CDCl_3$): -12.25, -17.33, -18.61, -20.26, -21.68, -24.67, -26.19, -43.68 ppm.

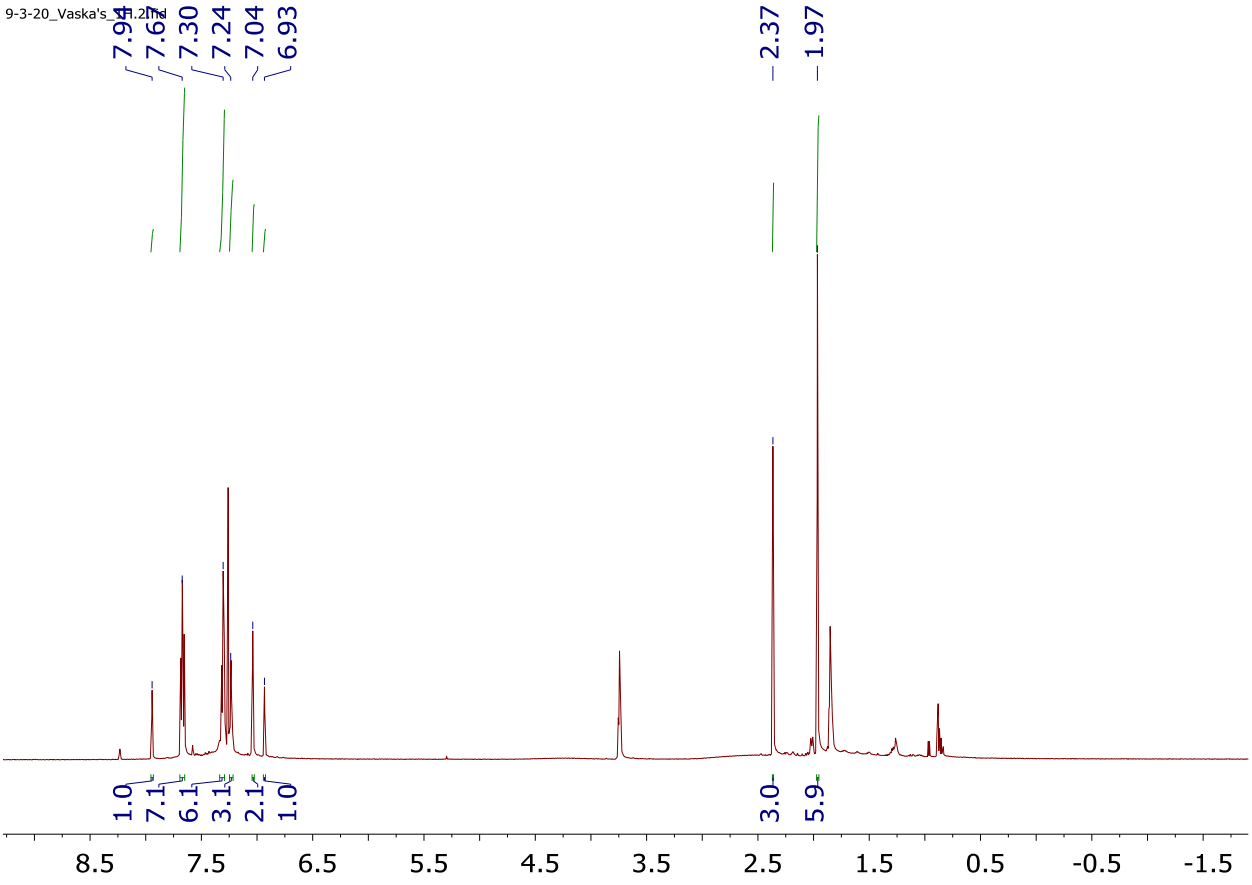

Fig. **7.56** ^{1}H NMR of complex **64** in $CDCl_3$

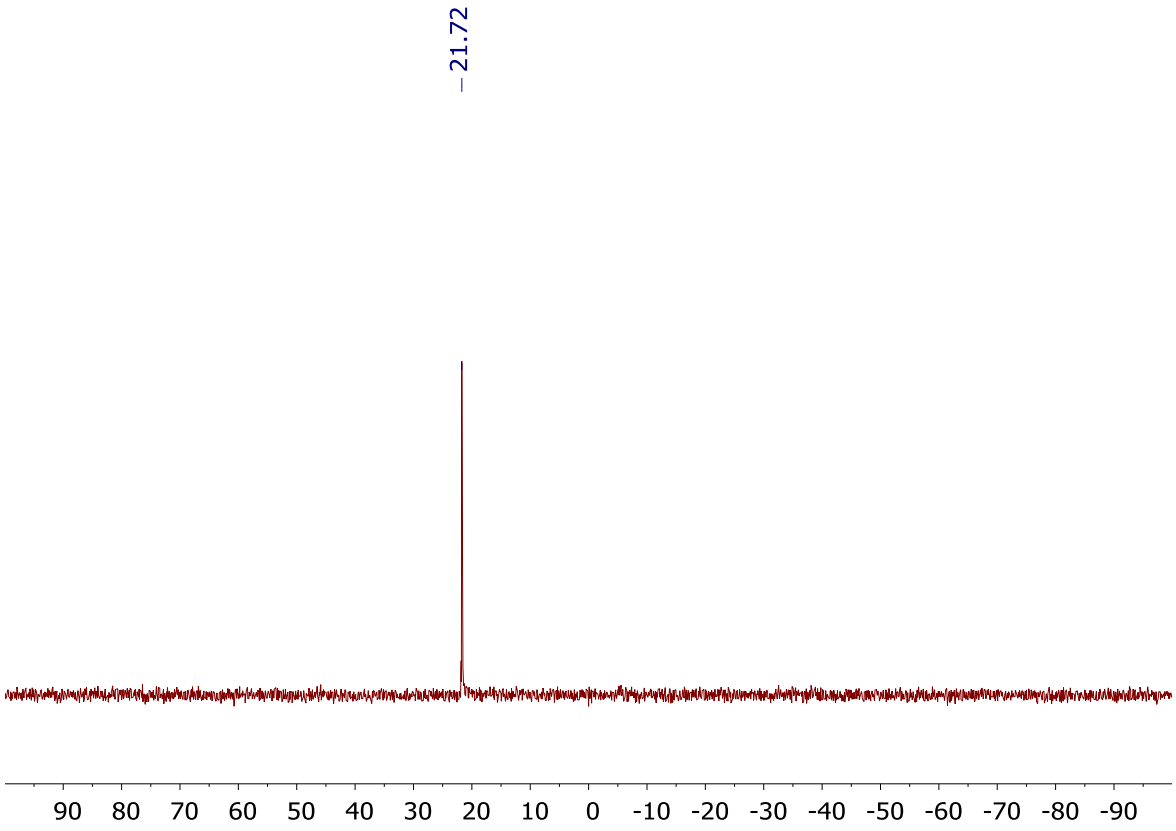

Fig. **7.57** $^{31}P[^{1}H]$ NMR of complex **64** in $CDCl_3$

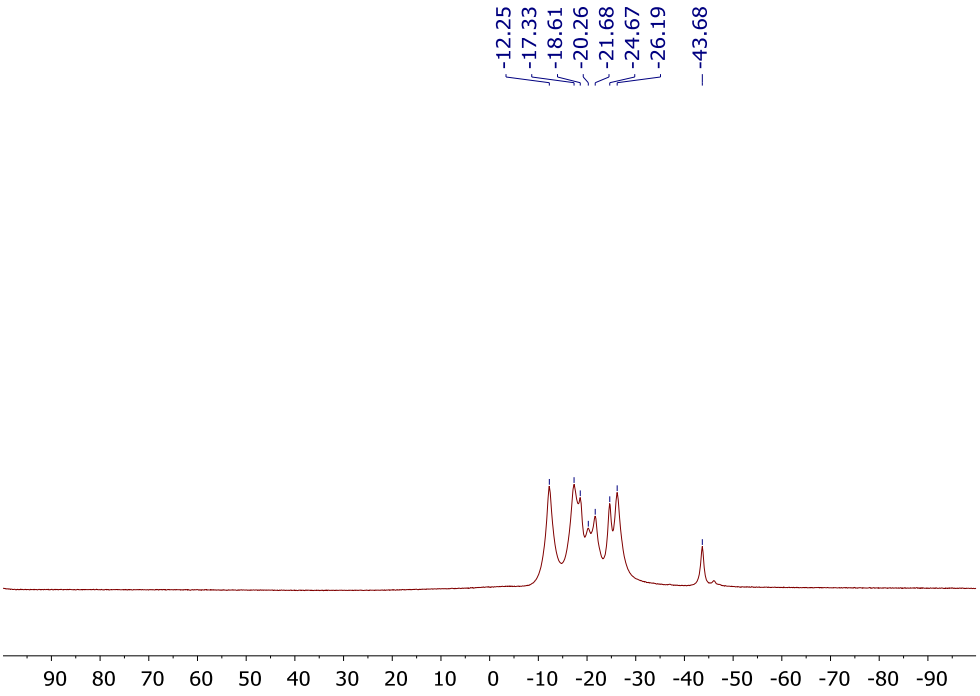

Fig. **7.58** $^{11}B[^{1}H]$ NMR of complex **64** in $CDCl_3$

Synthesis of 65:

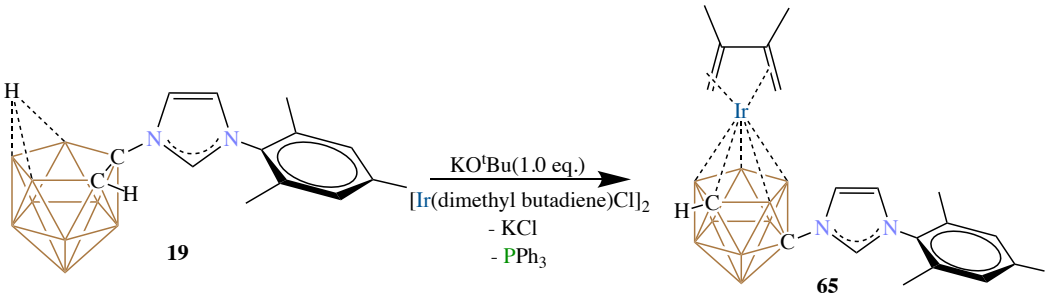

Scheme **7.13**. Synthesis of the Metallacarborane **65**

In a glass vial, the imidazolium **19** (50 mg, 0.156 mmol) was weighed out and dissolved in THF (2 mL). To this, a solution of KO^{t}Bu (22.4 mg, 0.2 mmol) in THF (4 mL) was added and stirred for 10 minutes. [Ir(dimethyl butadiene)Cl]$_2$ (48.3 mg, 0.078 mmol) dissolved in THF (4 mL) was then added to the reaction mixture and stirring continued overnight. The volatiles were pumped down under vacuum and the crude solid was dissolved in dichloromethane (10 mL) and filtered over celite. The DCM solution was then pumped

down under vacuum and the solid obtained was washed with hexanes (2x10 mL). The residual solid was pumped down to dryness producing compound **65** in 77% yield. ^{1}H NMR (400 MHz, 25°C, $CDCl_3$):

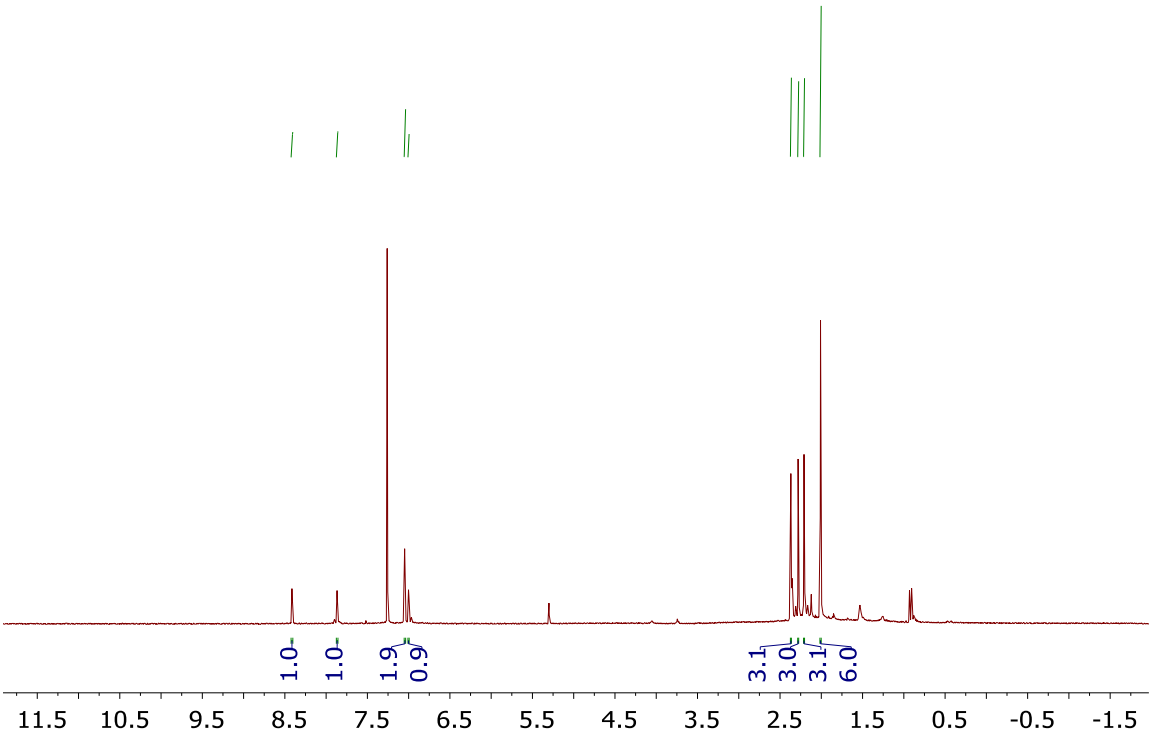

Fig. **7.59** ^{1}H NMR of compound **65** in $CDCl_3$

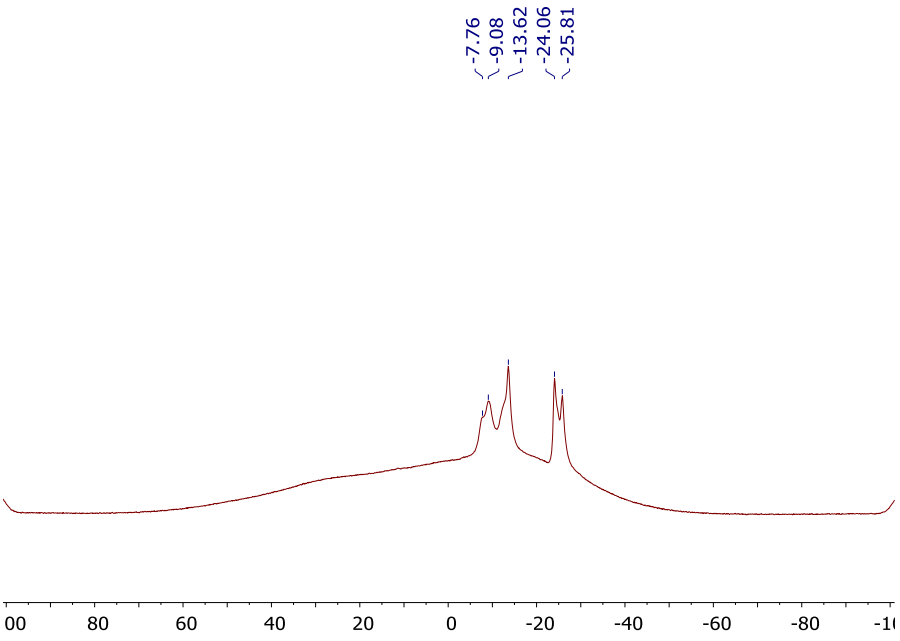

Fig. **7.60** $^{11}B[^{1}H]$ NMR of complex **65** in $CDCl_3$

Synthesis of 68:

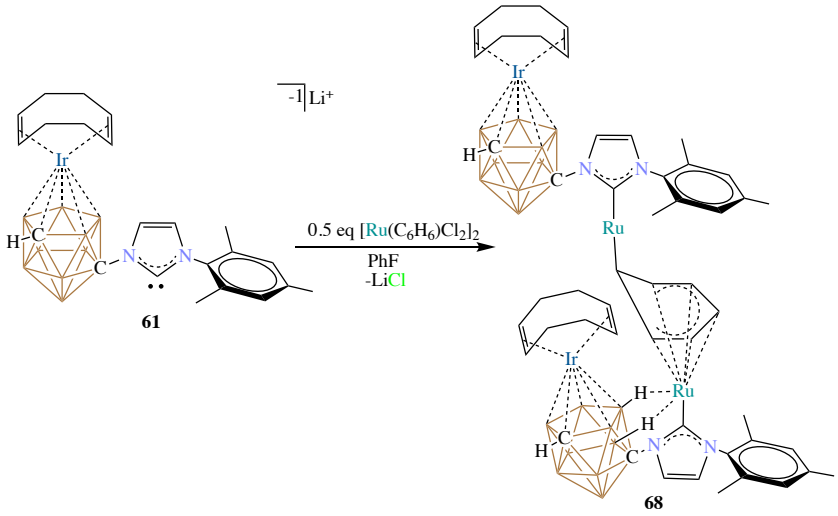

Scheme **7.17**. Synthesis of the Ir-Ru Bimetallic Complex **68**

In a vial, the NHC **61** (200 mg, 0.26 mmol) was weighed and loaded with a stir bar. To this, a suspension of $[Ru(C_6H_6)Cl_2]_2$ (65.02 mg, 0.13 mmol) in fluorobenzene (5 mL) was added while stirring and continued stirring vigorously for the next 2 hours at room

temperature. The suspension was then pumped down and filtered over celite in chloroform (5 mL). The chloroform solution was then pumped to dryness to produce a mixture of compounds. The compound **68** was identified and characterized using single crystal X-Ray diffraction. ^{1}H NMR (400 MHz, 25°C, $CDCl_3$): 7.75 (d, 2H, CH), 7.05 (s, 4H, CH), 6.99 (d, 2H, CH), 4.04 (m, 4H, COD), 3.87 (m, 4H, COD), 2.61 (bs, 2H, *carborane* CH), 2.44 (m, 16H, COD), 2.36 (s, 6H, *para*-CH_3), 2.00 (s, 12H, *ortho*-CH_3); ^{11}B[^{1}H] NMR (96 MHz, 25°C, $CDCl_3$): -7.72, -11.36, -12.82, -22.21, -24.41 ppm.

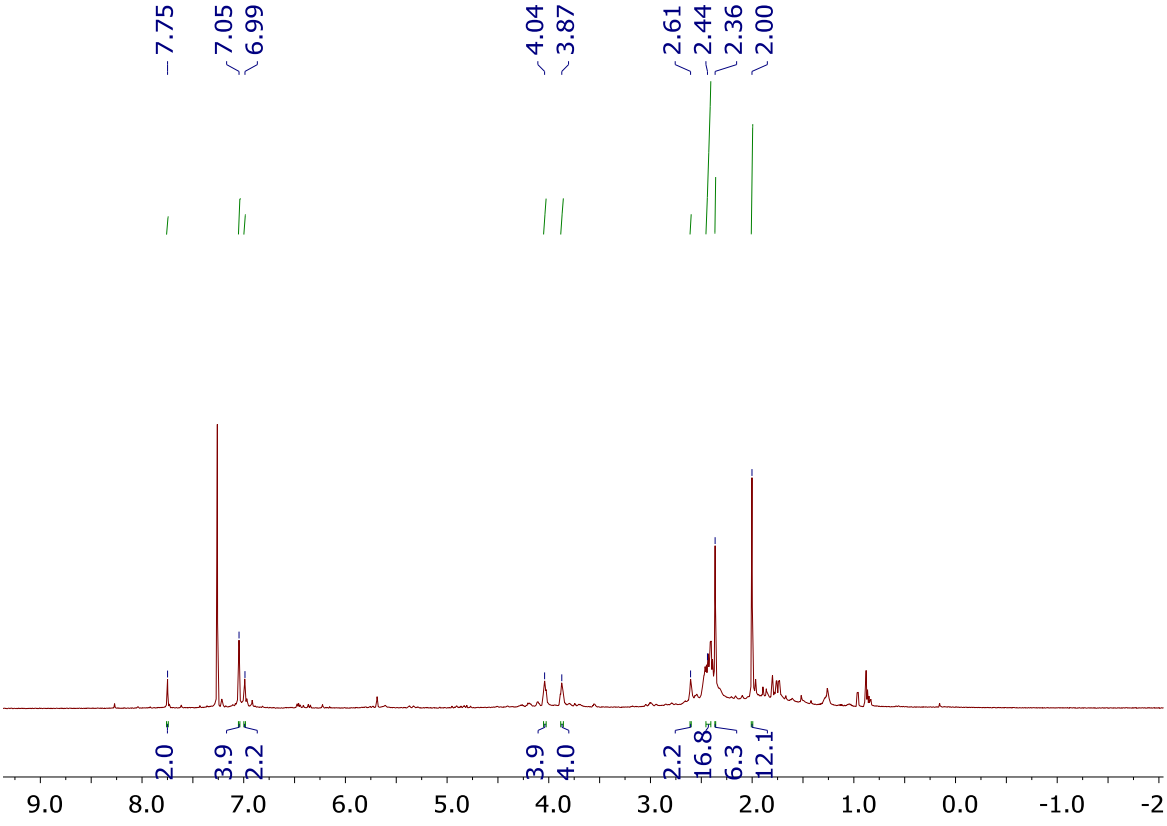

Fig. **7.61** ^{1}H NMR of crude reaction mixture containing compound **68** in $CDCl_3$

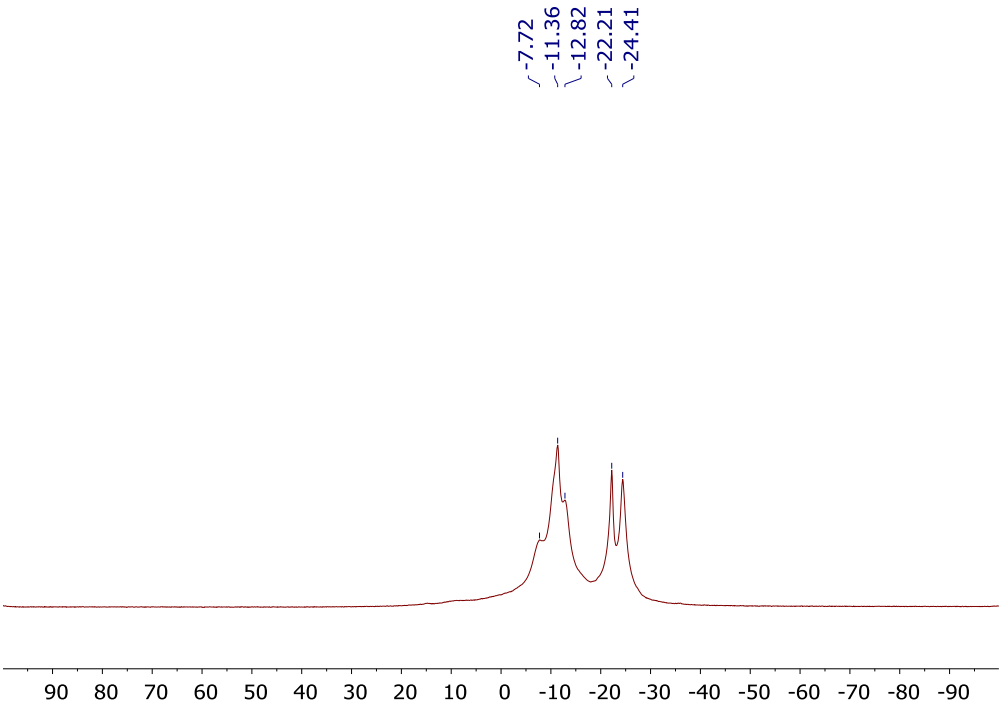

Fig. **7.62** $^{11}B[^{1}H]$ NMR of crude reaction mixture containing **68** in $CDCl_3$

X-Ray Structure Determination

X-Ray Structure of **13[K⁺]:**

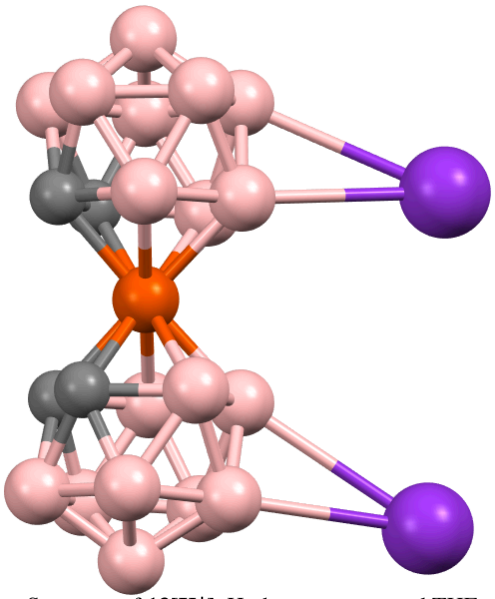

Fig. **7.6** Solid-State Structure of **13[K⁺]**. Hydrogen atoms and THF molecules coordinated to K^+ are omitted for clarity. B=pink, K=purple, Fe=maroon, C=grey

The sample was submitted by Varun Tej (research group of Professor Vincent Lavallo, Department of Chemistry, University of California, Riverside). The report was prepared by Dr. Veronica Carta.

Data collection

Single crystals suitable for X-ray diffraction were grown by solvent diffusion of tetrahydrofuran and hexane. A pink crystal (block, approximate dimensions 0.11 × 0.08 × 0.07 mm^3) was placed onto the tip of a MiTeGen pin and mounted on a Bruker Venture D8 diffractometer equipped with a PhotonIII detector at 100.00 K. The data collection was carried out using Mo Kα radiation (λ = 0.71073 Å, IμS micro-source) with a frame time of 15 seconds and a detector distance of 50 mm. A collection strategy was calculated and complete data to a resolution of 0.82 Å were collected. The frames were integrated with the Bruker SAINT[1] software package using a narrow-frame algorithm to 0.82 Å resolution. Data were corrected for absorption effects using the multi-scan method (SADABS).[2] Please refer to Table 1 for additional crystal and refinement information.

Structure solution and refinement

The space group P $2_1/c$ was determined based on intensity statistics and systematic absences. The structure was solved using the SHELX suite of programs[3] and refined using full-matrix least-squares on F^2 within the OLEX2 suite.[4] An intrinsic phasing solution was calculated, which provided most non-hydrogen atoms from the E-map. Full-matrix least squares / difference Fourier cycles were performed, which located the remaining non-hydrogen atoms. All non-hydrogen atoms were refined with anisotropic displacement parameters. The hydrogen atoms on the tetrahydrofuran molecules were placed in ideal

positions and refined as riding atoms with relative isotropic displacement parameters. The other hydrogen atoms were refined freely. The final full matrix least squares refinement converged to R1 = 0.0366 and wR2 = 0.0794 (F^2, all data). The goodness-of-fit was 1.146. On the basis of the final model, the calculated density was 1.325 g/cm^3 and F(000), 1120 e$^-$.

[1]SAINT, V8.30A, Bruker Analytical X-Ray Systems, Madison, WI, 2012.

[2]SADABS, 2.03, Bruker Analytical X-Ray Systems, Madison, WI, 2016.

[3]G. M. Sheldrick, Acta Cryst. A64, 112 - 122 (2008). Sheldrick, G.M. (2015). Acta Cryst. A71, 3-8.

[4]O. V. Dolomanov, L. J. Bourhis, R. J. Gildea, J. A. K. Howard and H. Puschmann, J. Appl. Crystallogr., 2009, 42, 339–341.

Table 7.1 Crystal data and structure refinement for **13[K$^+$]**

Empirical formula	C12 H38 B18 Fe K2 O2
Formula weight	543.05
Crystal color, shape, size	pink block, 0.11 × 0.08 × 0.07 mm^3
Temperature	100.00 K
Wavelength	0.71073 Å
Crystal system, space group	Monoclinic, P 2_1/c
Unit cell dimensions	a = 7.9511(5) Å α = 90°.
	b = 29.268(2) Å β = 94.012(2)°.
	c = 11.7289(8) Å γ = 90°.

Volume 2722.7(3) $Å^3$

Z 4

Density (calculated) 1.325 g/cm^3

Absorption coefficient 0.872 mm^{-1}

F(000) 1120

Data collection

Diffractometer Bruker D8 Venture

Theta range for data collection 1.874 to 25.755°.

Index ranges -9<=h<=9, -35<=k<=35, -14<=l<=14

Reflections collected 125272

Independent reflections 5199 [R_{int} = 0.0854]

Observed Reflections 4431

Completeness to theta = 25.242° 99.9 %

Solution and Refinement

Absorption correction Semi-empirical from equivalents

Max. and min. transmission 0.7410 and 0.7184

Solution Intrinsic methods

Refinement method Full-matrix least-squares on F^2

Weighting scheme $w = [\sigma^2 Fo^2 + AP^2 + BP]^{-1}$, with

	$P = (Fo^2 + 2\,Fc^2)/3$, A = 0.013, B = 3.68
Data / restraints / parameters	5199 / 26 / 426
Goodness-of-fit on F^2	1.146
Final R indices [I>2σ(I)]	R1 = 0.0366, wR2 = 0.0748
R indices (all data)	R1 = 0.0466, wR2 = 0.0794
Largest diff. peak and hole	0.402 and -0.331 e.Å^{-3}

X-Ray Structure of **58**:

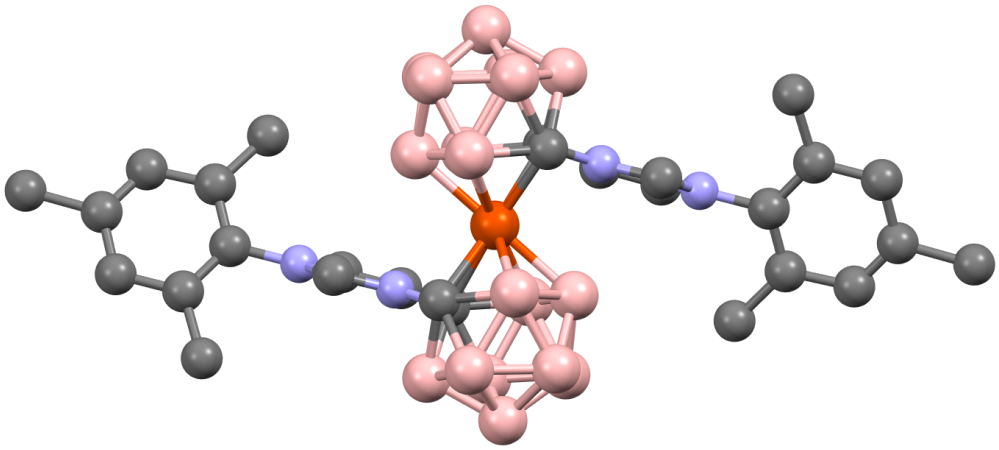

Fig. **7.4** Solid-State Structure of **58**. Hydrogen atoms omitted for clarity. N=blue, Fe=maroon, B=pink, C=grey,

Diffraction data were collected on a Bruker-AXS Apex II diffractometer with an Apex II CCD detector using Mo K_α radiation (λ = 0.71073 Å) from a fine-focus sealed tube source. Data were collected at 100 K by performing 0.5° ω-scans, integrated using SAINT[1], and absorption corrected using SADABS[2]. The structure was solved by direct methods using SHELXT[3] and refined against F^2 on all data by full-matrix least squares with SHELXL-

2018/3[4] following established refinement strategies[5]. All non-hydrogen atoms were refined anisotropically. With the exception of the two hydrogen atoms specified below, all hydrogen atoms were included into the model at geometrically calculated positions and refined using a riding model. The isotropic displacement parameters of all hydrogen atoms were fixed to 1.2 times the *U* value of the atoms to which they are bound (1.5 times for methyl groups). Crystal and data quality details, as well as a summary of the residual refinement values, are listed in the accompanying table.

Compound **vl353vt** crystallizes in the orthorhombic centrosymmetric space group *Pccn* with one half of one molecule of **vl353vt** and two and one half molecules of tetrahydrofuran per asymmetric unit.

The hydrogen atom on imidazolium carbon atom C1 was located in the Fourier synthesis and refined semi-freely with the help of a distance restraint (target C–H distance 0.95(2) Å), and the hydrogen atom on dicarbollide carbon atom C5 was also located in the Fourier synthesis and refined freely; the U_{iso} values of these hydrogen atoms were constrained to 1.2 times the U_{eq} value of the atom to which they bind.

The mesityl group on the ligand and two positions of tetrahydrofuran solvent each exhibit disorder that was modeled over two positions, while the disorder of the third position of tetrahydrofuran was modeled over five positions; the disorder ratios were refined freely and converged at 54:46, 60:40, 78:22, and 33:31:22:9:5, respectively. One disordered molecule of tetrahydrofuran resides on a two-fold rotation axis whose symmetry is not fulfilled by the arrangement of molecules. All disorders were refined with the help of

similarity restraints on 1,2- and 1,3- distances as well as similarity and rigid-bond restraints on anisotropic displacement parameters.

References

[1] SAINT, version 8.34A, Bruker (2012), Bruker AXS Inc., Madison, Wisconsin, USA.

[2] SADABS, version 2012/1, Bruker (2012), Bruker AXS Inc., Madison, Wisconsin, USA.

[3] Sheldrick, G. M., *Acta Cryst.* **2015**, *A71*, 3-8.

[4] Sheldrick, G. M., *Acta Cryst.* **2015**, *C71*, 3-8.

[5] Müller, P. *Crystallography Reviews* **2009**, *15*, 57-83.

Table 7.2 Crystal data and structure refinement for **58**

Identification code	vl353vt
Empirical formula	C48 H88 B18 Fe N4 O5
Formula weight	1051.65
Temperature	100(2) K
Wavelength	0.71073 Å
Crystal system	Orthorhombic
Space group	Pccn
Unit cell dimensions	a = 23.5018(4) Å α = 90°.

b = 14.5190(2) Å β = 90°.

c = 16.7222(3) Å γ = 90°.

Volume 5705.99(16) Å3

Z 4

Density (calculated) 1.224 Mg/m3

Absorption coefficient 0.312 mm-1

F(000) 2240

Crystal color purple

Crystal size 0.189 x 0.161 x 0.148 mm3

Theta range for data collection 1.649 to 29.130°

Index ranges -32 <= *h* <= 32, -19 <= *k* <= 19, -22 <= *l* <= 22

Reflections collected 117705

Independent reflections 7679 [R(int) = 0.0678]

Completeness to theta = 25.242° 100.0 %

Absorption correction Semi-empirical from equivalents

Refinement method Full-matrix least-squares on F2

Data / restraints / parameters 7679 / 2622 / 734

Goodness-of-fit on F2 1.053

Final R indices [I>2sigma(I) = 5865 data] R1 = 0.0440, wR2 = 0.1072

R indices (all data, 0.73 Å) R1 = 0.0640, wR2 = 0.1191

Largest diff. peak and hole 0.304 and -0.337 e.Å-3

X-Ray Structure of **59:**

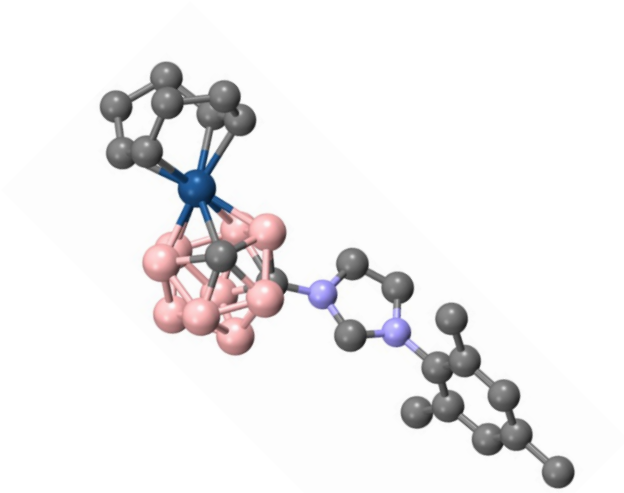

Fig. **7.5** Solid-State Structure of the Ir complex **59**. Hydrogen atoms omitted for clarity. N=Blue, B=pink, Ir=ocean blue, C=grey

The sample was submitted by Varun Tej (research group of Professor Vincent Lavallo, Department of Chemistry, University of California, Riverside). The report was prepared by Dr. Veronica Carta.

Data collection

Single crystals suitable for X-ray diffraction were grown by slow evaporation of dichloromethane. An orange crystal (block, approximate dimensions 0.12 × 0.08 × 0.06 mm^3) was placed onto the tip of a MiTeGen pin and mounted on a Bruker Venture D8 diffractometer equipped with a PhotonIII detector at 100.00 K. The data collection was carried out using Cu Kα radiation (λ = 1.54178 Å, IμS micro-source) with a frame time of 3 seconds and a detector distance of 40 mm. A collection strategy was calculated and complete data to a resolution of 0.82 Å were collected. The frames were integrated with the Bruker SAINT[1] software package using a narrow-frame algorithm to 0.84 Å resolution. Data were corrected for absorption effects using the multi-scan method (SADABS).[2] Please refer to Table 1 for additional crystal and refinement information.

Structure solution and refinement

The space group C 2/c was determined based on intensity statistics and systematic absences. The structure was solved using the SHELX suite of programs[3] and refined using full-matrix least-squares on F^2 within the OLEX2 suite.[4] An intrinsic phasing solution was calculated, which provided most non-hydrogen atoms from the E-map. Full-matrix least squares / difference Fourier cycles were performed, which located the remaining non-hydrogen atoms. All non-hydrogen atoms were refined with anisotropic displacement parameters. The hydrogen atoms were placed in ideal positions and refined as riding atoms with relative isotropic displacement parameters, with the exception of H1, which was refined freely. The final full matrix least squares refinement converged to R1 = 0.0352 and wR2 = 0.0775 (F^2, all data). The goodness-of-fit was 1.150. On the basis of the final model, the calculated density was 1.628 g/cm^3 and F(000), 2432 e^-.

[1]SAINT, V8.30A, Bruker Analytical X-Ray Systems, Madison, WI, 2012.

[2]SADABS, 2.03, Bruker Analytical X-Ray Systems, Madison, WI, 2016.

[3]G. M. Sheldrick, Acta Cryst. A64, 112 - 122 (2008). Sheldrick, G.M. (2015). Acta Cryst. A71, 3-8.

[4]O. V. Dolomanov, L. J. Bourhis, R. J. Gildea, J. A. K. Howard and H. Puschmann, J. Appl. Crystallogr., 2009, 42, 339–341.

Table 7.3 Crystal data and structure refinement for **59**

Empirical formula	C22 H36 B9 Ir N2
Formula weight	618.02
Crystal color, shape, size	orange block, 0.12 × 0.08 × 0.06 mm^3
Temperature	100.00 K
Wavelength	1.54178 Å
Crystal system, space group	Monoclinic, C 1 2/c 1
Unit cell dimensions	a = 22.7595(5) Å α = 90°.
	b = 7.3588(2) Å β = 102.137(2)°.
	c = 30.7951(8) Å γ = 90°.
Volume	5042.4(2) $Å^3$
Z	8
Density (calculated)	1.628 g/cm^3
Absorption coefficient	10.332 mm^{-1}
F(000)	2432

Data collection

Diffractometer Bruker D8 Venture

Theta range for data collection 2.935 to 66.949°.

Index ranges -26<=h<=26, -8<=k<=8, -36<=l<=30

Reflections collected 16820

Independent reflections 4361 [Rint = 0.0483]

Observed Reflections 3934

Completeness to theta = 66.949° 97.1 %

Solution and Refinement

Absorption correction Semi-empirical from equivalents

Max. and min. transmission 0.7528 and 0.5194

Solution Intrinsic methods

Refinement method Full-matrix least-squares on F^2

Weighting scheme $w = [\sigma^2 Fo^2 + AP^2 + BP]^{-1}$, with

$P = (Fo^2 + 2\,Fc^2)/3$, A = 0.00, B = 58.7

Data / restraints / parameters 4361 / 0 / 313

Goodness-of-fit on F^2 1.150

Final R indices [I>2σ(I)] R1 = 0.0352, wR2 = 0.0755

R indices (all data) R1 = 0.0406, wR2 = 0.0775

Largest diff. peak and hole 1.261 and -1.922 e.Å^{-3}

X-Ray Structure of **60[Li$^+$]:**

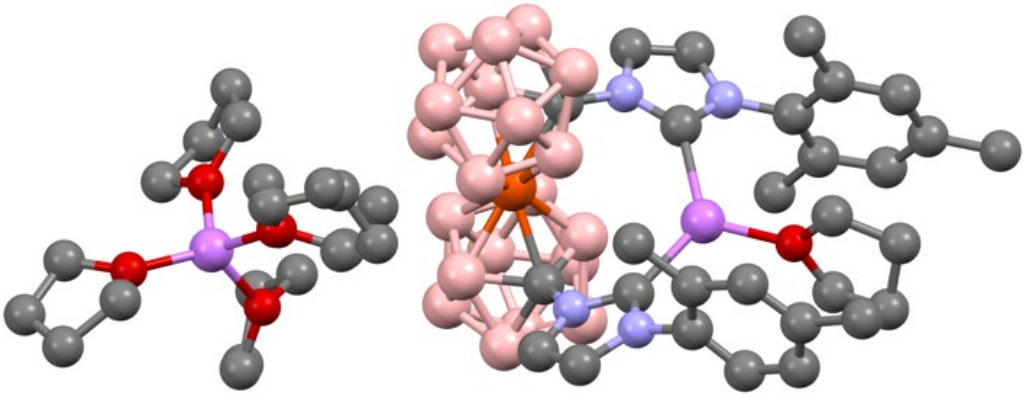

Fig. **7.8** Solid-State Structure of **60[Li$^+$]**. Hydrogen atoms omitted for clarity. N=Blue, C=grey, B=pink, Fe=maroon, O=red, Li=purple

The sample was submitted by Varun Tej (research group of Professor Vincent Lavallo, Department of Chemistry, University of California, Riverside). Data collection and structure solution were carried out by Dr. Charlene Tsay. The report was prepared by Dr. Veronica Carta.

Data collection

A red crystal (plate, approximate dimensions 0.21 × 0.114 × 0.018 mm^3) was placed onto the tip of a MiTeGen pin and mounted on a Bruker Venture D8 diffractometer equipped with a PhotonIII detector at 100.00 K. The data collection was carried out using Cu Kα radiation (λ = 1.54178 Å, IμS micro-source) with a frame time of 10 seconds and a detector distance of 50 mm. The frames were integrated with the Bruker SAINT[1] software package using a narrow-frame algorithm to 0.82 Å resolution. Data were corrected for absorption effects using TWINABS.[2] Please refer to Table 1 for additional crystal and refinement information.

Structure solution and refinement

The space group P $2_1/n$ was determined based on intensity statistics and systematic absences. The structure was solved using the SHELX suite of programs[3] and refined using full-matrix least-squares on F^2 within the OLEX2 suite.[4] An intrinsic phasing solution was calculated, which provided most non-hydrogen atoms from the E-map. Full-matrix least squares / difference Fourier cycles were performed, which located the remaining non-hydrogen atoms. All non-hydrogen atoms were refined with anisotropic displacement parameters. The hydrogen atoms were placed in ideal positions and refined as riding atoms with relative isotropic displacement parameters. The final full matrix least squares refinement converged to R1 = 0.1016 and wR2 = 0.2472 (F^2, all data). The goodness-of-fit was 1.054. On the basis of the final model, the calculated density was 1.217 g/cm^3 and F(000), 2248 e^-.

[1]SAINT, V8.30A, Bruker Analytical X-Ray Systems, Madison, WI, 2012.

[2]TWINABS, Bruker Analytical X-Ray Systems, Madison, WI, 2016.

[3]G. M. Sheldrick, Acta Cryst. A64, 112 - 122 (2008). Sheldrick, G.M. (2015). Acta Cryst. A71, 3-8.

[4]O. V. Dolomanov, L. J. Bourhis, R. J. Gildea, J. A. K. Howard and H. Puschmann, J. Appl. Crystallogr., 2009, 42, 339–341.

Table 7.4 Crystal data and structure refinement for **60[Li^+]**

Empirical formula	C46 H86 B20 Fe Li2 N4 O5
Formula weight	1061.11
Crystal color, shape, size	red plate, 0.21 × 0.114 × 0.018 mm^3
Temperature	100.00 K
Wavelength	1.54178 Å
Crystal system, space group	Monoclinic, P $2_1/n$
Unit cell dimensions	a = 20.3132(7) Å α = 90°.
	b = 14.5180(5) Å β = 114.7782(19)°.
	c = 21.6301(7) Å γ = 90°.
Volume	5791.6(3) $Å^3$
Z	4
Density (calculated)	1.217 g/cm^3
Absorption coefficient	2.434 mm^{-1}
F(000)	2248

Data collection

DiffractometerBruker D8 Venture

Theta range for data collection 2.507 to 70.069°.

Index ranges -24<=h<=22, 0<=k<=17, 0<=l<=26

Reflections collected 11941

Independent reflections 11074 [Rint = 0.1840]

Observed Reflections 7966

Completeness to theta = 67.679° 100.0 %

Solution and Refinement

Absorption correction Semi-empirical from equivalents

Max. and min. transmission 0.753576 and 0.533421

Solution Intrinsic methods

Refinement method Full-matrix least-squares on F^2

Weighting scheme $w = [\sigma^2 Fo^2 + AP^2 + BP]^{-1}$, with

$P = (Fo^2 + 2\,Fc^2)/3$, A = 0.052, B = 26.3

Data / restraints / parameters 11075 / 185 / 774

Goodness-of-fit on F^2 1.054

Final R indices [I>2σ(I)] R1 = 0.1016, wR2 = 0.2112

R indices (all data) R1 = 0.1527, wR2 = 0.2472

Largest diff. peak and hole 1.142 and -0.491 e.$Å^{-3}$

Twin Details

Type, twin law Non Merohedral, 0.12 0 -0.89, 0 -1 0, -1.11 0 -0.12

Twin element, domain ratio 180˚ rotation around reciprocal axis (1 0 -1), 65:35

X-Ray Structure of **61:**

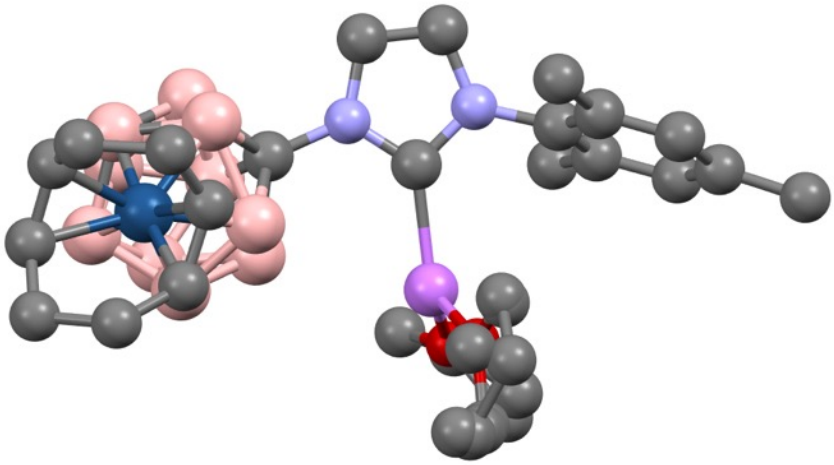

Fig. **7.9** Solid-State Structure of **61**. Hydrogen atoms omitted for clarity. N=Blue, C=grey, Li=purple, B=pink, O=red, Ir=ocean blue

Diffraction data were collected on a Bruker D8 Venture Duo diffractometer with a Bruker Photon III CPAD detector using Mo K_α radiation (λ = 0.71073 Å) from an IμS micro-source. Data were collected at 100 K by performing 0.5° φ- and ω-scans, integrated using SAINT[1], and scaled using SADABS[2]. The structure was solved by direct methods using SHELXT[3] and refined against F^2 on all data by full-matrix least squares with SHELXL-2018/3[4] following established refinement strategies[5]. All non-hydrogen atoms were refined anisotropically. Except where noted below, all hydrogen atoms were included into the model at geometrically calculated positions and refined using a riding model. The isotropic displacement parameters of all hydrogen atoms were fixed to 1.2 times the U

value of the atoms they are linked to (1.5 times for methyl groups). Crystal and data quality details, as well as a summary of the residual refinement values, are listed in the accompanying table.

Compound **vl359vt** crystallizes in the centrosymmetric monoclinic space group *P2₁/c* with one molecule of **vl359vt** per asymmetric unit.

The iridium-coordinated carborane carbon atom C5 is positionally disordered over two chemically equivalent carborane cage positions which are rendered inequivalent in the solid-state by an interaction between a carborane hydrogen atom and the lithium cation. This was modeled as an occupational disorder between carbon and boron at the two respective cage sites; the disorder ratio was refined freely and converged at 60:40. Simiarily restraints were used on the 1,2- distances involving the two occupationally disordered cage sites, and the anisotropic displacement parameters of the carbon/boron pairs that share a cage site were constrained to be equal. A model that includes two isotropic positions of the entire carborane cage (vl359vt_iso_full_split) is available for perusal.

One iridium-coordinated tetrahydrofuran molecule exhibits positional disorder which was modeled over two positions; the disorder ratio was refined freely and converged at 76:24. This disorder was refined with the help of similarity restraints on 1,2- and 1,3- distances as well as similarity and rigid bond restraints for anisotropic displacement parameters. The anisotropic displacement parameters of two nearly-overlapping major/minor atom pairs were constrained to be equivalent.

The hydrogen atoms of both C5 carborane cage positions as well as the alkenyl hydrogen atoms on the cyclooctadiene moiety were located in the Fourier synthesis and refined semi-freely with the help of distance restraints (target C–H distance 0.95(2) Å).

References

[1] SAINT, version 8.34A, Bruker (2012), Bruker AXS Inc., Madison, Wisconsin, USA.

[2] SADABS, version 2012/1, Bruker (2012), Bruker AXS Inc., Madison, Wisconsin, USA.

[3] Sheldrick, G. M., *Acta Cryst.* **2015**, *A71*, 3-8.

[4] Sheldrick, G. M., *Acta Cryst.* **2015**, *C71*, 3-8.

[5] Müller, P. *Crystallography Reviews* **2009**, *15*, 57-83.

Table 7.5 Crystal data and structure refinement for **61**

Identification code	vl359vt_r
Empirical formula	C30 H51 B9 Ir Li N2 O2
Formula weight	768.15
Temperature	100(2) K
Wavelength	0.71073 Å

Crystal system Monoclinic

Space group $P2_1/c$

Unit cell dimensions a = 12.1267(5) Å α = 90°.

b = 16.4077(6) Å β = 96.9395(16)°.

c = 17.0854(7) Å γ = 90°.

Volume 3374.6(2) Å3

Z 4

Density (calculated) 1.512 Mg/m3

Absorption coefficient 3.988 mm-1

F(000) 1544

Crystal color brown

Crystal size 0.157 x 0.145 x 0.117 mm3

Theta range for data collection 2.098 to 32.576°

Index ranges -18 <= *h* <= 18, -24 <= *k* <= 24, -25 <= *l* <= 25

Reflections collected 185427

Independent reflections 12281 [R(int) = 0.0420]

Completeness to theta = 25.242° 100.0 %

Absorption correction Semi-empirical from equivalents

Refinement method Full-matrix least-squares on F2

Data / restraints / parameters 12281 / 249 / 468

Goodness-of-fit on F2 1.037

Final R indices [I>2sigma(I) = 11070 data] R1 = 0.0159, wR2 = 0.0342

R indices (all data, 0.66 Å) R1 = 0.0198, wR2 = 0.0353

Largest diff. peak and hole 0.545 and -0.649 e.Å-3

X-Ray Structure of **66**:

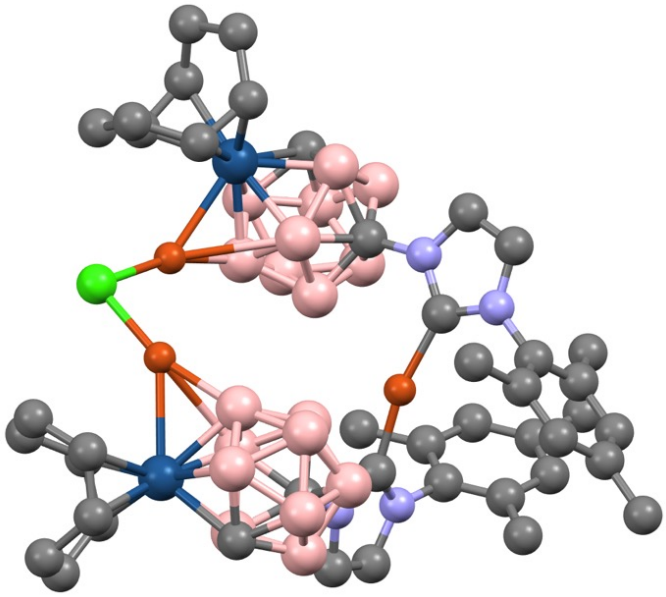

Fig. **7.13**. Solid-State Structure of **66**. Hydrogen atoms omitted for clarity. N=Blue, C=grey, B=pink, Cu=Brown, Cl=green, Ir=ocean blue

Diffraction data were collected on a Bruker D8 Venture Duo diffractometer with a Bruker Photon III CPAD detector using Mo K_α radiation (λ = 0.71073 Å) from an IμS micro-source. Data were collected at 100 K by performing 0.5° φ- and ω-scans, integrated using SAINT[1], and scaled using SADABS[2]. The structure was solved by direct methods using

SHELXT[3] and refined against F^2 on all data by full-matrix least squares with SHELXL-2018/3[4] following established refinement strategies[5]. All non-hydrogen atoms were refined anisotropically, and all hydrogen atoms were included into the model at geometrically calculated positions and refined using a riding model. The isotropic displacement parameters of all hydrogen atoms were fixed to 1.2 times the *U* value of the atoms they are linked to (1.5 times for methyl groups). Crystal and data quality details, as well as a summary of the residual refinement values, are listed in the accompanying table.

Compound **vl391vt** crystallizes in the centrosymmetric monoclinic space group *C*2/*c* with half of one molecule of **vl391vt** per asymmetric unit.

The hydrogen atoms of all carborane cage positions as well as the alkenyl hydrogen atoms on the cyclooctadiene moiety were located in the Fourier synthesis and refined semi-freely with the help of distance restraints (target $C_{carborane}$–H and $C_{cyclooctadiene}$-H distances = 0.95(2) Å, target $B_{carborane}$-H distance = 1.12(2) Å).

The SQUEEZE[6] program within the PLATON[7] suite was used to address a solvent pocket containing a heavily disordered molecule of dichloromethane that resides on an inversion center; a model that includes two positions of this dichloromethane molecule (vl391vt_DCM.res) is available for perusal.

This material is based upon work supported by the National Science Foundation under Award No. 1919677.

References

[1] SAINT, version 8.34A, Bruker (2012), Bruker AXS Inc., Madison, Wisconsin, USA.

[2] SADABS, version 2016/2, Bruker (2016), Bruker AXS Inc., Madison, Wisconsin, USA.

[3] Sheldrick, G. M., *Acta Cryst.* **2015**, *A71*, 3-8.

[4] Sheldrick, G. M., *Acta Cryst.* **2015**, *C71*, 3-8.

[5] Müller, P. *Crystallography Reviews* **2009**, *15*, 57-83.

[6] van der Sluis, P. & Spek, A. L., *Acta Cryst.* **1990**, *A46*, 194-201.

[7] Spek, A. L. *Acta Cryst.* **2009**, *D65*, 148-155.

Table 7.6 Crystal data and structure refinement for **66**

Identification code	vl391vt_sq
Empirical formula	C44 H70 B18 Cl Cu3 Ir2 N4
Formula weight	1460.09
Temperature	100(2) K
Wavelength	0.71073 Å
Crystal system	Monoclinic
Space group	C2/c
Unit cell dimensions	a = 15.7215(7) Å α = 90°.
	b = 14.6691(6) Å β = 101.7741(15)°.

c = 24.6032(11) Å γ = 90°.

Volume 5554.6(4) Å3

Z 4

Density (calculated) 1.746 Mg/m3

Absorption coefficient 5.989 mm-1

F(000) 2840

Crystal color colourless

Crystal size 0.160 x 0.160 x 0.057 mm3

Theta range for data collection 1.691 to 33.141°

Index ranges -23 <= *h* <= 24, -22 <= *k* <= 22, -37 <= *l* <= 37

Reflections collected 94028

Independent reflections 10598 [R(int) = 0.0359]

Completeness to theta = 25.242° 100.0 %

Absorption correction Semi-empirical from equivalents

Refinement method Full-matrix least-squares on F2

Data / restraints / parameters 10598 / 14 / 371

Goodness-of-fit on F2 1.052

Final R indices [I>2sigma(I) = 9696 data] R1 = 0.0247, wR2 = 0.0622

R indices (all data, 0.65 Å) R1 = 0.0283, wR2 = 0.0642

Largest diff. peak and hole 4.087 and -1.045 e.Å-3

X-Ray Structure of **62**:

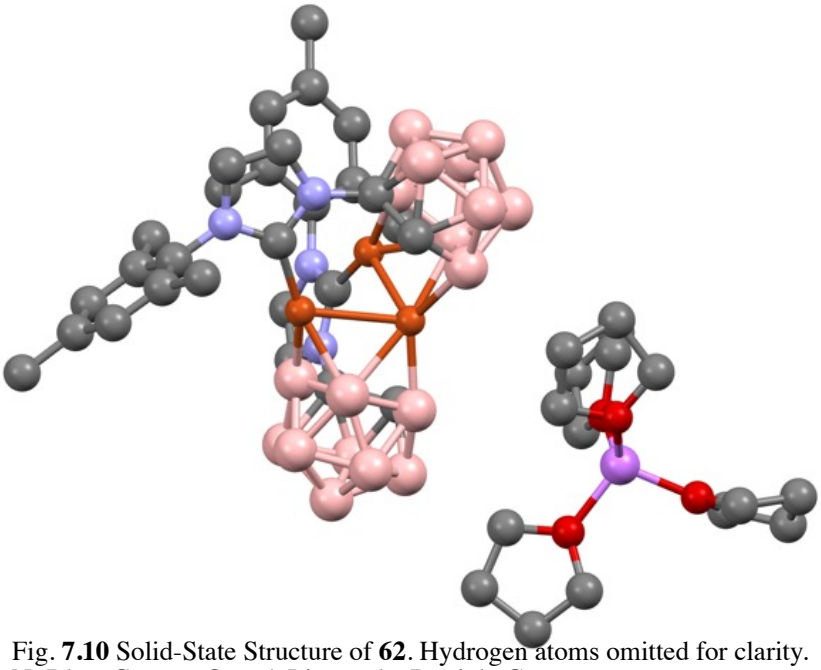

Fig. **7.10** Solid-State Structure of **62**. Hydrogen atoms omitted for clarity. N=Blue, C=grey, O=red, Li=purple, B=pink, Cu=orange

Data collection

The data collection was carried out using Mo Ka radiation (l = 0.71073 Å, ImS micro-source) with a frame time of 20 seconds and a detector distance of 45 mm. A collection strategy was calculated and complete data to a resolution of 0.83 Å were collected. The frames were integrated with the Bruker SAINT1 software package using a narrow-frame algorithm to 0.83 Å resolution. Data were corrected for absorption effects using the

multi-scan method (SADABS).2 Please refer to Table 1 for additional crystal and refinement information.

Structure solution and refinement

The space group P-1 was determined based on intensity statistics and systematic absences. The structure was solved using the SHELX suite of programs3 and refined using full-matrix least-squares on F2 within the OLEX2 suite.4 An intrinsic phasing solution was calculated, which provided most non-hydrogen atoms from the E-map. Full-matrix least squares / difference Fourier cycles were performed, which located the remaining non-hydrogen atoms. All non-hydrogen atoms were refined with anisotropic displacement parameters. The hydrogen atoms were placed in ideal positions and refined as riding atoms with relative isotropic displacement parameters. The final full matrix least squares refinement converged to R1 = 0.0642 and wR2 = 0.1872 (F2, all data). The goodness-of-fit was 1.034. On the basis of the final model, the calculated density was 1.325 g/cm3 and F(000), 1244 e-.

1SAINT, V8.30A, Bruker Analytical X-Ray Systems, Madison, WI, 2012.

2SADABS, 2.03, Bruker Analytical X-Ray Systems, Madison, WI, 2016.

3G. M. Sheldrick, Acta Cryst. A64, 112 - 122 (2008). Sheldrick, G.M. (2015). Acta Cryst. A71, 3-8.

4O. V. Dolomanov, L. J. Bourhis, R. J. Gildea, J. A. K. Howard and H. Puschmann, J. Appl.Crystallogr., 2009, 42, 339–341.

Table. **7.7** Crystal data and structure refinement for compound **62.**

Empirical formula C48 H86 B18 Cu3 Li N4 O5

Formula weight 1191.34

Crystal color and shape yellow block

Temperature 100.00 K

Wavelength 0.71073 Å

Crystal system, space group Triclinic, P-1

Unit cell dimensions a = 12.4406(10) Å a = 86.916(2)°.

b = 15.9529(13) Å b = 74.371(2)°.

c = 16.0714(14) Å g = 76.520(2)°.

Volume 2986.9(4) Å3

Z 2

Density (calculated) 1.325 g/cm3

Absorption coefficient 1.105 mm-1

F(000) 1244

Data collection

Diffractometer Bruker APEX-II CCD

Theta range for data collection 1.313 to 25.346°.

Index ranges -14<=h<=14, -19<=k<=19, -19<=l<=19

Reflections collected 34320

Independent reflections 10837 [Rint = 0.0509]

Observed Reflections 6941

Completeness to theta = 25.242° 99.5 %

Solution and Refinement

Absorption correction Semi-empirical from equivalents

Max. and min. transmission 0.5621 and 0.4776

Solution Intrinsic methods

Refinement method Full-matrix least-squares on F2

Weighting scheme w = [s2Fo2+ AP2+ BP]-1, with

P = (Fo2+ 2 Fc2)/3, A = 0.087, B = 7.21

Data / restraints / parameters 10837 / 10 / 728

Goodness-of-fit on F2 1.034

Final R indices [I>2s(I)] R1 = 0.0642, wR2 = 0.1590

R indices (all data) R1 = 0.1087, wR2 = 0.1872

Largest diff. peak and hole 1.080 and -0.600 e.Å-3

References

1. Kealy, T. J.; Pauson, P. L., A New Type of Organo-Iron Compound. *Nature* **1951,** 168 (4285), 1039-1040.

2. Wilkinson, G.; Rosenblum, M.; Whiting, M. C.; Woodward, R. B., THE STRUCTURE OF IRON BIS-CYCLOPENTADIENYL. *Journal of the American Chemical Society* **1952,** *74* (8), 2125-2126.

3. Pfab, W.; Fischer, E. O., Zur Kristallstruktur der Di-cyclopentadienyl-verbindungen des zweiwertigen Eisens, Kobalts und Nickels. *Zeitschrift für anorganische und allgemeine Chemie* **1953,** *274* (6), 316-322.

4. Hawthorne, M. F.; Young, D. C.; Garrett, P. M.; Owen, D. A.; Schwerin, S. G.; Tebbe, F. N.; Wegner, P. A., Preparation and characterization of the (3)-1,2- and (3)-1,7-dicarbadodecahydroundecaborate(-1) ions. *Journal of the American Chemical Society* **1968,** *90* (4), 862-868.

5. Hawthorne, M. F.; Young, D. C.; Andrews, T. D.; Howe, D. V.; Pilling, R. L.; Pitts, A. D.; Reintjes, M.; Warren, L. F., Jr.; Wegner, P. A., .pi.-Dicarbollyl derivatives of the transition metals. Metallocene analogs. *Journal of the American Chemical Society* **1968,** *90* (4), 879-896.

6. Kang, H. C.; Lee, S. S.; Knobler, C. B.; Hawthorne, M. F., Syntheses of charge-compensated dicarbollide ligand precursors and their use in the preparation of novel metallacarboranes. *Inorganic Chemistry* **1991,** *30* (9), 2024-2031.

7. Timofeev, S. V.; Sivaev, I. B.; Prikaznova, E. A.; Bregadze, V. I., Transition metal complexes with charge-compensated dicarbollide ligands. *Journal of Organometallic Chemistry* **2014,** *751*, 221-250.

8. Grimes, R. N., Metallacarboranes in the new millennium. *Coordination Chemistry Reviews* **2000,** *200-202*, 773-811.

9. Grimes, R. N., Chapter 13 - Metallacarboranes of the Transition and Lanthanide Elements. In *Carboranes (Third Edition)*, Grimes, R. N., Ed. Academic Press: Boston, 2016; pp 711-903.

10. Li, T. C.; Spokoyny, A. M.; She, C.; Farha, O. K.; Mirkin, C. A.; Marks, T. J.; Hupp, J. T., Ni(III)/(IV) Bis(dicarbollide) as a Fast, Noncorrosive Redox Shuttle for Dye-Sensitized Solar Cells. *Journal of the American Chemical Society* **2010,** *132* (13), 4580-4582.

11. Sivaev, I. B.; Bregadze, V. I., Chemistry of nickel and iron bis(dicarbollides). A review. *Journal of Organometallic Chemistry* **2000,** *614-615*, 27-36.

12. Stogniy, M. Y.; Kazheva, O. N.; Chudak, D. M.; Shilov, G. V.; Filippov, O. A.; Sivaev, I. B.; Kravchenko, A. V.; Starodub, V. A.; Buravov, L. I.; Bregadze, V. I.; Dyachenko, O. A., Synthesis and study of C-substituted methylthio derivatives of cobalt bis(dicarbollide). *RSC Advances* **2020,** *10* (5), 2887-2896.

13. Nelson, D. J.; Nolan, S. P., Quantifying and understanding the electronic properties of N-heterocyclic carbenes. *Chemical Society Reviews* **2013,** *42* (16), 6723-6753.

14. Lazreg, F.; Nahra, F.; Cazin, C. S. J., Copper–NHC complexes in catalysis. *Coordination Chemistry Reviews* **2015,** *293-294*, 48-79.

15. Arduengo, A. J., III; Harlow, R. L.; Kline, M., A stable crystalline carbene. *Journal of the American Chemical Society* **1991,** *113* (1), 361-363.

16. de Frémont, P.; Marion, N.; Nolan, S. P., Carbenes: Synthesis, properties, and organometallic chemistry. *Coordination Chemistry Reviews* **2009,** *253* (7), 862-892.

17. Fortman, G. C.; Nolan, S. P., N-Heterocyclic carbene (NHC) ligands and palladium in homogeneous cross-coupling catalysis: a perfect union. *Chemical Society Reviews* **2011,** *40* (10), 5151-5169.

18. Zhao, Q.; Meng, G.; Nolan, S. P.; Szostak, M., N-Heterocyclic Carbene Complexes in C–H Activation Reactions. *Chemical Reviews* **2020,** *120* (4), 1981-2048.

19. Marion, N.; Nolan, S. P., N-Heterocyclic carbenes in gold catalysis. *Chemical Society Reviews* **2008,** *37* (9), 1776-1782.

20. Martin, A. R.; Makida, Y.; Meiries, S.; Slawin, A. M. Z.; Nolan, S. P., Enhanced Activity of [Ni(NHC)CpCl] Complexes in Arylamination Catalysis. *Organometallics* **2013,** *32* (21), 6265-6270.

21. Kaur, H.; Zinn, F. K.; Stevens, E. D.; Nolan, S. P., (NHC)CuI (NHC = N-Heterocyclic Carbene) Complexes as Efficient Catalysts for the Reduction of Carbonyl Compounds. *Organometallics* **2004,** *23* (5), 1157-1160.

22. Díez-González, S.; Stevens, E. D.; Scott, N. M.; Petersen, J. L.; Nolan, S. P., Synthesis and Characterization of [Cu(NHC)2]X Complexes: Catalytic and Mechanistic Studies of Hydrosilylation Reactions. *Chemistry – A European Journal* **2008,** *14* (1), 158-168.

23. Izquierdo, F.; Manzini, S.; Nolan, S. P., The use of the sterically demanding IPr* and related ligands in catalysis. *Chemical Communications* **2014,** *50* (95), 14926-14937.

24. Tej Raviprolu, V.; McArthur, S. E.; Banda, I.; Gregory, A.; McArthur, S. G.; Fisher, S. P.; Lavallo, V., Fusing 10-vertex closo-carborane anions with N-heterocyclic carbenes. *Chemical Communications* **2022,** *58* (75), 10580-10582.

25. El-Hellani, A.; Lavallo, V., Fusing N-Heterocyclic Carbenes with Carborane Anions. *Angewandte Chemie International Edition* **2014,** *53* (17), 4489-4493.

26. Fisher, S. P.; McArthur, S. G.; Tej, V.; Lee, S. E.; Chan, A. L.; Banda, I.; Gregory, A.; Berkley, K.; Tsay, C.; Rheingold, A. L.; Guisado-Barrios, G.; Lavallo, V., Strongly Coordinating Ligands To Form Weakly Coordinating Yet Functional Organometallic Anions. *Journal of the American Chemical Society* **2020,** *142* (1), 251-256.

27. Estrada, J.; Lavallo, V., Fusing Dicarbollide Ions with N-Heterocyclic Carbenes. *Angewandte Chemie International Edition* **2017,** *56* (33), 9906-9909.

28. Vinogradov, M. M.; Nelyubina, Y. V.; Ikonnikov, N. S.; Strelkova, T. V.; Kudinov, A. R., First metallacarborane ethene complex [1,8-Me2-2,2-(C2H4)2-7-SMe2-2,1,8-IrC2B9H8] and its reaction with iodine. *Journal of Organometallic Chemistry* **2016,** *805*, 54-58.

29. Vinogradov, M. M.; Nelyubina, Y. V.; Pavlov, A. A.; Novikov, V. V.; Shvydkiy, N. V.; Kudinov, A. R., Polyhedral Rearrangements in the Complexes of Rhodium and Iridium with Isomeric Carborane Anions [7,8-Me2-X-SMe2-7,8-nido-C2B9H8]− (X = 9 and 10). *Organometallics* **2017,** *36* (4), 791-800.

30. Grafstein, D.; Dvorak, J., Neocarboranes, a new family of stable organoboranes isomeric with the carboranes. *Inorganic Chemistry* **1963,** *2* (6), 1128-1133.

31. Roa, A. E.; Salazar, V.; Mendoza-Espinosa, D.; Paneque, M.; Rodríguez-Diéguez, A.; Rodríguez, A. M.; Tejeda, J.; Castro-Osma, J. A.; Otero, A.; Lara-Sánchez, A., Study of the Coordination Modes of Hybrid NNCp Cyclopentadienyl/Scorpionate Ligands in Ir Compounds. *Inorganic Chemistry* **2019,** *58* (1), 900-908.

32. House, H. O.; Chu, C.-Y.; Wilkins, J. M.; Umen, M. J., Chemistry of carbanions. XXVII. Convenient precursor for the generation of lithium organocuprates. *The Journal of Organic Chemistry* **1975,** *40* (10), 1460-1469.

Chapter 8: Diverse Coordination Modes of the Dicarbollide and its Imidazolium Derivative

8.1 Introduction

Discovered by Hawthorne in 1965, the dicarbollides are obtained by the deboronation of the *o*-carborane followed by the deprotonation of the bridging hydride on the resulting *nido* face.[1] The frontier orbitals of the three borons and the two carbon atoms on the *nido* face of the cluster are isolobal with the classic cyclopentadienyl (Cp) ligand. Similar to Cp, the dicarbollides bind transition metals in an η^5 fashion forming the metallacarboranes, the dicarbollide analogues of metallocenes.[2]

In the previous chapter, we have shown that this analogy doesn't hold true when the dicarbollides are appended with a bulky electron withdrawing group like the imidazolium. The transmetalation of the bis(dicarbollide)iron derivatives like **58** to produce other metallacarboranes demonstrates a deviation from this long established trend. Subsequently, we became curious if other transition metal complexes of the dicarbollide-imidazolium ligand would display such interesting reactivity.

8.2 *Dicarbollide Pd Complexes*

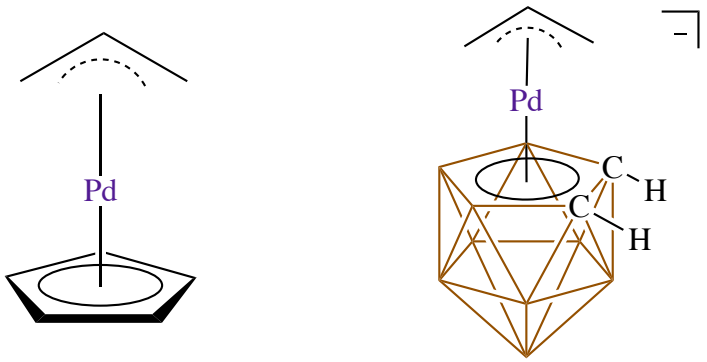

Fig. **8.1** CpPd(allyl) (left) and the corresponding dicarbollide analogue (right)

The group 10 allyl complexes serve as convenient precursors for organometallic complexes of nickel and palladium. The precursor $[Pd(allyl)Cl]_2$ dimer reacts with Cp^- to produce the well-known CpPd(allyl) complex (Fig. **8.1**). [3] This complex is widely used in catalysis for various organic transformations and in chemical vapor deposition of metallic palladium.[4-5] Despite this compound known since the 1970s, we were surprised to note that the dicarbollide analogue of this compound has not been reported so far.

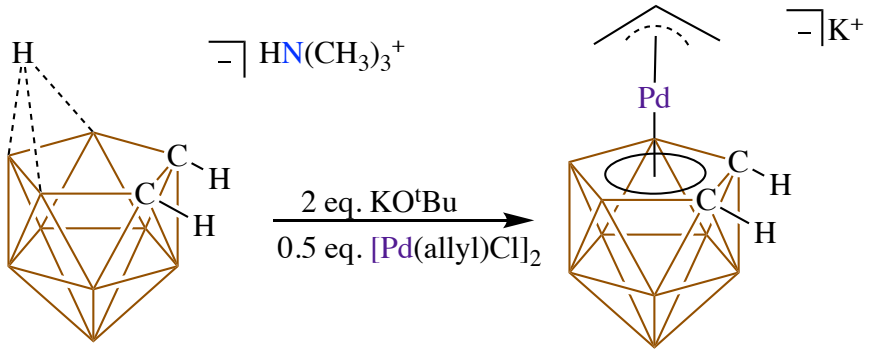

12 **69**

Scheme **8.1** Synthesis of the dicarbollide Pd(allyl) complex

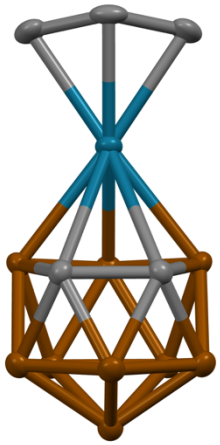

Fig. **8.2** Solid-State Structure of complex **69**. Hydrogen atoms, potassium counter-cation and THF molecules of solvation omitted for clarity. B=Brown, C=grey, Pd=ocean blue

When we reacted the $[Pd(allyl)Cl]_2$ precursor with the potassium salt of the dicarbollide in THF (Scheme **8.1**), a dark solution formed immediately. The crude ^1H NMR displayed

three distinct resonances at 2.3 ppm suggesting the formation of the expected [(dicarbollide) Pd(allyl)] complex. While the dicarbollide ligand displayed peaks at on the ^{11}B NMR, the crude reaction mixture displayed four peaks indicating the existence of one reaction product. The mass spectrometry performed on negative ion mode confirmed the identity of the complex. A single crystal X-Ray diffraction further established the structure of the compound unambiguously.

8.3 Dicarbollide-NHC Pd(II) Complex

We then reacted the same Pd precursor with the dicarbollide-imidazolium ligand **20**, expecting the formation of a complex similar to **69**. Given the precedence of the imidazolium carbon isomerization to the lower pentagonal belt of the cluster in case of Ir metallacarboranes,[6-8] we were curious if similar rearrangement would be observed

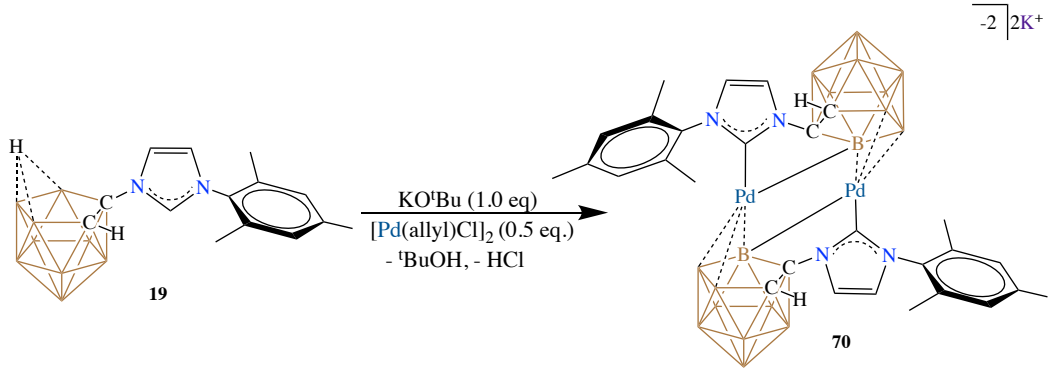

Scheme **8.2** Synthesis of the cyclometalated Pd(II) complex **70**

here.However, the crude ^{1}H NMR of the reaction mixture, displayed no resonances corresponding to the allyl ligand, unlike in the case of **69**. Moreover, the aromatic region displayed four resonances with all equal intensities corresponding to the two imidazolium backbone protons and two inequivalent mesityl ring protons. This probably indicates the formation of a Pd allyl complex initially with a concomitant C-H activation of the imidazolium ring C-2 proton. This might have been followed by reductive elimination of

the propene molecule, forming a Pd(II) complex that's coordinated both to the dicarbollide as well as the carbene ligands. This explains the reason behind the disappearance of the C-2 iminium proton and the allyl resonances on the ^{1}H NMR.

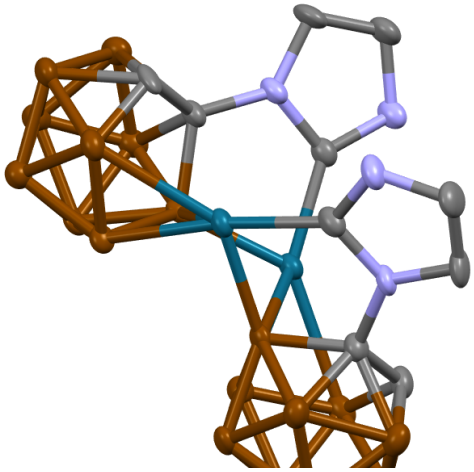

Fig. **8.3** Solid-State Structure of complex **70**. Hydrogen atoms, mesityl groups and potassium counter-cations omitted for clarity. B=Brown, C=grey, Pd=ocean blue, N=blue

To confirm the structure of the complex, X-Ray quality crystals were grown by diffusing fluorobenzene into a concentrated solution of the complex in acetonitrile. The solid-state structure revealed the dianionic dicarbollide-NHC coordinated Pd(II) complex (Fig. **8.2**). Interestingly, the dicarbollide is bound to Pd in a η^3 fashion via the three boron atoms unlike the classical η^5 way. Ring slipping to η^1 or η^3 coordination is more commonly seen in case of Cp ligands; this is one of the rare examples of a η^3 bound dicarbollide. The chloride abstracts a proton from one of the B-Hs in proximity and eliminates as HCl making a B-Pd covalent bond instead of the expected loss of KCl.

8.4 Conclusion

In this work, we show that although the dicarbollides are known to bind to transition metals in a η^5 bonding, this can be altered by functionalizing them with appropriate ligands. This

was demonstrated by the reaction of the dicarbollide and its imidazolium derivative with a Pd(II) precursor. This will provide insights into metallacarborane design that can potentially display novel coordination environment and reactivity.

8.5 Experimental

General Considerations:

Unless otherwise stated, all manipulations were performed inside a nitrogen filled glove box or under standard schlenk techniques (O_2, H_2O < 1 ppm). THF and diethyl ether were distilled under argon with K and NaK respectively. Fluorobenzene and acetonitrile were dried on CaH_2 and distilled under argon. Benzene, THF and toluene were dried on K and Na and distilled under argon respectively. Hexanes was dried in a solvent purification system and collected under argon. The imidazolium **19**,[9] and the *nido* carborane **12**,[1] were synthesized according to literature methods. All other reagents were purchased from commercial sources and used without any further purification. NMR spectra were recorded on Bruker Avance 300, Bruker Avance 600 and Varian Inova 400 MHz spectrometers. ^{1}H and ^{13}C NMRs are referenced to the residual solvents. ^{11}B NMRs were externally referenced to $BF_3.Et_2O$. ^{31}P NMRs were externally referenced to 80% H_3PO_4 in H_2O. High Resolution Mass Spectrometry data was recorded on Agilent Technologies 6210 (Time of Flight LC/MS) using ESI technique.

Synthesis of **69**:

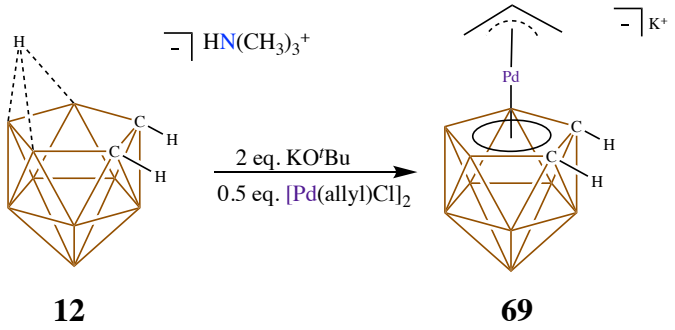

12 **69**

Scheme **8.1** Synthesis of the dicarbollide Pd(allyl) complex

In a vial, **12** (100 mg, 0.51 mmol) was dissolved in THF (2 mL). A solution of KO^{t}Bu (125.9 mg, 1.12 mmol, 2.2 eq) in THF (2 mL) was then added to **12** and stirred for 10 minutes. To the solution, $[Pd(allyl)Cl]_2$ (95.1 mg, 0.26 mmol) dissolved in THF (4 mL) was added. The dark solution was then stirred for 15 minutes after which the solution was filtered over celite, and the volatiles were pumped down under vacuum. Compound **69** was then obtained as a dark solid in 90% yield. ^{1}H NMR (600 MHz, THF-d_8, 25^{o}C): 5.11 (m, 1H, CH), 3.83 (d, 2H, CH_2 allyl), 2.99 (d, 2H, CH_2 allyl), 2.07 (bs, carborane CH); ^{11}B NMR (192 MHz, THF-d_8, 25^{o}C): -1.17, -13.49, -21.01, -23.45 ppm. ^{13}C[^{1}H] NMR (150 MHz, THF, 25^{o}C): 96.67, 67.32, 52.63, 33.23, 32.14 ppm.

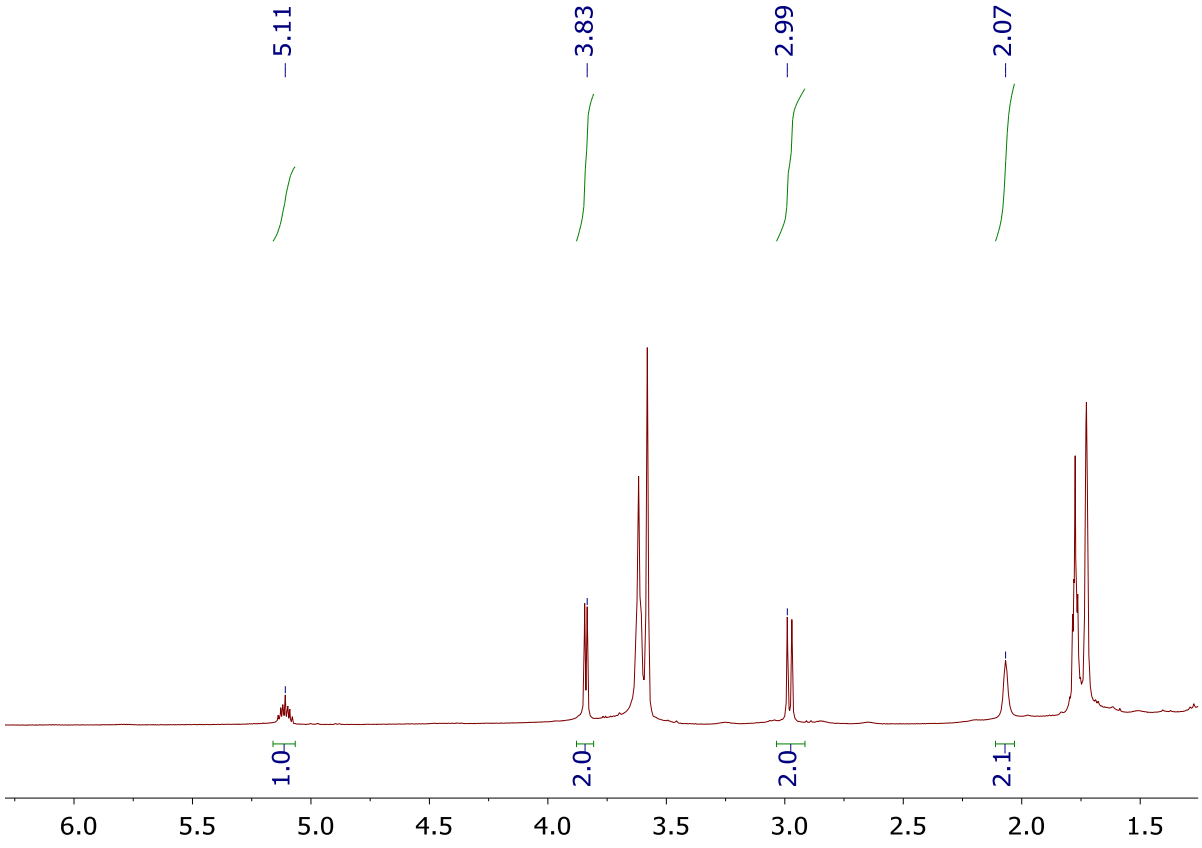

Fig. **8.4** ^{1}H NMR spectrum of compound **69** in THF-d_8

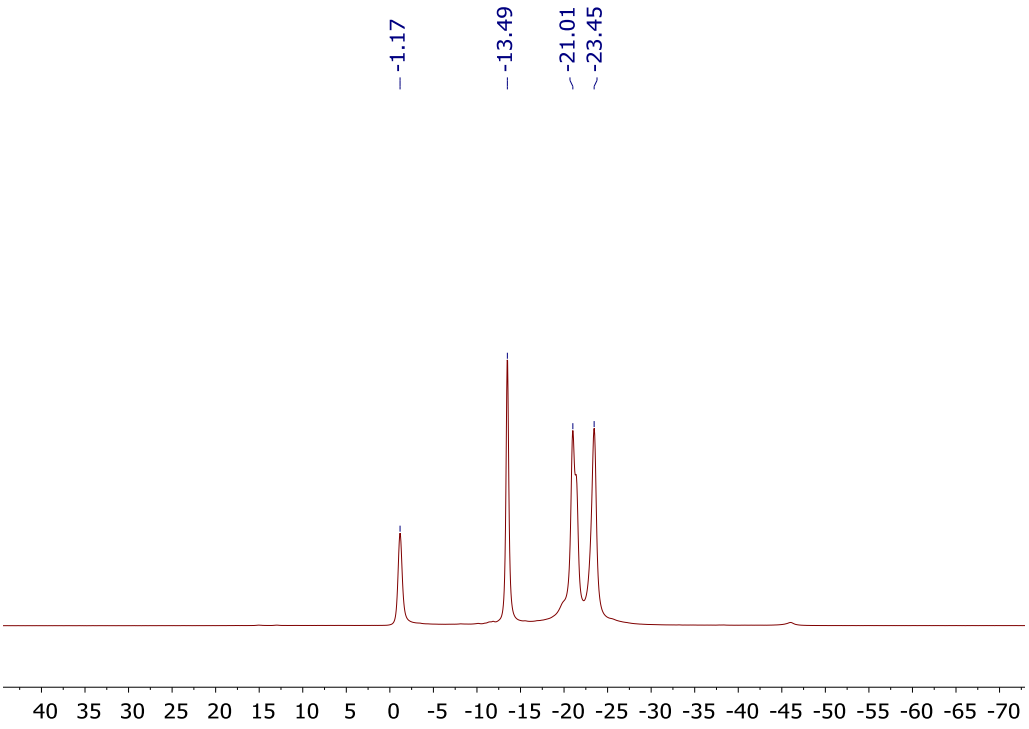

Fig. **8.5** $^{11}B[^{1}H]$ NMR spectrum of compound **69** in THF-d_8

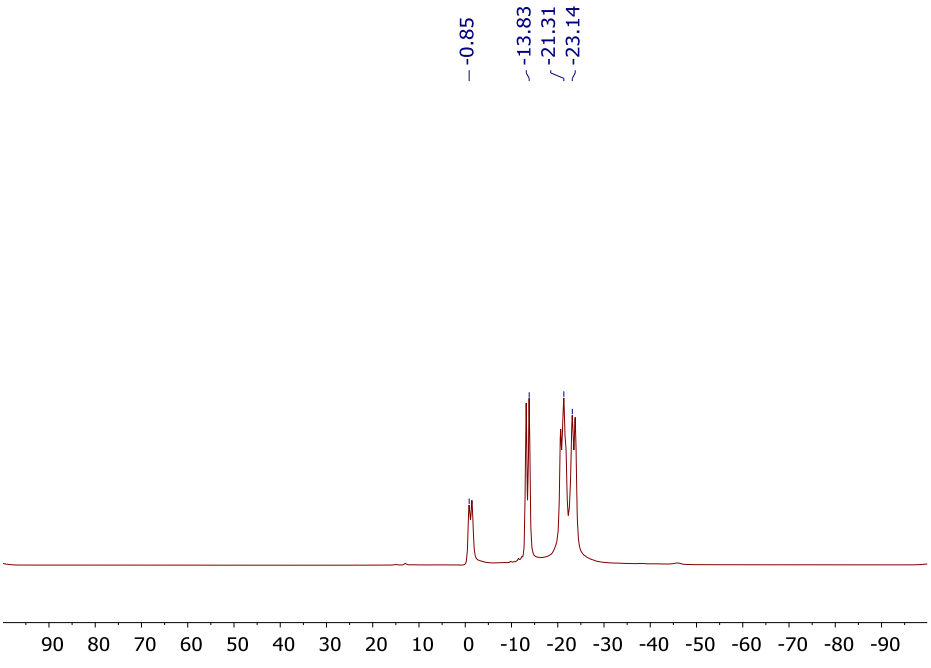

Fig. **8.6** ^{11}B NMR spectrum of compound **69** in THF-d_8

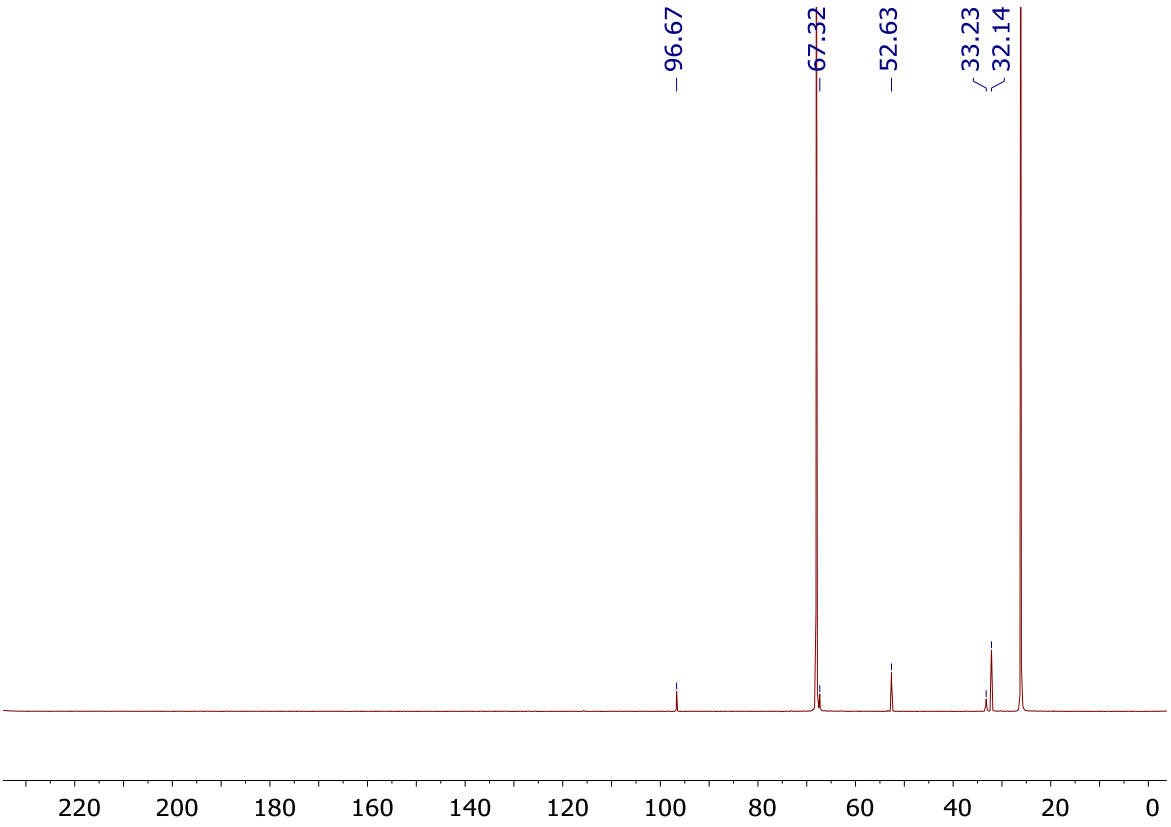

Fig. **8.7** $^{13}C[^{1}H]$ NMR spectrum of compound **69** in THF

Synthesis of **70**:

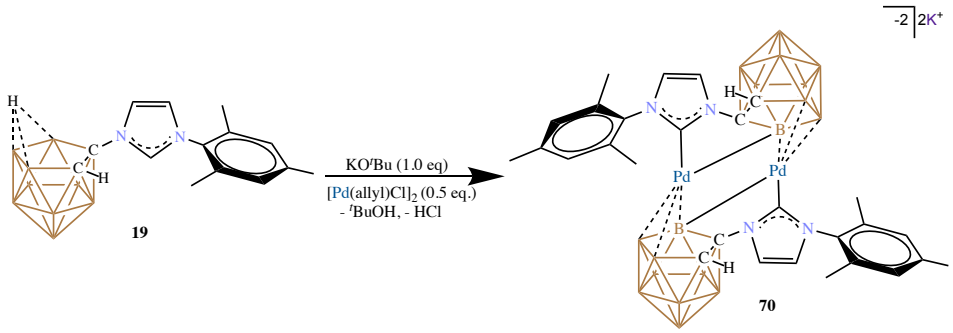

Scheme **8.2** Synthesis of the cyclometalated Pd(II) complex **70**

In a vial, **19** (100 mg, 0.31 mmol) was weighed and dissolved in THF (2 mL). To this, a solution of KO^{t}Bu (52.1 mg, 0.46 mmol, 1.5 eq) in THF (2 mL) was added and stirred for 5 minutes. A solution of [Pd(allyl)Cl]$_2$ (57.1 mg, 0.156 mmol) in THF (4 mL) was added. The solution turned deep red immediately and then dark. The dark solution was then stirred

for an hour. The volatiles were then pumped down under vacuum and the dark crude dissolved in acetonitrile (10 mL). The solution was then filtered over celite and the filtrate pumped down under vacuum to afford **70** as a dark brown microcrystalline powder in 75% yield. ^{1}H NMR (600 MHz, CD_3CN, 25°C): 6.96 (s, 1H, mesityl CH), 6.88 (s, 1H, mesityl CH), 6.71 (d, 1H, CH), 6.48 (d, 1H, CH), 2.28 (s, 3H, mesityl CH_3), 1.99 (s, 3H, mesityl CH_3), 1.76 (s, 3H, mesityl CH_3); ^{11}B NMR (192 MHz, CD_3CN, 25°C): -5.01, -15.17, -20.07, -24.70, -28.96, -33.40, -39.36 ppm. ^{13}C[^{1}H] NMR (100 MHz, CD_3CN, 25°C): 190.19, 138.67, 137.38, 136.82, 136.26, 129.34, 129.14, 116.48, 21.09, 18.96, 18.11 ppm.

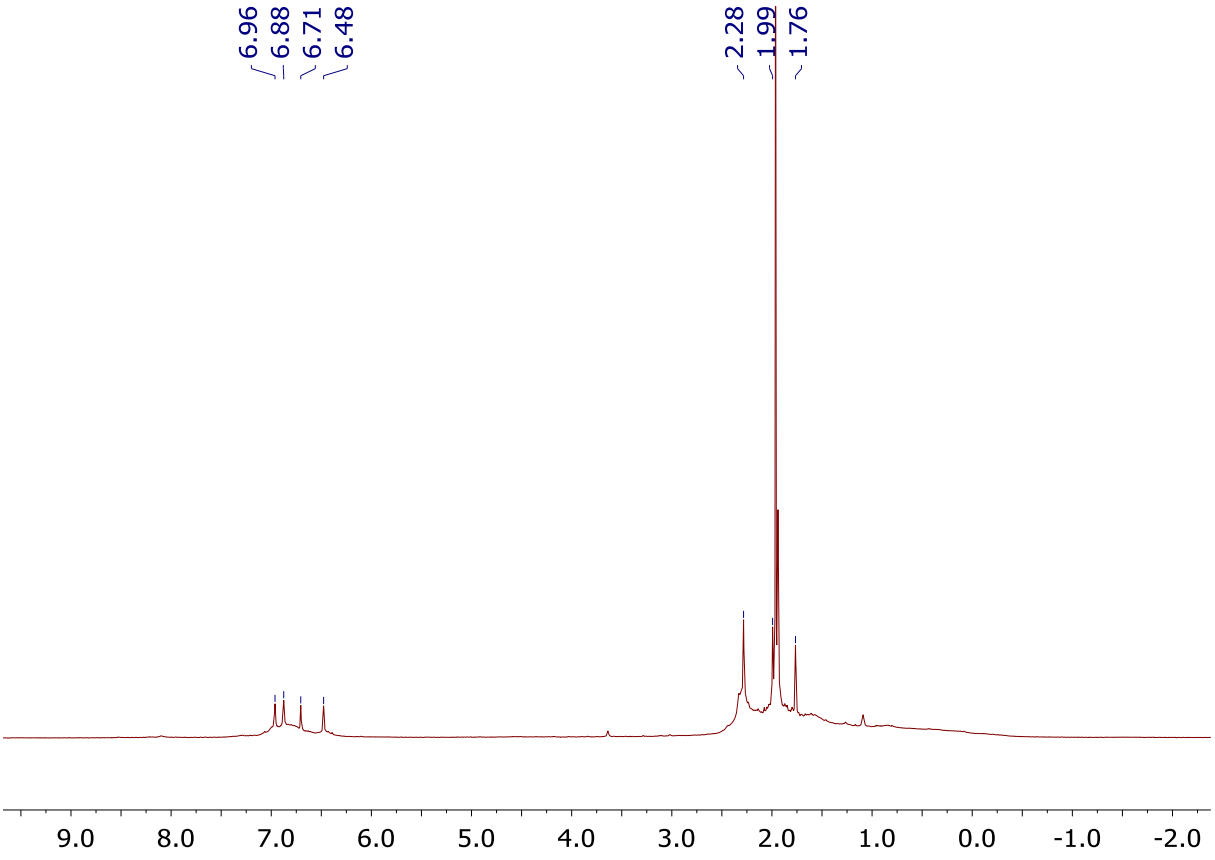

Fig. **8.8** ^{1}H NMR spectrum of **70** in CD_3CN

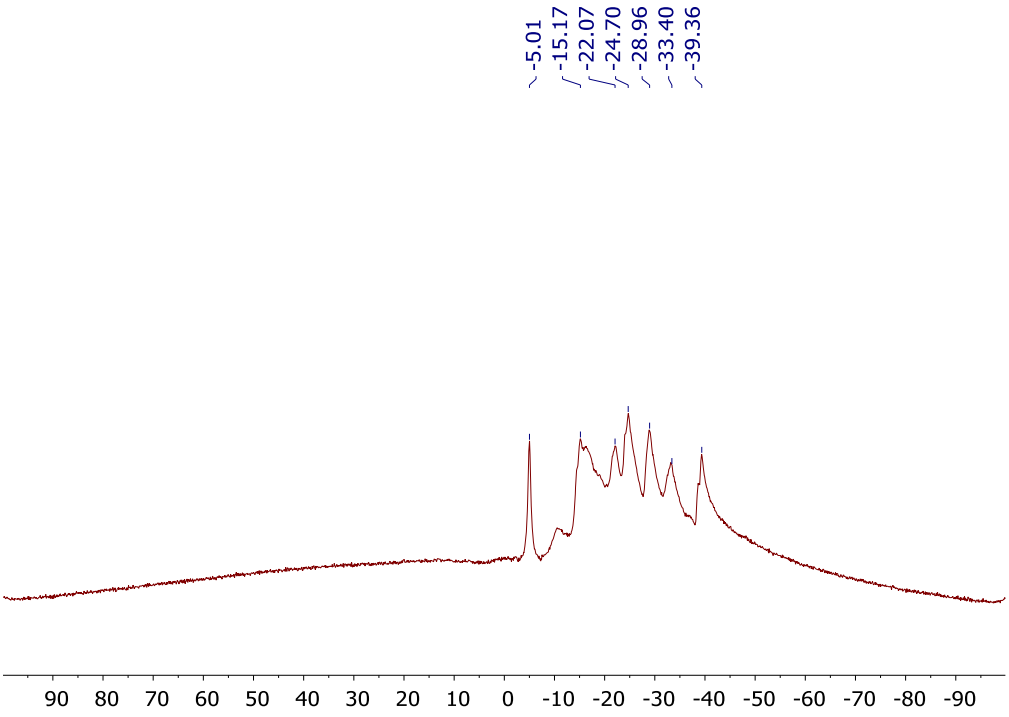

Fig. **8.9** ^{11}B NMR spectrum of **70** in CD_3CN

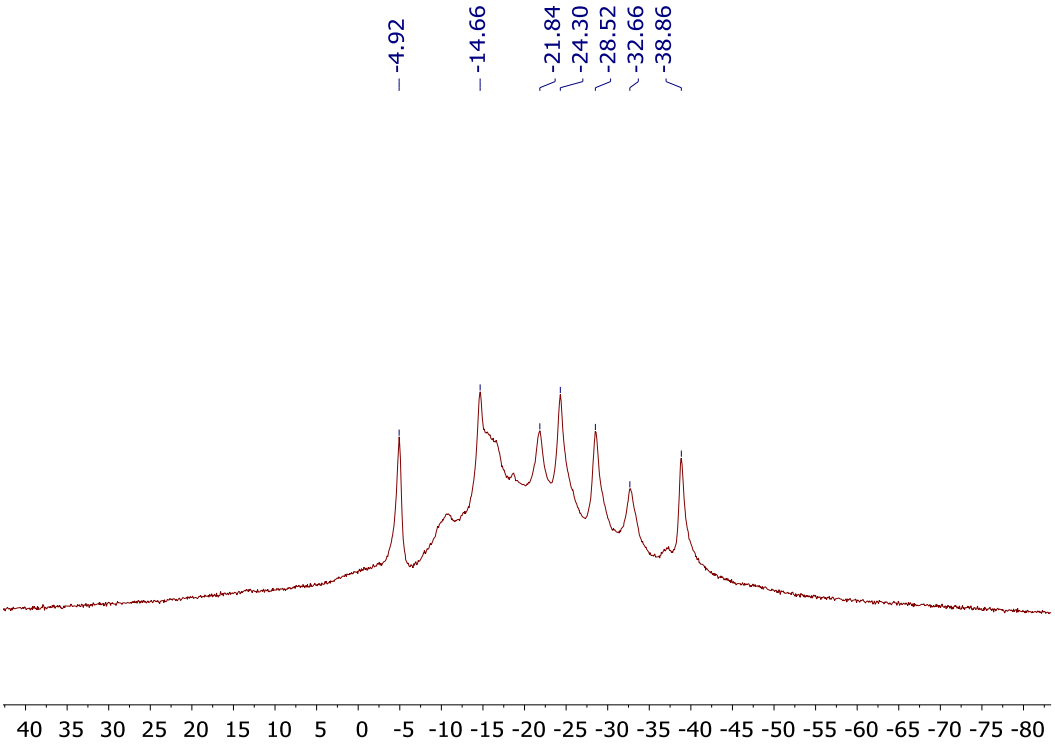

Fig. **8.10** $^{11}B[^{1}H]$ NMR spectrum of **70** in CD_3CN

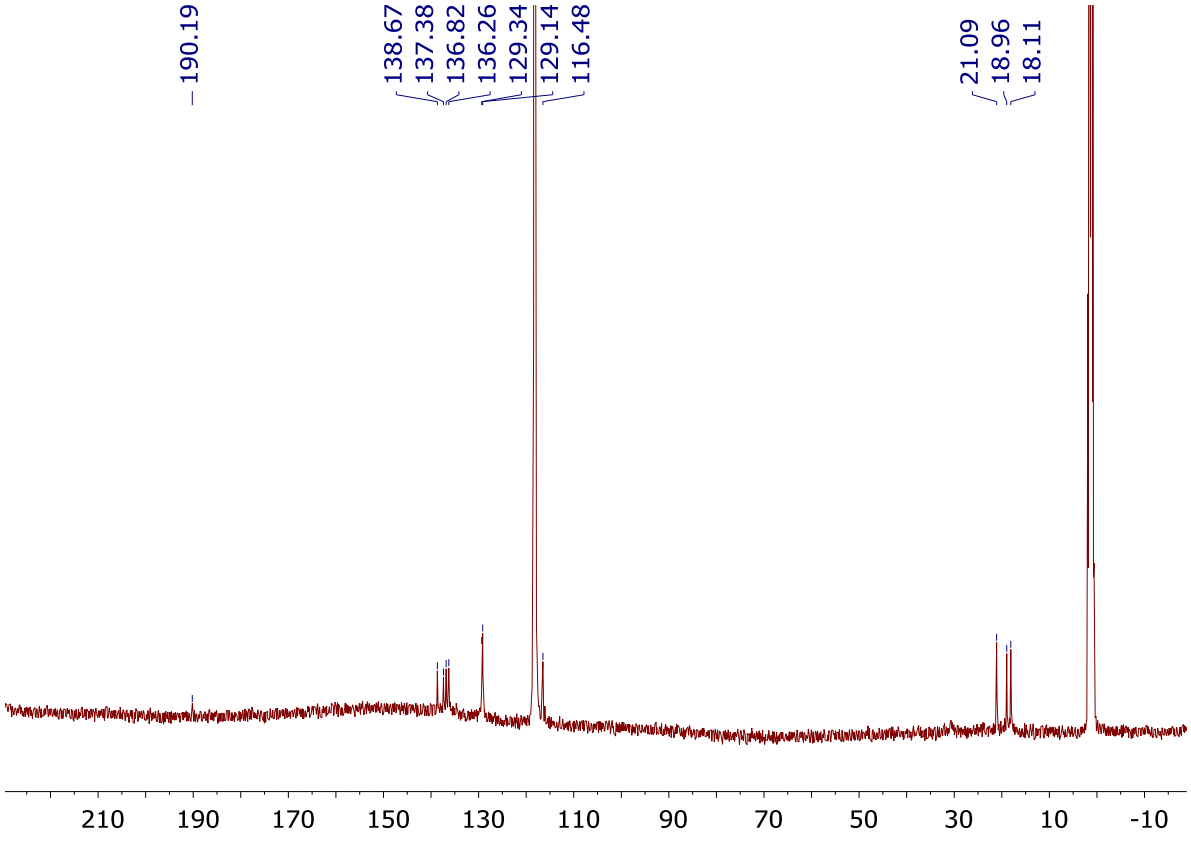

Fig. **8.11** $^{13}C[^{1}H]$ NMR spectrum of **70** in CD_3CN

X-Ray Structure Determination

X-Ray Structure of **70**:

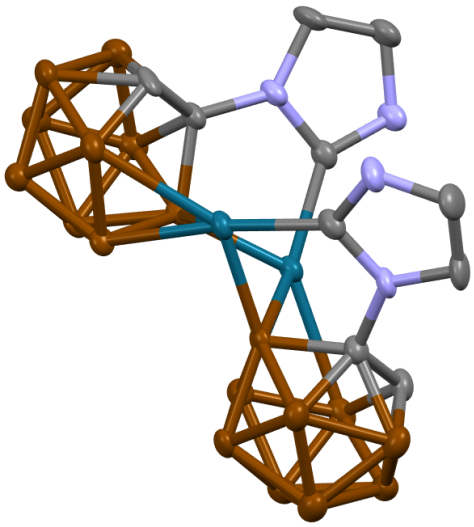

Fig. **8.12** Solid-State Structure of complex **70**. Hydrogen atoms, mesityl groups and potassium counter-cations omitted for clarity. B=Brown, C=grey, Pd=ocean blue, N=blue

The sample was submitted by Varun Tej (research group of Professor Vince Lavallo, Department of Chemistry, University of California, Riverside). The report was prepared by Dr. Veronica Carta.

Data collection

Single crystals suitable for X-ray diffraction were grown by slow evaporation of a solution of acetonitrile and fluorobenzene. An orange crystal (block, approximate dimensions 0.11 × 0.09 × 0.05 mm^3) was placed onto the tip of a MiTeGen pin and mounted on a Bruker Venture D8 diffractometer equipped with a PhotonIII detector at 123 K. The data collection was carried out using Mo Kα radiation (λ = 0.71073 Å, graphite monochromator) with a

frame time of 5 seconds and a detector distance of 50 mm. A collection strategy was calculated and complete data to a resolution of 0.80 Å with a redundancy of 6.5 were collected. The frames were integrated with the Bruker SAINT[1] software package using a narrow-frame algorithm. The integration of the data using a triclinic unit cell yielded a total of 207672 reflections to a maximum θ angle of 25.08° (0.84 Å resolution), of which 23987 were independent (average redundancy 8.658, completeness = 99.6%, Rint = 17.78%, Rsig = 9.92%) and 15634 (65.18%) were greater than 2σ(F2). The final cell constants of a = 17.0485(9) Å, b = 17.1271(10) Å, c = 25.0686(14) Å, α = 77.1804(18)°, β = 80.5761(17)°, γ = 72.4746(16)°, volume = 6769.0(7) Å3, are based upon the refinement of the XYZ-centroids of 9962 reflections above 20 σ(I) with 4.397° < 2θ < 48.27°. Data were corrected for absorption effects using the Multi-Scan method (SADABS).[2] The ratio of minimum to maximum apparent transmission was 0.960. The calculated minimum and maximum transmission coefficients (based on crystal size) are 0.6969 and 0.7318.

Structure solution and refinement

The space group P-1 was determined based on intensity statistics and systematic absences. The structure was solved using the SHELX suite of programs [3] and refined using full-matrix least-squares on F^2 within the OLEX2 suite.[4] An intrinsic phasing solution was calculated, which provided most non-hydrogen atoms from the E-map. Full-matrix least squares / difference Fourier cycles were performed, which located the remaining non-hydrogen atoms. All non-hydrogen atoms were refined with anisotropic displacement parameters. The hydrogen atoms were placed in ideal positions and refined as riding atoms with relative

isotropic displacement parameters, except for the hydrogen atoms involved in interactions with the potassium ions, which were refined unrestrained. The final full matrix least squares refinement converged to R1 = 0.0508 and wR2 = 0.1180 (F^2, all data). The goodness-of-fit was 1.015. On the basis of the final model, the calculated density was 1.475 g/cm^3 and F(000), 3014 e^-.

[1]SAINT, V8.30A, Bruker Analytical X-Ray Systems, Madison, WI, 2012.

[2]SADABS, 2.03, Bruker Analytical X-Ray Systems, Madison, WI, 2016.

[3]G. M. Sheldrick, Acta Cryst. A64, 112 - 122 (2008). Sheldrick, G.M. (2015). Acta Cryst. A71, 3-8.

[4]O. V. Dolomanov, L. J. Bourhis, R. J. Gildea, J. A. K. Howard and H. Puschmann, J. Appl. Crystallogr., 2009, 42, 339–341.

Table 8.1 Crystal data and structure refinement for **70**

Empirical formula	C194 H295 B108 F2 K12 N31 Pd12
Formula weight	6013.07
Crystal color, shape, size	orange block, 0.11 × 0.09 × 0.05 mm^3
Temperature	123 K
Wavelength	0.71073 Å
Crystal system, space group	Triclinic, P-1
Unit cell dimensions	a = 17.0485(9) Å α = 77.1804(18)°.
	b = 17.1271(10) Å β = 80.5761(17)°.
	c = 25.0686(14) Å γ = 72.4746(16)°.
Volume	6769.0(7) $Å^3$
Z	1

Density (calculated) 1.475 g/cm^3

Absorption coefficient 1.016 mm^{-1}

F(000) 3014

Data collection

DiffractometerBRUKER D8 VENTURE

Theta range for data collection 1.268 to 25.084°.

Index ranges -20<=h<=20, -20<=k<=20, -29<=l<=29

Reflections collected 207672

Independent reflections 23987 [Rint = 0.1778]

Observed Reflections 15634

Completeness to theta = 25.084° 99.6 %

Solution and Refinement

Absorption correction Semi-empirical from equivalents

Max. and min. transmission 0.7318 and 0.6969

Solution Intrinsic methods

Refinement method Full-matrix least-squares on F^2

Weighting scheme $w = [\sigma^2 Fo^2 + AP^2 + BP]^{-1}$, with

$P = (Fo^2 + 2\,Fc^2)/3$, A = 0.0388, B = 11.903999

Data / restraints / parameters 23987 / 3119 / 1668

Goodness-of-fit on F^2 1.015

Final R indices [I>2σ(I)] R1 = 0.0508, wR2 = 0.0988

R indices (all data) R1 = 0.1024, wR2 = 0.1180

Extinction coefficient 0.00008(2)

Largest diff. peak and hole 1.316 and -1.008 e.Å^{-3}

X-Ray Structure of **69**

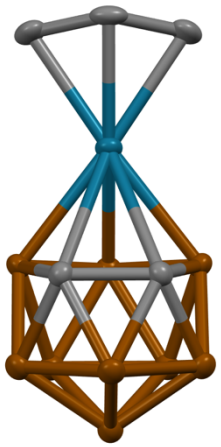

Fig. **8.13** Solid-State Structure of complex **69**. Hydrogen atoms, potassium counter-cation and THF molecules of solvation omitted for clarity. B=Brown, C=grey, Pd=ocean blue

Data collection

Single crystals suitable for X-ray diffraction were grown by solvent diffusion of hexane into tetrahydrofuran. An orange crystal (needle, approximate dimensions 0.3 × 0.03 × 0.02 mm3) was placed onto the tip of a MiTeGen pin and mounted on a Bruker Venture D8 diffractometer equipped with a PhotonIII detector at 100 K. The data collection was carried out using Mo Ka radiation (l = 0.71073 Å, ImS micro-source) with a frame time of 10 seconds and a detector distance of 40 mm. A collection strategy was calculated and complete data to a resolution of 0.77 Å were collected. The frames were integrated with the Bruker SAINT1 software package using a narrow-frame algorithm to 0.77 Å resolution. Data were corrected for absorption effects using the multi-scan method (SADABS).2 Please refer to Table 1 for additional crystal and refinement information.

Structure solution and refinement

The space group P 2 1 /m was determined based on intensity statistics and systematic absences. The structure was solved using the SHELX suite of programs3 and refined using full-matrix least-squares on F2 within the OLEX2 suite.4 An intrinsic phasing solution was calculated, which provided most non-hydrogen atoms from the E-map. Full-matrix least squares / difference Fourier cycles were performed, which located the remaining non-hydrogen atoms. All non-hydrogen atoms were refined with anisotropic displacement parameters. The hydrogen atoms were placed in ideal positions and refined as riding atoms with relative isotropic displacement parameters, except for H1A, H2, H5, and H6 which were refined freely. Disorder was modelled for a THF molecule on a special position. The final full matrix least squares refinement converged to R1 = 0.0342 and wR2 = 0.0805 (F2, all data). The goodness-of-fit was 1.032. On the basis of the final model, the calculated density was 1.557 g/cm3 and F(000), 392 e-.

1SAINT, V8.30A, Bruker Analytical X-Ray Systems, Madison, WI, 2012.

2SADABS, 2.03, Bruker Analytical X-Ray Systems, Madison, WI, 2016.

3G. M. Sheldrick, Acta Cryst. A64, 112 - 122 (2008). Sheldrick, G.M. (2015). Acta Cryst. A71, 3-8.

4O. V. Dolomanov, L. J. Bourhis, R. J. Gildea, J. A. K. Howard and H. Puschmann, J. Appl. Crystallogr.,

2009, 42, 339–341.

Table 8.2. Crystal data and structure refinement for compound **69**

Empirical formula C9 H24 B9 K O Pd

Formula weight 391.07

Crystal color, shape, size orange needle, 0.3 × 0.03 × 0.02 mm3

Temperature 100 K

Wavelength 0.71073 Å

Crystal system, space group Monoclinic, P 2 1 /m

Unit cell dimensions a = 9.1397(6) Å a = 90°.

b = 8.3508(6) Å b = 93.661(2)°.

c = 10.9550(8) Å g = 90°.

Volume 834.42(10) Å3

Z 2

Density (calculated) 1.557 g/cm3

Absorption coefficient 1.347 mm-1

F(000) 392

Data collection

Diffractometer Bruker D8 Venture

Theta range for data collection 1.863 to 27.527°.

Index ranges -11<=h<=11, -10<=k<=10, -14<=l<=14

Reflections collected 28515

Independent reflections 2039 [Rint = 0.0757]

Observed Reflections 1856

Completeness to theta = 25.242° 100.0 %

Solution and Refinement

Absorption correction Semi-empirical from equivalents

Max. and min. transmission 0.7456 and 0.6688

Solution Intrinsic methods

Refinement method Full-matrix least-squares on F2

Weighting scheme w = [s2Fo2+ AP2+ BP]-1, with

P = (Fo2+ 2 Fc2)/3, A = 0.031, B = 2.73

Data / restraints / parameters 2039 / 30 / 142

Goodness-of-fit on F2 1.032

Final R indices [I>2s(I)] R1 = 0.0342, wR2 = 0.0785

R indices (all data) R1 = 0.0384, wR2 = 0.0805

Largest diff. peak and hole 1.083 and -0.976 e.Å-3

References

1. Hawthorne, M. F.; Young, D. C.; Garrett, P. M.; Owen, D. A.; Schwerin, S. G.; Tebbe, F. N.; Wegner, P. A., Preparation and characterization of the (3)-1,2- and (3)-1,7-dicarbadodecahydroundecaborate(-1) ions. *Journal of the American Chemical Society* **1968,** *90* (4), 862-868.

2. Hawthorne, M. F.; Young, D. C.; Andrews, T. D.; Howe, D. V.; Pilling, R. L.; Pitts, A. D.; Reintjes, M.; Warren, L. F., Jr.; Wegner, P. A., .pi.-Dicarbollyl derivatives of the transition metals. Metallocene analogs. *Journal of the American Chemical Society* **1968,** *90* (4), 879-896.

3. McClellan, W. R.; Hoehn, H. H.; Cripps, H. N.; Muetterties, E. L.; Howk, B. W., π-Allyl Derivatives of Transition Metals. *Journal of the American Chemical Society* **1961,** *83* (7), 1601-1607.

4. Niklewski, A.; Strunskus, T.; Witte, G.; Wöll, C., Metal−Organic Chemical Vapor Deposition of Palladium: Spectroscopic Study of Cyclopentadienyl-allyl-palladium Deposition on a Palladium Substrate. *Chemistry of Materials* **2005,** *17* (4), 861-868.

5. Gozum, J. E.; Pollina, D. M.; Jensen, J. A.; Girolami, G. S., "Tailored" organometallics as precursors for the chemical vapor deposition of high-purity palladium and platinum thin films. *Journal of the American Chemical Society* **1988,** *110* (8), 2688-2689.

6. Vinogradov, M. M.; Nelyubina, Y. V.; Ikonnikov, N. S.; Strelkova, T. V.; Kudinov, A. R., First metallacarborane ethene complex [1,8-Me2-2,2-(C2H4)2-7-SMe2-2,1,8-IrC2B9H8] and its reaction with iodine. *Journal of Organometallic Chemistry* **2016,** *805*, 54-58.

7. Vinogradov, M. M.; Nelyubina, Y. V.; Pavlov, A. A.; Novikov, V. V.; Shvydkiy, N. V.; Kudinov, A. R., Polyhedral Rearrangements in the Complexes of Rhodium and Iridium with Isomeric Carborane Anions [7,8-Me2-X-SMe2-7,8-nido-C2B9H8]− (X = 9 and 10). *Organometallics* **2017,** *36* (4), 791-800.

8. Timofeev, S. V.; Sivaev, I. B.; Prikaznova, E. A.; Bregadze, V. I., Transition metal complexes with charge-compensated dicarbollide ligands. *Journal of Organometallic Chemistry* **2014,** *751*, 221-250.

9. Estrada, J.; Lavallo, V., Fusing Dicarbollide Ions with N-Heterocyclic Carbenes. *Angewandte Chemie International Edition* **2017,** *56* (33), 9906-9909.

Conclusion

In conclusion, the use of carboranes in NHC design unraveled their potential in unexplored avenues. The molecules that were studied as mere synthetic curiosities 50 years back were functionalized to produce some of the best catalysts discovered so far. Unlike the traditional transition metal chemistry focused primarily at the metal center, the inherent charge on these molecules was utilized to synthesize complex organometallic systems bound by electrostatic attraction forces. These systems were shown to cooperatively activate small molecules and catalyze multiple organic transformations. The flexible tuning of electronics and sterics of carboranes by halogenation allowed us to isolate a truly water stable dianionic carbene, only limited to theoretical predictions thus far. Unlike forming carbene complexes when reacted with transition metals, unprecedented transmetalation was observed when these NHCs were reacted with other transition metals. These reactivity and catalysis investigations open the door for exploration of carboranes as building blocks for ligands and metal complexes. These synthetic methodologies will be applicable to a broad range of fields like biology, medicine and material sciences and aid in their advancement.